OXYLIPINS: THE FRONT LINE OF PLANT INTERACTIONS

EDITED BY: Koichi Sugimoto, Silke Allmann and Michael V. Kolomiets

PUBLISHED IN: Frontiers in Plant Science

frontiers Research Topics

frontiers

Frontiers eBook Copyright Statement

The copyright in the text of individual articles in this eBook is the property of their respective authors or their respective institutions or funders. The copyright in graphics and images within each article may be subject to copyright of other parties. In both cases this is subject to a license granted to Frontiers.

The compilation of articles constituting this eBook is the property of Frontiers.

Each article within this eBook, and the eBook itself, are published under the most recent version of the Creative Commons CC-BY licence. The version current at the date of publication of this eBook is CC-BY 4.0. If the CC-BY licence is updated, the licence granted by Frontiers is automatically updated to the new version.

When exercising any right under the CC-BY licence, Frontiers must be attributed as the original publisher of the article or eBook, as applicable.

Authors have the responsibility of ensuring that any graphics or other materials which are the property of others may be included in the CC-BY licence, but this should be checked before relying on the CC-BY licence to reproduce those materials. Any copyright notices relating to those materials must be complied with.

Copyright and source acknowledgement notices may not be removed and must be displayed in any copy, derivative work or partial copy which includes the elements in question.

All copyright, and all rights therein, are protected by national and international copyright laws. The above represents a summary only. For further information please read Frontiers' Conditions for Website Use and Copyright Statement, and the applicable CC-BY licence.

ISSN 1664-8714
ISBN 978-2-88974-568-5
DOI 10.3389/978-2-88974-568-5

About Frontiers

Frontiers is more than just an open-access publisher of scholarly articles: it is a pioneering approach to the world of academia, radically improving the way scholarly research is managed. The grand vision of Frontiers is a world where all people have an equal opportunity to seek, share and generate knowledge. Frontiers provides immediate and permanent online open access to all its publications, but this alone is not enough to realize our grand goals.

Frontiers Journal Series

The Frontiers Journal Series is a multi-tier and interdisciplinary set of open-access, online journals, promising a paradigm shift from the current review, selection and dissemination processes in academic publishing. All Frontiers journals are driven by researchers for researchers; therefore, they constitute a service to the scholarly community. At the same time, the Frontiers Journal Series operates on a revolutionary invention, the tiered publishing system, initially addressing specific communities of scholars, and gradually climbing up to broader public understanding, thus serving the interests of the lay society, too.

Dedication to Quality

Each Frontiers article is a landmark of the highest quality, thanks to genuinely collaborative interactions between authors and review editors, who include some of the world's best academicians. Research must be certified by peers before entering a stream of knowledge that may eventually reach the public - and shape society; therefore, Frontiers only applies the most rigorous and unbiased reviews.
Frontiers revolutionizes research publishing by freely delivering the most outstanding research, evaluated with no bias from both the academic and social point of view. By applying the most advanced information technologies, Frontiers is catapulting scholarly publishing into a new generation.

What are Frontiers Research Topics?

Frontiers Research Topics are very popular trademarks of the Frontiers Journals Series: they are collections of at least ten articles, all centered on a particular subject. With their unique mix of varied contributions from Original Research to Review Articles, Frontiers Research Topics unify the most influential researchers, the latest key findings and historical advances in a hot research area! Find out more on how to host your own Frontiers Research Topic or contribute to one as an author by contacting the Frontiers Editorial Office: frontiersin.org/about/contact

OXYLIPINS: THE FRONT LINE OF PLANT INTERACTIONS

Topic Editors:
Koichi Sugimoto, University of Tsukuba, Japan
Silke Allmann, University of Amsterdam, Netherlands
Michael V. Kolomiets, Texas A&M University, United States

Citation: Sugimoto, K., Allmann, S., Kolomiets, M. V., eds. (2022). Oxylipins: The Front Line of Plant Interactions. Lausanne: Frontiers Media SA.
doi: 10.3389/978-2-88974-568-5

Table of Contents

frontiers in Plant Science

EDITORIAL
published: 28 March 2022
doi: 10.3389/fpls.2022.878765

Editorial: Oxylipins: The Front Line of Plant Interactions

Koichi Sugimoto[1]*, *Silke Allmann*[2]* and *Michael V. Kolomiets*[3]*

[1] Tsukuba-Plant Innovation Research Center, University of Tsukuba, Ibaraki, Japan, [2] Department of Plant Physiology, Green Life Sciences Research Cluster, Swammerdam Institute for Life Sciences, University of Amsterdam, Amsterdam, Netherlands, [3] Department of Plant Pathology and Microbiology, Texas A&M University, College Station, TX, United States

Keywords: plant oxylipins, oxidized lipids, volatile organic compounds, biotic interactions, abiotic stresses, jasmonates

Editorial on the Research Topic

Oxylipins: The Front Line of Plant Interactions

In this Research Topic, a collection of high-quality papers represents advances in our understanding of synthesis, biological functions and signaling activities of volatile and non-volatile plant oxylipins. Oxylipins are a large group of functionally and structurally diverse molecules produced from oxidized lipids and are widely known to have various roles in plant growth, development and interactions with biotic and abiotic stressors. Here we introduce 10 original research papers and two review papers on plant-environment, plant-pathogen, and plant-plant interactions. In this editorial piece, we overview the oxylipin metabolic pathways and introduce each research contribution in accordance with the corresponding metabolic pathway branches depicted in **Figure 1**.

Jasmonates (JAs) are the best-studied group of plant oxylipins and are widely known as defense phytohormones. JA biosynthesis is triggered by the reaction of 13-lipoxygenase (13-LOX) on polyunsaturated fatty acids, which are abundant in plant membrane lipids, to produce 13-hydroperoxides (**Figure 1**). 13-Hydroperoxides are catalyzed by 13-allene oxide synthase (13-AOS), a member of the CYP74 family, and subsequently converted into 12-oxo-phytodienoic acid (OPDA) and JA by the sequential reactions of allene oxide cyclase, OPDA reductase, and β-oxidation processes (Acosta and Farmer, 2010). The major bioactive JA in vascular plants is the JA-Isoleucine conjugate (JA-Ile), which is recognized by the COI1 receptor complex (Yan et al., 2013). The JA signal activates a group of downstream transcription factors responsible for the transcriptional upregulation of defense genes (Yan et al., 2013). One of the common defense responses in plants is the activation of secondary metabolite accumulation, such as alkaloids and terpenoids, which act as toxic compounds to pathogens and pests (Ding et al., 2021). Many drugs used in modern medicine are derived from such plant secondary metabolites. For example, *Catharanthus roseus* is known to produce the anticancer alkaloids vinblastine and vincristine, belonging to the class of monoterpenoid indole alkaloids. Colinas et al. combined newly generated and publicly available transcriptome data of *Catharanthus roseus* to identify new members of the BIS and ORCA transcription factors that specifically regulate genes involved in the synthesis of these alkaloids.

Although JA signaling strongly induces defense responses, such activation is tightly controlled not to impede plant growth while defending (Guo et al., 2018). To prevent excessive induction of the defense, the active form of JA is rapidly converted to the inactive forms through hydroxylation and/or other metabolic processes (Koo et al., 2011). Kimberlin et al. report novel translational regulation of proper JA responses through the analysis of an Arabidopsis double mutant of cytochrome P450s, CYP94B1 and CYP94B3, which convert active JA-Ile to 12OH-JA-Ile. Bioactive

OPEN ACCESS

Edited and reviewed by:
Reuben J. Peters,
Iowa State University, United States

***Correspondence:**
Koichi Sugimoto
sugimoto.koichi.gu@u.tsukuba.ac.jp
Silke Allmann
s.allmann@uva.nl
Michael V. Kolomiets
kolomiets@tamu.edu

Specialty section:
This article was submitted to Plant Metabolism and Chemodiversity, a section of the journal Frontiers in Plant Science

Received: *18 February 2022*
Accepted: *04 March 2022*
Published: *28 March 2022*

Citation:
Sugimoto K, Allmann S and Kolomiets MV (2022) Editorial: Oxylipins: The Front Line of Plant Interactions. Front. Plant Sci. 13:878765. doi: 10.3389/fpls.2022.878765

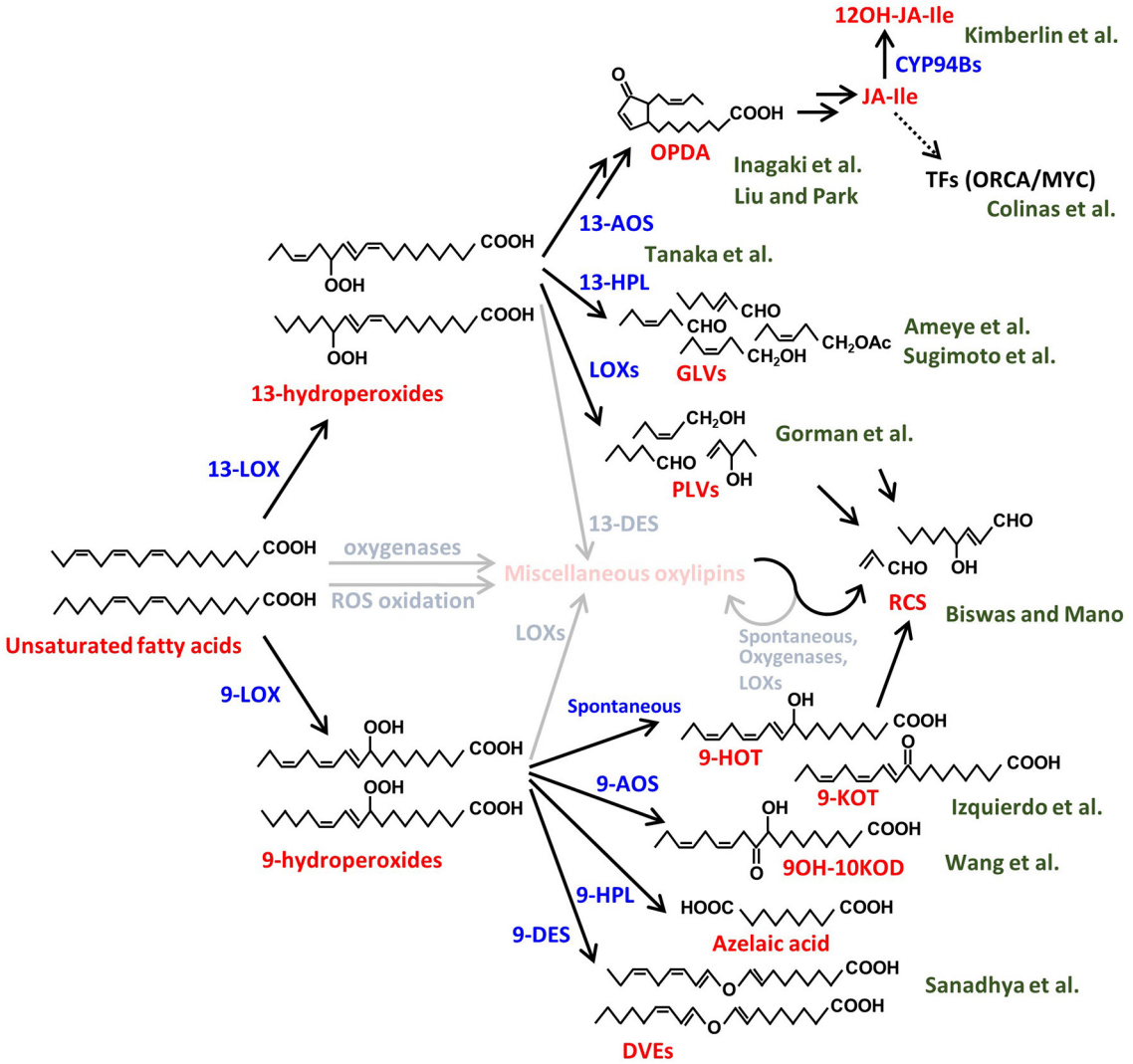

FIGURE 1 | Biosynthetic pathways of various plant oxylipins. Biosynthesis of the plant oxylipins is initiated by oxidation of the unsaturated fatty acids, e.g., linoleic acid and linolenic acid in this figure, enzymatically or nonenzymatically. The compound names are shown in red and the processes are shown in blue. The green characters behind the compounds show the author names in this Research Topic and the relationships between the authors' papers and the compounds. The miscellaneous compounds and processes that are not described well in this Research Topic are shown in faded colors. LOX, lipoxygenase; AOS, allene-oxide synthase; HPL, hydroperoxide lyase; DES, divinyl ether synthase; CYP, cytochrome P450; ROS, reactive oxygen species; OPDA, 12-oxo-phytodienoic acid; JA-Ile, jasmonic acid-isoleucine conjugate; 12OH-JA-Ile, 12-hydroxy JA-Ile; TFs, transcription factors; GLVs, green leaf volatiles; PLVs, pentyl leaf volatiles; RCS, reactive carbonyl species; 9-HOT, 9-hydroxy octadecatrienoic acid; 9-KOT, 9-keto-octadecatrienoic acid; 9OH-10KOD, 9-hydroxy-10keto-octadecadienoic acid; DVEs, divinyl ethers.

JA molecules in plants are not only JA-Ile but also its biosynthetic intermediate, OPDA. Liu and Park reviewed recent studies uncovering the biological functions of OPDA, especially in terms of growth-defense trade-offs and environmental responses in vascular plants. Unlike vascular plants, mosses do not produce JA or JA-Ile in response to mechanical damage but accumulate its cyclopentenone precursor compounds OPDA and dinor-OPDA, the latter of which is synthesized from hexadecatrienoic acid rather than linolenic acid (Yan et al., 2013). These compounds have been shown to function through both COI1-dependent and -independent signaling mechanisms in mosses (Monte et al., 2018, 2020). Inagaki et al. identified through transcriptome- and genome-mining the jasmonate signaling components, COI1 receptor, JAZ repressor, and MYC transcription factor, in the moss species, *Calohypnum plumiforme*, and suggested that OPDA is involved in primitive defense signaling, most likely via the COI1-dependent signaling pathway.

In addition to the 13-AOS-mediated JA biosynthesis, plants convert 13-hydroperoxides into green leaf volatiles (GLVs) and divinyl ethers (DVEs) by other CYP74 family proteins,

13-hydroperoxide lyase (13-HPL) and 13-divinyl ether synthase (13-DES), respectively (Matsui, 2006). GLVs are responsible for the leafy-green scent produced immediately after leaf damage, and the rapid production of GLVs, called GLV-burst, is commonly observed in vascular plants (e.g., D'Auria et al., 2007). Tanaka et al. studied whether the GLV-burst is a trait that has been conserved from primitive plants by comparing a wide range of plants and found that the GLV-burst occurs in all fern species, while being absent in most of the moss species. One of the well-studied biological functions of GLVs is the airborne communication between plants and surrounding organisms (Matsui, 2006; Scala et al., 2013). Ameye et al. utilized an untargeted metabolomics approach to investigate the effect of GLV, *Z*-3-hexenyl acetate, on the activation of wheat responses to infection by *Fusarium graminearum*, a major mycotoxin producing pathogen of wheat. Among the major metabolic changes identified were induction of ROS followed by production of diverse phenylpropanoids with antioxidative activities accompanied by a strong induction of glycosylation processes. Sugimoto et al. showed that various airborne GLVs, aldehydes, alcohols, and esters, could be glycosylated in tomato and Arabidopsis leaves through endogenous metabolic processes using mutants of GLV biosynthetic genes. Plants emit not only GLVs, with a six-carbon backbone, but also pentyl leaf volatiles (PLVs), which have a five-carbon backbone. Gorman et al. clarified the order of biosynthesis of diverse PLVs in Arabidopsis and maize and demonstrated that, in sharp contrast to the virulence-promoting effect of GLVs on the anthracnose pathogen, *Colletotrichum graminicola*, PLV treatment of maize increased resistance to this pathogen by activation of production of oxylipin ketols.

In addition to the 13-LOX-initiated pathways, plants have another oxylipin pathway initiated by 9-LOX to produce 9-hydroperoxides (Liavonchanka and Feussner, 2006). Similar to the 13-oxylipin pathways, 9-LOXs initiate synthesis of various 9-oxylipins by the reaction of 9-AOS, 9-HPL, 9-DES, and other unidentified enzymes (**Figure 1**). Sanadhya et al. reported that the biosynthesis of tomato DVEs, colneleic acid and colnelenic acid, produced by 9-DES are modulated by infection of root-knot nematode, *Meloidogyne javanica.* 9-DES expression is associated with the nematode feeding site and is modulated by auxin and salicylic acid and its overexpression results in increased resistance. Evidence is presented that DVEs have two modes of action, as they decrease motility of nematodes and act as defense signals. Wang et al. presented the physiological function of miscellaneous 9-oxylipins using 9-LOX mutants. The 9-LOX mutant of maize displayed increased susceptibility to Gibberella stalk rot caused by *Fusarium graminearum*, indicating that 9-oxylipins contribute to resistance to this pathogen. The transcriptome analysis and oxylipin profiling revealed that 9-oxylipin and JA pathway are antagonistically regulated and points to the previously unrecognized role of JA in promoting susceptibility to this hemi-biotrophic pathogen. On the other hand, Izquierdo et al. applied a different approach, forward genetic screening of a series of noxy (non-sensitive to oxylipin) mutants of mitochondrial proteins, which are insensitive to exogenous 9-HOT/9-KOT to clarify the role of 9-oxylipins. The authors clarified the oxidative stress targets of the 9-oxylipin signaling by showing that 9-oxylipins reduce respiration inhibitor-induced oxidative stress by activation of a specific mitochondria retrograde signaling pathway. Moreover, the authors showed that mitochondrial complex III is a target of the signaling activity of both 9- and 13-oxylipin pathways with α,β-unsaturated structure during oxidative stress responses.

As described above, plant oxylipins are produced by oxygenation of polyunsaturated fatty acids and downstream metabolic enzymes. In addition to the enzymes focused on in this Research Topic's papers, there are various oxylipin biosynthetic enzymes, such as those initiated by dioxygenases. Moreover, non-enzymatic oxidation by reactive oxygen species and subsequent cleavage/conversion of oxidized lipids also drives the production of a wide variety of oxylipins. Biswas and Mano categorized a series of compounds, which have α,β-unsaturated carbonyl structures, as reactive carbonyl species and reviewed their reaction targets and physiological functions. The functions of most oxylipins are still unclear. Although physiological roles of some of them are suggested, their mode of action is still not fully understood.

In conclusion, the papers collected in this Research Topic have presented some of the recent advances in oxylipin biology and will be informative for the researchers in this area and also help attract additional researchers to this growing research area of plant oxylipins.

AUTHOR CONTRIBUTIONS

All authors listed have made a substantial, direct, and intellectual contribution to the work and approved it for publication.

FUNDING

This work was supported by JSPS KAKENHI Grant Number JP20H03278 to KS, USDA-NIFA grant awards 2017-67013-26524 and 2021-67013-33568 to MK, and European Research Council (ERC) under the European Union's Horizon 2020 research and innovation programme (grant agreement no. 805074) to SA.

ACKNOWLEDGMENTS

The authors would like to thank all the handling editors and reviewers for their contribution to this Research Topic. We would also thank Dr. Fudge and Dr. Laurinavichute for their extensive help to our topic managements.

REFERENCES

Acosta, I. F., and Farmer, E. E. (2010). Jasmonates. *The Arabidopsis Book*. 8, e0129. doi: 10.1199/tab.0129

D'Auria, J. C., Pichersky, E., Schaub, A., Hansel, A., and Gershenzon, J. (2007). Characterization of a BAHD acyltransferase responsible for producing the green leaf colatile (*Z*)-3-hexen-1-yl acetate in *Arabidopsis thaliana*. *Plant J.* 49, 194–207. doi: 10.1111/j.1365-313X.2006.02946.x

Ding, Y., Northen, T. R., Khalil, A., Huffaker, A., and Schmelz, E. A. (2021). Getting back to the grass roots: harnessing specialized metabolites for improved crop stress resilience. *Curr. Opin. Biotechnol.* 70, 174–186. doi: 10.1016/j.copbio.2021.05.010

Guo, Q., Major, I. T., and Howe, G. A. (2018). Resolution of growth-defense conflict: mechanistic insights from jasmonate signaling. *Curr. Opin. Plant Biol.* 44, 72–81. doi: 10.1016/j.pbi.2018.02.009

Koo, A. J. K., Cook, T. F., and Howe, G. A. (2011). Cytochrome P450 CYP94B3 mediates catabolism and inactivation of the plant hormone jasmonoyl-L-isoleucine. *Proc. Natl. Acad Sci U.S.A.*, 108, 9298–9303. doi: 10.1073/pnas.1103542108

Liavonchanka, A., and Feussner, I. (2006). Lipoxygenases: Occurrence, functions and catalysis. *J. Plant Physiol.* 163, 348–357 doi: 10.1016/j.jplph.2005.11.006

Matsui, K. (2006). Green leaf volatiles: hydroperoxide lyase pathway of oxylipin metabolism. *Curr. Opin. Plant Biol.* 9, 274–280. doi: 10.1016/j.pbi.2006.03.002

Monte, I., Ishida, S., Zamarreño, A. M., Hamberg, M., Franco-Zorrilla, J. M., García-Casado, G., et al. (2018). Ligand-receptor co-evolution shaped the jasmonate pathway in land plants. *Nat. Chem. Biol.* 14, 480–488. doi: 10.1038/s41589-018-0033-4

Monte, I., Kneeshaw, S., Franco-Zorrilla, J. M., Chini, A., Zamarreño, A. M., García-Mina, J. M., et al. (2020). An ancient COI1-independent function for reactive electrophilic oxylipins in thermotolerance. *Curr. Biology.* 30, 962–971.e963. doi: 10.1016/j.cub.2020.01.023

Scala, A., Allmann, S., Mirabella, R., Haring, M., and Schuurink, R. (2013). Green leaf volatiles: a plant's multifunctional weapon against herbivores and pathogens. *Int. J. Mol. Sci.* 14, 17781–17811 doi: 10.3390/ijms140917781

Yan, Y., Borrego, E., and Kolomiets, M. V. (2013). "Jasmonate biosynthesis, perception and function in plant development and stress responses," in ed R. Baez, *Lipid Metabolism*. (London, UK: IntechOpen). doi: 10.5772/52675

Conflict of Interest: The authors declare that the research was conducted in the absence of any commercial or financial relationships that could be construed as a potential conflict of interest.

Publisher's Note: All claims expressed in this article are solely those of the authors and do not necessarily represent those of their affiliated organizations, or those of the publisher, the editors and the reviewers. Any product that may be evaluated in this article, or claim that may be made by its manufacturer, is not guaranteed or endorsed by the publisher.

Copyright © 2022 Sugimoto, Allmann and Kolomiets. This is an open-access article distributed under the terms of the Creative Commons Attribution License (CC BY). The use, distribution or reproduction in other forums is permitted, provided the original author(s) and the copyright owner(s) are credited and that the original publication in this journal is cited, in accordance with accepted academic practice. No use, distribution or reproduction is permitted which does not comply with these terms.

frontiers in Plant Science

ORIGINAL RESEARCH
published: 03 December 2020
doi: 10.3389/fpls.2020.596271

Metabolomics Reveal Induction of ROS Production and Glycosylation Events in Wheat Upon Exposure to the Green Leaf Volatile Z-3-Hexenyl Acetate

Maarten Ameye[1,2], Lieven Van Meulebroek[3], Bianca Meuninck[1], Lynn Vanhaecke[3], Guy Smagghe[2], Geert Haesaert[1] and Kris Audenaert[1]**

[1] Laboratory of Applied Mycology and Phenomics, Department of Plants and Crops, Faculty of Bioscience Engineering, Ghent University, Ghent, Belgium, [2] Laboratory of Agrozoology, Department of Plants and Crops, Faculty of Bioscience Engineering, Ghent University, Ghent, Belgium, [3] Laboratory of Chemical Analysis, Department of Veterinary Public Health and Food Safety, Faculty of Veterinary Medicine, Merelbeke, Belgium

OPEN ACCESS

Edited by:
Michael V. Kolomiets, Texas A&M University, United States

Reviewed by:
Jurgen Engelberth, University of Texas at San Antonio, United States
Kenji Matsui, Yamaguchi University, Japan

***Correspondence:**
Maarten Ameye
Maarten.ameye@ugent.be
Kris Audenaert
Kris.audenaert@ugent.be

Specialty section:
This article was submitted to Plant Pathogen Interactions, a section of the journal Frontiers in Plant Science

Received: *18 August 2020*
Accepted: *02 November 2020*
Published: *03 December 2020*

Citation:
Ameye M, Van Meulebroek L, Meuninck B, Vanhaecke L, Smagghe G, Haesaert G and Audenaert K (2020) Metabolomics Reveal Induction of ROS Production and Glycosylation Events in Wheat Upon Exposure to the Green Leaf Volatile Z-3-Hexenyl Acetate. Front. Plant Sci. 11:596271. doi: 10.3389/fpls.2020.596271

The activation and priming of plant defense upon perception of green leaf volatiles (GLVs) have often been reported. However, information as to which metabolic pathways in plants are affected by GLVs remains elusive. We report the production of reactive oxygen species in the tip of young wheat leaves followed by activation of antioxidant-related enzyme activity. In this study, we aimed to uncover metabolic signatures upon exposure to the GLV Z-3-hexenyl acetate (Z-3-HAC). By using an untargeted metabolomics approach, we observed changes in the phenylpropanoid pathways which yield metabolites that are involved in many anti-oxidative processes. Furthermore, exposure to GLV, followed by infection with *Fusarium graminearum* (Fg), induced significantly greater changes in the phenylpropanoid pathway compared to a sole Z-3-HAC treatment. Fragmentation of a selection of metabolites, which are significantly more upregulated in the Z-3-HAC + Fg treatment, showed D-glucose to be present as a substructure. This suggests that Z-3-HAC induces early glycosylation processes in plants. Additionally, we identified the presence of hexenyl diglycosides, which indicates that aerial Z-3-HAC is metabolized in the leaves by glycosyltransferases. Together these data indicate that GLV Z-3-HAC is taken up by leaves and incites oxidative stress. This subsequently results in the modulation of the phenylpropanoid pathway and an induction of glycosylation processes.

Keywords: green leaf volatile, metabolomic, wheat, fusarium, oxidative stress

INTRODUCTION

The production of biogenic volatile organic compounds is one of the defense strategies that plants mount at the advent of an attack by a pathogen or insect or by wounding (Dudareva et al., 2013). Green leaf volatiles (GLVs) are quickly (within seconds to minutes) produced upon biotic stress and can subsequently be perceived by neighboring plants (Fall et al., 1999; Ameye et al., 2018).

GLVs have often been described to play an important role in the defense of plants against deleterious insects (Turlings et al., 1991; Scala et al., 2013), pathogens (Nakamura and Hatanaka, 2002; Kishimoto et al., 2008) and abiotic stress (Yamauchi et al., 2015) by direct activation or by priming for enhanced defense (Engelberth et al., 2004; Ameye et al., 2015; Dombrowski et al., 2019). Being produced upon mechanical or biotic damage, GLVs have been assigned a role as long distance damage-associated molecular patterns, eliciting defense response (Quintana-Rodriguez et al., 2018). Recently, another defensive role for GLVs has been uncovered: GLV esters induce stomatal closure in several crops, thereby preventing infection by pathogens, as was shown for *Pseudomonas syringae* pv. *tomato* DC3000 in tomato (López-Gresa et al., 2018).

Despite its widespread occurrence throughout the plant kingdom, it remains enigmatic via which mechanism GLV perception and signal transduction occur (Heil, 2014; Ameye et al., 2018). However, there is evidence that GLVs influence the redox status of plants and hence induce plant stress responses (Cofer et al., 2018). Among the early reactions are plasma membrane potential depolarization, followed by an increase in cytosolic [Ca^{2+}] which, in turn, activates respiratory burst oxidase homologs (Asai et al., 2009; Zebelo et al., 2012). A transcriptomics study showed that Z-3-HOL induced the expression of genes involved in transcriptional regulation, lipid signaling, and cell wall reinforcement in maize (Engelberth et al., 2013). In *Arabidopsis*, it has been reported that, following exposure to GLV E-2-hexenal, one-third of the upregulated genes were unique and unrelated to plant hormones (Mirabella et al., 2015).

In a previous work, we have demonstrated that pre-exposure of wheat to Z-3-hexenyl acetate (Z-3-HAC) leads to enhanced defense against the hemi-biotrophic fungus *Fusarium graminearum* (Schwabe), a causal agent of the cereal disease fusarium head blight (Ameye et al., 2015). This enhanced defense coincided with a suppression of salicylic acid (SA)-related defense during the biotrophic phase of the fungus at 24 h after inoculation (hai) and an increase in JA-related defense during the necrotrophic phase of the fungus at 48 hai. However, to better understand which defense mechanisms were influenced upon Z-3-HAC exposure, a more detailed analysis of earlier plant responses is necessary.

Omics techniques, such as proteomics and metabolomics, are indispensable to bridge the genotype–phenotype gap (Patti et al., 2012; Feussner and Polle, 2015; Hong et al., 2016). Whereas proteins can be modified post-translationally, metabolites represent intermediary and downstream biochemical products and serve as signatures of metabolic pathways (Patti et al., 2012). The application of metabolomics in plant physiology is gaining traction. However, because of the lack of annotated databases, metabolite identification remains a major limitation for non-targeted plant metabolomics (Creek et al., 2014; Feussner and Polle, 2015; Razzaq et al., 2019). Consequently, current phytometabolome pathways are mostly restricted to genome-reconstructed pathways (Kind et al., 2009; Feussner and Polle, 2015). Due to this bottleneck, many studies have, in addition to untargeted analysis, also focused on how plant metabolites from *a priori* chosen pathways change in response to pathogen infections (Urano et al., 2009; Ward et al., 2010; Mhlongo et al., 2016).

As plant–pathogen interactions consist of a tightly regulated dynamic and transient activation of defense pathways, an analysis of the early effects of Z-3-HAC on plant defense is designated to uncover the changes in the plant metabolome. Using an untargeted metabolomics approach, we aimed to reveal hitherto unknown priming mechanisms by Z-3-HAC, which may aid in better understanding how the plants' metabolome changes after perceiving GLVs from the environment and how biological functionalities are controlled.

MATERIALS AND METHODS

Z-3-HAC Exposure Experiment

To test the effect of Z-3-HAC on plant health and reactive oxygen species (ROS) production, wheat seeds (var. Sahara, AVEVE, Belgium) were sterilized in NaOCl (14%) for 5 min and rinsed three times with distilled water and placed in 1.5 L glass jars filled with 250 mL growth medium [4.4 g L^{-1} MS salts with vitamins (Duchefa Biochemie, Haarlem, Netherlands), 10 g L^{-1} sucrose, and 8 g L^{-1} plant agar (Duchefa Biochemie, Haarlem, Netherlands)] at pH 5.7. After 1 week, the plants were exposed to 50 μM (corresponding to 5.9 g m^{-3}) Z-3-HAC by pipetting 9.9 μL on a piece of sterile filter paper placed inside the pot, followed by closing the lid and sealing it off with PTFE tape. At 0, 1, 2, 6, and 8 h after exposure (hae), the plants were removed from the jars, and multispectral images were taken.

Multispectral Imaging and Histochemical Staining

To automatically measure the effect of Z-3-HAC exposure on the health of wheat seedlings, we employed a custom-built phenotyping platform equipped with a multispectral camera (CropReporter, Phenovation, Wageningen, Netherlands). The color images and the maximum efficiency of PSII (F_v/F_m) (Baker, 2008) were measured according to the manufacturer's specifications. To detect H_2O_2 accumulation, staining by 3,3-diaminobenzidine (DAB) was executed according to the protocol of Thordal-Christensen et al. (1997), with minor modifications from De Vleesschauwer et al. (2010).

RT-qPCR and Enzyme Assay

The expression of genes involved in ROS production and quenching was measured using RT-qPCR. RNA from the leaf sheaths was extracted using TRI reagent (Sigma-Aldrich) according to the manufacturer's specifications and quantified with a fluorometer (Quantus, Promega Benelux, Leiden, Netherlands). First-strand complementary DNA was synthesized from 500 ng of total RNA using the Goscript kit (Promega Benelux, Leiden, Netherlands). The primers used for quantitative reverse transcription (qRT)-PCR analysis are listed in **Supplementary Table 1**. RT-qPCR analysis was performed using a CFX96 system (Bio-Rad). The thermal profile consisted

of an initial denaturation step for 2 min at 95°C, followed by 40 cycles of 95°C for 15 s and 60°C for 60 s. Finally, melting curve analysis was performed using a temperature profile of 95°C for 10 s, cooling to 65°C for 5 s, and subsequently heating to 95°C at a rate of 0.5°C per 10 s. Normalization of wheat defense genes was carried out using cell division control protein (Ta54227) and actin (Ta35284) as reference genes (Paolacci et al., 2009). All calculations and analyses of the quality of the reference genes were performed using qBase + software (Biogazelle, Zwijnaarde, Belgium).

Superoxide dismutase (706002, Cayman Chemical) and catalase enzyme activity (70002, Cayman Chemical) and phenolic content (K527, BioVision) were measured using colometric assays according to the manufacturer's specifications. Enzyme activity and phenolic content were normalized to the amount of protein measured according to the manufacturer's specifications (Roti Nanoquant, Carl Roth GmbH, Karlsruhe, Germany).

Sample Preparation for UHPLC–HRMS/MS

A total of 100 mg of 6–8 pooled leaf sheaths from the leaf sheath assay was crushed using liquid nitrogen. Afterward, 1 mL of cold (−20°C) modified Bieleski extraction buffer consisting of methanol, ultrapure water, and formic acid (75:20:5, v/v/v) was added. Additionally, the suspension was amended with a deuterium-labeled internal standard of 100 pg μL^{-1} d_6-abscisic acid (OlChemIm, Olomouc, Czech Republic). The samples were vortexed and placed at −20°C for 12 h of cold extraction. The samples were centrifuged for 10 min at 10,000 rpm, and 500 μL of the supernatant was transferred to a 30 kDa Amicon® Ultra centrifugal filter unit (Merck, Millipore Corporation, MA, United States). Finally, the extract was transferred to a high-performance liquid chromatography (HPLC) vial. Samples of different treatments were placed in the ultra-HPLC coupled to high-resolution tandem mass spectrometry (UHPLC–HRMS/MS) system in a randomized manner. Finally, 10 μL was injected directly on the column for UHPLC–HRMS/MS analysis. Two quality control (QC) samples were prepared by using aliquots of 10 randomly chosen samples, representing the different treatments. QC samples were run after each set of 10 samples and were used to correct for possible chromatographic and mass spectrometric variations.

UHPLC–HRMS/MS Analysis

The UHPLC–HRMS/MS system consisted of an Dionex UltiMate 3000 XRS UHPLC pumping system (Thermo Fisher Scientific, San Jose, CA, United States), coupled to a Q-Exactive™ hybrid quadrupole-Orbitrap mass spectrometer (Thermo Fisher Scientific, San Jose, CA, United States), being equipped with a heated electrospray ionization source (HESI-II) that was operated in switching polarity mode. The instrumental parameters for HESI-II ionization and mass spectrometric detection can be found in Van Meulebroek et al. (2012). Chromatographic separation of the compounds was achieved with a gradient elution program using a reversed phase Nucleodur Gravity C18 column (1.8 μm, 50 mm × 2.1 mm ID) (Macherey-Nagel, Düren, Germany). The mobile phase consisted of a binary solvent system: 0.1% formic acid in ultrapure water (solvent A) and methanol (solvent B) at a constant flow rate of 300 $\mu L\ min^{-1}$. A linear gradient profile with the following proportions (v/v) of solvent A was applied: 0–1 min at 98%, 1–2.50 min from 98 to 60%, 2.50–4 min from 60 to 50%, 4–5 min from 50 to 20%, 5–7 min at 20%, 7–7.10 min from 20 to 0%, 7.10–8 min at 0%, and 8–8.01 min from 0 to 98%, followed by 2 min of re-equilibration. The column oven temperature was set at 30°C. Phytohormones were identified based on both the retention time relative to the internal standard and accurate mass (*m/z*) using an analytical standard (**Supplementary Table 2**) (OlChemIm, Olomouc, Czech Republic). Instrument control and data processing were carried out by Xcalibur 3.1 software (Thermo Fisher Scientific, San Jose, CA, United States). For HRMS-MS, parallel reaction monitoring was used. An isolation window of 0.5 *m/z* was used, and ions were fragmented at 35 eV in the collision cell.

Pathway Analysis

In order to get an initial grasp of the pathways which are affected by the different treatments, we employed the mummichog algorithm (Li et al., 2013). This algorithm permitted to functionally characterize metabolites and map metabolite features from our HPLC-MS analysis to current metabolic models and to assess the significance and enrichment of metabolic pathways. For this, we used the *MS Peaks to Pathways* module in MetaboAnalyst (V4.0) (Chong et al., 2018). The molecular weight tolerance was set at 5 ppm. The *P*-value cutoff was 0.01, and the Kyoto Encyclopedia of Genes and Genomes (KEGG) pathway library was chosen, with *Oryza sativa japonica* as the model organism for monocotylydonous plants.

Chemometric Data Analysis

To identify metabolites which are differentially produced upon Z-3-HAC exposure, we employed the chemometrics strategy previously described in Van Meulebroek et al. (2015). A first step concerned the characterization of detected metabolite features in terms of retention time, *m/z* value, and abundance along the various samples. To this end, Sieve™ 2.1 (Thermo Fisher Scientific, San Jose, CA, United States) was used. Full-scan data were provided as input, and the following settings were applied: an *m/z* range of 100–800 Da, an *m/z* width of 5 ppm, a retention time range of 1.5–9.0 min, a peak intensity threshold of 10^6 arbitrary units, a maximum peak width of 0.5 min, and a maximum number of 15,000 frames. This step was preceded by a peak alignment process to correct for inherent chromatographic variability, thereby allowing a maximum retention time shift of 0.2 min. This step rendered 4,310 metabolite features for the positive ionization mode and 1,145 for the negative ionization mode.

Metabolite features and their abundances were used to construct predictive models, implementing multivariate data analysis techniques such as principal component analysis (PCA) and orthogonal partial least squares discriminant analysis (OPLS-DA) using SIMCA™ 15 software (Umetrics, Malmö, Sweden). Hereby Pareto scaling and log transformation were applied to

standardize the range of independent X variables and induce normality, respectively. For OPLS-DA, supervised models were established to classify samples according to their treatment and time points (**Table 1**). Model validity was tested with CV-ANOVA ($P < 0.05$) and permutation testing ($n = 100$). Additionally, according to Triba et al. (2015), a good OPLS-DA model should have $Q^2(Y) > 0.5$. It was concluded that the OPLS-DA models, as obtained for the positively ionized fingerprints, were valid and showed good predictability, which was not the case for the models that were constructed based on the negatively ionized metabolite features. In the following step, we selected the metabolites that contributed most to the predictability of the model by evaluating the variable importance in projection (VIP) scores (> 1), Jack-knifed confidence intervals (not across zero), and S-plots ($|$ correlation $p(\text{corr})| > 0.5$ and $|$ covariance $p| > 0.04$) (**Supplementary Figure 5**). As such, we initially retained 103 metabolite features. We further narrowed down this selection to a final number of 13 unique metabolites representing the highest VIP and S-plot scores. Hereby we also assessed whether a particular peak was not wrongly assigned various feature identity labels by SIEVE^{TM} and whether isotopes or different adducts of the same metabolite were present. Metabolites that were only important at a single time point were also omitted from further analysis.

Identification

Tentative identification of the retained selection of metabolites was performed using different data sources, i.e., isotope pattern, accurate mass (m/z), and HRMS/MS fragmentation pattern. For this purpose, Sirius software (Version 4.0.1, Jena, Germany) (Böcker and Dührkop, 2016) and the MetFrag web application (Ruttkies et al., 2016), linked to the public databases ChemSpider (Royal Society of Chemistry), PubChem (National Center for Biotechnology Information), and KEGG (Kyoto Encyclopedia of Genes and Genomes), were used.

Data Analysis

Data were analyzed and visualized by usage of SPSS (Version 22.0, IBM Corp., Armonk, NY, United States) and R (R Core Team, 2013).

Infection Assay

In order to study changes in the metabolome upon Z-3-HAC exposure and a subsequent *F. graminearum* infection, unless stated otherwise, four different treatments were used: (1) a control treatment, (2) a treatment in which wheat plants were exposed to Z-3-HAC, (3) a treatment in which Z-3-HAC-exposed wheat plants were subsequently challenged with a conidia suspension of *F. graminearum*, and (4) a treatment in which non-exposed plants were challenged with a conidia suspension of *F. graminearum*.

F. graminearum 8/1, containing a green fluorescent protein coding gene (Jansen et al., 2005), was used in this study. The strain was grown on potato dextrose agar for 10 days at 21°C under a regime of 12 h of dark and 12 h of combined UVC and UVA light (2 × TUV 8W T5 and 1 × TL 8W BLB; Philips). Macroconidia were harvested by adding 0.01% (v/v) Tween 80 to the Petri dishes and rubbing the mycelium with a sterile Drigalski spatula. Afterward, the suspension was adjusted to a final concentration of 10^5 conidia mL^{-1}.

Two weeks old winter wheat seedlings (var. Sahara) were exposed overnight to Z-3-HAC using a custom-built exposure system previously described in Ameye et al. (2015). The open flow system consisted of four nalophan bags which were supplied with purified air. In two of the bags (treatment 2 + 3), 70 μL of pure Z-3-HAC (Sigma-Aldrich) was applied to a piece of filter paper, thus avoiding direct contact with the plant. In the two other bags (treatment 1 + 4), distilled water was used. As nalophan bags were consistently flushed, the aerial concentrations of Z-3-HAC reached maximum values of 100 μM, which rapidly declined within minutes. Even though wheat seedlings were exposed to a high concentration of Z-3-HAC, the aerial Z-3-HAC concentration declined very rapidly to previously reported concentrations (Wenda-Piesik et al., 2010; Piesik et al., 2011). As stated by Matsui et al. (2012), aqueous concentrations of GLVs within cells can reach values up to 1 mM. Thus, using a high concentration for a short period of time mimics GLV concentrations in damaged cells (Heil, 2014). On the following morning, the seedlings were taken out of the bags and used in the infection described in Koga et al. (2004). Leaf sheaths were carefully peeled of the stem and subsequently inoculated

TABLE 1 | Orthogonal partial least squares discriminant analysis (OPLS-DA) models based on the metabolite features from the positive ionization mode provide better predictability compared to the negative ionization mode.

Time	Ionization mode	Model characteristics				
		Number of principal components (predictive + orthogonal)	R^2 (X)	R^2 (Y)	Q^2 (Y)	CV-ANOVA (P-value)
1 hai	+	1 + 2	0.624	0.99	0.976	4.95×10^{-6}
	-	1 + 2	0.786	0.913	0.57	0.222
6 hai	+	1 + 2	0.633	0.998	0.972	2.82×10^{-5}
	-	1 + 2	0.572	0.837	0.576	0.128
24 hai	+	1 + 2	0.721	0.996	0.936	0.0169
	-	1 + 2	0.742	0.992	0.837	0.098

Model characteristics for the different OPLS-DA models of Z-3-HAC + F. graminearum-treated plants vs. F. graminearum-treated plants at 1, 6, and 24 h after inoculation (hai).

with 10 μL of a conidia suspension (10^5 conidia mL^{-1}). At different time points, samples were taken and flash-frozen in liquid nitrogen. The samples were stored at −80°C until analysis.

RESULTS

ROS Production and Quenching Upon Z-3-HAC Exposure

Wheat seedlings were exposed in a closed environment to Z-3-HAC in order to investigate its effects on F_v/F_m values as a proxy for plant health. Two-way ANOVA revealed that there was an effect of the treatment ($P < 0.001$) and time after exposure ($P < 0.001$) and that there was an interaction between these factors ($P < 0.001$). Multispectral images revealed that, at 1 hae, F_v/F_m already started to decline, which continued until 8 hae (**Figure 1A**), of which the effect was significantly greater in Z-3-HAC-treated plants compared to the control plants. This effect on F_v/F_m values was only situated at the top of the leaves and does not further migrate downwards in the leaves (**Figure 1B**). Further microscopic analysis using DAB staining revealed that this decline in F_v/F_m values could be attributed to H_2O_2 accumulation surrounding the stomata which induced oxidative damage (**Figure 1C**). To examine this further in detail, we performed RT-qPCR (**Figure 2A**) and enzyme activity assays (**Figure 2B**) of genes and enzymes involved in ROS production and quenching by the wheat seedlings at 1 and 6 hae. The upper part of the leaf which showed reductions in F_v/F_m was selected. Genes *TaRBOH1* and *TaRBOH3*, responsible for O_2^- production, had a 16.1-fold ($P = 0.003$) and 5.4-fold ($P = 0.049$) increase at 1 hae and 4.7-fold ($P = 0.136$) and 7.5-fold ($P = 0.069$) at 6 hae, respectively, upon Z-3-HAC exposure. Concurrently, superoxide dismutase *CuSOD* ($P = 0.010$) and *MnSOD* ($P = 0.011$), which react with $2O_2^-$ to form H_2O_2, were significantly downregulated at 6 hae. *CAT*, coding for catalase, which reacts with H_2O_2 to form H_2O and O_2, was significantly downregulated at 1 hae ($P = 0.024$) (**Figure 2A**). Additionally, the gene ascorbate peroxidase (*APX*) was downregulated at 1 hae ($P = 0.003$). Glutathione peroxidase (*GPX*) was significantly downregulated at 6 hae ($P = 0.048$) (**Figure 2A**). When we look at enzyme activity, for SOD, we saw a significant effect of treatment ($P = 0.006$) and time ($P = 0.044$), but no interaction using a two-way ANOVA. *Post hoc* analysis showed that, at 6 hae, SOD activity was significantly higher in the Z-3-HAC treatment compared to the control (+ 86.8%, $P = 0.036$) at 6 hae. The two-way ANOVA for CAT activity revealed a significant effect of the treatment ($P = 0.02$), but not of the time after exposure ($P = 0.370$); also no interaction between the treatment and hae was present ($P = 0.144$). *Post hoc* analysis showed a significantly higher CAT activity (+ 117%, $P = 0.048$) upon Z-3-HAC exposure (**Figure 2B**) at 6 hae. Additionally, two-way ANOVA of the phenolic content, which is also implicated in the quenching of oxidative stress, revealed an effect of treatment ($P = 0.001$) and time ($P = 0.001$), and an interaction was present between treatment and time ($P = 0.018$). At 6 hae, phenolics were significantly higher in seedlings exposed to Z-3-HAC at 6 hae (+ 152%, $P = 0.009$) compared to the control treatment, and in the Z-3-HAC treatment, phenolic content was higher at 6 hae compared to that at 1 hae (+ 153%, $P = 0.009$) (**Figure 2B**).

Untargeted Metabolomics

Functional Pathway Analysis Upon Z-3-HAC Exposure

The previous results indirectly show the production of phenolic compounds in response to ROS accumulation. Several groups of plant metabolites have already been reported to be involved in the quenching of oxidative stress in plants such as phenolic compounds, carotenoids (Havaux, 2014), ascorbate (Caverzan et al., 2012), and glutathione (Szalai et al., 2009) among others (Škerget et al., 2005; Dai and Mumper, 2010; Akinwumi et al., 2018). However, a more holistic approach is warranted to elucidate the effects of Z-3-HAC exposure to wheat. Therefore, to uncover more detailed specific changes in the metabolome of wheat seedlings upon exposure to Z-3-HAC, we performed an untargeted metabolomics analysis. For this, the mummichog algorithm was chosen to functionally characterize unknown metabolites and assess which metabolic pathways in wheat were significantly changed. For this experiment, we used an open-flow system previously used in Ameye et al. (2015) to mimic sudden bursts in GLV production following foliar damage. At 1 hae, we observed the highest significant change in the metabolite content of compounds of the phenylpropanoid pathway, followed by ascorbate and aldarate metabolism, glutathione, stilbenoid, diarylheptanoid, and gingerol biosynthesis, and betalain biosynthesis, which are all involved in the quenching of oxidative stress in plants (**Figure 3**). At 6 hae, the pathways which were significantly up- or down-regulated are involved in the biosynthesis of phenylpropanoids, phenylalanine tyrosine and tryptophan, and isoquinoline alkaloids (**Figure 3**).

Functional Pathway Analysis Upon Z-3-HAC Exposure and *Fusarium graminearum* Infection

As we were primarily interested in the additional effect of pre-treating plants with Z-3-HAC on the metabolome following an infection with Fg, we compared the dataset of the Z-3-HAC + Fg treatment to the dataset of the Z-3-HAC treatment alone and the Fg treatment alone (**Figure 4**). This allowed us to distinguish the effects of the sole treatments Z-3-HAC and Fg, respectively, and to identify pathways which were more or less upregulated in plants that were pre-treated with Z-3-HAC and subsequently infected.

At 1, 6, and 24 hai, we observed that metabolites in the phenylalanine pathways and the more downstream phenylpropanoid and tryptophane pathways were significantly affected by the Z-3-HAC + Fg treatment, which goes beyond the separate effects of Z-3-HAC or Fg (**Figure 4**). To corroborate the observed results with respect to the phenylalanine pathway, we performed a targeted analysis using an analytical standard of L-phenylalanine (L-Phe), the starting product of the pathway. In the Z-3-HAC and Z-3-HAC + Fg-treated seedlings, L-Phe was significantly lower compared to the control and *Fg*-inoculated seedlings at 1 and 6 hai (**Supplementary Figure 1**). This either

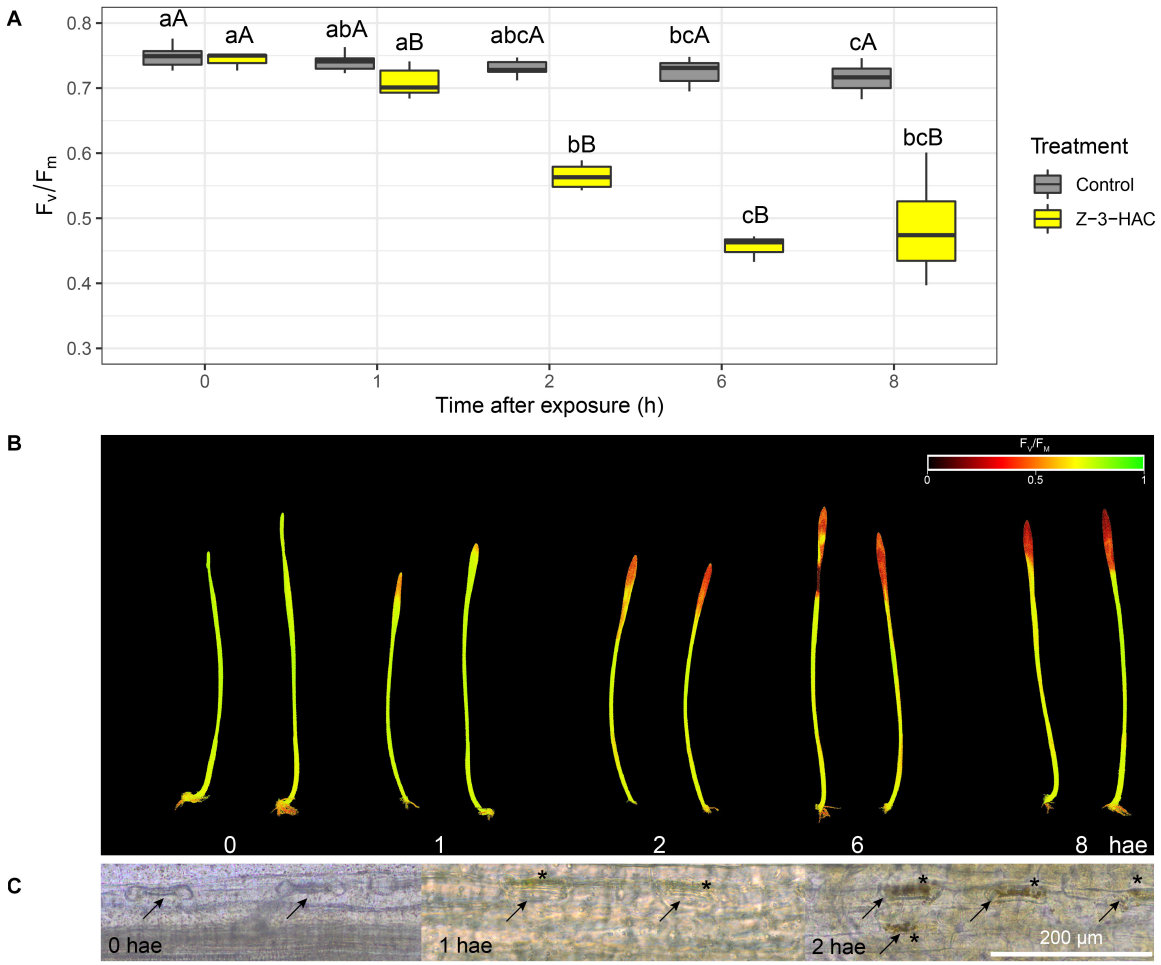

FIGURE 1 | Exposure to 50 μM Z-3-hexenyl acetate results in an initial decline in maximum efficiency of photosystem II (F_v/F_m) in 2 weeks old wheat plants concurrent with an accumulation of H_2O_2 around the stomata in the top of the leaves. **(A)** F_v/F_m values (n = 4 per time point) at different time points. Different lowercase letters above the box plots indicate significant differences between the time points per treatment level (Tukey's HSD test, α = 0.05). Different uppercase letters indicate significant differences between the treatments per time point (two-sample t-test, α = 0.05). **(B)** Corresponding images of the Z-3-HAC-treated leaves with the F_v/F_m values depicted using a continuous color scale. **(C)** Microscopic images of the stomata in which the H_2O_2 is shown to accumulate using 3,3-diaminobenzidine (DAB) staining. Arrows indicate the stomata, and asterisks depict locations of DAB accumulation.

suggests a decreased L-Phe production in these treatments or an increased demand of L-Phe from the downstream pathways.

Selection and Tentative Identification of Biologically Relevant Metabolites

The mummichog algorithm provided a powerful tool to get a first grasp on the changes in the metabolome related to Z-3-HAC exposure. However, as this strategy is limited to the available metabolites included in the KEGG database, we pursued a more tentative identification approach. First, we performed PCA, whereby the PCA-X score plots were based on 4,310 positively ionized metabolite features and showed that samples from the same treatment cluster together and separate from the other treatments, which became clear from 6 hai onward (**Figure 5**). This indicated that metabolic differences were present between the various treatments. The total variance explained by the first two principal model components was 45, 56, and 65% for 1, 6, and 24 hai, respectively. OPLS-DA models were constructed in order to reveal those metabolites that contributed to the differentiation between the Z-3-HAC and Z-3-HAC + Fg treatment. Initially, 103 metabolites from the positive ionization mode were retained for further chemical and biological assessment. Complete-linkage hierarchical clustering of the metabolites according to their abundance profiles along samples revealed two large clusters: one cluster in which a metabolite was most abundant in Z-3-HAC and Z-3-HAC + *Fg* treatments and another cluster in which the metabolites were least abundant in the Z-3-HAC + *Fg* treatment (**Figure 6**). The latter metabolites may be inhibited by Fg infection in Z-3-HAC-treated plants or serve as a substrate for the production of metabolites further downstream.

Metabolites were selected for HRMS/MS fragmentation, and tentative identification was established using full-scan data and the MS/MS patterns. Remarkably, the metabolites that were most abundantly present in the Z-3-HAC-treated plants

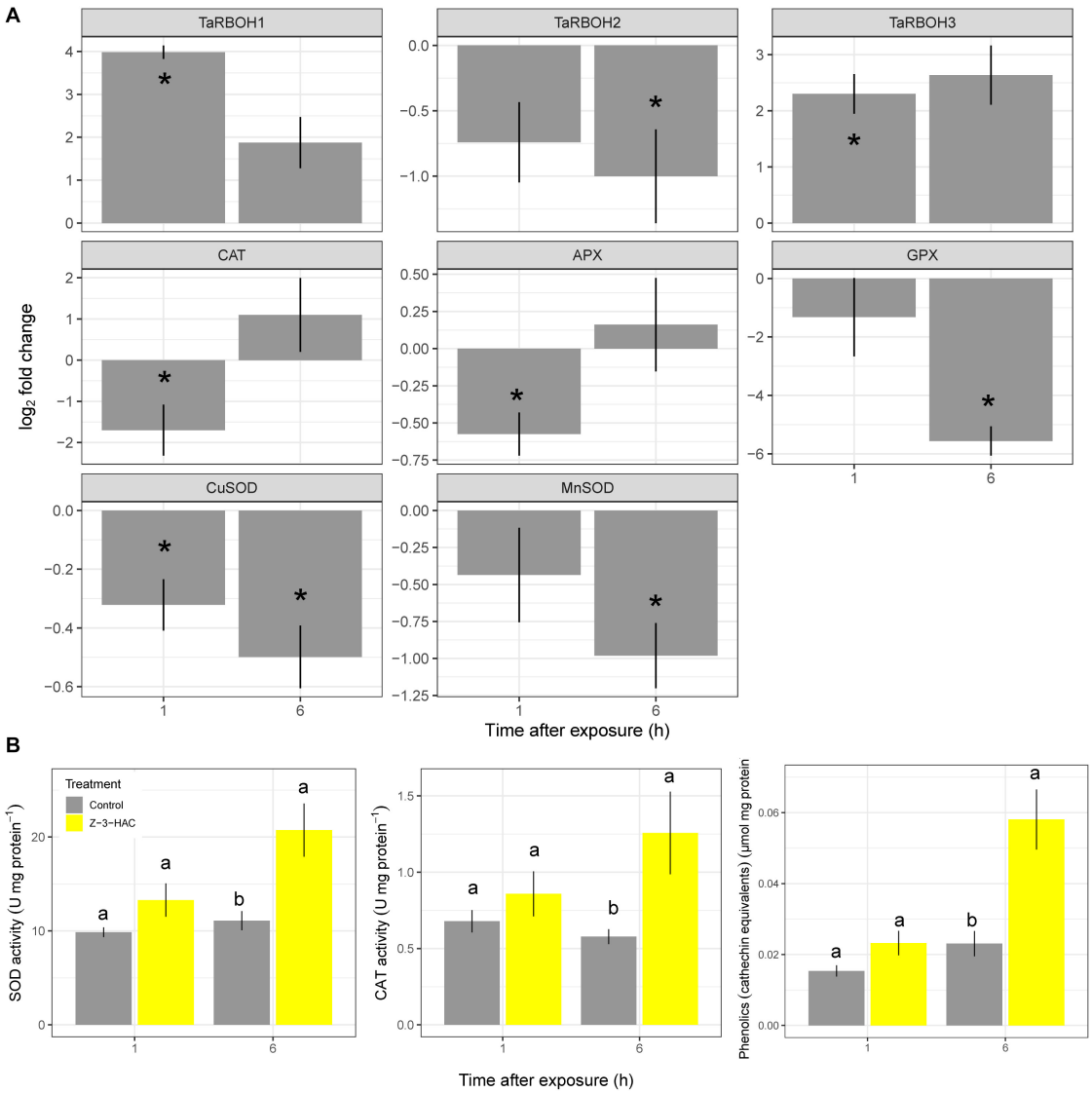

FIGURE 2 | Gene expression **(A)** and enzyme activity **(B)** of processes involved in the production and quenching of reactive oxygen species after exposure to Z-3-HAC. **(A)** Bars represent the $\log_2$-transformed means of four biological replicates, each consisting of three pooled upper part of leaves showing reductions in F_v/F_m. Fold change was calculated by dividing the CNRQ values of the Z-3-HAC-treated leaves to the control leaves. Asterisks depict significant changes (one-sample *t*-test, $\alpha = 0.05$). **(B)** Bars represent the means of four biological replicates from the same samples used for the RT-qPCR. Enzyme activity and phenolics content were normalized to the amount of protein present. Different uppercase letters above the box plots indicate significant differences between the time points per treatment (two-sample *t*-test, $\alpha = 0.05$) Different lowercase letters above the box plots indicate significant differences between the treatments per time point (two-sample *t*-test, $\alpha = 0.05$).

were tentatively identified as glycosylated compounds (**Table 2**, **Figure 7**, and **Supplementary Figure 2**). Using an analytical standard, we determined the MS/MS pattern of D-glucose (Merck, Darmstadt, Germany) and were able to confirm that various fragments of the metabolites under investigation were matching those of D-glucose, indicating the presence of a glucose group and pointing toward glycosylated metabolites (**Supplementary Figure 2** and **Supplementary Dataset 1**). The metabolites from the other cluster did not possess fragments matching those of D-glucose. Besides the fragments that were shared with those of D-glucose, 30 unique fragment ions were also shared between at least two different metabolites (**Supplementary Figure 3**), pointing to metabolites that share similar (sub)structures.

Among the metabolites, several have been described to be implicated in plant defense. Metabolite 2193 ($C_{14}H_{20}O_7$) was tentatively identified as rhodosin, a glycoside of tyrosol, a phenolic antioxidant. This compound was significantly induced in the Z-3-HAC + Fg treatment compared to the sole Z-3-HAC and Fg treatment (**Figure 7**). Metabolite 2778 ($C_{15}H_{24}O_9$) was tentatively identified as leonuridine. Those metabolites for which no glucose fragment ions were generated upon

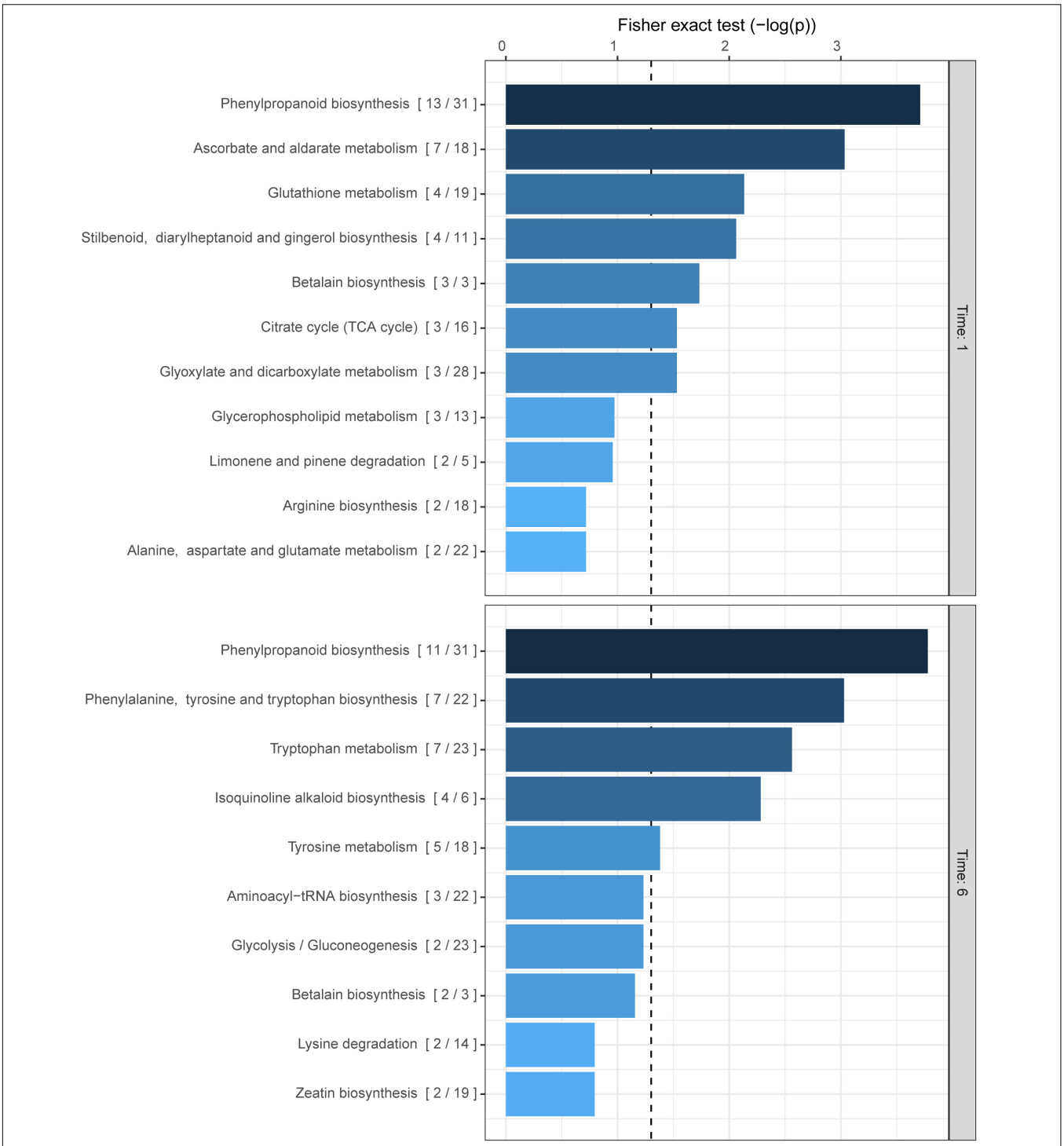

FIGURE 3 | Biochemical pathways in wheat which are affected by exposure to Z-3-HAC after 1 and 6 h. The mummichog algorithm was used on the *m/z* dataset of six biological replicates per treatment per time point. The ratio in brackets represents the number of significant matches to the total number of matched compounds in the pathway. Bars next to pathways represent the *p*-value of the Fisher exact test which represents the significance of change in the pathway following exposure to Z-3-HAC. The dashed line represents a *p*-value of 0.05.

HRMS/MS analysis were predicted to be phosphorylated: 3435 ($C_{12}H_{19}N_3O_9P_2$), 4208 ($C_{25}H_{25}N_2O_{14}P$), and 4302 ($C_{26}H_{32}N_{10}O_{14}P_2$). Additionally, based on the accurate mass of the $[M + NH_4]^+$ adduct of metabolite 3444 ($C_{17}H_{30}O_{10}$, *m/z* value of 412.21765) and HRMS/MS spectrum (fragment ions with mass 263, 295, 233, and 245 Da as well as fragments that are

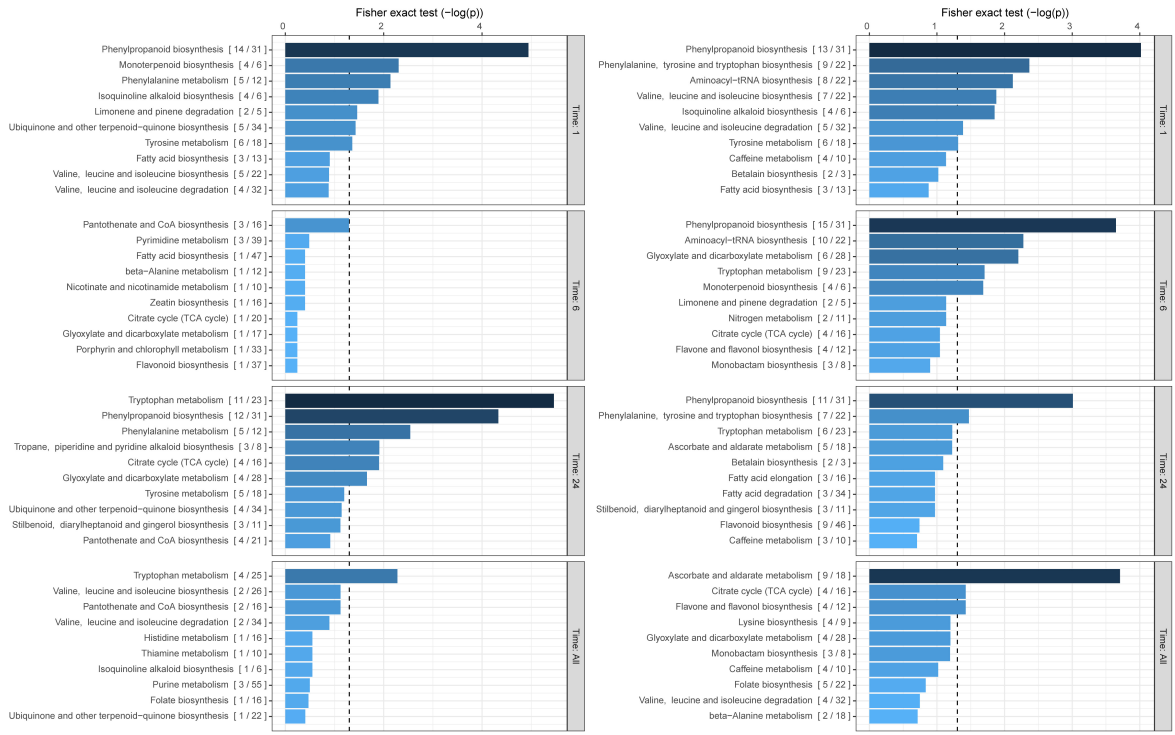

FIGURE 4 | Biochemical pathways in wheat which are affected by exposure to Z-3-HAC after 1, 6, and 24 h after infection. The mummichog algorithm was used on the *m/z* dataset of six biological replicates per treatment per time point. To analyze the added effect of pre-exposure to Z-3-HAC after infection, the *m/z* dataset of the Z-3-HAC + Fg treatment was compared to the *m/z* dataset of the Z-3-HAC treatment on the one hand (left panel) and to the *m/z* dataset of the Fg dataset on the other hand (right panel). Bars next to pathways represent the *p*-value of the Fisher exact test which represents the significance of change in the pathway when two treatments are compared. The ratio in brackets represents the number of significant matches to the total number of matched compounds in the pathway. The dashed line represents a *p*-value of 0.05.

linked to the sugar groups reported in the study of Sugimoto et al. (2014) (**Supplementary Dataset 1**), metabolite 3444 was identified as HexVic. This metabolite has been reported in the study of Sugimoto et al. (2014), in which 24 different plant species were exposed to Z-3-HOL and found to have an increased production of this diglycoside compound.

We observed an increase in glycosylated metabolites upon Z-3-HAC exposure, and glycosylation of defensive compounds is one of the proposed mechanisms of priming. As glycosylation of SA is a known priming mechanism, we retrospectively analyzed the metabolome data from the exposure experiment and the metabolome data from the inoculation experiment for the presence of SA and its glycoside, salicylic acid 2-O-β-D-glucoside (SAG) (**Figure 8**). To this end, an authentic reference standard was purchased for identification purposes (Toronto Research Chemicals, Toronto, ON, Canada).

At 1 hae, we already saw an induction of SA biosynthesis (+ 51.4%, $P = 0.004$) in the Z-3-HAC treatment compared to control leaves. At 6 hae, the SA contents in Z-3-HAC-treated seedlings was remarkably lower compared to those of the control seedlings (−43%, $P = 0.001$). For the inoculation experiment, we observed a threefold increase in seedlings which had been treated with Z-3-HAC and Z-3-HAC + *Fg* at 1 hai ($P < 0.01$), compared to the control treatment (**Figure 8**). No difference was observed between the Z-3-HAC and the Z-3-HAC + *Fg* treatments. Also, at 6 and 24 hai, the SA content was higher in Z-3-HAC and Z-3-HAC + *Fg*-treated seedlings, with significant differences at 24 hai, compared to the control. At 1 hae, SAG was significantly higher (+ 85.3%, $P = 0.003$), whereas at 6 hae SAG was not significantly different compared to the control treatment (**Figure 8B**). At 1 and 6 hai, SAG was higher in Z-3-HAC-treated plants, but not significantly different from the control treatment. At 24 hai, SAG was significantly higher ($P = 0.014$) in the Z-3-HAC + Fg treatment compared to those of the other treatments.

DISCUSSION

Z-3-HAC Induces Oxidative Stress and Transient SA Accumulation in Wheat

The notions that GLVs are quickly produced upon wounding (Fall et al., 1999) and that plants exposed to GLVs show the same activation patterns as plants which are wounded (Dombrowski and Martin, 2018; Dombrowski et al., 2019) fit within the framework of looking at GLVs as local "damaged-self signals" (Heil, 2014). Indeed GLVs are also released upon insect herbivory

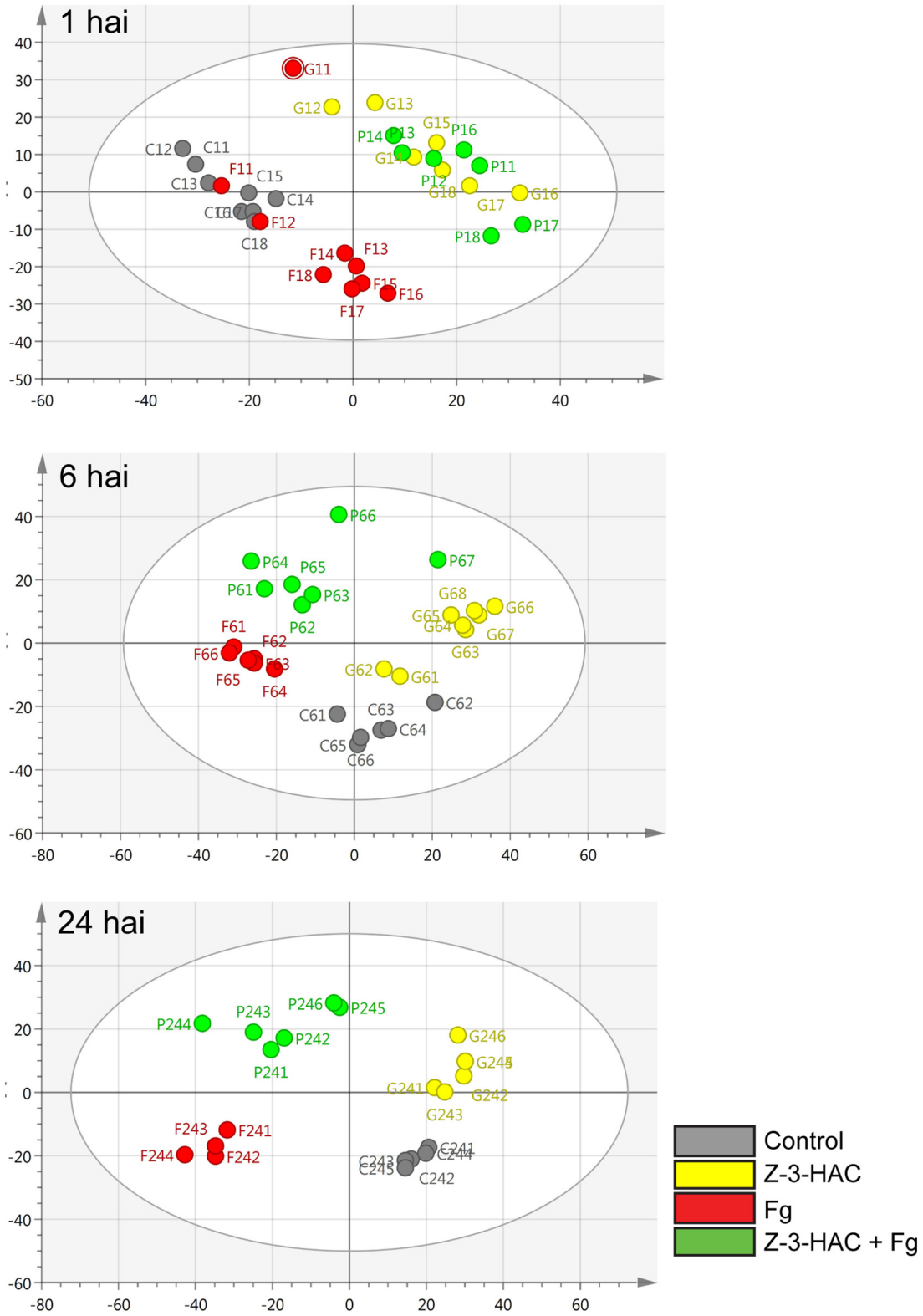

FIGURE 5 | Principal component analysis (PCA) score plots for the different time points. The PCA plots were constructed with metabolome data from the positive ionization mode for different time points: 1, 6, and 24 h after inoculation (hai). Each circle represents a single sample of 6–8 leaf sheaths. Control, gray; Z-3-HAC, yellow; Fg, red; Z-3-HAC + Fg, green. The ellipse depicts the Hotelling's T^2 95% confidence interval.

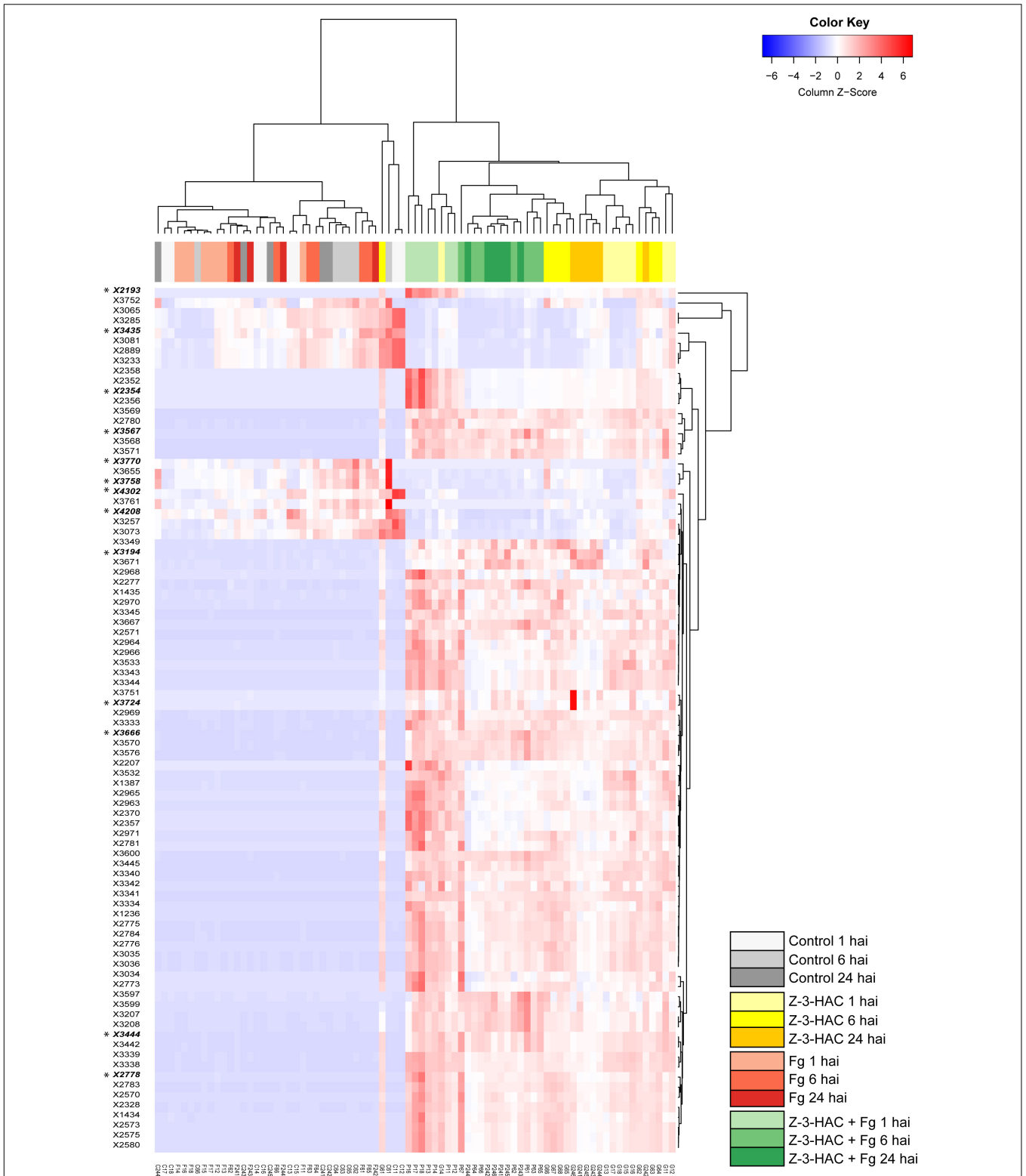

FIGURE 6 | Heat map and complete-linkage hierarchical clustering of the peak areas of the 103 metabolite features (horizontal lines) which contributed most to the orthogonal partial least squares discriminant analysis model for the positive ionization mode. A final set of 13 metabolite features was retained for further analysis, each one marked with an asterisk and in bold. Each vertical line has been assigned a color which corresponds to the treatment and time point of the sample. Metabolite feature codes (identity labels) were automatically assigned by Sieve™ 2.1 software (Thermo Fisher Scientific, San Jose, CA, United States). Z-3-HAC, Z-3-hexenyl acetate; Fg, *Fusarium graminearum*; hai, hours after inoculation.

TABLE 2 | Overview of metabolite ions which contribute the most to the predictability of the orthogonal partial least squares discriminant analysis model.

Metabolite ID	*m/z*[M + H]$^+$	RT (min)	Predicted elemental formula	Matching fragments	Candidate metabolite with highest score
2193	301.12560	3.69	$C_{14}H_{20}O_7$	8/17	Rhodosin (tyrosol glycoside)
2354	317.09949	3.43	$C_{10}H_{21}O_9P$	13/20	3-O-Butyl-alpha-D-glucopyranose 1-phosphoric acid
2778	349.14898	5.03	$C_{15}H_{24}O_9$	17/20	Leonuridine (iridoid glycoside)
3194	388.12930	3.9	$C_{22}H_{17}N_3O_4$	13/18	4-[[2-(4-Methoxyphenyl)-3H-benzimidazol-5-yl]carbamoyl]benzoic acid
3435	412.06369	4.06	$C_{12}H_{19}N_3O_9P_2$	16/21	N-[bis(Dimethoxyphosphoryl) methylideneamino]-2-methoxy-4-nitroaniline
3444 (NH_4^+)	412.21710	4.34	$C_{17}H_{30}O_{10}$	19/26	((Z)-3-Hexenyl-O-α-L-arabinopyranosyl-(1,6)-β-D-glucopyranoside
3567	424.21723	5.13	$C_{18}H_{33}NO_{10}$	17/21	β-Anthropyranosyl-(1→3)-α-L-rhamnopyranose
3666	445.14753	5.18	$C_{23}H_{24}O_9$	12/20	3-(Benzofuran-2-yl)-1-[2-hydroxy-6-[(2S,3R,4S,5S,6R)-3,4,5-trihydroxy-6-(hydroxymethyl)tetrahydropyran-2-yl]oxy-phenyl]propan-1-one
3724	456.20940	4.31	$C_{19}H_{29}N_5O_8$	15/21	tert-Butyl N-[1-[[(2R,3S,4R,5R)-5-(4-amino-2-oxopyrimidin-1-yl)-3,4-dihydroxyoxolan-2-yl]methylamino]-1,5-dioxopentan-2-yl]carbamate
3758	461.23476	6.03	$C_{22}H_{36}O_{10}$	8/20	(2E,4E)-8-(beta-D-Glucopyranosyloxy)-2,7-dimethyl-2,4-dodecadiene-1,10-dicarboxylic acid
3770	464.24035	6.06	$C_{24}H_{29}N_7O_3$	16/20	(2S)-2-[[(2S)-4-Cyclohexyloxy-2-[(2-methylpropan-2-yl)oxycarbonylamino]-4-oxobutanoyl]amino]-3-phenylpropanoic acid
4208	609.11274	3.99	$C_{25}H_{25}N_2O_{14}P$	4/18	Benzyl [[(2S,3S,4R,5R)-3-benzyloxycarbonyloxy-5-(2,4-dioxopyrimidin-1-yl)-4-hydroxy-tetrahydrofuran-2-yl]-phosphonooxy-methyl] carbonate
4302	771.16467	4.18	$C_{26}H_{32}N_{10}O_{14}P_2$	3/20	[[(2R,3S,4R,5R)-5-[6-amino-8-(4-Methoxyphenyl)purin-9-yl]-3,4-dihydroxy-tetrahydrofuran-2-yl]methoxy-hydroxy-phosphoryl] [(2R,3S,4R,5R)-5-(3-carbamoylpyridin-1-ium-1-yl)-3,4-dihydroxy-tetrahydrofuran-2-yl]methyl hydrogen phosphate

The metabolites are listed with their metabolite ID, mass over charge ratio (m/z) for the positive ionization mode, and retention time (RT). The predicted elemental formulas and in silico identifications were computed using the software package Sirius™ and the web application MetFrag™ Web beta. The numbers of the matching fragments from the high-resolution tandem mass spectrometry analysis are listed for the candidate metabolite with the highest score.

and fungal infection and quickly reach non-damaged parts of the plant (Ameye et al., 2018). This may then serve as a cue to induce plant defense responses against (a) biotic stress. To investigate the possible involvement of ROS in response to Z-3-HAC exposure, we performed several experiments.

We found the negative effects of 50 μM of Z-3-HAC on wheat leaves (**Figures 1A,B**). Remarkably, DAB staining revealed that H_2O_2 accumulation occurred around the stomata of the top of the leaves, which suggests that Z-3-HAC is taken up by the stomata and induces oxidative stress which is only limited to the top of the leaves. RT-qPCR analysis revealed an upregulation of genes *TaRBOH1* and *TaRBOH3* encoding for ROS-producing proteins and a suppression of genes coding for ROS-quenching enzymes. However, the enzyme activity of CAT and SOD was increased in Z-3-HAC-treated seedlings (**Figure 2**), which suggests that ROS quenching at these early time points is post-transcriptionally regulated and shows a delayed response. The induction of ROS and the parallel decreased expression of *CAT*, *APX*, *GPX*, and *SOD* isoforms are reminiscent of a hypersensitive response (HR) in which ROS accumulation leads to a type of programmed cell death of a number of cells to protect the plant from further biotic damage (De Gara et al., 2003; Balint-Kurti, 2019). Furthermore, this accumulation of ROS is an important hallmark to induce systemic acquired resistance (Durrant and Dong, 2004). We speculate that, during these early time points following GLV exposure, the expression of ROS-generating genes is induced, whereas the gene expression of ROS-quenching enzymes is negatively regulated, permitting the HR to carry on. However, at the protein level, the enzymes which are already present in the cells are post-transcriptionally activated (Rhee et al., 2005; Yamakura and Kawasaki, 2010), resulting in increased activity.

Pursuing a more holistic approach in which we aimed at uncovering pathways which are affected following Z-3-HAC exposure, we observed a significant effect of treating wheat with Z-3-HAC on the phenylpropanoid metabolism.

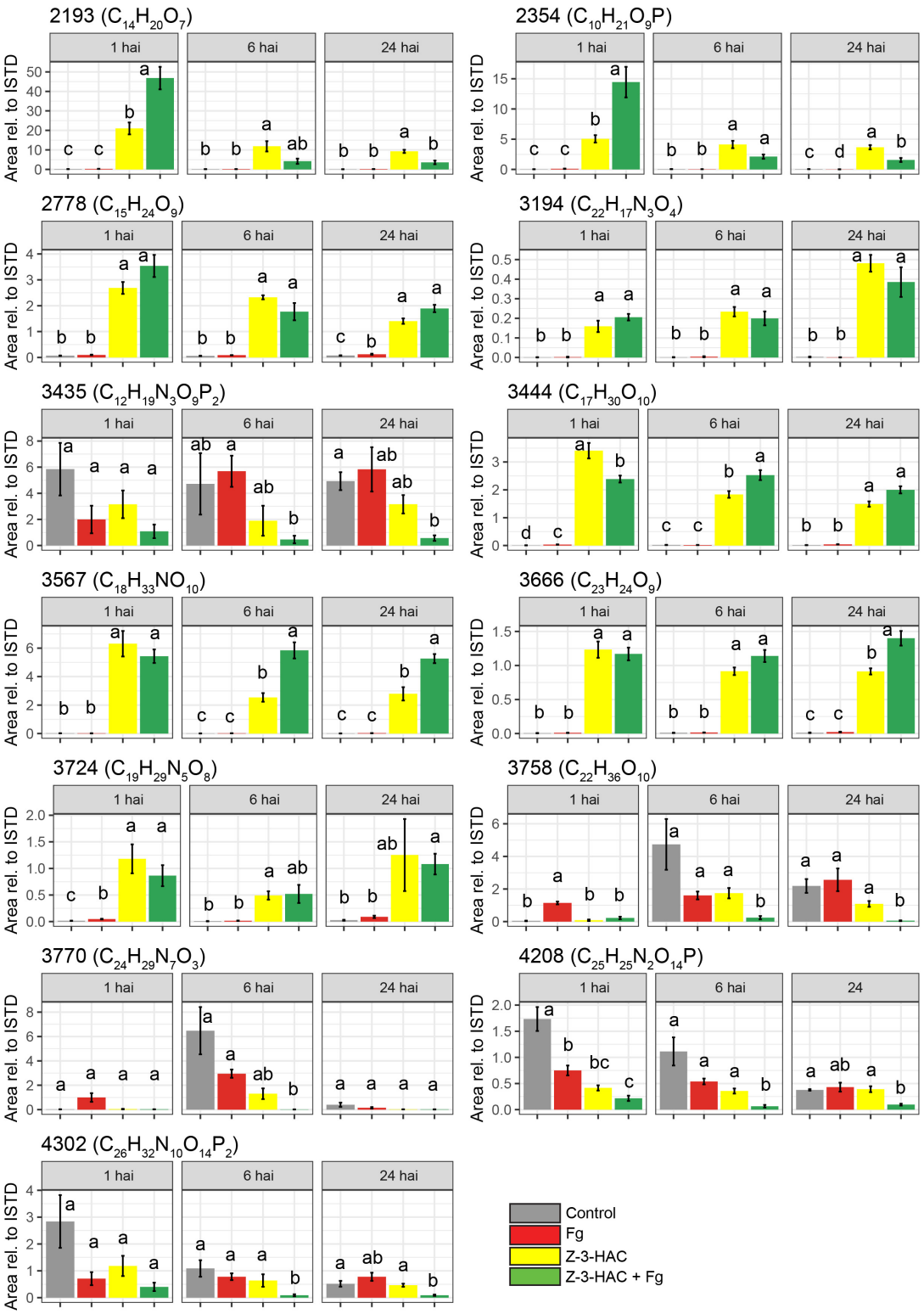

FIGURE 7 | Metabolite features which contribute most to the predictability of the orthogonal partial least squares discriminant analysis model for the positive ionization mode. Bars represent average integrated peak area values relative to the integrated peak area of the internal standard, and this is for 6–8 biological replicates. Treatments: control (gray bars); Fg, *F. graminearum* inoculation (red bars); Z-3-HAC, Z-3-hexenyl acetate exposure (yellow bars); Z-3-HAC + *Fg* inoculation (green bars); hai, hours after inoculation. Error bars represent ± SE. Significant differences between treatments per time point are depicted with different letters. The significance of differences was calculated using *post hoc* Dunett's T3 test ($\alpha = 0.05$). Metabolite codes were automatically assigned by Sieve™ 2.1 software (Thermo Fisher Scientific, San Jose, CA, United States).

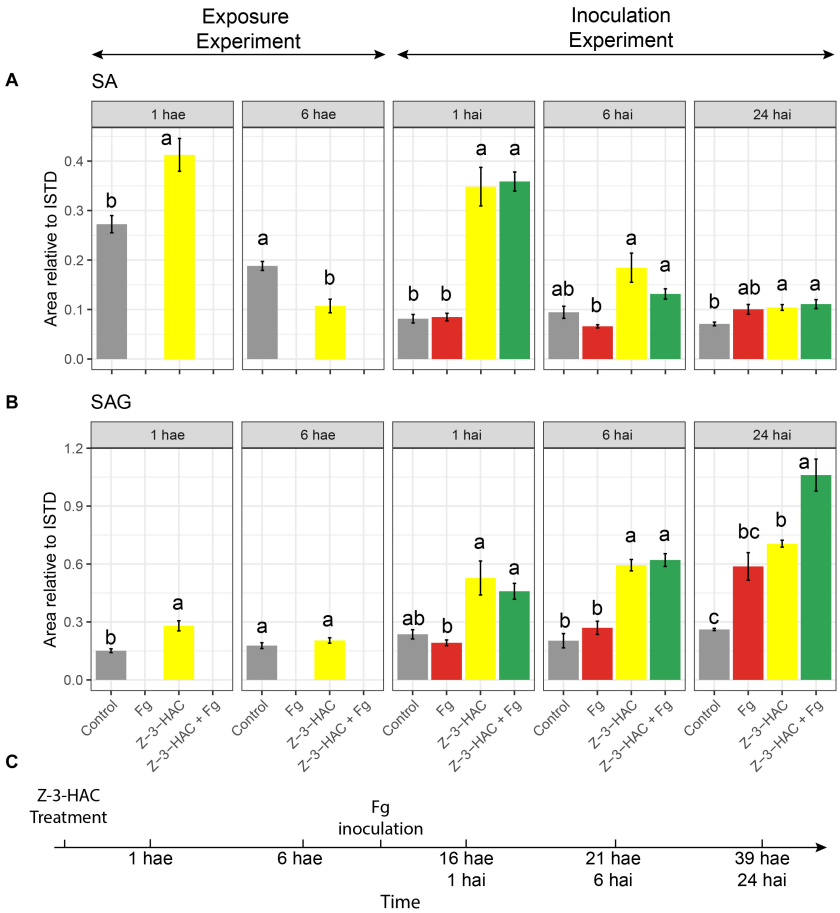

FIGURE 8 | (A) Salicylic acid and **(B)** salicylic acid 2-O-β-D-glucoside; bars represent integrated peak area relative to the internal standard of seedlings at 1 and 6 h after exposure (hae) to Z-3-HAC and at 1, 6, and 24 h after a combination of exposure to Z-3-HAC and inoculation with a conidia suspension (10^5 conidia mL^{-1}) of *F. graminearum* (*Fg*). **(C)** Timeline of the bioassays. Bars represent the average values of 6–8 biological replicates. Treatments: control (gray bars); Fg, *F. graminearum* inoculation (red bars); Z-3-HAC, Z-3-hexenyl acetate exposure (yellow bars); Z-3-HAC + Fg inoculation (green bars); hai, hours after inoculation. Error bars represent ± SE. Significant differences between treatments per time point are depicted with different letters and calculated using a two-sample Student's *t*-test for data at 1 and 6 hae and a *post hoc* Dunett's T3 test for data at 1, 6, and 24 hai (α = 0.05).

This is an important pathway in plants, yielding metabolites involved in (oxidative) stress responses such as flavonoids and hydroxycinnamic acids (Dixon et al., 2002). Additionally, other metabolic pathways which also play a role in the quenching of oxidative stress, such as glutathione and ascorbate, were also affected (**Figure 3**). However, if Z-3-HAC-treated plants were subsequently inoculated with Fg, we observed a different effect in the phenylpropanoid pathway compared to a sole Z-3-HAC or Fg treatment (**Figure 4**). However, whether this effect is due to the higher oxidative stress following infection in Z-3-HAC-treated plants or related to other processes should be further investigated in future research.

Besides accumulation of ROS, our results also disclosed a link between Z-3-HAC exposure and SA production (**Figure 8A**). Other studies have already shown that GLVs induce an upregulation of the expression of SA and JA biosynthesis genes (Bate and Rothstein, 1998; Arimura et al., 2001; Gomi et al., 2003; Farag et al., 2005; Kishimoto et al., 2006; Engelberth et al., 2007) during the first 6 hae. The effects of Z-3-HAC on SA levels and JA-dependent defense are not mutually exclusive as GLVs have been associated with both JA and SA responses (Ameye et al., 2018). This was shown in a transcriptomics study by Mirabella et al. (2015) who demonstrated the response of *Arabidopsis* after exposure to E-2-hexenal (E-2-HAL) during the first 3 h and reported that the differentially expressed genes showed a 49% overlap with the gene expression after exposure to SA, whereas there was also a 13% overlap after JA treatment. This suggests that E-2-HAL might activate SA- and JA-dependent responses, corroborating their findings. However, this does not entail that GLV signaling is solely SA or JA dependent as Mirabella et al. (2015) found that 32% of the differentially regulated genes were unique for E-2-HAL treatment. Thus, for our model system, a holistic transcriptomics approach at these early time points will be necessary to disclose whether the early increase in SA coincides with an early increase in SA defense gene expression and whether

Z-3-HAC influences defense genes downstream of SA-dependent defense signaling.

Z-3-HAC Induces Glycosylation of Metabolites Upon Infection With *F. graminearum*

While early responses of plants upon GLV exposure have been elucidated (Asai et al., 2009; Zebelo et al., 2012), mechanisms following these responses which contribute to increased defense remain less well understood (Ameye et al., 2018). In previous research, we have already determined that Z-3-HAC induces primed defense responses in wheat (Ameye et al., 2015). However, the mechanisms through which this primed state occurred still need to be further elucidated. The accumulation of conjugated defensive compounds is one of the proposed mechanisms for defense priming. Defense-related compounds such as ABA, SA, benzoxazinoids, and phytoanticipins, among others, can be glycosylated and transported to the vacuole, rendering them inactive. Following stress triggers, these can be quickly released from the vacuole and returned to their active state through hydroxylation by glucosidases (Conrath, 2011; Pastor et al., 2014). Our data are in line with this mechanism, as we observed an increase of metabolites upon exposure to Z-3-HAC, which shared several fragment ions with D-glucose (**Supplementary Dataset 1** and **Supplementary Figure 3**), indicating that Z-3-HAC induced the accumulation of glycosylated compounds. Furthermore, as some of these glycosylated metabolites were higher in the Z-3-HAC + Fg treatment, compared to the Z-3-HAC treatment [e.g., metabolites 2193 ($C_{14}H_{20}O_7$), 2354 ($C_{10}H_{21}O_9P$), and 3567 ($C_{18}H_{33}NO_{10}$)], these metabolites may point to mechanisms involved in the primed defense response of wheat plants following Z-3-HAC exposure.

Glycosyltransferases (GTs) play an important role in the biosynthesis and maintenance of the cell wall (Scheible and Pauly, 2004). GTs are also involved in plant defense by detoxifying xenobiotic compounds, such as mycotoxins (Lulin et al., 2010; Audenaert et al., 2013). Furthermore, GTs play a role in stabilizing and increasing the solubility of plant-defensive compounds such as phyto-anticipins, plant defense hormones, and their precursors. After glycosylation, these compounds can be transported and stored in the vacuole, from which they can be released upon stress or cellular damage and transformed into their active aglycons by glucosidases, which are located in different cell organelles (Bowles et al., 2006; Morant et al., 2008; Pastor et al., 2013). GTs constitute a large group of enzymes, with a restricted substrate specificity, entailing that different GTs glycosylate specific compounds (Jones and Vogt, 2001; Hansen et al., 2012). Several metabolites shared the same HRMS/MS fragment ions (**Supplementary Figure 3**), suggesting that some metabolites may have identical or similar aglycone substructure and thus may originate from the same, yet unknown, pathway(s). For example, metabolite 2193 has been identified as leonuridine, a glycosylated terpenoid, a member of the iridoid glycosides which exhibits antioxidant properties (Dinda et al., 2011). Leonuridine has additionally been reported to increase in *Quercus suber* following drought stress (Almeida et al., 2020). However, metabolite 2354 ($C_{10}H_{21}O_9P$) shares several fragment ions (**Supplementary Dataset 1**) and exhibits an identical pattern over time (**Figure 7**), which suggests that these may originate from the same pathway. Another glycoside was identified in our metabolomics study to be significantly produced upon Z-3-HAC exposure, the hexenyl diglycoside HexVic. The presence of hexenyl glycosides in plants has already been described in literature, whereby these compounds have primarily been reported to act as precursors for Z-3-HOL production (Jae-Hak et al., 1996; Nishikitani et al., 1999; Sugimoto et al., 2015). Moreover, it has been shown that one of the early responses (60 min) of maize following Z-3-HOL exposure involves the upregulation of putative glucosyltransferases and UDP-glucoside hydrogenase, which may result in concentration changes of glycosylated compounds (Engelberth et al., 2013). In a later study by Sugimoto et al. (2014), it has been shown for 24 different plant species, including *Arabidopsis* and *Triticum aestivum*, that hexenyl glucosides and hexenyl diglucosides increased after exposure to Z-3-HOL. The enzyme responsible for the synthesis of Z-3-hexenyl glycoside in *Camellia sinensis* was identified. Ohgami et al. (2015) demonstrated *in vitro* that AtUGT85A3 produced hexenyl-glycosides with UDP-glucose as a sugar donor and Z-3-hexenol as a sugar acceptor. Furthermore, they showed that homologs of the UGT85 family in several other plant species also formed hexenyl-glycosides. CsGT1, the AtUGT85A3 homolog in *C. sinensis*, was shown to have broad substrate specificity, including benzyl alcohol, linalool, geraniol, and Z-3-hexenol. However, GTs preferentially bind to hydroxyl groups, implying that, in our study, Z-3-HAC most likely must be hydrolyzed to Z-3-HOL by an esterase before it could be glycosylated.

We specifically investigated whether glycosylation of SA was also induced in Z-3-HAC-treated wheat. Indeed Z-3-HAC triggered an increased production of SAG (**Figure 8B**), corroborating that the defense-inducing action of GLVs may be attributed to the accumulation of glycosylated defensive compounds. These glycosylated compounds may be stored in the vacuole or transported through the xylem to other plant parts (Chen et al., 1995; Ratzinger et al., 2009). The time course of SA and its glycosylated derivate SAG accumulation follows the pattern for a priming response as stated by Martinez-Medina et al. (2016), i.e., following a priming stimulus (Z-3-HAC exposure), there is a transient induction of SA and SAG accumulation at 1 hae which returns to control levels at 6 hae, in the absence of a stress trigger (**Figures 8A,C**). However, following leaf sheath inoculation, a stress stimulus arises (wounding response because of the peeling of the leaf sheath and/or Fg inoculation), during which we observed a higher induction of SA and SAG formation in the Z-3-HAC and Z-3-HAC + Fg treatment at 1 and 6 hai. At 24 hai, SAG in the Z-3-HAC + Fg treatment is significantly higher than in the Z-3-HAC and the Fg treatment (**Figure 8B**), underlying the hypothesis that exposure to Z-3-HAC primes plant defense by glycosylating plant defense compounds.

These data together suggest that GLVs induce a transient production of defense signaling compounds (SA and SAG) on the first hours after exposure. After an (a)biotic stress trigger in

that tissue, SA and SAG formation are more strongly induced compared to plant tissue which was not previously exposed to Z-3-HAC. Then, Z-3-HAC directly induces glycosylation processes, which may play a role in plant defense. These glycosylation processes are activated upon Z-3-HAC perception and are even more enhanced when Z-3-HAC-treated plants encounter an (a)biotic stress trigger.

CONCLUSION

In conclusion, using a combined approach of the RT-qPCR analysis together with the metabolome data may point to a role for Z-3-HAC in the defense against pathogens by eliciting a ROS burst and increased activity of ROS-scavenging enzymes. This resulted in the activation of several pathways which are related to antioxidative processes. Indeed ROS production leading to HR constitutes a crude but effective means to fend off aggressors during the biotrophic phase of its infection phase in which living cells are needed to successfully infect the plant tissue. Additionally, our metabolomics approach showed an increase in glycosylation processes following Z-3-HAC exposure. However, further research is mandatory to elucidate the full identity of these glycosylated compounds which are produced more upon a combined treatment in order to unravel whether these involved plant defense.

DATA AVAILABILITY STATEMENT

The raw data supporting the conclusions of this article will be made available by the authors, without undue reservation, to any qualified researcher.

AUTHOR CONTRIBUTIONS

MA, GS, GH, KA, LM, and LV designed the experiments. MA performed all the experiments and wrote the manuscript. BM helped with the ROS experiment. LM and LV provided the valuable input for the metabolomics experiments. All authors read and revised the manuscript.

SUPPLEMENTARY MATERIAL

The Supplementary Material for this article can be found online at: https://www.frontiersin.org/articles/10.3389/fpls.2020.596271/full#supplementary-material

Supplementary Figure 1 | Levels of L-Phe in the infection assay.

Supplementary Figure 2 | Predicted chemical structures of the metabolites which contribute the most to the predictability of the orthogonal partial least squares discriminant analysis model.

Supplementary Figure 3 | High-resolution tandem mass spectrometry patterns of the metabolites which contributed most to the predictability of the orthogonal partial least squares discriminant analysis model for the positive ionization mode.

Supplementary Figure 4 | Principal component analysis score plots for the different time points of the negative ionization mode.

Supplementary Figure 5 | S-plot of the metabolite features for the samples at 6 h after inoculation, making the comparison between the Z-3-HAC and Z-3-HAC + Fg treatments.

Supplementary Table 1 | Accurate mass, ionization adduct, and retention time as determined based on analytical standards and used for the identification of salicylic acid.

Supplementary Dataset 1 | Excel datasheet containing fragment ions of metabolites which were most abundant in the Z-3-HAC and Z-3-HAC + Fg treatments.

REFERENCES

Akinwumi, B. C., Bordun, K.-A. M., and Anderson, H. D. (2018). Biological activities of stilbenoids. *Intern. J. Mol. Sci.* 19:792. doi: 10.3390/ijms19030792

Almeida, T., Pinto, G., Correia, B., Gonçalves, S., Meijón, M., and Escandón, M. (2020). In-depth analysis of the *Quercus suber* metabolome under drought stress and recovery reveals potential key metabolic players. *Plant Sci.* 299:110606. doi: 10.1016/j.plantsci.2020.110606

Ameye, M., Audenaert, K., De Zutter, N., Steppe, K., Van Meulebroek, L., Vanhaecke, L., et al. (2015). Priming of wheat with the green leaf volatile Z-3-hexenyl acetate enhances defense against *Fusarium graminearum* but boosts deoxynivalenol production. *Plant Physiol.* 167, 1671–1684. doi: 10.1104/pp.15.00107

Ameye, M., Van Meulebroek, L., Vanhaecke, L., Smagghe, G., Haesaert, G., and Audenaert, K. (2018). Green leaf volatile production by plants: a meta-analysis. *New Phytol.* 220, 666–683. doi: 10.1111/nph.14671

Arimura, G., Ozawa, R., Horiuchi, J., Nishioka, T., and Takabayashi, J. (2001). Plant-plant interactions mediated by volatiles emitted from plants infested by spider mites. *Biochem. Syst. Ecol.* 29, 1049–1061. doi: 10.1016/s0305-1978(01)00049-7

Asai, N., Nishioka, T., Takabayashi, J., and Furuichi, T. (2009). Plant volatiles regulate the activities of Ca2+-permeable channels and promote cytoplasmic calcium transients in *Arabidopsis* leaf cells. *Plant Signal. Behav.* 4, 294–300. doi: 10.4161/psb.4.4.8275

Audenaert, K., De Boevre, M., Vanheule, A., Callewaert, J., Bekaert, B., Höfte, M., et al. (2013). *Mycotoxin glucosylation* in commercial wheat varieties: impact on resistance to *Fusarium graminearum* under laboratory and field conditions. *Food Control* 34, 756–762. doi: 10.1016/j.foodcont.2013.06.019

Baker, N. R. (2008). Chlorophyll fluorescence: a probe of photosynthesis in vivo. *Annu. Rev. Plant Biol.* 59, 89–113. doi: 10.1146/annurev.arplant.59.032607.092759

Balint-Kurti, P. (2019). The plant hypersensitive response: concepts, control and consequences. *Mol. Plant Pathol.* 20, 1163–1178.

Bate, N. J., and Rothstein, S. J. (1998). C6-volatiles derived from the lipoxygenase pathway induce a subset of defense-related genes. *Plant J.* 16, 561–569. doi: 10.1046/j.1365-313x.1998.00324.x

Böcker, S., and Dührkop, K. (2016). Fragmentation trees reloaded. *J. Cheminform.* 8:5.

Bowles, D., Lim, E.-K., Poppenberger, B., and Vaistij, F. E. (2006). Glycosyltransferases of lipophilic small molecules. *Annu. Rev. Plant Biol.* 57, 567–597. doi: 10.1146/annurev.arplant.57.032905.105429

Caverzan, A., Passaia, G., Rosa, S. B., Ribeiro, C. W., Lazzarotto, F., and Margis-Pinheiro, M. (2012). Plant responses to stresses: role of ascorbate peroxidase in the antioxidant protection. *Genet. Mol. Biol.* 35, 1011–1019. doi: 10.1590/s1415-47572012000600016

Chen, Z., Malamy, J., Henning, J., Conrath, U., Sánchez-Casas, P., Silva, H., et al. (1995). Induction, modification, and transduction of the salicylic acid signal in plant defense responses. *Proc. Natl. Acad. Sci. U.S.A.* 92, 4134–4137. doi: 10.1073/pnas.92.10.4134

Chong, J., Soufan, O., Li, C., Caraus, I., Li, S., Bourque, G., et al. (2018). MetaboAnalyst 4.0: towards more transparent and integrative metabolomics analysis. *Nucleic Acids Res.* 46, W486–W494.

Cofer, T. M., Seidl-Adams, I., and Tumlinson, J. H. (2018). From acetoin to (Z)-3-hexen-1-ol: the diversity of volatile organic compounds that induce plant responses. *J. Agric. Food Chem.* 66, 11197–11208. doi: 10.1021/acs.jafc.8b03010

Conrath, U. (2011). Molecular aspects of defence priming. *Trends Plant Sci.* 16, 524–531. doi: 10.1016/j.tplants.2011.06.004

Creek, D. J., Dunn, W. B., Fiehn, O., Griffin, J. L., Hall, R. D., Lei, Z., et al. (2014). Metabolite identification: are you sure? And how do your peers gauge your confidence? *Metabolomics* 10:350. doi: 10.1007/s11306-014-0656-8

Dai, J., and Mumper, R. J. (2010). Plant phenolics: extraction, analysis and their antioxidant and anticancer properties. *Molecules* 15, 7313–7352. doi: 10.3390/molecules15107313

De Gara, L., De Pinto, M. C., and Tommasi, F. (2003). The antioxidant systems vis-à-vis reactive oxygen species during plant-pathogen interaction. *Plant Physiol. Biochem.* 41, 863–870. doi: 10.1016/s0981-9428(03)00135-9

De Vleesschauwer, D., Yang, Y., Cruz, C. V., and Höfte, M. (2010). Abscisic acid-induced resistance against the brown spot pathogen *Cochliobolus miyabeanus* in rice involves MAP kinase-mediated repression of ethylene signaling. *Plant Physiol.* 152, 2036–2052. doi: 10.1104/pp.109.152702

Dinda, B., Debnath, S., and Banik, R. (2011). Naturally occurring iridoids and secoiridoids. An updated review, Part 4. *Chem. Pharm. Bull.* 59, 803–833. doi: 10.1248/cpb.59.803

Dixon, R. A., Achnine, L., Kota, P., Liu, C.-J., Reddy, M. S. S., and Wang, L. (2002). The phenylpropanoid pathway and plant defence—a genomics perspective. *Mol. Plant Pathol.* 3, 371–390. doi: 10.1046/j.1364-3703.2002.00131.x

Dombrowski, J. E., Kronmiller, B. A., Hollenbeck, V. G., Rhodes, A. C., Henning, J. A., and Martin, R. C. (2019). Transcriptome analysis of the model grass *Lolium temulentum* exposed to green leaf volatiles. *BMC Plant Biol.* 19:222. doi: 10.1186/s12870-019-1799-6

Dombrowski, J. E., and Martin, R. C. (2018). Activation of MAP kinases by green leaf volatiles in grasses. *BMC Res. Notes* 11:79. doi: 10.1186/s13104-017-3076-9

Dudareva, N., Klempien, A., Muhlemann, J. K., and Kaplan, I. (2013). Biosynthesis, function and metabolic engineering of plant volatile organic compounds. *New Phytol.* 198, 16–32. doi: 10.1111/nph.12145

Durrant, W., and Dong, X. (2004). Systemic acquired resistance. *Annu. Rev. Phytopathol.* 42, 185–209.

Engelberth, J., Alborn, H. T., Schmelz, E. A., and Tumlinson, J. H. (2004). Airborne signals prime plants against insect herbivore attack. *Proc. Natl. Acad. Sci. U.S.A.* 101, 1781–1785. doi: 10.1073/pnas.0308037100

Engelberth, J., Contreras, C. F., Dalvi, C., Li, T., and Engelberth, M. (2013). Early transcriptome analyses of Z-3-hexenol-treated *Zea mays* revealed distinct transcriptional networks and anti-herbivore defense potential of green leaf volatiles. *PLoS One* 8:e0077465. doi: 10.1371/journal.pone.0077465

Engelberth, J., Seidl-Adams, I., Schultz, J. C., and Tumlinson, J. H. (2007). Insect elicitors and exposure to green leafy volatiles differentially upregulate major octadecanoids and transcripts of 12-oxo phytodienoic acid reductases in *Zea mays*. *Mol. Plant Microb. Interact.* 20, 707–716. doi: 10.1094/mpmi-20-6-0707

Fall, R., Karl, T., Hansel, A., Jordan, A., and Lindinger, W. (1999). Volatile organic compounds emitted after leaf wounding: on-line analysis by proton-transfer-reaction mass spectrometry. *J. Geophys. Res. Atmos.* 104, 15963–15974. doi: 10.1029/1999jd900144

Farag, M., Fokar, M., Abd, H., Zhang, H., Allen, R., and Paré, P. (2005). (*Z*)-3-Hexenol induces defense genes and downstream metabolites in maize. *Planta* 220, 900–909. doi: 10.1007/s00425-004-1404-5

Feussner, I., and Polle, A. (2015). What the transcriptome does not tell—proteomics and metabolomics are closer to the plants' patho-phenotype. *Curr. Opin. Plant Biol.* 26, 26–31. doi: 10.1016/j.pbi.2015.05.023

Gomi, K., Yamasaki, Y., Yamamoto, H., and Akimitsu, K. (2003). Characterization of a hydroperoxide lyase gene and effect of C6-volatiles on expression of genes of the oxylipin metabolism in Citrus. *J. Plant Physiol.* 160, 1219–1231. doi: 10.1078/0176-1617-01177

Hansen, S., Harholt, J., Oikawa, A., and Scheller, H. (2012). Plant glycosyltransferases beyond CAZy: a perspective on DUF families. *Front. Plant Sci.* 3:59. doi: 10.3389/fpls.2012.00059

Havaux, M. (2014). Carotenoid oxidation products as stress signals in plants. *Plant J.* 79, 597–606. doi: 10.1111/tpj.12386

Heil, M. (2014). Herbivore- induced plant volatiles: targets, perception and unanswered questions. *New Phytol.* 204, 297–306. doi: 10.1111/nph.12977

Hong, J., Yang, L. T., Zhang, D. B., and Shi, J. X. (2016). Plant metabolomics: an indispensable system biology tool for plant science. *Intern. J. Mol. Sci.* 17:767. doi: 10.3390/ijms17060767

Jae-Hak, M., Watanabe, N., Ijima, Y., and Sakata, K. (1996). cis-and trans-Linalool 3, 7-oxides and methyl salicylate glycosides and (Z)-3-hexenyl β-D-glucopyranoside as aroma precursors from tea leaves for oolong tea. *Biosci. Biotechnol. Biochem.* 60, 1815–1819. doi: 10.1271/bbb.60.1815

Jansen, C., Von Wettstein, D., Schafer, W., Kogel, K. H., Felk, A., and Maier, F. J. (2005). Infection patterns in barley and wheat spikes inoculated with wild-type and trichodiene synthase gene disrupted *Fusarium graminearum*. *Proc. Natl. Acad. Sci. India Sect. B. Biol. Sci.* 102, 16892–16897. doi: 10.1073/pnas.0508467102

Jones, P., and Vogt, T. (2001). Glycosyltransferases in secondary plant metabolism: tranquilizers and stimulant controllers. *Planta* 213, 164–174. doi: 10.1007/s004250000492

Kind, T., Scholz, M., and Fiehn, O. (2009). How large is the metabolome? A critical analysis of data exchange practices in chemistry. *PLoS One* 4:e5440. doi: 10.1371/journal.pone.05440

Kishimoto, K., Matsui, K., Ozawa, R., and Takabayashi, J. (2006). ETR1-, JAR1- and PAD2-dependent signaling pathways are involved in C6-aldehyde-induced defense responses of *Arabidopsis*. *Plant Sci.* 171, 415–423. doi: 10.1016/j.plantsci.2006.05.004

Kishimoto, K., Matsui, K., Ozawa, R., and Takabayashi, J. (2008). Direct fungicidal activities of C6-aldehydes are important constituents for defense responses in *Arabidopsis* against *Botrytis cinerea*. *Phytochemistry* 69, 2127–2132. doi: 10.1016/j.phytochem.2008.04.023

Koga, H., Dohi, K., Nakayachi, O., and Mori, M. (2004). A novel inoculation method of *Magnaporthe grisea* for cytological observation of the infection process using intact leaf sheaths of rice plants. *Physiol. Mol. Plant Pathol.* 64, 67–72. doi: 10.1016/j.pmpp.2004.07.002

Li, S., Park, Y., Duraisingham, S., Strobel, F. H., Khan, N., Soltow, Q. A., et al. (2013). Predicting network activity from high throughput metabolomics. *PLoS Comput. Biol.* 9:e1003123. doi: 10.1371/journal.pcbi.1003123

López-Gresa, M. P., Payá, C., Ozáez, M., Rodrigo, I., Conejero, V., Klee, H., et al. (2018). A new role for green leaf volatile esters in tomato stomatal defence against *Pseudomonas syringe* pv. tomato. *Front. Plant Sci.* 9:1855. doi: 10.3389/fpls.2018.01855

Lulin, M., Yi, S., Aizhong, C., Zengjun, Q., Liping, X., Peidu, C., et al. (2010). Molecular cloning and characterization of an up-regulated UDP-glucosyltransferase gene induced by DON from *Triticum aestivum* L. cv. Wangshuibai. *Mol. Biol. Rep.* 37:785. doi: 10.1007/s11033-009-9606-3

Martinez-Medina, A., Flors, V., Heil, M., Mauch-Mani, B., Pieterse, C. M., Pozo, M. J., et al. (2016). Recognizing plant defense priming. *Trends Plant Sci.* 21, 818–822. doi: 10.1016/j.tplants.2016.07.009

Matsui, K., Sugimoto, K., Mano, J., Ozawa, R., and Takabayashi, J. (2012). Differential metabolisms of green leaf volatiles in injured and intact parts of a wounded leaf meet distinct ecophysiological requirements. *PLoS One* 7:e36433. doi: 10.1371/journal.pone.0036433

Mhlongo, M. I., Piater, L. A., Madala, N. E., Steenkamp, P. A., and Dubery, I. A. (2016). Phenylpropanoid defences in *Nicotiana tabacum* cells: overlapping metabolomes indicate common aspects to priming responses induced by lipopolysaccharides, chitosan and flagellin-22. *PLoS One* 11:e0151350. doi: 10.1371/journal.pone.0151350

Mirabella, R., Rauwerda, H., Allmann, S., Scala, A., Spyropoulou, E. A., De Vries, M., et al. (2015). WRKY40 and WRKY6 act downstream of the green leaf volatile E-2-hexenal in *Arabidopsis*. *Plant J.* 83, 1082–1096. doi: 10.1111/tpj.12953

Morant, A. V., Jørgensen, K., Jørgensen, C., Paquette, S. M., Sánchez-Pérez, R., Møller, B. L., et al. (2008). β-Glucosidases as detonators of plant chemical defense. *Phytochemistry* 69, 1795–1813. doi: 10.1016/j.phytochem.2008.03.006

Nakamura, S., and Hatanaka, A. (2002). Green-leaf-derived C6-aroma compounds with potent antibacterial action that act on both gram-negative and gram-positive bacteria. *J. Agric. Food Chem.* 50, 7639–7644. doi: 10.1021/jf025808c

Nishikitani, M., Dongmei, W., Kubota, K., Kobayashi, A., and Sugawara, F. (1999). (Z)-3-hexenyl and trans-linalool 3, 7-oxide β-primeverosides isolated as aroma precursors from leaves of a green tea cultivar. *Biosci. Biotechnol. Biochem.* 63, 1631–1633. doi: 10.1271/bbb.63.1631

Ohgami, S., Ono, E., Horikawa, M., Murata, J., Totsuka, K., Toyonaga, H., et al. (2015). Volatile glycosylation in tea plants: sequential glycosylations for the biosynthesis of aroma β-primeverosides are catalyzed by two *Camellia sinensis* glycosyltransferases. *Plant Physiol.* 168, 464–477. doi: 10.1104/pp.15.00403

Paolacci, A. R., Tanzarella, O. A., Porceddu, E., and Ciaffi, M. (2009). Identification and validation of reference genes for quantitative RT-PCR normalization in wheat. *BMC Mol. Biol.* 10:11. doi: 10.1186/1471-2199-10-11

Pastor, V., Balmer, A., Gamir, J., Flors, V., and Mauch-Mani, B. (2014). Preparing to fight back: generation and storage of priming compounds. *Front. Plant Sci.* 5:295. doi: 10.3389/fpls.2014.00295

Pastor, V., Luna, E., Mauch-Mani, B., Ton, J., and Flors, V. (2013). Primed plants do not forget. *Environ. Exper. Bot.* 94, 46–56. doi: 10.1016/j.envexpbot.2012.02.013

Patti, G. J., Yanes, O., and Siuzdak, G. (2012). Metabolomics: the apogee of the omics trilogy. *Nat. Rev. Mol. Cell Biol.* 13, 263–269. doi: 10.1038/nrm3314

Piesik, D., Panka, D., Delaney, K. J., Skoczek, A., Lamparski, R., and Weaver, D. K. (2011). Cereal crop volatile organic compound induction after mechanical injury, beetle herbivory (*Oulema* spp.), or fungal infection (*Fusarium* spp.). *J. Plant Physiol.* 168, 878–886. doi: 10.1016/j.jplph.2010.11.010

Quintana-Rodriguez, E., Duran-Flores, D., Heil, M., and Camacho-Coronel, X. (2018). Damage-associated molecular patterns (DAMPs) as future plant vaccines that protect crops from pests. *Sci. Hortic.* 237, 207–220. doi: 10.1016/j.scienta.2018.03.026

R Core Team (2013). *R: A Language and Environment for Statistical Computing*. Vienna: R Core Team.

Ratzinger, A., Riediger, N., Von Tiedemann, A., and Karlovsky, P. (2009). Salicylic acid and salicylic acid glucoside in xylem sap of *Brassica napus* infected with *Verticillium longisporum*. *J. Plant Res.* 122, 571–579. doi: 10.1007/s10265-009-0237-5

Razzaq, A., Sadia, B., Raza, A., Khalid Hameed, M., and Saleem, F. (2019). Metabolomics: a way forward for crop improvement. *Metabolites* 9:303. doi: 10.3390/metabo9120303

Rhee, S. G., Yang, K.-S., Kang, S. W., Woo, H. A., and Chang, T.-S. (2005). Controlled elimination of intracellular H_2O_2: regulation of peroxiredoxin, catalase, and glutathione peroxidase via post-translational modification. *Antioxid. Redox Signal.* 7, 619–626. doi: 10.1089/ars.2005.7.619

Ruttkies, C., Schymanski, E. L., Wolf, S., Hollender, J., and Neumann, S. (2016). MetFrag relaunched: incorporating strategies beyond in silico fragmentation. *J. Cheminform.* 8:3.

Scala, A., Allmann, S., Mirabella, R., Haring, M. A., and Schuurink, R. C. (2013). Green leaf volatiles: a Plant's multifunctional weapon against herbivores and pathogens. *Intern. J. Mol. Sci.* 14, 17781–17811. doi: 10.3390/ijms140917781

Scheible, W.-R., and Pauly, M. (2004). Glycosyltransferases and cell wall biosynthesis: novel players and insights. *Curr. Opin. Plant Biol.* 7, 285–295. doi: 10.1016/j.pbi.2004.03.006

Škerget, M., Kotnik, P., Hadolin, M., Hraš, A. R., Simonič, M., and Knez, Ž (2005). Phenols, proanthocyanidins, flavones and flavonols in some plant materials and their antioxidant activities. *Food Chem.* 89, 191–198. doi: 10.1016/j.foodchem.2004.02.025

Sugimoto, K., Matsui, K., Iijima, Y., Akakabe, Y., Muramoto, S., Ozawa, R., et al. (2014). Intake and transformation to a glycoside of (Z)-3-hexenol from infested neighbors reveals a mode of plant odor reception and defense. *Proc. Natl. Acad. Sci. U.S.A.* 111, 7144–7149. doi: 10.1073/pnas.1320660111

Sugimoto, K., Matsui, K., and Takabayashi, J. (2015). Conversion of volatile alcohols into their glucosides in *Arabidopsis*. *Commun. Integrat. Biol.* 8:e992731. doi: 10.4161/19420889.2014.992731

Szalai, G., Kellös, T., Galiba, G., and Kocsy, G. (2009). Glutathione as an antioxidant and regulatory molecule in plants under abiotic stress conditions. *J. Plant Growth Regul.* 28, 66–80. doi: 10.1007/s00344-008-9075-2

Thordal-Christensen, H., Zhang, Z., Wei, Y., and Collinge, D. B. (1997). Subcellular localization of H_2O_2 in plants. HO_2 accumulation in papillae and hypersensitive response during the barley—powdery mildew interaction. *Plant J.* 11, 1187–1194. doi: 10.1046/j.1365-313x.1997.11061187.x

Triba, M. N., Le Moyec, L., Amathieu, R., Goossens, C., Bouchemal, N., Nahon, P., et al. (2015). PLS/OPLS models in metabolomics: the impact of permutation of dataset rows on the K-fold cross-validation quality parameters. *Mol. BioSyst.* 11, 13–19. doi: 10.1039/c4mb00414k

Turlings, T. C., Tumlinson, J. H., Heath, R. R., Proveaux, A. T., and Doolittle, R. E. (1991). Isolation and identification of allelochemicals that attract the larval parasitoid, *Cotesia marginiventris* (Cresson), to the microhabitat of one of its hosts. *J. Chem. Ecol.* 17, 2235–2251. doi: 10.1007/bf00988004

Urano, K., Maruyama, K., Ogata, Y., Morishita, Y., Takeda, M., Sakurai, N., et al. (2009). Characterization of the ABA-regulated global responses to dehydration in Arabidopsis by metabolomics. *Plant J.* 57, 1065–1078. doi: 10.1111/j.1365-313x.2008.03748.x

Van Meulebroek, L., Vanden Bussche, J., De Clercq, N., Steppe, K., and Vanhaecke, L. (2015). A metabolomics approach to unravel the regulating role of phytohormones towards carotenoid metabolism in tomato fruit. *Metabolomics* 11, 667–683. doi: 10.1007/s11306-014-0728-9

Van Meulebroek, L., Vanden Bussche, J., Steppe, K., and Vanhaecke, L. (2012). Ultra-high performance liquid chromatography coupled to high resolution Orbitrap mass spectrometry for metabolomic profiling of the endogenous phytohormonal status of the tomato plant. *J. Chromatogr. A* 1260, 67–80. doi: 10.1016/j.chroma.2012.08.047

Ward, J. L., Forcat, S., Beckmann, M., Bennett, M., Miller, S. J., Baker, J. M., et al. (2010). The metabolic transition during disease following infection of *Arabidopsis thaliana* by *Pseudomonas syringae* pv. tomato. *Plant J.* 63, 443–457. doi: 10.1111/j.1365-313x.2010.04254.x

Wenda-Piesik, A., Piesik, D., Ligor, T., and Buszewski, B. (2010). Volatile organic compounds (VOCs) from cereal plants infested with crown rot: their identity and their capacity for inducing production of VOCs in uninfested plants. *Intern. J. Pest Manag.* 56, 377–383. doi: 10.1080/09670874.2010.505668

Yamakura, F., and Kawasaki, H. (2010). Post-translational modifications of superoxide dismutase. *Biochim. Biophys. Acta Proteins Proteom.* 1804, 318–325. doi: 10.1016/j.bbapap.2009.10.010

Yamauchi, Y., Kunishima, M., Mizutani, M., and Sugimoto, Y. (2015). Reactive short-chain leaf volatiles act as powerful inducers of abiotic stress-related gene expression. *Sci. Rep.* 5:8030.

Zebelo, S. A., Matsui, K., Ozawa, R., and Maffei, M. E. (2012). Plasma membrane potential depolarization and cytosolic calcium flux are early events involved in tomato (*Solanum lycopersicon*) plant-to-plant communication. *Plant Sci.* 196, 93–100. doi: 10.1016/j.plantsci.2012.08.006

Conflict of Interest: The authors declare that the research was conducted in the absence of any commercial or financial relationships that could be construed as a potential conflict of interest.

Copyright © 2020 Ameye, Van Meulebroek, Meuninck, Vanhaecke, Smagghe, Haesaert and Audenaert. This is an open-access article distributed under the terms of the Creative Commons Attribution License (CC BY). The use, distribution or reproduction in other forums is permitted, provided the original author(s) and the copyright owner(s) are credited and that the original publication in this journal is cited, in accordance with accepted academic practice. No use, distribution or reproduction is permitted which does not comply with these terms.

frontiers in Plant Science

ORIGINAL RESEARCH
published: 11 March 2021
doi: 10.3389/fpls.2021.637959

Differential Regulation of the Ribosomal Association of mRNA Transcripts in an *Arabidopsis* Mutant Defective in Jasmonate-Dependent Wound Response

Athen Kimberlin[1,2†], Rebekah E. Holtsclaw[1,2†] and Abraham J. Koo[1,2]*

[1] Department of Biochemistry, University of Missouri, Columbia, MO, United States, [2] Interdisciplinary Plant Group, University of Missouri, Columbia, MO, United States

OPEN ACCESS

Edited by:
Koichi Sugimoto,
University of Tsukuba, Japan

Reviewed by:
Ian Major,
Michigan State University,
United States
Andrea Chini,
Centro Nacional de Biotecnología,
Consejo Superior de Investigaciones
Científicas (CSIC), Spain

***Correspondence:**
Abraham J. Koo
kooaj@missouri.edu

[†] These authors have contributed equally to this work

Specialty section:
This article was submitted to Plant Physiology, a section of the journal Frontiers in Plant Science

Received: 04 December 2020
Accepted: 01 February 2021
Published: 11 March 2021

Citation:
Kimberlin A, Holtsclaw RE and Koo AJ (2021) Differential Regulation of the Ribosomal Association of mRNA Transcripts in an Arabidopsis Mutant Defective in Jasmonate-Dependent Wound Response. Front. Plant Sci. 12:637959. doi: 10.3389/fpls.2021.637959

Jasmonoyl-L-isoleucine (JA-Ile) is a powerful oxylipin responsible for the genome-wide transcriptional reprogramming in plants that results in major physiological shifts from growth to defense. The double T-DNA insertion *Arabidopsis* mutant, *cyp94b1cyp94b3* (*b1b3*), defective in cytochrome p450s, CYP94B1 and CYP94B3, which are responsible for oxidizing JA-Ile, accumulates several fold higher levels of JA-Ile yet displays dampened JA-Ile–dependent wound responses—the opposite of what is expected. Transcriptomic and proteomic analyses showed that while the transcriptional response to wounding was largely unchanged in *b1b3* compared to wild type (WT), many proteins were found to be significantly reduced in the mutant, which was verified by immunoblot analyses of marker proteins. To understand this protein phenotype and their hypothesized contribution to the *b1b3* phenotypes, wounded rosette leaf samples from both WT and *b1b3* were subject to a translating ribosome affinity purification RNA sequencing analysis. More than 1,600 genes whose transcripts do not change in abundance by wounding changed their association with the ribosomes after wounding in WT leaves. Consistent with previous observations, the total pool of mRNA transcripts was similar between WT and *b1b3*; however, the ribosome-associated pool of transcripts was changed significantly. Most notably, fewer transcripts were associated with the ribosome pool in *b1b3* than in WT, potentially explaining the reduction of many proteins in the mutant. Among those genes with fewer ribosome-associated transcripts in *b1b3* were genes relating to stress response, specialized metabolism, protein metabolism, ribosomal subunits, and transcription factors, consistent with the biochemical phenotypes of the mutant. These results show previously unrecognized regulations at the translational level that are affected by misregulation of JA homeostasis during the wound response in plants.

Keywords: translatome, wound, JA-Ile, jasmonate, CYP94B, ribosomal profiling

INTRODUCTION

Much progress has been made in understanding the genome-wide transcriptional reprogramming after wounding. It has been estimated that several hundred to a few thousand genes change their expression upon wounding. and a majority of those genes are attributed to the jasmonate (JA) pathway (Reymond et al., 2000; Pauwels et al., 2009; Bhosale et al., 2013; Attaran et al., 2014; Hickman et al., 2017; Ikeuchi et al., 2017; Zander et al., 2020; Aerts et al., 2021). Among the changing genes are genes relating to the defense traits of plants against insects and pathogens such as those involved in production of defense compounds (Howe and Jander, 2008; Wasternack and Hause, 2013) and genes relating to growth inhibition (Zhang and Turner, 2008; Wu and Baldwin, 2010; Huot et al., 2014). The final outcome of these coordinated changes, which is commonly referred to as the defense versus growth trade-off, is expected to be complex and may come either as a passive result of the sum of the changes or an actively regulated process (e.g., cell cycle progression interference or hardwired transcriptional network) or both (Noir et al., 2013; Campos et al., 2016; Havko et al., 2020).

At the center of this transcriptional reprogramming is the biosynthesis of jasmonoyl-L-Ile (JA-Ile), a bioactive metabolite form of JA, which can activate transcriptional changes through physical binding to a nuclear-located hormone receptor co-complex consisting of CORONATINE INSENSITIVE1 (COI1) and JASMONATE ZIM-domain (JAZ) proteins (Chini et al., 2007; Thines et al., 2007; Yan et al., 2007; Fonseca et al., 2009; Sheard et al., 2010; Howe et al., 2018). The physical binding of JA-Ile with COI1-JAZ ultimately results in activation of transcription factors that in turn promotes transcription of hundreds to thousands of JA-responsive genes. As part of our investigation to understand how this pathway is inactivated, two genes belonging to the CYP94 clade of *Arabidopsis* cytochrome P450 enzymes, CYP94B1 and CYP94B3, were identified (Kitaoka et al., 2011; Koo et al., 2011, 2014; Heitz et al., 2012). These enzymes act as JA-Ile-12-hydroxylases in the so-called ω-oxidation pathway that oxidizes JA-Ile in a sequential manner to eventually catabolize the hormone (Koo and Howe, 2012; Koo, 2018). In support of the role of these enzymes in JA-Ile turnover, *Arabidopsis* plants overexpressing either enzyme display reduced JA-Ile content and associated JA-deficient phenotypes (Koo et al., 2011, 2014). Recently, in maize, it was discovered that the genetic lesion responsible for the feminized tassels of the classical *Tasselseed5* mutant results from overexpression of *ZmCYP94B1* that depletes the bioactive pool of JA-Ile that is required to abort silks in the tassel (Lunde et al., 2019), consistent with the role of CYP94s in JA-Ile turnover.

Conversely to the overexpression, *Arabidopsis* double homozygous T-DNA insertion mutant *cyp94b1cyp94b3* (*b1b3*) overaccumulates JA-Ile due to the blockage of its turnover (Poudel et al., 2016). However, in contrast to the straightforward biochemical phenotypes of the CYP94B overexpressing mutants, puzzling results were obtained while analyzing the *b1b3* mutant (Poudel et al., 2016). Despite the increased level of bioactive JA-Ile [at the expense of 12-hydroxy-JA-Ile (12OH-JA-Ile), the product of CYP94Bs catalysis] in this mutant, the plants displayed a range of phenotypes that are more typical of plants lacking JA-Ile. For example, *b1b3* plants were more susceptible to insect attack, were more resistant to the growth inhibitory effects of wounding, accumulated fewer trichomes, and experienced a global reduction in specialized metabolites when compared to wild type (WT) (Poudel et al., 2016). Exogenous JA application and following transcriptomic analysis confirmed that these phenotypes were not due to *b1b3* being insensitive to JA and that the perception of JA and JA-regulated transcription was happening normally in the mutant. Subsequent studies have revealed bioactivity of 12OH-JA-Ile similar to that of JA-Ile (Jimenez-Aleman et al., 2019; Poudel et al., 2019). Exogenous 12OH-JA-Ile induced a large number of JA-Ile–inducible genes, promoted anthocyanin and other specialized metabolite accumulation, increased the number of trichome cells, inhibited root growth, and reduced insect larvae growth, and its signaling was blocked by mutation in COI1 (Jimenez-Aleman et al., 2019; Poudel et al., 2019). Based on these findings, it was suggested that the lack of 12OH-JA-Ile in *b1b3* may contribute to its attenuated wound response (Poudel et al., 2019). This explanation was supported by genetic analysis of several pathway-engineered plants that either mimicked or offset the JA profile of *b1b3* (Poudel et al., 2019). Even though the surprisingly strong impact of altered 12OH-JA-Ile levels *in planta* was discovered in that study, they still did not completely resolve the problem of why *b1b3*, containing a more than threefold higher level of JA-Ile, shows a weakened wound phenotype (Poudel et al., 2016).

These collective observations and the additional discovery of proteome changes described in this article have led us to an unbiased genome-scale studies in the *b1b3* mutant. In particular, we have applied a technique known as translating ribosome affinity purification RNA sequencing (TRAP-Seq) (Zanetti et al., 2005) to study JA and wound signaling in plants. The collective multiomics results provide potential explanations for phenotypic changes in *b1b3* and also reveal previously unrecognized regulations at the translational level in response to wounding in *Arabidopsis*.

MATERIALS AND METHODS

Plant Materials, Growth Conditions, and Wounding Treatment

All plants were grown under long day conditions (16-h light, 100–120 μE m^{-2} s^{-1}) in growth chambers kept at 22°C. *Arabidopsis thaliana* ecotype Columbia-0 (Col-0) was used as the WT, and the double T-DNA insertion mutant *cyp94b1-1cyp94b3-1* (*b1b3*) was described earlier (Koo et al., 2014). Plants used for TRAP-Seq experiments harbor a transgene consisting of the 6X histidine-FLAG-epitope tagged ribosomal protein (RP) L18 (HF-RPL18) gene under a cauliflower mosaic virus (CaMV) 35S promoter (35S:HF-RPL18). The WT seeds harboring 35S:HF-RPL18 were a gift from Dr. David Mendoza from the University of Missouri, who received them from previously published work (Mustroph et al., 2009). The binary vector (pGreen2 35S:HF-RPL18) used to transform *b1b3* was also a gift from the Mendoza laboratory. Plant transformation was done according to the floral

dip method (Clough and Bent, 1998). Seeds harvested from the resulting plants (T1) were screened for resistance to hygromycin (50 $\mu g\ mL^{-1}$) and expression of RPL18.

Wounding treatment was executed by firmly pressing a pair of serrated-tip hemostats across the leaf midvein three times, with two leaves per plant being wounded in general. For anthocyanin measurements and immunoblot for systemic induction of marker proteins, plants were wounded according to the wound-induced growth inhibition (WIGI) wounding scheme described previously (Poudel et al., 2016). Data generated from two biological replicates for proteomics and three biological replicates for transcriptomics and TRAP-seq were used in this study. All tissues were collected at their respective time points and immediately frozen in liquid nitrogen and stored in −80°C until use. The anthocyanin measurement method was performed as described (Poudel et al., 2016).

Protein Extraction, Immunoblots, and Proteomics

Rosette leaves from untreated (control, unwounded) or wounded (8 h) 3- to 4-week-old WT and *b1b3* plants were used as tissue to extract proteins. Frozen tissue was ground to a powder in a prechilled mortar and pestle, and protein was extracted with 50 mM sodium phosphate buffer, pH 7.0, containing 10% glycerol, 50 mM NaCl, and protease inhibitor tablets (Pierce/Thermo Fisher Scientific). Samples were briefly spun down to remove debris. Proteins were quantified by the bicinchoninic acid method (Pierce/Thermo Fisher Scientific).

Equal amounts (20 μg) of protein were loaded and separated by sodium dodecyl sulfate–polyacrylamide gel electrophoresis (SDS-PAGE). Proteins were transferred to polyvinylidene fluoride membrane overnight at 4°C at constant 40 mA. Anti-LOX2 (Agrisera, Sweden) antibody was used at a 1:15,000 dilution, whereas anti-JAR1 (Cocalico Biologicals Inc., PA) and Anti-AOC [gift from Dr. Bettina Hause, Leibniz Institute of Plant Biochemistry, Halle (Saale), Germany] were used at a 1:3,000 dilution. Secondary antibody was horseradish peroxidase–conjugated ECL anti–rabbit immunoglobulin G from donkey (GE Healthcare) and was used at a 1:15,000 dilution. Blots were visualized using SuperSignal West Pico Chemiluminescent Substrate (Pierce/Thermo Fisher Scientific) and x-ray films (Midwest Scientific, MO).

Approximately 120 μg of protein was used per sample for proteomics analysis. The samples were acetone precipitated, and protein pellets were resuspended in 100 mM ammonium bicarbonate, 6 M urea, and 2 M thiourea. Samples were reduced in 200 mM DTT for 1 h and alkylated in 200 mM iodoacetamide for 1 h. Unreacted iodoacetamide was consumed by addition of excess DTT. Water was then added to dilute urea in samples to ∼0.6 M. Trypsin (Promega, WI, United States) was then added at a ratio of ∼1:50 (protease:substrate), and digestion was carried out at 37°C overnight. The reaction was stopped by the addition of formic acid (1% vol/vol). Sample peptides were then purified and concentrated by C18 tip (Pierce/Thermo Fisher Scientific). Samples were lyophilized and resuspended in 5:1% acetonitrile:formic acid, and data acquired on a Bruker timsTOF pro at the University of Missouri Gehrke Proteomics Center. Approximately 0.8 μg of suspended peptide was separated on Bruker nanoElute fifteen C18 ReproSil AQ column (150 mm × 75 μm, 1.9 μm) (packing material from Dr. Maisch GmbH, Ammerbuch-Entringen, Germany) with a step gradient of acetonitrile at 400 nL min^{-1} flow rate. The Bruker nanoElute system is connected to a timsTOF pro mass spectrometer. Initial LC gradient conditions were as follows: 3% B (A: 0.1% formic acid in water, B: 99.9% acetonitrile, 0.1% formic acid), followed by 51-min ramp to 30% B, 30–50% B over 7.5 min, gradient of 50% B to 80% B over 5.5 min, held at 80% B for 6 min with total run time of 70 min. MS data were collected over an *m/z* range of 100 to 1,700. During MS/MS data collection, each TIMS cycle included 1 MS an average of 10 PASEF MS/MS scans. The acquired data were submitted to the PEAKS X+ search engine for protein identifications against TAIR10 protein database. Data search parameters included trypsin as enzyme, two missed cleavages allowed; carbamidomethyl cysteine as a fixed modification; oxidized methionine and deamidation of asparagine and glutamine as variable modification; 50 ppm mass tolerance on precursor ions; and 0.5 Da on fragment ions. The PEAKS X+ search estimates false discovery rate (FDR) using a "decoy fusion" approach (Zhang et al., 2012). Data were filtered for peptide-spectrum match (PSM)–FDR of < 0.1%. PSM-FDR is the total number of decoy database assignments to spectra relative to the total number of target database assignments to spectra represented as a percentage. Entry with an average spectral count of two or more in at least one of the three treatment replicates was included, and fold change (FC) of 2 was applied as cutoff.

Translating RNA Affinity Purification

The method of isolating the FLAG-tagged ribosomes was described previously (Zanetti et al., 2005; Castro-Guerrero et al., 2016). Briefly, frozen tissue samples were ground using a mortar and pestle yielding approximately 10 to 15 g of powdered tissue per sample. Ice-cold ribosome extraction buffer (200 mM Tris-HCl pH 9.0, 200 mM KCl, 25 mM EGTA, 36 mM $MgCl_2$, 1 mM DTT, 50 $\mu g\ mL^{-1}$ cycloheximide, 50 $\mu g\ mL^{-1}$ chloramphenicol, 1 mM phenylmethylsulfonyl fluoride, 1% igepal CA-630, 1% Brij 35, 1% triton X-100, 1% tween 20, 1% tridecyl ether, 1% sodium deoxycholate, 0.5 mg mL^{-1} heparin) was added at a 2:1 ratio (buffer:tissue). The samples were gently rocked at 4°C for 30 min. The samples were then centrifuged at 16,000 × *g* for 15 min at 4°C. The supernatant was gently filtered through miracloth and collected in a separate tube. To the supernatant, 300 μL of EZ view Red Anti-FLAG M2 Affinity Gel (Sigma) was added and incubated with gentle rocking for 2 h at 4°C. Samples were briefly centrifuged to recover beads and were washed four times with 10 mL of wash buffer (200 mM Tris-HCl pH 9.0, 200 mM KCl, 25 mM EGTA, 36 mM $MgCl_2$, 1 mM DTT, 50 $\mu g\ mL^{-1}$ cycloheximide, 50 $\mu g\ mL^{-1}$ chloramphenicol). Beads were collected by centrifugation, and RNA was extracted immediately from them using the Direct-zol RNA MiniPrep Plus Kit (Zymo Research, CA, United States). RNA samples were normalized to ∼100 ng mL^{-1}, and approximately 3 μg of RNA

was sent to Novogene Corporation Inc (Sacramento, CA) for RNA sequencing (RNA-Seq) analysis.

Total RNA Isolation and RNA-Seq

Approximately 15 g of rosette leaf tissue from either wounded or untreated (unwounded) plants was ground up with prechilled mortar and pestle while frozen in liquid nitrogen. A 50-mg aliquot of the ground tissue was used for total RNA extraction, and the remaining tissue was used for the TRAP experiment. The total RNA was extracted using the Direct-zol RNA MiniPrep Plus Kit (Zymo Research, CA, United States) and was treated with TURBO DNA-free kit (Thermo Fisher Scientific, MA, United States). Both total and TRAP RNA was sent for sequencing by Novogene (Sacramento, CA), which describes using the following procedures. Briefly, after the standard RNA quality control assessments, mRNA was enriched using oligo(dT) beads after which the cDNA library was constructed. Library concentration was first quantified using a Qubit 2.0 fluorometer (Life Technologies) and then diluted to 1 ng μL^{-1} before checking insert size on an Agilent 2100 and quantifying to greater accuracy by quantitative polymerase chain reaction (qPCR). Libraries were fed into respective Illumina sequencers according to activity and expected data volume. Raw reads were filtered to remove reads containing adapters or reads of low quality, so that downstream analyses were based on clean reads. The sequences were mapped to the reference genome using Tophat2 (Kim et al., 2013) with the mismatch parameter set to 2 and all others set to default. Read counts were normalized and used for differential expression using DEseq (Anders and Huber, 2010). Negative binomial distribution after normalization by DEseq (adjusted *P* value) of less than 0.05 and $\log_2$ FC of 1 (twofold) was used to determine differential expression.

qPCR

One microgram of RNA from each biological replicate from both the total and TRAP samples was reverse transcribed using oligo$(dT)_{20}$ primers and Moloney murine leukemia virus reverse transcriptase (Promega, WI, United States) and was used as the template for semiquantitative reverse transcription (qRT)–PCR reaction using SYBR^{TM} Green PCR Master Mix (Thermo Fisher Scientific, MA, United States) in a CFX96 Touch^{TM} real-time PCR detection system (Bio-Rad, CA, United States). ACTIN8 (AT1G49240) was used as an internal reference gene, and the relative transcript abundance was expressed as FC relative to the mock treatment. Primers (5′-3′) used for qRT-PCR were JAZ7qPCRF: CGACTTGGAACTTCGCCTTCTTA, JAZ7 qPCRR: ACATCTCTACTCGCTAGCGATAG; JAR1qPCRF: CA TCGATGTCTCGACAGATCCAGGA, JAR1qPCRR: GCTCC AAGGCTCCAATAGTCTTGC. Primers for *OPR3* and *ACTIN8* have been described earlier (Poudel et al., 2016).

Data Mining

For data analysis and visualization, the following web-based programs and public databases were used. For area proportional Venn diagrams, BioVenn was used[1] (Hulsen et al., 2008). For hierarchical clustering and heatmapping exercises, the online tool, Morpheus[2], from the Broad Institute, Cambridge, MA, United States, was used. For cluster analysis, Euclidean distance with complete linkage was used. Correlation coefficient chart was also generated using Morpheus tool. The program MapMan[3] (Thimm et al., 2004) was utilized for pathway mapping and visualization using the most up-to-date TAIR10 genome. For further pathway analysis, Kyoto Encyclopedia of Genes and Genomes (KEGG) Pathway Analysis tools were used[4]. Gene Ontology (GO) terms were assigned by the protein analysis through evolutionary relationships classification system, Protein ANalysis THrough Evolutionary Relationships (PANTHER) version 14[5] (Mi et al., 2018). All GO term categories were found using the GO aspect, GO biological process, except for the categories for up-regulated WT_U_TRAP/WT_U (**Figure 4**), where the GO aspect, PANTHER GO-Slim Biological process was used. All GO term datasets were calculated using the Fisher exact test and Bonferroni correction for multiple testing.

RESULTS

There Is a Global Reduction in the Proteome of Wounded b1b3 Leaves Compared to WT

It has previously been observed through multiple biochemical and physiological studies that much of the downstream JA-dependent wound responses including anthocyanin accumulation (**Figure 1A**) are down-regulated in the *cyp94b1cyp94b3* (*b1b3*) mutant when compared to WT despite containing threefold to fourfold higher levels of JA-Ile in the mutant (Koo et al., 2014; Poudel et al., 2016). Gene expression studies showed either similar or increased levels of mRNA transcripts for several JA-responsive marker genes in the wounded leaves of *b1b3* (Poudel et al., 2016), making it difficult to explain the phenotype by differential gene expression. In an attempt to close the gap in our understanding between transcription and downstream responses in this mutant, protein immunoblots were carried out (**Figures 1B–D**). Total proteins extracted from wounded leaf samples collected 4, 8, and 12 h after wounding along with unwounded (0 h) leaves from WT and *b1b3* were separated on an SDS-PAGE gel and probed with antibodies against three wound response marker proteins in the JA pathway, LOX2, AOC, and JAR1. All three proteins detected were induced by wounding in 4 h, peaking around 8 h (**Figure 1B**). Surprisingly, all three marker proteins were recognizably reduced in *b1b3* compared to WT. A variation of wound time course was carried out over 3 days (**Figure 1C**). In this case, the same set of leaves (two leaves per plant, leaf numbers 3 and 4) was wounded once every day for 3 days, and leaves were collected 12 h after wounding each day. This type of wounding had been used for WIGI assays before (Poudel et al., 2016),

[1]http://www.biovenn.nl/index.php

[2]https://software.broadinstitute.org/morpheus/

[3]https://mapman.gabipd.org/

[4]https://www.genome.jp/kegg/

[5]http://pantherdb.org

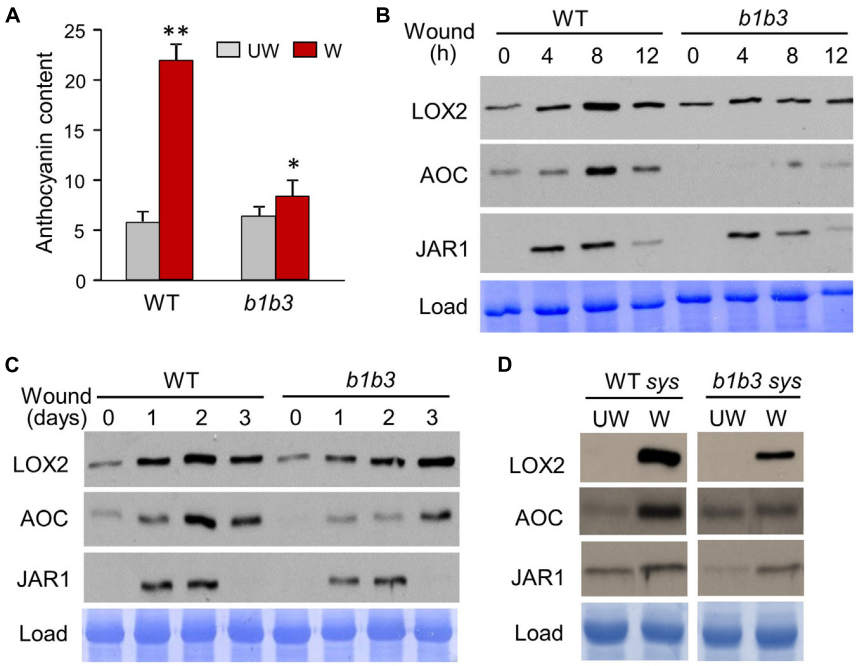

FIGURE 1 | Wound-inducible proteins accumulate to a lesser extent in *b1b3*. **(A)** Anthocyanin levels in wounded (W) and unwounded (UW) WT and *b1b3* plants. Plants were wounded multiple times following the WIGI (wound-induced growth inhibition) wounding scheme described in the section "Materials and Methods." Bar graphs represent means ± SD ($n = 5$). Asterisks denote statistical significance by Student *t* test compared to UW WT: $^{*}P < 0.05$, $^{**}P < 0.01$. **(B)** Immunoblots showing a 12-h wounding time course of LOX2, AOC, and JAR1 in WT and *b1b3*. Fully expanded rosette leaves of 25-day-old plants were crushed two times across the midrib per leaf with a hemostat. **(C)** A 3-day wound time course showing lower protein accumulation for *b1b3*. Two leaves per plant were wounded once every day for 3 days and samples collected 12 h after wounding each day. **(D)** Protein accumulation in the undamaged systemic leaves of unwounded (UW) and wounded (W) WT and *b1b3* plants. Plants were wounded according to the WIGI wounding scheme as in **(A)**. Remaining undamaged leaves were harvested 1 day after final wounding and used as systemic samples.

which resulted in differential growth suppression between the two genotypes. Immunoblot signals for LOX2 and AOC intensified until days 2 and 3 in the WT and *b1b3*, respectively (**Figure 1C**). Importantly, signals for all three markers were either weaker or delayed in *b1b3* compared to WT, similarly, to the short time course (**Figure 1B**). Marker protein changes in the systemic leaves of the wounded plant were also assessed (**Figure 1D**). Most of the differential response to wounding in *b1b3* was attributed to systemic wound signaling (Poudel et al., 2016). Clear induction of proteins in the systemic leaves was detected for LOX2 and AOC. Systemic induction of JAR1 was less obvious. However, both LOX2 and AOC induction was weaker in *b1b3* than in WT (**Figure 1D**).

The protein markers used so far are limited to the JA pathway, and so the next question was whether this phenomenon is limited to JA responsive proteins or is widespread across proteins outside the known JA regulatory network. To address this question, an unbiased proteomics experiment was carried out. Wounded leaf samples were collected 8 h after wounding based on earlier immunoblot results that showed the greatest discrepancy in protein amount between *b1b3* and WT (**Figure 1B**). Upon clearing of crude debris by medium speed centrifugation at 23,000×*g* for 45 min, all soluble fractions from both unwounded and wounded samples from WT and *b1b3* were analyzed by the nanoElute LC-timsTOF Pro mass spectrometer. A total of 1,956 proteins were identified with an average spectral count of two or more in at least one of the three treatment replicates with no other statistical constraints. Relatively low stringency criteria were used here in order to be more inclusive because our goal was to take a broader survey of the proteome rather than to identify specific proteins with a high level of confidence. The majority of proteins did not differ in spectral counts between WT and *b1b3*, but 204 (10%) in unwounded and 135 (6.9%) in wounded leaves were different by more than twofold between the two genotypes. These were mostly not the proteins encoded by those typically known as JA responsive genes (Reymond et al., 2000; Pauwels et al., 2008; Bhosale et al., 2013; Attaran et al., 2014; Poudel et al., 2019), indicating that the differentially regulated proteins in the mutant were not restricted to JA pathway. A comparable number (7%–10%) of proteins changed in abundance either up or down twofold or more in response to wounding in both genotypes (**Figure 2A**) (**Supplementary Table 1**). However, more proteins were notably repressed than induced by wounding in *b1b3* (**Figure 2A**). Compared to 82 induced and 46 repressed in WT, only 38 proteins were induced in wounded *b1b3*, whereas as many as 154 proteins were repressed in *b1b3* (**Figure 2A**). This is consistent with the downward trend of the marker protein levels observed by the immunoblots (**Figure 1**). **Figure 2B** displays the functional classification of 211 proteins induced or repressed by wounding. This clearly shows the predominant downward

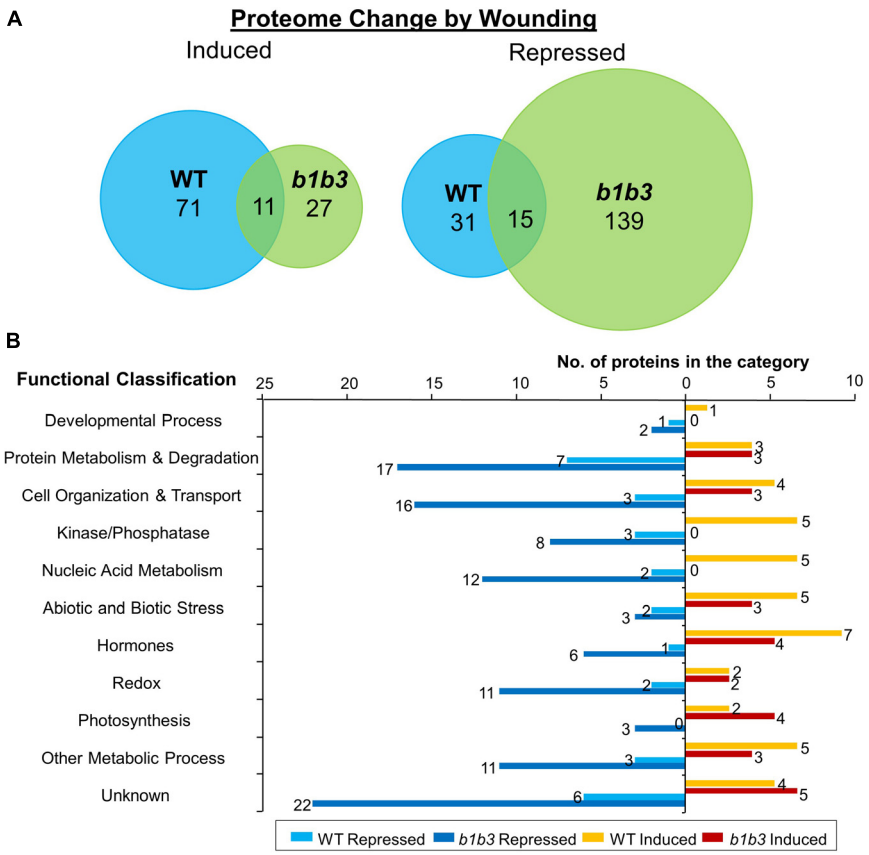

C

Oppositely Regulated

Locus ID	Description	Log2 FC (wound/unwound) WT	b1b3
RNA Processing, Transport and Translation			
AT1G43190	POLYPYRIMIDINE TRACT-BINDING PROTEIN 3 (PTB3)	4.39	-4.39
AT1G78010	tRNA modification GTPase (TRME)	4.39	-1.24
AT5G58470	TBP-ASSOCIATED FACTOR 15B (TAF15b)	2.58	-4.70
AT2G30060	Pleckstrin homology (PH) domain superfamily protein	1.81	-1.81
AT3G20810	JUMONJI DOMAIN CONTAINING 5 (JMJD5)	1.42	-1.90
AT1G07140	putative Ran-binding protein (siRanBP)	1.36	-1.20
Protein Metabolism			
AT5G04710	M18 ASPARTYL AMINOPEPTIDASE2 (DAP2)	3.46	-1.24
AT3G59990	METHIONINE AMINOPEPTIDASE 2B (MAP2B)	1.42	-2.12
AT3G13235	DNA-DAMAGE INDUCIBLE 1 (DDI1)	1.20	-1.88
AT1G71950	SUBTILISIN PROPEPTIDE-LIKE INHIBITOR 1 (SPI-1)	1.17	-1.49
Cell Wall, Plasma Membrane, Cell Organization and Development			
AT3G45970	EXPANSIN-LIKE A1 (EXLA1)	4.00	-1.24
AT5G10760	APOPLASTIC, EDS1-DEPENDENT 1 (AED1)	3.46	-5.17
AT1G05850	CHITINASE-LIKE PROTEIN 1 (CTL1) / POM-POM1 (POM1)	3.46	-5.17
AT1G66250	O-Glycosyl hydrolases family 17 protein	3.46	-4.39
AT3G57240	BETA-1,3-GLUCANASE 3 (BG3)	3.22	-3.35
AT2G26890	GRAVITROPISM DEFECTIVE 2 (GRV2) / (KAM2)	2.58	-4.39
AT2G17120	LYSM-CONTAINING RECEPTOR PROTEIN 1 (LYP1) / CEBIP-LIKE 1	2.12	-1.81
Stress Response and Signaling			
AT3G57260	BETA-1,3-GLUCANASE 2 (BG2) / (PR-2)	2.09	-1.93
AT1G04510	MOS4-ASSOCIATED COMPLEX 3A (MAC3A)	1.81	-2.37
AT3G45640	MITOGEN-ACTIVATED PROTEIN KINASE 3 (MPK3)	1.71	-4.95
AT2G43590	Chitinase family protein	1.52	-5.93
AT4G28730	GLUTAREDOXIN C5 (GrxC5)	1.49	-2.04
AT5G16590	LEUCINE RICH REPEAT PROTEIN 1 (LRR1)	1.42	-5.36
AT1G49670	(NQR) / response to oxidative stress	-1.42	2.12
AT1G19670	CHLOROPHYLLASE 1 (CLH1) / CORONATINE-INDUCED PROTEIN 1	-1.42	2.12
Other metabolic processes			
AT4G02860	D-AMINO ACID RACEMASE2 (DAAR2)	2.58	-2.12
AT2G33845	Nucleic acid-binding, OB-fold-like protein	2.58	-1.81
AT3G03630	CYSTEINE SYNTHASE 26 (CS26)	2.37	-4.70
AT1G55980	FAD/NAD(P)-binding oxidoreductase family protein	1.90	-1.67
AT1G56560	ALKALINE/NEUTRAL INVERTASE A (A/N-InvA)	1.36	-1.13

FIGURE 2 | Protein changes by wounding in WT and *b1b3* leaves. **(A)** Area-proportional Venn diagrams showing number of proteins induced or repressed twofold or more by wounding compared to unwounded leaves of WT and *b1b3*. **(B)** Functional classification of proteins differentially regulated by wounding [fold change (FC) ≥ 2]. GO assignment was based on TAIR. **(C)** List of oppositely regulated proteins in WT and *b1b3* grouped into functional categories. The values are $-1 \geq \log_2$ FC (wound/unwound) ≥ 1 and displayed as a heatmap. Average spectral counts from LC-MS/MS analysis of two biological replicates were used to calculate the FC.

regulation in *b1b3* across all 11 functional categories. The top two known categories with the largest number of proteins were the "Protein Metabolism & Degradation" and "Cell Organization and Transport" classes. These may be related to the reduction in proteins and dampened growth responses to wounding in *b1b3* (Poudel et al., 2016).

Thirty proteins were even oppositely regulated between the two genotypes (**Figure 2C**). Interestingly, except for two that were repressed in WT, all the rest were repressed in *b1b3*, again reflecting the downward trend of protein abundance in wounded *b1b3*. These include several proteins involved in RNA processing and protein metabolism such as POLYPYRIMIDINE TRACT-BINDING PROTEIN 3 (Rühl et al., 2012) that showed the most extreme changes in abundance ($\log_2$FC (wound/unwound) of 4.39 in WT and -4.39 in *b1b3*). Additional genes that were oppositely regulated include those encoding pathogenesis-related proteins such as the BETA-1,3-GLUCANASES 2 (BG2), BG3 (Dong et al., 1991; Zavaliev et al., 2013), and APOPLASTIC EDS1-DEPENDENT 1 (Breitenbach et al., 2014). Together, these results show that there is a widespread reduction in proteome in the wounded leaves of *b1b3*.

Many Transcripts Change Their Association With Ribosomes Upon Wounding in WT Leaves

The distinctive proteomic features between WT and *b1b3* led us to wonder what might be the reason behind such difference. Protein abundance can be affected by both the synthesis of protein and the turnover of protein, so we hypothesized that the mRNA translation into protein may be differentially regulated in the two genotypes. Although less studied than the transcriptional responses, increasing evidence indicates changes occur at the level of translation in response to biotic as well as abiotic stresses (Branco-Price et al., 2005; Merchante et al., 2017; Merret et al., 2017; Sablok et al., 2017; Xu et al., 2017). Alterations in the translating pools of mRNA can have direct effects on protein abundance because increased association with the ribosomes increases the chance of them being translated. Although mRNA association with ribosomes does not always guarantee translation, it has been widely used as a proxy to gauge translational activity (Bailey-Serres et al., 2009; Reynoso et al., 2015; Mazzoni-Putman and Stepanova, 2018). In order to compare the relative levels of translation between WT and *b1b3*, a procedure called TRAP-Seq was employed (Reynoso et al., 2015). Briefly, RPL18, one of the subunits of the ribosomal complex, is tagged with an epitope tag (FLAG in our case) that can be used later to pull down the entire ribosomal complex bound with the mRNA from the total cell lysate using antibody-conjugated beads (**Figure 3A**). Total mRNA (bound and unbound to ribosome) and the ribosome-bound mRNA from wounded (20 min) and unwounded leaves of WT and *b1b3*, both harboring the FLAG-tagged RPL18, were subject to RNA-Seq analysis (**Figure 3B**). A 20-min wounding time point was used to capture early changes in ribosomal association that may result in later differences in protein levels. By 20 min, there is a significant increase in both JA hormone and early JA-responsive genes (Chung et al., 2008; Koo et al., 2009). For data analysis, we first studied wound-induced changes in WT followed by comparisons between the two genotypes. The total number of clean reads after filtering in each sample ranged from 74 to 113 million reads. For quality control measures, Pearson correlation coefficients for all biological replicates were calculated across all 24 sample replicates (**Figure 3C**). The darker the blue color is in the figure, the closer the R2 correlation value is to 1 or perfect correlation (squares aligned at the center diagonal line). All of the three biological replicates had an R2 correlation value greater than 0.96 (except one 0.875 and majority greater than 0.99) among themselves, showing low variation within sample replicates. RNA-Seq data were validated by qRT-PCR analyses of four marker genes, OXOPHYTODIENOATE-REDUCTASE 3 (OPR3), JASMONATE-ZIM-DOMAIN PROTEIN 7 (JAZ7), JASMONATE RESISTANT 1 (JAR1), and LIPOXYGENASE 2 (LOX2) (**Figure 3D**). Early genes, OPR3 and JAZ7, were strongly induced by wounding, whereas JAR1 and LOX2 transcripts were not increased upon wounding consistent with the delayed expression observed before (Reymond et al., 2000; Suza and Staswick, 2008; Koo et al., 2009; Body et al., 2019). In all cases, similar trends were seen between qRT-PCR and RNA-Seq data [expressed as fragments per kilobase of transcript per million mapped reads (FPKM)] for wounded and unwounded total and TRAP mRNA samples (**Figure 3D**).

As we begin to analyze the data, in order to simplify the analysis and to ensure that we are dealing with the genes that are differentially regulated exclusively at the level of ribosomal association and not at the level of transcription, transcripts that did not change in abundance after wounding were preselected from the WT total RNA-Seq data (**Figure 4A**). There were 19,739 genes that did not change (FC $>$ 0.5 and $<$ 2) in total transcript abundance upon wounding compared to unwounded controls (WT_Wound/WT_Unwound). These represent the majority (73.12%) of genes that were similar in transcript levels between the wound versus unwounded samples. Among these 19,739 transcripts, as many as 18,101 representing $>$ 91% were not different when total mRNA (WT_Wound) and those associated with ribosomes (WT_Wound_TRAP) were compared, indicating that wounding did not have a colossal effect on mRNA association with ribosomes for a large swath of genes in the genome in 20 min after wounding in leaf tissue. However, still a significant number of genes (1,636) were either more (FC $\geq$ 2; 381 genes) or less (FC $\leq$ 0.5; 1,255 genes) preferentially associated with the ribosomes after wounding (WT_Wound_TRAP/WT_Wound) (**Figure 4A**). Within these 1,636 genes whose ribosomal versus total transcripts differ more than twofold in wounded leaves, a predominant number was changed toward less associated (1,255) than more associated (381) with the ribosomes, indicating that for a larger number of genes, translation activity could be reduced when cells are wounded despite no change in overall transcriptional activity (**Figure 4A** and **Supplementary Table 2**). Those transcripts fell into some distinctive functional groups according to GO terms assigned by the PANTHER classification system (see text footnote 5) (**Figures 4B,C**) (Gaudet et al., 2011). GO terms for those transcripts that were more associated with the ribosomes (FC $\geq$ 2; 381 genes) were as follows: "regulation of amino acid transport," "mRNA transcription,"

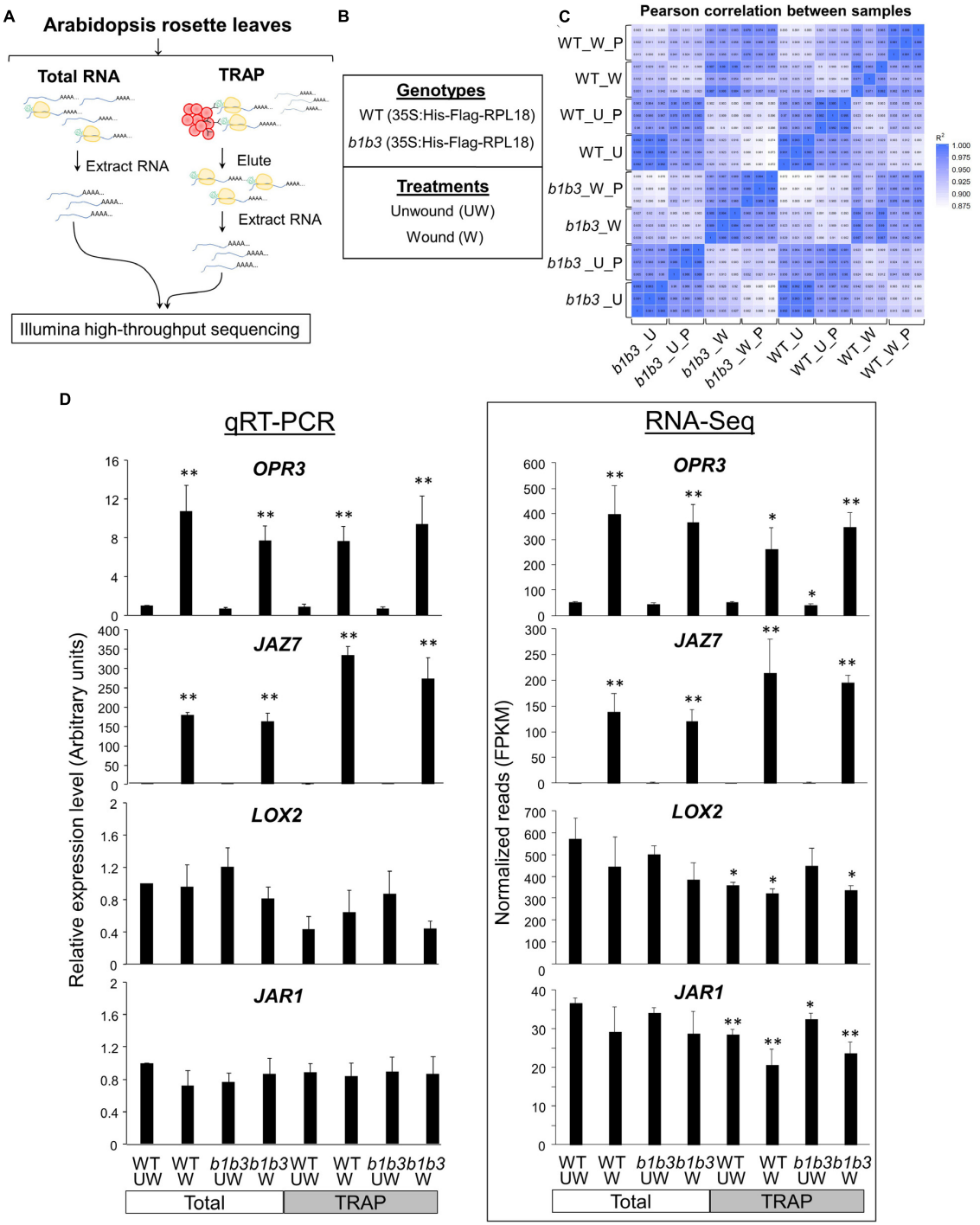

FIGURE 3 | Overview of TRAP-Seq experiment and qPCR validation. **(A)** Schematics of total RNA-Seq and TRAP-Seq. Tissue samples were divided into two for total RNA extraction and TRAP. RPL18 of ribosomes (yellow) are epitope-tagged with 6X histidine (His)-FLAG (green), which is used to pull down by affinity to anti–FLAG-conjugated beads (red circles) to collect associated RNA. **(B)** Plant genotypes and treatments. **(C)** Pearson correlation between samples as an indicator of experiment reliability. The color gradient scale is shown where darkest blue indicates the R^2 correlation value of 1 or perfect correlation. U, unwounded; W, wounded; P, polysomal. Each sample group labeled on the x- and y-axes consists of three sample replicates. Samples are ordered by experiment type. **(D)** Semiquantitative RT-PCR (qRT-PCR) (left) of *OPR3*, *JAZ7*, *LOX2*, and *JAR1* genes compared with RNA-Seq data (right). Transcript abundance is indicated by FPKM (fragments per kilobase of transcript sequence per million base pairs sequenced). *ACTIN8* was used as an internal reference gene, and the expression levels are displayed relative to the unwounded WT total RNA values. Data represent the mean + SE of three biological replicates. Asterisks denote statistical significance by Student *t* test compared to UW WT: $*P < 0.05$, $**P < 0.01$.

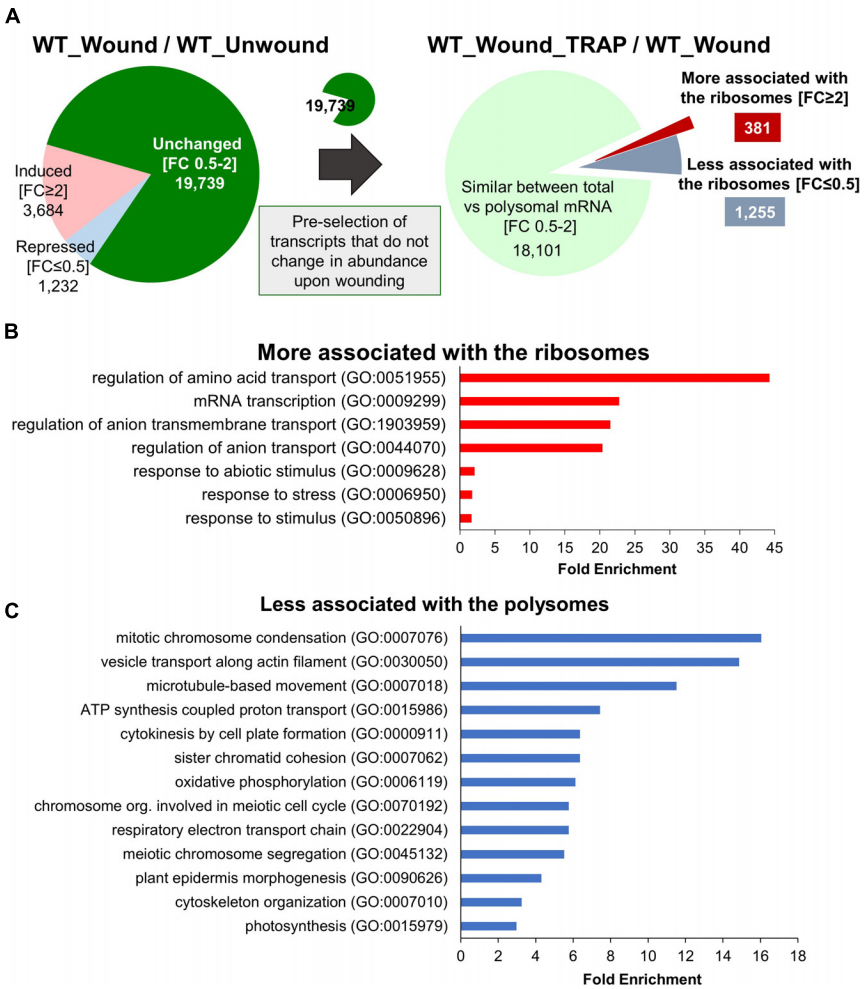

FIGURE 4 | Genes with transcripts exclusively changing their ribosomal association after wounding without change in their net transcription. **(A)** Among 19,739 genes that do not change (FC 0.5–2) in total transcript abundance upon wounding (WT_Wound/WT_Unwound), 381 were more (FC ≥ 2) and 1,256 were less (FC ≤ 0.5) associated with the ribosomes (WT_Wound_TRAP/WT_Wound). **(B,C)** PANTHER GO Enrichment Analysis of the 1,636 transcripts that either increased **(B)** or decreased **(C)** in ribosomal association from **(A)**. Statistically significant GO terms were selected using Fisher exact test and Bonferroni correction for multiple testing ($P < 0.05$). Representative biological processes with fold enrichment above 1.5 are displayed. The full list of GO and genes in each category is provided in **Supplementary Table 3**.

"regulation of ion transport," "response to abiotic stimulus," and "response to stress." Those transcripts that were less associated with the ribosomes (FC ≤ 0.5; 1,256 genes) fell in the GO categories of "mitotic chromosome condensation," "vesicle transport along actin-filament," "microtubule-based movement," "ATP synthesis coupled proton transport," "cytokinesis by cell-plate formation," "respiratory electron transport chain," "oxidative phosphorylation," and "photosynthesis" (**Figure 3C**). These GO term assignments are indicative of a shift in priority by the plant from those that are important for cell division and growth to transcription, stress response, and various transport function by wounding.

We also carried out similar GO classification studies with a set of genes that have not been preselected for transcriptional changes (**Supplementary Figure 1**). This was to have a more general view about the translatome regardless of their transcriptional inducibility by wounding. This was done both with unwounded (U) and wounded (W) WT samples. In total, 2,113 genes were found to be different in their abundance between ribosomal versus total mRNA fraction. Before wounding, there were 538 that were differentially regulated [FC (WT_U_TRAP/WT_U) ≥ 2 and ≤ 0.5, $p < 0.05$] that did not overlap with those from wounded samples. They were roughly evenly split between increased (286) or decreased (252) in their association with the ribosomes. Those more associated with ribosomes were involved in cell division and metabolism (copper ion, glutathione, sulfur, amino acid), whereas those less associated with ribosomes were involved in signal transduction (ARF, small GTPase, Ras) and DNA repair (**Supplementary Figures 1B,E**). In wounded leaves (WT_W_TRAP/WT_W), there was a similar number (617) of genes that were differentially expressed exclusively in the

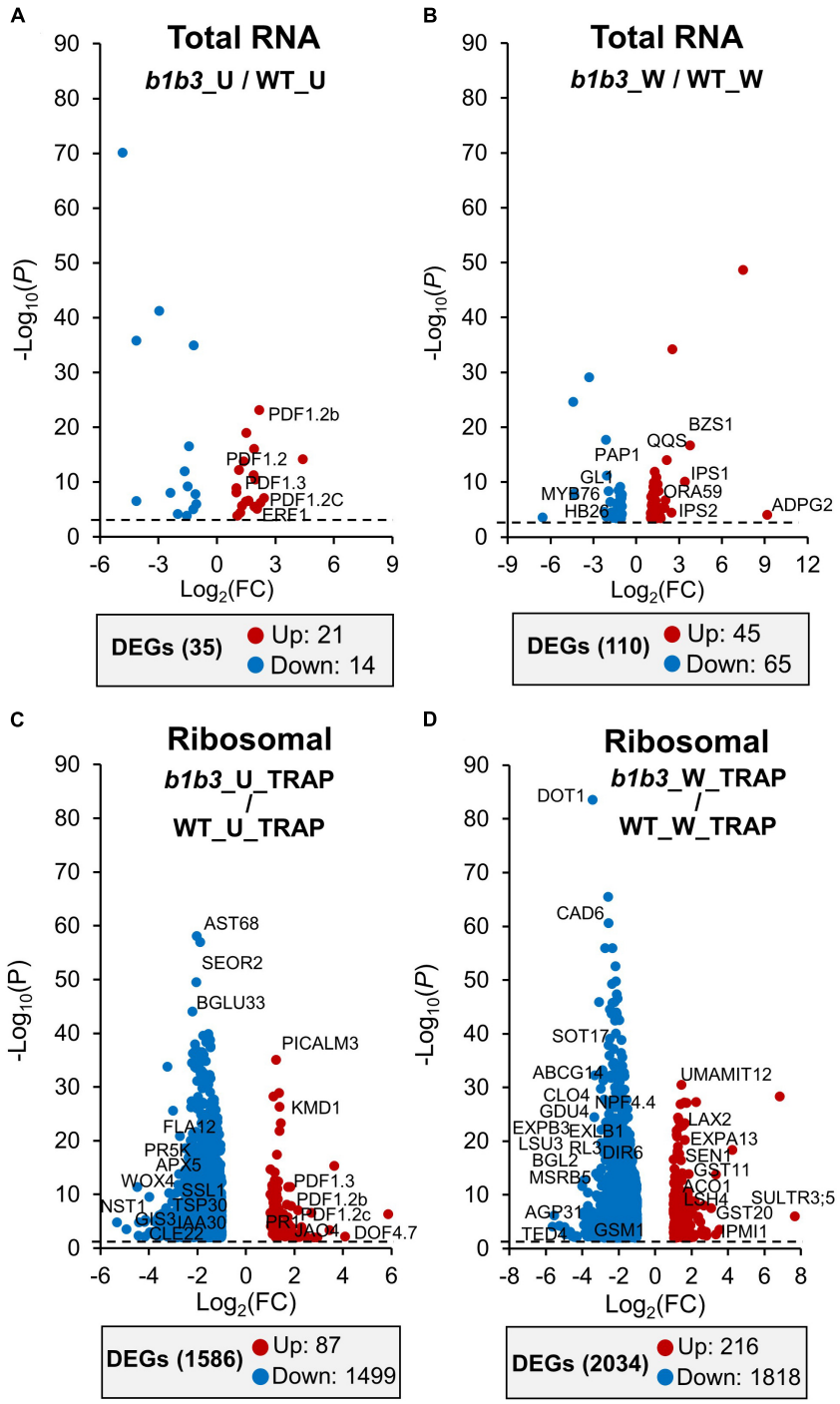

FIGURE 5 | Transcript abundance comparisons between WT and *b1b3* in the total and TRAP RNA pools. **(A,B)** Volcano plots of differentially expressed genes (DEGs) in total RNA of unwounded (U) **(A)** and wounded (W) **(B)** samples of WT and *b1b3*. **(C,D)** DEGs in TRAP RNA preparations of U and W leaf samples. Comparisons of $\log_2$FC of FPKM ≤ -1 and ≥ 1 per indicated sample were plotted (*x*-axis). Dotted line indicates the *P* value cutoff of < 0.05. Names of representative genes are displayed. Full list of gene names is provided in **Supplementary Table 4**. The numbers of up-regulated and down-regulated DEGs are shown in the gray boxes below each graph.

wounded tissues with more genes with transcripts that are less associated with ribosomes after wounding (385) than those more ribosome-associated (232) (**Supplementary Figure 1A**), consistent with what was observed earlier with the 19,739 preselected set (**Figure 4A**). GO terms for these less-ribosome–associating transcripts were also related to cell division,

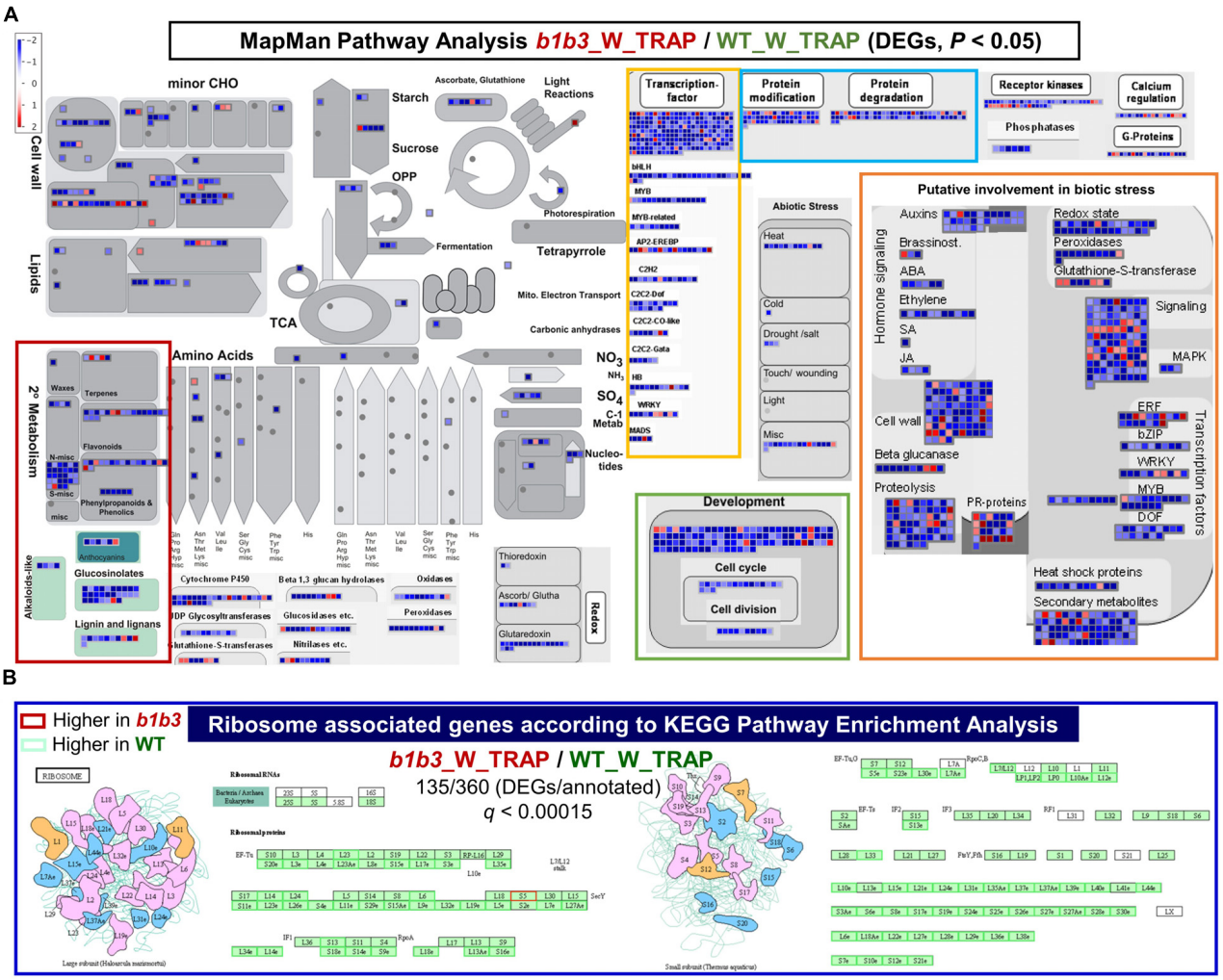

FIGURE 6 | Pathway analysis of differentially expressed TRAP transcripts in wounded WT and *b1b3*. **(A)** MapMan pathways analysis of the *b1b3*_W_TRAP/WT_W_TRAP comparisons. All transcripts included in the figure met the *P* value cutoff ($P < 0.05$) and the FC cutoff ($\log_2 FC \leq -1$ and ≥ 1). Each colored square is representative of a single gene, and the color indicates either up- or down-regulation with scales from red to blue as shown in the key. **(B)** Ribosome-associated genes found to be most significantly ($q < 0.00015$) overrepresented in the *b1b3*_W_TRAP/WT_W_TRAP comparisons according to the KEGG Pathway Enrichment Analysis. Red and green boxes indicate higher and lower, respectively, expression in *b1b3* compared to WT. Cartoons represent large and small ribosomal protein complexes.

cell cycle, and DNA metabolic processes (**Supplementary Figure 1F**). Those transcripts more associated with ribosomes after wounding were related to various stress responses, cellular responses to oxygen levels, and transcription (**Supplementary Figure 1C**), similar to the results from the 19,739 preselect set (**Figure 4A**). The largest number of genes (958) that were differentially regulated between the ribosomal and total RNA fraction comparison fell under the category that maintained consistent ratio between the two fractions regardless of wounding state (the common area in the Venn diagram) (**Supplementary Figure 1A**). The predominant number (724 out of 958) in this group was less associated with the ribosomes, indicating that among those that are differentially partitioned between ribosome and total, more transcripts tend to be in the free state than engaged in translation. As will be described later, this phenomenon of a greater number of genes whose transcripts are in greater abundance in the total than in ribosomal fraction is exacerbated in the *b1b3* mutant.

Direct Comparison of Translatomes Between WT Versus b1b3

Coming back to the main issue of the large influence the *b1b3* mutation has on both the wound phenotype and the proteome, the RNA-Seq and TRAP-Seq data for the two genotypes (WT and *b1b3*) were directly compared. A volcano plot of differentially expressed genes (DEGs) immediately illustrated the stark difference between the two genotypes (**Figure 5** and **Supplementary Table 4**). First, when comparing only the total mRNA fractions of unwounded and wounded

samples (*b1b3*_U/WT_U and *b1b3*_W/WT_W), there were only 35 and 110 DEGs, respectively, between the two genotypes (**Figures 5A,B**). This is a remarkably small number of DEGs given the large number of genes in the genome (∼30,000) and the relatively strong phenotypes displayed by *b1b3* plants upon wounding, although this had been predicted based on the earlier targeted gene expression studies showing that the marker gene transcript abundances did not differ much between the two genotypes (Poudel et al., 2016). Even the 145 (35 + 110) DEGs displayed a similar trend of changes; that is, those induced in one genotype were also induced in the other genotype (with only the degree of differences qualifying them as DEGs), and the same with the down-regulated genes, instead of displaying opposite trends. However, a completely different picture emerged when the TRAP-Seq datasets were compared between the two genotypes (*b1b3*_U_TRAP/WT_U_TRAP and *b1b3*_W_TRAP/WT_W_TRAP) (**Figures 5C,D**). The number of DEGs in unwounded and wounded datasets was 1,586 and 2,034, respectively. Most importantly, the changes that occurred were predominantly toward down-regulation in the *b1b3* (blue dots in **Figures 5C,D**). In the *b1b3*_U_TRAP/WT_U_TRAP comparison, there were 1,499 out of 1,586 DEGs that were less abundant in *b1b3* ribosome-associated transcripts, representing 94.5% of all DEGs in that comparison. Similarly, in the *b1b3*_W_TRAP v WT_W_TRAP comparison, 1,818 out of 2,034 DEGs (89%) were less abundant in the *b1b3*. This supports the hypothesis that the large reduction in proteome observed in *b1b3* (**Figures 1**, **2**) may be in part caused by the reduction in number of transcripts associated with the ribosomes in *b1b3* compared to WT.

Differential Focus on Cellular Function Between WT Versus b1b3 Translatome

Next, we looked at what kind of genes are in those DEGs between WT and *b1b3* translatome. DEGs in the unwounded (*b1b3*_U_TRAP/WT_U_TRAP) and wounded (*b1b3*_W_TRAP/WT_W_TRAP) TRAP-Seq comparisons were subject to GO Enrichment Analysis using PANTHER (**Supplementary Figure 2** and **Supplementary Table 6**). Among the most enriched functional categories in the unwounded TRAP-Seq comparisons (*b1b3*_U_TRAP/WT_U_TRAP) were those related to vascular and secondary cell wall biogenesis (**Supplementary Figure 2A**). This shows that although unstressed *b1b3* does not display obvious growth or developmental defects (Poudel et al., 2016), there are basal differences in ribosome-associated transcripts that could potentially prime the plant for response to external stimuli (i.e., wounding). Glucosinolate metabolic genes were also highly enriched as down-regulated in this unwounded TRAP-Seq comparison (*b1b3*_U_TRAP/WT_U_TRAP).

The trend of GO enrichment in vascular development, secondary cell wall biogenesis, cell cycle, and glucosinolate metabolism–related functional categories continued with the wounded WT and *b1b3* TRAP-Seq comparisons (*b1b3*_W_TRAP/WT_W_TRAP) (**Supplementary Figure 2B**). These wounded sample comparison data were further analyzed by MapMan (Thimm et al., 2004) and KEGG pathway analyses (**Figure 6**). The 2,034 genes identified earlier (**Figure 5D**) to be differentially expressed from the direct comparison of *b1b3*_W_TRAP/WT_W_TRAP including both up- and down-regulated in *b1b3* were mapped into various cellular pathways, including those relating to transcription factors, protein modification, protein degradation, development, cell cycle and division, primary and secondary metabolism, and biotic and abiotic stresses (**Figure 6A**). One striking aspect made visible from this analysis was that the less-ribosomal-association trend dominated across all listed pathways indicating that there was a large underrepresentation of transcripts associated with the ribosomes in *b1b3*. Among the transcription factors representing various classes were MYC4 and MYC5 that work redundantly with MYC2 and MYC3 to mediate multiple JA responses including root growth inhibition, specialized metabolite biosynthesis, and defense against insects (Chini et al., 2007; Kazan and Manners, 2008; Fernandez-Calvo et al., 2011; Figueroa and Browse, 2012; Song et al., 2017). Down-regulation of these functional pathways correlates well with the biochemical and growth phenotypes of wounded *b1b3*, namely, resistance to growth inhibition, reduced glucosinolates and other secondary metabolites, increased susceptibility to insects (Poudel et al., 2016), and reduced protein levels (**Figures 1**, **2**).

One interesting class of gene transcripts identified by KEGG enrichment analysis that stood out to be differentially affected in their association with the ribosomes by the *b1b3* mutation was that related to ribosomes themselves (**Figure 6B**). Ribosomes are a complex assembly of RNA and RPs with at least ∼80 RP members making up a ribosome, and each RP unit is encoded by several paralogs in *Arabidopsis*. In wounded *b1b3,* a large fraction of the transcripts encoding RPs (135/360) are less associated with ribosomes. This may result in a significant reduction in certain ribosome combinations that may be involved in translating proteins of certain pathways in line with the increasing evidence of specialization of ribosomal function (Martinez-Seidel et al., 2020).

Comparisons Between Transcriptome (RNA-Seq), Proteome, and Translatome (TRAP-Seq)

Finally, correlation between the three types of omics data was assessed using two approaches, correlation coefficient measurements and hierarchical clustering, both by using Morpheus tools (**Supplementary Figure 3**). Instead of using all data sets, data corresponding to the 1,956 genes that were identified by the proteomics approach (**Figure 2**), which was limiting among the three data sets, were used for this comparison. In other words, data were available for all three analyses (RNA-Seq, proteomics, and TRAP-Seq) for these 1,956 genes. To normalize across different types of data, $\log_2$(FC) values were used.

Data were grouped largely according to the types of analysis rather than by genotypes or treatments (**Supplementary Figure 3**). The transcriptomics data, regardless of genotype, gave correlation coefficient values (r) > 0.8, indicating a high level

of correlation within the group. The correlations between the W_TRAP/U_TRAP of the TRAP-Seq datasets and the RNA-Seq datasets were relatively high at $r > 0.77$ for both genotypes. This is likely because albeit being TRAP-Seq data, the TRAP versus TRAP comparisons are more reflective of the transcriptional changes than the translational changes, which is measured by translational efficiency (ribosome-associated transcripts/total transcripts or TRAP-Seq/RNA-Seq) (Merret et al., 2017; Xu et al., 2017). The proteomics data for WT and *b1b3*, although appearing to group together in the figure (**Supplementary Figure 3**), had no correlation with each other ($r < 0.1$). This was true using either all 1,956 protein entries identified from the proteomics analysis (**Supplementary Figure 3A**) or a subset of 239 selected proteins whose abundance changed up or down twofold or more by wounding (**Supplementary Figure 3B**). The proteomics data for these 239 subsets had negative *r* scores reflecting the earlier observation of vast differences between the two genotypes (**Figure 2**). Next, the *r* values for the translatome data (TRAP/total RNA) against proteome and transcriptome were assessed. Somewhat contrary to our expectation, no correlation was observed between the translatome versus proteome comparisons ($r < 0.02$) for both genotypes, whether wounded or not. Similarly, no correlations were observed between ($r < 0.1$) the translatome datasets and the transcriptome datasets.

A similar trend of clustering among data sets emerged with hierarchical clustering and heatmap visualization (**Supplementary Figure 3C**). The transcriptome and translatome data clustered by themselves, whereas the proteome data for WT and *b1b3* formed their own independent branches. The translatome data clustered between the same genotypes rather than across different treatments (i.e., wound or unwound), indicating that the genotype had greater influence on ribosomal association of mRNA than wounding.

DISCUSSION

Various gene expression studies have been undertaken to investigate the transcriptional reprogramming occurring in plants after wounding or treatment with JA (Reymond et al., 2000; Lorenzo et al., 2004; Devoto et al., 2005; Mandaokar et al., 2006; Memelink, 2009; Pauwels et al., 2009; Attaran et al., 2014; Ikeuchi et al., 2017; Zander et al., 2020). The JA signaling pathway is responsible for up to 80% of the wound-induced transcriptome changes (Reymond et al., 2004; Gfeller et al., 2011). The molecular mechanism of JA controlled transcriptional regulation through COI1-JAZ coreceptor and transcription factors (e.g., MYC2/3/4/5) was elucidated at the mechanistic and structural level (Xie et al., 1998; Chini et al., 2007; Dombrecht et al., 2007; Thines et al., 2007; Sheard et al., 2010; Zhang et al., 2015; Howe et al., 2018; Chico et al., 2020). In contrast, the direct involvement JA signaling has in processes outside transcriptional control is largely unknown. Although the data presented in this research also do not determine the molecular mechanism of how JA might be involved in posttranscriptional regulation of genetic information flow from DNA to protein, the data showing changes in proteome and ribosomal association of transcripts caused by genetic mutations that alter the JA profile in *b1b3* have offered a first peek at the influence of the JA pathway on these processes.

The striking phenotypes of the *b1b3* mutant could not be easily explained by its transcriptional differences compared to WT (Poudel et al., 2016), which is in itself surprising given how the major way in which JA exerts its effect on plant physiology is via transcription (Kazan and Manners, 2008; Howe et al., 2018). Our transcriptome data (**Figure 5**) again confirmed earlier qRT-PCR results of marker genes showing normal behavior in terms of transcriptional response in the mutant (Poudel et al., 2016). Exogenous application of JA also resulted in normal induction of marker gene expression in *b1b3*, discounting the possibility of its defect in molecular perception or transcriptional mechanism of JA (Poudel et al., 2016, 2019). The possibility of *b1b3* phenotypes being merely pleiotropic or random can be raised, but the mutant displaying phenotypes consistently in most, if not all, classical JA-dependent wound responses such as growth inhibition, anthocyanin accumulation, trichome biogenesis, specialized metabolite induction, and insect resistance, albeit in an exact opposite direction of the expectation, implied that the phenotypes must still be somehow influenced by the altered JA pathway in *b1b3*.

Protein changes provided an alternative mechanism to explain the gap between the normal transcription and abnormal downstream phenotypes of *b1b3* (**Figure 1**). The proteomics data confirmed that the unusual decrease in marker proteins in the wounded *b1b3* was not an isolated event restricted to a few JA marker proteins but a more widely spread phenomenon in the mutant (**Figure 2**). However, it is important to note that although there is a prevalent reduction in abundance of many proteins in *b1b3*, still the vast majority (>90%) of the proteome was unchanged from the WT at the given moment. This indicates a certain degree of specificity to the effect of the mutation on the proteome. The identity of those proteins repressed by wounding in *b1b3* (compared to WT) was also not restricted to typical JA-responsive marker genes/proteins, but rather was distributed across several functional classes. Somewhat related to this observation, earlier proteomic studies by Gfeller et al. (2011) in *Arabidopsis* have found that many proteins differentially regulated by wounding were not regulated by transcription (Gfeller et al., 2011). However, a majority of the wound-regulated proteins they found were deregulated by blocking JA biosynthesis. Collection of these differentially expressed proteins may be useful in the future to elucidate the protein-level regulation of JA during wound responses. Selection of proteins for such purpose will require additional work to confirm the results provided by our first-pass proteomic study. The degree of protein level changes must also be determined through more quantitative targeted and comprehensive proteomic studies with higher-stringency selection criteria.

One potential way protein levels could be altered is through translation. We found that there is a large change in the ribosomal-associated pool of mRNA after wounding in WT. Many transcripts (>90%) did not change their ribosomal association after wounding at 20 min, but among the 10% that did change (1,638), vast majority (1,256 or 77%) became

less associated with the ribosomes. There was an increase in the ribosomal association of transcripts relating to mRNA transcription and abiotic stimulus, whereas there was a decrease in those relating to cell division and energy metabolism (**Figure 4** and **Supplementary Figure 1**). A similar trend has been observed in other stress responses (Branco-Price et al., 2008; Merchante et al., 2017; Merret et al., 2017; Meteignier et al., 2017; Martinez-Seidel et al., 2020). This also shows that not only is there transcriptional adjustment in activating defense while pausing growth in response to wounding, but similar regulation is found in terms of ribosomal association.

As many as 1,586 and 2,034 gene transcripts in the unwounded and wounded samples, respectively, were differentially regulated in the ribosomal fraction in a direct comparison between WT and *b1b3* (**Figure 5**). While those numbers may be considered to be minor in a backdrop of 25,000 to 30,000 genes in the *Arabidopsis* genome, they were significant compared to the total transcript comparisons that yielded a mere 35 in unwounded and 110 in wounded DEGs between the two genotypes. More strikingly, the majority (1,499 and 1,818 representing 95% and 89%, respectively) of these DEGs in the ribosomal fraction had a smaller number of ribosome-associated transcripts occurring in *b1b3* compared to WT. This is in line with the reduced protein abundance seen in the *b1b3* proteome (**Figure 2**) and suggests an exacerbating effect of *b1b3* mutation on wound-induced reduction of ribosome-associated transcripts seen in WT (**Figure 4**). Most notable changes in the wounded *b1b3* ribosomal fraction were in the down-regulation of transcripts associated with specialized metabolism, development, protein degradation, and abiotic and biotic stress (**Figure 6A**). These pathways are related to various phenotypes exhibited by *b1b3* plants (Poudel et al., 2016).

The more difficult question to answer lies on the issue of specificity. As mentioned earlier, the numbers of differentially expressed ribosome-associated transcripts between wounded WT and *b1b3* were in the order of few thousands (**Figure 5D**). These are not evenly distributed across all functional categories, which would have indicated random reduction in overall ribosome association in *b1b3* but are rather enriched in the aforementioned functional classes indicating specificity. Generally speaking, at least two types of translational regulation can be considered—global regulation and gene−specific control—although they are not always inseparable (Merchante et al., 2017). During global or whole-genome translation regulation, which can happen during stress conditions, such as hypoxia, there are several mechanisms at work including the phosphorylation of poly(A)−binding proteins and elongation initiation factors (Browning and Bailey-Serres, 2015). Global translation regulation can also be achieved through exchanging protein composition of the general translational machinery (Merchante et al., 2017; Martinez-Seidel et al., 2020) (which will be discussed in more detail below). Gene-specific translational regulation refers to uneven translational activity among specific mRNAs that create disproportional representation of proteins encoded by those transcripts compared to others in the cell. Some known mechanisms of this type of regulation involve small RNAs, specific RNA-binding proteins and translation factors, small molecules, and *cis*-regulatory elements internal and external of the mRNA (Brodersen et al., 2008; Liu et al., 2013; Cui et al., 2015; Merchante et al., 2015, 2017; Hou et al., 2016). Although yet to be completed, our ongoing investigation into the conserved sequence features of mRNA repressed in the ribosome-associated fraction of *b1b3* mRNA could potentially add to the mechanisms conferring the specificity.

Protein composition of ribosomal super-complex can also play a role in specific translational regulation (Martinez-Seidel et al., 2020). As many as 135 genes encoding RPs were differentially expressed in wounded *b1b3*, predominantly less abundant in the mutant than WT (**Figure 6B**). The proteomics data could not independently verify many of the TRAP-seq results probably due to multiple factors, including differences between steady-state level of proteins and more transient ribosome-associated mRNAs levels. Differences in tissue sampling times, different data sizes, and similarity among RP paralogs could have also contributed to the proteomic detection failure. However, evidence supporting functional heterogeneity of RPs as opposed to homogenous mRNA translational machineries have increased over the years in plants (Martinez-Seidel et al., 2020), similar to cases in yeast and mammals (Gilbert, 2011; Shi et al., 2017). There can be two to seven paralogs per RP for a total of more than 230 proteins identified as RPs in the *Arabidopsis* genome rendering an immense number (10^{34}) of possible ribosomal combinations (Barakat et al., 2001; Browning and Bailey-Serres, 2015; Martinez-Seidel et al., 2020). Although the basic functions of ribosomes are likely conserved, it is not unreasonable to expect that this ribosomal heterogeneity would contribute to functional and regulatory specialization. In fact, there is growing evidence supporting differential regulation of a subset of RPs at the transcriptional, posttranscriptional, translational, and posttranslational levels in response to developmental cues, environmental conditions, and phytohormones (Barakat et al., 2001; McIntosh and Bonham-Smith, 2006; Muench et al., 2012; Asensi-Fabado et al., 2017; Schepetilnikov and Ryabova, 2017; Wang et al., 2017; Cheong et al., 2020).

Other modes of regulations for translation that could confer specificity include a set of proteins called ribosome-inactivating proteins (RIPs) that irreversibly inhibit protein translation by depurination of ribosomal RNA (Barbieri et al., 1993; Chaudhry et al., 1994; Reinbothe et al., 1994; Nielsen and Boston, 2001; Jiang et al., 2008; Bolognesi et al., 2016). The expression of several RIPs is regulated by JA and abiotic and biotic stress, thereby alluding to their potential regulatory roles as a regulator of various environmental cues and hormone signaling (Jiang et al., 2008; Rustgi et al., 2014; Genuth and Barna, 2018; Zhu et al., 2018). Various types of RIPs have been reported (Stirpe and Battelli, 2006; Bolognesi et al., 2016), the most prominent example being ricin from *Ricinus communis* L. (caster bean), but none have been reported in *Arabidopsis* and hence have not been detected among our data. However, their wide distribution among plant species would predict existence of their functional counterpart in *Arabidopsis*.

As such, there are a number of potential mechanisms to explain how a specific pool of translating mRNAs can be differentially regulated, but how that exactly relates to the *b1b3*

mutation is still not known. The immediate metabolic defect caused by the mutation is changes in JA-Ile and 12OH-JA-Ile hormone levels. The molecular target of 12OH-JA-Ile was shown to be the COI1-JAZ coreceptor system. This was shown by 12OH-JA-Ile's ability to promote molecular interaction between COI1 and JAZ *in vitro* and *in silico*, and that its signaling effect *in planta* can be blocked by mutation in COI1 (Koo et al., 2011; Jimenez-Aleman et al., 2019; Poudel et al., 2019). However, this signaling system that mainly regulates transcription is not altered in *b1b3*. This leads to at least several hypotheses. One, there are alternative molecular targets of these JAs or their derivatives related to ribosomal loading or translational control. Alternatively, there could be alternative novel substrates for CYP94Bs besides JA metabolites. In this case, those alternative substrates should have as profound effect on the wound response as JAs in order to explain the broad spectrum of JA-related *b1b3* phenotypes. In addition, small transcriptional changes in the *b1b3* mutant could still lead to downstream production (or inhibition) of effectors that could target translation. The general lack of a mechanistic understanding of many of the translational mechanisms in plants is both a challenge and an opportunity to understand plant adaptation to their environment. The *b1b3* mutant can be used as a tool to further study translational regulation and its interplay with stressors such as wounding.

There have been mixed reports about the correlation between transcriptomics and proteomics data, but the dominant consensus has been that they are generally not correlated very well (Baerenfaller et al., 2008; Gfeller et al., 2011; Fernie and Stitt, 2012; Walley et al., 2016; Fan et al., 2017; Zander et al., 2020). Our analysis also showed poor correlation between transcriptome and proteome data. This may have been in part caused by different time points used for those two analyses. However, even comparison between current proteomics and transcriptome data generated at various timepoints produced in-house still resulted in low correlation. This observation advises caution against common practices among researchers to explain phenotypic data based solely on gene transcription and underscores the importance of taking into account the discordant behavior between transcript and protein abundance. Regarding the translatome data, our intuitive expectation was that they would capture somewhat intermediary dynamics between the transcriptome and proteome. However, the translatome data formed their own cluster and did not show clear correlation with neither the transcriptome nor proteome data. However, this may again be due to different sampling times. Our conclusion and discussion, in general, are based on observations made at particular time points in a particular tissue type (i.e., leaf). Higher time resolution data at various developmental stages in different tissue types as well as information about their kinetic behavior are needed to provide a more accurate picture of the collective changes occurring after wounding stress in the future.

DATA AVAILABILITY STATEMENT

The datasets presented in this study can be found in online repositories. The names of the repository/repositories and accession number(s) can be found below: Bioproject SRA data: PRJNA692417.

AUTHOR CONTRIBUTIONS

AKi and AKo designed experiments. AKi performed experiments. RH performed computational data analysis. AKi, RH, and AKo analyzed the data and wrote the manuscript. All authors contributed to the article and approved the submitted version.

FUNDING

This work was supported by funds awarded to AKo from the National Science Foundation (grant nos. IOS-1557439 and IOS-1829365), the Hatch Multi-State Research program from the USDA National Institute of Food and Agriculture (project accession no. 1010448), and Food for the 21st Century Program, University of Missouri.

ACKNOWLEDGMENTS

We thank Dr. Bettina Hause from Leibniz Institute of Plant Biochemistry, Halle (Saale), Germany and Dr. David Mendoza from the University of Missouri for sharing AOC antibody and 35S:HF-RPL18 construct and seeds, respectively. Dr. Tong Zhang was acknowledged for the production of JAR1 antibody. We also thank MU Gehrke Proteomics Center for assistance with protein mass spectrometry.

SUPPLEMENTARY MATERIAL

The Supplementary Material for this article can be found online at: https://www.frontiersin.org/articles/10.3389/fpls.2021.637959/full#supplementary-material

Supplementary Figure 1 | GO term classification of genes with transcripts that are differentially associated with the ribosomes (TRAP/total RNA) in unwounded and wounded Wt leaves.

Supplementary Figure 2 | GO term classification of genes that are less-associated with ribosomes in *b1b3* through a direct comparison with unwounded and wounded Wt TRAP datasets.

Supplementary Figure 3 | Correlation coefficient chart and hierarchical clustering map illustrating the relationship between the transcriptome, translatome, and proteome of Wt and *b1b3*.

Supplementary Table 1 | Proteins changed by wounding in Wt and *b1b3* leaves.

Supplementary Table 2 | Genes with transcripts exclusively changing their ribosomal association after wounding without changing their net transcription.

Supplementary Table 3 | GO Enrichment Analysis of genes with transcripts that do not change transcriptionally but are differentially associating with the ribosomes (TRAP/total RNA) in unwounded and wounded Wt leaves.

Supplementary Table 4 | Transcript abundance difference between Wt and *b1b3* in the total and TRAP RNA pools.

Supplementary Table 5 | GO Enrichment Analysis of genes with transcripts that are differentially associating with the ribosomes (TRAP/total RNA) in unwounded and wounded Wt leaves.

Supplementary Table 6 | GO Enrichment Analysis of genes that are less-associated with ribosomes in *b1b3* through a direct comparison with unwounded and wounded Wt TRAP datasets.

REFERENCES

Aerts, N., Pereira Mendes, M., and Van Wees, S. C. M. (2021). Multiple levels of crosstalk in hormone networks regulating plant defense. *Plant* J. 105, 489–504. doi: 10.1111/tpj.15124

Anders, S., and Huber, W. (2010). Differential expression analysis for sequence count data. *Genome Biol* 11, R106. doi: 10.1186/gb-2010-11-10-r106

Asensi-Fabado, M. A., Amtmann, A., and Perrella, G. (2017). Plant responses to abiotic stress: The chromatin context of transcriptional regulation. *Biochim Biophys Acta Gene Regul Mech* 1860, 106–122. doi: 10.1016/j.bbagrm.2016.07.015

Attaran, E., Major, I. T., Cruz, J. A., Rosa, B. A., Koo, A. J., Chen, J., et al. (2014). Temporal dynamics of growth and photosynthesis suppression in response to jasmonate signaling. *Plant Physiol* 165, 1302–1314. doi: 10.1104/pp.114.239004

Baerenfaller, K., Grossmann, J., Grobei, M. A., Hull, R., Hirsch-Hoffmann, M., Yalovsky, S., et al. (2008). Genome-scale proteomics reveals Arabidopsis thaliana gene models and proteome dynamics. *Science* 320, 938–941. doi: 10.1126/science.1157956

Bailey-Serres, J., Sorenson, R., and Juntawong, P. (2009). Getting the message across: cytoplasmic ribonucleoprotein complexes. *Trends Plant Sci* 14, 443–453. doi: 10.1016/j.tplants.2009.05.004

Barakat, A., Szick-Miranda, K., Chang, I. F., Guyot, R., Blanc, G., Cooke, R., et al. (2001). The organization of cytoplasmic ribosomal protein genes in the Arabidopsis genome. *Plant Physiol* 127, 398–415. doi: 10.1104/pp.010265

Barbieri, L., Battelli, M. G., and Stirpe, F. (1993). Ribosome-inactivating proteins from plants. *Biochim Biophys Acta* 1154, 237–282. doi: 10.1016/0304-4157(93)90002-6

Bhosale, R., Jewell, J. B., Hollunder, J., Koo, A. J., Vuylsteke, M., Michoel, T., et al. (2013). Predicting gene function from uncontrolled expression variation among individual wild-type Arabidopsis plants. *Plant Cell* 25, 2865–2877. doi: 10.1105/tpc.113.112268

Body, M. J. A., Dave, D. F., Coffman, C. M., Paret, T. Y., Koo, A. J., Cocroft, R. B., et al. (2019). Use of yellow fluorescent protein fluorescence to track OPR3 expression in Arabidopsis thaliana responses to insect herbivory. *Front Plant Sci* 10:1586. doi: 10.3389/fpls.2019.01586

Bolognesi, A., Bortolotti, M., Maiello, S., Battelli, M. G., and Polito, L. (2016). Ribosome-Inactivating Proteins from Plants: A Historical Overview. *Molecules* 21, 1627. doi: 10.3390/molecules21121627

Branco-Price, C., Kaiser, K. A., Jang, C. J., Larive, C. K., and Bailey-Serres, J. (2008). Selective mRNA translation coordinates energetic and metabolic adjustments to cellular oxygen deprivation and reoxygenation in Arabidopsis thaliana. *Plant J* 56, 743–755. doi: 10.1111/j.1365-313X.2008.03642.x

Branco-Price, C., Kawaguchi, R., Ferreira, R. B., and Bailey-Serres, J. (2005). Genome-wide analysis of transcript abundance and translation in Arabidopsis seedlings subjected to oxygen deprivation. *Ann Bot* 96, 647–660. doi: 10.1093/aob/mci217

Breitenbach, H. H., Wenig, M., Wittek, F., Jordá, L., Maldonado-Alconada, A. M., Sarioglu, H., et al. (2014). Contrasting Roles of the Apoplastic Aspartyl Protease apoplastic, enhanced disease susceptibility1-dependent1 and legume lectin-like protein1 in *Arabidopsis* systemic acquired resistance. *Plant Physiol.* 165, 791–809. doi: 10.1104/pp.114.239665

Brodersen, P., Sakvarelidze-Achard, L., Bruun-Rasmussen, M., Dunoyer, P., Yamamoto, Y. Y., Sieburth, L., et al. (2008). Widespread translational inhibition by plant miRNAs and siRNAs. *Science* 320, 1185–1190. doi: 10.1126/science.1159151

Browning, K. S., and Bailey-Serres, J. (2015). Mechanism of cytoplasmic mRNA translation. *Arabidopsis Book* 13, e0176. doi: 10.1199/tab.0176

Campos, M. L., Yoshida, Y., Major, I. T., De Oliveira Ferreira, D., Weraduwage, S. M., Froehlich, J. E., et al. (2016). Rewiring of jasmonate and phytochrome B signalling uncouples plant growth-defense tradeoffs. *Nat Commun* 7, 12570. doi: 10.1038/ncomms12570

Castro-Guerrero, N. A., Cui, Y., and Mendoza-Cozatl, D. G. (2016). Purification of Translating Ribosomes and Associated mRNAs from Soybean (Glycine max). *Curr Protoc Plant Biol* 1, 185–196. doi: 10.1002/cppb.20011

Chaudhry, B., Muller-Uri, F., Cameron-Mills, V., Gough, S., Simpson, D., Skriver, K., et al. (1994). The barley 60 kDa jasmonate-induced protein (JIP60) is a novel ribosome-inactivating protein. *Plant J* 6, 815–824. doi: 10.1046/j.1365-313X.1994.6060815.x

Cheong, B. E., Beine-Golovchuk, O., Gorka, M., Ho, W. W. H., Martinez-Seidel, F., Firmino, A. A. P., et al. (2020). Arabidopsis REI-LIKE proteins activate ribosome biogenesis during cold acclimation. *bioRxiv [Preprint]* doi: 10.1101/2020.02.18.954396

Chico, J. M., Lechner, E., Fernandez-Barbero, G., Canibano, E., García-Casado, G., Franco-Zorrilla, J. M., et al. (2020). CUL3(BPM) E3 ubiquitin ligases regulate MYC2, MYC3, and MYC4 stability and JA responses. *Proc Natl Acad Sci U S A* 117, 6205–6215. doi: 10.1073/pnas.1912199117

Chini, A., Fonseca, S., Fernandez, G., Adie, B., Chico, J. M., Lorenzo, O., et al. (2007). The JAZ family of repressors is the missing link in jasmonate signalling. *Nature* 448, 666–671. doi: 10.1038/nature06006

Chung, H. S., Koo, A. J., Gao, X., Jayanty, S., Thines, B., Jones, A. D., et al. (2008). Regulation and function of Arabidopsis JASMONATE ZIM-domain genes in response to wounding and herbivory. *Plant Physiol* 146, 952–964. doi: 10.1104/pp.107.115691

Clough, S. J., and Bent, A. F. (1998). Floral dip: a simplified method for Agrobacterium-mediated transformation of Arabidopsis thaliana. *Plant J.* 16, 735–743. doi: 10.1046/j.1365-313x.1998.00343.x

Cui, Y., Rao, S., Chang, B., Wang, X., Zhang, K., Hou, X., et al. (2015). AtLa1 protein initiates IRES-dependent translation of WUSCHEL mRNA and regulates the stem cell homeostasis of Arabidopsis in response to environmental hazards. *Plant Cell Environ* 38, 2098–2114. doi: 10.1111/pce.12535

Devoto, A., Ellis, C., Magusin, A., Chang, H. S., Chilcott, C., Zhu, T., et al. (2005). Expression profiling reveals COI1 to be a key regulator of genes involved in wound- and methyl jasmonate-induced secondary metabolism, defence, and hormone interactions. *Plant Molecular Biology* 58, 497–513. doi: 10.1007/s11103-005-7306-5

Dombrecht, B., Xue, G. P., Sprague, S. J., Kirkegaard, J. A., Ross, J. J., Reid, J. B., et al. (2007). MYC2 differentially modulates diverse jasmonate-dependent functions in Arabidopsis. *Plant Cell* 19, 2225–2245. doi: 10.1105/tpc.106.048017

Dong, X., Mindrinos, M., Davis, K. R., and Ausubel, F. M. (1991). Induction of Arabidopsis defense genes by virulent and avirulent *Pseudomonas* syringae strains and by a cloned avirulence gene. *Plant Cell* 3, 61–72. doi: 10.1105/tpc.3.1.61

Fan, M., Sun, X., Xu, N., Liao, Z., Li, Y., Wang, J., et al. (2017). Integration of deep transcriptome and proteome analyses of salicylic acid regulation high temperature stress in Ulva prolifera. *Scientific Reports* 7, 11052. doi: 10.1038/s41598-017-11449-w

Fernandez-Calvo, P., Chini, A., Fernandez-Barbero, G., Chico, J. M., Gimenez-Ibanez, S., Geerinck, J., et al. (2011). The Arabidopsis bHLH transcription factors MYC3 and MYC4 are targets of JAZ repressors and act additively with MYC2 in the activation of jasmonate responses. *Plant Cell* 23, 701–715. doi: 10.1105/tpc.110.080788

Fernie, A. R., and Stitt, M. (2012). On the discordance of metabolomics with proteomics and transcriptomics: coping with increasing complexity in logic, chemistry, and network interactions scientific correspondence. *Plant Physiol* 158, 1139–1145. doi: 10.1104/pp.112.193235

Figueroa, P., and Browse, J. (2012). The Arabidopsis JAZ2 promoter contains a G-Box and thymidine-rich module that are necessary and sufficient for jasmonate-dependent activation by MYC transcription factors and repression by JAZ proteins. *Plant Cell Physiol* 53, 330–343. doi: 10.1093/pcp/pcr178

Fonseca, S., Chini, A., Hamberg, M., Adie, B., Porzel, A., Kramell, R., et al. (2009). (+)-7-iso-Jasmonoyl-L-isoleucine is the endogenous bioactive jasmonate. *Nat Chem Biol* 5, 344–350. doi: 10.1038/nchembio.161

Gaudet, P., Livstone, M. S., Lewis, S. E., and Thomas, P. D. (2011). Phylogenetic-based propagation of functional annotations within the Gene Ontology consortium. *Brief Bioinform* 12, 449–462. doi: 10.1093/bib/bbr042

Genuth, N. R., and Barna, M. (2018). The Discovery of Ribosome Heterogeneity and Its Implications for Gene Regulation and Organismal Life. *Mol Cell* 71, 364–374. doi: 10.1016/j.molcel.2018.07.018

Gfeller, A., Baerenfaller, K., Loscos, J., Chetelat, A., Baginsky, S., and Farmer, E. E. (2011). Jasmonate controls polypeptide patterning in undamaged tissue in wounded Arabidopsis leaves. *Plant Physiol* 156, 1797–1807. doi: 10.1104/pp.111.181008

Gilbert, W. V. (2011). Functional specialization of ribosomes? *Trends Biochem Sci* 36, 127–132. doi: 10.1016/j.tibs.2010.12.002

Havko, N. E., Kapali, G., Das, M. R., and Howe, G. A. (2020). Stimulation of Insect Herbivory by Elevated Temperature Outweighs Protection by the Jasmonate Pathway. *Plants (Basel)* 9, 172. doi: 10.3390/plants9020172

Heitz, T., Widemann, E., Lugan, R., Miesch, L., Ullmann, P., Desaubry, L., et al. (2012). Cytochromes P450 CYP94C1 and CYP94B3 catalyze two successive oxidation steps of plant hormone Jasmonoyl-isoleucine for catabolic turnover. *J Biol Chem* 287, 6296–6306. doi: 10.1074/jbc.M111.316364

Hickman, R., Van Verk, M. C., Van Dijken, A. J. H., Pereira Mendes, M., Vroegop-Vos, I. A., Caarls, L., et al. (2017). Architecture and dynamics of the jasmonic acid gene regulatory network. *The Plant Cell* 29, 2086–2105. doi: 10.1105/tpc.16.00958

Hou, C. Y., Lee, W. C., Chou, H. C., Chen, A. P., Chou, S. J., and Chen, H. M. (2016). Global Analysis of Truncated RNA Ends Reveals New Insights into Ribosome Stalling in Plants. *Plant Cell* 28, 2398–2416. doi: 10.1105/tpc.16.00295

Howe, G. A., and Jander, G. (2008). Plant immunity to insect herbivores. *Annu Rev Plant Biol* 59, 41–66. doi: 10.1146/annurev.arplant.59.032607.092825

Howe, G. A., Major, I. T., and Koo, A. J. (2018). Modularity in jasmonate signaling for multistress resilience. *Annu Rev Plant Biol* 69, 387–415. doi: 10.1146/annurev-arplant-042817-040047

Hulsen, T., De Vlieg, J., and Alkema, W. (2008). BioVenn - a web application for the comparison and visualization of biological lists using area-proportional Venn diagrams. *BMC Genomics* 9:488. doi: 10.1186/1471-2164-9-488

Huot, B., Yao, J., Montgomery, B. L., and He, S. Y. (2014). Growth-defense tradeoffs in plants: a balancing act to optimize fitness. *Mol Plant* 7, 1267–1287. doi: 10.1093/mp/ssu049

Ikeuchi, M., Iwase, A., Rymen, B., Lambolez, A., Kojima, M., Takebayashi, Y., et al. (2017). Wounding triggers callus formation via dynamic hormonal and transcriptional changes. *Plant Physiol* 175, 1158–1174. doi: 10.1104/pp.17.01035

Jiang, S. Y., Ramamoorthy, R., Bhalla, R., Luan, H. F., Venkatesh, P. N., Cai, M., et al. (2008). Genome-wide survey of the RIP domain family in Oryza sativa and their expression profiles under various abiotic and biotic stresses. *Plant Mol Biol* 67, 603–614. doi: 10.1007/s11103-008-9342-4

Jimenez-Aleman, G. H., Almeida-Trapp, M., Fernández-Barbero, G., Gimenez-Ibanez, S., Reichelt, M., Vadassery, J., et al. (2019). Omega hydroxylated JA-Ile is an endogenous bioactive jasmonate that signals through the canonical jasmonate signaling pathway. *Biochim Biophys Acta Mol Cell Biol Lipids* 1864, 158520. doi: 10.1016/j.bbalip.2019.158520

Kazan, K., and Manners, J. M. (2008). Jasmonate signaling: toward an integrated view. *Plant Physiol.* 146, 1459–1468. doi: 10.1104/pp.107.115717

Kim, D., Pertea, G., Trapnell, C., Pimentel, H., Kelley, R., and Salzberg, S. L. (2013). TopHat2: accurate alignment of transcriptomes in the presence of insertions, deletions and gene fusions. *Genome Biol* 14, R36. doi: 10.1186/gb-2013-14-4-r36

Kitaoka, N., Matsubara, T., Sato, M., Takahashi, K., Wakuta, S., Kawaide, H., et al. (2011). Arabidopsis CYP94B3 encodes jasmonyl-L-isoleucine 12-hydroxylase, a key enzyme in the oxidative catabolism of jasmonate. *Plant Cell Physiol* 52, 1757–1765. doi: 10.1093/pcp/pcr110

Koo, A. J. (2018). Metabolism of the plant hormone jasmonate: a sentinel for tissue damage and master regulator of stress response. *Phytochemistry Reviews* 17, 51–80. doi: 10.1007/s11101-017-9510-8

Koo, A. J., Cooke, T. F., and Howe, G. A. (2011). Cytochrome P450 CYP94B3 mediates catabolism and inactivation of the plant hormone jasmonoyl-L-isoleucine. *Proc Natl Acad Sci U S A* 108, 9298–9303. doi: 10.1073/pnas.1103542108

Koo, A. J., Gao, X., Jones, A. D., and Howe, G. A. (2009). A rapid wound signal activates the systemic synthesis of bioactive jasmonates in Arabidopsis. *Plant J* 59, 974–986. doi: 10.1111/j.1365-313X.2009.03924.x

Koo, A. J., and Howe, G. A. (2012). Catabolism and deactivation of the lipid-derived hormone jasmonoyl-isoleucine. *Front Plant Sci* 3:19. doi: 10.3389/fpls.2012.00019

Koo, A. J., Thireault, C., Zemelis, S., Poudel, A. N., Zhang, T., Kitaoka, N., et al. (2014). Endoplasmic reticulum-associated inactivation of the hormone jasmonoyl-L-isoleucine by multiple members of the cytochrome P450 94 family in Arabidopsis. *J Biol Chem* 289, 29728–29738. doi: 10.1074/jbc.M114.603084

Liu, M. J., Wu, S. H., Wu, J. F., Lin, W. D., Wu, Y. C., Tsai, T. Y., et al. (2013). Translational landscape of photomorphogenic Arabidopsis. *Plant Cell* 25, 3699–3710. doi: 10.1105/tpc.113.114769

Lorenzo, O., Chico, J. M., Sanchez-Serrano, J. J., and Solano, R. (2004). JASMONATE-INSENSITIVE1 encodes a MYC transcription factor essential to discriminate between different jasmonate-regulated defense responses in Arabidopsis. *Plant Cell* 16, 1938–1950. doi: 10.1105/tpc.022319

Lunde, C., Kimberlin, A., Leiboff, S., Koo, A. J., and Hake, S. (2019). Tasselseed5 overexpresses a wound-inducible enzyme, ZmCYP94B1, that affects jasmonate catabolism, sex determination, and plant architecture in maize. *Commun. Biol.* 2, 114. doi: 10.1038/s42003-019-0354-1

Mandaokar, A., Thines, B., Shin, B., Lange, B. M., Choi, G., Koo, Y. J., et al. (2006). Transcriptional regulators of stamen development in Arabidopsis identified by transcriptional profiling. *Plant Journal* 46, 984–1008. doi: 10.1111/j.1365-313X.2006.02756.x

Martinez-Seidel, F., Beine-Golovchuk, O., Hsieh, Y.-C., and Kopka, J. (2020). Systematic Review of Plant Ribosome Heterogeneity and Specialization. *Frontiers in Plant Science* 11:948. doi: 10.3389/fpls.2020.00948

Mazzoni-Putman, S. M., and Stepanova, A. N. (2018). A Plant Biologist's Toolbox to Study Translation. *Frontiers in Plant Science* 9:873. doi: 10.3389/fpls.2018.00873

McIntosh, K. B. M. B., and Bonham-Smith, P. C. B.-S. C. (2006). Ribosomal protein gene regulation: what about plants? *Canadian Journal of Botany* 84, 342–362. doi: 10.1139/b06-014

Memelink, J. (2009). Regulation of gene expression by jasmonate hormones. *Phytochemistry* 70, 1560–1570. doi: 10.1016/j.phytochem.2009.09.004

Merchante, C., Brumos, J., Yun, J., Hu, Q., Spencer, K. R., Enriquez, P., et al. (2015). Gene-specific translation regulation mediated by the hormone-signaling molecule EIN2. *Cell* 163, 684–697. doi: 10.1016/j.cell.2015.09.036

Merchante, C., Stepanova, A. N., and Alonso, J. M. (2017). Translation regulation in plants: an interesting past, an exciting present and a promising future. *The Plant Journal* 90, 628–653. doi: 10.1111/tpj.13520

Merret, R., Carpentier, M. C., Favory, J. J., Picart, C., Descombin, J., Bousquet-Antonelli, C., et al. (2017). Heat Shock Protein HSP101 Affects the Release of Ribosomal Protein mRNAs for Recovery after Heat Shock. *Plant Physiol* 174, 1216–1225.

Meteignier, L. V., El Oirdi, M., Cohen, M., Barff, T., Matteau, D., Lucier, J. F., et al. (2017). Translatome analysis of an NB-LRR immune response identifies important contributors to plant immunity in Arabidopsis. *J Exp Bot* 68, 2333–2344.

Mi, H., Muruganujan, A., Ebert, D., Huang, X., and Thomas, P. D. (2018). PANTHER version 14: more genomes, a new PANTHER GO-slim and improvements in enrichment analysis tools. *Nucleic Acids Research* 47, D419–D426.

Muench, D. G., Zhang, C., and Dahodwala, M. (2012). Control of cytoplasmic translation in plants. *WIREs RNA* 3, 178–194.

Mustroph, A., Zanetti, M. E., Jang, C. J., Holtan, H. E., Repetti, P. P., Galbraith, D. W., et al. (2009). Profiling translatomes of discrete cell populations resolves altered cellular priorities during hypoxia in Arabidopsis. *Proc Natl Acad Sci U S A* 106, 18843–18848.

Nielsen, K., and Boston, R. S. (2001). RIBOSOME-INACTIVATING PROTEINS: A Plant Perspective. *Annu Rev Plant Physiol Plant Mol Biol* 52, 785–816.

Noir, S., Bomer, M., Takahashi, N., Ishida, T., Tsui, T. L., Balbi, V., et al. (2013). Jasmonate controls leaf growth by repressing cell proliferation and the onset of endoreduplication while maintaining a potential stand-by mode. *Plant Physiol* 161, 1930–1951.

Pauwels, L., Inze, D., and Goossens, A. (2009). Jasmonate-inducible gene: what does it mean? *Trends Plant Sci.* 14, 87–91.

Pauwels, L., Morreel, K., De Witte, E., Lammertyn, F., Van Montagu, M., Boerjan, W., et al. (2008). Mapping methyl jasmonate-mediated transcriptional reprogramming of metabolism and cell cycle progression in cultured Arabidopsis cells. *Proc Natl Acad Sci U S A* 105, 1380–1385.

Poudel, A. N., Holtsclaw, R. E., Kimberlin, A., Sen, S., Zeng, S., Joshi, T., et al. (2019). 12-Hydroxy-jasmonoyl-l-isoleucine is an active jasmonate that signals through CORONATINE INSENSITIVE 1 and contributes to the wound response in Arabidopsis. *Plant Cell Physiol* 60, 2152–2166.

Poudel, A. N., Zhang, T., Kwasniewski, M., Nakabayashi, R., Saito, K., and Koo, A. J. (2016). Mutations in jasmonoyl-L-isoleucine-12-hydroxylases suppress multiple JA-dependent wound responses in Arabidopsis thaliana. *Biochim Biophys Acta* 1861, 1396–1408.

Reinbothe, S., Mollenhauer, B., and Reinbothe, C. (1994). Jips And Rips - The Regulation Of Plant Gene-Expression By Jasmonates In Response To Environmental Cues And Pathogens. *Plant Cell* 6, 1197–1209.

Reymond, P., Bodenhausen, N., Van Poecke, R. M., Krishnamurthy, V., Dicke, M., and Farmer, E. E. (2004). A conserved transcript pattern in response to a specialist and a generalist herbivore. *Plant Cell* 16, 3132–3147.

Reymond, P., Weber, H., Damond, M., and Farmer, E. E. (2000). Differential gene expression in response to mechanical wounding and insect feeding in Arabidopsis. *Plant Cell* 12, 707–720.

Reynoso, M. A., Juntawong, P., Lancia, M., Blanco, F. A., Bailey-Serres, J., and Zanetti, M. E. (2015). Translating Ribosome Affinity Purification (TRAP) followed by RNA sequencing technology (TRAP-SEQ) for quantitative assessment of plant translatomes. *Methods Mol Biol* 1284, 185–207.

Rühl, C., Stauffer, E., Kahles, A., Wagner, G., Drechsel, G., Rätsch, G., et al. (2012). Polypyrimidine tract binding protein homologs from Arabidopsis are key regulators of alternative splicing with implications in fundamental developmental processes. *Plant Cell* 24, 4360–4375.

Rustgi, S., Pollmann, S., Buhr, F., Springer, A., Reinbothe, C., Von Wettstein, D., et al. (2014). JIP60-mediated, jasmonate- and senescence-induced molecular switch in translation toward stress and defense protein synthesis. *Proc Natl Acad Sci U S A* 111, 14181–14186.

Sablok, G., Powell, J. J., and Kazan, K. (2017). Emerging Roles and Landscape of Translating mRNAs in Plants. *Frontiers in Plant Science* 8:1443. doi: 10.3389/fpls.2017.01443

Schepetilnikov, M., and Ryabova, L. A. (2017). Auxin Signaling in Regulation of Plant Translation Reinitiation. *Front Plant Sci* 8:1014.

Sheard, L. B., Tan, X., Mao, H., Withers, J., Ben-Nissan, G., Hinds, T. R., et al. (2010). Jasmonate perception by inositol-phosphate-potentiated COI1-JAZ co-receptor. *Nature* 468, 400–405.

Shi, Z., Fujii, K., Kovary, K. M., Genuth, N. R., Röst, H. L., Teruel, M. N., et al. (2017). Heterogeneous Ribosomes Preferentially Translate Distinct Subpools of mRNAs Genome-wide. *Mol Cell* 67, 71–83e7.

Song, S., Huang, H., Wang, J., Liu, B., Qi, T., and Xie, D. (2017). MYC5 is Involved in Jasmonate-Regulated Plant Growth, Leaf Senescence and Defense Responses. *Plant Cell Physiol* 58, 1752–1763.

Stirpe, F., and Battelli, M. G. (2006). Ribosome-inactivating proteins: progress and problems. *Cell Mol Life Sci* 63, 1850–1866.

Suza, W. P., and Staswick, P. E. (2008). The role of JAR1 in Jasmonoyl-L: -isoleucine production during Arabidopsis wound response. *Planta* 227, 1221–1232.

Thimm, O., Blasing, O., Gibon, Y., Nagel, A., Meyer, S., Kruger, P., et al. (2004). MAPMAN: a user-driven tool to display genomics data sets onto diagrams of metabolic pathways and other biological processes. *Plant J* 37, 914–939.

Thines, B., Katsir, L., Melotto, M., Niu, Y., Mandaokar, A., Liu, G., et al. (2007). JAZ repressor proteins are targets of the SCF(COI1) complex during jasmonate signalling. *Nature* 448, 661–665.

Walley, J. W., Sartor, R. C., Shen, Z., Schmitz, R. J., Wu, K. J., Urich, M. A., et al. (2016). Integration of omic networks in a developmental atlas of maize. *Science* 353, 814–818.

Wang, L., Li, H., Zhao, C., Li, S., Kong, L., Wu, W., et al. (2017). The inhibition of protein translation mediated by AtGCN1 is essential for cold tolerance in Arabidopsis thaliana. *Plant Cell Environ* 40, 56–68.

Wasternack, C., and Hause, B. (2013). Jasmonates: biosynthesis, perception, signal transduction and action in plant stress response, growth and development. An update to the 2007 review in Annals of Botany. *Ann Bot* 111, 1021–1058.

Wu, J., and Baldwin, I. T. (2010). New insights into plant responses to the attack from insect herbivores. *Annu Rev Genet* 44, 1–24.

Xie, D. X., Feys, B. F., James, S., Nieto-Rostro, M., and Turner, J. G. (1998). COI1: an Arabidopsis gene required for jasmonate-regulated defense and fertility. *Science* 280, 1091–1094.

Xu, G., Greene, G. H., Yoo, H., Liu, L., Marques, J., Motley, J., et al. (2017). Global translational reprogramming is a fundamental layer of immune regulation in plants. *Nature* 545, 487–490.

Yan, Y., Stolz, S., Chetelat, A., Reymond, P., Pagni, M., Dubugnon, L., et al. (2007). A downstream mediator in the growth repression limb of the jasmonate pathway. *Plant Cell* 19, 2470–2483.

Zander, M., Lewsey, M. G., Clark, N. M., Yin, L., Bartlett, A., Saldierna Guzmán, J. P., et al. (2020). Integrated multi-omics framework of the plant response to jasmonic acid. *Nature Plants* 6, 290–302.

Zanetti, M. E., Chang, I. F., Gong, F., Galbraith, D. W., and Bailey-Serres, J. (2005). Immunopurification of polyribosomal complexes of Arabidopsis for global analysis of gene expression. *Plant Physiol* 138, 624–635.

Zavaliev, R., Levy, A., Gera, A., and Epel, B. L. (2013). Subcellular dynamics and role of Arabidopsis β-1,3-glucanases in cell-to-cell movement of tobamoviruses. *Mol Plant Microbe Interact* 26, 1016–1030.

Zhang, F., Yao, J., Ke, J., Zhang, L., Lam, V. Q., Xin, X. F., et al. (2015). Structural basis of JAZ repression of MYC transcription factors in jasmonate signalling. *Nature* 525, 269–273.

Zhang, J., Xin, L., Shan, B., Chen, W., Xie, M., Yuen, D., et al. (2012). PEAKS DB: de novo sequencing assisted database search for sensitive and accurate peptide identification. *Mol Cell Proteomics* 11, M111.010587.

Zhang, Y., and Turner, J. G. (2008). Wound-induced endogenous jasmonates stunt plant growth by inhibiting mitosis. *PLoS ONE* 3:e3699.

Zhu, F., Zhou, Y.-K., Ji, Z.-L., and Chen, X.-R. (2018). The Plant Ribosome-Inactivating Proteins Play Important Roles in Defense against Pathogens and Insect Pest Attacks. *Frontiers in Plant Science* 9:146. doi: 10.3389/fpls.2018.00146

Conflict of Interest: The authors declare that the research was conducted in the absence of any commercial or financial relationships that could be construed as a potential conflict of interest.

Copyright © 2021 Kimberlin, Holtsclaw and Koo. This is an open-access article distributed under the terms of the Creative Commons Attribution License (CC BY). The use, distribution or reproduction in other forums is permitted, provided the original author(s) and the copyright owner(s) are credited and that the original publication in this journal is cited, in accordance with accepted academic practice. No use, distribution or reproduction is permitted which does not comply with these terms.

frontiers in Plant Science

ORIGINAL RESEARCH
published: 25 May 2021
doi: 10.3389/fpls.2021.687406

Subfunctionalization of Paralog Transcription Factors Contributes to Regulation of Alkaloid Pathway Branch Choice in *Catharanthus roseus*

Maite Colinas[1,2*†], Jacob Pollier[1,3], Dries Vaneechoutte[1,2], Deniz G. Malat[1,2], Fabian Schweizer[1,2], Liesbeth De Milde[1,2], Rebecca De Clercq[1,2], Joana G. Guedes[4,5,6], Teresa Martínez-Cortés[4†], Francisco J. Molina-Hidalgo[1,2†], Mariana Sottomayor[4,7], Klaas Vandepoele[1,2] and Alain Goossens[1,2*]

[1] Department of Plant Biotechnology and Bioinformatics, Ghent University, Ghent, Belgium, [2] VIB Center for Plant Systems Biology, Ghent, Belgium, [3] VIB Metabolomics Core, Ghent, Belgium, [4] CIBIO/InBIO, Centro de Investigação em Biodiversidade e Recursos Genéticos, Universidade do Porto, Vairaão, Portugal, [5] I3S-Instituto de Investigação e Inovação em Saúde, IBMC-Instituto de Biologia Molecular e Celular, Universidade do Porto, Porto, Portugal, [6] ICBAS–Instituto de Ciências Biomédicas Abel Salazar, Universidade do Porto, Porto, Portugal, [7] Faculdade de Ciências, Universidade do Porto, Porto, Portugal

Catharanthus roseus produces a diverse range of specialized metabolites of the monoterpenoid indole alkaloid (MIA) class in a heavily branched pathway. Recent great progress in identification of MIA biosynthesis genes revealed that the different pathway branch genes are expressed in a highly cell type- and organ-specific and stress-dependent manner. This implies a complex control by specific transcription factors (TFs), only partly revealed today. We generated and mined a comprehensive compendium of publicly available *C. roseus* transcriptome data for MIA pathway branch-specific TFs. Functional analysis was performed through extensive comparative gene expression analysis and profiling of over 40 MIA metabolites in the *C. roseus* flower petal expression system. We identified additional members of the known BIS and ORCA regulators. Further detailed study of the ORCA TFs suggests subfunctionalization of ORCA paralogs in terms of target gene-specific regulation and synergistic activity with the central jasmonate response regulator MYC2. Moreover, we identified specific amino acid residues within the ORCA DNA-binding domains that contribute to the differential regulation of some MIA pathway branches. Our results advance our understanding of TF paralog specificity for which, despite the common occurrence of closely related paralogs in many species, comparative studies are scarce.

Keywords: AP2/ERF transcription factor, bHLH transcription factor, *Catharanthus roseus*, Madagascar periwinkle, monoterpenoid indole alkaloids, transcription factor gene clusters, transcription factor paralogs, synergistic regulation

OPEN ACCESS

Edited by:
Koichi Sugimoto, University of Tsukuba, Japan

Reviewed by:
Tsubasa Shoji, RIKEN Center for Sustainable Resource Science (CSRS), Japan
Vincent Courdavault, Université de Tours, France

***Correspondence:**
Maite Colinas
mmartinez@ice.mpg.de
Alain Goossens
alain.goossens@psb.vib-ugent.be; algoo@psb.vib-ugent.be

†Present address:
Maite Colinas, Department of Natural Product Biosynthesis, Max Planck Institute for Chemical Ecology, Jena, Germany
Francisco J. Molina-Hidalgo Department of Biochemistry and Molecular Biology, University of Cordoba, Edificio Severo Ochoa, Campus de Rabanales, Córdoba, Spain
Teresa Martínez-Cortés, Universidade da Coruña, Facultad de Ciencias–Departamento de Biologia Animal, Centro de Investigaciones Científicas Avanzadas (CICA), A Coruña, Spain

Specialty section:
This article was submitted to Plant Metabolism and Chemodiversity, a section of the journal Frontiers in Plant Science

Received: *29 March 2021*
Accepted: *27 April 2021*
Published: *25 May 2021*

INTRODUCTION

Plant specialized metabolites are chemically diverse, typically species- or taxa-specific and have often evolved in adaptation to the ecological niche of the plant. Within the plant, their production often exclusively takes place in specific organs or cell types and may be up-regulated precisely in response to defined environmental conditions [for a review, see Colinas and Goossens (2018)]. The integration of internal cues, such as cell type environment and developmental stage, and external cues, such as the presence of pathogens or herbivores, is predominantly regulated at the transcriptional level by specific transcription factors (TFs). Different TFs might act independently or cooperatively, forming regulatory modules that ensure the optimal spatiotemporal expression of specific metabolic pathway genes.

The medicinal plant *Catharanthus roseus* is well-known as being the only source of the important anti-cancer compounds vinblastine and vincristine (Van Der Heijden et al., 2004). These complex molecules belong to the class of monoterpenoid indole alkaloids (MIAs); around 150 different MIAs are estimated to occur in *C. roseus* (Van Der Heijden et al., 2004). The identification of many of the involved biosynthetic enzymes has revealed that genes involved in the different MIA pathway steps and branches are expressed in a cell type-specific, organ-specific and stress-dependent manner, making this species an ideal model to study how a modular system of different TFs possibly regulates specialized metabolism (Courdavault et al., 2014; Dugé De Bernonville et al., 2015).

Different MIA pathway steps and branches can be organized into *subdivisions* with connected gene expression patterns (**Figure 1**). The first of such *subdivisions* is the *iridoid pathway*, i.e., the biosynthesis of the precursor loganic acid from geranyl diphosphate (GPP) via seven enzymatic steps occurring in the specialized internal phloem-associated parenchyma (IPAP) cells (Geu-Flores et al., 2012; Asada et al., 2013; Simkin et al., 2013; Miettinen et al., 2014; Salim et al., 2014). An iridoid intermediate, presumably loganic acid, is then transported to the epidermis, possibly by the recently characterized nitrate/peptide family (NPF) transporters (NPF2.4, NPF2.5, and NPF2.6) (Yamamoto et al., 2016, 2019; Larsen et al., 2017). The coupling of the then converted iridoid secologanin to the tryptophan-derived indole moiety tryptamine marks the formation of the first MIA strictosidine, from which, after deglycosylation, all MIAs derive (*strictosidine pathway*). A single enzymatic step is needed to convert the strictosidine aglycone either into the heterohymbines ajmalicine or tetrahydroalstonine (and subsequently alstonine) (Stavrinides et al., 2016; Dang et al., 2018), or into nitrosamine (Stavrinides et al., 2018). The branch leading to the precursors of the anti-cancer compounds has recently been resolved and involves seven enzymatic steps to yield the unstable intermediate dehydrosecodine (named *stemmadenine pathway* according to the name of one of the intermediates) (Tatsis et al., 2017; Caputi et al., 2018; Qu et al., 2018, 2019). From the latter either tabersonine or catharanthine are formed by two different enzymes (Caputi et al., 2018; Qu et al., 2018). Catharanthine forms one moiety of the MIA dimers vinblastine and vincristine and has been additionally suggested to have a repellent function as a monomer after secretion to the leaf surface by an epidermal ATP-binding cassette (ABC) transporter (Roepke et al., 2010; Yu and De Luca, 2013). The second monomer, vindoline, is produced from tabersonine via seven enzymatic steps, from which the two last steps are thought to take place in specialized idioblasts or laticifers (St-Pierre and De Luca, 1995; St-Pierre et al., 1999; Levac et al., 2008; Liscombe et al., 2010; Guirimand et al., 2011; Liscombe and O'connor, 2011; Besseau et al., 2013; Qu et al., 2015). Noteworthy, the *vindoline pathway* exclusively occurs in the green aerial parts of the plant (Liu et al., 2019). By contrast, in roots (particularly hairy roots), a different set of interconvertible *root-specific MIAs* (lochnericine, hörhammericine, minovincinine among others) is formed (Laflamme et al., 2001; Giddings et al., 2011; Carqueijeiro et al., 2018a,b; Williams et al., 2019). Finally, the assumed spatially separated monomers vindoline and catharanthine are dimerized to α-3′,4′-anhydrovinblastine, the direct precursor of vinblastine and vincristine, presumably by a peroxidase (Costa et al., 2008). Noteworthy, a very recent study suggests that catharanthine, as well as ajmalicine and its oxidation product serpentine, may also accumulate in idioblasts and laticifers in addition to the epidermis (Yamamoto et al., 2019). Thus, more research is needed in order to clarify the hypothesis of spatial separation of the monomers and differences in the sites of biosynthesis and accumulation of MIA monomers.

There has been a substantial increase in knowledge about which specific TFs from different families control the different MIA pathway steps and branches, although not complete yet. The main focus has been on the jasmonate (JA)-dependent transcriptional activation, because many (but not all, see below) MIA pathway steps are up-regulated upon exposure to this phytohormone that mainly mediates defense against necrotrophic pathogens and herbivores (Aerts et al., 1994; Zhang et al., 2011; De Geyter et al., 2012; Goossens et al., 2016, 2017; Zhou and Memelink, 2016). The primary response regulator of JA-dependent up-regulation of target genes is the basic helix-loop-helix (bHLH) TF MYC2, whose activity is post-translationally suppressed in the absence of JA (Chini et al., 2007; Goossens et al., 2017; Wasternack and Strnad, 2019). Recently, we have described how overexpression of the de-repressed *CrMYC2a*^{D126N} variant can boost the expression of the JA-responsive MIA biosynthesis genes (Schweizer et al., 2018). This up-regulation may partly occur directly and/or via the up-regulation of branch-specific TFs described below (Schweizer et al., 2018). For instance the regulators clade IVa bHLH iridoid synthesis (BIS) 1 and 2 TFs exclusively up-regulate the *iridoid pathway* genes (Van Moerkercke et al., 2015; Van Moerkercke et al., 2016). The expression of *strictosidine pathway* genes is controlled by members of the octadecanoid derivative-responsive *catharanthus* apetala2-domain (ORCA) clade (Menke et al., 1999; Van Der Fits and Memelink, 2000;Van Der Fits and Memelink, 2001; Paul et al., 2016; Paul et al., 2020; Singh et al., 2020). In addition, overexpression of ORCA3 has been shown to increase the expression of the *iridoid pathway* genes to some extent, part of the *stemmadenine pathway* genes and, when overexpressed in combination with *CrMYC2a*^{D126N}, *root specific MIA* genes in a highly synergistic manner (Schweizer et al., 2018). While there is some knowledge about the target gene profiles of the other

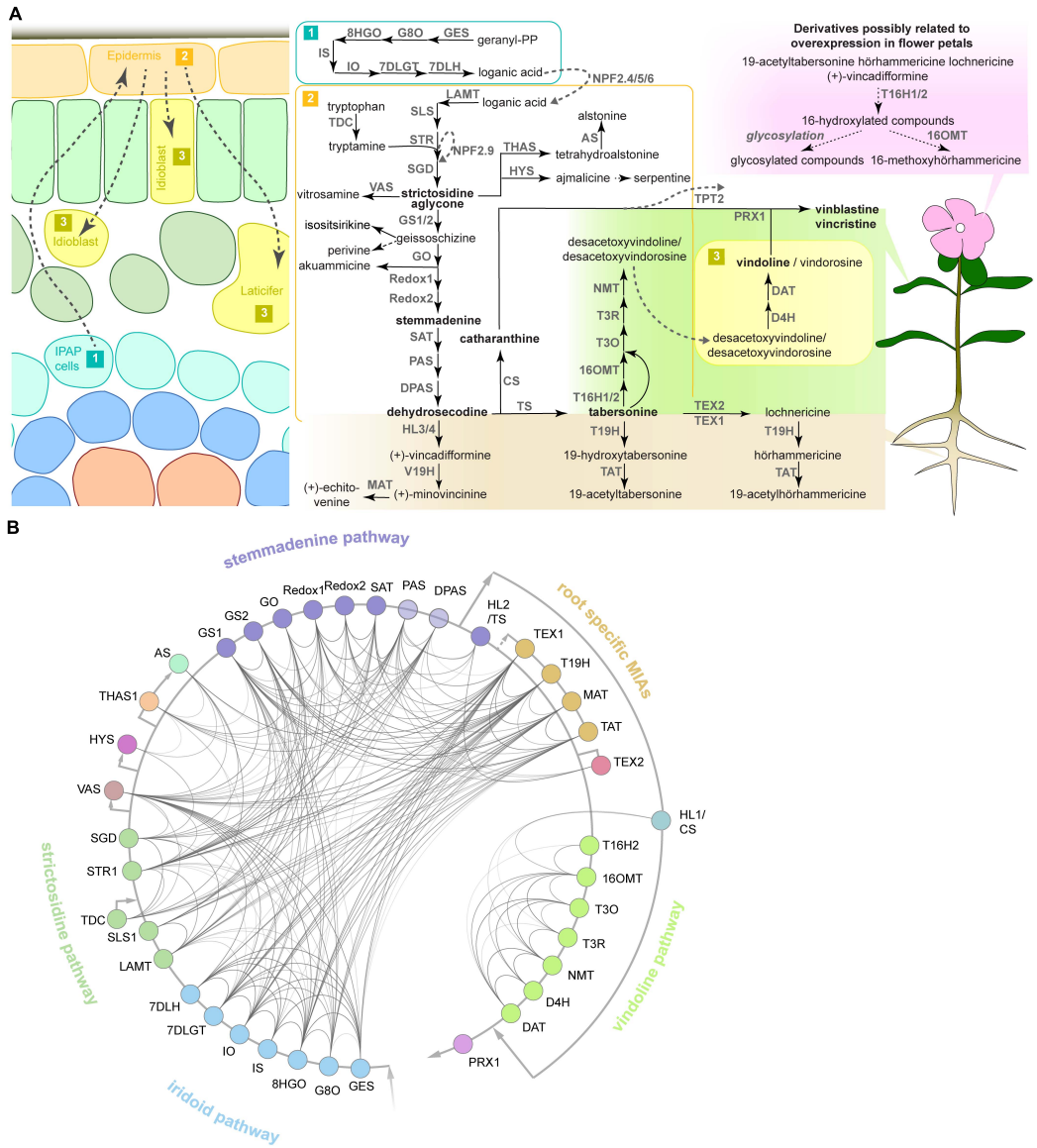

FIGURE 1 | The MIA pathway consists of different branches with corresponding co-expression networks. **(A)** The MIA network and known or presumed cellular and organ-specific expression of the encoding MIA biosynthesis genes based on the current knowledge and available data. MIA biosynthesis is compartmentalized into the three different cell types shown on the left, although a cell type-specific expression has not been experimentally verified for all MIA biosynthesis genes such as the root MIA biosynthesis genes. Available organ-specific transcriptome data revealed that in particular two MIA branches are either root- or leaf-specific as shown on the right. In our study, transient overexpression of TFs in *C. roseus* flower petals is used to assess the impact on MIA biosynthesis at the gene expression level (by qPCR) and MIA metabolite level (by LC-MS analysis). Some MIA derivatives are detected in this flower petal expression system in this study, but it is not known where they occur in wild-type plants (upper right). Arrows indicate known characterized enzymatic reactions and corresponding enzymes; dashed black arrows indicate assumed enzymatic or chemical reactions for which no specific enzyme has been identified. Dashed gray arrows indicate transport and corresponding transporters. Note that NPF2.9 is an intracellular transporter conferring vacuolar export of strictosidine and TPT2 is an epidermis-specific transporter exporting catharanthine to the leaf surface. For clarity, only selected MIA metabolites are shown. **(B)** Co-expression network of MIA biosynthesis genes. From an expression atlas of 82 samples KNN networks were created. A line between genes indicates co-expression. Opacity of the lines is scaled according to the mutual rank of co-expression between two genes in their KNN 500 clusters (darker = stronger co-expression). To simplify the complex MIA biosynthesis network, we have colored the different pathway branches. Abbreviations: GES, geraniol synthase; G8O, geraniol-8-oxidase; 8HGO, 8-hydroxygeraniol oxidoreductase; IS, iridoid synthase; IO, iridoid oxidase; 7DLGT, 7-deoxyloganetic acid glucosyl transferase; 7DLH, 7-deoxyloganic acid hydroxylase; LAMT, loganic acid *O*-methyltransferase; SLS, secologanin synthase; TDC, tryptophan decarboxylase; STR, strictosidine synthase; NPF, nitrate/peptide family; SGD, strictosidine β-glucosidase; VAS, nitrosamine synthase; THAS, tetrahydroalstonine synthase; AS, a lstonine synthase: HYS, heteroyohimbine synthase; GS, geissoschizine synthase; GO, geissoschizine oxidase; SAT, stemmadenine-*O*-acetyl- transferase; PAS, precondylocarpine acetate synthase; DPAS, dihydroprecondylocarpine synthase; CS, catharanthine synthase; TPT, catharanthine transporter; T16H, tabersonine 16-hydroxylase; 16OMT, 16-hydroxytabersonine *O*-methyltransferase; T3O, tabersonine 3-oxygenase; T3R, tabersonine 3-reductase; NMT, 2,3-dihydro-3-hydroxytabersonine-N-methyltransferase; D4H, desacetoxyvindoline 4-hydroxylase; DAT, deacetylvindoline 4-*O*-acetyltransferase; PRX, peroxidase; HL, hydrolase; V19H, vincadifformine-19-hydroxylase; MAT, minovincinine-19-*O*-acetyltransferase; T19H, tabersonine 19-hydroxylase; TAT, 19-hydroxytabersonine 19-*O*-acetyltransferase; TEX, tabersonine epoxidase.

ORCAs (Paul et al., 2016, 2020; Singh et al., 2020), a direct comparison of them under the same experimental condition is currently lacking. Moreover, it has not been clarified, which, if any, of the ORCAs, in addition to ORCA3, act synergistically with CrMYC2a^{D126N}. Noteworthy, the *vindoline pathway* does not appear to be up-regulated by JA and seems to be rather repressed upon overexpression of *CrMYC2a*^{D126N} (Schweizer et al., 2018). Very recently it has been shown that, the *vindoline pathway* is at least in part up-regulated by a GATA TF and down-regulated by phytochrome-interacting factor TFs in a light-dependent manner (Liu et al., 2019). However, the moderate changes in expression of the vindoline pathway genes and metabolite levels induced by these TFs suggest the presence of additional regulators. Other TFs, with a more limited impact on MIA biosynthesis have been described [for a review, see Liu et al. (2017)].

Together, the increasing identification of MIA biosynthesis genes over the recent years revealed a network of pathway branches (*subdivisions*) with differential gene expression profiles. This suggests the existence of specific regulatory factors acting independently or cooperatively in a branch-specific manner. Here, we sought out for regulators for pathway branches for which regulation was unclear or unknown by using co-expression analysis of publicly available and hitherto unpublished in-house generated RNA-Seq datasets. We identified additional members of well-known BIS, ORCA, and MYB clades. Our results further suggest that subfunctionalization of the ORCA TFs leads to differential regulation of particular subsets of MIA pathway genes. Likewise, synergistic up-regulation of MIA pathway genes in combination with de-repressed CrMYC2a appears to be paralog dependent.

MATERIALS AND METHODS

Compilation and Generation of RNA-Seq Datasets

In total, 82 RNA-Seq samples were mapped to the latest *C. roseus* draft genome version (Kellner et al., 2015)[1]and compiled in our compendium. In addition to publicly available datasets, RNA-Seq data from additional in-house experiments were included (see **Supplementary Table 1**). Two datasets consist of cell-type enriched transcriptomes obtained from macro-dissected stem (peeled) and leaf tissue (central vein compared to rest of leaf) as described previously (Van Moerkercke et al., 2015). A third dataset consists of RNA-Seq data from flower petals infiltrated with *Agrobacterium tumefaciens* C58C1 or infiltration buffer as control. The fourth dataset consists of transcriptomes of stably transformed hairy root lines constitutively overexpressing *BIS1*, *ORCA3* or the *green fluorescent protein* (*GFP*) (Van Moerkercke et al., 2015). In all cases, RNA was extracted from three biological replicates, as described previously (Van Moerkercke et al., 2015) and described below, and sequenced (50 bp, single-end) with an Illumina HiSeq2500 by GATC Biotech[2].

[1]http://medicinalplantgenomics.msu.edu/index.shtml

[2]https://eurofinsgenomics.eu

RNA-Seq Data Processing

RNA-Seq data was obtained from eight publicly available and unpublished datasets, covering 81 samples listed in **Supplementary Table 1**. Raw RNA-Seq data was processed with Prose from the Curse toolset (Vaneechoutte and Vandepoele, 2019). Prose uses FastQC (v0.11.7) (Andrews, 2012) and Trimmomatic (v0.38) (Bolger et al., 2014) to perform adapter clipping and quality trimming, and Kallisto (v0.44.0) (Bray et al., 2016) to quantify gene and transcript expression levels in Transcript Per Million (TPM) normalized values. For adapter clipping, Trimmomatic was run with the sliding window size set to 4 and the seed mismatches set to 2. Adapters were detected by FastQC and clipped in each sample separately. For quality trimming, Trimmomatic was run with a simple clip threshold of 10 and a minimum required quality of 15. Reads shorter than 32 bp after quality control were discarded. For Kallisto, an index of the *C. roseus* transcripts was created with a k-mer size of 31. The wrongly split transcript sequence for the *SGD* gene was manually corrected by merging the two CRO_T111319 and CRO_T111320. To process single-end reads with Kallisto, the mean fragment length was set to 200 and the standard deviation to 20. The *C. roseus* expression atlas is available in **Supplementary Dataset 1**. Prose was used to generate k-nearest neighbor (KNN) networks from the expression atlas of 82 samples. In this network, each gene was connected to its top 500 most co-expressing genes. This co-expression information was used for network and heatmap visualization.

Candidate Selection

To search for potential regulators of gene expression, *C. roseus* transcripts were submitted to TRAPID (Van Bel et al., 2013). TRAPID was used to generate functional annotation for these transcripts based on sequence similarity and the presences of protein domains. In total, TRAPID annotated 1,586 genes with the Gene Ontology term "regulation of gene expression" (GO:0010468). Next, 44 genes with known involvement in the catharanthine and vindoline biosynthesis pathways were used as baits to select candidate regulators of these processes. For each bait gene, the top 500 most co-expressing genes in the KNN network were searched for the 1,586 genes that were predicted as regulators of gene expression by TRAPID. Genes that matched this selection were considered to be candidate regulators of the catharanthine or vindoline pathways, since they are both predicted regulators of gene expression and are co-expressed with known pathway genes. If more than 10 matches could be found for a single bait gene, only the top 10 most co-expressing candidates were kept. With 44 bait genes, this could result in at most 440 candidate genes, but due to overlap between the top 10 s of different baits, a final list of 111 candidates was selected (**Figure 2A**).

Generation of DNA Constructs

Coding sequences (CDSs) of TFs were amplified using cDNA from *C. roseus* var. "Little bright eyes" or *C. roseus* var. "Sunstorm apricot" as templates. Amplification was performed using Q5® High-Fidelity DNA Polymerase (New England BioLabs®)

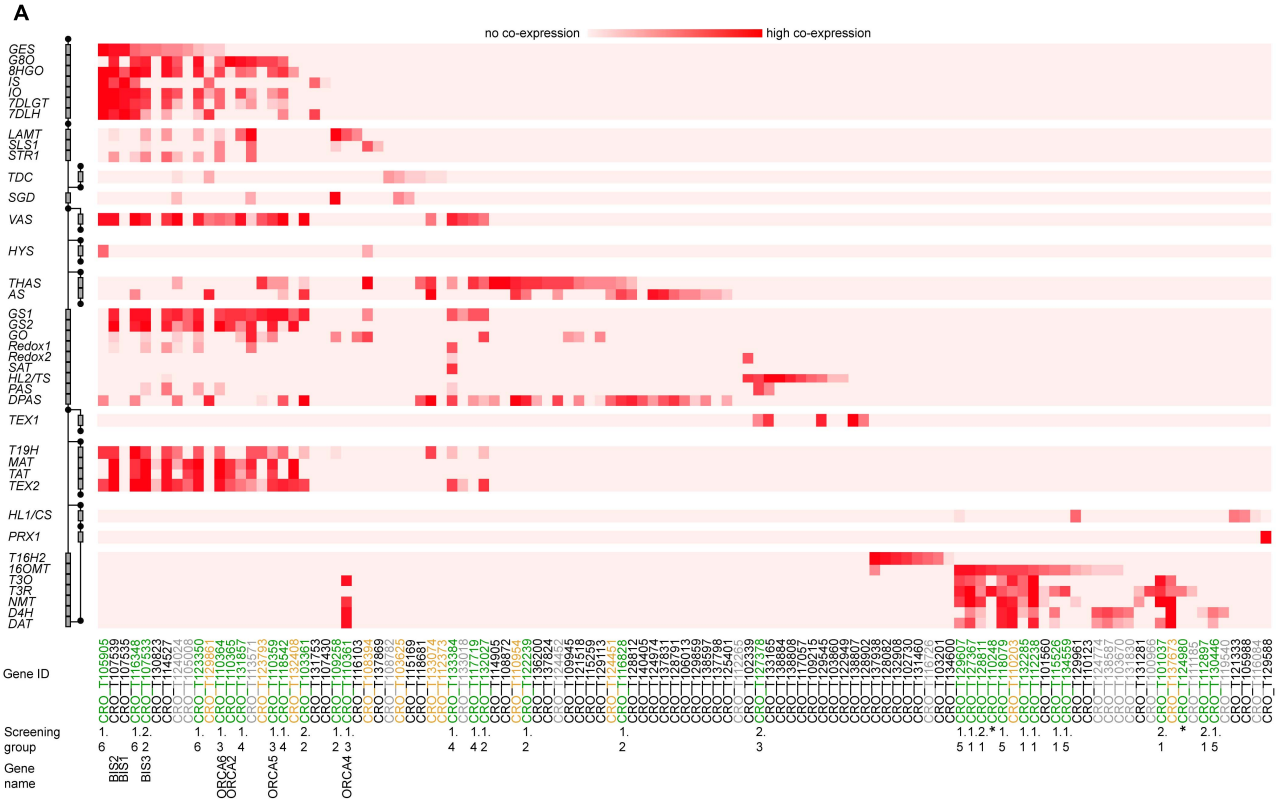

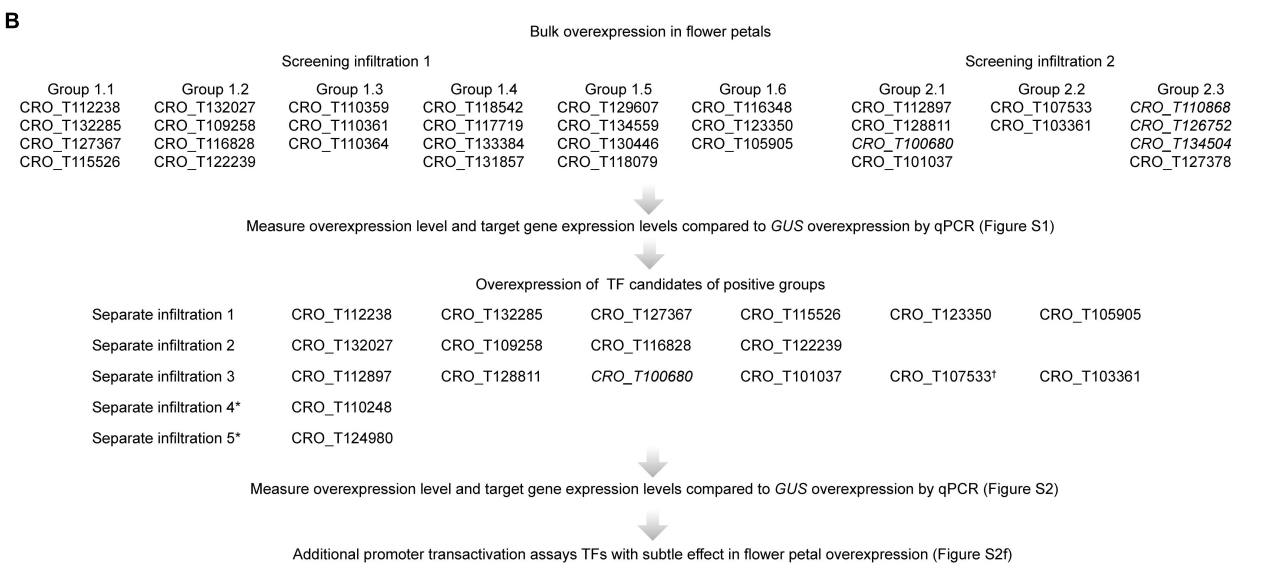

FIGURE 2 | MIA regulator candidate selection and screening procedure. **(A)** Pathway genes (left) are plotted against regulator candidates (below); the relative rank of a regulator in the top 500 most co-expressed genes is depicted in red, with dark red indicating low ranks and strong associations between regulator and pathway gene. TF gene IDs are color-coded, indicating which genes by manual sequence analyses are likely not specific TFs and were thus not further considered (gray), which were considered for screening but cloning failed (yellow), and which were tested (green). Previously characterized TFs are labeled with their names in addition to "BIS3," identified in this study. **(B)** Overview about the screening procedure. To enhance the output, TF candidates were bulk-overexpressed ("Screening groups") by mixing *A. tumefaciens* strains containing the respective constructs. The screening was performed in two independent rounds of infiltration ("Screening infiltration 1 and 2"). In case of a detected up-regulation of target genes >2-fold and $P < 0.05$ (tested by Student's *t*-test) (**Supplementary Figure 1**), the TF candidates from the respective group were overexpressed separately (**Supplementary Figure 2**). Gene IDs in italics were not picked in this co-expression analysis but in a previous one.

or iProof™ (Bio-Rad) and gene-specific oligonucleotides containing attB Gateway® recombination sites (**Supplementary Table 2**). Fragments were gel-purified (GeneJET Gel Extraction Kit, Thermo Fisher) and recombined into pDONR™207 using Gateway® BP clonase™ II enzyme mix (Thermo Fisher), and the resulting clones sequence verified. ENTRY clones containing *CrMYC2a*^{D126N}, *BIS1*, *BIS2* were cloned previously (Van Moerkercke et al., 2015; Van Moerkercke et al., 2016; Schweizer et al., 2018). ORCA3 protein mutants were constructed by site-directed mutagenesis using iProof™ (Bio-Rad) and pDONR207_CrORCA3 as a template and complementary primers. Chimeric CrORCA3-4 and CrORCA4-3 were constructed by overlap extension PCR using chimeric primers. ENTRY clones containing TFs were recombined using LR Clonase™ II enzyme mix (Thermo Fisher) into pH7WG2D or pK7WG2D for overexpression in flower petals, or p2GW7 for promoter transactivation assays in tobacco protoplasts (Karimi et al., 2002).

The promoter fragment of *STR* had been cloned previously (Vom Endt et al., 2007). The promoter fragments of *GO*, *MAT*, *TAT*, *T3O*, *T3R*, *D4H*, and *DAT* were amplified from *C. roseus* var. "Sunstorm apricot" genomic DNA using specific oligonucleotides (**Supplementary Table 3**), recombined into pDONR™207 and sequence verified, as described for the TF CDSs. The resulting ENTRY clones containing promoter fragments were recombined into pGWL7 (Karimi et al., 2002) for transient expression assays in tobacco protoplasts.

Transient Expression Assays in *Nicotiana tabacum* Protoplasts

Promoter transactivation of *C. roseus* gene promoters by *C. roseus* TFs was measured via transient expression assays in *Nicotiana tabacum* "Bright Yellow-2" protoplasts exactly as described previously (Vanden Bossche et al., 2013; Schweizer et al., 2018). Statistical analysis (ANOVA with Tukey's test for multiple comparisons) was performed using PRISM GraphPad 8 software.

Plant Material and Flower Petal Transformation

Catharanthus roseus var. "Little bright eyes" plants were grown in the greenhouse under 16-h/8-h light/dark conditions. Plants of the same age (6 months to 2 years) were used for flower petal infiltration with *A. tumefaciens* C58C1 harboring overexpression constructs as previously described (Schweizer et al., 2018) with minor adaptations. Briefly, all opened flowers were removed 2 days prior to infiltration. *A. tumefaciens* pre-cultures were inoculated from glycerol stocks 2 days prior to infiltration to inoculate final overnight cultures 1 day prior to infiltration. Cultures were washed and re-suspended as described (Schweizer et al., 2018). The suspensions were diluted and mixed (in case of combined overexpression of up to four TF overexpression constructs) to obtain a final concentration of OD_{600} = 0.4. Infiltration took place as described using four to five flowers, each from different individual plants. Samples were harvested in four biological replicates as described (Schweizer et al., 2018). In case of parallel analysis of gene expression and metabolite profiling, each sample was divided in two immediately before freezing.

Gene Expression Analysis by qPCR

RNA extraction and reverse transcription were performed as described (Schweizer et al., 2018) with modifications. Up to 500 ng of RNA was used for reverse transcription using either the iScript™ cDNA synthesis kit (Bio-Rad) or the qScript cDNA Synthesis Kit (Quantabio). qPCR was performed using a JANUS pipetting robot (PerkinElmer) and a LightCycler® 480 (Roche) using SYBR Green qPCR master Mix (Agilent) and gene-specific oligonucleotides (**Supplementary Table 5**) in two technical replicates. The data was normalized to *N2227* and *SAND* as reference genes (Pollier et al., 2014) using qBase (Hellemans et al., 2007). Statistical analyses (ANOVA with Tukey's test for multiple comparisons or Student's *t*-test, as indicated) were performed on log2-transformed data using PRISM GraphPad 8 software. Principle component analyses (PCAs) of MIA target gene profiles were performed with ClustVis (Metsalu and Vilo, 2015).

Metabolite Profiling

For metabolite extraction, around 100 mg of infiltrated flower petal samples were ground in liquid nitrogen, lyophilized and extracted with 1 ml methanol containing 100 μM caffeine as an internal standard. Extraction took place exactly as described previously (Schweizer et al., 2018). For LC-MS, 10 μL of the sample was injected in an Acquity UPLC BEH C18 column (150 × 2.1 mm, 1.7 μm; Waters, Milford, MA, United States) mounted on an Acquity UPLC system (Waters) connected to a Synapt HDMS qTOF-MS (Micromass) with an electrospray ionization source. A gradient was run at flow rate of 350 μL/min using acidified [0.1% (v/v) formic acid] solvents A [water/acetonitrile (99:1, v/v)] and B [acetonitrile/water; 99:1, v/v)]: time 0 min, 5% B; 30 min, 50% B; 33 min, 100% B. The mass spectrometer was set to positive ionization mode with the following parameter values: capillary voltage, 2.5 kV; sampling cone, 40 V; extraction cone, 4 V; source temperature, 120°C; desolvation temperature, 400°C; cone gas flow, 50 L/h; and desolvation gas flow, 750 L/h. Centroid data were recorded between *m*/*z* 100 and *m*/*z* 1,200 at a scan speed of 0.2 s/scan. Peak areas were determined using Progenesis QI software (Waters). PCAs were performed with MetaboAnalyst 4.0[3] using Pareto-scaled mass spectrometry data with standard settings (Chong et al., 2018). Statistical analyses of identified MIAs (ANOVA with Tukey's test for multiple comparisons) were performed using PRISM GraphPad 8 software. Identifications of the MIAs were done using FT-MS and MS^n data generated as described (Schweizer et al., 2018) and are shown in **Supplementary Dataset 2**.

Gene IDs and Data Deposition

Gene IDs (*C. roseus* genome version 2) are listed with the corresponding primer sequences in **Supplementary Table 4**. In some cases, the cloned sequences differed from publicly available genome and transcriptome data. All sequences cloned for this

[3]https://www.metaboanalyst.ca/

study have been deposited in the GenBank database; accession numbers are also listed in **Supplementary Table 4**.

RESULTS

TF Candidate Selection and Screening Impact on MIA Biosynthesis

To enable comprehensive mining of *C. roseus* transcriptomes for novel MIA regulators, first a total of 82 RNA-Seq datasets were mapped to the latest *C. roseus* draft genome version (Kellner et al., 2015) (see text footnote 1). In addition to publicly available datasets, RNA-Seq data from hitherto unpublished in-house experiments were included, including data of cell type-enriched transcriptomes (see methods and **Supplementary Table 1**). Across these datasets, branches of MIA pathway genes (**Figure 1B**) showed a high level of co-expression. Noteworthy, in particular the *vindoline* branch and catharanthine biosynthesis were not co-expressed with other MIA pathway branches (**Figure 1B**). A KNN network was created and for each MIA biosynthesis gene the top 500 most co-expressing genes were searched for genes with the GO term "regulation of gene expression" (GO:0010468) (see "Materials and Methods" section for details) yielding a list of 111 candidates (**Figure 2A**). Manual sequence analysis of the candidates revealed that 15 were likely not unambiguously corresponding to genuine TFs and thus not considered for further analysis. Consistent with previous results, among the co-expressed candidates we found the previously characterized TFs BIS1 and 2 and ORCA2, 4, 5, and 6, but not ORCA3. We further selected those TFs that showed co-expression with (i) multiple pathway genes and (ii) MIA pathway genes for which till now no transcriptional regulators are known, in particular genes belonging to the *stemmadenine* or *vindoline* branches or involved in catharanthine biosynthesis, and that were not predicted to act as repressors. Out of the 40 selected candidates, 28 were successfully cloned comprising all but two candidates that were ranked as candidates of highest priority and subjected to agroinfiltration in *C. roseus* flower petals. Four additional candidates, that were not found through this co-expression analysis but through a preceding, preliminary, analysis, were also tested in this screening (gene IDs in italic font in **Figure 2B**). The latter preceding co-expression analysis was performed exactly as described above but on 72 RNA-Seq samples because one dataset (Pan et al., 2018) had not yet been available at the start of this project (data not shown). While the candidate lists of the two analyses greatly overlapped those four candidates were exclusively found in the first analysis. Thus altogether 32 candidates were tested by bulk overexpression in *C. roseus* flower petals as described hereafter.

To enhance the throughput, up to four TF candidates were co-overexpressed under the control of the *CaMV35S* promoter (p35S). We specifically combined those candidates that were co-expressed with the same (or overlapping) subsets of MIA pathway genes. This resulted in nine overexpression groups of candidates (**Figure 2B**). *A. tumefaciens* harboring a plasmid for *p35S:GUS* expression was infiltrated as a control. The overexpression level of the candidate TFs and the expression level of the MIA pathway genes were then measured by qPCR (**Supplementary Figure 1**). In case of successful overexpression (>5-fold) and observed increase(s) (>2-fold, *P*-value according to Student's *t*-test < 0.05) in expression level(s) of potential target MIA pathway genes compared to the *p35S:GUS* control, the TF candidates from the respective group were overexpressed separately (**Figure 2B**; **Supplementary Figure 2**). In the case of CRO_T132285 and CRO_T127367, for which the increase in target gene expression level was at the threshold level, additional promoter transactivation assays were carried out that did not confirm a (direct) up-regulation of MIA target genes (**Supplementary Figure 2F**). Altogether the results from the screening suggested that only the ORCA TFs (CRO_T110359, CRO_T110361, and CRO_T110364) and clade IVa bHLH TFs (CRO_T123350, CRO_T105905, and CRO_T107533) reproducibly led to an increase in MIA biosynthesis gene expression levels (**Supplementary Figures 1**, **2** and below).

The *Iridoid* Regulatory Module: Identification of an Additional *BIS* Paralog That Clusters With *BIS1* and *2*

Overexpression of the three newly identified iridoid pathway co-expressed (**Figure 2**) clade IVa bHLHs (CRO_T123350, CRO_T105905, and CRO_T107533) led to enhanced expression of the iridoid genes, albeit to very different levels (**Figure 3A**). Only overexpression of CRO_T107533 (referred to as *BIS3* hereafter) led to increases in *iridoid pathway* transcript levels (28- to 480-fold) similar to overexpression of *BIS1* and *2* in our previous study (Van Moerkercke et al., 2016). This high up-regulation of iridoid pathway genes by BIS1, 2, and 3 in comparison to the CRO_T123350 and CRO_T105905 was further confirmed by promoter transactivation assays in transient expression assays in *N. tabacum* (tobacco) protoplasts on (**Figure 3B**). We did not observe consistent differential or synergistic effects of combinations of the three BIS on iridoid pathway gene promoters (**Supplementary Figure 3**), suggesting that homo- or heterodimers of BIS1/2/3 have similar transactivation capacities and specificities. A ClustalW alignment of the highly conserved bHLH domains of the five clade IVa factors reveals a higher level of sequence identity between the three BIS (BIS2 and 3 bHLH sequences are identical) compared to CRO_T123350 and CRO_T105905 (**Figure 3C**). Noteworthy, all three *BIS* TFs cluster within a 120-kb locus in the genome and are probably the result of recent tandem gene duplication events (**Figure 3D**). This was previously not known but could now be detected because of the recent update (v2) of the *C. roseus* genome (see text footnote 1).

The ORCA Cluster: Functional Diversification Into Branch-Specific Regulatory Modules

In addition to the long-known *ORCA2* and *3*, *ORCA4*, *5*, and *6* have recently been found to be members of a gene cluster together with *ORCA3*, and their target gene profile has partly been elucidated (Paul et al., 2016, 2020). All ORCA TFs together form a cluster spreading over 70 kb, which can be subdivided into an ORCA3, 4, and 5 subcluster (around 25 kb)

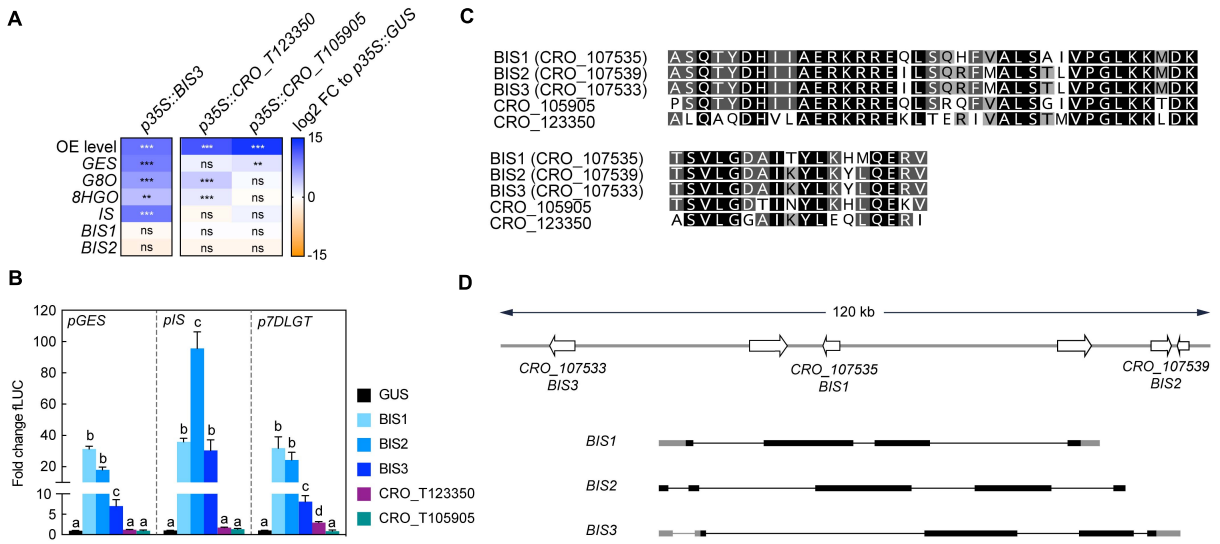

FIGURE 3 | BIS3 up-regulates iridoid pathway genes. **(A)** Overexpression of *BIS3* leads to increased expression levels of iridoid pathway genes similar to those previously observed for *BIS1* and *2*, whereas overexpression of the other clade IVa TFs CRO_T123350 and CRO_T105905 leads to comparably much lower increases. *BIS1* and *2* themselves are not up-regulated by BIS3, suggesting that the iridoid pathway up-regulation is directly caused by BIS3 and that there is no cross up-regulation between the three BIS TFs. Asterisks indicate statistically significant differences in expression (**$P < 0.01$, ***$P < 0.01$) as calculated by Student's *t*-test for each gene compared to GUS control (not included in this graph). **(B)** *N. tabacum* protoplasts were co-transfected with constructs containing the *firefly luciferase* gene (*fLUC*) expressed under control of the indicated promoter fragments and constructs for overexpression of *bHLHs* as indicated or *GUS* as a control. The *y*-axis shows fold change in normalized fLUC activity relative to the control transfection with GUS, set at 1. The error bars depict SEM of four biological replicates. For each promoter, columns labeled with different letters represent statistically significant differences ($P < 0.05$, ANOVA with Tukey's correction for multiple comparisons). BIS1-3 redundantly highly transactivate iridoid pathway promoters whereas CRO_T123350 and CRO_T105905 have no effect. **(C)** A MUSCLE alignment of the bHLH domain protein sequences reveals a high level of sequence identity between the five clade IVa bHLHs. However, BIS1, 2 and 3 show a slightly higher level of identity than CRO_T123350 and CRO_T105905 potentially explaining the differential level of up-regulation of iridoid pathway genes. Sites that are identical in all five sequences are colored in black; sites identical in four out of five sequences are colored in dark gray and sites identical in 3 out of 5 sequences are colored in light gray. **(D)** The latest version of the *C. roseus* genome revealed that the previously published BIS1 and 2, and BIS3 identified in this study, are all located in close proximity and have similarly organized gene structures suggesting that they probably arose from recent gene duplications. Exons are depicted as bars with untranslated regions (UTRs) in gray and CDS' in black. Introns are depicted as black lines.

and an ORCA2 and 6 subcluster (around 10 kb) (**Figure 4A**). A combination of different computational sequence analyses led us to hypothesize that the five ORCA TFs are possibly not fully functionally redundant. First, key amino acid residues (AARs) within the DNA-binding domain (DBD) differ between the ORCAs and are predicted to confer direct interaction with DNA differ (**Figure 5A**). Second, it is generally accepted that the activation domains (ADs) of TFs are mostly poorly conserved at sequence level, but it is rather the structural properties defining the level of activation (Staby et al., 2017). The combined information of different prediction programs suggested that the ORCA TFs differ significantly in their structural organization, further hinting toward a certain degree of diversification (**Supplementary Figure 4**). Third, ORCA3-5 contain a serine-rich C-terminal domain that ORCA2 and 6 lack. Fourth, the five ORCA TFs showed a differential expression profile (**Figure 4B** and **Supplementary Figure 5**) and our co-expression analysis revealed that they co-express with different subsets of MIA pathway genes (**Figure 2A**). Despite the occurrence of clusters of ORCA orthologs in other species, such as tomato and tobacco, it has not been systematically analyzed in any of these species if and to which level they are functionally redundant (Cárdenas et al., 2016; Kajikawa et al., 2017). Therefore, we sought out to decipher their specific regulatory roles by comparing their target gene and metabolite profile upon overexpression in flower petals. A PCA analysis of the MIA gene expression levels revealed that ORCA2-4 showed only partly overlapping target gene profiles (**Figure 4C**). Particularly the expression of early and intermediate MIA pathway genes increased to similar levels upon overexpression of ORCA2-4 (**Figure 4D**, for instance *SLS1*, *STR1*, *GS1*, *GS2*, *REDOX1*,*2*). However, in other cases, the fold changes differed considerably. For instance, *GO*, which encodes an enzyme producing the intermediate geissoschizine but also akuammicine (see **Figure 1A**), as well as the iridoid pathway genes including the regulator BIS1, were considerably more highly up-regulated upon overexpression of *ORCA4*, and to a lesser extent of *ORCA2* compared to overexpression of the other *ORCAs* (**Figure 4D**). Conversely, the *root MIA* genes *T19H* and *MAT* were more highly up-regulated when *ORCA3* was overexpressed. It should be noted that the overexpression level of the different *ORCA* paralogs differed considerably, with *ORCA3*, *4*, and *6* being highly overexpressed (around 510-, 440-, and 960-fold, respectively) and with *ORCA2* and in particular *ORCA5* somewhat less (93-, and 15-fold, respectively) overexpressed (**Figure 4D**). Thus, the overall lower MIA biosynthesis gene up-regulation levels observed for *ORCA5* overexpression might

be partly due to the lower overexpression level of *ORCA5*. We did not observe any "intra-cluster" up-regulation between the different ORCA TFs. We next performed metabolite profiling on samples from this experiment (**Figures 4F,G**, **Supplementary Figure 6** and **Supplementary Table 6**). A PCA analysis of the Mass spectrometry (MS) data revealed a (partially) differential profile (**Figure 4E**), which was caused by differential accumulation of MIA metabolites (**Figure 4F**). In addition to MIAs identified in a previous study (Schweizer et al., 2018), the loadings plot further showed differentially accumulating compounds that we identified as MIAs (**Figure 4F** (red), Supporting Dataset S2). In particular, akuammicine, 16-hydroxytabersonine and 16-hydroxylochnericine accumulation increased more when *ORCA4* was overexpressed and that of the root MIA derivative 16-methoxyhörhammericine when *ORCA3* was overexpressed (**Figure 4G**). Overexpression of *ORCA6* had only mild effects on MIA pathway gene expression and no noticeable effects on MIA abundance. Promoter transactivation assays in tobacco protoplasts with promoter fragments of *STR*, *GO*, *MAT*, and *TAT* expressed with and without the addition of CrMYC2a^{D126N} overall confirmed these observations (**Figure 6**). ORCA4 transactivated *pGO* to a much higher extent than the other ORCA TFs, whereas ORCA3 transactivated *pTAT* higher than other ORCAs, whereas *pSTR* was similarly transactivated by ORCA3, 4, and 5. Together, these data support both redundant and specific functions of the different ORCA TFs in the regulation of MIA biosynthesis.

Specific AARs Within ORCA DBDs Contribute to Target Gene Specificity

Generally, the DBD is thought to define the specificity to the DNA motif, whereas the AD defines the level of up-regulation by recruiting the transcriptional machinery. In a previous study, the affinities of different orthologs of group IXa AP2/ERFs, i.e., ORCA3 and its orthologs from tobacco and *Arabidopsis thaliana*, to the DNA motif were compared (Shoji et al., 2013). The results suggested that the specific binding affinity to different DNA motifs is indeed mediated by specific AARs in the DBD. However, specific AARs mediating target gene specificity among paralogs from the same species have never been characterized in detail to our knowledge. A protein sequence alignment of the DBDs of the ORCAs shows the expected overall high level of sequence conservation (**Figure 5A**). Likewise, structural models of the ORCA DBDs are almost identical and highly align with the solved structure (PDB 1gcc) of the Arabidopsis ortholog AtERF1 (Allen et al., 1998; **Figure 5B**). While the paralog-specific AARs corresponding to K101, P107, K110, and D117 in ORCA3 are not predicted to directly interact with DNA in the shown model, they are nevertheless predicted to be part of the beta-sheets in close proximity to the DNA (**Figure 5B**). To compare a potential impact of these AARs on MIA target gene specificity, we performed site-directed mutagenesis on ORCA3 to obtain single (K101R, P107L, K110R, K110T, and D117N) and double (K101R/P107L, K101R/K110R_K101R/K110T) mutants, whose sequence would correspond to that of the other paralogs. The mutated versions were then overexpressed alongside native *ORCA3* in flower petals in two independent infiltration series (**Figures 5C–F** and **Supplementary Figure 7**, respectively). Overall, our results pointed to two key AARs leading to changes in MIA target gene expression. Compared to overexpression of native *ORCA3*, overexpression of *ORCA3*^{K101R} (corresponding to an AAR change occurring in ORCA2, 4, 5, and 6) generally enhanced the expression of MIA pathway genes (**Figure 5C**, **Supplementary Figure 7**). By contrast, overexpression of *ORCA3*^{P107L} (corresponding to one of the AAR changes in ORCA4) led to reduced or abolished levels of MIA pathway genes that were partly recovered in the double mutant *ORCA3*^{K101RP107L} (corresponding to AARs in ORCA4) (**Figure 5C**). Noteworthy, overexpression of *ORCA3*^{K101RP107L} still led to a lower up-regulation of *root MIA* genes than *ORCA3* or *ORCA3*^{K101R}, suggesting that the combination of these two AARs contributes to the differential target gene profile of ORCA3 and 4. The impact of the other AARs appeared to be less specific. Overexpression of the *ORCA5*-like *ORCA3*^{K101RK110R} led to an expression profile similar to that upon overexpression of *ORCA3*^{K101R}. Also, the much lower level of MIA target gene up-regulation by ORCA6 compared to the other ORCAs was not explained by the selected AARs [compare the overexpression of *ORCA3*^{K101RK110T} (**Figure 5C**) and *ORCA3*^{D117N} (**Supplementary Figure 7**)]. However, we did not produce a triple mutant in which all three AARs would correspond to those of ORCA6. The observed differential target gene profiles upon overexpression of *ORCA3* mutants were also reflected at the metabolite level (**Figures 5D–F**, **Supplementary Figure 8** and **Supplementary Table 7**). Noteworthy, in particular the levels of 16-hydroxytabersonine, akuammicine, 16-methoxyhörhammericine and 16-hydroxylochnericine (among others) upon overexpression of *ORCA3* versus the ORCA2-like *ORCA3*^{K101R} and the ORCA4-like *ORCA3*^{K101RP107L} were very similar to those upon overexpression of the actual *ORCA2*, *3*, and *4* (**Figure 4G** and **Supplementary Figure 6**). We further performed transactivation assays with ORCA3, ORCA3^{K101R}, ORCA3^{P107L}, ORCA3^{K101RP107L}, and ORCA3^{K101K110R} on *pSTR*, *pGO*, *pTAT* and *pMAT* (**Figure 5G**). Similarly to what was observed in the flower petal overexpression experiments ORCA3^{K101R} appeared to have a higher overall transactivation effect than ORCA3 on the four promoters whereas the double mutant ORCA3^{K101RP107L} transactivated pGO at significantly higher levels than ORCA3 but not the other promoters.

Synergistic Up-Regulation in Combination With De-Repressed CrMYC2a^{D126N} Is Both ORCA- and Target Gene-Dependent

Previously, we have shown that combinatorial overexpression of *ORCA3* and the de-repressed *CrMYC2a*^{D126N} variant leads to a synergistic up-regulation in particular of the *root MIA genes* compared to independent overexpression (Schweizer et al., 2018). Based on this and our experiments above that suggest that the ORCA TFs to some extent up-regulate different subsets of MIA pathway genes, we next investigated whether the combined overexpression of *CrMYC2a*^{D126N}

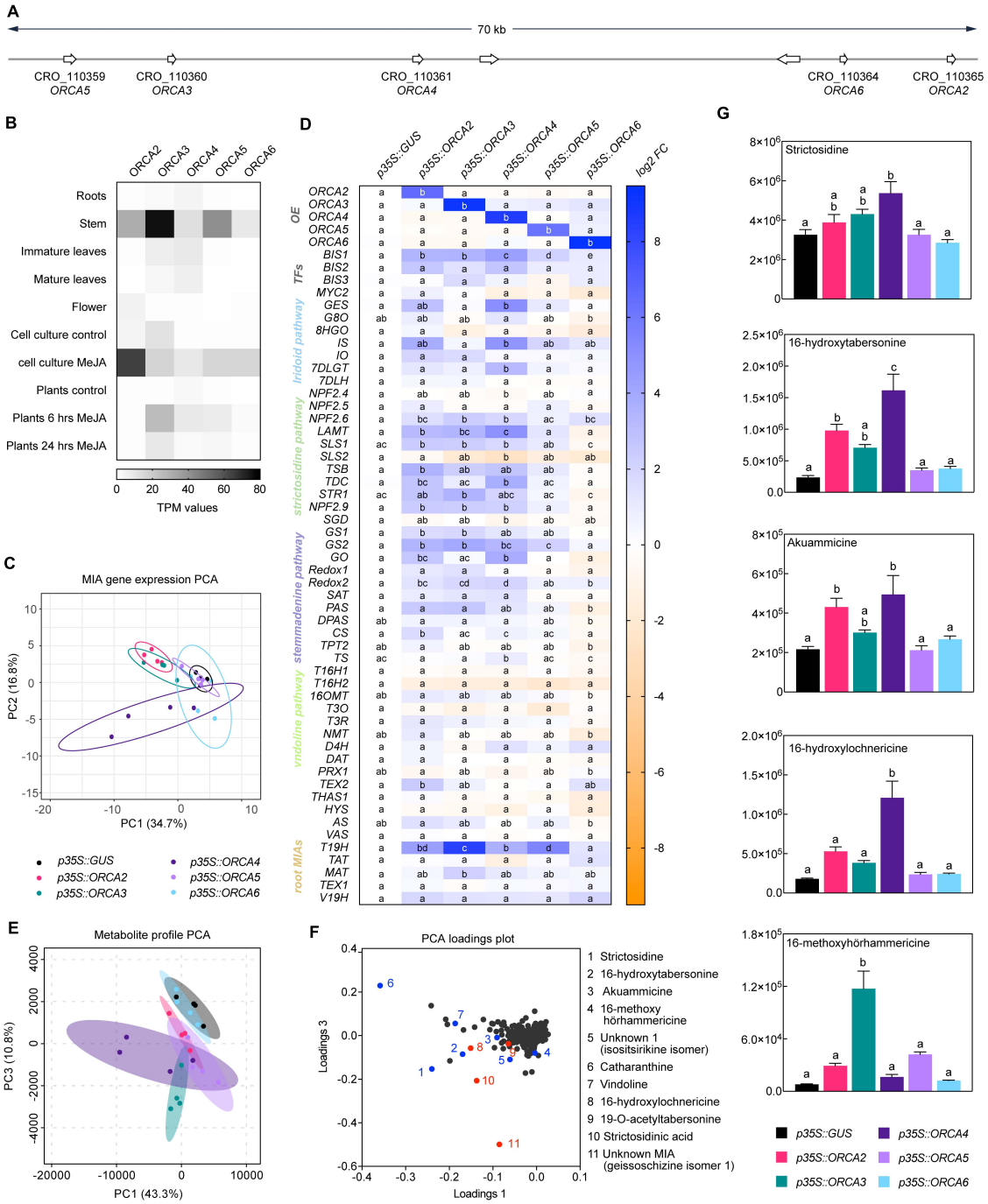

FIGURE 4 | Members of the ORCA TF cluster differentially up-regulate MIA biosynthesis genes. **(A)** Localization of the *ORCA* genes within the cluster. **(B)** Expression pattern of *ORCA* paralogs extracted from publicly available RNA-Seq data from indicated tissues and conditions. TPM, Transcripts Per Kilobase Million. **(C)** A PCA of MIA pathway genes measured by qPCR upon *ORCA* overexpression [shown in panel **(D)**] suggests overlapping but also differential MIA target gene expression patterns in particular between *ORCA2*, *3*, and *4*. PCA was performed with ClustVis (Metsalu and Vilo, 2015). **(D)** Expression of MIA biosynthesis genes measured by qPCR upon *ORCA* overexpression shown as log2 fold changes (FC) compared to the overexpression of *GUS* as a control. For each pathway gene, cells labeled with different letters represent statistically significant differences ($P < 0.05$, ANOVA with Tukey's correction for multiple comparisons). Note that the overexpression levels of *ORCA3*, *4*, and *6* were higher than those of *ORCA2* and *5*. **(E)** PCA of metabolite profiling data from *ORCA* overexpression samples. **(F)** Loading plot of the PCA shown in panel **(E)**, indicating that the differences found in the PCA are indeed predominantly caused by MIA metabolite levels. Selected known MIAs are labeled in blue; MIAs identified in this study (see Supporting Dataset S1) are labeled in red. **(G)** Levels of selected MIA metabolites expressed in average total ion current (TIC). The levels of all measured MIA metabolites can be found in the supporting information (**Supplementary Figure 6**; **Supplementary Table 6**). Columns labeled with different letters represent statistically significant differences ($P < 0.05$, ANOVA with Tukey's correction for multiple comparisons). Error bars are standard error of the mean (SEM) of four biological replicates.

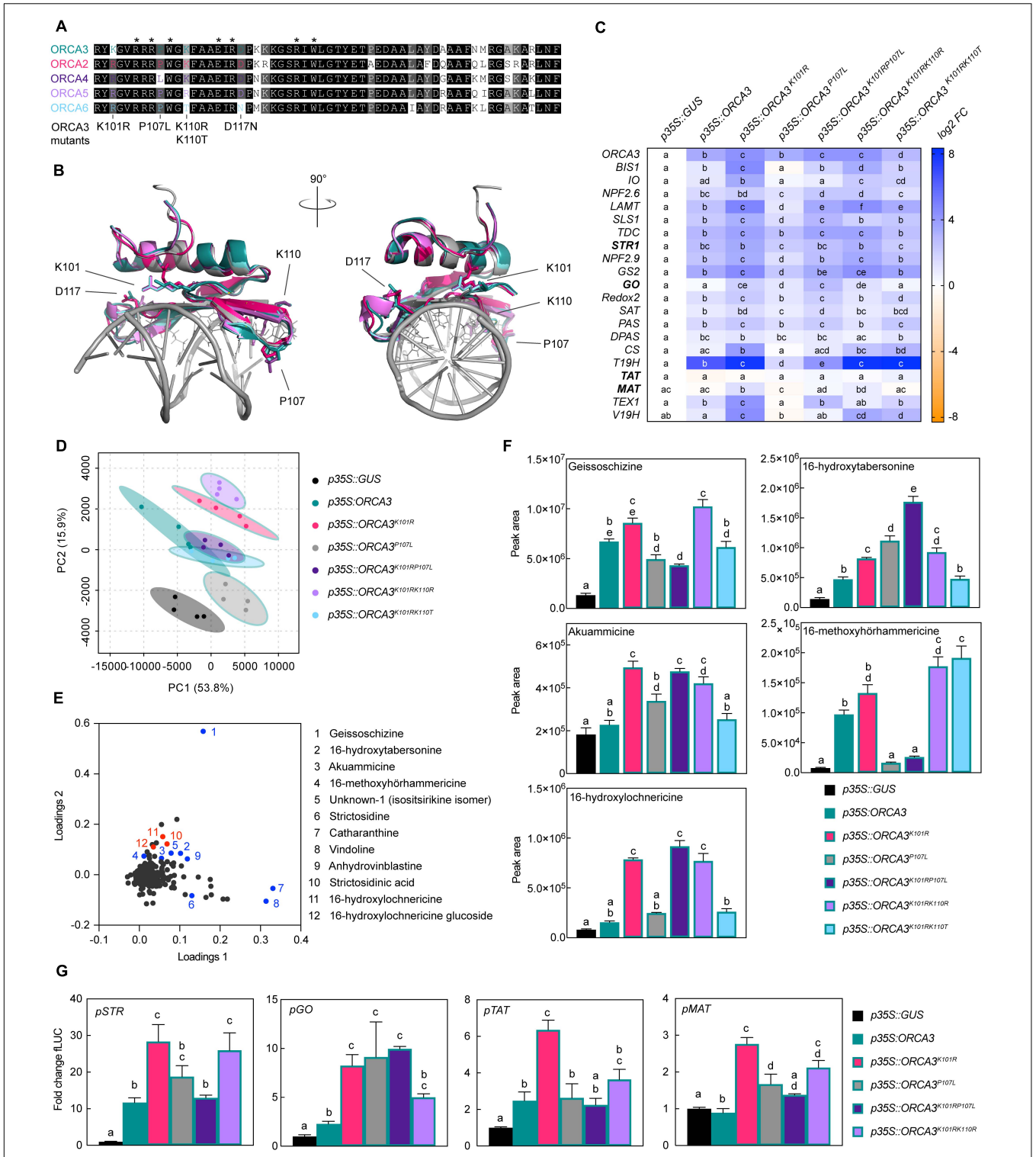

FIGURE 5 | Specific amino acid residues (AARs) in the DNA-binding domain (DBD) of ORCA TFs influence target gene specificity. **(A)** Alignment of the DBDs of ORCAs. AARs labeled with an asterisk were identified previously as directly interacting with the DNA based on the solved crystal structure of the *Arabidopsis* AP2/ERF member AtERF1 DBD (Allen et al., 1998; Shoji et al., 2013). ORCA3 was used as a template to exchange AARs so that they would correspond to AARs in other ORCA TFs. The respective mutated AARs are indicated below the alignment. **(B)** Homology models of ORCA DBDs. The models [made by Phyre2 "intensive mode" (Kelley et al., 2015); colored as in panel **(A)**] are overlaid with the AtERF1 structure bound to DNA (PDB 1GCC) colored in gray. AARs identified as directly interacting with the DNA [asterisks in panel **(A)**] are shown as lines of AtERF1. AARs differing in the ORCA DBDs and selected for site-directed mutagenesis are

(Continued)

FIGURE 5 | Continued
shown as sticks for all ORCA models, while the AAR numbering refers to ORCA3. The models suggest that the differing AARs are unlikely to interact directly with the DNA, but are in close proximity to the DNA and might thereby modulate DNA binding affinity. **(C)** Overexpression of *ORCA3* mutants in *C. roseus* flower petals and expression level of selected MIA target genes as measured by qPCR. Two AAR changes, K101R and P107L, seem to significantly modulate the MIA target gene profile. While K101R appears to increase the level of up-regulation, up-regulation is greatly reduced and in some cases nearly abolished when overexpressing the $ORCA3^{P107L}$ mutant. The double mutant $ORCA3^{K101RP107L}$, corresponding to the native ORCA4 sequence, recovers some activation potential, and reaches similar levels than observed upon overexpression of *ORCA4* (**Figure 4D**). This suggests that the combination of these AARs may account for the differences between ORCA3 and 4. For each pathway gene, cells labeled with different letters represent statistically significant differences ($P < 0.05$, ANOVA with Tukey's correction for multiple comparisons). Results from overexpression of all *ORCA3* single AAR mutants (including $ORCA3^{D117N}$) can be found in **Supplementary Figure 6**. **(D)** PCA of metabolite profiling data. **(E)** Loading plot indicating that sample separation shown in the PCA plot is largely due to changes in MIA metabolite levels. Selected known MIAs are labeled in blue; MIAs identified in this study are labeled in red. **(F)** Levels of selected MIA metabolites expressed in average total ion current (TIC). The levels of all measured MIA metabolites can be found in the supporting information (**Supplementary Figure 8**; **Supplementary Table 7**). Columns labeled with different letters represent statistically significant differences ($P < 0.05$, ANOVA with Tukey's correction for multiple comparisons). Error bars are standard error of the mean (SEM) of four biological replicates. **(G)** Transactivation assays of *pSTR*, *pGO*, *pTAT*, and *pMAT* performed in tobacco protoplasts. Columns labeled with different letters represent statistically significant differences ($P < 0.05$, ANOVA with Tukey's correction for multiple comparisons). Error bars are standard error of the mean (SEM) of four biological replicates.

with *ORCA2*, *4*, *5*, or *6* leads to a synergistic up-regulation of target genes similar as with *ORCA3* and if different subsets of MIA pathway genes would be up-regulated (**Figure 7A**). Indeed, a PCA depicted that in particular the combined overexpression of $CrMYC2a^{D126N}$ with *ORCA2*, *3*, or *4* led to differences in the overlapping MIA pathway gene expression profiles (**Figure 7B**). Accordingly, PCA analysis of the MS data (**Figure 7C**) revealed somewhat differential metabolite profiles for the combination of $CrMYC2a^{D126N}$ with these three *ORCA* genes rather than with *ORCA5* or *6*, or upon overexpression of $CrMYC2a^{D126N}$ alone; these changes were due to differential accumulation of MIAs (**Figure 7D**). With regard to synergistic effects, the combined overexpression of $CrMYC2a^{D126N}$ with *ORCA2* or *4*, synergistically up-regulated the *root MIA* genes, but to a lower extent than with *ORCA3* (**Figure 7A**). Accordingly, at the metabolite level, the *root MIAs* 19-hydroxytabersonine and 16-hydroxy-19-O-acetyltabersonine accumulated to much higher levels upon $CrMYC2a^{D126N}$/*ORCA3* overexpression than upon overexpression of any of the other combinations (**Figure 7E**). Notably, no synergistic, if anything an additive up-regulation was observed for *GO*, although it was up-regulated upon overexpression of $CrMYC2a^{D126N}$ and *ORCA4* alone (**Figures 4D**, **7A**). Likewise, the level of the respective metabolic product akuammicine was only less than 2-fold higher in the samples with combined overexpression of $CrMYC2a^{D126N}$ with *ORCA4*, compared to when $CrMYC2a^{D126N}$ was overexpressed alone (**Figure 7E**). These two observations suggest that the ORCA-CrMYC2a^{D126N} synergistic module is partly TF-dependent, i.e., more pronounced for ORCA3 and, moreover, target gene-dependent, i.e., specific to some of the *root MIA* genes. To further confirm these observations promoter transactivation assays on *pSTR*, *pGO*, *pTAT*, and *pMAT* were carried out (**Figure 6**). Synergistic transactivation occurred particularly in the case of the *root MIA* gene promoter *pTAT* in combination with ORCA3 but could not be confirmed for the other root MIA promoter *pMAT*. However, transactivation levels for *pMAT* were generally low and it is possible that the 2-kB fragment did not contain all necessary *cis* regulatory sites. We were unable to clone the promoter region of *T19H* in several attempts. Transactivation of *pGO* by CrMYC2a^{D126N} and ORCA4 was not synergistic, again as observed in overexpression in flower petals.

To gain more insight into how a synergistic up-regulation could be mediated at the molecular level and to possibly shift the subset of target genes of this synergy, we next made chimeric constructs. Here, we focused on *ORCA3* and *4*, because their level of overexpression was most similar and the level of up-regulation of target genes was the strongest for these two paralogs. In these chimeric constructs, the N-terminal AD of ORCA3 was fused to the C-terminal DBD of ORCA4 (ORCA3-ORCA4) and *vice versa* (ORCA4-ORCA3) (**Figure 8A**). Overexpression of these "*ORCA*-swaps" in combination with $CrMYC2a^{D126N}$ led to shifts in the up-regulation of root MIA genes (**Figure 8B**). Overexpression of *ORCA3-ORCA4* led to a 2 to 4 fold higher up-regulation of *root MIA genes* than overexpression of native *ORCA4*, whereas overexpression of *ORCA4-ORCA3* led to around 4-fold lower up-regulation than overexpression of native *ORCA3*. These results indicate that the AD of ORCA3 might at least in part be necessary for the synergistic up-regulation. On the other hand, overexpression of $CrMYC2a^{D126N}$/*ORCA3-ORCA4* did not lead to a higher up-regulation of *GO* than overexpression of $CrMYC2a^{D126N}$/*ORCA4*, further supporting the previous observation that the synergistic up-regulation is specific to *root MIA* genes, i.e., target gene specific.

Putative Cell-Specific Regulation of the *Vindoline* Branch

Data from the cell type-enriched transcriptomes pointed toward a number of epidermis-specific TFs that might be candidate regulators of the epidermis-specific expression of some MIA pathway genes (*strictosidine* and *stemmadenine* branches and parts of the *vindoline* branch and catharanthine biosynthesis). Among these potential candidates, two MYB TFs were highly expressed in the stem epidermis (**Supplementary Figure 10B**). Both MYB TFs, hereafter named MYB96 and MYB96b, appeared to be potential orthologs of AtMYB96 and 94 (**Supplementary Figure 10A**), which amongst others positively regulate cuticular wax biosynthesis genes in *Arabidopsis* (Seo et al., 2011; Lee and Suh, 2015; Lee et al., 2016). In a preliminary screen, both MYB TFs were found to transactivate the *T3R* promoter in tobacco protoplasts, albeit not additively (**Supplementary Figure 10C**).

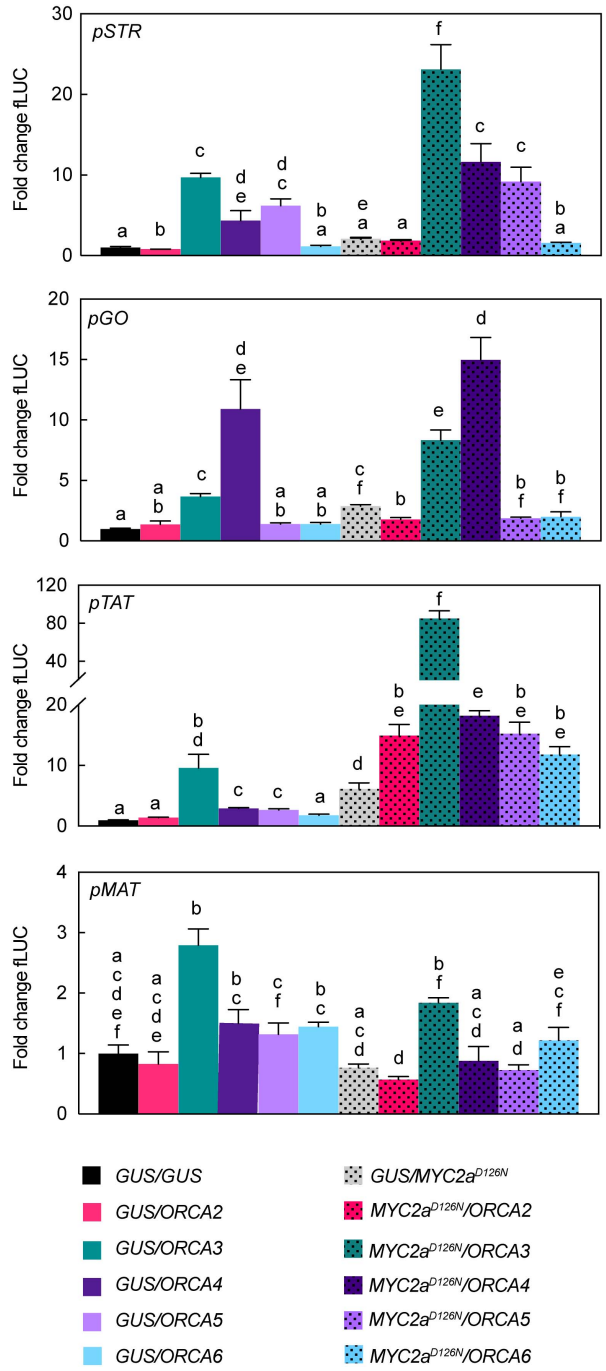

FIGURE 6 | Transactivation of *STR*, *GO*, *TAT*, and *MAT* promoter fragments by ORCAs and CrMYC2a^{D126N}. *N. tabacum* protoplasts were co-transfected with constructs containing the *fLUC* gene expressed under control of the indicated promoter fragments and constructs for overexpression of *ORCAs*, *CrMYC2a*^{D126N}, or *GUS* as a control. Note in particular differential transactivation of *pGO* and *pTAT* upon *ORCA3* versus *ORCA4* expression and synergistic effects on *pTAT* upon combined overexpression of *ORCA3* and *CrMYC2a*^{D126N} in combination. The *y*-axis shows fold change in normalized fLUC activity relative to the control transfection with GUS, set at 1. The error bars depict SEM of four biological replicates. For each promoter, columns labeled with different letters represent statistically significant differences ($P < 0.05$, ANOVA with Tukey's correction for multiple comparisons).

Overexpression of *MYB96* in flower petals also led to an up-regulation of expression of *T3R* and of a putative ortholog of the *Arabidopsis* cuticular wax biosynthesis gene *CER1*, but this was not the case for *MYB96b* (**Supplementary Figure 10D**). Nonetheless, the combined overexpression of *MYB96* and *MYB96b* led to a very small increase in catharanthine levels, which was not observed upon overexpression of *MYB96* alone (**Supplementary Figures 10G,H**). Notably however, because we neither detected any up-regulation of other *vindoline pathway* genes by *MYB96* (**Supplementary Figure 10D**) nor did MYB96 transactivate promoters of other vindoline pathway genes in tobacco protoplasts (**Supplementary Figure 10C**), MYB96 appears to be specific to *T3R*. In an attempt to enhance the vindoline content we further overexpressed *MYB96* in combination with the above-described *MYC2a*^{D126N}*-ORCA4* module, which led to a higher availability of the vindoline precursor 16-hydroxytabersonine (**Supplementary Figure 11**). We observed that overexpression of *MYB96*, in addition to the observed up-regulation of *T3R* and *CER1*, also led to a slight but statistically significant up-regulation (around 2-fold) of *stemmadenine pathway* genes and to a significant up-regulation of the catharanthine exporter gene *TPT2* (at least 4-fold) (**Supplementary Figure 11**). However, at the metabolite level, the overexpression of *MYB96* solely or in combination with *ORCA4* and/or *CrMYC2a*^{D126N} did not lead to increased vindoline or catharanthine content (**Supplementary Figure 11D** and **Supplementary Table 10**). Furthermore, it should be noted that overexpression of *CrMYC2a*^{D126} appeared to lead to a down-regulation of most vindoline pathway genes except *T3R* (**Supplementary Figure 11A**), further suggesting that a synergistic/additive action between these TFs seems unlikely.

DISCUSSION

While *C. roseus* is traditionally known as a medicinal plant, it is also increasingly being established as a model species for plant specialized metabolism in general. Thanks to the extensive work in the past decades by several labs, including ours, our knowledge about the network of MIA pathway branches represents one of the most detailed known biosynthesis networks of specialized metabolites, both at the enzyme and regulator level. In this study, we first aimed to identify new regulators for the different MIA branches, using the currently available pathway information. Thereby, we further underscore the importance of specific ORCA and bHLH TFs as modular regulatory hubs for different MIA pathway branches. While these TF families have been already generally implicated in the regulation of specialized metabolism, our study additionally provides evidence for the functional specialization of TF paralogs due to specific AAR changes in the DBD. These results are predominantly based on overexpression in flower petals. Despite being a powerful experimental system, it comes with the limitation that levels of overexpression of different TFs may differ and thus skew the results. By additionally performing promoter transactivation assays in tobacco protoplasts we were however able to generally confirm our results for a selection of available

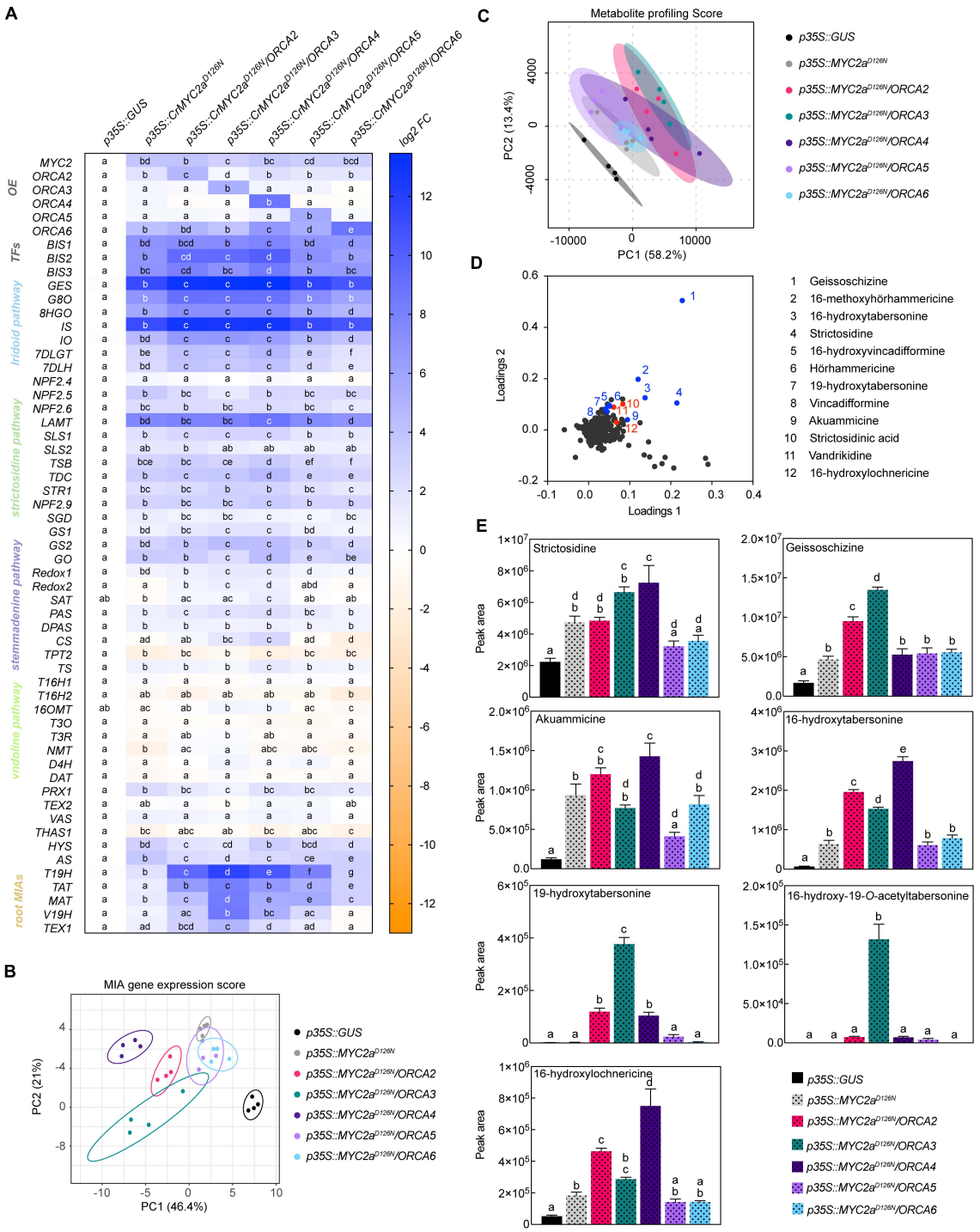

FIGURE 7 | Combinatorial overexpression of *CrMYC2a*^{D216N} and *ORCAs*. **(A)** Expression profile of MIA pathway genes and overexpression levels. For each pathway gene, cells labeled with different letters represent statistically significant differences ($P < 0.05$, ANOVA with Tukey's correction for multiple comparisons). Note that synergistic up-regulation of particularly root MIA genes is most pronounced by combinatorial overexpression of *CrMYC2a*^{D126N} and *ORCA3*. **(B)** PCA of the MIA gene expression data is suggesting that in particular the combinatorial overexpression of *CrMYC2a*^{D126N} and *ORCA2*, *3*, and *4* lead to differential changes in the MIA gene expression pattern, whereas combinatorial overexpression with *ORCA5* or *6* does not differ substantially from overexpression of *CrMYC2a*^{D126N} alone. PCA was performed with ClustVis (Metsalu and Vilo, 2015). **(C)** PCA of metabolite profiling data. **(D)** Loading plot of PCA with selected known MIAs (blue) and MIAs identified in this study (red). **(E)** Levels of selected MIA metabolites expressed in average total ion current (TIC). The levels of all measured MIA metabolites can be found in the supporting information (**Supplementary Figure 9**; **Supplementary Table 8**). Columns labeled with different letters represent statistically significant differences ($P < 0.05$, ANOVA with Tukey's correction for multiple comparisons). Error bars are standard error of the mean (SEM).

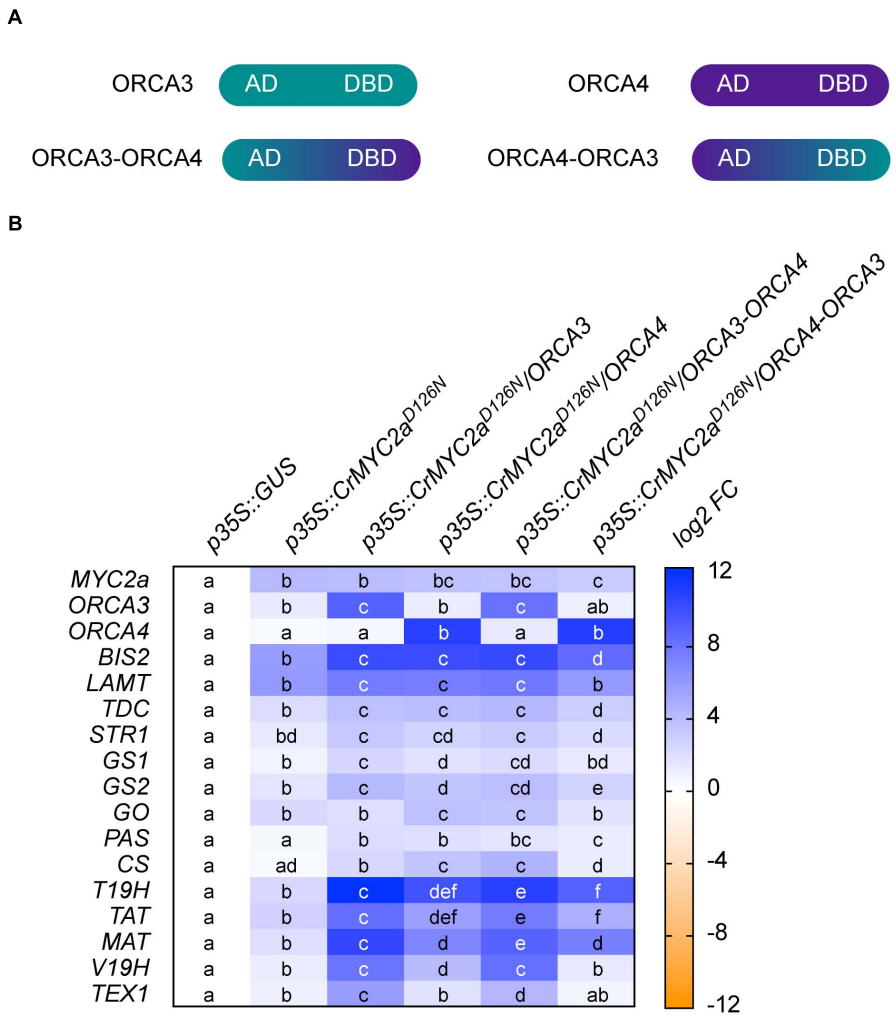

FIGURE 8 | Swapping of DNA-binding domain (DBD) and activation domain (AD) of ORCA3 and 4. In order to get insight into the role of the AD in the synergistic up-regulation of MIA target genes, the respective DBDs and ADs of ORCA3 and 4 were swapped. **(A)** Cartoon showing the domain organization of ORCA3 and 4 and the respective chimeric proteins. **(B)** Combinatorial overexpression of *CrMYC2a*^{D126N} with *ORCA3*, *4* or chimeric proteins *ORCA3-ORCA4* or *ORCA4-ORCA3*. These results suggest that the AD of ORCA3 improves the synergistic up-regulation of target genes. Cells labeled with different letters represent statistically significant differences ($P < 0.05$, ANOVA with Tukey's correction for multiple comparisons).

promoter fragments. In the future additional experiments such as individual knocking down of specific ORCAs by Virus Induced Gene Silencing (VIGS) (Liscombe and O'connor, 2011) or knocking out by genome editing could be performed to further clarify the specific roles of the different ORCAs.

Functional Redundancy and Diversification Among BIS and ORCA TF Clusters

Clusters of TF paralogs appear among various species and families; the orthologs of *ORCA* genes occur for instance also as gene clusters in tobacco, tomato and potato (Shoji et al., 2010; Cárdenas et al., 2016; Kajikawa et al., 2017; Shoji and Yuan, 2021) and so do the *Arabidopsis* BIS orthologs *bHLH18*, *19*, and *20* (Cui et al., 2018). Our findings indicate that redundancy and sub-functionalization may occur at the same time for different target genes. In case of the ORCA cluster, we observed that they activate those pathway genes necessary to synthesize common precursors, i.e., "early pathway genes" in a redundant manner. Conversely, later MIA pathway branches are then to some extent controlled by individual members. ORCA3, for instance, is more specific to some of the root MIAs and ORCA4 to the akuammicine branch. ORCA6 seems to have a rather limited impact on known MIA pathway genes, with the exception of a moderate up-regulation of the root MIA genes. The latter results are consistent with a recent study (Singh et al., 2020). These observations are similar to what has been described for the *Medicago truncatula* BIS orthologs, which redundantly activate early triterpene saponin biosynthesis genes but differentially activate downstream branches in the triterpene biosynthesis pathways and/or in different organs

(Mertens et al., 2016; Ribeiro et al., 2020). The members of the ORCA orthologous ERF gene clusters in tobacco and tomato also show differences with regard to their sequences and their tissue and environmental specific expression profiles (Shoji et al., 2010; Cárdenas et al., 2016; Kajikawa et al., 2017; Shoji and Yuan, 2021). It has been suggested that members of these ERF gene clusters acquired a level of sub-functionalization similar to what is found for the ORCAs (Shoji and Yuan, 2021). For instance, in the case of the tobacco ERF genes it was very recently shown that two members have more impact on nicotine biosynthesis than the other members further indicating sub-functionalization (Hayashi et al., 2020). Although more research is needed to unravel the specific roles of individual members of TF clusters in more species it is tempting to speculate that TF gene duplications resulting in clusters and subsequent sub-functionalization might be a common strategy for plants to achieve a more specific regulation of specialized metabolic pathway branches.

Specific AARs in the DBDs of ORCA TFs Modulate Target Gene Specificity

Despite increasing knowledge about the DNA binding motifs of different TF families, much less is known about the specific binding affinities of TFs belonging to the same clade. A previous study compared the differential DNA binding affinities of ORCA3 and its orthologs from different species and defined some AARs conferring DNA binding specificity (Shoji et al., 2013). Here, we specifically compare all members of clade XIa AP2/ERFs within the same species under the same experimental conditions and determine AARs conferring specificity that had not been identified previously. It will be interesting to further investigate whether similar AAR changes also confer target gene specialization in the other species with several paralogs and, moreover, determine paralog-specific DNA binding site sequences. Ultimately, further knowledge about such key AARs may offer more precise possibilities for metabolic engineering. For instance, the native version of a given TF might not be the most desirable one for flux into a specific pathway branch but an engineered version in which a key amino acid is substituted might do so. This smallest change for metabolic engineering purposes might be referred to as metabolic editing (Swinnen et al., 2019). Similarly, once the respective DNA binding motifs of a TF are known, specific target genes could be brought under control of that TF by promoter base editing (Swinnen et al., 2016).

MYC2-a Long-Known Hub With Remaining Mechanistic Mysteries

As described here and elsewhere, many MIA pathway genes are up-regulated by JA, which can be mimicked by overexpression of the de-repressed *CrMYC2a*^{D126N} (Schweizer et al., 2018). In addition, we have previously shown that the combinatorial overexpression with *ORCA3* leads to an up-regulation of the *root MIA pathway* genes and other target genes in a synergistic manner (Schweizer et al., 2018). A similar synergistic up-regulation of target genes has previously been observed between the respective tomato and tobacco MYC2 and AP2/ERF orthologs, suggesting an evolutionary conservation of this combinatorial TF module (De Boer et al., 2011; Cárdenas et al., 2016). Here, we observe that in *C. roseus* the synergistic transactivation is to some extent paralog specific, as the level of synergy is higher in combination with ORCA3 than with ORCA4 for instance. Although we cannot rule out that this is (in part) invoked by different protein stabilities, our results further suggest that this is at least in part due to the AD as we could observe that the AD of ORCA3 significantly enhanced the level of target gene up-regulation when fused to the DBD of ORCA4, whereas the reverse swap rather led to a reduced up-regulation. Although ADs are generally little conserved at the sequence level, it has been shown that specific structural features or subdomains are essential for the TF activity, for instance for the recruitment of the transcriptional machinery (Staby et al., 2017). Noteworthy, *in silico* analyses of the ORCA ADs predict structural differences, which further supports that they are diverse. It remains to be uncovered if and which of these structural differences confer the ORCA3-specific synergistic up-regulation of target genes and if this is for instance mediated by direct physical interaction between the TFs or by other mechanisms. Likewise, more investigation is needed to clarify how the synergistic up-regulation is restricted to specific target genes, i.e., the *root MIA* genes, whereas the up-regulation of other target genes, for instance the BIS TFs, does not appear synergistic.

Outlook: Touching the Boundaries of Co-expression Analysis as a Tool to Find Regulator Candidates

Co-expression analysis, which is based on the assumption that the expression profiles of functionally related genes correlate, remains one of the most popular and successful strategies to identify both metabolic pathway genes and regulatory TFs (Movahedi et al., 2012; Goossens, 2015; Wisecaver et al., 2017). However, it has also been noted previously that a successful outcome is greatly dependent on the combination of datasets included in the analysis, the specific methodology used and others (Goossens, 2015; Uygun et al., 2016). In the case of our study, there are a number of conceivable reasons, technical or mechanistic, why we were not able to unambiguously uncover regulators for all MIA branches yet, e.g., the *vindoline pathway*. First, the number of available expression datasets for *C. roseus* is still limited to around 80. Hence, if the pathway branch of interest does not show a (highly) differential expression profile among these datasets, the correlation with expression profiles of regulator candidates might be low. More specifically, the induction of regulatory TFs identified in past studies on *C. roseus* and of their target MIA pathway genes upon JA exposure is highly correlated because of the renowned amplification loops in the JA signaling cascade (De Geyter et al., 2012), which facilitated their discoveries. By contrast, the *vindoline pathway* is not induced upon JA exposure and, apart from a higher expression in green tissues, it is not differentially expressed otherwise. Hence, this pathway branch is either not differentially expressed in response to a specific environmental condition, or a discriminating RNA-Seq dataset for this hypothetical condition is not yet available.

Further, transcriptional regulation may involve independently acting TFs individually mediating the specific responses to environment, development, cell type and others. The expression of such a condition-related TF might thus only be strongly correlated to its MIA target genes in a subselection of datasets and not across all datasets. Mining of selected dataset combinations or application of a bi-clustering approach to identify significant co-expression in a subset of samples, could improve this and could be recommended for future co-expression analyses, but would possibly also yield a much longer list of candidates. Next, at the experimental level, it is possible that the candidate list indeed contains positive regulators but that (i) their cloning failed, (ii) they were not sufficiently overexpressed, (iii) their target gene induction required the combined action of TFs (analogous to the ORCA3-CrMYC2a^{D126N} module) but the respective TFs did not happen to be in the same co-overexpression group, (iv) they were not active in flower petals due to epigenetic or post-translational mechanisms.

Our study, together with the vast work previously published by different research groups extensively illustrates that MYC2 TFs globally up-regulate MIA biosynthesis together with the branch-specific ORCA and BIS TFs with the exception of the *vindoline* branch. This raises questions about the biological function of vindoline and/or the intermediates in this pathway branch. While MIA biosynthesis has been generally connected to defense against for instance caterpillars to some extent (Dugé De Bernonville et al., 2017), the chemical ecology of the different specific MIAs is largely unknown. The decoupled expression profile of the *vindoline pathway* from other MIA branches and the absence of up-regulation by CrMYC2a^{D126N} (rather a potential down-regulation) concomitant with a light-induced regulation raise the possibility of other or additional biological functions of vindoline. Nevertheless, the biosynthesis (and/or putative transport) of precursors must be assured, a process that appears not to be light regulated. It is clear that additional studies, likely not based on transcriptome mining solely, are therefore necessary to further investigate how these different signals are integrated to regulate flux through the distinct MIA pathway branches.

DATA AVAILABILITY STATEMENT

The datasets presented in this study can be found in online repositories. The names of the repository/repositories and accession number(s) can be found in the article/ **Supplementary Material**.

AUTHOR CONTRIBUTIONS

MC and AG designed the research and wrote the manuscript with consent from all other authors. MC performed the research and data analysis with contributions from DM, FS, LD, RD, JG, TM-C, FM-H, and MS. DV and KV performed RNA-Seq data and co-expression analysis and inferred candidate regulators. JP collected and analyzed metabolite data and performed compound identification. All authors contributed to the article and approved the submitted version.

FUNDING

MC and FS are indebted to the Swiss National Science Foundation (P300PA_177831 and P300PA_167772). This work was supported by European Union's Horizon 2020 Research and Innovation Program under Grant Agreement No 760331 (Newcotiana). This work was supported by the Agency for Innovation by Science and Technology (IWT) in Flanders (predoctoral fellowship to DV). JG is indebted to the Portuguese Fundação para a Ciência e Tecnologia (FCT) and FEDER Funds (SFRH/BD/97590/2013).

ACKNOWLEDGMENTS

We thank Robin Vanden Bossche for excellent technical assistance, Alex Van Moerkercke for generating the RNA-Seq data of transformed *C. roseus* hairy root lines and Annick Bleys for help with manuscript preparation.

SUPPLEMENTARY MATERIAL

The Supplementary Material for this article can be found online at: https://www.frontiersin.org/articles/10.3389/fpls.2021.687406/full#supplementary-material

Supplementary Figure 1 | MIA gene expression levels upon bulk overexpression of TF candidates.

Supplementary Figure 2 | Separate overexpression of positive TF candidates.

Supplementary Figure 3 | Promoter transactivation of iridoid pathway genes by combinations of BIS.

Supplementary Figure 4 | Comparison of structural features and motifs of ORCA activation domains (ADs).

Supplementary Figure 5 | Expression profiles of MIA biosynthesis genes and regulators in analyzed RNA-seq data.

Supplementary Figure 6 | MIA levels upon overexpression of *ORCAs*.

Supplementary Figure 7 | MIA gene expression levels upon overexpression of *ORCA3* single mutants.

Supplementary Figure 8 | MIA levels upon overexpression of *ORCA3* mutants.

Supplementary Figure 9 | MIA levels upon combinatorial overexpression of *CrMYC2a*^{D126N} and *ORCAs*.

Supplementary Figure 10 | Orthologs of cuticular wax regulators up-regulate the vindoline pathway gene *T3R*.

Supplementary Figure 11 | Combinatorial overexpression of *ORCA4, CrMYB96, CrMYC2a*^{D126N}.

Supplementary Table 1 | List of RNA-Seq datasets used.

Supplementary Table 2 | Oligonucleotide primers used for cloning of coding sequences.

Supplementary Table 3 | Oligonucleotide primers used for cloning of promoter fragments.

Supplementary Table 4 | List of all cloned TFs and promoter fragments and GeneBank IDs.

Supplementary Table 5 | Oligonucleotide primers used for qPCR.

Supplementary Table 6 | MIA levels upon overexpression of *ORCAs*.

Supplementary Table 7 | MIA levels upon overexpression of *ORCA3* mutants.

Supplementary Table 8 | MIA levels upon combinatorial overexpression of *CrMYC2a*^{D126N} and *ORCAs*.

Supplementary Table 9 | MIA levels upon overexpression of *MYB96/b*.

Supplementary Table 10 | MIA levels upon overexpression of *MYB96/b*, *CrMYC2a*^{D126N}, and *ORCA4*.

Supporting Dataset I | *C. roseus* expression atlas.

Supporting Dataset II | MIAs identified in this study.

REFERENCES

Aerts, R. J., Gisi, D., Decarolis, E., Deluca, V., and Baumann, T. W. (1994). Methyl jasmonate vapor increases the developmentally controlled synthesis of alkaloids in *Catharanthus* and *Cinchona* seedlings. *Plant J.* 5, 635–643. doi: 10.1111/j.1365-313X.1994.00635.x

Allen, M. D., Yamasaki, K., Ohme-Takagi, M., Tateno, M., and Suzuki, M. (1998). A novel mode of DNA recognition by a β-sheet revealed by the solution structure of the GCC-box binding domain in complex with DNA. *EMBO J.* 17, 5484–5496. doi: 10.1093/emboj/17.18.5484

Andrews, S. (2012). *FastQC: A quality control tool for high throughput sequence data. 3-5-12: Version 0.10.1*. Available Online at: (http://www.bioinformatics.babraham.ac.uk/projects/fastqc/)

Asada, K., Salim, V., Masada-Atsumi, S., Edmunds, E., Nagatoshi, M., Terasaka, K., et al. (2013). A 7-deoxyloganetic acid glucosyltransferase contributes a key step in secologanin biosynthesis in madagascar periwinkle. *Plant Cell.* 25, 4123–4134. doi: 10.1105/tpc.113.115154

Besseau, S., Kellner, F., Lanoue, A., Thamm, A. M. K., Salim, V., Schneider, B., et al. (2013). A pair of tabersonine 16-hydroxylases initiates the synthesis of vindoline in an organ-dependent manner in *Catharanthus roseus*. *Plant Physiol.* 163, 1792–1803. doi: 10.1104/pp.113.222828

Bolger, A. M., Lohse, M., and Usadel, B. (2014). Trimmomatic: a flexible trimmer for illumina sequence data. *Bioinformatics* 30, 2114–2120. doi: 10.1093/bioinformatics/btu170

Bray, N. L., Pimentel, H., Melsted, P., and Pachter, L. (2016). Near-optimal probabilistic RNA-seq quantification. *Nat. Biotechnol.* 34, 525–527. doi: 10.1038/nbt.3519

Caputi, L., Franke, J., Farrow, S. C., Chung, K., Payne, R. M. E., Nguyen, T.-D., et al. (2018). Missing enzymes in the biosynthesis of the anticancer drug vinblastine in madagascar periwinkle. *Science* 360, 1235–1239. doi: 10.1126/science.aat4100

Cárdenas, P. D., Sonawane, P. D., Pollier, J., Vanden Bossche, R., Dewangan, V., Weithorn, E., et al. (2016). GAME9 regulates the biosynthesis of steroidal alkaloids and upstream isoprenoids in the plant mevalonate pathway. *Nat. Commun.* 7:10654. doi: 10.1038/ncomms10654

Carqueijeiro, I., Dugé De Bernonville, T., Lanoue, A., Dang, T.-T., Teijaro, C. N., Paetz, C., et al. (2018a). A BAHD acyltransferase catalyzing 19-*O*-acetylation of tabersonine derivatives in roots of *Catharanthus roseus* enables combinatorial synthesis of monoterpene indole alkaloids. *Plant J.* 84, 469–484. doi: 10.1111/tpj.13868

Carqueijeiro, I. T., Brown, S., Chung, K., Dang, T.-T., Walia, M., Besseau, S., et al. (2018b). Two tabersonine 6,7-epoxidases start synthesis of lochnericine-type alkaloids in *Catharanthus roseus*. *Plant Physiol.* 177, 1473–1486. doi: 10.1104/pp.18.00549

Chini, A., Fonseca, S., Fernández, G., Adie, B., Chico, J. M., Lorenzo, O., et al. (2007). The JAZ family of repressors is the missing link in jasmonate signalling. *Nature* 448, 666–671. doi: 10.1038/nature06006

Chong, J., Soufan, O., Li, C., Caraus, I., Li, S., Bourque, G., et al. (2018). MetaboAnalyst 4.0: towards more transparent and integrative metabolomics analysis. *Nucleic Acids Res.* 46, W486–W494. doi: 10.1093/nar/gky310

Colinas, M., and Goossens, A. (2018). Combinatorial transcriptional control of plant specialized metabolism. *Trends Plant Sci.* 23, 324–336. doi: 10.1016/j.tplants.2017.12.006

Costa, M. M., Hilliou, F., Duarte, P., Pereira, L. G., Almeida, I., Leech, M., et al. (2008). Molecular cloning and characterization of a vacuolar class III peroxidase involved in the metabolism of anticancer alkaloids in *Catharanthus roseus*. *Plant Physiol.* 146, 403–417. doi: 10.1104/pp.107.107060

Courdavault, V., Papon, N., Clastre, M., Giglioli-Guivarc'h, N., St-Pierre, B., and Burlat, V. (2014). A look inside an alkaloid multisite plant: the *Catharanthus* logistics. *Curr. Opin. Plant Biol.* 19, 43–50. doi: 10.1016/j.pbi.2014.03.010

Cui, Y., Chen, C.-L., Cui, M., Zhou, W.-J., Wu, H.-L., and Ling, H.-Q. (2018). Four IVa bHLH transcription factors are novel interactors of fit and mediate JA inhibition of iron uptake in *Arabidopsis*. *Mol. Plant* 11, 1166–1183. doi: 10.1016/j.molp.2018.06.005

Dang, T.-T. T., Franke, J., Carqueijeiro, I. S. T., Langley, C., Courdavault, V., and O'connor, S. E. (2018). Sarpagan bridge enzyme has substrate-controlled cyclization and aromatization modes. *Nat. Chem. Biol.* 14, 760–763. doi: 10.1038/s41589-018-0078-4

De Boer, K., Tilleman, S., Pauwels, L., Vanden Bossche, R., De Sutter, V., Vanderhaeghen, R., et al. (2011). Apetala2/Ethylene response factor and basic helix-loop-helix tobacco transcription factors cooperatively mediate jasmonate-elicited nicotine biosynthesis. *Plant J.* 66, 1053–1065. doi: 10.1111/j.1365-313X.2011.04566.x

De Geyter, N., Gholami, A., Goormachtig, S., and Goossens, A. (2012). Transcriptional machineries in jasmonate-elicited plant secondary metabolism. *Trends Plant Sci.* 17, 349–359. doi: 10.1016/j.tplants.2012.03.001

Dugé De Bernonville, T., Carqueijeiro, I., Lanoue, A., Lafontaine, F., Sánchez Bel, P., Liesecke, F., et al. (2017). Folivory elicits a strong defense reaction in *Catharanthus roseus*: metabolomic and transcriptomic analyses reveal distinct local and systemic responses. *Sci. Rep.* 7:40453. doi: 10.1038/srep40453

Dugé De Bernonville, T., Clastre, M., Besseau, S., Oudin, A., Burlat, V., Glévarec, G., et al. (2015). Phytochemical genomics of the madagascar periwinkle: unravelling the last twists of the alkaloid engine. *Phytochemistry* 113, 9–23. doi: 10.1016/j.phytochem.2014.07.023

Geu-Flores, F., Sherden, N. H., Courdavault, V., Burlat, V., Glenn, W. S., Wu, C., et al. (2012). An alternative route to cyclic terpenes by reductive cyclization in iridoid biosynthesis. *Nature* 492, 138–142. doi: 10.1038/nature11692

Giddings, L.-A., Liscombe, D. K., Hamilton, J. P., Childs, K. L., Dellapenna, D., Buell, C. R., et al. (2011). A stereoselective hydroxylation step of alkaloid biosynthesis by a unique cytochrome P450 in *Catharanthus roseus*. *J. Biol. Chem.* 286, 16751–16757. doi: 10.1074/jbc.M111.225383

Goossens, A. (2015). It is easy to get huge candidate gene lists for plant metabolism now, but how to get beyond? *Mol. Plant* 8, 2–5. doi: 10.1016/j.molp.2014.08.001

Goossens, J., Fernández-Calvo, P., Schweizer, F., and Goossens, A. (2016). Jasmonates: signal transduction components and their roles in environmental stress responses. *Plant Mol. Biol.* 91, 673–689. doi: 10.1007/s11103-016-0480-9

Goossens, J., Mertens, J., and Goossens, A. (2017). Role and functioning of bHLH transcription factors in jasmonate signalling. *J. Exp. Bot.* 68, 1333–1347. doi: 10.1093/jxb/erw440

Guirimand, G., Guihur, A., Poutrain, P., Héricourt, F., Mahroug, S., St-Pierre, B., et al. (2011). Spatial organization of the vindoline biosynthetic pathway in *Catharanthus roseus*. *J. Plant Physiol.* 168, 549–557. doi: 10.1016/j.jplph.2010.08.018

Hayashi, S., Watanabe, M., Kobayashi, M., Tohge, T., Hashimoto, T., and Shoji, T. (2020). Genetic manipulation of transcriptional regulators alters nicotine biosynthesis in tobacco. *Plant Cell Physiol.* 61, 1041–1053. doi: 10.1093/pcp/pcaa036

Hellemans, J., Mortier, G., De Paepe, A., Speleman, F., and Vandesompele, J. (2007). qBase relative quantification framework and software for management and automated analysis of real-time quantitative PCR data. *Genome Biol.* 8:R19. doi: 10.1186/gb-2007-8-2-r19

Kajikawa, M., Sierro, N., Kawaguchi, H., Bakaher, N., Ivanov, N. V., Hashimoto, T., et al. (2017). Genomic insights into the evolution of the nicotine biosynthesis pathway in tobacco. *Plant Physiol.* 174, 999–1011. doi: 10.1104/pp.17.00070

Karimi, M., Inzé, D., and Depicker, A. (2002). GATEWAY^{TM} vectors for *Agrobacterium*-mediated plant transformation. *Trends Plant Sci.* 7, 193–195. doi: 10.1016/S1360-1385(02)02251-3

Kelley, L. A., Mezulis, S., Yates, C. M., Wass, M. N., and Sternberg, M. J. E. (2015). The Phyre2 web portal for protein modeling, prediction and analysis. *Nat. Protoc.* 10, 845–858. doi: 10.1038/nprot.2015.053

Kellner, F., Kim, J., Clavijo, B. J., Hamilton, J. P., Childs, K. L., Vaillancourt, B., et al. (2015). Genome-guided investigation of plant natural product biosynthesis. *Plant J.* 82, 680–692. doi: 10.1111/tpj.12827

Laflamme, P., St-Pierre, B., and De Luca, V. (2001). Molecular and biochemical analysis of a madagascar periwinkle root-specific minovincinine-19-hydroxy-O-acetyltransferase. *Plant Physiol.* 125, 189–198. doi: 10.1104/pp.125.1.189

Larsen, B., Fuller, V. L., Pollier, J., Van Moerkercke, A., Schweizer, F., Payne, R., et al. (2017). Identification of iridoid glucoside transporters in *Catharanthus roseus*. *Plant Cell Physiol.* 58, 1507–1518. doi: 10.1093/pcp/pcx097

Lee, S. B., Kim, H. U., and Suh, M. C. (2016). MYB94 and MYB96 additively activate cuticular wax biosynthesis in arabidopsis. *Plant Cell. Physiol.* 57, 2300–2311. doi: 10.1093/pcp/pcw147

Lee, S. B., and Suh, M. C. (2015). Cuticular wax biosynthesis is up-regulated by the MYB94 transcription factor in arabidopsis. *Plant Cell Physiol.* 56, 48–60. doi: 10.1093/pcp/pcu142

Levac, D., Murata, J., Kim, W. S., and De Luca, V. (2008). Application of carborundum abrasion for investigating the leaf epidermis: molecular cloning of *Catharanthus roseus* 16-hydroxytabersonine-16-*O*-methyltransferase. *Plant J.* 53, 225–236. doi: 10.1111/j.1365-313X.2007.03337.x

Liscombe, D. K., and O'connor, S. E. (2011). A virus-induced gene silencing approach to understanding alkaloid metabolism in *Catharanthus roseus*. *Phytochemistry* 72, 1969–1977. doi: 10.1016/j.phytochem.2011.07.001

Liscombe, D. K., Usera, A. R., and O'connor, S. E. (2010). Homolog of tocopherol C methyltransferases catalyzes *N* methylation in anticancer alkaloid biosynthesis. *Proc. Natl. Acad. Sci. USA* 107, 18793–18798. doi: 10.1073/pnas.1009003107

Liu, J., Cai, J., Wang, R., and Yang, S. (2017). Transcriptional regulation and transport of terpenoid indole alkaloid in *Catharanthus roseus*: exploration of new research directions. *Int. J. Mol. Sci.* 18:53. doi: 10.3390/ijms18010053

Liu, Y., Patra, B., Pattanaik, S., Wang, Y., and Yuan, L. (2019). GATA and phytochrome interacting factor transcription factors regulate light-induced vindoline biosynthesis in *Catharanthus roseus*. *Plant Physiol.* 180, 1336–1350. doi: 10.1104/pp.19.00489

Menke, F. L. H., Champion, A., Kijne, J. W., and Memelink, J. (1999). A novel jasmonate- and elicitor-responsive element in the periwinkle secondary metabolite biosynthetic gene *Str* interacts with a jasmonate- and elicitor-inducible AP2-domain transcription factor, ORCA2. *EMBO J.* 18, 4455–4463. doi: 10.1093/emboj/18.16.4455

Mertens, J., Pollier, J., Vanden Bossche, R., Lopez-Vidriero, I., Franco-Zorrilla, J. M., and Goossens, A. (2016). The bHLH transcription factors TSAR1 and TSAR2 regulate triterpene saponin biosynthesis in *Medicago truncatula*. *Plant Physiol.* 170, 194–210. doi: 10.1104/pp.15.01645

Metsalu, T., and Vilo, J. (2015). ClustVis: a web tool for visualizing clustering of multivariate data using principal component analysis and heatmap. *Nucleic Acids Res.* 43, W566–W570. doi: 10.1093/nar/gkv468

Miettinen, K., Dong, L., Navrot, N., Schneider, T., Burlat, V., Pollier, J., et al. (2014). The seco-iridoid pathway from *Catharanthus roseus*. *Nat. Commun.* 5:3606. doi: 10.1038/ncomms4606

Movahedi, S., Van Bel, M., Heyndrickx, K. S., and Vandepoele, K. (2012). Comparative co-expression analysis in plant biology. *Plant Cell Environ.* 35, 1787–1798. doi: 10.1111/j.1365-3040.2012.02517.x

Pan, Y.-J., Lin, Y.-C., Yu, B.-F., Zu, Y.-G., Yu, F., and Tang, Z.-H. (2018). Transcriptomics comparison reveals the diversity of ethylene and methyl-jasmonate in roles of TIA metabolism in *Catharanthus roseus*. *BMC Genom.* 19:508. doi: 10.1186/s12864-018-4879-3

Paul, P., Singh, S. K., Patra, B., Liu, X., Pattanaik, S., and Yuan, L. (2020). Mutually regulated AP2/ERF gene clusters modulate biosynthesis of specialized metabolites in plants. *Plant Physiol.* 182, 840–856. doi: 10.1104/pp.19.00772

Paul, P., Singh, S. K., Patra, B., Sui, X., Pattanaik, S., and Yuan, L. (2016). A differentially regulated AP2/ERF transcription factor gene cluster acts downstream of a MAP kinase cascade to modulate terpenoid indole alkaloid biosynthesis in *Catharanthus roseus*. *New Phytol.* 213, 1107–1123. doi: 10.1111/nph.14252

Pollier, J., Vanden Bossche, R., Rischer, H., and Goossens, A. (2014). Selection and validation of reference genes for transcript normalization in gene expression studies in *Catharanthus roseus*. *Plant Physiol. Biochem.* 83, 20–25. doi: 10.1016/j.plaphy.2014.07.004

Qu, Y., Easson, M. E. A. M., Simionescu, R., Hajicek, J., Thamm, A. M. K., Salim, V., et al. (2018). Solution of the multistep pathway for assembly of corynanthean, strychnos, iboga, and aspidosperma monoterpenoid indole alkaloids from 19*E*-geissoschizine. *Proc. Natl. Acad. Sci. USA* 115, 3180–3185. doi: 10.1073/pnas.1719979115

Qu, Y., Easson, M. L. A. E., Froese, J., Simionescu, R., Hudlicky, T., De Luca, V., et al. (2015). Completion of the seven-step pathway from tabersonine to the anticancer drug precursor vindoline and its assembly in yeast. *Proc. Natl. Acad. Sci. USA* 112, 6224–6229. doi: 10.1073/pnas.1501821112

Qu, Y., Safonova, O., and Luca, V. (2019). Completion of the canonical pathway for assembly of anticancer drugs vincristine/vinblastine in *Catharanthus roseus*. *Plant J.* 97, 257–266. doi: 10.1111/tpj.14111

Ribeiro, B., Lacchini, E., Bicalho, K. U., Mertens, J., Arendt, P., Vanden Bossche, R., et al. (2020). A seed-specific regulator of triterpene saponin biosynthesis in *Medicago truncatula*. *Plant Cell* 32, 2020–2042. doi: 10.1105/tpc.19.00609

Roepke, J., Salim, V., Wu, M., Thamm, A. M. K., Murata, J., Ploss, K., et al. (2010). Vinca drug components accumulate exclusively in leaf exudates of madagascar periwinkle. *Proc. Natl. Acad. Sci. USA* 107, 15287–15292. doi: 10.1073/pnas.0911451107

Salim, V., Wiens, B., Masada-Atsumi, S., Yu, F., and De Luca, V. (2014). 7-deoxyloganetic acid synthase catalyzes a key 3 step oxidation to form 7-deoxyloganetic acid in *Catharanthus roseus* iridoid biosynthesis. *Phytochemistry* 101, 23–31. doi: 10.1016/j.phytochem.2014.02.009

Schweizer, F., Colinas, M., Pollier, J., Van Moerkercke, A., Vanden Bossche, R., De Clercq, R., et al. (2018). An engineered combinatorial module of transcription factors boosts production of monoterpenoid indole alkaloids in *Catharanthus roseus*. *Metab. Eng.* 48, 150–162. doi: 10.1016/j.ymben.2018.05.016

Seo, P. J., Lee, S. B., Suh, M. C., Park, M.-J., Go, Y. S., Park, C.-M., et al. (2011). The MYB96 transcription factor regulates cuticular wax biosynthesis under drought conditions in *Arabidopsis*. *Plant Cell* 23, 1138–1152. doi: 10.1105/tpc.111.083485

Shoji, T., Kajikawa, M., and Hashimoto, T. (2010). Clustered transcription factor genes regulate nicotine biosynthesis in tobacco. *Plant Cell* 22, 3390–3409. doi: 10.1105/tpc.110.078543

Shoji, T., Mishima, M., and Hashimoto, T. (2013). Divergent DNA-binding specificities of a group of ethylene response factor transcription factors involved in plant defense. *Plant Physiol.* 162, 977–990. doi: 10.1104/pp.113.217455

Shoji, T., and Yuan, L. (2021). ERF gene clusters: working together to regulate metabolism. *Trends Plant Sci.* 26, 23–32. doi: 10.1016/j.tplants.2020.07.015

Simkin, A. J., Miettinen, K., Claudel, P., Burlat, V., Guirimand, G., Courdavault, V., et al. (2013). Characterization of the plastidial geraniol synthase from madagascar periwinkle which initiates the monoterpenoid branch of the alkaloid pathway in internal phloem associated parenchyma. *Phytochemistry* 85, 36–43. doi: 10.1016/j.phytochem.2012.09.014

Singh, S. K., Patra, B., Paul, P., Liu, Y., Pattanaik, S., and Yuan, L. (2020). Revisiting the ORCA gene cluster that regulates terpenoid indole alkaloid biosynthesis in *Catharanthus roseus*. *Plant Sci.* 293:110408. doi: 10.1016/j.plantsci.2020.110408

Staby, L., O'shea, C., Willemoës, M., Theisen, F., Kragelund, B. B., and Skriver, K. (2017). Eukaryotic transcription factors: paradigms of protein intrinsic disorder. *Biochem. J.* 474, 2509–2532. doi: 10.1042/BCJ20160631

Stavrinides, A., Tatsis, E. C., Caputi, L., Foureau, E., Stevenson, C. E. M., Lawson, D. M., et al. (2016). Structural investigation of heteroyohimbine alkaloid synthesis reveals active site elements that control stereoselectivity. *Nat. Commun.* 7:12116. doi: 10.1038/ncomms12116

Stavrinides, A. K., Tatsis, E. C., Dang, T.-T., Caputi, L., Stevenson, C. E. M., Lawson, D. M., et al. (2018). Discovery of a short-chain dehydrogenase from *Catharanthus roseus* that produces a new monoterpene indole alkaloid. *Chem.BioChem.* 19, 940–948. doi: 10.1002/cbic.201700621

St-Pierre, B., and De Luca, V. (1995). A cytochrome P-450 monooxygenase catalyzes the first step in the conversion of tabersonine to vindoline in *Catharanthus roseus*. *Plant Physiol.* 109, 131–139. doi: 10.1104/pp.109.1.131

St-Pierre, B., Vazquez-Flota, F. A., and De Luca, V. (1999). Multicellular compartmentation of *Catharanthus roseus* alkaloid biosynthesis predicts intercellular translocation of a pathway intermediate. *Plant Cell* 11, 887–900. doi: 10.1105/tpc.11.5.887

Swinnen, G., Goossens, A., and Colinas, M. (2019). Metabolic editing: small measures, great impact. *Curr. Opin. Biotechnol.* 59, 16–23. doi: 10.1016/j.copbio.2019.02.002

Swinnen, G., Goossens, A., and Pauwels, L. (2016). Lessons from domestication: targeting *cis*-regulatory elements for crop improvement. *Trends Plant Sci.* 21, 506–515. doi: 10.1016/j.tplants.2016.01.014

Tatsis, E. C., Carqueijeiro, I., Dugé De Bernonville, T., Franke, J., Dang, T.-T., Oudin, A., et al. (2017). A three enzyme system to generate the *Strychnos* alkaloid scaffold from a central biosynthetic intermediate. *Nat. Commun.* 8:316. doi: 10.1038/s41467-017-00154-x

Uygun, S., Peng, C., Lehti-Shiu, M. D., Last, R. L., and Shiu, S.-H. (2016). Utility and limitations of using gene expression data to identify functional associations. *PLoS Comput. Biol.* 12:e1005244. doi: 10.1371/journal.pcbi.1005244

Van Bel, M., Proost, S., Van Neste, C., Deforce, D., Van De Peer, Y., and Vandepoele, K. (2013). TRAPID: an efficient online tool for the functional and comparative analysis of *de novo* RNA-Seq transcriptomes. *Genome Biol.* 14:R134. doi: 10.1186/gb-2013-14-12-r134

Van Der Fits, L., and Memelink, J. (2000). ORCA3, a jasmonate-responsive transcriptional regulator of plant primary and secondary metabolism. *Science* 289, 295–297. doi: 10.1126/science.289.5477.295

Van Der Fits, L., and Memelink, J. (2001). The jasmonate-inducible AP2/ERF-domain transcription factor ORCA3 activates gene expression via interaction with a jasmonate-responsive promoter element. *Plant J.* 25, 43–53. doi: 10.1046/j.1365-313x.2001.00932.x

Van Der Heijden, R., Jacobs, D. I., Snoeijer, W., Hallard, D., and Verpoorte, R. (2004). The *Catharanthus* alkaloids: pharmacognosy and biotechnology. *Curr. Med. Chem.* 11, 607–628. doi: 10.2174/0929867043455846

Van Moerkercke, A., Steensma, P., Gariboldi, I., Espoz, J., Purnama, P. C., Schweizer, F., et al. (2016). The basic helix-loop-helix transcription factor BIS2 is essential for monoterpenoid indole alkaloid production in the medicinal plant *Catharanthus roseus*. *Plant J.* 88, 3–12. doi: 10.1111/tpj.13230

Van Moerkercke, A., Steensma, P., Schweizer, F., Pollier, J., Gariboldi, I., Payne, R., et al. (2015). The bHLH transcription factor BIS1 controls the iridoid branch of the monoterpenoid indole alkaloid pathway in *Catharanthus roseus*. *Proc. Natl. Acad. Sci. USA* 112, 8130–8135. doi: 10.1073/pnas.1504951112

Vanden Bossche, R., Demedts, B., Vanderhaeghen, R., and Goossens, A. (2013). Transient expression assays in tobacco protoplasts. *Methods Mol. Biol.* 1011, 227–239. doi: 10.1007/978-1-62703-414-2_18

Vaneechoutte, D., and Vandepoele, K. (2019). Curse: building expression atlases and co-expression networks from public RNA-Seq data. *Bioinformatics* 35, 2880–2881. doi: 10.1093/bioinformatics/bty1052

Vom Endt, D., Soares, E., Silva, M., Kijne, J. W., Pasquali, G., and Memelink, J. (2007). Identification of a bipartite jasmonate-responsive promoter element in the *Catharanthus roseus ORCA3* transcription factor gene that interacts specifically with AT-hook DNA-binding proteins. *Plant Physiol.* 144, 1680–1689. doi: 10.1104/pp.107.096115

Wasternack, C., and Strnad, M. (2019). Jasmonates are signals in the biosynthesis of secondary metabolites — pathways, transcription factors and applied aspects — a brief review. *New Biotechnol.* 48, 1–11. doi: 10.1016/j.nbt.2017.09.007

Williams, D., Qu, Y., Simionescu, R., and De Luca, V. (2019). The assembly of (+)-vincadifformine- and (−)-tabersonine-derived monoterpenoid indole alkaloids in *Catharanthus roseus* involves separate branch pathways. *Plant J.* 99, 626–636. doi: 10.1111/tpj.14346

Wisecaver, J. H., Borowsky, A. T., Tzin, V., Jander, G., Kliebenstein, D. J., and Rokas, A. (2017). A global coexpression network approach for connecting genes to specialized metabolic pathways in plants. *Plant Cell* 29, 944–959. doi: 10.1105/tpc.17.00009

Yamamoto, K., Takahashi, K., Caputi, L., Mizuno, H., Rodriguez-Lopez, C. E., Iwasaki, T., et al. (2019). The complexity of intercellular localisation of alkaloids revealed by single-cell metabolomics. *New Phytol.* 224, 848–859. doi: 10.1111/nph.16138

Yamamoto, K., Takahashi, K., Mizuno, H., Anegawa, A., Ishizaki, K., Fukaki, H., et al. (2016). Cell-specific localization of alkaloids in *Catharanthus roseus* stem tissue measured with imaging MS and single-cell MS. *Proc. Natl. Acad. Sci. USA* 113, 3891–3896. doi: 10.1073/pnas.1521959113

Yu, F., and De Luca, V. (2013). ATP-binding cassette transporter controls leaf surface secretion of anticancer drug components in *Catharanthus roseus*. *Proc. Natl. Acad. Sci. USA* 110, 15830–15835. doi: 10.1073/pnas.1307504110

Zhang, H., Hedhili, S., Montiel, G., Zhang, Y., Chatel, G., Pré, M., et al. (2011). The basic helix-loop-helix transcription factor CrMYC2 controls the jasmonate-responsive expression of the *ORCA* genes that regulate alkaloid biosynthesis in *Catharanthus roseus*. *Plant J.* 67, 61–71. doi: 10.1111/j.1365-313X.2011.04575.x

Zhou, M., and Memelink, J. (2016). Jasmonate-responsive transcription factors regulating plant secondary metabolism. *Biotechnol. Adv.* 34, 441–449. doi: 10.1016/j.biotechadv.2016.02.004

Conflict of Interest: The authors declare that the research was conducted in the absence of any commercial or financial relationships that could be construed as a potential conflict of interest.

Citation: Colinas M, Pollier J, Vaneechoutte D, Malat DG, Schweizer F, De Milde L, De Clercq R, Guedes JG, Martínez-Cortés T, Molina-Hidalgo FJ, Sottomayor M, Vandepoele K and Goossens A (2021) Subfunctionalization of Paralog Transcription Factors Contributes to Regulation of Alkaloid Pathway Branch Choice in Catharanthus roseus. Front. Plant Sci. 12:687406. doi: 10.3389/fpls.2021.687406

Copyright © 2021 Colinas, Pollier, Vaneechoutte, Malat, Schweizer, De Milde, De Clercq, Guedes, Martínez-Cortés, Molina-Hidalgo, Sottomayor, Vandepoele and Goossens. This is an open-access article distributed under the terms of the Creative Commons Attribution License (CC BY). The use, distribution or reproduction in other forums is permitted, provided the original author(s) and the copyright owner(s) are credited and that the original publication in this journal is cited, in accordance with accepted academic practice. No use, distribution or reproduction is permitted which does not comply with these terms.

frontiers in Plant Science

ORIGINAL RESEARCH
published: 31 May 2021
doi: 10.3389/fpls.2021.688565

Deciphering OPDA Signaling Components in the Momilactone-Producing Moss *Calohypnum plumiforme*

Hideo Inagaki[1], Koji Miyamoto[1,2], Noriko Ando[2], Kohei Murakami[2], Koki Sugisawa[2], Shion Morita[2], Emi Yumoto[3], Miyu Teruya[4], Kenichi Uchida[1,2,3], Nobuki Kato[5], Takuya Kaji[5], Yousuke Takaoka[5], Yuko Hojo[6], Tomonori Shinya[6], Ivan Galis[6], Akira Nozawa[7], Tatsuya Sawasaki[7], Hideaki Nojiri[4,8], Minoru Ueda[5,9] and Kazunori Okada[4]*

[1] Graduate School of Science and Engineering, Teikyo University, Utsunomiya, Japan, [2] Department of Biosciences, Faculty of Science and Engineering, Teikyo University, Utsunomiya, Japan, [3] Advanced Instrumental Analysis Center, Teikyo University, Utsunomiya, Japan, [4] Agro-Biotechnology Research Center, Graduate School of Agricultural and Life Sciences, The University of Tokyo, Tokyo, Japan, [5] Graduate School of Science, Tohoku University, Sendai, Japan, [6] Institute of Plant Science and Resources, Okayama University, Kurashiki, Japan, [7] Proteo-Science Center, Ehime University, Matsuyama, Japan, [8] Collaborative Research Institute for Innovative Microbiology, The University of Tokyo, Tokyo, Japan, [9] Graduate School of Life Sciences, Tohoku University, Sendai, Japan

OPEN ACCESS

Edited by:
Koichi Sugimoto, University of Tsukuba, Japan

Reviewed by:
Isabel Monte, University of Zurich, Switzerland
Marcelo Lattarulo Campos, Federal University of Mato Grosso, Brazil

***Correspondence:**
Koji Miyamoto
miyamoto@nasu.bio.teikyo-u.ac.jp

Specialty section:
This article was submitted to Plant Metabolism and Chemodiversity, a section of the journal Frontiers in Plant Science

Received: *31 March 2021*
Accepted: *03 May 2021*
Published: *31 May 2021*

Citation:
Inagaki H, Miyamoto K, Ando N, Murakami K, Sugisawa K, Morita S, Yumoto E, Teruya M, Uchida K, Kato N, Kaji T, Takaoka Y, Hojo Y, Shinya T, Galis I, Nozawa A, Sawasaki T, Nojiri H, Ueda M and Okada K (2021) Deciphering OPDA Signaling Components in the Momilactone-Producing Moss Calohypnum plumiforme. Front. Plant Sci. 12:688565. doi: 10.3389/fpls.2021.688565

Jasmonic acid (JA) and its biologically active form jasmonoyl-L-isoleucine (JA-Ile) regulate defense responses to various environmental stresses and developmental processes in plants. JA and JA-Ile are synthesized from α-linolenic acids derived from membrane lipids *via* 12-oxo-phytodienoic acid (OPDA). In the presence of JA-Ile, the COI1 receptor physically interacts with JAZ repressors, leading to their degradation, resulting in the transcription of JA-responsive genes by MYC transcription factors. Although the biosynthesis of JA-Ile is conserved in vascular plants, it is not recognized by COI1 in bryophytes and is not biologically active. In the liverwort *Marchantia polymorpha*, dinor-OPDA (dn-OPDA), a homolog of OPDA with two fewer carbons, and its isomer dn-*iso*-OPDA accumulate after wounding and are recognized by COI1 to activate downstream signaling. The moss *Calohypnum plumiforme* produces the antimicrobial-specialized metabolites, momilactones. It has been reported that JA and JA-Ile are not detected in *C. plumiforme* and that OPDA, but not JA, can induce momilactone accumulation and the expression of these biosynthetic genes, suggesting that OPDA or its derivative is a biologically active molecule in *C. plumiforme* that induces chemical defense. In the present study, we investigated the biological functions of OPDA and its derivatives in *C. plumiforme*. Searching for the components potentially involving oxylipin signaling from transcriptomic and genomic data revealed that two *COI1*, three *JAZ*, and two *MYC* genes were present. Quantification analyses revealed that OPDA and its isomer *iso*-OPDA accumulated in larger amounts than dn-OPDA and dn-*iso*-OPDA after wounding. Moreover, exogenously applied OPDA, dn-OPDA, or dn-*iso*-OPDA induced the transcription of *JAZ* genes. These results imply that OPDA, dn-OPDA, and/or their isomers potentially act as biologically active molecules to induce the signaling downstream of COI1-JAZ. Furthermore, co-immunoprecipitation analysis showed the

physical interaction between JAZs and MYCs, indicating the functional conservation of JAZs in *C. plumiforme* with other plants. These results suggest that COI1-JAZ-MYC mediated signaling is conserved and functional in *C. plumiforme*.

Keywords: oxylipin, plant hormone, 12-oxo-phytodienoic acid, moss, *Calohypnum plumiforme*

INTRODUCTION

The phytohormone jasmonic acid (JA; **1**) and its biologically active form jasmonoyl-L-isoleucine (JA-Ile) regulate defense responses to various environmental stresses such as wounding, and plant growth and development (Wasternack and Hause, 2013; Wasternack, 2015; Guo et al., 2018; Ballaré and Austin, 2019). JA and JA-Ile are synthesized from fatty acids, α-linolenic acid or hexadecatrienoic acid, derived from membrane lipids. Oxygenation by lipoxygenase and dehydration-cyclization by allene oxide synthase and allene oxide cyclase (AOC) converts α-linolenic acid to 12-oxo-phytodienoic acid (OPDA; **2**). The double bond hydrogenation by OPDA reductase (OPR3) and three sequential β-oxidations convert OPDA to JA (Wasternack and Hause, 2013). Finally, the GH3 family protein JAR1 conjugates JA to isoleucine to produce the biologically active form (+)-7-*iso*-JA-Ile (Staswick and Tiryaki, 2004; Fonseca et al., 2009).

JA-Ile is recognized by the F-box protein COI1 (Xie et al., 1998; Yan et al., 2009; Sheard et al., 2010). JAZ proteins repress transcription factors such as MYC, which activate the transcription of JA-responsive genes, when JA-Ile is at low levels. In the presence of high JA-Ile levels, COI1 physically interacts with JAZ repressors, leading to their degradation, and the transcription of JA-responsive genes by MYC and other transcription factors (Chini et al., 2007; Thines et al., 2007).

Although its biosynthesis is conserved in vascular plants (Wasternack and Hause, 2013; Wasternack, 2015; Pratiwi et al., 2017), JA-Ile is not a biologically active form recognized by COI1 in bryophytes. In the liverwort *Marchantia polymorpha*, 2,3-dinor-OPDA (dn-OPDA; **3**) and its isomer 2,3-dinor-12-oxo-9(13),15(*Z*)-phytodienoic acid (dn-*iso*-OPDA; **4**) accumulate after wounding, whereas JA-Ile is not found. dn-OPDA and dn-*iso*-OPDA are recognized by MpCOI1 to activate downstream signaling (Monte et al., 2018). The model moss *Physcomitrium patens*, formerly known as *Physcomitrella patens*, also produces dn-OPDA and dn-*iso*-OPDA (Stumpe et al., 2010; Mukhtarova et al., 2020). Additionally, 12-oxo-9(13),15(*Z*)-phytodienoic acid (*iso*-OPDA; **5**) has been found in *P. patens*, but its biological activity has not been revealed (Mukhtarova et al., 2020). Comparative genomics and metabolomics suggest that dn-OPDA and dn-*iso*-OPDA might act as COI1 ligands in mosses (Monte et al., 2018; Mukhtarova et al., 2020).

The moss *Calohypnum plumiforme* like rice and barnyard grass produces specialized metabolites, momilactones, which have antimicrobial and allelochemical activities (Nozaki et al., 2007; Yamane, 2013; Miyamoto et al., 2014; Guo et al., 2017). These momilactone-producing plants possess the momilactone biosynthetic gene cluster, which is formed by the concentration of biosynthetic genes in a narrow region of the chromosome (Shimura et al., 2007; Guo et al., 2017; Mao et al., 2020). Therefore, the investigation of the regulatory mechanism(s) of momilactone production in *C. plumiforme* will contribute to a better understanding of the diversity and evolution of plant chemical defenses. Previous studies have revealed that JA and JA-Ile are not detected in *C. plumiforme* and that OPDA, but not JA, induces momilactone accumulation and the expression of these biosynthetic genes (Okada et al., 2016; Mao et al., 2020). These results suggest that OPDA or its derivative is a biologically active molecule in *C. plumiforme* that induces the production of momilactones.

In the present study, we focused on the function of OPDA and its derivatives and explored the potential involvement of protein components in oxylipin signaling in the moss *C. plumiforme*. We found two *COI1*, three *JAZ*, and two *MYC* genes from the transcriptome and genome data. The quantification of endogenous oxylipins revealed that OPDA and *iso*-OPDA accumulated in larger amounts than dn-OPDA and dn-*iso*-OPDA. We also found that exogenously applied OPDA, dn-OPDA, or dn-*iso*-OPDA induced the transcription of *JAZ* genes. Moreover, co-immunoprecipitation analysis revealed the physical interaction between JAZs and MYCs. These results imply that OPDA, dn-OPDA, and/or their isomers act as biologically active molecules to induce downstream signaling and that COI1-JAZ-MYC-mediated signaling is conserved in *C. plumiforme*.

MATERIALS AND METHODS

Plant Materials and Growth Conditions

Calohypnum plumiforme kindly provided by Prof. Kenichiro Hayashi (Okayama University of Science) was the same line as that used in a previous report (Okada et al., 2016). Gametophores were cultured on BCDATG agar medium under continuous white light at 23°C (Nishiyama et al., 2000), transferred to a new BCDATG agar medium every 2 months, and used for chemical and wounding treatments 1 month after each transfer.

Chemicals

Racemic JA was purchased from Tokyo Chemical Industry Co. (Tokyo, Japan) and used as a standard for quantification analysis. (–)-JA was prepared as previously described (Miyamoto et al., 2019) and used for the treatment of *C. plumiforme*. [$^2H_5$]-JA was obtained from Nacalai Tesque, Inc. (Kyoto, Japan). (–)-JA-Ile and [$^{13}C_6$]-JA-Ile were synthesized as previously described (Jikumaru et al., 2004).

OPDA and [$^2H_5$]-OPDA were purchased from Olchemim (Olomouc, Czechia Republic) and used as standards for

quantification analysis. For the treatment of *C. plumiforme*, OPDA and [$^2H_5$]-OPDA were synthesized from α-linolenic acid (FUJIFILM Wako Pure Chemical Co., Osaka, Japan) and [$^2H_5$]-α-linolenic acid (Cayman Chemical Company, MI, United States), respectively, as previously described with slight modifications (Zimmerman and Feng, 1978; Kajiwara et al., 2012). Briefly, the extracted protein fraction of flaxseed acetone powder supplemented with recombinant *Oryza sativa* AOC (OsAOC) was used for enzymatic conversion. Glutathione-*S*-transferase (GST)-fused OsAOC was expressed in *Escherichia coli* Rosetta2 (DE3) (Merck, Darmstadt, Germany) according to the manufacturer's instructions (Riemann et al., 2013), precipitated with ammonium sulfate and suspended in 50 mM potassium phosphate (pH 7.0). α-Linolenic acid and [$^2H_5$]-α-linolenic acid were suspended in 200 mM borate-NaOH buffer (pH 9.0) containing 5% (v/v) Tween 20, mixed with the extract of flaxseed acetone powder supplemented with recombinant GST-OsAOC, and incubated at 25°C for 150 min. The reaction was stopped by adding 1 N HCl to adjust the pH to 3.0–4.0, and the mixture was flushed with N_2 gas for 30 min. The products were extracted with ethyl acetate, dried using an evaporator, and dissolved in methanol.

iso-OPDA was synthesized as shown in **Scheme 1**. All chemical reagents and solvents for chemical synthesis of *iso*-OPDA were obtained from Kanto Chemical Co., FUJIFILM Wako Pure Chemical Co., Nacalai Tesque Co., Tokyo Chemical Industry Co. (Tokyo, Japan), Sigma-Aldrich Co. (MO, United States), and GE Healthcare (IL, United States) and used without further purification. All anhydrous solvents were either dried by standard techniques and freshly distilled before use or purchased in anhydrous form and used as supplied.

^{1}H and ^{13}C NMR spectra were recorded on a JNM–ECS–400 spectrometer (JEOL, Tokyo, Japan) in deuterated chloroform using TMS as an internal standard. Fourier transform infrared (FT/IR) spectra were recorded on an FT/IR–4100 (JASCO, Tokyo, Japan). High–resolution (HR) electrospray ionization (ESI)–mass spectrometry (MS) analyses were conducted using a microTOF II (Bruker Daltonics Inc., MA, United States).

To a solution of THPO$(CH_2)_8$MgBr (0.53 M in THF, 5.3 mL, 2.81 mmol) was added a solution of 6 (Wang et al., 2021) (127 mg, 702 μmol) in THF (6.5 mL) at reflux temperature under argon atmosphere. After being stirred at 60°C for 2 h, the reaction mixture was allowed to cool to rt and 2 M HCl aq. (10 mL) was added. After 12 h of stirring, H_2O was added and the water layer was extracted with EtOAc. The combined organic layers were washed with saturated aqueous NaCl, dried over Na_2SO_4 and concentrated under reduced pressure. After evaporation, the residue was purified by medium-pressure chromatography (Isolera, eluent: 40:60 *n*-hexane/EtOAc to EtOAc) to give the mixture contained **7** (73.2 mg). The mixture was carried on to the next step.

To a solution of the mixture (73.2 mg) in acetone (20 mL) was added Jones reagent (4.0 M solution, 2.5 mL, 10 mmol) at −20°C. After 1 h of stirring at −20°C, *i*-PrOH was added to quench the remaining reagent. Then, H_2O (200 mL) was added and the water layer was extracted with EtOAc. The combined organic layers were washed with saturated aqueous NaCl, dried over Na_2SO_4 and concentrated under reduced pressure. The residue was purified by medium-pressure chromatography (Isolera, eluent: 0.5:50:50 AcOH/*n*-hexane/EtOAc to 0.5:99.5 AcOH/EtOAc) to give *iso*-OPDA (68.3 mg, 33% in two steps) as a colorless oil. ^{1}H NMR (400 MHz, $CDCl_3$); δ_H 5.37 (dtt, J = 10.6, 7.4, 1.6 Hz, 1H), 5.21 (dtt, J = 10.6, 7.0, 1.5 Hz, 1H), 2.93 (brd, J = 7.0 Hz, 2H), 2.52–2.45 (m, 2H), 2.42 (t, J = 7.4 Hz, 2 H), 2.39–2.32 (m, 4H), 2.15 (quintet, J = 7.4 Hz, 2H), 1.64 (brquintet, J = 7.5 Hz, 2H), 1.52 (brquintet, J = 7.5 Hz, 2H), 1.34 (brs. 6H), 0.99 (t, J = 7.4 Hz, 3H); ^{13}C NMR (100 MHz, $CDCl_3$); δ_C 209.49, 178.88, 174.35, 139.16, 132.19, 125.33, 34.18, 33.81, 31.27, 29.52, 29.16, 29.04, 28.89, 27.35, 24.59, 21.23, 20.60, 14.16; IR (film) cm^{-1}: 3205, 2931, 2858, 1732, 1701; HRMS (ESI, positive) m/z $[M + Na]^+$ Calcd. for $C_{18}H_{28}O_3$: 2315.1936, found: 315.1927. The ^{1}H and ^{13}C NMR spectra of *iso*-OPDA are shown in **Supplementary Figures 1**, **2**, respectively.

dn-OPDA and dn-*iso*-OPDA were prepared as previously described (Wang et al., 2021). [$^2H_5$]-dn-OPDA was purchased from Cayman Chemical Company.

Chemical and Wounding Treatments

12-Oxo-phytodienoic acid, dn-OPDA, dn-*iso*-OPDA, JA, and JA-Ile were dissolved in dimethyl sulfoxide at a concentration of 10 mM and added to BCDATG liquid media to a final concentration of 50 μM, whereas [$^2H_5$]-OPDA, dissolved in 20% (v/v) aqueous dimethyl sulfoxide solution at a concentration of 1 mM, was added to BCDATG liquid media to 25 μM. *C. plumiforme* gametophores were incubated with media containing the chemicals for 2 h under continuous white light at 23°C.

For wounding treatment, *C. plumiforme* gametophores were cut by scissors into 5-mm long pieces, incubated under continuous white light at 23°C, and collected after 0, 0.5, 1, 2, and 4 h.

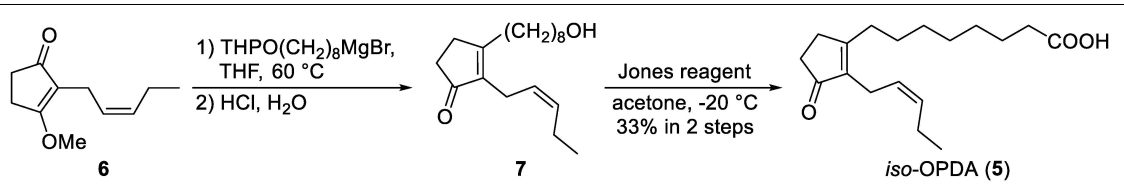

SCHEME 1 | Chemical synthesis of *iso*-OPDA.

5′- and 3′-Rapid Amplification of cDNA Ends

To determine the nucleotide sequence of full-length *CpJAZ2* cDNA, total RNA was extracted from *C. plumiforme* gametophores 1 h after wounding using an RNeasy Plant Mini Kit (QIAGEN, Venlo, Netherlands). 5′- and 3′-RACE analyses of *CpJAZ2* were performed using the SMARTer RACE cDNA Amplification Kit (Clontech, CA, United States) and KOD FX (TOYOBO Co., Osaka, Japan) according to the manufacturer's protocol. Amplified RACE products were cloned into pRACE using the In-Fusion HD Cloning Kit (Clontech) and sequenced to determine the full-length cDNA of *CpJAZ2*, which was amplified by end-to-end RT-PCR using KOD FX and a cDNA template prepared for 5′-RACE analysis. The full-length cDNA was cloned into the pCR-II-Blunt-TOPO vector (Thermo Fisher Scientific, MA, United States) to generate pCR-CpJAZ2, and the inserted fragment was sequenced. Sequences of primers used for RACE and cloning are provided in **Supplementary Table 1**.

Cloning of COI1, JAZ, and MYC2 Genes

According to information from the genome database, coding sequences of *COI1*, *JAZ*, and *MYC2* genes of *C. plumiforme* were amplified by RT-PCR using KOD Plus Neo (TOYOBO Co.) and a cDNA template that was prepared for the 5′-RACE analysis. pCR-CpJAZ2 was used as a template for the amplification of *CpJAZ2*. Sequences of primers used for cloning are provided in **Supplementary Table 1**. Amplified fragments were cloned into pEU vectors (CellFree Sciences Co., Ehime, Japan), which are the expression vectors for a wheat germ cell-free protein expression system, using the In-Fusion HD Cloning Kit (Clontech) or SLiCE (Motohashi, 2015). *COI1* and *MYC2* genes were cloned into pEU-E01-GST-PS-MCS-N1, and *JAZ* genes were cloned into pEU-E01-DYKDDDDK-MCS-N1. The inserted fragments were sequenced.

Sequence Identification and Phylogenetic Analyses

Transcriptome data of *C. plumiforme* treated with $CuCl_2$, which induces oxidative stress and defense responses in plants, were available based on our previous RNA-seq analyses, the results of which are deposited in the DDBJ Sequence Read Archive under accession no. DRA010138 (Okada et al., 2016). The *C. plumiforme* genome sequence and annotation for estimated coding proteins are deposited in the Genome Sequence Archive under accession no. PRJCA001833 (Mao et al., 2020). *C. plumiforme* genes homologous to *COI1*, *JAZ*, and *MYC* were obtained using the corresponding genes in *M. polymorpha* as a query for a BLAST search using transcriptome data and the genome sequence.

Phylogenetic and molecular evolutionary analyses were conducted using MEGA version X (Kumar et al., 2018) with the neighbor-joining method (Saitou and Nei, 1987). Sequence alignments were constructed in MEGA using Muscle (Edgar, 2004). Neighbor-joining trees were also constructed. Bootstrap values were evaluated with 1,000 replications. Sequence alignments were performed using the BioEdit software version 7.2.5.

Statistical Analysis

One-way ANOVA with Tukey's *post hoc* test was performed using Excel (Microsoft Co., WA, United States) and Statcel 4 (OMS Publishing Inc., Saitama, Japan) software.

Quantification of OPDAs, JA, and JA-Ile

Wounded *C. plumiforme* gametophores (approximately 50 mg fresh weight) were homogenized and suspended in 2 mL of 80% (v/v) aqueous methanol, and $[^2H_5]$-OPDA (2.5 ng), $[^2H_5]$-JA (10 ng), $[^{13}C_6]$-JA-Ile (10 ng), and $[^2H_5]$-dn-OPDA (10 ng) were added as internal standards. The extracts were purified and concentrated as previously described (Miyamoto et al., 2016). $[^2H_5]$-OPDA-fed gametophores (approximately 7 mg fresh weight) were homogenized and purified using the same method without internal standards. The resultant samples were subjected to liquid chromatography with electrospray ionization tandem mass spectrometry (LC-ESI-MS/MS) composed of a quadrupole tandem mass spectrometer (Agilent 6460 Triple Quadrupole mass spectrometer) with an electrospray ion source and an Agilent 1200 separation module. OPDAs, JA, and JA-Ile were quantified as previously described, with slight modifications (Tamiru et al., 2016). The mobile phase consisted of 0.05% acetic acid in water (solvent A) and 0.05% acetic acid in acetonitrile (solvent B). Elution was conducted using a linear gradient of solvent B from 3 to 70% over 15 min and 70 to 98% over 5 min at a flow rate of 0.2 mL/min. The retention times of OPDA, *iso*-OPDA, dn-OPDA, dn-*iso*-OPDA, JA, and JA-Ile were 17.1, 16.8, 15.9, 15.5, 13.4, and 15.0 min, respectively. The precursor-to-product transitions monitored were *m*/*z* 291/165 for OPDA and *iso*-OPDA, *m*/*z* 296/170 for $[^2H_5]$-OPDA and $[^2H_5]$-*iso*-OPDA, *m*/*z* 263/165 for dn-OPDA and dn-*iso*-OPDA, *m*/*z* 268/170 for $[^2H_5]$-dn-OPDA and $[^2H_5]$-dn-*iso*-OPDA, m/z 209/59 for JA; *m*/*z* 214/62 for $[^2H_5]$-JA, *m*/*z* 322/130 for JA-Ile, and *m*/*z* 328/136 for $[^{13}C_6]$-JA-Ile. The concentrations of OPDAs and JA in the wounded samples were calculated based on the relative proportions of the peak area relative to the internal standards, whereas those of OPDAs in the $[^2H_5]$-OPDA-fed samples were determined based on the concentration of the authentic standard run under the same analysis conditions.

Gene Expression Analysis

Total RNA was extracted from *C. plumiforme* gametophores using an RNeasy Plant Mini Kit (QIAGEN) and subjected to cDNA synthesis using a PrimeScript RT Reagent Kit with gDNA Eraser (Takara Bio, Shiga, Japan). Quantitative RT-PCR (qRT-PCR) was performed using a THUNDERBIRD SYBR qPCR Mix (TOYOBO Co.) on an ABI 7500 Fast Real-Time PCR System (Applied Biosystems, CA, United States). The ddCt method was used to calculate transcript levels. *CpACT3* (DDBJ ID: LC129863) was used as an internal control to normalize the amount of mRNA. For each sample, the mean value from biological triplicate samples was used to calculate the transcript abundance. Sequences of primers used for qRT-PCR analysis are provided in **Supplementary Table 1**.

In vitro Cell-Free Protein Expression

GST- or FLAG tag-fused CpMYC2 and CpJAZ proteins were expressed using a WEPRO7240 Expression Kit (CellFree Sciences Co.), which is a wheat germ cell-free protein expression system, according to the manufacturer's protocol. Expressed samples were centrifuged at 17,800 × *g* for 5 min at 4°C, and the supernatants were used for subsequent analyses. FLAG-CpJAZ2 was diluted five times before use because its expression was higher than that of FLAG-CpJAZ1 and FLAG-CpJAZ3. A portion of the supernatant was mixed with Laemmli SDS sample buffer and boiled at 96°C for 10 min; the boiled proteins were subjected to protein gel blot analysis. The remaining supernatants were subjected to co-immunoprecipitation analysis.

Co-immunoprecipitation Analysis

For each sample, 10 μL of the supernatant was used. GST-CpMYC2a, GST-CpMYC2b, and GST were mixed with FLAG-CpJAZ1, FLAG-CpJAZ2, or FLAG-CpJAZ3 in IP buffer [25 mM Tris pH 7.8, 50 mM NaCl, 5% (v/v) glycerol, 20 mM 2-mercaptoethanol, and 0.05% (v/v) Tween 20] in the presence of a cOmplete EDTA-free protease inhibitor cocktail (Merck). After incubation at 4°C for 60 min, 0.2 μg of anti-FLAG M2 monoclonal antibody (Merck) was added to each sample. The samples were further incubated at 4°C for 60 min with rotation, and SureBeads Protein G Magnetic Beads (Bio-Rad, CA, United States) were added. Finally, after incubation at 4°C for 60 min with rotation, the beads were washed three times with PBS containing 0.1% (v/v) Tween 20. The resultant beads were boiled in double-diluted sample buffer solution (2ME +) (× 2) (Fujifilm Co.) containing 100 mM dithiothreitol at 60°C for 10 min. The boiled proteins were subjected to protein gel blot analysis.

Protein Gel Blot Analysis

The boiled samples were subjected to SDS-PAGE on 10% (w/v) polyacrylamide gels and transferred to a nitrocellulose membrane (Bio-Rad). GST-CpMYC2a, GST-CpMYC2b, and GST were detected using an anti-GST HRP conjugate [dilution 1:5,000 (v/v)] (Cytiva, Tokyo, Japan) and iBind Flex Western Device (Thermo Fisher Scientific), whereas FLAG-CpJAZ1, FLAG-CpJAZ2, and FLAG-CpJAZ3 were detected using anti-FLAG M2 monoclonal antibody (Merck) [dilution 1:1,000 (v/v)] as the primary antibody and anti-mouse IgG, HRP-linked whole antibody sheep [dilution 1:10,000 (v/v)] (Cytiva) as the secondary antibody with an iBind Flex Western Device. Chemiluminescent detection was carried out using Immobilon Western Chemiluminescent HRP Substrate (Merck) and a ChemiDoc imaging system (Bio-Rad).

RESULTS

Genomic Mining of COI1, JAZ, and MYC2 Gene Homologs in *Calohypnum plumiforme*

In the process of elucidating the molecular mechanism that induces momilactone production in *C. plumiforme*, we previously reported that OPDA induces momilactone accumulation, suggesting that OPDA or its derivatives act as signaling molecules (Okada et al., 2016). The OPDA/dn-OPDA signaling pathway has been identified in the bryophyte *M. polymorpha*. Therefore, we first searched for genes homologous to *COI1*, *JAZ*, and *MYC* using the corresponding genes in *M. polymorpha* as a query using transcriptome data and the genome sequence of *C. plumiforme*.

COI1 in *Calohypnum plumiforme*

We found two genes similar to *MpCOI1* (Monte et al., 2018) from transcriptome data, and these genes were also found in the *C. plumiforme* genome database. These genes were designated as *CpCOI1a* and *CpCOI1b* (**Table 1**). We cloned the coding sequences of *CpCOI1a* and *CpCOI1b* based on the information from the genome annotation, which were identical to annotated sequences in the genome database and deposited in GenBank under accession no. MW775560 (*CpCOI1a*) and MW775561 (*CpCOI1b*).

Phylogenetic analysis was conducted using the amino acid sequences of COI1 in *C. plumiforme*, *M. polymorpha*, and *P. patens* with *Arabidopsis thaliana* COI1 as an outgroup. CpCOI1a and three sequences from *P. patens*, were grouped in the same clade as MpCOI1 (**Figure 1A**), suggesting that these COI1s are conserved in both mosses and liverworts. However, CpCOI1b and COI1 of *P. patens* formed another clade (**Figure 1A**), suggesting that these two COI1s are moss-specific. The alignment of these sequences revealed that the residues involved in the recognition of ligands or the interaction with JAZ proteins reported by Sheard et al. (2010) were conserved in COI1 of *C. plumiforme* (**Supplementary Figure 3**). Monte et al. (2018) reported that valine at position 377 in MpCOI1 is essential for the recognition of dn-OPDA and dn-*iso*-OPDA and that this residue is substituted with alanine on COI1s recognizing a JA-Ile such as AtCOI1. COIs in the mosses predominantly show isoleucine in this position, which is a hydrophobic residue similar to valine (Monte et al., 2018). Consistent with this, the isoleucine residue is conserved in CpCOI1a, although the corresponding residue in CpCOI1b is valine (**Figure 1B**).

JAZ in *Calohypnum plumiforme*

We found three genes similar to *MpJAZ* (Monte et al., 2019) from transcriptome data designated as *CpJAZ1, CpJAZ2,* and *CpJAZ3* (**Table 1**). *CpJAZ1* and *CpJAZ3* were also annotated in the

TABLE 1 | *COI1*, *JAZ*, and *MYC2* genes in *C. plumiforme*.

Gene name	ID in genome sequence archive	GenBank accession number
CpCOI1a	GWHTAMMO020093	MW775560
CpCOI1b	GWHTAMMO007259	MW775561
CpJAZ1	GWHTAMMO005348	MW775562
CpJAZ2	Not annotated	MW775563
CpJAZ3	GWHTAMMO025074	MW775564
CpMYC2a	GWHTAMMO011051	MW775565
CpMYC2b	GWHTAMMO007338	MW775566

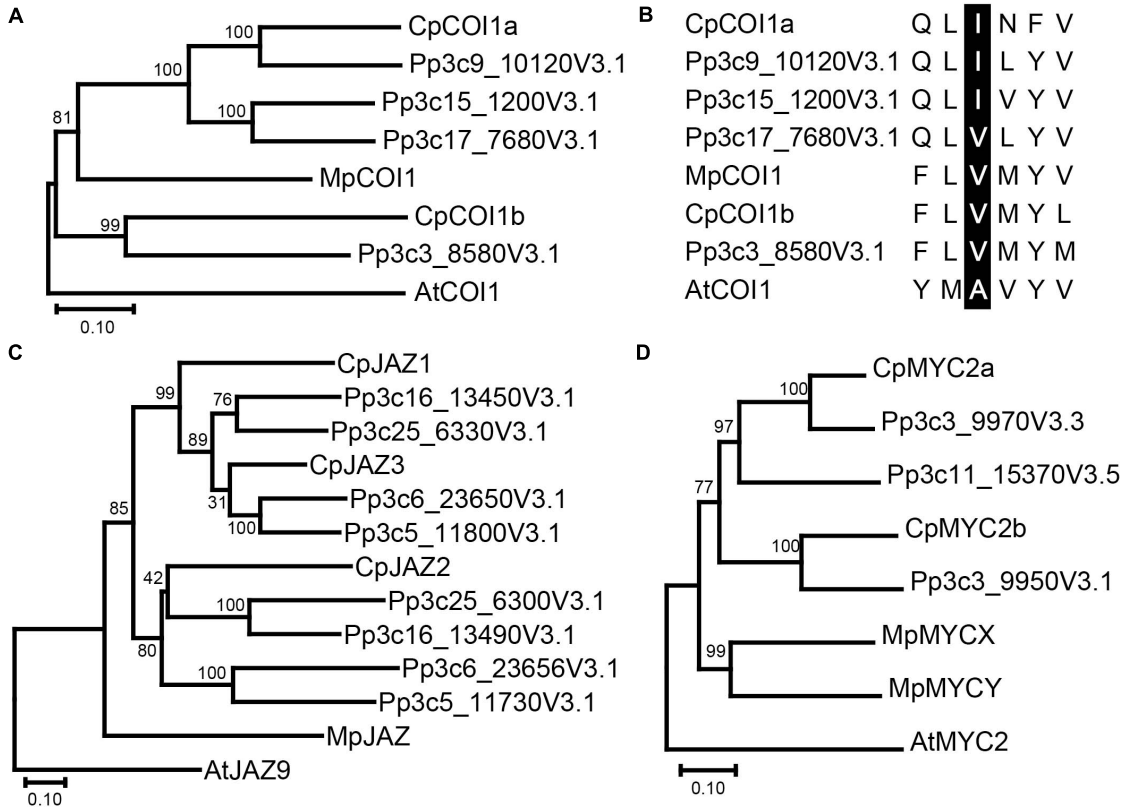

FIGURE 1 | Phylogenetic analysis of COI1 **(A)**, JAZ **(C)**, MYC2 **(D)** homologs, and the residue essential for dn-OPDA and dn-*iso*-OPDA recognition **(B)**. **(A)** Phylogenetic trees (amino acid sequences) were obtained using the neighbor-joining method as described in the "Materials and Methods." The percentage of replicate trees in which the associated taxa clustered together in the bootstrap test (1000 replicates) is shown next to the branches. COI1 homologs in *M. polymorpha* and *P. patens* are also included. The phylogenetic tree was rooted in AtCOI1. Gene IDs are as follows: MpCOI1: Mapoly0025s0025 and AtCOI1: AT2G39940. **(B)** The amino acid sequence of the valine residue at position 377 (V377) of MpCOI1 and its surroundings is shown with the corresponding sequences of other COI1 homologs. V377 in MpCOI1 and its corresponding residues in other COI1 homologs are highlighted by black. **(C)** Phylogenetic trees (amino acid sequences) were obtained using the neighbor-joining method as described in the "Materials and Methods." The percentage of replicate trees in which the associated taxa clustered together in the bootstrap test (1000 replicates) is shown next to the branches. JAZ homologs in *M. polymorpha* and *P. patens* are also included. The phylogenetic tree was rooted in AtJAZ9. Gene IDs are as follows: MpJAZ: Mapoly0097s0021 and AtJAZ9: AT1G70700. **(D)** Phylogenetic trees (amino acid sequences) were obtained using the neighbor-joining method as described in the "Materials and Methods." The percentage of replicate trees in which the associated taxa clustered together in the bootstrap test (1,000 replicates) is shown next to the branches. MYC2 homologs in *M. polymorpha* and *P. patens* are also included. The phylogenetic tree was rooted in AtMYC2. Gene IDs are as follows: MpMYCX: Mapoly0018s0019; MpMYCY: MapolyY_B0018; and AtMYC2: AT1G32640.

C. plumiforme genome database. We cloned the coding sequences of *CpJAZ1* and *CpJAZ3* according to the information from the genome database, which were identical to annotated sequences in the genome database and deposited in GenBank under accession no. MW775562 (*CpJAZ1*) and MW775564 (*CpJAZ3*). *CpJAZ2* was not annotated in the genome database, and only a partial sequence of *CpJAZ2* was obtained from the RNA-seq data. Therefore, we performed 5′- and 3′- RACE to obtain the full-length sequence of *CpJAZ2*, which was deposited in GenBank under accession no. MW775563. Phylogenetic analysis was conducted using the amino acid sequences of JAZ in *C. plumiforme*, *M. polymorpha*, and *P. patens*, with *A. thaliana* JAZ9 as an outgroup. CpJAZ1 and CpJAZ3, along with four sequences from *P. patens*, were grouped in the same clade, whereas CpJAZ2 and four sequences of *P. patens* formed another clade (**Figure 1C**), suggesting that JAZ proteins evolved into two groups in mosses. The alignment of these sequences revealed that the Jas motif and TIFY domain were conserved in CpJAZ1, CpJAZ2, and CpJAZ3 (**Figure 2**). N-terminal sequences were conserved among several JAZs in *C. plumiforme* and *P. patens*, including CpJAZ1 and CpJAZ3. This conserved sequence was not found in MpJAZ or AtJAZ9 (**Figure 2**).

MYC2 in *Calohypnum plumiforme*

We found two genes similar to the *M. polymorpha* MYC2 ortholog gene, *MpMYCY* (Peñuelas et al., 2019), from transcriptome data, and these genes were also found in the *C. plumiforme* genome database. These two genes were designated as *CpMYC2a,* and *CpMYC2b* (**Table 1**). We cloned the coding sequences of *CpMYC2a* and *CpMYC2b* according to the information from the genome database; that of *CpMYC2a* had a 12 bp substitution with the annotation of the genome database, possibly due to misassembly of the genome sequence or polymorphism among the *C. plumiforme* lines used in genome

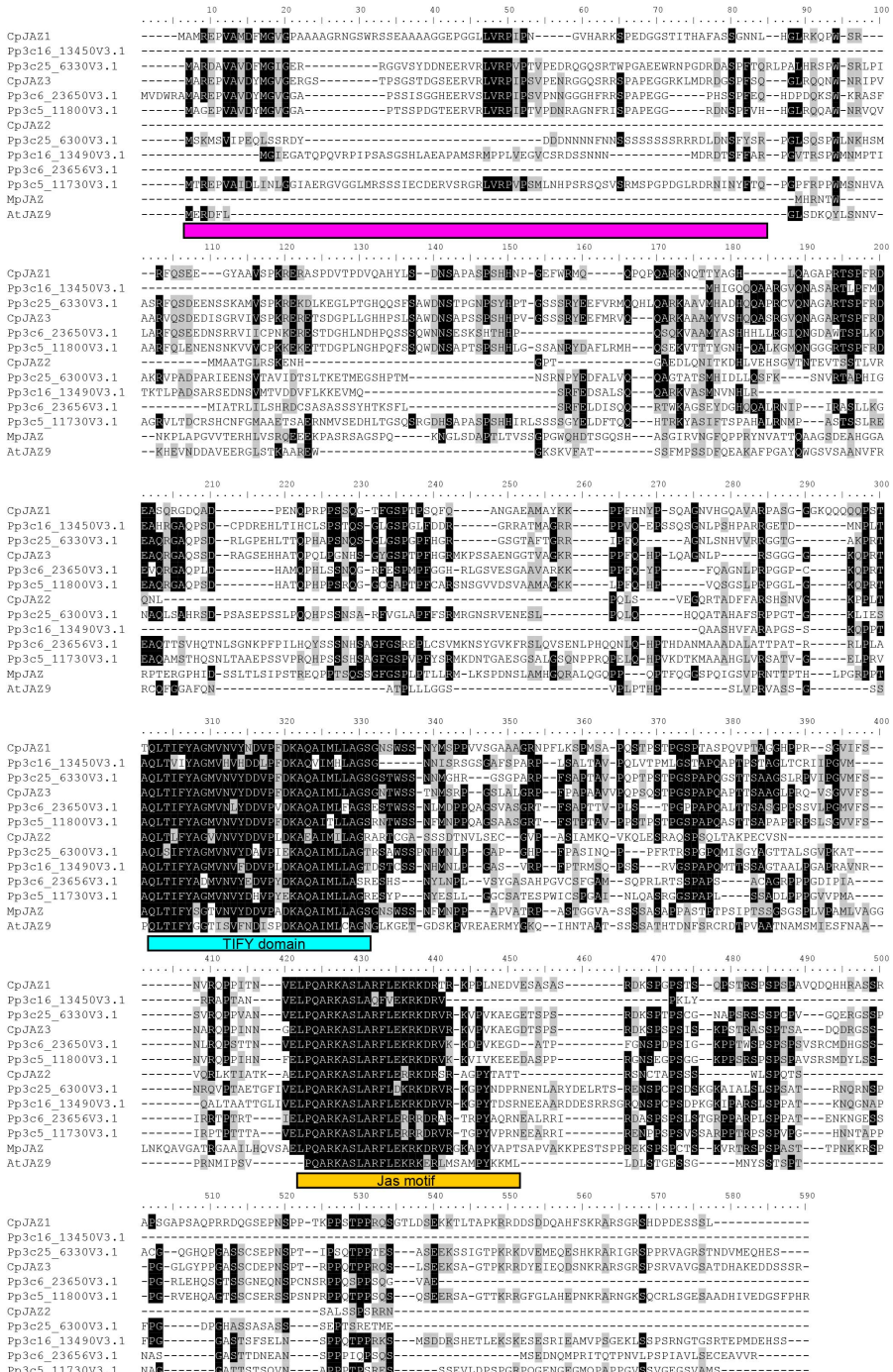

FIGURE 2 | Sequence alignment of JAZ proteins. Sequences of JAZ homologs were aligned using MEGA version X using Muscle. Sequence alignments were drawn using the BioEdit software version 7.2.5. The shading thresholds for identical or similar residues were 40%. Identical and similar residues are highlighted by black and gray, respectively. The TIFY domain and Jas motifs are indicated by blue and orange squares, respectively. The conserved sequence in the N-terminus of the moss JAZs is indicated by magenta squares.

sequencing and our experiments (**Supplementary Figure 4A**), whereas that of *CpMYC2b* lacked a 99 bp sequence that was annotated as exons in the genome database. This sequence had a putative 3′-splice site (5′-AG-3′) and branchpoint sequence (5′-CTNAN-3′; Brown et al., 1996), suggesting that the longer region was removed in the *C. plumiforme* gametophores used in the present study (**Supplementary Figure 4B**). The cloned coding sequences were deposited in GenBank under accession

no. MW775565 (*CpMYC2a*) and MW775566 (*CpMYC2b*) and used for subsequent analyses.

Phylogenetic analysis was conducted using the amino acid sequences of MYC2 in *C. plumiforme*, *M. polymorpha*, and *P. patens* with *A. thaliana* MYC2 as an outgroup. CpMYC2a and two sequences from *P. patens* were grouped in the same clade, whereas CpMYC2b and one sequence from *P. patens* formed another clade (**Figure 1D**), suggesting that MYC2 proteins evolved into two groups in mosses. The alignment of these sequences revealed that the JID and bHLH domains were conserved in CpMYC2a and CpMYC2b (**Supplementary Figure 5**).

Quantification of Endogenous Levels of OPDA, dn-OPDA, and Their Isomers

We found putative OPDA/dn-OPDA signaling components in *C. plumiforme*; however, the endogenous levels of OPDA, dn-OPDA, and their isomers, which accumulate in gametophores after wounding, have not yet been investigated. Therefore, we measured these. The levels of OPDA and dn-OPDA increased and peaked at 30 min after wounding and then decreased (**Figure 3**). *iso*-OPDA and dn-*iso*-OPDA also accumulated after 30 min but remained at a high level for 4 h after wounding. After wounding, the level of OPDA was highest, followed by that of *iso*-OPDA, which was approximately one-tenth of that of OPDA. The amounts of dn-OPDA and dn-*iso*-OPDA were less than one-hundredth that of OPDA. We detected a small amount of JA, although this was below the detection limit of a previous study (Okada et al., 2016). Additionally, the level of JA 4 h after wounding was significantly higher than that in unwounded *C. plumiforme* gametophores (**Figure 3**). The amount of JA was about 1/1000 of that of OPDA, and it was almost consistent with a steady-state level of JA in angiosperms, such as *A. thaliana* and rice (Park et al., 2002; Riemann et al., 2013). JA-Ile, which is a biologically active form in seed plants, was not detected with or without wounding.

In planta Conversion of Labeled-OPDA to *iso*-OPDA, dn-OPDA, and dn-*iso*-OPDA

Two synthetic pathways for dn-OPDA and dn-*iso*-OPDA are shown in *M. polymorpha*. One is the conversion of OPDA to dn-OPDA and dn-*iso*-OPDA; the other is the direct synthesis of dn-OPDA and dn-*iso*-OPDA from hexadecatrienoic acid, but not *via* OPDA (Monte et al., 2018). To investigate the conversion of OPDA to dn-OPDA and dn-*iso*-OPDA, we fed 25 μM deuterium-labeled OPDA [($^2H_5$)-OPDA] to *C. plumiforme* gametophores and then measured the level of deuterium-labeled

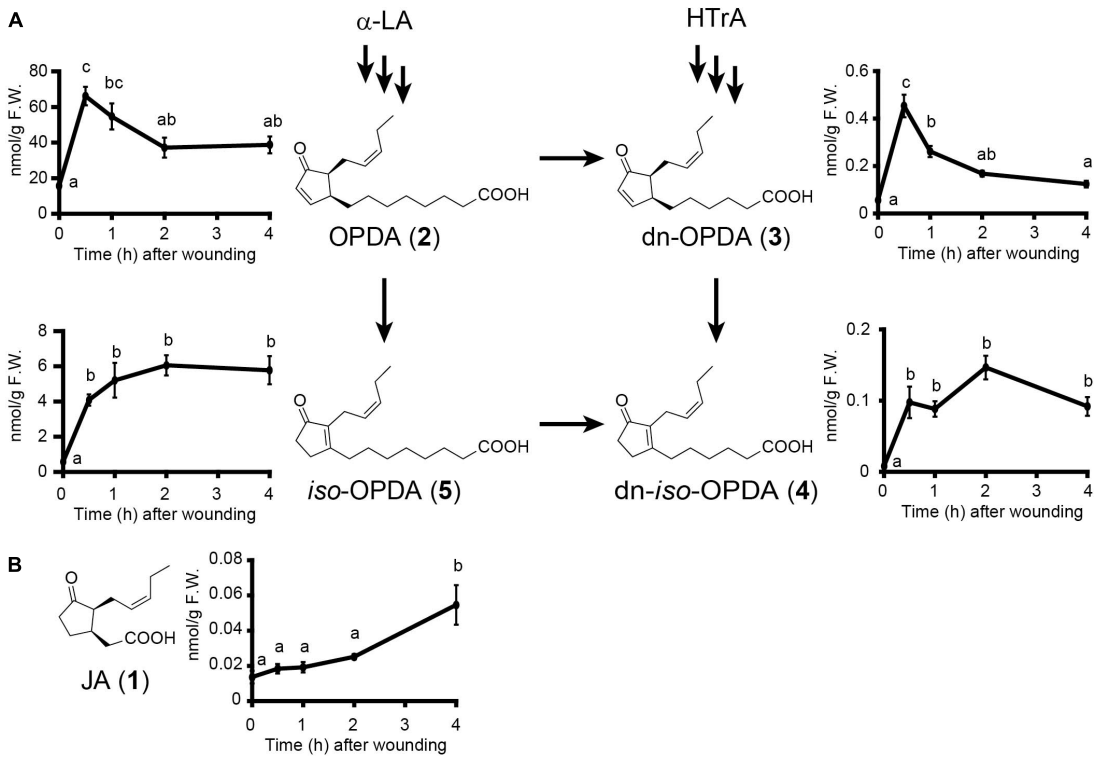

FIGURE 3 | Effects of wounding on accumulation levels of endogenous OPDA, *iso*-OPDA, dn-OPDA, dn-*iso*-OPDA **(A)**, and JA **(B)**. **(A)** Values indicate the amount of OPDA, *iso*-OPDA, dn-OPDA, and dn-*iso*-OPDA in *C. plumiforme* gametophores after wounding ($n = 3$). **(B)** Values indicate the amount of JA in *C. plumiforme* gametophores after wounding ($n = 3$). Arrows indicate the proposed biosynthetic pathways in *M. polymorpha*. Bars indicate standard errors of the means. Statistically different data groups are indicated with different letters ($p < 0.05$, one-way ANOVA with Tukey's *post hoc* test). LA, linolenic acid; HTrA, hexadecatrienoic acid.

derivatives by LC-MS/MS. Both [$^2H_5$]-dn-OPDA and [$^2H_5$]-dn-*iso*-OPDA accumulated after [$^2H_5$]-OPDA treatment, indicating that OPDA can be efficiently converted to dn-OPDA in *C. plumiforme* (**Figure 4**). Isomerization of OPDA to *iso*-OPDA was also observed because [$^2H_5$]-*iso*-OPDA also accumulated after [$^2H_5$]-OPDA treatment (**Figure 4**). The ratio of the amounts of [$^2H_5$]-OPDA, [$^2H_5$]-*iso*-OPDA, [$^2H_5$]-dn-OPDA, and [$^2H_5$]-dn-*iso*-OPDA in [$^2H_5$]-OPDA-treated *C. plumiforme* was similar to that of the unlabeled compounds in wounded plants.

OPDA, dn-OPDA, and dn-*iso*-OPDA Induce the Expression of CpJAZ Genes

The expression of *JAZ* genes encoding repressors is induced by the ligand for COI1 to repress the signal (Chini et al., 2007; Thines et al., 2007; Monte et al., 2019). We examined the expression of *JAZ* genes after OPDA, dn-OPDA, or dn-*iso*-OPDA treatment in *C. plumiforme*. As shown in **Figure 5**, the expression of *CpJAZ1*, *CpJAZ2*, and *CpJAZ3* was induced by treatment with OPDA, dn-OPDA, or dn-*iso*-OPDA. JA and JA-Ile did not affect the expression of these genes. These results suggest that OPDA and/or both isomers of dn-OPDA are biologically active. dn-OPDA and dn-*iso*-OPDA might be recognized by CpCOI1 as in *M. polymorpha*, although there remains the possibility that another metabolite from OPDA and dn-OPDA acts as a ligand of CpCOI1.

Physical Interaction Between CpJAZs and CpMYC2s

JAZ proteins physically interact with MYC2, MYC3 and MYC4 transcription factors to repress downstream signaling (Chini et al., 2007; Thines et al., 2007; Fernández-Calvo et al., 2011; Peñuelas et al., 2019). To investigate the physical interaction between JAZ and MYC2 proteins from *C. plumiforme*, we performed co-immunoprecipitation analyses. GST- or FLAG tag-fused CpMYC2 and CpJAZ proteins were expressed using a wheat germ cell-free protein expression system and detected by protein gel blot analysis at a position consistent with the predicted molecular weight; GST: 29.3 kDa, GST-CpMYC2a: 105.7 kDa, GST-CpMYC2b: 111.1 kDa, FLAG-CpJAZ1: 53.6 kDa, FLAG-CpJAZ2: 25.5 kDa, and FLAG-CpJAZ3: 54.8 kDa (**Supplementary Figure 6**). Expressed MYC2 and JAZ proteins were mixed and then immunoprecipitated using an anti-FLAG antibody. Immunoprecipitated proteins were analyzed by protein gel blot analysis using anti-GST or anti-FLAG antibodies. GST-CpMYC2a and CpMYC2b, but not GST, were detected after immunoprecipitation with CpJAZ1, CpJAZ2, or CpJAZ3 (**Figure 6A**). Additionally, GST-CpMYC2a and CpMYC2b in immunoprecipitated proteins with CpJAZs were more strongly detected than those without FLAG-tagged proteins. Immunoprecipitated FLAG-CpJAZs were detected using an anti-FLAG antibody (**Figure 6B**). These results indicate that CpJAZ1, CpJAZ2, and CpJAZ3 directly interact with CpMYC2a or CpMYC2b *in vitro*.

DISCUSSION

COI1, JAZ, and MYC2 Genes Were Conserved in *Calohypnum plumiforme*

In this study, we investigated signaling mechanisms promoted by OPDA and its derivatives in *C. plumiforme*. We found

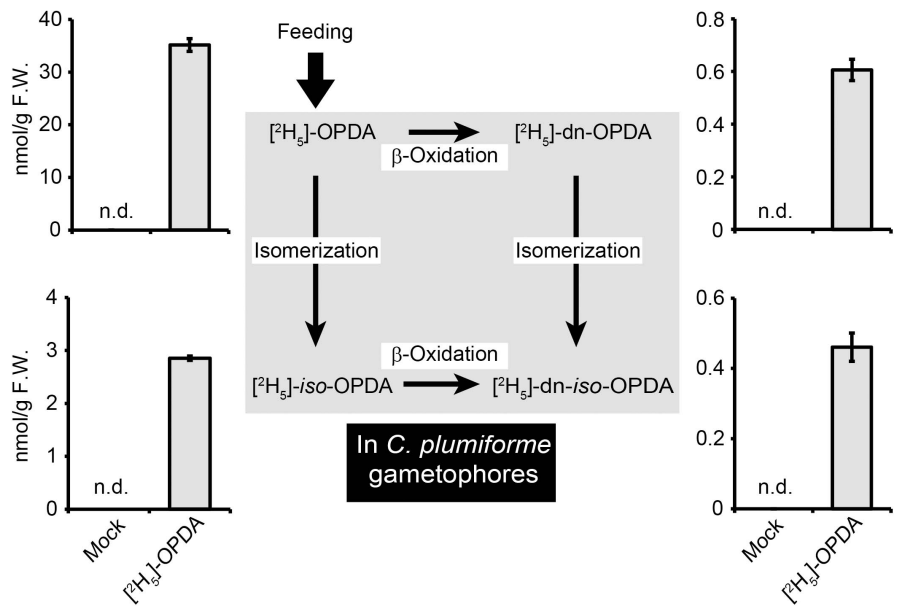

FIGURE 4 | Conversion of deuterium-labeled OPDA [($^2H_5$)-OPDA] in *C. plumiforme* gametophores. The values indicate the amount of [$^2H_5$]-OPDA, *iso*-OPDA, dn-OPDA, and dn-*iso*-OPDA in *C. plumiforme* gametophores after [$^2H_5$]-OPDA treatment at 25 μM (n = 3). Mock samples were treated with BCDATG liquid media containing 0.5% (v/v) dimethyl sulfoxide as a negative control. The arrows indicate the proposed biosynthetic pathways in *M. polymorpha.*

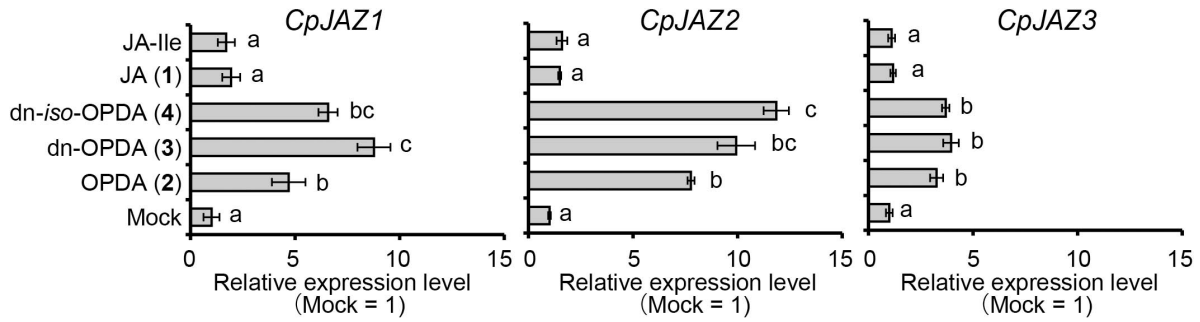

FIGURE 5 | Effect of wounding on the expression of *CpJAZ1*, *CpJAZ2*, and *CpJAZ3* as determined by qRT-PCR. Values indicate relative expression levels after treatment with OPDA, dn-OPDA, dn-*iso*-OPDA, JA, and JA-Ile at 50 μM ($n = 3$). Mock samples were treated with BCDATG liquid media containing 0.5% (v/v) dimethyl sulfoxide as a negative control. Expression levels were normalized to the expression of *CpACT3*, and the bars indicate the standard errors of the means. Statistically different data groups are indicated with different letters ($p < 0.05$, one-way ANOVA with Tukey's *post hoc* test).

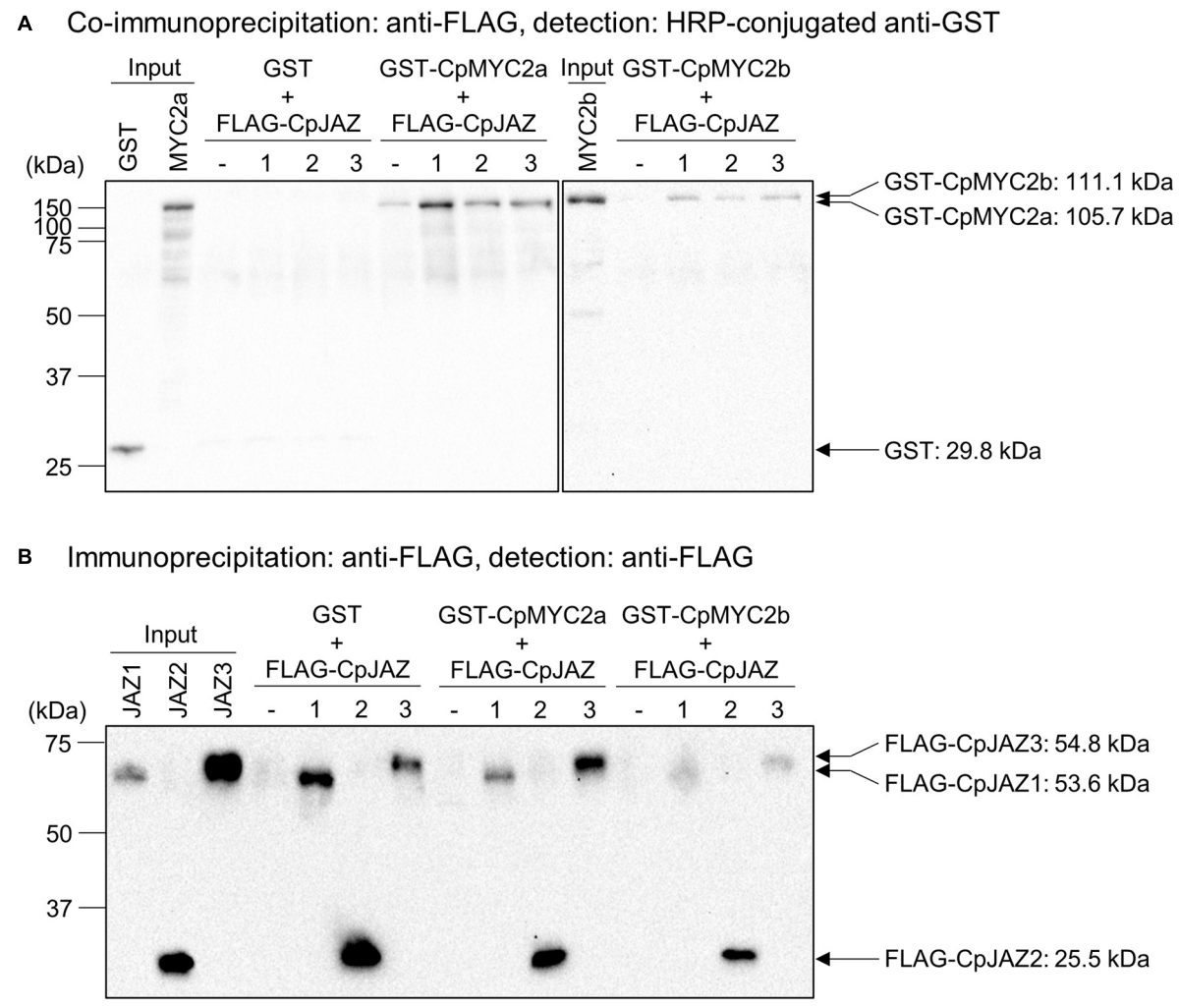

FIGURE 6 | Co-immunoprecipitation analysis investigating the interaction between CpJAZs and CpMYC2s. **(A)** Proteins co-immunoprecipitated by anti-FLAG antibodies were analyzed. GST and GST-fused proteins were detected by protein gel blot analysis using a horseradish peroxidase-conjugated anti-GST antibody. **(B)** Proteins immunoprecipitated by anti-FLAG antibody were analyzed. FLAG-tagged proteins were detected by protein gel blot analysis using an anti-FLAG antibody.

that COI, JAZ, and MYC2 sequences, including domains important for their functions, were conserved (**Figures 1**, **2** and **Supplementary Figures 3**, **5**). Moreover, in CpCOI1a and CpCOI1b, a hydrophobic residue that is important for the recognition of dn-OPDA and dn-*iso*-OPDA was conserved (**Figure 1B**), suggesting that CpCOI1a and CpCOI1b recognize dn-OPDA and its related derivatives.

CpJAZ1, CpJAZ2, and CpJAZ3 conserved the Jas motif and TIFY domain as MpJAZ and AtJAZ9, implying that JAZs of *C. plumiforme* have similar functions to repress the downstream signaling of COI1 and MYCs. Several JAZs from mosses had conserved N-terminal sequences, which were not found in MpJAZ and AtJAZ9 (**Figure 2**). These sequences might be involved in the specific function of JAZs in mosses, although we could not find a similar sequence with identifiable functions by the BLAST search. Although the liverwort *M. polymorpha* has a single *JAZ* gene, mosses *C. plumiforme* and *P. patens* have at least three and eight *JAZ* genes, respectively. The number of JAZs in seed plants is even higher; for example, there are 13 and 15 JAZs in *Arabidopsis* and rice, respectively (Pauwels and Goossens, 2011; Chini et al., 2016; Uji et al., 2016). Genome duplication has been reported in mosses (Rensing et al., 2007; Gao et al., 2021), which may explain why there are more JAZs in mosses than in liverworts.

As *C. plumiforme* possessed fewer *COI1*, *JAZ*, and *MYC2* genes than *P. patens* (**Figure 1**), less redundancy is expected. Unfortunately, we could not use reverse genetics approaches because of the absence of a transformation system in *C. plumiforme*. Because of the small number of COI1, JAZ, and MYC2 homologs and their importance in the research on the evolution of plant chemical defenses, the development of a transformation system for *C. plumiforme* is needed.

OPDA, dn-OPDA, and Their Isomers Accumulated After Wounding Treatment in *Calohypnum plumiforme*

To determine a biologically active molecule in OPDA signaling in *C. plumiforme*, we performed quantification analyses of OPDA, dn-OPDA, and their isomers. We observed that OPDA, *iso*-OPDA, dn-OPDA, and dn-*iso*-OPDA accumulated after wounding (**Figure 3**). A small amount of JA was detected and increased by wounding, although JA-Ile was not detected (**Figure 3**). Bryophytes do not have OPR3 orthologs, which catalyze the reduction of OPDA, but homologous genes to *AtOPR2*, which catalyzes 4,5-didehydro-JA reduction to produce JA (Han, 2016; Chini et al., 2018; Wasternack and Hause, 2018). Consistent with these reports, genes homologous to AtOPR2 were found in the *C. plumiforme* genome. These translation products possibly catalyze the reduction of OPDA homologs, such as dn-OPDA. However, the contribution of OPR should be small in *C. plumiforme*, since the level of JA is very low.

We conducted a feeding experiment using [$^2H_5$]-OPDA to investigate whether *iso*-OPDA, dn-OPDA, and dn-*iso*-OPDA were synthesized from OPDA. [$^2H_5$]-dn-OPDA was detected after the feeding of [$^2H_5$]-OPDA (**Figure 4**), indicating that OPDA was converted to dn-OPDA by β-oxidation in *C. plumiforme* as reported in *M. polymorpha* (Monte et al., 2018). The detection of [$^2H_5$]-*iso*-OPDA in [$^2H_5$]-OPDA-fed plants revealed that the isomerization of OPDA occurred (**Figure 4**). [$^2H_5$]-dn-*iso*-OPDA was observed after feeding [$^2H_5$]-OPDA (**Figure 4**). dn-*iso*-OPDA may be synthesized from OPDA by the β-oxidation of *iso*-OPDA and/or isomerization of dn-OPDA as proposed in *M. polymorpha* and *P. patens* (Monte et al., 2018; Mukhtarova et al., 2020). In *M. polymorpha*, dn-OPDA is synthesized from hexadecatrienoic acid, not *via* OPDA, in addition to the pathway from OPDA. It is unknown whether a biosynthetic pathway from hexadecatrienoic acid exists in *C. plumiforme*. The ratio of [$^2H_5$]-OPDA, [$^2H_5$]-*iso*-OPDA, [$^2H_5$]-dn-OPDA, and [$^2H_5$]-dn-*iso*-OPDA in [$^2H_5$]-OPDA-treated plants was approximately 60:5:1:1, which is similar to that of the corresponding endogenous compounds after wounding. Therefore, the pathway for the synthesis of dn-OPDA from OPDA may also be functional in *C. plumiforme* after wounding. However, the metabolic flow of the β-oxidation of OPDA and/or *iso*-OPDA seems to be moderate compared with that in *M. polymorpha*.

OPDA, dn-OPDA, and dn-*iso*-OPDA Induce CpJAZ Gene Expression

We investigated the inductive activity of OPDA, dn-OPDA, and dn-*iso*-OPDA on the expression of *JAZ* genes. Although they induced the expression of *CpJAZ1*, *CpJAZ2*, and *CpJAZ3*, JA and JA-Ile did not (**Figure 5**). We attempted to reveal the ligand for CpCOI1a and CpCOI1b by analyzing the physical interaction between COI1-JAZ using co-immunoprecipitation and yeast two-hybrid assays in the presence of OPDA, dn-OPDA, or dn-*iso*-OPDA, but we could not prove this interaction. This may be because the expressed COI1 protein did not retain its activity or another molecule is the ligand for COI1 of *C. plumiforme*.

Difference in OPDA Profiles of Bryophytes

We showed that OPDA was the most abundant in wounded *C. plumiforme*, followed by *iso*-OPDA, dn-OPDA, and dn-*iso*-OPDA (**Figure 3**). In the model liverwort *M. polymorpha*, dn-*iso*-OPDA is most abundant after wounding, followed by OPDA and dn-OPDA, the levels of which are almost comparable (Monte et al., 2018). Additionally, in the model moss *P. patens*, *iso*-OPDA is predominant, and smaller amounts of OPDA and dn-*iso*-OPDA exist with or without the feeding of α-linolenic acid (Mukhtarova et al., 2020). The differences in the profiles of OPDA and its derivatives among the three species indicate that the metabolic rates of isomerization and β-oxidation are different. The biological significance of the different profiles of OPDAs requires further study.

CpJAZs Interact With CpMYC2s

JAZ proteins interact with MYC2, MYC3 and MYC4 and repress downstream genes in various plants (Chini et al., 2007; Thines et al., 2007; Fernández-Calvo et al., 2011; Wasternack and Hause, 2013; Peñuelas et al., 2019). Co-immunoprecipitation

analyses revealed that CpJAZ1, CpJAZ2, and CpJAZ3 physically interacted with CpMYC2a or CpMYC2b (**Figure 6**). Although the target genes of CpMYC2s are still unknown, CpJAZs might repress the transcription of these target genes at a steady state. Because a histidine residue in the bHLH domain that determines which DNA sequence to bind was conserved in CpMYC2s (**Supplementary Figure 5**), we assumed that CpMYC2s might bind to a G-box motif (CACGTG), similar to AtMYC2 and MpMYCs (Chini et al., 2007; Peñuelas et al., 2019). We found a G-box motif approximately 60 and 100 bp upstream of the transcription start site of *CpJAZ1* and *CpJAZ2*, respectively. There is no G-box motif in the 2,000 bp upstream region from the transcription start site of *CpJAZ3*, but a G-box motif exists in the 5′- untranslated region of *CpJAZ3*. CpMYC2a and CpMYC2b possibly bind to these G-box motifs and regulate the inductive expression of *CpJAZ* genes in response to OPDA or its derivatives.

Conclusion

We found that OPDA, dn-OPDA, and their isomers accumulated in *C. plumiforme* after wounding at different abundance ratios than in *M. polymorpha* and *P. patens*, and that OPDA, dn-OPDA, and dn-*iso*-OPDA induced *CpJAZ* gene expression, indicating that they all have biological activity in *C. plumiforme*. *COI1*, *JAZ*, and *MYC2* genes were conserved, as were the physical interactions between JAZ and MYC2 proteins. These results indicate that COI1-JAZ-MYC mediated signaling is conserved. At this time, the ligand(s) of CpCOI1s remain unknown. Future research using genetic approaches and/or other biochemical methods will reveal the interaction between CpCOI1s and CpJAZs and the ligand(s) of CpCOI1.

DATA AVAILABILITY STATEMENT

The datasets presented in this study can be found in online repositories. The names of the repository/repositories and accession number(s) are as follows: https://www.ncbi.nlm.nih.gov/genbank/, MW775560; MW775561; MW775562; MW775563; MW775564; MW775565; MW775566.

AUTHOR CONTRIBUTIONS

KMi and KO designed the study. HI, NA, KMu, KS, SM, and MT performed the biological experiments. EY carried out LC/MS/MS analyses. KU synthesized (–)-JA and JA-Ile. NK and MU synthesized dn-OPDA, dn-*iso*-OPDA, and *iso*-OPDA. YH, TSh, and IG synthesized OPDA and [$^2H_5$]-OPDA. TK, YT, and MU performed the protein-protein interaction analyses. AN and TSa expressed JAZ proteins. HI and KMi performed all the computational analyses. KMi, HN, and KO supervised the experiments. KMi and KO wrote the manuscript. HI, NK, TSh, and IG revised the manuscript. All authors read and approved the final manuscript.

FUNDING

This work was supported by JSPS KAKENHI (Grant Numbers JP18K14399 to KMi; JP20H02922 to KO; JP17H06407, JP18KK0162, and JP20H00402 to MU; JP18H02101 and JP19H05283 to YT), JSPS A3 Foresight Program to MU, Japan-Austria Research Cooperative Program between JSPS and FWF (Grant Number JPJSBP120202002) to KO, and the Joint Usage/Research Center, Institute of Plant Science and Resources, Okayama University.

ACKNOWLEDGMENTS

We would like to thank Hisakazu Yamane (The University of Tokyo) for his advice; Peter Nick and Michael Riemann for providing an expression vector for OsAOC; Ryosuke Sato (Teikyo University) for providing the SLiCE; and Kenichiro Hayashi (Okayama University of Science) for providing *C. plumiforme* plants. We would also like to thank Izumi C. Mori and Takakazu Matsuura (Okayama University) for their insights and technical assistance in [$^2H_5$]-dn-OPDA synthesis.

SUPPLEMENTARY MATERIAL

The Supplementary Material for this article can be found online at: https://www.frontiersin.org/articles/10.3389/fpls.2021.688565/full#supplementary-material

Supplementary Figure 1 | ^{1}H NMR spectrum of *iso*-OPDA.

Supplementary Figure 2 | ^{13}C NMR spectrum of *iso*-OPDA.

Supplementary Figure 3 | Sequence alignment of COIs.

Supplementary Figure 4 | Differences between cloned CpMYC2s sequences and annotated sequences in the genome database.

Supplementary Figure 5 | Sequence alignment of MYC2.

Supplementary Figure 6 | Expression of GST-CpMYC2s and FLAG-JAZs.

Supplementary Table 1 | Primers used in this study.

REFERENCES

Ballaré, C. L., and Austin, A. T. (2019). Recalculating growth and defense strategies under competition: key roles of photoreceptors and jasmonates. *J. Exp. Bot.* 70, 3425–3434. doi: 10.1093/jxb/erz237

Brown, J. W. S., Smith, P., and Simpson, C. G. (1996). Arabidopsis consensus intron sequences. *Plant Mol. Biol.* 32, 531–535. doi: 10.1007/bf00019105

Chini, A., Fonseca, S., Fernández, G., Adie, B., Chico, J. M., Lorenzo, O., et al. (2007). The JAZ family of repressors is the missing link in jasmonate signalling. *Nature* 448, 666–671. doi: 10.1038/nature06006

Chini, A., Gimenez-Ibanez, S., Goossens, A., and Solano, R. (2016). Redundancy and specificity in jasmonate signalling. *Curr. Opin. Plant Biol.* 33, 147–156. doi: 10.1016/j.pbi.2016.07.005

Chini, A., Monte, I., Zamarreño, A. M., Hamberg, M., Lassueur, S., Reymond, P., et al. (2018). An OPR3-independent pathway uses 4,5-didehydrojasmonate for jasmonate synthesis. *Nat. Chem. Biol.* 14, 171–178. doi: 10.1038/nchembio.2540

Edgar, R. C. (2004). MUSCLE: multiple sequence alignment with high accuracy and high throughput. *Nucleic Acids Res.* 32, 1792–1797. doi: 10.1093/nar/gkh340

Fernández-Calvo, P., Chini, A., Fernández-Barbero, G., Chico, J.-M., Gimenez-Ibanez, S., Geerinck, J., et al. (2011). The Arabidopsis bHLH transcription factors MYC3 and MYC4 are targets of JAZ repressors and act additively with MYC2 in the activation of jasmonate responses. *Plant Cell* 23, 701–715. doi: 10.1105/tpc.110.080788

Fonseca, S., Chini, A., Hamberg, M., Adie, B., Porzel, A., Kramell, R., et al. (2009). (+)-7-iso-Jasmonoyl-l-isoleucine is the endogenous bioactive jasmonate. *Nat. Chem. Biol.* 5, 344–350. doi: 10.1038/nchembio.161

Gao, B., Chen, M.-X., Li, X.-S., Liang, Y.-Q., Zhang, D.-Y., Wood, A. J., et al. (2021). Ancestral gene duplications in mosses characterized by integrated phylogenomic analyses. *J. Syst. Evol.* (in press). doi: 10.1111/jse.12683

Guo, L., Qiu, J., Ye, C., Jin, G., Mao, L., Zhang, H., et al. (2017). Echinochloa crus-galli genome analysis provides insight into its adaptation and invasiveness as a weed. *Nat. Commun.* 8:1031. doi: 10.1038/s41467-017-01067-5

Guo, Q., Yoshida, Y., Major, I. T., Wang, K., Sugimoto, K., Kapali, G., et al. (2018). JAZ repressors of metabolic defense promote growth and reproductive fitness in Arabidopsis. *Proc. Natl. Acad. Sci. U.S.A.* 115, E10768–E10777. doi: 10.1073/pnas.1811828115

Han, G.-Z. (2016). Evolution of jasmonate biosynthesis and signaling mechanisms. *J. Exp. Bot.* 68, 1323–1331. doi: 10.1093/jxb/erw470

Jikumaru, Y., Asami, T., Seto, H., Yoshida, S., Yokoyama, T., Obara, N., et al. (2004). Preparation and biological activity of molecular probes to identify and analyze jasmonic acid-binding proteins. *Biosci. Biotechnol. Biochem.* 68, 1461–1466. doi: 10.1271/bbb.68.1461

Kajiwara, A., Abe, T., Hashimoto, T., Matsuura, H., and Takahashi, K. (2012). Efficient synthesis of (+)-cis-12-oxo-phytodienoic acid by an in vitro enzymatic reaction. *Biosci. Biotechnol. Biochem.* 76, 2325–2328. doi: 10.1271/bbb.120506

Kumar, S., Stecher, G., Li, M., Knyaz, C., and Tamura, K. (2018). MEGA X: molecular evolutionary genetics analysis across computing platforms. *Mol. Biol. Evol.* 35, 1547–1549. doi: 10.1093/molbev/msy096

Mao, L., Kawaide, H., Higuchi, T., Chen, M., Miyamoto, K., Hirata, Y., et al. (2020). Genomic evidence for convergent evolution of gene clusters for momilactone biosynthesis in land plants. *Proc. Natl. Acad. Sci. U.S.A.* 117, 12472–12480. doi: 10.1073/pnas.1914373117

Miyamoto, K., Enda, I., Okada, T., Sato, Y., Watanabe, K., Sakazawa, T., et al. (2016). Jasmonoyl-l-isoleucine is required for the production of a flavonoid phytoalexin but not diterpenoid phytoalexins in ultraviolet-irradiated rice leaves. *Biosci. Biotechnol. Biochem.* 80, 1934–1938. doi: 10.1080/09168451.2016.1189319

Miyamoto, K., Matsumoto, T., Yumoto, E., Sakazawa, T., Yokota, T., Yamane, H., et al. (2019). Facile preparation of optically active jasmonates and their biological activities in rice. *Biosci. Biotechnol. Biochem.* 83, 876–881. doi: 10.1080/09168451.2019.1569500

Miyamoto, K., Shimizu, T., and Okada, K. (2014). Transcriptional regulation of the biosynthesis of phytoalexin: a lesson from specialized metabolites in rice. *Plant Biotechnol.* 31, 377–388. doi: 10.5511/plantbiotechnology.14.0730a

Monte, I., Franco-Zorrilla, J. M., García-Casado, G., Zamarreño, A. M., García-Mina, J. M., Nishihama, R., et al. (2019). A single JAZ repressor controls the jasmonate pathway in *Marchantia polymorpha*. *Mol. Plant* 12, 185–198. doi: 10.1016/j.molp.2018.12.017

Monte, I., Ishida, S., Zamarreño, A. M., Hamberg, M., Franco-Zorrilla, J. M., García-Casado, G., et al. (2018). Ligand-receptor co-evolution shaped the jasmonate pathway in land plants. *Nat. Chem. Biol.* 14, 480–488. doi: 10.1038/s41589-018-0033-4

Motohashi, K. (2015). A simple and efficient seamless DNA cloning method using SLiCE from *Escherichia coli* laboratory strains and its application to SLiP site-directed mutagenesis. *BMC Biotechnol.* 15:47. doi: 10.1186/s12896-015-0162-8

Mukhtarova, L. S., Lantsova, N. V., Khairutdinov, B. I., and Grechkin, A. N. (2020). Lipoxygenase pathway in model bryophytes: 12-Oxo-9(13),15-phytodienoic acid is a predominant oxylipin in *Physcomitrella patens*. *Phytochemistry* 180:112533. doi: 10.1016/j.phytochem.2020.112533

Nishiyama, T., Hiwatashi, Y., Sakakibara, K., Kato, M., and Hasebe, M. (2000). Tagged mutagenesis and gene-trap in the moss, *Physcomitrella patens* by shuttle mutagenesis. *DNA Res.* 7, 9–17. doi: 10.1093/dnares/7.1.9

Nozaki, H., Hayashi, K., Nishimura, N., Kawaide, H., Matsuo, A., and Takaoka, D. (2007). Momilactone A and B as allelochemicals from moss *Hypnum plumaeforme*: first occurrence in bryophytes. *Biosci. Biotechnol. Biochem.* 71, 3127–3130. doi: 10.1271/bbb.70625

Okada, K., Kawaide, H., Miyamoto, K., Miyazaki, S., Kainuma, R., Kimura, H., et al. (2016). HpDTC1, a stress-inducible bifunctional diterpene cyclase involved in momilactone biosynthesis, functions in chemical defence in the moss *Hypnum plumaeforme*. *Sci. Rep.* 6:25316. doi: 10.1038/srep25316

Park, J.-H., Halitschke, R., Kim, H. B., Baldwin, I. T., Feldmann, K. A., and Feyereisen, R. (2002). A knock-out mutation in allene oxide synthase results in male sterility and defective wound signal transduction in Arabidopsis due to a block in jasmonic acid biosynthesis. *Plant J.* 31, 1–12. doi: 10.1046/j.1365-313X.2002.01328.x

Pauwels, L., and Goossens, A. (2011). The JAZ proteins: a crucial interface in the jasmonate signaling cascade. *Plant Cell* 23, 3089–3100. doi: 10.1105/tpc.111.089300

Peñuelas, M., Monte, I., Schweizer, F., Vallat, A., Reymond, P., García-Casado, G., et al. (2019). Jasmonate-related MYC transcription factors are functionally conserved in *Marchantia polymorpha*. *Plant Cell* 31, 2491–2509. doi: 10.1105/tpc.18.00974

Pratiwi, P., Tanaka, G., Takahashi, T., Xie, X., Yoneyama, K., Matsuura, H., et al. (2017). Identification of jasmonic acid and jasmonoyl-isoleucine, and characterization of AOS, AOC, OPR and JAR1 in the model lycophyte *Selaginella moellendorffii*. *Plant Cell Physiol.* 58, 789–801. doi: 10.1093/pcp/pcx031

Rensing, S. A., Ick, J., Fawcett, J. A., Lang, D., Zimmer, A., Van de Peer, Y., et al. (2007). An ancient genome duplication contributed to the abundance of metabolic genes in the moss *Physcomitrella patens*. *BMC Evol. Biol.* 7:130. doi: 10.1186/1471-2148-7-130

Riemann, M., Haga, K., Shimizu, T., Okada, K., Ando, S., Mochizuki, S., et al. (2013). Identification of rice Allene Oxide Cyclase mutants and the function of jasmonate for defence against *Magnaporthe oryzae*. *Plant J.* 74, 226–238. doi: 10.1111/tpj.12115

Saitou, N., and Nei, M. (1987). The neighbor-joining method: a new method for reconstructing phylogenetic trees. *Mol. Biol. Evol.* 4, 406–425. doi: 10.1093/oxfordjournals.molbev.a040454

Sheard, L. B., Tan, X., Mao, H., Withers, J., Ben-Nissan, G., Hinds, T. R., et al. (2010). Jasmonate perception by inositol-phosphate-potentiated COI1–JAZ co-receptor. *Nature* 468, 400–405. doi: 10.1038/nature09430

Shimura, K., Okada, A., Okada, K., Jikumaru, Y., Ko, K.-W., Toyomasu, T., et al. (2007). Identification of a biosynthetic gene cluster in rice for momilactones. *J. Biol. Chem.* 282, 34013–34018. doi: 10.1074/jbc.M703344200

Staswick, P. E., and Tiryaki, I. (2004). The oxylipin signal jasmonic acid Is activated by an enzyme that conjugates it to isoleucine in Arabidopsis. *Plant Cell* 16, 2117–2127. doi: 10.1105/tpc.104.023549

Stumpe, M., Göbel, C., Faltin, B., Beike, A. K., Hause, B., Himmelsbach, K., et al. (2010). The moss *Physcomitrella patens* contains cyclopentenones but no jasmonates: mutations in allene oxide cyclase lead to reduced fertility and altered sporophyte morphology. *New Phytol.* 188, 740–749. doi: 10.1111/j.1469-8137.2010.03406.x

Tamiru, M., Takagi, H., Abe, A., Yokota, T., Kanzaki, H., Okamoto, H., et al. (2016). A chloroplast-localized protein LESION AND LAMINA BENDING affects defence and growth responses in rice. *New Phytol.* 210, 1282–1297. doi: 10.1111/nph.13864

Thines, B., Katsir, L., Melotto, M., Niu, Y., Mandaokar, A., Liu, G., et al. (2007). JAZ repressor proteins are targets of the SCFCOI1 complex during jasmonate signalling. *Nature* 448, 661–665. doi: 10.1038/nature05960

Uji, Y., Taniguchi, S., Tamaoki, D., Shishido, H., Akimitsu, K., and Gomi, K. (2016). Overexpression of OsMYC2 results in the up-regulation of early JA-responsive genes and bacterial blight resistance in rice. *Plant Cell Physiol.* 57, 1814–1827. doi: 10.1093/pcp/pcw101

Wang, J., Sakurai, H., Kato, N., Kaji, T., and Ueda, M. (2021). Syntheses of dinor-cis/iso-12-oxo-phytodienoic acid (dn-cis/iso-OPDAs), ancestral jasmonate phytohormones of the bryophyte *Marchantia polymorpha* L., and their catabolites. *Sci. Rep.* 11:2033. doi: 10.1038/s41598-021-81575-z

Wasternack, C. (2015). How jasmonates earned their laurels: past and present. *J. Plant Growth Regul.* 34, 761–794. doi: 10.1007/s00344-015-9526-5

Wasternack, C., and Hause, B. (2013). Jasmonates: biosynthesis, perception, signal transduction and action in plant stress response, growth and development. An update to the 2007 review in Annals of Botany. *Ann. Bot.* 111, 1021–1058. doi: 10.1093/aob/mct067

Wasternack, C., and Hause, B. (2018). A bypass in jasmonate biosynthesis – the OPR3-independent formation. *Trends Plant Sci.* 23, 276–279. doi: 10.1016/j.tplants.2018.02.011

Xie, D.-X., Feys, B. F., James, S., Nieto-Rostro, M., and Turner, J. G. (1998). COI1: an Arabidopsis gene required for jasmonate-regulated defense and fertility. *Science* 280, 1091–1094. doi: 10.1126/science.280.5366.1091

Yamane, H. (2013). Biosynthesis of phytoalexins and regulatory mechanisms of it in rice. *Biosci. Biotechnol. Biochem.* 77, 1141–1148. doi: 10.1271/bbb.130109

Yan, J., Zhang, C., Gu, M., Bai, Z., Zhang, W., Qi, T., et al. (2009). The *Arabidopsis* CORONATINE INSENSITIVE1 protein is a jasmonate receptor. *Plant Cell* 21, 2220–2236. doi: 10.1105/tpc.109.065730

Zimmerman, D. C., and Feng, P. (1978). Characterization of a prostaglandin-like metabolite of linolenic acid produced by a flaxseed extract. *Lipids* 13:313. doi: 10.1007/bf02533720

Conflict of Interest: The authors declare that the research was conducted in the absence of any commercial or financial relationships that could be construed as a potential conflict of interest.

Copyright © 2021 Inagaki, Miyamoto, Ando, Murakami, Sugisawa, Morita, Yumoto, Teruya, Uchida, Kato, Kaji, Takaoka, Hojo, Shinya, Galis, Nozawa, Sawasaki, Nojiri, Ueda and Okada. This is an open-access article distributed under the terms of the Creative Commons Attribution License (CC BY). The use, distribution or reproduction in other forums is permitted, provided the original author(s) and the copyright owner(s) are credited and that the original publication in this journal is cited, in accordance with accepted academic practice. No use, distribution or reproduction is permitted which does not comply with these terms.

frontiers in Plant Science

ORIGINAL RESEARCH
published: 29 July 2021
doi: 10.3389/fpls.2021.705373

Oxylipins From Different Pathways Trigger Mitochondrial Stress Signaling Through Respiratory Complex III

Yovanny Izquierdo[1], Luis Muñiz[1†], Jorge Vicente[1,2], Satish Kulasekaran[1†], Verónica Aguilera[1], Ana López Sánchez[1], Ada Martínez-Ayala[1], Bran López[1], Tomás Cascón[1] and Carmen Castresana[1]**

[1] Department of Plant Molecular Genetics, Centro Nacional de Biotecnología (CNB-CSIC), Madrid, Spain, [2] School of Biosciences, University of Nottingham, Nottingham, United Kingdom

OPEN ACCESS

Edited by:
Michael V. Kolomiets,
Texas A&M University, United States

Reviewed by:
Jun'ichi Mano,
Yamaguchi University, Japan
Autar Krishen Mattoo,
Agricultural Research Service (USDA), United States

***Correspondence:**
Yovanny Izquierdo
yizquierdo@cnb.csic.es
Carmen Castresana
ccastreana@cnb.csic.es

†Present address:
Luis Muñiz,
Miltenyi Biotec, Madrid, Spain
Satish Kulasekaran,
Biopharm Discovery, GlaxoSmithKline, Brentford, United Kingdom

Specialty section:
This article was submitted to Plant Physiology, a section of the journal Frontiers in Plant Science

Received: 05 May 2021
Accepted: 02 July 2021
Published: 29 July 2021

Citation:
Izquierdo Y, Muñiz L, Vicente J, Kulasekaran S, Aguilera V, López Sánchez A, Martínez-Ayala A, López B, Cascón T and Castresana C (2021) Oxylipins From Different Pathways Trigger Mitochondrial Stress Signaling Through Respiratory Complex III. Front. Plant Sci. 12:705373. doi: 10.3389/fpls.2021.705373

Plant oxylipins are signaling molecules produced from fatty acids by oxidative pathways, mainly initiated by 9- and 13-lipoxygenases (9-LOX and 13-LOX), alpha-dioxygenases or non-enzymatic oxidation. Oxylipins from the 9-LOX pathway induce oxidative stress and control root development and plant defense. These activities have been associated with mitochondrial processes, but precise cellular targets and pathways remain unknown. In order to study oxylipin signaling, we previously generated a collection of *Arabidopsis thaliana* mutants that were insensitive to the 9-LOX products 9(S)-hydroxy-10,12, 15-octadecatrienoic acid (9-HOT) and its ketone derivative 9-KOT (*noxy* mutants). Here, we describe *noxy1*, *noxy3*, *noxy5*, *noxy23*, and *noxy54* mutants, all affected in nucleus-encoded mitochondrial proteins, and use them to study the role of mitochondria in oxylipin signaling. Functional and phenotypic analyses showed that *noxy* plants displayed mitochondrial aggregation, reduced respiration rates and resistance to the complex III inhibitor Antimycin A (AA), thus indicating a close similarity of the oxylipin signaling and mitochondrial stress. Application of 9-HOT and 9-KOT protected plants against subsequent mitochondrial stress, whereas they boosted root growth reduction when applied in combination with complex III inhibitors but did not with inhibitors of other respiratory complexes. A similar effect was caused by linear-chain oxylipins from 13-LOX or non-enzymatic pathways having α,β-unsaturated hydroxyl or keto groups in their structure. Studies to investigate 9-HOT and 9-KOT activity indicated that they do not reduce respiration rates, but their action is primarily associated with enhanced ROS responses. This was supported by the results showing that 9-HOT or 9-KOT combined with AA amplified the expression of oxylipin- and ROS-responding genes but not of the AA marker *AOX1a*, thus implying the activation of a specific mitochondria retrograde signaling pathway. Our results implicate mitochondrial complex III as a hub in the signaling activity of multiple oxylipin pathways and point at downstream ROS responses as components of oxylipin function.

Keywords: arabidopsis, oxylipins, mitochondria, Antimycin A, reactive oxygen species, complex III, retrograde signaling

INTRODUCTION

The term oxylipin is generically used to group oxidized lipid derivatives produced from the oxidation of fatty acids. Oxylipins are ubiquitous throughout life kingdoms and usually have signaling functions. In animals, prostaglandins and leukotrienes mediate inflammatory responses (Haeggström and Funk, 2011), whereas in bacteria, oleic-acid derived oxylipins participate in quorum sensing and virulence (Martínez and Campos-Gómez, 2016). In plants, hundreds of different oxylipins have been reported, but there are vast differences in our knowledge of different existing pathways (Wasternack and Feussner, 2018).

Plant oxylipins are produced mainly during stress responses. Biosynthesis occurs by both enzymatic or non-enzymatic incorporation of oxygen, mainly to polyunsaturated fatty acids such as linoleic (18:2, LA) or linolenic acid (18:3, LNA). **Figure 1** shows a schematic representation of the major oxylipin biosynthesis pathways, focused on the derivatives used in this study. The first step of oxylipin synthesis is usually the formation of a lipid hydroperoxide, followed by secondary modifications leading to a vast array of compounds (Wasternack and Feussner, 2018). Depending on the position of the initial oxygenation, several enzymatic pathways can be defined. Taking LNA as initial substrate, α-dioxygenases (α-DOX) lead to 2(*R*)-hydroxy-9(*Z*),12(*Z*),15(*Z*)-octadecatrienoic acid (2-HOT, Hamberg et al., 2003), whereas 9- and 13- lipoxygenases (9-LOX and 13-LOX) catalyze stereospecific oxidation in positions 9 and 13, respectively. Hydroperoxides derived from LNA and 13-LOX can be either committed to jasmonic acid synthesis or transformed into 13(*S*)-hydroxy-9(*Z*),11(*E*),15(*Z*)-octadecatrienoic acid (13-HOT) and 13-keto-9(*Z*),11(*E*),15(*Z*)-octadecatrienoic acid (13-KOT). Likewise, 9-LOX activity generates mainly 9(*S*)-hydroxy-10(*E*),12(*Z*),15(*Z*)-octadecatrienoic acid (9-HOT) and 9-keto-10(*E*),12(*Z*),15(*Z*)-octadecatrienoic acid (9-KOT; Blée, 2002; Andreou and Feussner, 2009; Mosblech et al., 2009). LNA peroxidation can also take place non-enzymatically during severe oxidative stress, by reaction with singlet oxygen or hydroxyl radicals. In these cases, oxygen addition can occur at any unsaturated carbon, leading to HOT and possibly KOT derivatives in positions 9, 10, 12, 13, 15, and 16 (Göbel et al., 2003; Mosblech et al., 2009). Lipid fragmentation is also common, leading to short chain α,β-unsaturated aldehydes or ketones such as malondialdehyde, 2-hexenal and acrolein (Alméras et al., 2003; Farmer and Mueller, 2013; Mochizuki et al., 2016). These reactive electrophilic species (RES) are considered universal lipid peroxidation markers and can bind covalently to cysteine residues (Mueller and Berger, 2009; Ameye et al., 2018). Some lipoxygenase products, such as 9-KOT and 13-KOT, also contain α,β-unsaturated carbonyl, but little is known about their specific reactivity.

13-LOX-derived jasmonic acid is by far the most studied oxylipin. As a key hormone controlling both developmental and stress-related processes, its receptor, co-receptors, and downstream-regulated transcription factors and target genes are well defined (Chini et al., 2009; Ruan et al., 2019). In addition to jasmonates, oxylipins from the 9-LOX and non-enzymatic pathways are also implicated in plant stress responses. In Arabidopsis roots, 9-HOT induces a characteristic waving phenotype, accompanied by oxidative stress and callose deposition (Vellosillo et al., 2007). These processes are mediated by brassinosteroid signaling and contribute to defense against pathogens (Marcos et al., 2015). In leaves, 9-HOT and 9-KOT (and other hydroxy and keto derivatives of LNA) accumulate in response to infection with avirulent bacteria, contributing to the hypersensitive response (HR) in different plant species (Rustérucci et al., 1999; Göbel et al., 2002; Jalloul et al., 2002; Battilani et al., 2018). Moreover, inoculation of 9-KOT induces local and systemic acquired resistance (SAR) against subsequent *Pseudomonas* infection (Vicente et al., 2012). Oxylipins produced exclusively by non-enzymatic reactions (e.g., 10, 12, 15, and 16-HOT) have also been detected in strong oxidative conditions leading to lipid peroxidation, like the onset of HR and cell death (Göbel et al., 2003), but very little is known about their functions.

Despite abundant evidence on 9-LOX-oxylipin functions in plant responses, their precise perception and signaling pathways remain elusive. In an attempt to identify specific signaling pathways, Walper et al. (2016) identified transcription factors involved in 9-HOT response, but concluded these were mostly related to oxylipin detoxification instead of signal transduction. In a previous study, we took advantage of the waving phenotype induced by 9-HOT to generate a collection of non-sensitive to oxylipin (*noxy*) mutants (Vellosillo et al., 2007). Three of these signaling mutants (*noxy2*, *noxy15/drp3a-1* and *noxy38/fmt-1*) displayed abnormal mitochondrial aggregates and were affected in mitochondrial stress responses (Vellosillo et al., 2013). In the same study, 9-HOT was found to decrease the mitochondrial membrane potential, collectively suggesting that 9-LOX oxylipin signaling was associated to mitochondrial processes.

Here, we describe five additional *noxy* mutants (*noxy1*, *noxy3*, *noxy5*, *noxy23,* and *noxy54*), all affected in mitochondrial distribution and function, and at the same time resistant to Antimycin A (AA), a mitochondrial complex III (C-III) inhibitor commonly used to study mitochondrial retrograde signaling (Yu et al., 2001). Studies with mitochondrial respiration inhibitors in combination with 9-HOT and 9-KOT, showed that these oxylipins exacerbate the root growth arrest caused by inhibitors of C-III, but not of other respiratory complexes. This effect was associated to an increment of ROS production and changes in stress gene expression. The application of 9-HOT and 9-KOT protected plants against subsequent mitochondrial stress. These activities were extensive not only to 9-LOX derivatives, but also to structurally related oxylipins from 13-LOX and non-enzymatic pathways (collectively named here as mitochondria-active oxylipins) suggesting a common mitochondrial effect. Altogether, our results point to mitochondrial C-III as a hub in oxylipin signaling that would cause mild mitochondrial damage to trigger a stress response protecting plants against cellular injury.

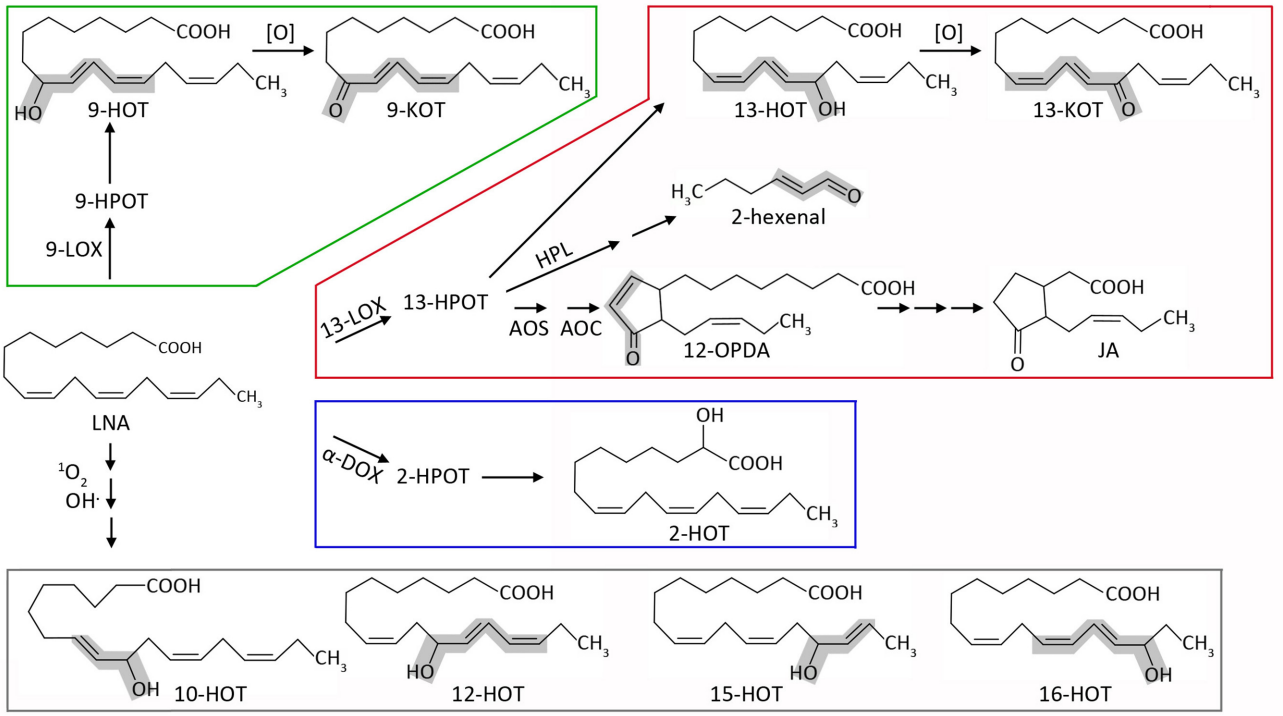

FIGURE 1 | Schematic representation of the major oxylipin biosynthesis pathways, focused on the derivatives used in this work. Starting from linolenic acid (LNA), oxygenation can be carried out by 9-lipoxygenases (9-LOX, green), 13-lipoxygenases (13-LOX, red), α-dioxygenases (α-DOX, blue), or non-enzymatic reactions (gray). Lipoxygenases generate the hydroperoxides 9-HPOT and 13-HPOT, which are then reduced to hydroxyl-acids 9-HOT and 13-HOT. These can be further oxidized to 9-KOT and 13-KOT (alternatively, lipoxygenases could directly generate keto-acids from hydroperoxides, which is not shown for simplicity). 13-HPOT can be fragmented by hydroperoxide lyase (HPL) to 2-hexenal or committed to the jasmonate pathway by the sequential action of allene oxide synthase (AOS) and allene oxide cyclase (AOC) leading to 12-OPDA. The latter can be reduced and subjected to three β-oxidation cycles leading to jasmonic acid (JA). α-dioxygenases mainly yield 2-HOT *in vivo*, also through a hydroperoxide intermediate (2-HPOT). LNA can also react directly with singlet oxygen or hydroxyl radical. This pathway can lead to 9-HOT and 13-HOT (not shown), but also to oxylipins exclusively generated by non-enzymatic reactions (10-HOT, 12-HOT, 15-HOT and 16-HOT). α,β-unsaturated carbonyl (RES) or hydroxyl (RES precursor) moieties are highlighted in gray. For simplicity, stereochemistry details have been omitted (e.g., 13-LOX and 9-LOX yield *S*-enantiomers whereas non-enzymatic reactions produce racemic mixtures) as well as additional oxylipins generated by secondary enzymatic or non-enzymatic reactions.

MATERIALS AND METHODS

Plant Material, Mutant Characterization and Growth Conditions

Arabidopsis thaliana wild type and mutant plants were derived from Columbia-0 ecotype. *noxy1, noxy3, noxy5, noxy23,* and *noxy54* mutants were generated in a previous screening of an EMS-mutagenized population (Vellosillo et al., 2007). Therein, *noxy* mutants were selected due to their inability to show a root waving phenotype in presence of 9-HOT. To identify mutations, *noxy* plants were crossed to wild type Landsberg erecta ecotype and F2 mutants were selected. DNA from *noxy* and 400 recombinant mutants was used to analyze mutation linkage as described by Ponce et al. (2006). Massive genome sequencing performed at BGI genomics (http://www.genomics.cn) was used to identify *noxy* mutations in the mapped region. For microscopy analysis, Col-0;*35S:mtYFP* plants (Nelson et al., 2007; Vellosillo et al., 2013) were crossed with *noxy* mutants. Additional mutants used were *ahg2-1*(Nishimura et al., 2004) and T-DNA insertion lines *lon1-4* (SALK_013817) and *noxy23-2* (SALK_036918) which were obtained from the Nottingham Arabidopsis Stock Center (Nottingham, UK).

For *in vitro* analysis, seeds were sterilized with 75% bleach and vernalized for 3 days. Germinated seedlings were grown vertically in controlled chambers at 22°C with 14 h light (120 μmol $s^{-1}m^{-2}$) and 10 h dark, in fluorescent illumination. Culture medium was 0.5 × MS with 1.5% (w/v) agar and 1.5% (w/v) sucrose. For phenotype analysis, seedlings were transferred after 4 days to the same medium supplemented with specific products at the indicated concentrations. In pretreatment assays, plants were germinated directly in oxylipins (25 μM), LNA (25 μM) or AA (2.5 μM) and transferred after 4 days to AA-containing (15 μM) MS medium. In all cases, root growth was measured 3 days after transference to the new medium. For gene expression analysis, 7-day-old seedlings were moved to liquid medium (0.5 × MS with 1.5% sucrose), kept overnight for acclimation, and treated with oxylipins (20 μM), AA (20 μM), or their combinations.

Reagents and Chemicals

Oxylipins used in this study (**Supplementary Table 1**) were obtained as previously described. 9-LOX and 13-LOX derivatives (9-HOT, 9-KOT, 13-HOT, and 13-KOT) were produced as in Prost et al. (2005); α-DOX derivative 2-HOT was synthesized as in Hamberg et al. (1999); non-enzymatically produced 10-HOT, 12-HOT, and the mixture 15-HOT/16-HOT, were obtained by singlet oxygen oxygenation (Przybyla et al., 2008). Oxylipin stocks were prepared in 95% ethanol and diluted in buffer or culture media to reach appropriate concentrations. OPDA and JA were purchased from Larodan Fine Chemicals. Additional products used for phenotype analysis and respiration assays were purchased from Sigma Aldrich with at least 95% purity: Antimycin A (A8674), Myxothiazol (T5580), Rotenone (R8875), Carboxin (45371), Sodium malonate (63409), KCN (60178), Oligomycin A (75351), Sodium ascorbate (A7631), *tert*-butyl hydroperoxyde (458139), 2(*E*)-hexenal (132659), Paraquat (36541), NADH (10107735001), ATP (A1852), ADP (01905), Sodium succinate (S2378), Dithiothreitol (D0632) and n-Propyl gallate (P3130).

Root Phenotype Analysis

Vertically grown plants were photographed and root lengths were measured with Fiji software (https://fiji.sc/). For each genotype, measurements were presented as relative root growth with respect to plants grown in control conditions. In single treatments, statistical differences were determined by Student's *t*-test. Interaction in combined treatments was determined by two-way ANOVA with R functions "aov" and "Anova."

Confocal Microscopy

Mitochondrial distribution in wild type and *noxy* plants expressing mt-YFP was observed in the elongation zone of 7-day-old seedling roots. Images were taken with a Leica Stellaris microscope using a 20 × objective and 4 × zoom amplification. A 488 nm laser line was used for excitation, and fluorescence was detected in the range 500-636 nm. Localization of NOXY1:GFP was determined by co-localization with the mitochondrial marker mt-mCherry in *Nicothiana benthamiana* leaves. NOXY1:GFP construct was prepared by cloning the genomic sequence of NOXY1 into the pGWB5 vector, and it was transiently coexpressed with mt-mCherry (Nelson et al., 2007) in *N. benthamiana* by Agrobacterium-mediated transformation. Images were taken with a Leica TCS-SP8 microscope using a 63x objective. Sequential scanning was done with 488 nm (for GFP) and 575 nm (for mCherry) excitation laser lines. Fluorescence emission bands 496–550 and 585–660 nm were used to detect GFP and mCherry, respectively. Raw images were exported to jpeg format with LASX software (https://www.leica-microsystems.com/).

Mitochondrial Isolation

Mitochondria were isolated as described by Whelan and Murcha (2015). Briefly, 10 g of 2-week-old, plate-grown plants were collected and immediately ground with 7 g of sea sand in 40 ml of cold extraction buffer (0.3 M sucrose, 25 mM tetrasodium pyrophosphate, 10 mM KH_2PO_4, 2 mM EDTA, 1% w/v PVP-40, 1% w/v defatted BSA, 18 mM sodium ascorbate, 20 mM cysteine, pH 7.5). Homogenate was filtered and centrifuged at 2,450 × *g*. Supernatant was collected and centrifuged 20 min at 17,400 × *g*. The resultant pellet was collected by gently resuspending in 1 ml wash buffer (0.3 M sucrose, 10 mM TES, 0.1% defatted BSA, pH 7.5) using a paintbrush. This suspension contained crude mitochondria and chloroplasts, and was cleaned up by repeating both previous centrifugation steps, and finally resuspended in 400 μl of wash buffer. The resulting chloroplast/mitochondria preparation was overlaid in continuous PVP-40/Percoll gradients and ultracentrifuged in a SW40Ti rotor (Beckman Coulter) for 40 min, at 40,000 × *g* (no brake). Mitochondria formed a yellowish band close to the bottom. They were carefully aspirated, placed in a new ultracentrifuge tube, and washed by filling with wash buffer and centrifuging 20 min at 31,000 × *g* with light brake. This washing step was repeated with 15 min centrifugation at 18,000 × *g* and supernatant was carefully removed. The mitochondrial pellet was collected by aspiration with a Pasteur pipette in a minimum volume (∼200 μl). Protein concentration was measured with Bio-Rad Protein Assay kit (Bio-Rad).

Respiration Measurement

Mitochondria respiratory capacity was estimated by measuring oxygen consumption of purified mitochondria (30–50 μg protein) with a Clark electrode (Oxygraph, Hansatech) using 5 mM sodium succinate and 1 mM NADPH as substrates, as described by Whelan and Murcha (2015).

Western Blot

Western blot was performed by standard procedures. Samples were extracted in 4 M urea, 50 mM TrisHCl pH 7.5, 150 mM NaCl, 0.1% (w/v) Nonidet P40, 1 mM PMSF and 1X complete protease inhibitor cocktail (Roche). Protein-containing supernatants were collected by centrifugation (10,000 × *g*, 10 min, 4°C). 25 μg protein per sample were separated by SDS-PAGE in 10% acrylamide gels, transferred to nitrocellulose membranes (GE Health Care), stained with red Ponceau (0.1%), washed, blocked with 5% defatted powder milk in TBS and incubated with an antibody specific to plant AOX1/2 (Agrisera) diluted 1:1000 in TBS with 1% defatted powder milk. Blots were then incubated with a peroxidase-labeled anti-rabbit antibody (Agrisera) and revealed with ECL Select™ (Amersham). Blot images were taken in a ChemiDoc™ imaging system (BioRad).

RNA Isolation and RT-qPCR

For each treatment, RNA was isolated from three biological replicates by Guanidine hydrochloride/Phenol-chloroform extraction (Logemann et al., 1987). Contaminant DNA was removed using Turbo DNA-free™ kit (ThermoFisher). cDNA was synthesized with Transcriptor First Strand cDNA Synthesis Kit (Roche) using hexamer random primers and RNA denaturation at 60°C. qPCR was performed in a 7500 thermocycler (Applied Biosystems), using NZYSpeedy qPCR Green Master Mix (2x) and specific primers (**Supplementary Table 2**). Expression was normalized combining 18S rRNA and *SAND* gene (At2g28390, described in Czechowski et al., 2005) as references.

RESULTS

Identification of *noxy* Mutants With Mitochondrial Dysfunction

Previous studies with the 9-LOX product 9(*S*)-hydroxy-10,12,15-octadecatrienoic acid (9-HOT) demonstrated the importance of mitochondria in 9-LOX-derived oxylipin signaling (Vellosillo et al., 2013; Marcos et al., 2015). 9-HOT caused mitochondrial aggregation and loss of inner membrane potential when added to wild type plants, whereas 9-HOT insensitive mutants *noxy2*, *noxy15/drp3a-1* and *noxy38/fmt-1* exhibited constitutive mitochondrial alterations (Vellosillo et al., 2013).

The activity of 9-HOT on mitochondria was further investigated here by using additional *noxy* mutants (*noxy1*, *noxy3,* *noxy5*, *noxy23,* and *noxy54*). They all had shorter roots than wild type plants and were impeded in characteristic 9-HOT responses such as root waving and callose deposition (**Supplementary Figure 1**), similar to other oxylipin-insensitive *noxy* mutants (Vellosillo et al., 2007, 2013; López et al., 2011; Marcos et al., 2015; Izquierdo et al., 2018).

A combination of classical map-based positional cloning and next-generation sequencing allowed the identification of *noxy* mutations, summarized in **Table 1**. This genetic analysis indicated that all *noxy* mutations were monogenic and recessive. *noxy1* and *noxy5* were located at loci At1g43980 and At3g02010, respectively. Both encode mitochondrial Pentatricopeptide Repeat (PPR) proteins, which are usually associated with post-transcriptional processing of chloroplast or mitochondrial RNA (Lurin et al., 2004). The *noxy1* mutation is a G-to-A transition between repeats 11 and 12 that changes Gly-366 to Glu in the protein sequence. The *noxy5* mutation is a C-to-T transition that converts Thr-227, within repeat 6, to Met. *noxy3* was located at locus At5g26860 encoding the mitochondrial protease LON1, involved in the control of protein turnover (Rigas et al., 2009). *noxy3* mutant contains two G-to-A nucleotide mutations in *LON1* gene, changing Arg-441 and Glu-444 to Lys residues. As mutant alleles *lon1-1* and *lon1-2* were previously described (Solheim et al., 2012), *noxy3* was renamed as *lon1-3*. The *noxy23* mutation is a G-to-A transition changing Glu-199 to Lys in locus At1g64880, which encodes a member of the S5 ribosomal protein family with mitochondrial localization (Bonen and Calixte, 2006). Finally, mutation *noxy54* was located at the locus At1g55870 encoding AHG2 (ABA Hypersensitive Germination 2), a mitochondrial poly(A)-specific exoribonuclease (AtPARN) that controls mRNA levels in this organelle (Hirayama et al., 2013). *noxy54* plants contain a G-to-A transition that turns Trp-552 into a stop codon and produces a truncated protein. As mutant alleles *ahg2-1* and *ahg2-2* were previously characterized (Nishimura et al., 2004; Hirayama et al., 2013), *noxy54* was renamed as *ahg2-3*.

NOXY3/LON1, NOXY5, NOXY23, and NOXY54/AHG2 had been demonstrated to be nuclear-encoded mitochondrial proteins (Lurin et al., 2004; Bonen and Calixte, 2006; Ostersetzer et al., 2007; Hirayama et al., 2013), whereas experimental evidence for subcellular localization of *NOXY1* gene product was still lacking. To examine NOXY1 cellular localization, we transiently coexpressed a *35S:NOXY1-GFP* construct together with the mitochondrial marker mt-mCherry in *N. benthamiana* leaves. Fluorescence microscopy showed that GFP and mt-mCherry colocalized, supporting the mitochondrial localization of NOXY1 protein (**Supplementary Figure 2**).

We previously described that both 9-HOT treatment and *noxy* mutations produced abnormal mitochondrial aggregation (Vellosillo et al., 2013). To analyze the mitochondrial morphology of *noxy1*, *noxy3/lon1-3*, *noxy5*, *noxy23,* and *noxy54/ahg2-3*, these mutations were crossed into a transgenic Col-0 line expressing a mitochondria-targeted yellow fluorescent protein (mt-YFP) allowing mitochondrial visualization (Nelson et al., 2007; Vellosillo et al., 2013). Whereas small, individual mitochondria were visible in transgenic Col-0 plants, fluorescence imaging showed abnormal mitochondria accumulates in the roots of all *noxy* mutants. This pattern was more evident in the vascular bundle, where mitochondrial aggregates were accompanied by a noticeable reduction of mitochondrial density in the remaining cells (**Figure 2A**).

We then addressed whether this abnormal distribution was associated with mitochondrial dysfunction. To this end, we measured the respiratory capacities of mitochondria isolated from *in vitro* grown wild type and *noxy* plants. A significantly reduced cytochrome respiration was detected in all mutants, ranging from ∼30% of wild type in *noxy3/lon1-3* to ∼70% in *noxy1* (**Figure 2B**). By contrast, no significant differences were detected in alternative respiration rates (**Figure 2B**).

noxy Mutants Are Resistant to Antimycin A

Given that all five *noxy* mutations affected mitochondrial functionality, we tested the response of *noxy* mutants to Antimycin A (AA), a widely used and well characterized inhibitor of mitochondrial respiratory complex III (Li et al., 2014). Wild type plants were first exposed to different concentrations of AA to identify a root phenotype allowing subsequent analysis. Root growth reduction was observed with increasing concentrations of AA, until complete growth arrest at 15 μM. Based on this result, AA treatments at 2.5 and 15 μM were selected as inducers of moderate and severe mitochondrial stress, respectively. Growth in AA-containing medium showed that all *noxy* mutants were resistant to both levels of AA; this difference was particularly evident at 15 μM, where complete root growth arrest in wild type plants contrasted with only ∼50% reduction in *noxy* mutants (**Figures 3A,B**). We extended this analysis to previously identified *noxy* mutants with mitochondrial dysfunction (*noxy2*, *noxy15/drp3a-1*, *noxy38/fmt-1*, Vellosillo et al., 2013) and the ethylene overproducer *noxy22* (López et al., 2011); in all cases, root growth was not arrested by 15 μM AA (**Supplementary Figure 3**).

Both AA resistance and 9-HOT insensitivity phenotypes were useful to validate the identity of *noxy* mutations (**Supplementary Figure 4**). *lon1-4* and *ahg2-1* plants responded similarly to their original mutant alleles *noxy3/lon1-3* and *noxy54/ahg2-3* (**Supplementary Figure 4**), whereas *noxy23-2* showed an intermediate phenotype compared to *noxy23*, probably due to a lower penetration of the *noxy23-2* mutation (a T-DNA insertion at the promoter region of At1g64880) (**Supplementary Figure 4**). As no mutant alleles were available

TABLE 1 | Mutants used in this study.

Mutant	Renamed as	Gene name	AGI	Localization	Description (Uniprot)
noxy1	*noxy1*	*NOXY1*	At1g43980	Mitochondria[a,e]	PPR-containing protein, mitochondrial
noxy3	*lon1-3*	*LON1*	At5g26860	Mitochondria[b]	Lon protease homolog 1, mitochondrial
noxy5	*noxy5*	*NOXY5*	At3g02010	Mitochondria[a]	Putative PPR-containing protein
noxy23	*noxy23*	*NOXY23*	At1g64880	Mitochondria[c]	Ribosomal protein S5 family protein
noxy54	*ahg2-3*	*AtPARN*	At1g55870	Mitochondria[d]	Poly(A)-specific ribonuclease (PARN)

[a]*Lurin et al. (2004)*, [b]*Ostersetzer et al. (2007)*, [c]*Bonen and Calixte (2006)*, [d]*Hirayama et al. (2013)*, [e]*This study.*

for *noxy1* and *noxy5*, we tested the complementation of mutant phenotypes with wild type versions of *NOXY1* and *NOXY5* genes under the 35S promoter. *noxy1*;*35S:NOXY1* plants recovered wild type phenotypes in response to 9-HOT and AA, confirming the identity of *noxy1* mutation. In the case of *noxy5*, phenotype complementation was observed by transformation with wild type *NOXY5* cDNA (**Supplementary Figure 4**).

In order to overcome AA damage, plants induce alternative oxidases (AOX) to restore electron transport after C-III inhibition (Saisho et al., 1997; Woodson and Chory, 2008). We therefore performed western blot analyses to test whether AOX accumulation in response to AA was affected in *noxy* mutants. In accordance to their resistance to AA, AOX induction was stronger in all *noxy* mutants than in wild type plants. In untreated or control *noxy* plants, AOX levels were also higher than in the wild type. This was particularly evident in *noxy3/lon1-3* plants, which showed constitutively induced AOX expression (**Figure 3C**).

Altogether, our results indicate that *noxy1*, *noxy3/lon1-3*, *noxy5*, *noxy23,* and *noxy54/ahg2-3* are mutants affected in nucleus-encoded mitochondrial proteins, exhibiting both 9-HOT insensitivity and AA resistance.

Structurally Related Oxylipins From Different Pathways Modulate Mitochondrial Stress Associated With Complex III

The coincidence between insensitivity to 9-HOT and AA resistance in *noxy* mutants raised the possibility that both treatments could target a common process, thus we applied both treatments simultaneously and evaluated root phenotypes. A combination of moderate concentrations of 9-HOT (12.5 μM) and AA (2.5 μM) caused complete root growth arrest in wild type plants when added to culture medium (**Figure 4A**). At these concentrations, 9-HOT alone did not reduce root growth, whereas individual application of AA caused ∼50% reduction compared to control seedlings, indicating that 9-HOT amplifies AA-driven root growth reduction. A statistical analysis (two-way ANOVA) confirmed the synergistic interaction between 9-HOT and AA treatments, proving that the root growth reduction observed in the AA/9-HOT combination is stronger to what would be expected from the additive effects of each product (**Figure 4B**).

We extended this experiment to a collection of oxylipins generated by 9-LOX, 13-LOX, α-DOX and non-enzymatic oxidative pathways, all derived from linolenic acid (LNA) (**Figure 1**; **Supplementary Table 1**). Our aim was to identify additional oxylipins that could amplify the response to mitochondrial stress caused by AA (hereafter referred to as mitochondria-active oxylipins). Similar to 9-HOT, amplification of root shortening was observed in AA combined with 9-KOT (from the 9-LOX pathway) as well as with 13-HOT and 13-KOT (13-LOX pathway) (**Figure 4B**). Plant response to hydroxy fatty acids generated by non-enzymatic pathways varied for different oxylipins. Thus, AA in combination with 12-HOT produced a strong root growth arrest, whereas an intermediate effect was observed with a mixture of 15-HOT/16-HOT, and a marginal response was observed in the combination of AA and 10-HOT. By contrast, LNA and α-DOX-derived 2-HOT did not cause any extra root growth reduction combined with AA (**Figure 4B**). Amplification of AA root growth arrest was also observed when oxylipin concentration was reduced to 10 μM (with the exception of 10-HOT), however, further reduction to 5 μM caused only a marginal effect (**Supplementary Figure 5**).

Since 9-KOT and 13-KOT are RES structures, we tested whether other oxylipins bearing α,β-unsaturated carbonyl could amplify the AA-induced root phenotype. The oxylipins 2-hexenal (short chain, linear RES), OPDA (long chain, cyclic RES) and jasmonic acid (non-RES oxylipin control) reduced root growth when applied alone, but their combinations with AA led to an additive response rather than amplification of root growth arrest (**Figures 4C,D**).

We then examined whether *in vivo* generation of oxylipins by application of tert-butyl hydroperoxide (tBuOOH), an inducer of lipid peroxidation, could amplify AA root growth inhibition. tBuOOH did not arrest root growth when applied at 10 or 20 μM, but reduced root length by ∼80% at 50 μM. The combination of tBuOOH with 2.5 μM AA caused a stronger root growth reduction than expected by an additive effect (>60% at 20 μM and complete growth arrest at 50 μM tBuOOH) (**Figures 4E,F**).

In order to know if a pre-existing oxylipin signal influences the AA response, we pre-treated wild type plants with oxylipins before AA exposure. Pre-treatments were 25 μM oxylipins, 2.5 μM AA (mild mitochondrial stress control), 25 μM LNA (fatty acid control) and MS (negative control). After 4 days, seedlings were transferred to 15 μM AA or MS and root growth was measured (**Figure 5A**). As expected, roots of MS pre-treated plants were completely arrested by 15 μM AA. A higher root growth was observed in plants pre-treated with mitochondria-active oxylipins or 2.5 μM AA (∼30–40% of MS

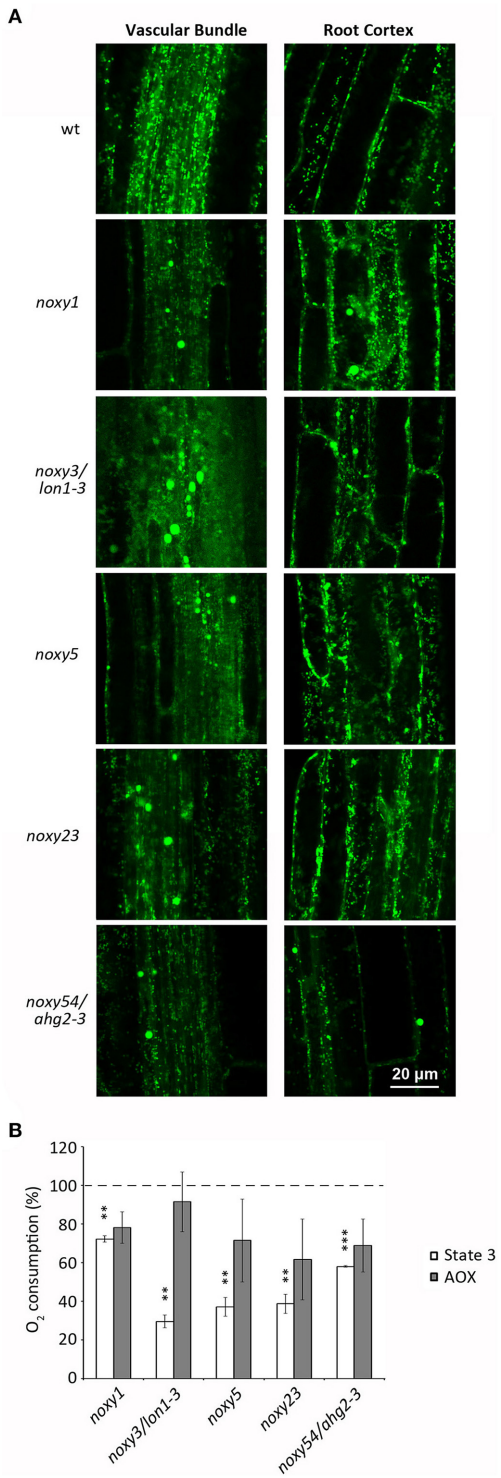

FIGURE 2 | Analysis of mitochondrial distribution and function in wild type, *noxy1*, *noxy3/lon1-3*, *noxy5*, *noxy23*, and *noxy54/ahg2-3* plants. **(A)** Confocal images of mitochondria-tagged mt-YFP in the root vascular bundle (left) and cortex (right) showing abnormal accumulates in *noxy* plants. **(B)** Oxygen consumption rates of cytochrome (State 3) and alternative (AOX) pathways in mitochondria isolated from *noxy* mutants, relative to wild type mitochondria. Asterisks indicate significant differences with wild type plants in each condition ($n = 4$, Student's *t*-test, $^{***}P < 0.001$, $^{**}P < 0.01$.

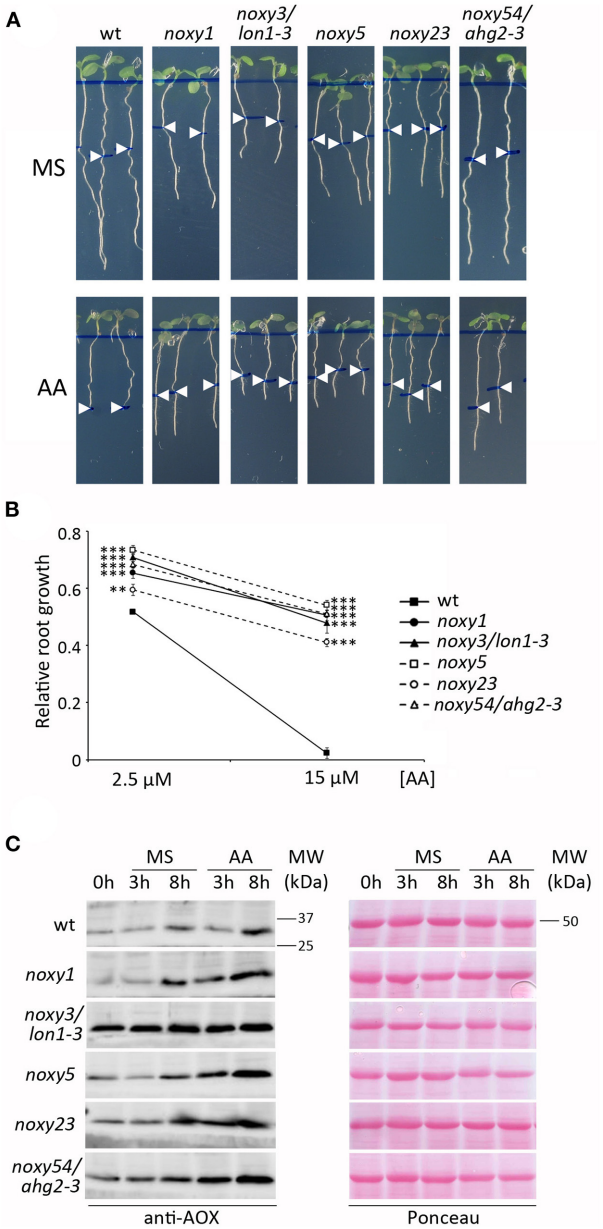

FIGURE 3 | Response of wild type, *noxy1*, *noxy3/lon1-3*, *noxy5*, *noxy23*, and *noxy54/ahg2-3* plants to Antimycin A (AA). **(A)** Root phenotypes of seedlings grown for 3 days on MS medium and then transferred to MS with or without 15 µM AA. Arrow heads indicate root length at the moment of transfer. **(B)** Relative root growth of seedlings in 2.5 and 15 µM AA, defined as the fraction of growth on MS. Asterisks indicate significant differences with wild type plants in each condition ($n \geq 8$, Student's *t*-test, $^{***}P < 0.001$, $^{**}P < 0.01$. **(C)** Western blot showing AOX accumulation in seedlings treated with 20 µM AA. Proteins were extracted and examined at the indicated times. Left: immunoblots with anti-AOX antibody; right: Red Ponceau staining used as loading control. MW, Molecular weight.

control, **Figure 5**). This protection was also observed in plants pre-treated with 10-HOT, 2-HOT, and LNA, suggesting these can be metabolized to mitochondria-active oxylipins.

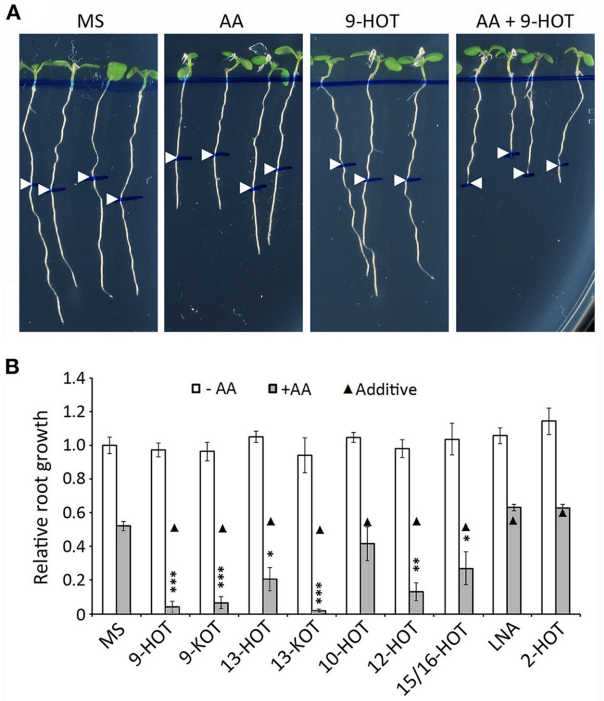

FIGURE 4 | Continued

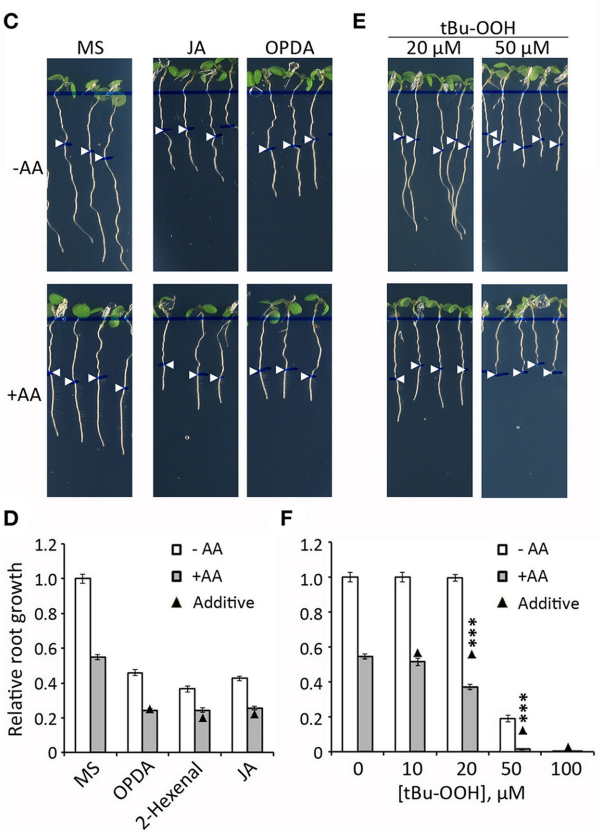

FIGURE 4 | Root growth phenotype in seedlings treated with oxylipins and AA. **(A)** Root phenotypes of wild type plants grown for 4 days on MS medium and then transferred to MS or MS with 2.5 µM AA, 12.5 µM 9-HOT or AA+9-HOT. **(B)** Root growth (relative to MS) of wild type plants in MS, 9-HOT, 9-KOT, 13-HOT, 13-KOT, 10-HOT, 12-HOT, 15/16-HOT, LNA and 2-HOT, alone or in combination with 2.5 µM AA. Oxylipins and LNA were used at 12.5 µM. **(C)** Root phenotypes of wild type plants grown for 3 days on MS medium and then transferred to MS, or to MS with 1 µM OPDA or 10 µM JA, alone or in combination with 2.5 µM AA. **(D)** Root growth (relative to MS) of wild type plants in MS, 1 µM OPDA, 12.5 µM 2-hexenal or 10 µM JA, alone or in combination with 2.5 µM AA. **(E)** Root phenotypes and **(F)** root growth (relative to MS) of wild type plants in different concentrations of tBuOOH, alone or in combination with 2.5 µM AA. In all cases, pictures and measurements were taken on plants 3 days after passing to the indicated media. In **(A,C,E)** root lengths at the moment of medium transfer are pointed by white arrowheads. In **(B,D,F)** black triangles represent expected root growths in combined treatments if both effects were additive (no interaction). Asterisks represent a significant interaction between treatments ($n \geq 8$, Two way ANOVA, $^{***}P < 0.001$, $^{**}P < 0.01$, $^{*}P < 0.05$).

Oxylipin Action Is Specific to Complex III, Not Inhibitory and ROS-dependent

To examine whether oxylipins could also enhance the response to inhibitors of other respiratory complexes, we measured the root length of seedlings grown in 9-KOT combined with Rotenone (complex I), Carboxin (Ubiquinone reductase of complex II), Malonate (Succinate dehydrogenase of complex II), KCN (complex IV), Oligomycin A (complex V), and Myxothiazol (another C-III inhibitor). For comparison with AA control, we selected inhibitor concentrations causing intermediate growth reductions (between 40 and 70%) compared to MS. **Figure 6A** shows that addition of 9-KOT did not change the root growth reduction caused by inhibitors of complexes I, II, IV or V. In the case of Myxothiazol (C-III inhibitor) root growth reduction was amplified by 9-KOT, although full growth arrest as in the 9-KOT/AA combination was not reached (**Figures 6A,B**). Hence, oxylipins amplify the respiration inhibition phenotype in a C-III specific manner.

These data could be consistent with the action of oxylipins as inhibitors of the cytochrome or alternative respiration pathways. To test this hypothesis, we evaluated the effect of 9-HOT and 9-KOT on the respiratory capacity of isolated mitochondria. Oxygen consumption rates were not changed by these oxylipins in State 2 (with ATP and respiration substrates, but not ADP) or State 3 respiration (after ADP addition), implying that cytochrome respiration was not affected (**Figure 7A**). Similarly, oxylipin treatment did not affect oxygen consumption after inhibiting the cytochrome pathway while triggering AOX activity, showing that alternative respiration was not affected. We also considered the possibility that oxylipins could inhibit respiration conditionally, that is, only when a C-III inhibitor was present. In our conditions, addition of 1 nM AA inhibited ∼70% of oxygen consumption in State 3 (**Figure 7B**). This value was consistently lower (close to 60%) in the presence of 9-KOT, indicating that instead of reinforcing it, 9-KOT seems to ameliorate AA inhibition of cytochrome respiration capacity.

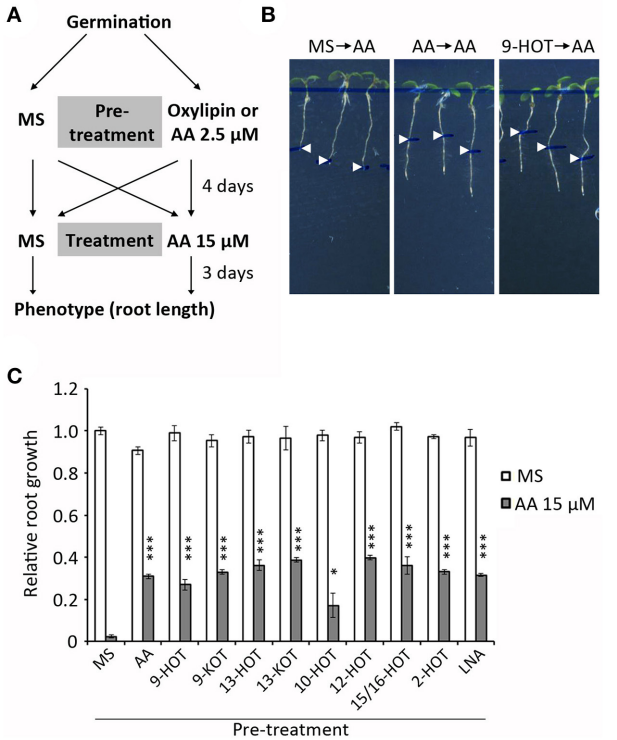

FIGURE 5 | Pretreatment with oxylipins or mild mitochondrial stress protects seedlings against severe mitochondrial damage **(A)** Experiment design: wild type plants were grown 4 days on MS medium with 2.5 µM AA, 20 µM oxylipins (9-HOT, 9-KOT, 13-HOT, 13-KOT, 10-HOT, 12-HOT, 15/16-HOT and 2-HOT) linolenic acid or MS, and then transferred to MS or 15 µM AA to grow for 3 additional days. **(B)** Representative phenotype of plants grown on MS, MS with 2.5 µM AA or 20 µM 9-HOT and transferred to MS with 15 µM AA. Root lengths at the moment of transfer are indicated by arrowheads **(C)** Root growth (relative to plants transferred from MS to MS) of wild type plants transferred from different pre-treatments to MS or MS with 15 µM AA. Asterisks represent significant differences with control plants pre-treated with MS ($n \geq 8$, Student's *t*-test, $^{***}P < 0.001$, $^{*}P < 0.05$).

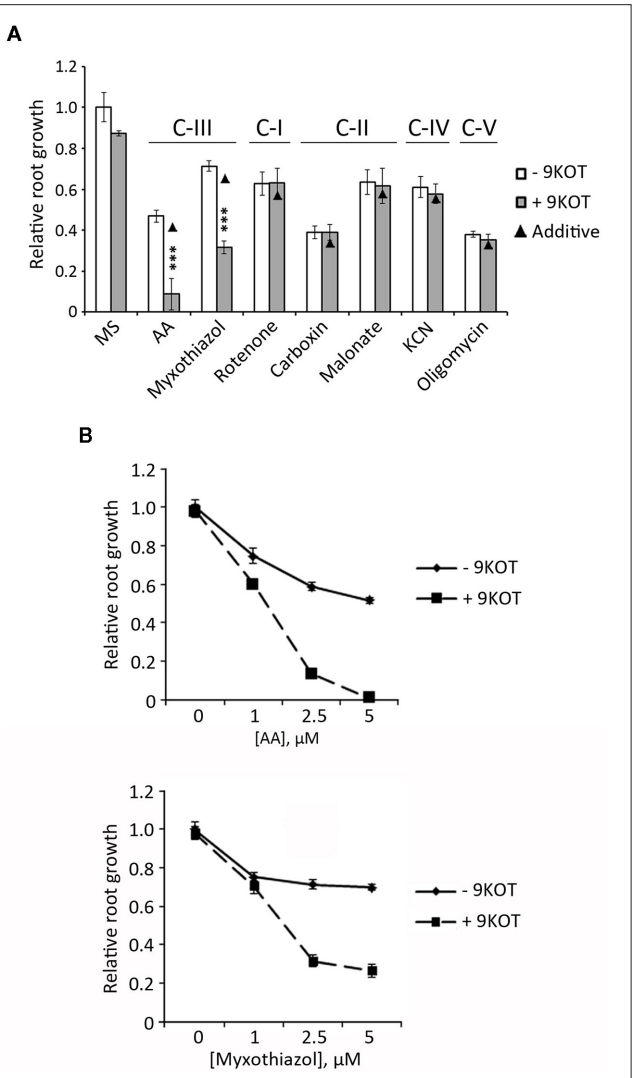

FIGURE 6 | Root growth phenotype in seedlings treated with 9-KOT and inhibitors of respiratory complexes. **(A)** Root growth (relative to MS) of wild type plants grown for 4 days in MS, and then transferred to MS with 2.5 µM AA (C-III), 2.5 µM Myxothiazol (C-III), 50 µM Rotenone (C-I), 100 µM Carboxin (C-II), 2 mM Malonate (C-II), 100 µM KCN (C-IV) or 1 µM Oligomycin A (C-V), alone or in combination with 12.5 µM 9-KOT. Black triangles represent expected root growths in combined treatments if both effects were additive (no interaction). Asterisks represent a significant interaction between treatments ($n \geq 8$, Two way ANOVA, $^{***}P < 0.001$. **(B)** Effect on root growth of 12.5 µM 9-KOT in combination with different concentrations of AA and Myxothiazol. Treatments were applied as in **(A)**.

Taken together, these results indicate that 9-HOT and 9-KOT do not seem to act as direct inhibitors of mitochondrial respiration.

One side effect of AA inhibition of C-III is superoxide generation due to over-reduction of the ubiquinone pool and electron transfer to molecular oxygen (Bleier and Dröse, 2013). In order to know if oxylipins affect ROS production/signaling by C-III, we analyzed the effect of ascorbate (a ROS scavenger) on the root growth arrest phenotype caused by AA/oxylipin mixtures. We first selected 500 µM as the highest concentration of ascorbate at which root growth was not severely affected (data not shown). At this amount, ascorbate did not influence the root growth arrest caused by 2.5 µM AA (**Figure 8A**). By contrast, it caused a partial reversion of the root growth inhibition produced by AA/9-HOT or AA/9-KOT combinations, indicating that oxylipin action on mitochondria is associated with ROS production (**Figures 8A,B**). Moreover, 500 µM ascorbate relieved the root arrest caused by high concentrations of AA (10 and 15 µM), but not of KCN, which inhibits respiration without producing superoxide (**Supplementary Figure 6**). To test whether 9-HOT or 9-KOT enhance the root growth reduction caused by a superoxide source not related to C-III inhibition, we combined these oxylipins with paraquat in the culture media. In our conditions, 2 nM paraquat reduced the root growth of wild type seedlings by ∼60%. This value was not changed significantly by addition of 12.5 µM 9-HOT or 9-KOT (**Figure 8C**), indicating that oxylipin association with ROS production is specific to C-III inhibition.

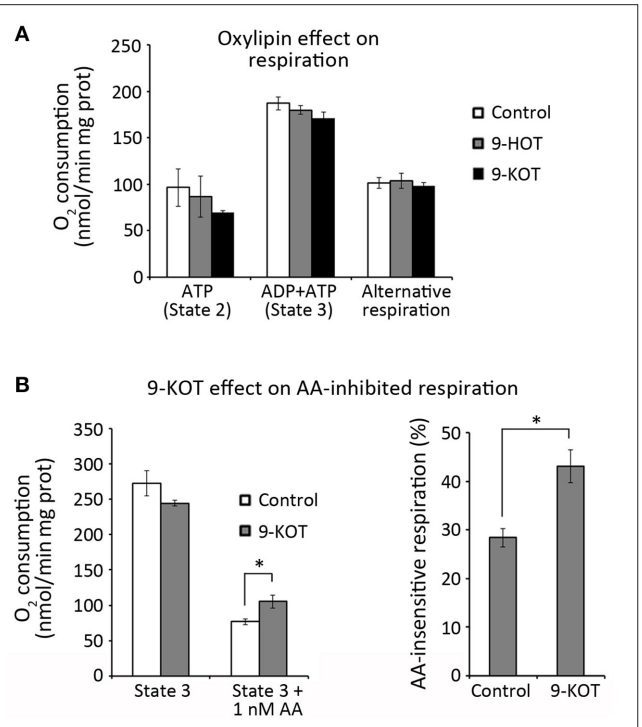

FIGURE 7 | Oxylipin effect on respiration rates of isolated mitochondria. **(A)** O_2 consumption by the cytochrome (State 2 and State 3) and alternative pathways in the presence of 9-HOT or 9-KOT. **(B)** Effect of 12.5 μM 9-KOT on respiration partially inhibited by 1 nM AA. Left: O_2 consumption by State 3 mitochondria with or without 9-KOT and AA. Right: Effect of 9-KOT on AA-insensitive respiration, defined as the percent of O_2 consumed by mitochondria after AA treatment, with or without 9-KOT. Asterisks represent significant differences with controls, as indicated ($n = 4$, Student's t-test, $^*P < 0.05$).

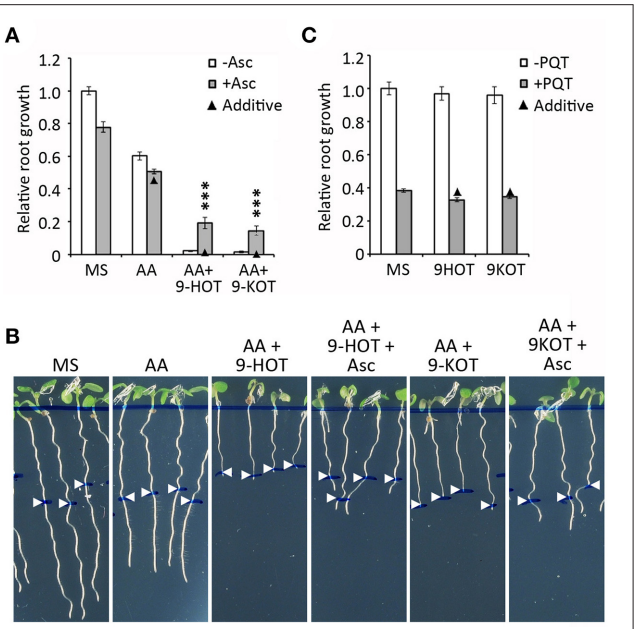

FIGURE 8 | Effect of superoxide on the root growth arrest caused by AA or AA/oxylipin combinations. **(A)** Relative root growth of wild type plants grown for 4 days on MS and then transferred to MS with AA, AA/9-HOT, and AA/9-KOT, with or without the superoxide scavenger Ascorbate (500 μM). **(B)** Representative images of plants from **(A)**. **(C)** Relative root growth of wild type plants in MS, 9-HOT or 9-KOT, with or without addition of the superoxide generator Paraquat (2 nM). In **(A,B)**, AA concentration was 2.5 μM. In all cases, 9-HOT and 9-KOT concentration was 12.5 μM. Black triangles represent expected root growths in combined treatments if both effects were additive (no interaction). Asterisks represent a significant interaction between treatments ($n \geq 8$, Two way ANOVA, $^{***}P < 0.001$.

Mitochondria-Active Oxylipins Influence Complex III Retrograde Signaling

After mitochondrial damage, nuclear gene expression is activated by retrograde signaling to restore mitochondrial homeostasis. In order to know if oxylipin amplification of AA stress was associated with altered signaling, we analyzed the expression of marker genes of the mitochondrial retrograde pathway (*AOX1A*; Saisho et al., 1997), ROS signaling (transcription factors ZAT12 and WRKY33; Willems et al., 2016; Xu et al., 2017) and 9HOT/9KOT response (ABCG40; López et al., 2011; Marcos et al., 2015). Transcript levels were measured in wild type plants treated for 3 and 8 h with AA, 9-HOT, 9-KOT or AA/oxylipin combinations.

ABCG40 was strongly induced (∼30–40-fold) 3 h after treatment with oxylipins alone or in combination with AA, whereas the application of AA alone caused a milder induction (8-fold). At 8 h, expression increased slightly in AA-treated plants (13-fold) but decreased in oxylipin treatments (to ∼10–15-fold). By contrast, AA/oxylipin combinations amplified *ABCG40* expression 8 h after treatment, with transcript levels reaching 50 and 70-fold in response to AA/9-HOT and AA/9-KOT, respectively (**Figure 9A**). A similar pattern was observed for *WRKY33* and *ZAT12* transcripts, which expression increased at 3 h after treatment with AA, 9-HOT or 9-KOT, and later descended in 8 h samples. In response to AA/9-HOT or AA/9-KOT combinations, induction of both genes was sustained, and transcript levels at 8 h were higher than in single AA or oxylipin treatments (**Figures 9B,C**). As expected, the level of *AOX1A* transcripts increased in response to AA treatment (20 and 15-fold at 3 and 8 h, respectively). Application of 9-HOT or 9-KOT, either alone or in combination with AA, did not markedly change *AOX1A* expression (**Figure 9D**).

noxy Mutants Are More Tolerant to Oxidative Stress

Our results indicate that oxylipin action on mitochondria could be primarily associated with superoxide production. Accordingly, insensitivity of *noxy* plants to oxylipins could be accompanied by enhanced resistance to this type of ROS. To test this possibility, we examined the root phenotypes of *noxy* plants grown in paraquat-containing medium. In wild type plants, addition of this herbicide at concentrations 1 and 5 nM reduced root growth by ∼30 and ∼70%, respectively. Compared to these values, root growth reduction was milder in all *noxy* mutants, which thus appear partially resistant to superoxide damage (**Figure 10A**).

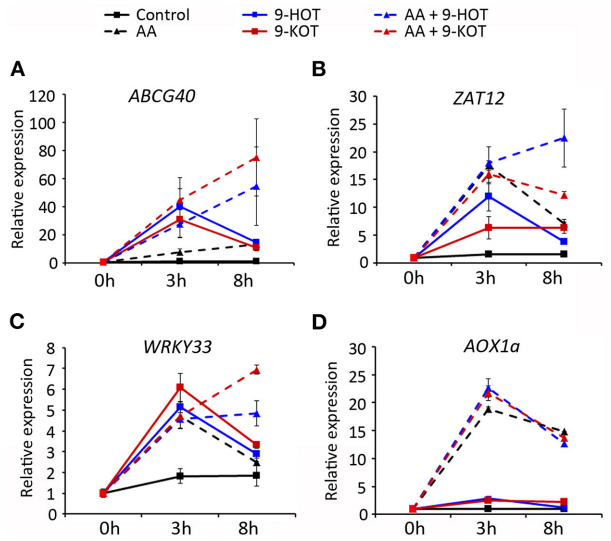

FIGURE 9 | Gene expression in response to 20 μM oxylipins (9-HOT or 9-KOT), 20 μM AA or AA/oxylipin combinations. RNA was extracted and examined at the indicated times after treatment. Selected genes were the oxylipin signaling marker *ABCG40* **(A)**, ROS-specific transcription factors *ZAT12* **(B)** and *WRKY33* **(C)** and the mitochondria retrograde signaling marker *AOX1A* **(D)**. Expression values are relative to untreated plants, using 18S rRNA and *SAND* as reference genes.

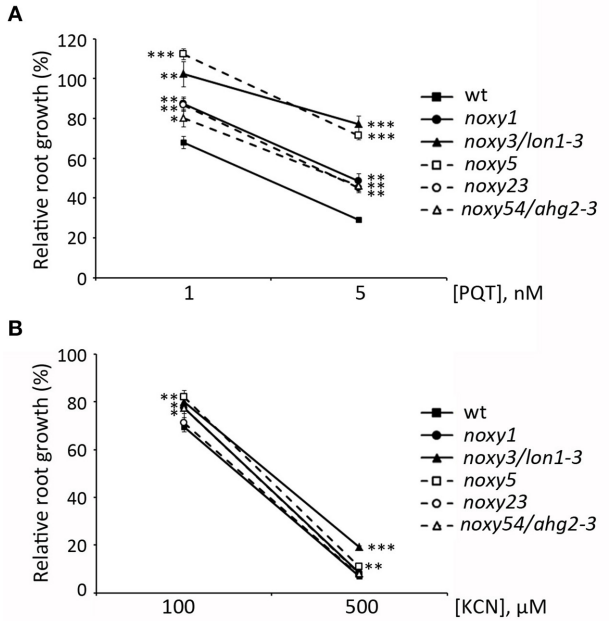

FIGURE 10 | Effect of ROS-generating Paraquat (PQT) and non-ROS-generating KCN on the root growth of *noxy* mutants. Relative root growth of wild type and *noxy1*, *noxy3/lon1-3*, *noxy5*, *noxy23*, and *noxy54/ahg2-3* plants in Paraquat **(A)** and KCN **(B)**. Asterisks indicate significant differences with wild type plants in each condition ($n \geq 8$, Student's *t*-test, $^{***}P < 0.001$, $^{**}P < 0.01$, $^{*}P < 0.05$).

Conversely, KCN is an inhibitor of cytochrome respiration that does not induce ROS production (Chen et al., 2003). In contrast to AA, *noxy* mutants responded like wild type plants to KCN at the two concentrations tested (100 and 500 μM), showing only minor differences probably due to specific compensation mechanisms (**Figure 10B**).

DISCUSSION

Oxylipins are a diverse group of oxidized lipid derivatives with relevant signaling activities in developmental and stress responses. However, precise assignment of their functions is challenging due to multiple enzymatic and non-enzymatic sources, biosynthetic genes and metabolic interaction of the existing pathways (summarized in **Figure 1**). Here, we report that oxylipins generated from 9-LOX, 13-LOX and non-enzymatic pathways converge as enhancers of the stress response produced by Antimycin A, a ROS-generating inhibitor of mitochondrial complex III.

noxy Mutants and Oxylipin Function

The identification of five *noxy* mutations (*noxy1*, *noxy3*, *noxy5*, *noxy23,* and *noxy54*) in nuclear genes encoding mitochondrial proteins supports the participation of mitochondria in 9-LOX-derived oxylipin signaling as described (Vellosillo et al., 2013). As the majority of mitochondrial proteins are nuclear-encoded, any perturbation in this organelle needs to be signaled to the nucleus (retrograde signaling) to modulate gene expression and restore mitochondrial homeostasis (Rhoads and Subbaiah, 2007).

The inhibition of C-III by AA is a mitochondrial stress model that has allowed the identification of key components of the retrograde pathway such as the transcription factor ANAC17 and the protein kinase CDKE1, both mediating the induction of AOX proteins to restore electron transport (Ng et al., 2013a,b). The *noxy* mutations described here alter mitochondrial morphology and respiration rates, which is consistent with higher AOX levels in these *noxy* mutants before and/or after AA treatment. These alterations are indicative of mitochondrial stress likely caused by altered mitochondrial RNA or protein homeostasis, as suggested by the functions of the mutated genes. Accordingly, *ahg2-1* affects C-III levels (Hirayama et al., 2013) and *lon1-1* impairs the accumulation of electron transport chain (ETC) components (Solheim et al., 2012). Likewise, *noxy1* and *noxy5* mutations in PPR proteins could lead to aberrant RNA editing, whereas *noxy23* could result in impaired mitochondrial protein synthesis, ultimately leading to mitochondrial stress. This rationale can also be applied to previously described *noxy* mutants with abnormal mitochondria, which are also AA-resistant (Vellosillo et al., 2013 and **Supplementary Figure 3**). Since 9-HOT and 9-KOT are associated to mitochondrial stress, *noxy* mutant insensibility to these oxylipins could be a consequence of upregulated mitochondrial retrograde signaling. Interestingly, other *noxy* mutations not directly associated with mitochondria, such as *noxy7/gcn1-3*, *gcn20-2* (general translation control) and *noxy22* (ethylene signaling) also confer resistance to AA (López et al., 2011; Izquierdo et al., 2018 and **Supplementary Figure 3**)

making non-mitochondrial *noxy* mutants an interesting tool to search for new mitochondrial-nucleus communication pathways.

9-HOT induces mitochondria aggregation and decreases inner membrane potential (Vellosillo et al., 2013). Similarly to moderate AA (2.5 μM) pre-treatment, this mild mitochondrial stress protects plants against subsequent, root-arresting AA levels. Oxylipin functions could therefore include the induction of retrograde signals to protect plants against mitochondrial damage. It is intriguing how, alongside this protective role, mitochondria-active oxylipins potentiate AA damage when applied simultaneously. This opens the question of whether natural C-III inhibitors exist in plants, whose action would be enhanced by endogenously produced oxylipins. For instance, salicylic acid has been proposed to inhibit C-III and activate C-II to induce mitochondrial ROS production (Nie et al., 2015; Belt et al., 2017), which could be linked to oxylipin roles in plant defense.

9-HOT and 9-KOT amplification of AA root phenotype was accompanied by induction of stress-responsive genes, illustrating the activation of retrograde signaling pathways. Thus, sustained induction of *ABCG40* (9-HOT responsive gene), *ZAT12* and *WRKY33* (ROS-responsive transcription factors) suggests that oxylipin-triggered mitochondrial signals mediate the stress responses reportedly associated with these genes (Davletova et al., 2005; Zheng et al., 2006; Borghi et al., 2015). Interestingly, induction of *AOX1a* by AA is not affected by these oxylipins. As this gene is considered the hallmark of the retrograde pathway (Woodson and Chory, 2008; Ng et al., 2013b), oxylipin retrograde signaling could be independent of ANAC17 and CDKE1.

Mitochondria-Active Oxylipins Affect Complex III-Derived ROS Signaling

Evidence points to C-III as the primary target of a vast array of oxylipins derived from 9-LOX, 13-LOX and non-enzymatic pathways, presenting the challenge to understand how this common feature fits into the negative and positive interactions among oxylipin pathways (Vicente et al., 2012; Zoeller et al., 2012; Wang et al., 2020). Instead of being *bona fide* C-III inhibitors, our results indicate that mitochondria-active oxylipins might act by enhancing ROS production and signaling by this complex. A first indication was that 9-KOT arrests root growth in combination with AA but not with KCN, both inhibitors of cytochrome respiration which differ in ROS production. Secondly, root arrest caused by AA/9-HOT and AA/9-KOT combinations can be partially reversed by the superoxide scavenger ascorbate. An increment of superoxide production by AA/oxylipins is also consistent with the higher oxygen consumption rate observed in mitochondria treated with AA/9-KOT, compared to AA alone. Nevertheless, specific measurements or imaging analyses will be needed to determine specific ROS contribution to oxylipin signaling.

How mitochondria-active oxylipins act on C-III remains an open question. Based on their chemical structure, they are α,β-unsaturated keto acids (9-KOT and 13-KOT) or hydroxy acids (9,12,13,15 and 16-HOT). The former are RES that could bind directly to cysteine residues, whereas oxidation of the latter to RES structures is thermodynamically favored (House et al., 1972). It is therefore tempting to speculate that oxylipins could bind covalently to their targets to promote C-III ROS production. In basal conditions, about 1–5% of ETC electrons are "lost" at C-III by collateral superoxide generation (Osyczka et al., 2005). This rate increases after AA inhibition, as well as in response to environmental stress conditions such as hypoxia, salt, drought and pathogen attack (Mittova et al., 2003; Rhoads et al., 2006; Cruz De Carvalho, 2008; Colombatti et al., 2014; Wagner et al., 2018), all situations in which oxylipin production has been reported (Blée, 2002; Ghanem et al., 2012; Moradi et al., 2017; Savchenko et al., 2019). Superoxide can generate a second wave of highly oxidant ROS, causing extensive oxidation of lipids and proteins and ultimately cell death. In this scenario, the oxidative stress caused by high AA, or low AA combined with mitochondria-active oxylipins, could exceed the cell antioxidant capacity leading to full growth arrest. Alternatively, oxylipins could enhance C-III superoxide production indirectly through modulation of AOX activity. Although we did not detect any influence of 9-HOT or 9-KOT on the alternative respiration capacity of isolated mitochondria, we cannot rule out that AOX activity could be affected *in vivo* by mitochondria-active oxylipins.

CONCLUSION

Taken together, our results show that oxylipins from different pathways converge as activators of mitochondrial retrograde signaling through complex III, potentially controlling cell responses to a wide range of stress conditions. Future studies will be needed to determine how this pathway influences plant acclimation and fitness.

DATA AVAILABILITY STATEMENT

The original contributions presented in the study are included in the article/**Supplementary Material**, further inquiries can be directed to the corresponding authors.

AUTHOR CONTRIBUTIONS

CC, YI, and LM designed the study. YI, JV, SK, VA, and TC mapped the *noxy* mutations. LM and AM-A generated transgenic *noxy* lines. YI, LM, and BL performed *in vitro* phenotypic analyses. YI and CC generated confocal images. YI, AL and CC wrote the paper. YI, TC, and AL conducted gene expression analyses. YI performed respiration measurements. All authors read and approved the final version of the manuscript.

FUNDING

This work was supported by grants BIO2015-68130-R (Ministry of Economy and Competitiveness/European Regional Development Fund) and RTI2018- 097102-B-100 (Ministry of Science, Innovation and Universities) to CC. Ph.D. scholarship to BL was supported by BES-2016-076425

(Severo Ochoa Centers of Excellence Program, Ministry of Economy and Competitiveness) and post-doctoral contract to AL was supported by grant 20172SEV647 (Severo Ochoa Centers of Excellence Program, Ministry of Science, Innovation and Universities).

ACKNOWLEDGMENTS

We are grateful to Mats Hamberg (Karolinska Institutet, Stockholm, Sweden) for critical reading of the manuscript and providing oxylipins used in this study, Gunvor Hamberg (Karolinska Institutet, Stockholm, Sweden) for oxylipin preparation, María Rosa Ponce and José Luis Micol (Universidad Miguel Hernández Gene, Elche, Spain) for help in positional cloning of *noxy* mutations, and Takashi Hirayama (Okayama University, Japan) for providing *ahg2-1* seeds.

SUPPLEMENTARY MATERIAL

The Supplementary Material for this article can be found online at: https://www.frontiersin.org/articles/10.3389/fpls.2021.705373/full#supplementary-material

REFERENCES

Alméras, E., Stolz, S., Vollenweider, S., Reymond, P., Mène-Saffrané, L., and Farmer, E. E. (2003). Reactive electrophile species activate defense gene expression in Arabidopsis. *Plant J.* 34, 205–216. doi: 10.1046/j.1365-313X.2003.01718.x

Ameye, M., Allmann, S., Verwaeren, J., Smagghe, G., Haesaert, G., Schuurink, R. C., et al. (2018). Green leaf volatile production by plants: a meta-analysis. *New Phytol.* 220, 666–683. doi: 10.1111/nph.14671

Andreou, A., and Feussner, I. (2009). Lipoxygenases—structure and reaction mechanism. *Phytochemistry* 70, 1504–1510. doi: 10.1016/j.phytochem.2009.05.008

Battilani, P., Lanubile, A., Scala, V., Reverberi, M., Gregori, R., Falavigna, C., et al. (2018). Oxylipins from both pathogen and host antagonize jasmonic acid-mediated defence via the 9-lipoxygenase pathway in Fusarium verticillioides infection of maize. *Mol. Plant Pathol.* 19, 2162–2176. doi: 10.1111/mpp.12690

Belt, K., Huang, S., Thatcher, L. F., Casarotto, H., Singh, K. B., Van Aken, O., et al. (2017). Salicylic acid-dependent plant stress signaling via mitochondrial succinate dehydrogenase. *Plant Physiol.* 173, 2029–2040. doi: 10.1104/pp.16.00060

Blée, E. (2002). Impact of phyto-oxylipins in plant defense. *Trends Plant Sci.* 7, 315–322. doi: 10.1016/S1360-1385(02)02290-2

Bleier, L., and Dröse, S. (2013). Superoxide generation by complex III: From mechanistic rationales to functional consequences. *Biochim. Biophys Acta Bioenerg.* 1827, 1320–1331. doi: 10.1016/j.bbabio.2012.12.002

Bonen, L., and Calixte, S. (2006). Comparative analysis of bacterial-origin genes for plant mitochondrial ribosomal proteins. *Mol. Biol. Evol.* 23, 701–712. doi: 10.1093/molbev/msj080

Borghi, L., Kang, J., Ko, D., Lee, Y., and Martinoia, E. (2015). The role of ABCG-type ABC transporters in phytohormone transport. *Biochem. Soc. Trans.* 43, 924–930. doi: 10.1042/BST20150106

Chen, Q., Vazquez, E. J., Moghaddas, S., Hoppel, C. L., and Lesnefsky, E. J. (2003). Production of reactive oxygen species by mitochondria: central role of complex III. *J. Biol. Chem.* 278, 36027–36031. doi: 10.1074/jbc.M304854200

Chini, A., Boter, M., and Solano, R. (2009). Plant oxylipins : COI1/JAZs/MYC2 as the core jasmonic acid-signalling module. *FEBS J.* 276, 4682–4692. doi: 10.1111/j.1742-4658.2009.07194.x

Colombatti, F., Gonzalez, D. H., and Welchen, E. (2014). Mitochondrion Plant mitochondria under pathogen attack: a sigh of relief or a last breath? *MITOCH* 19, 238–244. doi: 10.1016/j.mito.2014.03.006

Cruz De Carvalho, M. H. (2008). Drought stress and reactive oxygen species: production, scavenging and signaling. *Plant Signal. Behav.* 3, 156–165. doi: 10.4161/psb.3.3.5536

Czechowski, T., Stitt, M., Altmann, T., and Udvardi, M. K. (2005). Genome-wide identification and testing of superior reference genes for transcript normalization. *Plant Physiol.* 139, 5–17. doi: 10.1104/pp.105.063743

Davletova, S., Schlauch, K., Coutu, J., and Mittler, R. (2005). The zinc-finger protein Zat12 plays a central role in reactive oxygen and abiotic stress signaling in Arabidopsis. *Plant Physiol.* 139, 847–856. doi: 10.1104/pp.105.068254

Farmer, E. E., and Mueller, M. J. (2013). ROS-mediated lipid peroxidation and RES-activated signaling. *Annu. Rev. Plant Biol.* 64, 429–450. doi: 10.1146/annurev-arplant-050312-120132

Ghanem, M. E., Ghars, M. A., Frettinger, P., Pérez-Alfocea, F., Lutts, S., Wathelet, J. P., et al. (2012). Organ-dependent oxylipin signature in leaves and roots of salinized tomato plants (Solanum lycopersicum). *J. Plant Physiol.* 169, 1090–1101. doi: 10.1016/j.jplph.2012.03.015

Göbel, C., Feussner, I., Hamberg, M., and Rosahl, S. (2002). Oxylipin profiling in pathogen-infected potato leaves. *Biochim. Biophys. Acta—Mol. Cell Biol. Lipids* 1584, 55–64. doi: 10.1016/S1388-1981(02)00268-8

Göbel, C., Feussner, I., and Rosahl, S. (2003). Lipid peroxidation during the hypersensitive response in potato in the absence of 9-lipoxygenases. *J. Biol. Chem.* 278, 52834–52840. doi: 10.1074/jbc.M310833200

Haeggström, J. Z., and Funk, C. D. (2011). Lipoxygenase and leukotriene pathways: biochemistry, biology, and roles in disease. *Chem. Rev.* 111, 5866–5896. doi: 10.1021/cr200246d

Hamberg, M., Sanz, A., and Castresana, C. (1999). α-Oxidation of Fatty Acids in Higher Plants. Identification of a pathogen-inducible oxygenase (PIOX) as an α-dioxygenase and biosynthesis of 2-hydroperoxylinolenic acid. *J. Biol. Chem.* 274, 24503–24513. doi: 10.1074/jbc.274.35.24503

Hamberg, M., Sanz, A., Rodriguez, M. J., Calvo, A. P., and Castresana, C. (2003). Activation of the fatty acid α-dioxygenase pathway during bacterial infection of tobacco leaves: formation of oxylipins protecting against cell death. *J. Biol. Chem.* 278, 51796–51805. doi: 10.1074/jbc.M310514200

Hirayama, T., Matsuura, T., Ushiyama, S., Narusaka, M., Kurihara, Y., Yasuda, M., et al. (2013). A poly(A)-specific ribonuclease directly regulates the poly(A) status of mitochondrial mRNA in Arabidopsis. *Nat. Commun.* 4, 1–7. doi: 10.1038/ncomms3247

House, H. O., Huber, L. E., and Umen, M. J. (1972). Empirical rules for estimating the reduction potential of α,β-unsaturated carbonyl compounds. *J. Am. Chem. Soc.* 94, 8471–8475. doi: 10.1021/ja00779a028

Izquierdo, Y., Kulasekaran, S., Benito, P., López, B., Marcos, R., Cascón, T., et al. (2018). Arabidopsis nonresponding to oxylipins locus NOXY7 encodes a yeast GCN1 homolog that mediates noncanonical translation regulation and stress adaptation. *Plant Cell Environ.* 41, 1438–1452. doi: 10.1111/pce.13182

Jalloul, A., Montillet, J. L., Assigbets,é, K., Agnel, J. P., Delannoy, E., Triantaphylidès, C., et al. (2002). Lipid peroxidation in cotton: Xanthomonas interactions and the role of lipoxygenases during the hypersensitive reaction. *Plant J.* 32, 1–12. doi: 10.1046/j.1365-313X.2002.01393.x

Li, H., Zhu, X.-L., Yang, W.-C., and Yang, G.-F. (2014). Comparative kinetics of Qi site inhibitors of cytochrome bc1 complex: picomolar antimycin and micromolar cyazofamid. *Chem. Biol. Drug Des.* 83, 71–80. doi: 10.1111/cbdd.12199

Logemann, J., Schell, J., and Willmitzer, L. (1987). Improved method for the isolation of RNA from plant tissues. *Anal. Biochem.* 163, 16–20. doi: 10.1016/0003-2697(87)90086-8

López, M. A., Vicente, J., Kulasekaran, S., Vellosillo, T., Martínez, M., Irigoyen, M. L., et al. (2011). Antagonistic role of 9-lipoxygenase-derived oxylipins and ethylene in the control of oxidative stress, lipid peroxidation and plant defence. *Plant J.* 67, 447–458. doi: 10.1111/j.1365-313X.2011.04608.x

Lurin, C., Andrés, C., Aubourg, S., Bellaoui, M., Bitton, F., Bruyère, C., et al. (2004). Genome-wide analysis of arabidopsis pentatricopeptide repeat proteins reveals their essential role in organelle biogenesis. *Plant Cell* 16, 2089–2103. doi: 10.1105/tpc.104.022236

Marcos, R., Izquierdo, Y., Vellosillo, T., Kulasekaran, S., Cascón, T., Hamberg, M., et al. (2015). 9-Lipoxygenase-derived oxylipins activate brassinosteroid signaling to promote cell wall-based defense and limit pathogen infection. *Plant Physiol.* 169, 2324–2334. doi: 10.1104/pp.15.00992

Martínez, E., and Campos-Gómez, J. (2016). Oxylipins produced by Pseudomonas aeruginosa promote biofilm formation and virulence. *Nat. Commun.* 7, 1–10. doi: 10.1038/ncomms13823

Mittova, V., Tal, M., Volokita, M., and Guy, M. (2003). Up-regulation of the leaf mitochondrial and peroxisomal antioxidative systems in response to salt-induced oxidative stress in the wild salt-tolerant tomato species Lycopersicon pennellii. *Plant, Cell Environ.* 26, 845–856. doi: 10.1046/j.1365-3040.2003.01016.x

Mochizuki, S., Sugimoto, K., Koeduka, T., and Matsui, K. (2016). Arabidopsis lipoxygenase 2 is essential for formation of green leaf volatiles and five-carbon volatiles. *FEBS Lett.* 590, 1017–1027. doi: 10.1002/1873-3468.12133

Moradi, P., Mahdavi, A., Khoshkam, M., and Iriti, M. (2017). Lipidomics unravels the role of leaf lipids in thyme plant response to drought stress. *Int. J. Mol. Sci.* 18:2067. doi: 10.3390/ijms18102067

Mosblech, A., Feussner, I., and Heilmann, I. (2009). Oxylipins: Structurally diverse metabolites from fatty acid oxidation. *Plant Physiol. Biochem.* 47, 511–517. doi: 10.1016/j.plaphy.2008.12.011

Mueller, M. J., and Berger, S. (2009). Reactive electrophilic oxylipins: pattern recognition and signalling. *Phytochemistry* 70, 1511–1521. doi: 10.1016/j.phytochem.2009.05.018

Nelson, B. K., Cai, X., and Nebenführ, A. (2007). A multicolored set of in vivo organelle markers for co-localization studies in Arabidopsis and other plants. *Plant J.* 51, 1126–1136. doi: 10.1111/j.1365-313X.2007.03212.x

Ng, S., Giraud, E., Duncan, O., Law, S. R., Wang, Y., Xu, L., et al. (2013a). Cyclin-dependent kinase E1 (CDKE1) provides a cellular switch in plants between growth and stress responses. *J. Biol. Chem.* 288, 3449–3459. doi: 10.1074/jbc.M112.416727

Ng, S., Ivanova, A., Duncan, O., Law, S. R., Van Aken, O., De Clercq, I., et al. (2013b). A membrane-bound NAC transcription factor, ANAC017, mediates mitochondrial retrograde signaling in Arabidopsis. *Plant Cell* 25, 3450–3471. doi: 10.1105/tpc.113.113985

Nie, S., Yue, H., Zhou, J., and Xing, D. (2015). Mitochondrial-derived reactive oxygen species play a vital role in the salicylic acid signaling pathway in arabidopsis thaliana. *PLoS ONE* 10, 1–25. doi: 10.1371/journal.pone.0119853

Nishimura, N., Yoshida, T., Murayama, M., Asami, T., Shinozaki, K., and Hirayama, T. (2004). Isolation and characterization of novel mutants affecting the abscisic acid sensitivity of Arabidopsis germination and seedling growth. *Plant Cell Physiol.* 45, 1485–1499. doi: 10.1093/pcp/pch171

Ostersetzer, O., Kato, Y., Adam, Z., and Sakamoto, W. (2007). Multiple intracellular locations of lon protease in Arabidopsis: Evidence for the localization of AtLon4 to chloroplasts. *Plant Cell Physiol.* 48, 881–885. doi: 10.1093/pcp/pcm052

Osyczka, A., Moser, C. C., and Dutton, P. L. (2005). Fixing the Q cycle. *Trends Biochem. Sci.* 30, 176–182. doi: 10.1016/j.tibs.2005.02.001

Ponce, M. R., Robles, P., Lozano, F. M., Brotóns, M. A., and Micol, J. L. (2006). Low-resolution mapping of untagged mutations. *Methods Mol. Biol.* 323, 105–113. doi: 10.1385/1-59745-003-0:105

Prost, I., Dhondt, S., Rothe, G., Vicente, J., Rodriguez, M. J., Kift, N., et al. (2005). Evaluation of the antimicrobial activities of plant oxylipins supports their involvement in defense against pathogens. *Plant Physiol.* 139, 1902–1913. doi: 10.1104/pp.105.066274

Przybyla, D., Göbel, C., Imboden, A., Hamberg, M., Feussner, I., and Apel, K. (2008). Enzymatic, but not non-enzymatic, 1O2-mediated peroxidation of polyunsaturated fatty acids forms part of the EXECUTER1-dependent stress response program in the flu mutant of Arabidopsis thaliana. *Plant J.* 54, 236–248. doi: 10.1111/j.1365-313X.2008.03409.x

Rhoads, D. M., and Subbaiah, C. C. (2007). Mitochondrial retrograde regulation in plants. *Mitochondrion* 7, 177–194. doi: 10.1016/j.mito.2007.01.002

Rhoads, D. M., Umbach, A. L., Subbaiah, C. C., and Siedow, J. N. (2006). Mitochondrial reactive oxygen species. contribution to oxidative stress and interorganellar signaling. *Plant Physiol.* 141, 357–366. doi: 10.1104/pp.106.079129

Rigas, S., Daras, G., Sweetlove, L. J., and Hatzopoulos, P. (2009). Mitochondria biogenesis via Lon1 selective proteolysis: who dares to live for ever? *Plant Signal. Behav.* 4, 221–224. doi: 10.4161/psb.4.3.7863

Ruan, J., Zhou, Y., Zhou, M., Yan, J., Khurshid, M., Weng, W., et al. (2019). Jasmonic acid signaling pathway in plants. *Int. J. Mol. Sci.* 20:2479. doi: 10.3390/ijms20102479

Rustérucci, C., Montillet, J. L., Agnel, J. P., Battesti, C., Alonso, B., Knoll, A., et al. (1999). Involvement of lipoxygenase-dependent production of fatty acid hydroperoxides in the development of the hypersensitive cell death induced by cryptogein on tobacco leaves. *J. Biol. Chem.* 274, 36446–36455. doi: 10.1074/jbc.274.51.36446

Saisho, D., Nambara, E., Naito, S., Tsutsumi, N., Hirai, A., and Nakazono, M. (1997). Characterization of the gene family for alternative oxidase from Arabidopsis thaliana. *Plant Mol. Biol.* 35, 585–596. doi: 10.1023/A:1005818507743

Savchenko, T., Rolletschek, H., Heinzel, N., Tikhonov, K., and Dehesh, K. (2019). Waterlogging tolerance rendered by oxylipin-mediated metabolic reprogramming in Arabidopsis. *J. Exp. Bot.* 70, 2919–2932. doi: 10.1093/jxb/erz110

Solheim, C., Li, L., Hatzopoulos, P., and Harvey Millar, A. (2012). Loss of Lon1 in Arabidopsis changes the mitochondrial proteome leading to altered metabolite profiles and growth retardation without an accumulation of oxidative damage. *Plant Physiol.* 160, 1187–1203. doi: 10.1104/pp.112.203711

Vellosillo, T., Aguilera, V., Marcos, R., Bartsch, M., Vicente, J., Cascón, T., et al. (2013). Defense activated by 9-Lipoxygenase-derived oxylipins requires specific mitochondrial proteins. *Plant Physiol.* 161, 617–627. doi: 10.1104/pp.112.207514

Vellosillo, T., Martínez, M., López, M. A., Vicente, J., Cascón, T., Dolan, L., et al. (2007). Oxylipins produced by the 9-lipoxygenase pathway in Arabidopsis regulate lateral root development and defense responses through a specific signaling cascade. *Plant Cell* 19, 831–846. doi: 10.1105/tpc.106.046052

Vicente, J., Cascón, T., Vicedo, B., García-Agustín, P., Hamberg, M., and Castresana, C. (2012). Role of 9-lipoxygenase and α-dioxygenase oxylipin pathways as modulators of local and systemic defense. *Mol. Plant* 5, 914–928. doi: 10.1093/mp/ssr105

Wagner, S., Van Aken, O., Elsässer, M., and Schwarzländer, M. (2018). Mitochondrial energy signaling and its role in the low oxygen stress response of plants. *Plant Physiol.* 176, 1156–1170. doi: 10.1104/pp.17.01387

Walper, E., Weiste, C., Mueller, M. J., Hamberg, M., and Dröge-Laser, W. (2016). Screen identifying arabidopsis transcription factors involved in the response to 9-lipoxygenase-derived oxylipins. *PLoS ONE* 11, 1–17. doi: 10.1371/journal.pone.0153216

Wang, K., Der, B.orrego, E. J., Kenerley, C. M., and Kolomiets, M. V. (2020). Oxylipins other than jasmonic acid are xylem-resident signals regulating systemic resistance induced by trichoderma virens in maize. *Plant Cell* 32, 166–185. doi: 10.1105/tpc.19.00487

Wasternack, C., and Feussner, I. (2018). The oxylipin pathways: biochemistry and function. *Annu. Rev. Plant Biol.* 69, 363–386. doi: 10.1146/annurev-arplant-042817-040440

Whelan, J., and Murcha, M. W. (2015). *Plant Mitochondria: Methods and Protocols.* New York, NY: Humana Press.

Willems, P., Mhamdi, A., Stael, S., Storme, V., Kerchev, P., Noctor, G., et al. (2016). The ROS wheel: Refining ROS transcriptional footprints. *Plant Physiol.* 171, 1720–1733. doi: 10.1104/pp.16.00420

Woodson, J. D., and Chory, J. (2008). Coordination of gene expression between organellar and nuclear genomes. *Nat. Rev. Genet.* 9, 383–395. doi: 10.1038/nrg2348

Xu, J., Tran, T., Padilla Marcia, C. S., Braun, D. M., and Goggin, F. L. (2017). Superoxide-responsive gene expression in Arabidopsis thaliana and Zea mays. *Plant Physiol. Biochem.* 117, 51–60. doi: 10.1016/j.plaphy.2017.05.018

Yu, J., Nickels, R., and McIntosh, L. (2001). A genome approach to mitochondrial-nuclear communication in Arabidopsis. *Plant Physiol. Biochem.* 39, 345–353. doi: 10.1016/S0981-9428(01)01254-2

Zheng, Z., Qamar, S. A., Chen, Z., and Mengiste, T. (2006). Arabidopsis WRKY33 transcription factor is required for resistance to necrotrophic fungal pathogens. *Plant J.* 48, 592–605. doi: 10.1111/j.1365-313X.2006.02901.x

Zoeller, M., Stingl, N., Krischke, M., Fekete, A., Waller, F., Berger, S., et al. (2012). Lipid profiling of the Arabidopsis hypersensitive response reveals specific lipid peroxidation and fragmentation processes: Biogenesis of pimelic and azelaic acid. *Plant Physiol.* 160, 365–378. doi: 10.1104/pp.112.202846

Conflict of Interest: SK conducted his research work at Centro Nacional de Biotecnología and is currently employed by GlaxoSmithKline.

The remaining authors declare that the research was conducted in the absence of any commercial or financial relationships that could be construed as a potential conflict of interest.

Publisher's Note: All claims expressed in this article are solely those of the authors and do not necessarily represent those of their affiliated organizations, or those of the publisher, the editors and the reviewers. Any product that may be evaluated in this article, or claim that may be made by its manufacturer, is not guaranteed or endorsed by the publisher.

Copyright © 2021 Izquierdo, Muñiz, Vicente, Kulasekaran, Aguilera, López Sánchez, Martínez-Ayala, López, Cascón and Castresana. This is an open-access article distributed under the terms of the Creative Commons Attribution License (CC BY). The use, distribution or reproduction in other forums is permitted, provided the original author(s) and the copyright owner(s) are credited and that the original publication in this journal is cited, in accordance with accepted academic practice. No use, distribution or reproduction is permitted which does not comply with these terms.

frontiers in Plant Science

REVIEW
published: 17 August 2021
doi: 10.3389/fpls.2021.724079

12-*oxo*-Phytodienoic Acid: A Fuse and/or Switch of Plant Growth and Defense Responses?

*Wenshan Liu and Sang-Wook Park**

Department of Entomology and Plant Pathology, Auburn University, Auburn, AL, United States

12-oxo-Phytodienoic acid (OPDA) is a primary precursor of (-)-jasmonic acid (JA), able to trigger autonomous signaling pathways that regulate a unique subset of jasmonate-responsive genes, activating and fine-tuning defense responses, as well as growth processes in plants. Recently, a number of studies have illuminated the physiol-molecular activities of OPDA signaling in plants, which interconnect the regulatory loop of photosynthesis, cellular redox homeostasis, and transcriptional regulatory networks, together shedding new light on (*i*) the underlying modes of cellular interfaces between growth and defense responses (e.g., fitness trade-offs or balances) and (*ii*) vital information in genetic engineering or molecular breeding approaches to upgrade own survival capacities of plants. However, our current knowledge regarding its mode of actions is still far from complete. This review will briefly revisit recent progresses on the roles and mechanisms of OPDA and information gaps within, which help in understanding the phenotypic and environmental plasticity of plants.

Keywords: cyclophilin 20-3, fitness tradeoffs/balances, light-dependent redox reactions, redox signaling, retrograde signaling

OPEN ACCESS

Edited by:
Koichi Sugimoto,
University of Tsukuba, Japan

Reviewed by:
Tomonori Shinya,
Okayama University, Japan
Sajjan Grover,
University of Nebraska-Lincoln, United States

****Correspondence:***
Sang-Wook Park
swpark@auburn.edu

Specialty section:
This article was submitted to Plant Metabolism and Chemodiversity, a section of the journal Frontiers in Plant Science

Received: *11 June 2021*
Accepted: *19 July 2021*
Published: *17 August 2021*

Citation:
Liu W and Park SW (2021) 12-oxo-Phytodienoic Acid: A Fuse and/or Switch of Plant Growth and Defense Responses? Front. Plant Sci. 12:724079. doi: 10.3389/fpls.2021.724079

PHYTO-OXYLIPINS: JASMONATE SIGNALING IN PLANTS

Oxylipins, the oxygenated derivative of fatty acids (FAs), are critical signal molecules in diverse physiological processes in life, including plants and animals (Marnett, 2008). In plants, oxylipins are involved in a layer of defense and ontogenetic pathways, while mammalian oxylipins (eicosanoids) control intricate regulatory mechanisms in immunity, functioning as messengers in the central nervous system, and participating in the resolution process following tissue injury (Funk, 2001; Mosblech et al., 2010). Recent studies, moreover, have illuminated the medicinal values of phyto-oxylipins, presenting their anticancer, anti-inflammatory, and antioxidative activities (Flescher, 2007; Dang et al., 2008; Taki-Nakano et al., 2014). Noticeably, the molecular components and metabolic pathways, involved in oxylipin biogenesis and signaling, share common ancestry and evolutionary processes across Kingdoms (Marnett, 2008). Hence, uncovering the modes of actions associated with oxylipins will not only assist the development of agricultural strategies in advancing disease resistance and stress adaptation, as well as yield and biomass increases in plants, but also assist the improvement of drug development through facilitating the rational design of more potent and safe anticancer (and anti-inflammation) drugs. However, our current knowledge regarding oxylipin signaling is still incomplete, despite decades of investigations (Funk, 2001; Mosblech et al., 2010).

Lately, molecular underpinnings have been investigated for 12-oxo-phytodienoic acid (OPDA) signaling in plant defense responses. OPDA is a primary precursor of the jasmonate family of oxylipins, which includes jasmonic acid (JA) and its precursors and derivatives. Jasmonates are derived from trienoic-FA *via* the octadecanoid pathway in the chloroplasts. Lipase-mediated oxidation of trienoic-FA leads to the release of OPDA that travels to the peroxisomes through plastid envelope proteins (e.g., OPDAT1 and JASSY, Guan et al., 2019; Zhao et al., 2020) and/or peroxisomal ATP-binding transporters (e.g., COMATOSE, Theodoulou et al., 2005) and undergoes β-oxidations to form JA. JA can be further metabolized to several derivatives, including JA-isoleucine (JA-Ile), JA-tryptophan (JA-Trp), methyl-JA, and hydroxyl-JA. Signaling of these jasmonate molecules then controls a large number of gene expressions in the nucleus and mediates defense (adaptive) responses to various forms of biotic and abiotic stresses, including microbial pathogens and insect herbivores, tissue injury, and light damage. Jasmonate signaling also plays essential roles in reproduction and other developmental processes such as senescence, root growth and tuberization, fruit ripening, and tendril coiling (reviewed in Acosta and Farmer, 2010; Pieterse et al., 2012). These important, yet diverse activities of jasmonates must be tied to their versatility as major molecular and cellular modulators.

The most well-characterized jasmonate-associated signaling pathway revolves around JA-Ile. Once it is produced, JA-Ile binds a F-box protein, CORONATINE INSENSITIVE 1 (COI1, a part of SCF ubiquitin E3 ligase). This complex then binds and ubiquitinates jasmonate ZIM-domain (JAZ) proteins, which are negative transcription regulators of JA-responsive genes (JRGs). Thus, JAZ degradation by 26S proteasomes frees transcription factors (TFs, e.g., bHLH-containing MYCs) and allows subsequent gene expressions (Chini et al., 2007; Thines et al., 2007). Jasmonate signaling, however, must involve a much more complex network, given that a number of JRGs respond independently of COI1 (Devoto et al., 2005). For example, JA induction of *GRX480* and *AOC3* is mediated *via* a COI1-independent MYC2 regulatory pathway, whereas JA-activated MAP kinase cascades (e.g., *MPK1*, *MPK2* and *BIK1*) and *GST25* are regulated in a COI1- and/or MYC2-independent manner (Veronese et al., 2006; Ortiz-Masia et al., 2007; Stotz et al., 2013). In addition, OPDA is capable of triggering autonomous signaling pathways that regulate unique subsets of JRGs, coordinated with and without the canonical JA pathway (Taki et al., 2005). OPDA signaling is presumed to be independent of COI1, as it is unable to bind the COI1/JAZ complex (Thines et al., 2007). However, OPDA induction of *PHO1;H10* needs COI1 activity (Ribot et al., 2008), suggesting additional layers of complexity in jasmonate signaling. In fact, ancestral plants such as the bryophyte *Marchantia polymorpha* are able to synthesize only a set of OPDAs (OPDA, dinor-*cis*-OPDA and dinor-*iso*-OPDA), but not JA/JA-Ile, though their genomes still express a functional COI1 (Monte et al., 2018). Hence, *M. polymorpha* deploys OPDAs, instead of JA-Ile, to activate COI1/JAZ signaling for defense activations and growth processes (Monte et al., 2018, 2019). The other study also established a distinct role of JA-Trp conjugate, linking jasmonate with auxin signaling (Staswick, 2009), further supporting the notion that distinct messages sent out by specific jasmonate coordinate essential molecular and cellular processes.

BIOSYNTHESIS OF OPDA AND ITS DERIVATIVES

As alluded, jasmonates are synthesized in the chloroplasts from oxygenized FAs, linolenic acid (18:3) and hexadecatrienoic acid (16:3), that are stored mostly as the esterified monogalactosyldiacylglycerol (MGDG). The first step, hydroperoxidation, is began by 13-lipoxygenases adding molecular oxygen to 18:3 and 16:3 and forming 13(*S*)-hydroperoxy-octadecatrienoic acid and 11(*S*)-hydroperoxy-hexadecatrienoic acid, respectively. These compounds are then transformed *via* allene oxide synthase into (*13S*)12,13-epoxy-octadecatrienoic acid and (11*S*)10,11-epoxy-octadecatrienoic acid, which are subsequently cyclized through allene oxide cyclase to yield *cis*-(+)-OPDA and dinor-OPDA (collectively, OPDA); containing a reactive electrophilic α,β-unsaturated carbonyl group. These metabolic pathways are known to be activated in response to various herbivories and microbial pathogens, as well as abiotic stresses such as extreme temperatures and tissue injury (Stintzi et al., 2001; Kourtchenko et al., 2007; Vu et al., 2012; Bosch et al., 2014a,b; Monte et al., 2020). Some portion of OPDA is then further derivatized to a glutathione (GSH) conjugate, or galactolipids (later named "arabidopsides") by its binding with MGDG and digalactosyl DG (Hisamatsu et al., 2003, 2005; Davoine et al., 2005, 2006; Andersson et al., 2006; Buseman et al., 2006). The biological roles of OPDA-GSH and arabidopsides are yet largely elusive, but have been hypothesized as the vacuolar delivery and storage forms, respectively, in maintaining the cellular-level homeostasis of OPDA to avoid their potential toxicity and/or negative effects on physiol-molecular processes in plants (Böttcher and Pollmann, 2009; Ohkama-Ohtsu et al., 2011). Alternatively, recent studies have been suggested that arabidopsides could interact with plant plasma membrane lipids such as glycosyl inositol phosphor ceramides, which thus lead them to locate and modify membrane organizations, and such changes could signal defense mechanism activations (Genva et al., 2019).

SIGNALING OF OPDA IN PLANT DEFENSE RESPONSES

In plants, OPDA signaling plays intrinsic roles in activating and fine-tuning defense (adaptive) responses against an array of biotic and abiotic stresses, as well as growth processes (Böttcher and Pollmann, 2009; Dave and Graham, 2012; Maynard et al., 2018). Its distinctive activity in plant defense activations was first described by the pathoanalyses of a mutant Arabidopsis plant (*opr3*) arresting the conversion of OPDA to JA/JA-Ile (Stintzi et al., 2001). WT-like resistance of *opr3*, in contrast to enhanced susceptibility in other mutants disrupting trienoic-FA biosynthesis (*fad3*/*7*/*8*) and the octadecanoid pathway (*dde2* and *aos*), against fungal pathogens (*Alternaria brassicicola*

and *Scerotinia sclerotiarum*) and an insect herbivory (*Bradysia impatiens*), underlined a critical activity of OPDA signaling in plant disease resistance in the absence of JA/JA-Ile (Stintzi et al., 2001; Zhang and Turner, 2008; Stotz et al., 2011). Following studies with genetically modified (GM) plants reducing or impairing JA productions (*OPR3-RNAi*, *SiOPR3*s, and *opr7opr8*) or enhancing OPDA accumulations (*OPR3ox*) further substantiate that OPDA signaling is essential for the full activation of basal defense responses in tomato, maize, and rice against microbial and/or pest attacks such as *Botrytis cinerea*, tobacco hornworm (*Manduca sexta* larvae), beet armyworm (*Spodoptera exigua* larvae), brown plant hopper (*Nilaparvata lugens*), green peach aphid (*Myxus persicae*), and corn leaf aphid (*Rhopalosiphum maidis*) (Bosch et al., 2014a,b; Guo et al., 2014; Scalschi et al., 2015; Varsani et al., 2019; Grover et al., 2020b; Wang et al., 2020). Upon their infections, OPDA is induced rapidly in the chloroplasts and triggers the retrograde signaling toward the nucleus, which coordinates large-scale changes in defense gene expressions (Taki et al., 2005). These then lead to (*i*) the spatiotemporal induction of protease inhibitors (PIs) such as miraculin-like proteins, which likely serve as antinutrients against insect attackers by reducing their digestibility of dietary proteins (Felton, 2005; López-Galiano et al., 2017), (*ii*) the actuation of other hormone and metabolite biosynthesis (**Figure 1**) in maximizing defense capacity and survival of plants, and (*iii*) the stimulation of callose deposition (Scalschi et al., 2015; Varsani et al., 2019), a multifaceted cell wall barrier developed at the sites of infection, preventing the cell-to-cell spread of microbes and limiting the feeding capacity and colonization of insects (Luna et al., 2010; De Storme and Geelen, 2014). OPDA signaling appeared to trigger abscisic acid (ABA) accumulations (Dave et al., 2016) that activate a NADPH oxidase subunit of RBOHF (Respiratory Burst Oxidase Homolog Protein F) leading to transient reactive oxygen species (ROS) productions (Sirichandra et al., 2009; **Figure 1**) and in consequence stimulating callose synthesis (Luna et al., 2010). However, OPDA signal alone did not elevate the expression levels of callose synthase gene such as *Tie-dyed2* in maize, suggesting rather the need of additional or alternative, yet unknown, defense and/or OPDA-inducible element(s), perhaps free thiols such as GSH and glucosinolates (Park et al., 2013; Zhou and Memelink, 2016; Varsani et al., 2019).

Indeed, it is still largely elusive how OPDA is perceived for signaling. Recently, in search of OPDA derivatives potentially binding SCF^{COI}, OPDA conjugated with Ile (OPDA-Ile) was identified in Arabidopsis (Floková et al., 2016) and described its ability to induce OPDA-responsive genes (ORGs) such as *GRX480* and *ZAT10* in JA/JA-Ile-deficient mutant (*opr3* and *jar1*) plants (Arnold et al., 2016). The latter suggests that OPDA-Ile is a bioactive signal and conveys JA/JA-Ile-independent, OPDA-dependent signaling pathway. OPDA-Ile is though only active under specific conditions as it was found exclusively in wounded leaves of flowering plants (Floková et al., 2016). It would be interesting to delineate mechanisms underlying the perception of OPDA-Ile and its cross-networking with other OPDA signaling pathways (see "Summary: Mode of Action of OPDA Signaling").

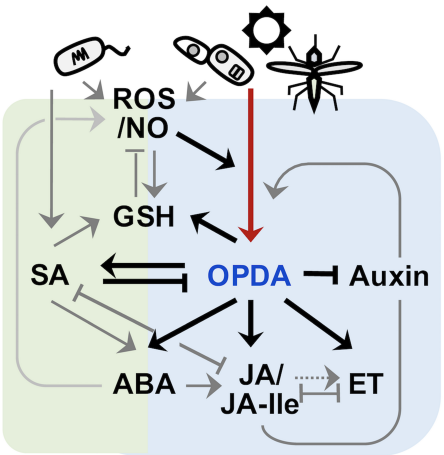

FIGURE 1 | Schematic crosstalk of OPDA with the signaling pathways of other phytohormones. OPDA and JA/JA-Ile (collectively, jasmonate) signaling activates defense responses to various forms of biotic and abiotic stresses, including necrotroph infection, insect attack, wounding, and UV damage, whereas salicylic acid (SA) signaling confers disease resistance against mostly biotrophic pathogens. Once recognized "non-self," plants rapidly produce ROS including nitric oxide (NO) (Huang et al., 2004; Wang et al., 2013), which in turn actuates jamonate biosynthesis (Palmieri et al., 2008). OPDA signaling then stimulates and coordinates with different defense signaling, e.g., JA/JA-Ile, SA, ABA, ethylene (ET), and GSH pathways (Taki et al., 2005; Park et al., 2013; Dave et al., 2016; Varsani et al., 2019; Scalschi et al., 2020), while suppressing growth hormone (e.g., auxin) signaling (Taki et al., 2005) to optimize defense capability of plants. On the other hand, JA/JA-Ile signaling can feedback induce own jasmonate biosynthesis (Taki et al., 2005), whereas SA signaling antagonizes both OPDA and JA/JA-Ile signaling (Leon-Reyes et al., 2010; Shim et al., 2013; Wei et al., 2014).

Besides its roles in local defenses, a new study has proposed that OPDA is a long-distance signal for "induced systemic resistance" (ISR) (Wang et al., 2020), a state of heightened defense that is activated throughout the plant following an initial encounter with plant growth-promoting rhizobacteria/fungi (PGPR/F) (Pieterse et al., 2014). Their oxylipin profiling of xylem saps collected from ISR-induced maize leaves detected uniquely OPDA and KODA (α-ketol-octadecadienoic acid). In addition, the transfusion of OPDA and KODA into naïve plants led to develop systemic resistance against an anamorphic fungus *Collectotrichum graminicola* in a dose-dependent manner (Wang et al., 2020), together proposing their role in conveying ISR signaling. A caveat is that OPDA appears to be stationary exhibiting little or no distal accumulation under pathogen attacks (Christensen et al., 2015). This speculates if an ISR receptor of OPDA is present in xylem. Alternatively, OPDA may be rapidly converted to and activate JA/JA-Ile signaling, upon arrival to systemic tissues, for priming systemic defense (Koo et al., 2009; Bosch et al., 2014a). In this context, an earlier grafting experiment using WT and JA/JA-deficient (*OPR3-RNAi*) plants showed that OPDA can substitute for JA/JA-Ile in the local induction of defense gene expressions, but the production of JA/JA-Ile is required for systemic responses (Bosch et al., 2014b). It will be intriguing to find out whether

OPDA is "truly" moved from local to vascular to systemic tissues, and if OPDA can autonomously signal ISR priming or is converted to JA/JA-Ile for ISR development. In addition, we cannot still rule out a potential role of phloem in channeling a mobile signal of ISR development (Varsani et al., 2019). Perhaps, ISR may also involve multiple signals and transduction pathways as does in systemic acquired resistance (Klessig et al., 2018).

On the other hand, a recent report argued that only a biologically active jasmonate molecule is JA-Ile (Chini et al., 2018). Using a new mutant allele (*opr3-3*) completely lacking OPR3 reductase activity, the study demonstrated the increased accumulation levels (∼fifteen-folds) of non-reduced cyclopente none, 4,5-didehydrojasmoante, in *opr3* and its provisional reduction to JA by one of OPR3 isoforms, OPR2 reductase, together postulating that WT-like resistance of *opr3* is actuated not by OPDA signaling, rather by COI1-dependent JA-Ile signaling. However, the OPR3-independent pathway of JA biosynthesis appeared to contribute to the accumulation of dismal amounts of JA-Ile (<2.0 % [less than its basal levels] of WT) under stress conditions, while conferring tenable strength defense responses against pathogen infections, prompting speculation that *opr3-3* mutants may exert alternative, OPDA-associated defense pathways. In fact, *coi1* mutants feedback suppress JA biosynthesis so that lack stress-induced OPDA and JA accumulations (Chung et al., 2008; Park et al., 2013). Thus, *coi1*-like increased susceptibility shown in *coi1*/*opr3-3* against insect and fungal attacks (Chini et al., 2018) might be, not because WT-like resistance of *opr3-3* requires COI1, due to auxiliary side effects led by double mutagenesis, perhaps lowering the level threshold of OPDA and JA-Ile signaling.

SIGNALING OF OPDA IN PLANT GROWTH AND DEVELOPMENTAL PROCESSES

An earlier study of COMATOSE, a peroxisomal ATP-binding cassette transporter, and its mutant plants (*cts*) disrupted the transport of OPDA into the peroxisome, where JA biosynthesis occurs, illuminated a critical activity of OPDA signaling in coordinating seed germination and dormancy (Russell et al., 2000). The mutant *cts* seeds exhibited increased accumulation level of OPDA and low germination rates (Russell et al., 2000; Dave et al., 2011), while exogenous OPDA applications stimulated the repression of the germination of WT seeds (Dave et al., 2011). Such an inhibitory effect of OPDA signaling is perhaps mediated through its activation of ABA biosynthesis by upregulating the expression of an ABA biosynthesis gene (*ABA1* and *ABA-deficient 1*) and an inducer (*RGL2*, *Repressor of Gibberellic Acid-like 2*) of RING-H2 XERICO (ABA biosynthesis regulator) (Ko et al., 2006; Piskurewicz et al., 2008; Dave et al., 2016). OPDA and ABA both are then able to induce and/or stabilize the activity of GRL2 and ABI5 (ABA insensitive 5) bZIP TF, which in subsequence promotes the expression of *MET* (*Mother-of FT and TFL1*),

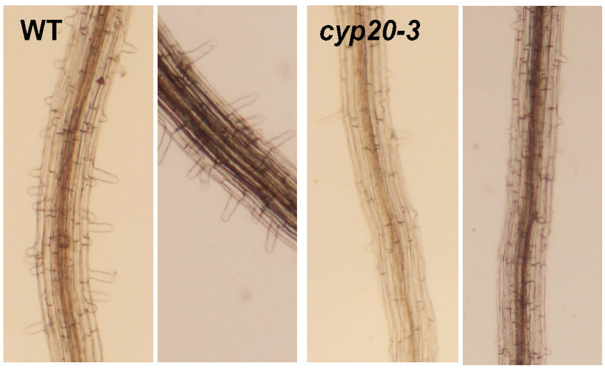

FIGURE 2 | Important roles of OPDA signaling in root morphogenesis. OPDA signaling mutant Arabidopsis (*cyp20-3*) demonstrated the impairment of root hair growth.

an inhibitor of seed germination or early seedling growth (Skubacz et al., 2016; Vaistij et al., 2018), so that it suppresses seed germinations (Dave et al., 2016; Barros-Galvão et al., 2019). Two hormones, however, displayed different mechanistic outcomes that ABA signal ruptures seed coats and endosperm tissues, whereas OPDA-treated seeds keep intact endosperm and seed coats (Dave et al., 2011), indicating that OPDA signal, besides coordinating ABA biosynthesis/signaling, can execute its autonomous, unique regulatory metabolic pathways in plant organismal development.

OPDA-responsive ABA accumulations also convey the inhibition of root growth and morphogenesis in plants (Mueller et al., 2008; Park et al., 2013; Sun et al., 2018; Vissenberg et al., 2020). ABA could suppress primary root growth and lateral root branching, mediated *via* balancing the cellular homeostasis of several growth components (Arc et al., 2013; Sun et al., 2018) that enhance the production of ROS, Ca^{2+}, and ethylene but reduce auxin levels (Wang et al., 2002; He et al., 2012; Jiao et al., 2013; Luo et al., 2014). These changes then stimulate the expression of *PLETHORA* TFs, rhizotatic regulators, and some cell cycle-related genes (e.g., *Cyclin-dependent Protein Kinase* and *Cell Cycle B-type Cyclins*), thus affecting DNA replication, cell division, and cell elongation in roots and inhibiting root growth (Wang et al., 2008, 2011; Yin et al., 2009; Xu et al., 2010; Hofhuis et al., 2013; Yao et al., 2013). However, the effects of OPDA signal on roots did also not entirely depend on ABA signaling. Our recent study indicated that OPDA signaling could act as a positive regulator in root growth and development (**Figure 2**). Disruption of OPDA signaling in Arabidopsis (*cyp20-3*, Park et al., 2013) engendered the impairment of root hair growth. It is though unclear if the opposite is correct; the increased accumulation level of OPDA under stress conditions could enhance root growth and branching; further studies are needed to reconstitute the complete, functional networks of OPDA signaling in plant growth and development.

A MODE OF OPDA SIGNALING BY ITS BINDING PROTEIN CYCLOPHILIN 20-3

Previously, our search of jasmonate receptors uncovered that a small plastid protein, cyclophilin 20-3 (CYP20-3), can physically interact with OPDA, and its T-DNA insertion mutant Arabidopsis (*cyp20-3*) attenuates the expression of ORGs (Park et al., 2013). The Arabidopsis genome encodes 29 CYP and CYP-like proteins, belonging to the family of, namely, immunophilins that possess binding abilities toward immunosuppressive drugs, cyclosporin A, and functions in broad ranges of cellular processes, including transcriptional regulation, organogenesis, photosynthetic and hormone signaling pathways, stress adaptation, and defense responses (Dos Santos and Park, 2019). CYP20-3 is the only isoform localized in the chloroplast stroma and acts as a dual-enzyme able to chaperone protein folding (peptidyl-prolyl *cis-trans* isomerase; PPlase) and transfers electrons (e^-) to peroxide substrates (reductase) in cysteine (Cys) biosynthesis (i.e., sulfur assimilation; Romano et al., 2004; Laxa et al., 2007; Dominguez-Solis et al., 2008; Park et al., 2013). In line with this scenario, OPDA, once accumulated under stress states, binds and stimulates CYP20-3 to form a complex with serine acetyltransferase1 (SAT1), which triggers the formation of a hetero-oligomeric Cys synthase complex (CSC) with *O*-acetylserine(thiol)lyase B (OASTL-B) (**Figure 3**, left side). CSC formation then leads to the production of Cys and subsequently thiol metabolites (e.g., GSH), which builds up cellular reduction potentials. The enhanced redox capacity in turn coordinates the expression of a subset of ORGs that activate and calibrate pathogen defense and stress adaptation processes. Thus, the KO of *CYP20-3* (*cyp20-3*) displays enhanced susceptibility against necrotrophic fungal (e.g., *A. brassicicola* and *B. cinerea*) and oomycete (*Pythium irregulare*) infections, as well as nematode (*Meloidogyne hapla*) infestations, compared with WT (Park et al., 2013; Gleason et al., 2016; Dos Santos and Park, 2019), together concurring with the conclusion that OPDA is an autonomous metabolic messenger, connecting stress cues to the readjustment of cellular redox homeostasis in actuating retro-directional signaling from the chloroplasts to the nucleus for regulating defense gene expressions.

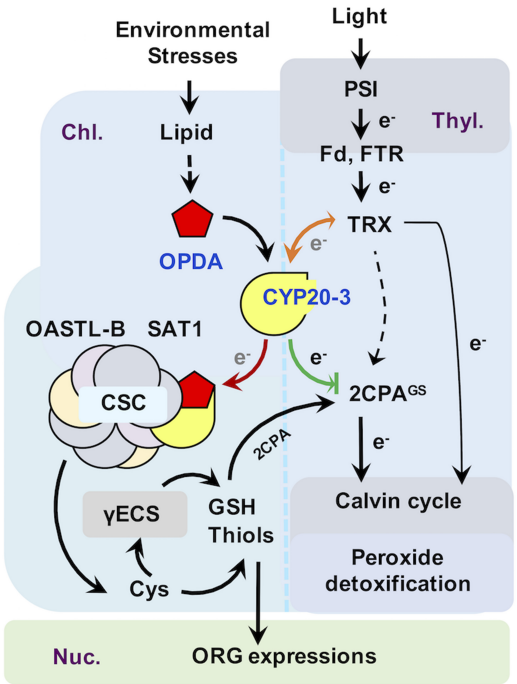

FIGURE 3 | Proposed model of CYP20-3 as a regulatory hub in the interplay between light and OPDA signaling. In optimal conditions, CYP20-3 relays light signaling in buffering cellular redox homeostasis, whereas, in stressed states, CYP20-3 interfaces light and OPDA signaling, which fine-tunes plant fitness between growth (light-dependent detoxification and Calvin cycle) and defense response (redox-mediated retrograde signaling). Colored arrows indicate the enhanced interactions of CYP20-3 with TRXs (orange), SAT1 (red), and 2CPA (green) during stress (OPDA-signaling) defense responses. Hypothesized passage of electron (e^-) transfers is noted in gray.

CYP20-3 RELAYS OPDA SIGNALING BETWEEN PLANT DEFENSE AND GROWTH REGULATORY PATHWAYS

Emerging evidence from a number of recent studies has underpinned that CYP20-3 is a versatile metabolite in plants, proposed to be a key regulator in controlling the interface between OPDA (defense) and light-dependent redox (growth) signaling (Dos Santos and Park, 2019, **Figure 3**). The latter, also known as the e^- transport chain (ETC) photosystem I (PSI), is a primary metabolism converting solar energy into biologically useful chemical energies, necessary for the production of overall biomass of plants and living organisms (Chitnis, 2001; Jensen et al., 2007). When the PSI captures solar energy, it excites e^- that reduce thioredoxins (TRXs) *via* a ferredoxin (Fd) and a Fd-TRX reductase (FTR). TRXs, small oxidoreductases, then deliver e^- and activate target enzymes in the Calvin cycle that balances consumption in photosynthesis (Meyer et al., 2009; Serrato et al., 2013; Nikkanen and Rintamäki, 2014). Recent studies, however, have revealed that TRXs can also reduce other Calvin cycle-unrelated proteins, including CYP20-3, a regulator of OPDA defense signaling (see above), and photosynthetic ETC as an e^- donor of 2-cysteine peroxiredoxin A (2CPA; Motohashi et al., 2001; Peltier et al., 2006; Laxa et al., 2007). Plastid 2CPA is a thiol-based peroxidase involved in protecting and optimizing photosynthesis. When arrived at the chloroplasts, 2CPA is activated by either different e^- donors such as NADPH-dependent TRX reductase C (NTRC), TRXs, and CYP20-3, or—as recently proposed—oxidation folding with GSH (also called S-glutathionylation), which in turn reduces toxic by-products (e.g., H_2O_2) in photosynthesis or activates Calvin cycle enzymes such as a fructose 1,6-bisphosphatase (Konig et al., 2002; Peltier et al., 2006; Caporaletti et al., 2007; Laxa et al., 2007; Muthuramalingam et al., 2009; Liebthal et al., 2016; Pérez-Ruiz et al., 2017; Liu et al., 2020).

In this context, OPDA binding promotes the interaction of CYP20-3 with TRXs (e.g., type-f2 and x; Cheong et al., 2017),

illuminating a mode of OPDA/CYP20-3 signaling in transferring e^- from TRXs to 2CPA and/or SAT1 (**Figure 3**, orange arrow). The latter then stimulates plastid sulfur assimilations (e.g., GSH and thiol accumulations), which coordinate redox-resolved nucleus gene expressions in defense responses against biotic and abiotic stresses (Park et al., 2013), while accelerating the S-glutathionylation (activation) of 2CPA that promotes photosynthetic energy productions (Liu et al., 2020), postulating that OPDA/CYP20-3 signaling optimizes the growth, reproduction, and survival of plants under constant environmental stresses. Traditionally, the cost of resistance (often referred to as growth and defense tradeoff) has been typically described as a teeter-totter model where for defense to increase, growth must decrease and vice versa (Huot et al., 2014). This model well circumstantiates the response of plants to the persistent and excess surge of environmental stresses. However, in nature, plants are more often situated to encounter a consistent array of temporal and modest levels of environmental changes, while concurrently trying to ensure normal growth and developmental processes, in order to maximize their yields and production. For instance, a sorghum inbred line tolerant to sugarcane aphid (*Melanaphis sacchari*) accumulates significantly higher levels of OPDA, but little if any increase in JA/JA-Ile levels, compared to susceptible lines, as supporting insect growth (tolerance, defense) while concomitantly maintaining enhanced photosynthesis (growth, Grover et al., 2020a). Hence, recent studies have begun to elaborate an alternative model, "growth and defense coordination," wherein a balancing act between growth and defense can synergistically optimize plant fitness (Kliebenstein, 2016). In agreement, plants' acclimations toward environmental changes and pressures causing oxidative stresses (e.g., insect and pathogen attack, tissue injury, excess light and temperature, and drought and salinity) accompany the accumulation of OPDA on a time sale of hours with attendant accumulation of reduced, non-protein thiols (Riemann et al., 2003; Kazan and Manners, 2011; Noctor et al., 2011; Savchenko and Dehesh, 2014; Hazman et al., 2015; Muench et al., 2016). This initial response subsequently reprograms cellular redox homeostasis and elevates net photosynthesis and nutrient acquisition, together providing plant tolerance to constant and multitudinous biological/ecological constraints (Koch et al., 2016).

SIGNALING OF OPDA IN THE PLANT ACCLIMATION AND ADAPTATION OF HEAT SHOCK (HS)

In parallel, our recent study has unveiled that OPDA/CYP20-3 signaling also conveys e^- transfers toward peroxidatic (S-glutathionylated) 2CPA ($2CPA^{GS}$) under HS stress (**Figure 3**, green arrow). The deglutathionylation then dimerized and inactivated 2CPA that removes HS- and PSI-induced H_2O_2 bursts and/or activates Calvin cycle enzymes. Hence, it enables the actuation of oxidative stress (defense) signaling and potentially counteracts plant growth, to some extent, elucidating the mode of OPDA in growth and defense tradeoff (Dave et al., 2011; Hazman et al., 2015). On the other hand, HS promoted the increased accumulation and S-glutathionylation of, in part through OPDA/CYP20-3 signaling, 2CPB (another 2CP isoform in the chloroplasts) that constitutes a stable, decameric conformation conferring a chaperone activity (Liu et al., 2020). The expression and activation of a battery of molecular chaperones (i.e., heat shock proteins, HSPs) in protecting native folding and/or assembly of cellular proteins are major defense machinery in plant acclimations of HS (Finka et al., 2011), supporting the critical role of OPDA signaling in thermotolerance (Dave et al., 2011; Muench et al., 2016; Monte et al., 2020). In Arabidopsis when HS occurred, OPDA is mainly, but not JA and JA-Ile, accumulated in the leaves and is only able to dramatically induce HSPs (Taki et al., 2005; Mueller et al., 2008; Balfagón et al., 2019). These HSPs are also induced in *coi1* mutants further delineating that OPDA is involved in COI1-independent HS-responsive pathways (Monte et al., 2020). As known from the previous study (Mueller et al., 2008), ORG expressions are largely dependent on TGA TFs (a group of bZIP TFs containing the TGACG motif) TFs. However, the induction of HSPs does not employ TGA TFs but rather a key HS TFs (HSFA1s) or CYP20-3 (Muench et al., 2016). CYP20-3 relays HS-responsive OPDA signaling in the regulation of cellular redox homeostasis that induces and/or stabilizes HSPs (e.g., decameric $2CPB^{GS}$), while deglutathionylating $2CPA^{GS}$ (suppressing peroxide detoxification) allowing to trigger the rapid ROS signaling, together enhancing heat tolerance in plants (Park et al., 2013; Hazman et al., 2015; Liu et al., 2020). This HS response subsequently leads to induce the short-term acquired tolerance and/or cross-defense responses against following abiotic and biotic stresses such as extreme temperatures, high light, salinity, drought, heavy metal, and insect (*Mayetiola destuctor*) herbivory (Cheng et al., 2018; Hossain et al., 2018; Balfagón et al., 2019), which highlights the vital activity of OPDA signaling in broad-spectrum, induced systemic tolerance/resistance against a wide range of environmental stresses, improving and optimizing growth and yield potential across economically important crops.

SUMMARY: MODE OF ACTION OF OPDA SIGNALING

As sessile organisms, plants cope with constant encounters with a wide range of biotic competitors and consumers, and abiotic constraints, through mobilizing a number of primary and secondary metabolites, and intricate signaling networks that interconnect and orchestrate large-scale changes in transcriptome, proteome, and metabolome. As described in this review, the emerging evidence has espied that OPDA is a versatile signal molecule involved in a variety of metabolic pathways, coordinating plant growth and survival in optimal condition as well as under various forms of environmental stresses (**Table 1**). In the recent decade, a large number of efforts have been devoted and begun to delineate the mechanistical modus operandi of OPDA signaling; thus far, three working

TABLE 1 | Biophysiological activities and functions of OPDA across diverse plant genres.

Crops	Defense responses	Growth	References
Arabidopsis thaliana	Local defense against infections of fungal pathogens (*A. brassicacola* and *S. sclerotiarum*), insect (*B. impatiens*), and root-knot nematode (*M. hapla*). Enhanced resolution of tissue injury and tolerance to high light and heat stress.	Regulation of seed dormancy and germination Inhibition of primary root growth	Stintzi et al., 2001; Buseman et al., 2006; Mueller et al., 2008; Park et al., 2013; Dave et al., 2016; Gleason et al., 2016; Balfagón et al., 2019; Liu et al., 2020.
Marchantia polymorpha	Enhanced protection against heat stress.		Monte et al., 2020.
Oryza sativa	Local defense against insect (*N. lugens* and *M. persicae*) infections and increased tolerance toward salt stress.		Guo et al., 2014; Hazman et al., 2015.
Populus trichocarpa	Local defense against spider mite (*T. urticae*) infestations and enhanced adaptation of tissue injury.		Zhao et al., 2020.
Sorghum bicolar	Enhance tolerance to aphids (*M. sacchari*).		Grover et al., 2020a.
Solanum lycopersicum	Local defense against fungal (*B. cinerea*) and insect (*M. sexta* larvae) infections.	Regulation of embryo development and seed dormancy	Goetz et al., 2012; Bosch et al., 2014a; Scalschi et al., 2015.
Solanum melongena	Hexanoci acid-mediated systemic defense against insect (*L. decemlineata*) infestations.		López-Galiano et al., 2017.
Triticum aestivum	Enhanced resistance to Hessian fly (Diptera: *Cecidomyiidae*) under heat stress		Cheng et al., 2018.
Zea mays	Local defense against aphids (*R. maidis*) and *T. virens*-primed IST against parasites (*C. graminicola*).		Varsani et al., 2019; Wang et al., 2020.

models have been proposed. Once it is produced in the chloroplasts, OPDA is *i*) conjugated with galactolipids, GSH, and/or amino acids (e.g., Ile) before/after being released to the cytosol, in turn targets yet unknown effector/receptor proteins, and conveys ORG expressions (Böttcher and Pollmann, 2009; Ohkama-Ohtsu et al., 2011; Floková et al., 2016). Alternatively, OPDA itself can *ii*) serve as a reactive electrophile that targets and modifies thiol residues of, e.g., cysteine, histidine, and lysine in proteins (Mueller and Berger, 2009; Monte et al., 2020) triggering downstream signal transductions and metabolic cascades, or *iii*) covalently bind a CYP20-3 receptor and builds up a reduction capacity that modulates the cellular activity of oxidoreductase cascades in controlling retrograde signaling, rapidly adjusting nuclear gene expressions (Tada et al., 2008; Park et al., 2013; Cheong et al., 2017). It is, however, still unclear how these signaling mechanisms ultimately stimulate global, spatiotemporal gene expression dynamics with both distinctive and redundant transcriptional outputs. Our study suggests though that OPDA can target and fine-tune an interface between photosynthesis-derived ETC and sulfur assimilation processes in the chloroplasts (Cheong et al., 2017; Liu et al., 2020). This interplay enables plants to make an adaptive decision in allocating resources (e^-) between growth and defense responses (e.g., fitness trade-offs or balances) toward different ecological challenges such as pathogens, pests, tissue injury as well as light and oxidative stresses, in the end, ensuring optimal growth, reproduction, and survival of plants. Therefore, furthering our understanding of functional and biological activities of OPDA and associated molecular mechanisms (a) will not only provide new insights into a "broad-spectrum" defense responses and (b) can enrich plant breeding and engineering strategies for the selection of elite genetic traits that will maximize plant fitness, but also (c) will address fundamental gaps in the immune activation of a mammalian system, and (d) help in improving drug developments through facilitating the rational design of more potent and safe reagents.

AUTHOR CONTRIBUTIONS

SWP and WL, designed and wrote the article. All authors contributed to the article and approved the submitted version.

ACKNOWLEDGMENTS

This work was supported by the Alabama Agricultural Experiment Station (Auburn University), the Hatch Program of the National Institute of Food and Agriculture (United States Department of Agriculture), the Alabama Cotton Commission, and the Alabama Farmers Federation.

REFERENCES

Acosta, I. F., and Farmer, E. E. (2010). "Jasmonates," in *Arabidopsis Book*, eds C.R. Somerville, E.M. Meyerowitz (Rockville: American Society of Plant Biologists) 8, e0129.

Andersson, M. X., Hamberg, M., Kourtchenko, O., Brunnström, A., McPhail, K. L., Gerwick, W. H., et al. (2006). Oxylipin profiling of the hypersensitive response in *Arabidopsis thaliana*: formation of a novel oxo-phytodienoic acid-containing galactolipid, arabidopsides E. *J. Biol. Chem.* 281, 31528–31537. doi: 10.1074/jbc.M604820200

Arc, E., Sechet, J., Corbineau, F., Rajjou, L., and Marion-Poll, A. (2013). ABA crosstalk with ethylene and nitric oxide in seed dormancy and germination. *Front. Plant Sci.* 4:63. doi: 10.3389/fpls.2013.00063

Arnold, M. D., Gruber, C., Flokov,á, K., Miersch, O., Strnad, M., Novák, O., et al. (2016). The recently identified isoleucine conjugate of *cis*-12-oxo-phytodienoic acid is partially active in *cis*-12-oxo-phytodienoic acid-specific gene expression of *Arabidopsis thaliana*. *PLoS ONE* 11:e0162829. doi: 10.1371/journal.pone.0162829

Balfagón, D., Sengupta, S., Gómez-Cadenas, A., Fritschi, F. B., Azad, R. K., Mittler, R., et al. (2019). Jasmonic acid is required for plant acclimation to a combination of high light and heat stress. *Plant Physiol.* 181, 1668–1682. doi: 10.1104/pp.19.00956

Barros-Galvão, T., Dave, A., Cole, A., Harvey, D., Langer, S., Larson, T. R., et al. (2019). *cis*-12-Oxo phytodienoic acid represses Arabidopsis seed germination in shade conditions. *J. Exp. Bot.* 70, 5919–5927. doi: 10.1093/jxb/erz337

Bosch, M., Berger, S., Schaller, A., and Stintzi, A. (2014a). Jasmonate-dependent induction of polyphenol oxidase activity in tomato foliage is important for defense against *Spodoptera exigua* but not against *Manduca sexta*. *BMC Plant Biol.* 14:257. doi: 10.1186/s12870-014-0257-8

Bosch, M., Wright, L. P., Gershenzon, J., Wasternack, C., Hause, B., Schaller, A., et al. (2014b). Jasmonic acid and its precursor 12-oxophytodienoci acid control different aspects of constitutive and induced herbivore defenses in tomato. *Plant Physiol.* 116, 396–410. doi: 10.1104/pp.114.237388

Böttcher, C., and Pollmann, S. (2009). Plant oxylipins: Plant responses to 12-oxo-phytodienoic acid are governed by its specific structural and functional properties. *FEBS J.* 17, 4693–4703. doi: 10.1111/j.1742-4658.2009.07195.x

Buseman, C. M., Tamura, P., Sparks, A. A., Gaughman, E. J., Maatta, S., Zhao, J., et al. (2006). Wounding stimulates the accumulation of glycerolipids containing oxophytodienoic acid and dinor-oxophytodienoic acid in Arabidopsis leaves. *Plant Physiol.* 142, 28–39. doi: 10.1104/pp.106.082115

Caporaletti, D., D'Alessio, A. C., Rodriguez-Suarez, R. J., Senn, A. M., Duek, P. D., and Wolosiuk, R. A. (2007). Non-reductive modulation of chloroplast fructose-1,6-bisphos-phatase by 2-Cys peroxiredoxin. *Biochem. Biophys. Res. Commun.* 355, 722–727. doi: 10.1016/j.bbrc.2007.02.013

Cheng, G., Chen, M. S., and Zhu, L. (2018). 12-oxo-phytodienoic acid enhances wheat resistance to Hessian Fly (Diptera: Cecidomyiidae) under heat stress. *J. Econ. Entomol.* 111, 917–922. doi: 10.1093/jee/tox374

Cheong, H., Dos Santos, I. B., Liu, W., Gosse, H. N., and Park, S. W. (2017). Cyclophilin 20-3 is positioned as a regulatory hub between light-dependent redox and 12-oxo-phytodienoic acid signaling. *Plant Signal. Behav.* 12:e1362520. doi: 10.1080/15592324.2017.1362520

Chini, A., Fomseca, S., Fernández, G., Adie, B., Chico, J. M., Lorenzo, O., et al. (2007). The JAZ family of repressors is the missing link in jasmonate signaling. *Nature* 448, 666–671. doi: 10.1038/nature06006

Chini, A., Monte, I., Zamarreño, A. M., Hamberg, M., Lassueur, S., Reymond, P., et al. (2018). An OPR3-independent pathway uses 4,5-didehydrojasmonate for jasmonate synthesis. *Nat. Chem. Biol.* 14, 171–178. doi: 10.1038/nchembio.2540

Chitnis, P. R. (2001). Photosystme I: function and physiology. *Annu. Rev. Plant Physiol. Mol. Biol.* 52, 593–626. doi: 10.1146/annurev.arplant.52.1.593

Christensen, S. A., Huffaker, A., Kaplan, F., Slims, J., Ziemann, S., Doehlemann, G., et al. (2015). Maize death acids, 9-lipoxygenase-derived cyclopente(a)nones, display activity as cytotoxic phytoalexins and transcriptional mediators. *Proc. Natl. Acad. Sci. U.S.A.* 112, 11407–11412. doi: 10.1073/pnas.1511131112

Chung, H. S., Koo, A. J. K., Gao, X., Jayanty, S., Thines, B., Jones, A. D., et al. (2008). Regulation and function of *Arabidopsis JAMONATE ZIM*-domain genes in response to wounding and herbivory. *Plant Physiol.* 146, 952–964. doi: 10.1104/pp.107.115691

Dang, H. T., Lee, H. J., Yoo, E. S., Hong, J., Bao, B., Choi, J. S., et al. (2008). New jasmonate analogues as potential anti-inflammatory agents. *Bioorg. Med. Chem.* 16, 10228–10235. doi: 10.1016/j.bmc.2008.10.050

Dave, A., and Graham, I. A. (2012). Oxylipin signaling: A distinct role for the jasmonic acid precursor *cis*-(+)-12-oxo-phytodienoic acid (*cis*-OPDA). *Front. Plant Sci.* 3, 42. doi: 10.3389/fpls.2012.00042

Dave, A., Hernández, M. L., He, Z., Andriotix, V. M. E., Vaistij, F. E., Larson, T. R., et al. (2011). 12-oxo-phytodienoic acid accumulation during seed development represses seed germination in *Arabidopsis*. *Plant Cell* 23, 583–599. doi: 10.1105/tpc.110.081489

Dave, A., Vaistij, F. E., Gilday, A. D., Penfield, S. D., and Graham, I. A. (2016). Regulation of *Arabidopsis thaliana* seed dormancy and germination by 12-oxo-phytodienoci acid. *J. Exp. Bot.* 67, 2277–2284. doi: 10.1093/jxb/erw028

Davoine, C., Douki, T., Iacazio, G., Montillet, J. L., and Triantaphylidès, C. (2005). Conjugation of keto fatty acids to glutathione in plant tissues. characterization and quantification by HPLC-tandem mass spectrometry. *Anal. Chem.* 77, 7366–7372. doi: 10.1021/ac051155y

Davoine, D., Falletti, O., Douki, T., Iacazio, G., Ennar, N., Montillet, J. L., et al. (2006). Adducts of oxylipin electrophiles to gluatathione reflect a 13 specificity of the downstream lipoxygenase pathway in the tobacco hypersensitive response. *Plant Physiol.* 140, 1484–01493. doi: 10.1104/pp.105.074690

De Storme, N., and Geelen, D. (2014). Callose homeostasis at plasmodesmata: molecular regulators and developmental relevance. *Front. Plant Sci.* 5, 138. doi: 10.3389/fpls.2014.00138

Devoto, A., Ellis, C., Magusin, A., Chang, H. S., Chilcott, C., Xhu, T., et al. (2005). Expression profiling reveals COI1 to be a key regulator of genes involved in wound- and methyl jasmonate-induced secondary metabolism, defence, and hormone interactions. *Plant Mol. Biol.* 58, 497–513. doi: 10.1007/s11103-005-7306-5

Dominguez-Solis, J. R., He, Z., Lima, A., Ting, J., Buchanan, B. B., and Luan, S. (2008). A cyclophilin links redox and light signals to cysteine biosynthesis and stress responses in chloroplasts. *Proc. Natl. Acad. Sci. U.S.A.* 105, 16386–16391. doi: 10.1073/pnas.0808204105

Dos Santos, I. B., and Park, S. W. (2019). Versatility of cyclophilins in plant growth and survival: a case study in *Arabidopsis*. *Biomolecules* 9:20. doi: 10.3390/biom9010020

Felton, G. W. (2005). Indigestion is a plant's best defense. *Proc. Natl. Acad. Sci. U.S.A.* 92, 407–411. doi: 10.1073/pnas.0509895102

Finka, A., Mattoo, R. U., and Goloubinoff, P. (2011). Meta-analysis of heat- and chemically upregulated chaperone genes in plant and human cells. *Cell Stress Chaperones* 16, 15–31. doi: 10.1007/s12192-010-0216-8

Flescher, E. (2007). Jasmonates in cancer therapy. *Cancer Lett.* 245, 1–10. doi: 10.1016/j.canlet.2006.03.001

Floková, K., Feussner, K., Herrfurth, C., Miersch, O., Mik, V., Tarkowsk,á, D., et al. (2016). A previously undescribed jasmonate compound in flowering *Arabidopsis thaliana*—the identification of cis-(+)-OPDA-Ile. *Phytochemistry* 122, 230–237. doi: 10.1016/j.phytochem.2015.11.012

Funk, C. D. (2001). Prostaglandins and leukotrienes: advances in eicosanoid biology. *Science.* 294, 1871–1875. doi: 10.1126/science.294.5548.1871

Genva, M., Deleu, M., Andersson, M. X., Lins, L., and Fauconnier, M. L. (2019). "Evaluation of interactions between arabidopsides and plant plasma membrane lipids," in Scientific Congresses and Symposiums. Available online at: https://orbi.uliege.be/bitstream/2268/222461/1/Bruxelles%20congress.pdf.

Gleason, C., Leelarasamee, N., Meldau, D., and Feussner, I. (2016). OPDA has key role in regulating plant susceptibility to the root-knot nematode *Meloidogyne hapla* in *Arabidopsis*. *Front. Plant Sci.* 7:1565. doi: 10.3389/fpls.2016.01565

Goetz, S., Hellwege, A., Stenzel, I., Kutter, C., Hauptmann, V., Forner, S., et al. (2012). Role of Cis-12-Oxo-Phytodienoic Acid in Tomato Embryo Development. *Plant Physiol.* 4, 1715–1727. doi: 10.1104/pp.111.192658

Grover, S., Agpawa, E., Sarath, G., Sattler, S. E., and Louis, J. (2020a). Interplay of phytohormones facilitate sorghum tolerance to aphids. *Plant Mol. Biol.* 1–12. doi: 10.1007/s11103-020-01083-y

Grover, S., Versani, S., Kolomietx, M. V., and Louis, J. (2020b). Maize defense elicitor, 12-oxo-phytodienoic acid, prolongs aphid salivation. *Commun. Integr. Biol.* 13, 63–66. doi: 10.1080/19420889.2020.1763562

Guan, L., Denkert, N., Eisa, A., Lehmann, M., Sjuts, I., Weiberg, A., et al. (2019). JASSY, a chloroplast outer membrane protein required for

jasmonate biosynthesis. *Proc. Natl. Acad. Sci. U.S.A.* 116, 10568–10575. doi: 10.1073/pnas.1900482116

Guo, H. M., Li, H. C., Zhou, S. H., Xue, H. W., and Miao, X. X. (2014). *Cis*-12-oxo-phytodienoic acid stimulates rice defense response to a piercing-sucking insect. *Mol. Plant* 7, 1683–1692. doi: 10.1093/mp/ssu098

Hazman, M., Hause, B., Eiche, E., Nick, P., and Riemann, M. (2015). Increased tolerance to salt stress in OPDA-deficient rice *ALLENE OXDE CYCLASE* mutants is linked to an increase ROS-scavenging activity. *J. Exp. Bot.* 66, 3339–3352. doi: 10.1093/jxb/erv142

He, J., Duan, Y., Hua, D., Fan, G., Wang, L., Liu, Y., et al. (2012). DEXH box RNA helicase-mediated mitochondrial reactive oxygen species production in Arabidopsis mediates crosstalk between abscisic acid and auxin signaling. *Plant Cell* 24, 1815–1833. doi: 10.1105/tpc.112.098707

Hisamatsu, Y., Goto, N., Hasegawa, K., and Shigemori, H. (2003). Arabidopsides A and B, two new oxylipins from *Arabidopsis thaliana*. *Tetrahedron Lett.* 44, 5553–5556. doi: 10.1016/S0040-4039(03)01148-1

Hisamatsu, Y., Goto, N., Sekiguchi, M., Hasegawa, K., and Shigemori, H. (2005). Oxylipins arabidopsides C and D from *Arabidopsis thaliana*. *J. Nat. Prod.* 68, 600–603. doi: 10.1021/np0495938

Hofhuis, H., Laskowski, M., Du, Y., Prasad, K., Grigg, S., Pinon, V., et al. (2013). Phyllotaxis and rhizotaxis in Arabidopsis are modified by three PLETHORA transcription factors. *Curr. Biol.* 23, 965–962. doi: 10.1016/j.cub.2013.04.048

Hossain, M. A., Li, A. G., Hoque, T. S., Burritt, D. J., Fujita, M., and Munnè-Bosch, S. (2018). Heat or cold priming-induced cross-tolerance to abiotic stresses in plants: key regulators and possible mechanisms. *Protoplasma* 255, 399–412. doi: 10.1007/s00709-017-1150-8

Huang, X., Stettmaier, K., Michel, C., Hutzler, P., Mueller, M. J., and Durner, J. (2004). Nitric oxide is induced by wounding and influences jasmonic acid signaling in Arabidopsis thaliana. *Planta* 218, 938–946. doi: 10.1007/s00425-003-1178-1

Huot, B., Yao, J., Montgomery, B. L., and He, S. Y. (2014). Growth-defense tradeoffs in plants: a balancing act to optimize fitness. *Mol. Plant* 7, 1267–1287. doi: 10.1093/mp/ssu049

Jensen, P. E., Bassi, R., Boekema, E. J., Dekker, J. P., Jansson, S., Leister, D., et al. (2007). Structure, function and regulation of plant photosystem I. *Biochim. Biophys. Acta.* 1767, 335–352. doi: 10.1016/j.bbabio.2007.03.004

Jiao, Y., Sun, L., Song, Y., Wang, L., Liu, L., Zhang, L., et al. (2013). AtrbohD and atrbohF positively regulate abscisic acid-inhibited primary root growth by affecting Ca^{2+} signaling and auxin response of roots in Arabidopsis. *J. Exp. Bot.* 64, 4183–4192. doi: 10.1093/jxb/ert228

Kazan, K., and Manners, J. M. (2011). The interplay between light and jasmonate signaling during defence and development. *J. Exp. Bot.* 62, 4087–4100. doi: 10.1093/jxb/err142

Klessig, D. F., Choi, H. W., and Dempsey, D. A. (2018). Systemic acquired resistance and salicylic acid: past, present and future. *Mol. Plant Microbe Interact.* 31, 871–888. doi: 10.1094/MPMI-03-18-0067-CR

Kliebenstein, D. J. (2016). False idolatry of the mythical growth versus immunity tradeoff in molecular systems plant pathology. *Physiol. Mol. Plant Pathol.* 95, 55–59. doi: 10.1016/j.pmpp.2016.02.004

Ko, J. H., Yang, S. H., and Han, K. H. (2006). Upregulation of an Arabidopsis RING-H2 gene, *XERICO*, confers drought tolerance through increased abscisic acid biosynthesis. *Plant J.* 47, 343–355. doi: 10.1111/j.1365-313X.2006.02782.x

Koch, K. G., Chapman, K., Louis, J., Heng-Moss, T., and Sarath, G. (2016). Plant tolerance: a unique approach to control hemipteran pests. *Front. Plant Sci.* 7:1363. doi: 10.3389/fpls.2016.01363

Konig, J., Baier, M., Horling, F., Kahmann, U., Harris, G., and Schurmann, P. (2002). The plant-specific function of 2-Cys peroxiredoxin-mediated detoxification of peroxides in the redox-hierarchy of photosynthetic electron flux. *Proc. Natl. Acad. Sci. U.S.A.* 99, 5738–5743. doi: 10.1073/pnas.072644999

Koo, A. J. K., Gao, X., Jones, A. D., and Howe, G. A. (2009). A rapid wound signal activates the systemic synthesis of bioactive jasmonates in Arabidopsis. *Plant J.* 59, 974–986. doi: 10.1111/j.1365-313X.2009.03924

Kourtchenko, O., Andersson, M. X., Hamberg, M., Brunnström, A., Göbel, C., McPhail, K. L., et al. (2007). Oxo-phytodienoic acid-containing galactolipids in Arabidopsis: jasmonate signaling dependence. *Plant Physiol.* 145, 1658–1669. doi: 10.1104/pp.107.104752

Laxa, M., Konig, J., Dietz, K. J., and Kandlbinder, A. (2007). Role of the cysteine residues in *Arabidopsis thaliana* cyclophilin CYP20-3 in peptidylprolyl *cis-trans* isomerase and redox-related function. *Biochem. J.* 401, 287–297. doi: 10.1042/BJ20061092

Leon-Reyes, A., Van der Does, D., De Lange, E. S., Delker, C., Wasternack, C., Van Wees, S. C., et al. (2010). Salicylate-mediated suppression of jasmonate-responsive gene expression in Arabidopsis is targeted downstream of the jasmonate biosynthesis pathway. *Planta* 232, 1423–1432. doi: 10.1007/s00425-010-1265-z

Liebthal, M., Strüve, M., Li, X., Hertle, Y., Maynard, D., Hellweg, T., et al. (2016). Redox-dependent conformational dynamics of decameric 2-cys-teine peroxiredoxin and its interaction with cyclophilin 20-3. *Plant Cell Physiol.* 57, 1415–1425. doi: 10.1093/pcp/pcw031

Liu, W., Barbosa dos Santos, I., Moye, A., and Park, S. W. (2020). CYP20-3 deglutathionylates 2-CysPRX A and suppresses peroxide detoxification during heat stress. *Life Sci. Alliance* 3:e202000775. doi: 10.26508/lsa.202000775

López-Galiano, M. J., Ruiz-Arroyo, V. M., Fernández-Crespo, E., Rausell, C., Real, M. D., García-Agustín, P., et al. (2017). Oxylipin mediated stress response of a miraculin-like protease inhibitor in hexanoic acid primed eggplant plants infested by Colorado potato beetle. *J. Plant Physiol.* 215, 59–64. doi: 10.1016/j.jplph.2017.04.013

Luna, E., Pastor, V., Robert, J., Flors, V., Mauch-Mani, B., and Ton, J. (2010). Callose deposition: a multifaceted plant defense response. *Mol. Plant Microbe. Interact.* 24, 183–193. doi: 10.1094/MPMI-07-10-0149

Luo, X., Chen, Z., Gao, J., and Gong, Z. (2014). Abscisic acid inhibits root growth in Arabidopsis through ethylene biosynthesis. *Plant J.* 79, 44–58. doi: 10.1111/tpj.12534

Marnett, L. J. (2008). Divergence from the superfamily. *Nature* 455, 300–301. doi: 10.1038/455300a

Maynard, D., Gröger, H., Dierks, T., and Dietz, K. J. (2018). The function of the oxylipin, 12-oxo-phytodienoic acid in cell signaling, stress acclimation, and development. *J. Exp. Bot.* 69, 5341–5354. doi: 10.1093/jxb/ery316

Meyer, Y., Buchanan, B. B., Vignols, F., and Reichheld, J. P. (2009). Thioredoxins and glutaredoxins: unifying elements in redox biology. *Annu. Rev. Genet.* 43, 335–367. doi: 10.1146/annurev-genet-102108-134201

Monte, I., Kneeshaw, S., Franco-Zorrilla, J. M., Chini, A., Zamarreño, A. M., García-Mina, J. M., et al. (2020). An ancient COI1-independent function for reactive electrophilic oxylipins in thermotolerance. *Curr. Biol.* 30, 962–971. doi: 10.1016/j.cub.2020.01.023

Monte, L., Franco-Zorrilla, J. M., García-Mina, J. M., Zamarreño, A. M., García-Mina, J. M., Nishihama, R., et al. (2019). A single JAZ repressor controls the jasmonate pathway in *Marchantia polymorpha*. *Mol. Plant* 12, 185–198. doi: 10.1016/j.molp.2018.12.017

Monte, L., Ishida, S., Zamarreño, A. M., Hamberg, M., Franco-Zorrilla, J. M., García-Mina, J. M., et al. (2018). Ligand-receptor co-evolution shaped the jasmonate pathway in land plants. *Nat. Chem. Biol.* 14, 480–488. doi: 10.1038/s41589-018-0033-4

Mosblech, A., Feussner, I., and Heilmann, I. (2010). "Oxylipin signaling and plant growth," in *Lipid Signaling in Plants*, ed. T. Munnik (Springer-Verlag, Berlin, Heidelberg) 277–291.

Motohashi, K., Kondoh, A., Stumpp, M. T., and Hisabori, T. (2001). Comprehensive survey of proteins targeted by chloroplast thioredoxin. *Proc. Natl. Acad. Sci. U.S.A.* 98, 11224–11229. doi: 10.1073/pnas.191282098

Mueller, S., and Berger, S. (2009). Reactive electrophilic oxylipins: Pattern recognition and signalling. *Phytochemistry* 70, 1511–1521. doi: 10.1016/j.phytochem.2009.05.018

Mueller, S., Hilbert, B., Dueckershoff, K., Roitsch, T., Krischke, M., Mueller, M. J., et al. (2008). General detoxification and stress responses are mediated by oxidized lipids through TGA transcription factors in *Arabidopsis*. *Plant Cell* 20, 768–785. doi: 10.1105/tpc.107.054809

Muench, M., Hsin, C. H., Ferber, E., Berger, S., and Mueller, M. J. (2016). Reactive electrophilic oxylipins triggers a heat stress-like response through HSFA1 transcription factors. *J. Exp. Bot.* 67, 6139–6148. doi: 10.1093/jxb/erw376

Muthuramalingam, M., Seidel, T., Laxa, M., de Miranda, S. M. N., Gärtner, F., Ströher, E., et al. (2009). Multiple redox and non-redox interactions define 2-Cys peroxiredoxin as a regulatory hub in the chloroplast. *Mol. Plant* 2, 1273–1288. doi: 10.1093/mp/ssp089

Nikkanen, L., and Rintamäki, E. (2014). Thioredoxin-dependent regulatory networks in chloroplasts under fluctuating light conditions. *Phil. Trans. R. Soc. B.* 369, 20130224. doi: 10.1098/rstb.2013.0224

Noctor, G., Queval, G., Mhamdi, A., Chaouch, S., and Foyer, C. H. (2011). "Glutathione," in *Arabidopsis Book*, eds. C.R. Somerville, E.M. Meyerowitz, (Rockville: American Society of Plant Biologists) 9, e0142.

Ohkama-Ohtsu, N., Sasaki-Sekimoto, Y., Oikawa, A., Jikumaru, Y., Shinoda, S., Inoue, E., et al. (2011). 12-oxo-phytodienoic acid-glutathione conjugate is transported into the vacuole in Arabidopsis. *Plant Cell Physiol.* 52, 205–209. doi: 10.1093/pcp/pcq181

Ortiz-Masia, D., Perez-Amdor, M. A., Carbonell, J., and Marcote, M. J. (2007). Diverse stress signals activate the C1 subgroup MAP Kinases of *Arabidopsis*. *FEBS Lett.* 58, 1834–1840. doi: 10.1016/j.febslet.2007.03.075

Palmieri, M. C., Sell, S., Huang, X., Scherf, M., Werner, T., Durner, J., et al. (2008). Nitric oxide-resposive genes and promoters in Arabidopsis thaliana: a bioinformatics approach. *J. Exp. Bot.* 59, 177–186. doi: 10.1093/jxb/erm345

Park, S. W., Li, W., Voejjaiser, A., He, B., Kim, S., Nilsson, A. K., et al. (2013). Cyclophilin 20-3 relays a 12-oxo-phytodienoic acid signal during stress responsive regulation of cellular redox homeostasis. *Proc. Natl. Acad. Sci. U.S.A.* 110, 9559–9564. doi: 10.1073/pnas.1218872110

Peltier, J. B., Cai, Y., Sun, Q., Zabrouskov, V., Giacomelli, L., Rudella, A., et al. (2006). The oligomeric stromal proteome of *Arabidopsis thaliana* chloroplasts. *Mol. Cell Proteomics* 5, 114–133. doi: 10.1074/mcp.M500180-MCP200

Pérez-Ruiz, J. M., Naranjo, B., Ojeda, V., Guinea, M., and Cejudo, F. J. (2017). NTRC-dependent redox balance of 2-Cys peroxiredoxins is needed for optimal function of the photosynthetic apparatus. *Proc. Natl. Acad. Sci. U.S.A.* 114, 12069–12074. doi: 10.1073/pnas.1706003114

Pieterse, C. M. J., Van der Does, D., Zamioudis, C., Leon-Reyes, A., and Van Wees, S. C. M. (2012). Hormonal modulation of plant immunity. *Annu. Rev. Cell Dev. Biol.* 28, 489–521. doi: 10.1146/annurev-cellbio-092910-154055

Pieterse, C. M. J., Zamioudis, C., Berendsen, R. L., Weller, D. M., Van Wees, S. C. M., and Bakker, P. A. H. M. (2014). Induced systemic resistance by beneficial microbes. *Annu. Rev. Phytophahtol.* 52, 347–375. doi: 10.1146/annurev-phyto-082712-102340

Piskurewicz, U., Jikumaru, Y., Kinoshita, N., Nambara, E., Kamiya, Y., and Lopez-Molina, L. (2008). The gibberellic acid signaling repressor RGL2 inhibits *Arabidopsis* seed germination by stimulating abscisic acid synthesis and ABI5 activity. *Plant Cell* 20, 2729–2745. doi: 10.1105/tpc.108.061515

Ribot, C., Zimmerili, C., Farmer, E. E., Reymond, P., and Poirier, Y. (2008). Induction of the Arabidopsis *PHO1;H10* gene by 12-oxo-phytodienoic acid but not jasmonic acid via a CORONATINE INSENSITIVE1-dependent pathway. *Plant Physiol.* 147, 696–706. doi: 10.1104/pp.108.119321

Riemann, M., Müller, A., Korte, A., Furuya, M., Wiler, E. W., and Nick, P. (2003). Impaired induction of the jasmonate pathway in the rice mutant hebiba. *Plant Physiol.* 133, 1820–1830. doi: 10.1104/pp.103.027490

Romano, P. G. N., Horton, P., and Gray, J. E. (2004). The *Arabidopsis* cyclophilin gene family. *Plant Physiol.* 134, 1268–1282. doi: 10.1104/pp.103.022160

Russell, L., Larner, V., Kurup, S., Bougourd, S., and Holdsworth, M. (2000). The *Arabidopsis COMATOSE* locus regulates germination potential. *Development* 127, 3759–3767. doi: 10.1242/dev.127.17.3759

Savchenko, T., and Dehesh, K. (2014). Drought stress modulates oxylipin signature by eliciting 12-OPDA as a potent regulator of stomatal sperture. *Plant Signal. Behav.* 9:e28304. doi: 10.4161/psb.28304

Scalschi, L., Llorens, E., García-Agustín, P., and Vicedo, B. (2020). Role of jasmonic acid pathway in tomato plant-*Pseudomonas syringae* interaction. *Plants* 9, 136. doi: 10.3390/plants9020136

Scalschi, L., Sanmartin, M., Camañes, G., Troncho, P., Sánchez-Serrano, J. J., García-Agustín, P., et al. (2015). Silencing of *OPR3* in tomato reveals the role of OPDA in callose deposition during the activation of defense responses against *Botrytis cinerea*. *Plant J.* 81, 304–315. doi: 10.1111/tpj.12728

Serrato, A. J., Fernández-Trijueque, J., Barajas-López, J., Chueca, A., and Sahrawy, M. (2013). Plastid thioredoxins: a "one-for-all" redox-signaling system in plants. *Front. Plant Sci.* 4, 463. doi: 10.3389/fpls.2013.00463

Shim, J. S., Jung, C., Lee, S., Min, K., Lee, Y. W., Choi, Y., et al. (2013). AtMYB44 regulates WRKY70 expression and modulates antagonistic interaction between salicylic acid and jasmonic acid signaling. *Plant J.* 73, 483–495. doi: 10.1111/tpj.12051

Sirichandra, C., Gu, D., Hu, H. C., Davanture, M., Lee, S., Djaoui, M., et al. (2009). Phosphorylation of the Arabidopsis AtrbohF NADPH oxidase by OST1 protein kinase. *FEBS Lett.* 583, 2982–2986. doi: 10.1016/j.febslet.2009.08.033

Skubacz, A., Daszkowska-Golec, A., and Szarejko, I. (2016). The role and regulation of ABI5 (ABA-insensitive 5) in plant development, abiotic stress responses and phytohormone crosstalk. *Front. Plant Sci.* 7:1884. doi: 10.3389/fpls.2016.01884

Staswick, P. E. (2009). The tryptophan conjugates of jasmonic and idole-3-acetic acids are endoge-nous auxin inhibitors. *Plant Physiol.* 150, 1310–1321. doi: 10.1104/pp.109.138529

Stintzi, A., Weber, H., Reymond, P., Browse, J., and Farmer, E. E. (2001). Plant defense in the absence of jasmonic acid: The role of cyclopentenones. *Proc. Natl. Acad. Sci. U.S.A.* 97, 10625–10630. doi: 10.1073/pnas.190264497

Stotz, H. U., Jikumaru, Y., Shimada, Y., Sasaki, E., Stingl, N., Mueller, M. J., et al. (2011). Jasmonate-dependent and COI1-independent defense responses against *Sclerotinia sclerotiorum* in *Arabidopsis thaliana*: Auxin is part of COI1-independent defense signaling. *Plant Cell Physiol.* 52, 1941–1951. doi: 10.1093/pcp/pcr127

Stotz, H. U., Mueller, S., Zoeller, M., Mueller, M. J., and Berger, S. (2013). TGA transcription factors and jasmonate-independent COI1 signalling regulate specific plant responses to reactive oxylipins. *J. Exp. Bot.* 64, 963–975. doi: 10.1093/jxb/ers389

Sun, L. R., Wang, Y. B., He, S. B., and Hao, F. S. (2018). Mechanisms for abscisic acid inhibition of primary root growth. *Plant Signal. Behav.* 13, 9. doi: 10.1080/15592324.2018.1500069

Tada, Y., Spoel, S. H., Paferowska-Mukhtar, K., Mou, Z., Song, J., Wang, C., et al. (2008). Plant immunity requires conformational changes of NPR1 via S-nitrosylation and thioredoxins. *Science* 321, 952–956. doi: 10.1126/science.1156970

Taki, N., Sasaki-Sekimoto, Y., Obayashi, T., Kikuta, A., Kobayashi, K., Ainai, T., et al. (2005). 12-oxo-phytodienoic acid triggers expression of a distinct set of genes and plays a role in wound-induced gene expression in *Arabidopsis*. *Plant Physiol.* 139, 1268–1283. doi: 10.1104/pp.105.067058

Taki-Nakano, N., Ohzeki, H., Kotera, J., and Ohta, H. (2014). Cytoprotective effects of 12-oxo-phytodienoci acid, a plant-derived oxylipin jasmonate, on oxidative stress-induced toxicity in human neuroblastoma SH-SY5Y cells. *Biochim. Biophys. Acta*. 1840, 3413–3422. doi: 10.1016/j.bbagen.2014.09.003

Theodoulou, F. L., Job, K., Slocombe, S. P., Footitt, S., Holdsworth, M., Baker, A., et al. (2005). Jasmonic acid levels are reduced in COMATOSE ATP-binding cassette transporter mutants. Implications for transport of jasmonate precursors into peroxisomes. *Plant Physiol.* 137, 835–840. doi: 10.1104/pp.105.059352

Thines, B., Katsir, L., Melotto, M., Niu, Y., Mandaokar, A., Liu, G., et al. (2007). JAZ repressor proteins are targets of the SCF^{COI1} complex during jasmonate signalling. *Nature* 448, 661–665. doi: 10.1038/nature05960

Vaistij, F. E., Barros-Galvão, T., Cole, A. F., Gilday, A., He, Z., Li, Y., et al. (2018). *MOTHER-OF-FT-AND-TFL1* represses seed germination under far-red light by modulating phytohormone responses in *Arabidopsis thaliana*. *Proc. Natl. Acad. Sci. U.S.A.* 115, 8442–8447. doi: 10.1073/pnas.1806460115

Varsani, S., Grover, S., Zhou, S., Koch, K. G., Huang, P. C., Kolomiets, M. V., et al. (2019). 12-oxo-phytodienoic acid acts as a regulator of maize defense against corn leaf aphid. *Plant Physiol.* 179, 1402–1415. doi: 10.1104/pp.18.01472

Veronese, P., Nakagami, H., Bluhm, B., Abuqamar, S., Chen, X., Salmeron, J., et al. (2006). The membrane-anchored *BOTRYTIS-INDUCED KINASE1* plays distinct roles in Arabidopsis resistance to necrotrophic and biotrophic pathogens. *Plant Cell* 18, 257–273. doi: 10.1105/tpc.105.035576

Vissenberg, K., Claeijs, N., Balcerowicz, D., and Schoenaers, S. (2020). Hormonal regulation of root hair growth and responses to the environment in Arabidopsis. *J. Exp. Bot.* 71, 2412–2427. doi: 10.1093/jxb/eraa048

Vu, H. S., Tamura, P., Galeva, N. A., Chaturvedi, R., Roth, M. R., Williams, T. D., et al. (2012). Direct infusion mass spectrometry of oxylipin-containing Arabidopsis membrane lipids reveals varied patterns in different stress responses. *Plant Physiol.* 158, 324–339. doi: 10.1104/pp.111.190280

Wang, H., Qi, Q., Schorr, P., Cutler, A. J., Crosby, W. L., and Fowke, L. C. (2008). ICK1, a cyclin-dependent protein kinase inhibitor from Arabidopsis interacts

with both Cdc2a and CycD3, and its expression is induced by abscisic acid. *Plant J.* 15, 501–510. doi: 10.1046/j.1365-313X.1998.00231.x

Wang, K. D., Borrego, E. J., Kenerley, C. M., and Kolemiets, M. V. (2020). Oxylipins other than jasmonic acid are xylem-resident signals regulating systemic resistance induced by *Trichoderma virens* in maize. *Plant Cell* 32, 166–185. doi: 10.1105/tpc.19.00487

Wang, K. L., Li, H., and Ecker, J. R. (2002). Ethylene biosynthesis and signaling networks. *Plant Cell* 14, S131–S151. doi: 10.1105/tpc.001768

Wang, L., Hua, D., He, J., Duan, Y., Chen, Z., Hong, X., et al. (2011). Auxin response factor2 (ARF2) and its regulated homeodomain gene HB33 mediate abscisic acid response in Arabidopsis. *PLoS Genet.* 7:e1002172. doi: 10.1371/journal.pgen.1002172

Wang, Y., Loake, G. J., and Chu, C. (2013). Cross-talk of nitric oxide and reactive oxygen species in plant programed cell death. *Front Plant Sci.* 4:314. doi: 10.3389/fpls.2013.00314

Wei, J., van Loon, J. J., Gols, R., Menzel, T. R., Li, N., Kang, L., et al. (2014). Reciprocal crosstalk between jasmonate and salicylate defence-signalling pathways modulates plant volatile emission and berbivore host-selection behaviour. *J. Exp. Bot.* 65, 3289–3298. doi: 10.1093/jxb/eru181

Xu, J., Gao, G. L., Du, J. J., Guo, Y., and Yang, C. W. (2010). Cell cycle modulation in response to the primary root of Arabidopsis. *Pak. J. Bot.* 42, 2703–2710.

Yao, T., Jin, D., Liu, Q., and Gong, Z. (2013). Abscisic acid suppresses the highly occurred somatic homologous recombination in Arabidopsis rfc1 mutant. *J. Genet. Genomics* 40, 465–471. doi: 10.1016/j.jgg.2013.05.006

Yin, H., Zhang, X., Liu, J., Wang, Y., He, J., Yang, T., et al. (2009). Epigenetic regulation, somatic homologous recombination, and abscisic acid signaling are influenced by DNA polymerase epsilon mutation in Arabidopsis. *Plant Cell* 21, 386–402. doi: 10.1105/tpc.108.061549

Zhang, Y., and Turner, J. G. (2008). Wound-induced endogenous jasmonates stunt plant growth by inhibiting mitosis. *PLoS ONE* 3:e3699. doi: 10.1371/journal.pone.0003699

Zhao, X., Li, N., Song, Q., Li, X., Meng, H., and Luo, K. (2020). OPDAT1, a plastid envelope protein involved in 12-oxo-phytodienoci acid export for jasmonic acid biosynthesis in *Populus*. *Tree Physiol.* 9:tpab037. doi: 10.1093/treephys/tpab037

Zhou, M., and Memelink, J. (2016). Jasmonate-responsive transcription factors regulating plant secondary metabolism. *Biotechnol. Adv.* 34, 441–449. doi: 10.1016/j.biotechadv.2016.02.004

Conflict of Interest: The authors declare that the research was conducted in the absence of any commercial or financial relationships that could be construed as a potential conflict of interest.

Publisher's Note: All claims expressed in this article are solely those of the authors and do not necessarily represent those of their affiliated organizations, or those of the publisher, the editors and the reviewers. Any product that may be evaluated in this article, or claim that may be made by its manufacturer, is not guaranteed or endorsed by the publisher.

Copyright © 2021 Liu and Park. This is an open-access article distributed under the terms of the Creative Commons Attribution License (CC BY). The use, distribution or reproduction in other forums is permitted, provided the original author(s) and the copyright owner(s) are credited and that the original publication in this journal is cited, in accordance with accepted academic practice. No use, distribution or reproduction is permitted which does not comply with these terms.

frontiers in Plant Science

ORIGINAL RESEARCH
published: 25 August 2021
doi: 10.3389/fpls.2021.670772

Tomato Divinyl Ether-Biosynthesis Pathway Is Implicated in Modulating of Root-Knot Nematode *Meloidogyne javanica*'s Parasitic Ability

*Payal Sanadhya[1], Anil Kumar[1], Patricia Bucki[1], Nathalia Fitoussi[1,2], Mira Carmeli-Weissberg[3], Menachem Borenstein[4] and Sigal Brown-Miyara[1]**

[1] Department of Entomology, Nematology and Chemistry Units, Agricultural Research Organization, The Volcani Center, Bet Dagan, Israel, [2] Department of Plant Pathology and Microbiology, The Faculty of Agriculture, Food and Environment, The Hebrew University of Jerusalem, Rehovot, Israel, [3] Metabolomics, Institute of Plant Sciences, Agricultural Research Organization, The Volcani Center, Bet Dagan, Israel, [4] Department of Plant Pathology and Weed Research, Agricultural Research Organization (ARO), The Volcani Center, Bet Dagan, Israel

OPEN ACCESS

Edited by:
Michael V. Kolomiets,
Texas A&M University, United States

Reviewed by:
Sofia R. Costa,
University of Minho, Portugal
Ana López Sánchez,
National Center of Biotechnology (CSIC), Spain
Carmen Castresana,
National Center of Biotechnology (CSIC), Spain, in collaboration with reviewer AS

***Correspondence:**
Sigal Brown-Miyara
sigalhor@volcani.agri.gov.il

Specialty section:
This article was submitted to Plant Pathogen Interactions, a section of the journal Frontiers in Plant Science

Received: 22 February 2021
Accepted: 21 July 2021
Published: 25 August 2021

Citation:
Sanadhya P, Kumar A, Bucki P, Fitoussi N, Carmeli-Weissberg M, Borenstein M and Brown-Miyara S (2021) Tomato Divinyl Ether-Biosynthesis Pathway Is Implicated in Modulating of Root-Knot Nematode Meloidogyne javanica's Parasitic Ability. Front. Plant Sci. 12:670772. doi: 10.3389/fpls.2021.670772

The role of the 9-lipoxygenase (9-LOX)-derived oxylipins in plant defense is mainly known in solanaceous plants. In this work, we identify the functional role of the tomato divinyl ether synthase (LeDES) branch, which exclusively converts 9-hydroperoxides to the 9-divinyl ethers (DVEs) colneleic acid (CA) and colnelenic acid (CnA), during infection by the root-knot nematode *Meloidogyne javanica*. Analysis of *LeDES* expression in roots indicated a concurrent response to nematode infection, demonstrating a sharp increase in expression during the molting of third/fourth-stage juveniles, 15 days after inoculation. Spatiotemporal expression analysis using an *LeDES promoter:GUS* tomato line showed high GUS activity associated with the developing gall; however the GUS signal became more constricted as infection progressed to the mature nematode feeding sites, and eventually disappeared. Wounding did not activate the LeDES promoter, but auxins and methyl salicylate triggered *LeDES* expression, indicating a hormone-mediated function of DVEs. Heterologous expression of *LeDES* in *Arabidopsis thaliana* rendered the plants more resistant to nematode infection and resulted in a significant reduction in third/fourth-stage juveniles and adult females as compared to a vector control and the wild type. To further evaluate the nematotoxic activity of the DVEs CA and CnA, recombinant yeast that catalyzes the formation of CA and CnA from 9-hydroperoxides was generated. Transgenic yeast accumulating CnA was tested for its impact on *M. javanica* juveniles, indicating a decrease in second-stage juvenile motility. Taken together, our results suggest an important role for *LeDES* as a determinant in the defense response during *M. javanica* parasitism, and indicate two functional modes: directly via DVE motility inhibition effect and through signal molecule-mediated defense reactions to nematodes that depend on methyl salicylate.

Keywords: divinyl ether synthase, *Meloidogyne javanica*, plant defense signaling, oxylipins, hormone signaling, innate immunity

INTRODUCTION

Root knot nematodes (RKNs) are devastating pathogens of a wide variety of plants, causing substantial annual losses in yield worldwide (McCarter, 2009). They also incur the intensive use of toxic nematicides that pose a great threat to human and environmental health (Hague and Gowen, 1987; Johnson and Feldmesser, 1987; Thomason, 1987; Desaeger et al., 2020). The consequent withdrawal of frontline nematicides has put a significant dent in our ability to control RKNs, as well as all other plant-parasitic nematodes. The *Meloidogyne* life cycle consists of six stages: eggs, J1 (first-stage juvenile), J2 (second-stage juvenile), J3 (third-stage juvenile), J4 (fourth-stage juvenile), and adults (female and male). The J2, which are motile and infective, pierce the elongation zone of the plant root near its tip and migrate intercellularly through the root apex to the vascular cylinder (Bird et al., 2009). Once they reach the differentiation zone in the vascular bundle, they become sessile and induce the transformation of 4–8 root cells into coenocytic giant cells that operate as feeding sites, supplying the RKNs with the nutrients required for their development and reproduction (Wyss et al., 1992; Davis et al., 2004; Bird et al., 2009).

Transcriptomic studies of *Arabidopsis thaliana*, *Glycine max* (soybean), and *Solanum lycopersicum* (tomato) plants in response to RKN infection have revealed complicated multistep signaling cascades that are instigated by pathogen attack (Bar-Or et al., 2005; Jammes et al., 2005; Alkharouf et al., 2006; Szakasits et al., 2009). Among them, fatty acid signaling produces oxygenated fatty acids known as oxylipins, which are involved in defense against pathogen attack (Feussner and Wasternack, 2002). Studies have shown that various oxylipin-biosynthesis pathway genes are induced in plants by pathogen attack (Deboever et al., 2020; Estelle et al., 2020), along with a spike in the concentration of related oxylipins as shown in oxylipin-profiling studies (Weber et al., 1999; Göbel et al., 2001; Mariutto et al., 2014; Fitoussi et al., 2021). Several studies on mutant or transgenic plants with altered synthesis or signaling of oxylipins have suggested a direct signaling role for oxylipins in the plant's response to pathogen attack (Deboever et al., 2020), acting as antimicrobial (Croft et al., 1993; Weber et al., 1999; Granér et al., 2003; Prost et al., 2005) or nematicidal agents (Naor et al., 2018). Overexpression of jasmonic acid carboxyl methyltransferase in *Arabidopsis* or 9-lipoxygenase (9-LOX) in tobacco conferred resistance against the necrotrophic pathogen *Botrytis cinerea* (Seo et al., 2001) and the oomycete pathogen *Phytophthora parasitica* (Mène-Saffrané et al., 2003). Ozalvo et al. (2014) also demonstrated the role of 13-LOXs in *Arabidopsis*; they found that LOX3 and LOX4 are involved in the response to nematodes, and that LOX4 is required for resistance to nematode infection. High expression levels of the divinyl ether synthase (*DES*) and *9-LOX* genes was also detected in pepper (*Capsicum annuum*) leaves inoculated with *Obuda pepper virus* (Gullner et al., 2010; Juhász et al., 2015). Moreover, disruption of *LOX1* in pepper plants renders them more susceptible to *Xanthomonas campestris* pv. *vesicatoria* and *Colletotrichum coccodes* infection, further emphasizing the role of LOX-biosynthesis pathway products in pepper plants defense response (Hwang and Hwang, 2010).

Infection of potato leaves by the pathogens *Phytophthora infestans* and *Pseudomonas syringae* leads to elevated transcription of *DES* and accumulation of the 9-divinyl ethers (DVEs) colneleic acid and colnelenic acid (CA and CnA, respectively; Weber et al., 1999; Stumpe et al., 2001). The involvement of CA and CnA in plant defense was also demonstrated by Fammartino et al. (2007), who reported high concentrations of CA and CnA in wild-type (WT) tobacco roots challenged with *P. parasitica* var. *nicotianae*, whereas silencing of *NtLOX1* downregulated the production of CA and CnA. The *DES* genes involved in the synthesis of CA and CnA in potato and tomato have been cloned and characterized (Itoh and Howe, 2001; Stumpe et al., 2001). 9-Divinyl ethers have an important role in defense mechanisms against different plant pathogens and can act as antimicrobial agents (Weber et al., 1999; Göbel et al., 2001; Stumpe et al., 2001; Granér et al., 2003; Fammartino et al., 2007) or signaling components that induce further defense responses. Although much literature is available on the structural diversity of DVEs (Göbel and Feussner, 2009) their occurrence in different plants and their role as antimicrobial agents (Weber et al., 1999; Prost et al., 2005; Fammartino et al., 2007); information on transcriptional regulation of *DES* and its potential role in mediating defense responses is rather scarce, with no knowledge of its function in the tomato–RKN system. Here, we investigated the functional role of *DES* from tomato (*S. lycopersicum*) in response to nematode infection. To further study the spatial and temporal expression of *LeDES*, we generated *pLeDES::GUS* transgenic hairy root lines which show induced expression of *LeDES* in response to early and middle–late stages (15 days) of *Meloidogyne javanica* infection. In addition, the full-length *LeDES* was functionally characterized by heterologous expression in *Arabidopsis* plants. Characterization of transgenic lines indicated a significant reduction in the number of *M. javanica* developmental stages and suggests a role for the DVEs in modulating *M. javanica* disease development in the host root.

MATERIALS AND METHODS

Plant Materials and Growth Conditions

Tomato (*Lycopersicon esculentum*) cv Avigail 870 was used as the background line for the transformation in experiments involved tomato plants. For the transformation protocol, tomato seeds were treated with 1.6% NaOCl for 10 min with continuous shaking, washed with sterile water for 5 min, and placed on standard-strength Gambourg's B5 medium supplemented with 2% sucrose and 0.8% Gelrite agar (Duchefa, Haarlem, The Netherlands). The plates were kept in darkness at 26°C for 2 days, followed by 2 weeks under a 16/8-h photoperiod until cotyledons emerged. They then were used immediately for cocultivation as described by Chinnapandi et al. (2017). Similarly, tomato roots sections were subculture, by placing one root per Petri dish (Miniplast, Ein Shemer, Israel), containing B5 medium. Branching roots were used for inoculation as described below. For experiments conducted on Arabidopsis, *A. thaliana* WT and transgenic lines were grown in a growth chamber at 24°C on MS medium (Murashige and Skoog, 1962) or in pots filled with cocopeat. The plants

were maintained under a 14 h/10 h day/night cycle at a light intensity of 50–60 μmol/m^2s. *Arabidopsis thaliana* ecotype Columbia-0 (Col-0) was used as the genetic background for all transgenic lines.

Nematode Inoculation and Infection of Tomato and Arabidopsis Plants

Meloidogyne javanica was propagated on greenhouse-grown tomato "Avigail" (870) plants. Nematode egg masses were extracted from roots with 0.05% (v/v) sodium hypochlorite followed by sucrose flotation (Hussey and Baker, 1973). For sterilization, eggs were placed on a cellulose–acetate filter membrane (Sartorius Stedim Biotech GmbH, Goettingen, Germany, pore size 5 μm) in a sterile Whatman® filter holder (Whatman International Ltd., Dassel, Germany). Eggs on the filter were exposed for 10 min to 0.01% (w/v) mercuric chloride (Sigma-Aldrich, St Louis, MO, USA), followed by 0.7% (v/v) streptomycin solution (Sigma-Aldrich), and three washing steps with 50 ml sterilized distilled water (Jansen van Vuuren and Woodward, 2001). The sterilized eggs were collected from the membrane and placed on 25-μm-pore sieves in 0.01 M 2-morpholinoethanesulfonic acid buffer (Sigma-Aldrich) under aseptic dark conditions for 3 days, allowing J2s to hatch. Freshly hatched preparasitic J2s were collected in a 50 ml falcon tube. For nematode infection, 1-week-old transgenic tomato root hairy root lines, growing on standard-strength Gamborg's B5 salt medium, were inoculated with 200 sterile freshly hatched *M. javanica* preparasitic J2s. Plates were left uncovered in a laminar flow hood until water had completely soaked into the medium (Sijmons et al., 1991). The inoculated and non-inoculated roots were incubated horizontally in the dark, and root samples were taken for GUS bioassay at the designated time points after wounding or inoculation. To test the response of transgenic Arabidopsis plants to nematode infection, three transgenic lines were used, 10 plants per line in each experiment. Seeds of WT, vector-only and transgenic *Arabidopsis* lines were surface sterilized and germinated on standard-strength GB media with 2% (w/v) sucrose and 0.8% (w/v) Gelrite as described previously by Joshi et al. (2019). One-week-old seedlings grown *in vitro* were gently transferred with a forceps to a petri dish containing GB media, one plant per dish. Each seedling was inoculated with 300 sterile freshly hatched *M. javanica* J2s applied near the roots; the plates were left open until the solution was completely absorbed into the media (Sijmons et al., 1991). The infected seedlings were kept vertically and root samples were gently harvested 28 days post-infection (dpi).

LeDES Transcript Accumulation, RNA Isolation, and Quantitative RT-PCR (qRT-PCR) Analysis

Expression of *LeDES* in infected tomato roots (non-transgenic) at different time points was analyzed by qRT-PCR using gene-specific primers LeDes-rtF: 5′-CCGGATGAGTTTGTACCTGA-3′ and LeDes-rtR: 5′-ATCTTTGCCTGGACATTGCT-3′(López-Ráez et al., 2010). Ten root systems (100 mg) from each time point were pooled from uninfected and infected roots. Total RNA was extracted using Trizol reagent (Invitrogen, Carlsbad, CA, USA) and subjected to Turbo DNase (Ambion, Thermo Fisher Scientific, Waltham, MA, USA). One microgram of total RNA was reverse-transcribed to cDNA using the Verso cDNA Synthesis Kit (Thermo Scientific, Waltham, MA, USA) according to the manufacturer's instructions; qRT-PCR was carried out in a StepOne Real Time PCR system (Applied Biosystems, Foster City, CA, USA) in 10 μl reaction mix comprised of 3.4 μl cDNA, SYBR-Green ROX Mix (Abgene, Portsmouth, NH, USA), 150 nM forward primer and 150 nM reverse primer as described in Chinnapandi et al. (2019). Reactions were performed in MicroAmp 96-well plates (Applied Biosystems) and PCR cycles consisted of initial denaturation at 95°C for 10 min; 40 cycles at 95°C for 15 s, 56°C for 20 s, and 72°C for 20 s, and a final extension at 72°C for 2 min. Reactions were conducted in triplicate, with a control with no template, and the presented results are the means of two independent biological experiments. The qRT-PCR results were analyzed and interpreted using the $2^{-\Delta\Delta Ct}$ method (Livak and Schmittgen, 2001) integrated into StepOne v2.3 of the StepOne Plus (Applied Biosystems) real-time PCR instrument. Tomato β-*tubulin* gene (GenBank accession number NM_001247878.1) was used as the internal reference to normalize the expression of *LeDES*.

Plasmid Construction and Generation of pLeDES::GUS Reporter Hairy-Root Cultures

Genomic DNA was isolated from soil-grown tomato seedlings, cv. Avigail 870, according to the cetyltrimethylammonium bromide (CTAB) method (Murray and Thompson, 1980). A promoter–GUS construct, to study the expression pattern of *LeDES*, was generated by Gateway Technology (Invitrogen). A 1,602-bp sequence upstream of the ATG start codon of *LeDES* was amplified with Platinum Taq DNA polymerase (Invitrogen) using the primers LeDESprom (attB1) 5′-GGGGACAAGTTTGTACAAAAAAGCAGGCT-GTATAGTGTAGCTACGCGCTT-3′ and LeDESprom (attB2) 5′-GGGGACCACTTTGTACAAGAAAGCTGGGT-TTTTCTTA ACAAGTTTTGG-3′ and tomato genomic DNA as the template. The purified product was first cloned into the *pDONR221* vector (Invitrogen) by BP reaction, generating the entry vector. The entry vector was then cloned by LR Clonase II (Thermo Fisher Scientific) into the destination vector pKGWFS7 (VIB-Ugent Center for Plant System Biology, Ghent, Belgium) upstream of *GFP::GUS*-coding sequences, generating the *pKGWFS7:prom-LeDES* (*pLeDES::GUS*) construct. The resulting promoter construct was confirmed by sequencing prior to *Rhizobium rhizogenes* transformation. The *pLeDES::GUS* construct was mobilized to *Rhizobium rhizogenes* ATCC 15834 by freeze–thaw procedure as described by Xu and Li (2008). The transformed *R. rhizogenes* colonies were confirmed by colony PCR using LeDES promoter-specific primers (pLeDESF: 5′-GTATAGTGGAGCTCCGCGCTT-3′ and pLeDESR: 5′-CCCCCGGGTTTTCTTAACAAGTTTTGG-3′) and kanamycin primers (kanF: 5′-GCTCTTCGTCCAGATCATCC-3′ and kanR: 5′-GCGTTCAAAAGTCGCCTAAG-3′).

R. rhizogenes-mediated transformation of tomato cotyledons was carried out according to the protocol described by Chinnapandi et al. (2017). Two weeks after transformation, cotyledons with emerging kanamycin-resistant roots were transferred to Gamborg's B5 salts medium (GB; Duchefa Biochemie, Haarlem, The Netherlands) containing 0.8% (w/v) Gelrite + cefotaxime (200 mg/L) + kanamycin (50 mg/L). Roots were excised from the cotyledons once they were 1.0 cm long. The excised roots were transferred to individual GB medium plates (with 200 mg/L cefotaxime + 50 mg/L kanamycin). After two rounds of subculture, cefotaxime was eliminated from the media and transgenic roots were maintained on GB medium plates (with 50 mg/L kanamycin) for further analysis. The genomic DNA of the hairy roots was isolated and used as a template for identification of the positive transgenic lines with promoter-specific (*pLeDESF* and *pLeDESR*) and kanamycin (*kanF* and *kanR*) primers.

Histochemical Localization of GUS Activity and Microscopic Analysis

For the wounding treatment, transgenic roots were subcultured in GB media for 1 week. Roots were mechanically wounded at several points across their length using sterile forceps. Wounded roots were kept on the GB plates in the dark and collected after 6 and 24 h. GUS activity was assessed histochemically by incubating root samples in GUS staining buffer: 50 mM sodium phosphate (pH 7.0), 10 mM EDTA, 5 mM $K_4[Fe_2(CN)_6]$, 5 mM $K_3[Fe_2(CN)_6]$, 0.2% (v/v) Triton X-100, and 2 mM 5-bromo-4-chloro-3-indolyl ß- D-glucuronide (X-Gluc) overnight at 37°C as described previously (Iberkleid et al., 2015). The stained roots were washed twice with distilled water, and then suspended in water in petri plates or mounted on slides and observed under a Leica DMLB light microscope (Leica Microsystems GmbH, Wetzlar, Germany) and photographed with a Nikon Eclipse 90i (Nikon Corporation, Tokyo, Japan), or observed under a stereomicroscope (Leica MZFLIII, Leica Microsystems GmbH) equipped with a Nikon DS-Fi1 camera.

To study the effect of hormones on the expression of *LeDES*, 1-week-old pLeDES::GUS roots were subcultured on a GB plate supplemented with indoleacetic acid (IAA; 1 and 5 μM), indolebutyric acid (IBA; 1 and 10 μM), methyl jasmonate (Me-JA; 0.01 and 0.1 mM), or methyl salicylate (Me-SA; 1 and 5 mM) for 16 h. One-week-old roots grown on GB medium were used as a control. Treated roots were harvested and analyzed by GUS staining as described above.

Prior to the infection assay with *M. javanica* J2s, the established root cultures were transferred to antibiotic-free GB media for 1 week. Control and *pLeDES::GUS* root cultures were inoculated with 300 J2s per culture previously sterilized as described above. Non-infected transgenic roots served as the control. The inoculated and non-inoculated transgenic roots were placed in the dark, and the roots were gently harvested for analysis of histochemical GUS activity at designated time points post-inoculation.

For tissue localization of GUS signal within galls, stained galls were dissected, fixed in 1% (w/v) glutaraldehyde and 4% (v/v) formaldehyde in 50 mM sodium phosphate buffer pH 7.2, dehydrated, and embedded in Technovit 7100 (Heraeus Kulzer, Wehrheim, Germany) according to the manufacturer's instructions. Semi-thin sections (3 μm) were cut, mounted in DePeX (Sigma-Aldrich) and observed under a Nikon DS Ri2-equipped microscope with dark-field illumination (Leica Microsystems GmbH).

Plasmid Construction and *Agrobacterium tumefaciens*-Mediated Transformation of *Arabidopsis* Plants

For amplification of *LeDES*, PCR was performed with cDNA from 1-month-old tomato plants as the template. The full-length *LeDES* (1,437 bp) coding sequence was amplified using gene-specific primers (*LeDESF* 5′-GTATGGGTACCATGGATACAAA CTTGG-3′ and *LeDESR* 5′-CCTAGAAGCTTTTATATAATTTTTTGCATTTGA-3′), with *Kpn*I and *Hind*III restriction enzyme cutting sites in the forward and reverse primers, respectively. The PCR products were digested with *Kpn*I/*Hind*III and ligated into the *pHANNIBAL* vector. The expression cassette (3,700 bp) containing *LeDES* flanked by the *CaMV35S* promoter and *OCS* terminator was obtained as fallout after digestion with *Not*I restriction enzyme, which was subsequently cloned into the *pART27* binary vector to generate expression plasmid *pART27::LeDES*. The identity, orientation, and vector-insert junctions for *pART27::LeDES* were checked by restriction enzyme digestion and sequencing. The *pART27::LeDES* and *pART27* empty vector were transferred into *Agrobacterium tumefaciens* strain GV3101 by freeze–thaw method as described in Xu and Li (2008). Positive *Agrobacterium* transformants containing *pART27::LeDES* and *pART27* were transformed into *Arabidopsis* Col-0 plants (5-week-old flowering plants) by floral dipping method (Clough and Bent, 1998). The T_1 transformants were screened on agar plates containing half-strength MS medium supplemented with 50 mg/L kanamycin. Segregation ratios of T_2 lines with kanamycin resistance were calculated and lines showing an insertional event were selected. Independent T_3 plants homozygous for kanamycin resistance were used for the infection experiments. The presence of *LeDES* was confirmed by PCR on genomic DNA isolated from the transgenic lines. Expression of *LeDES* for each homozygous line was determined by RT-PCR using cDNA.

DVE Extraction and Analysis by LC–MS

Analysis for the presence of CnA and CA in transgenic *Arabidopsis* roots was performed according to method described by Kuroda with minor modifications (Kuroda et al., 2005). Production of CnA and CA from (9S)-hydroperoxy linoleic acid (9-HPODE; Cayman Chemicals, Ann Arbor, MI, USA) by root lysate of transgenic *Arabidopsis* lines (D1, D2, and D3) and control lines was measured by LC–MS as follows. *Arabidopsis* root samples were harvested 2 weeks after germination and homogenized in Bead Ruptor Elite (OMNI International, Kennesaw, GA, USA) and 500 μl of 50 mM sodium phosphate buffer pH 7. Samples were centrifuged at 15,000 g and the

supernatant was collected and incubated with 5 μg/ml 9-HPODE at 30°C overnight. The reaction was terminated by adding an equal amount of 1 ppm 2-hydroxydecanoic acid (Cayman Chemicals) in ethanol. LC–MS analyses were conducted using a UPLC-Triple Quadrupole mass spectrometer (Waters Xevo TQ MS, Waters Corp., Milford, MA, USA). Separation was performed on a Waters Acquity UPLC BEH C18 1.7 μm, 2.1 × 100 mm column with a VanGuard precolumn (BEH C18 1.7 μm, 2.1 × 5 mm). Chromatographic and MS parameters were as follows: the mobile phase consisted of water (phase A) and acetonitrile (phase B), both containing 0.1% (v/v) formic acid in gradient elution mode. The flow rate was 0.3 ml/min, and the column temperature was kept at 35 °C. LC–MS analysis was performed using the ESI source in positive ion mode for CA and CnA and in negative ion mode for 2-hydroxydecanoic acid with the following settings: capillary voltage 3.1 kV, cone voltage 30 V, desolvation temperature 350°C, desolvation gas flow 650 L/h, source temperature 150°C. Quantification was performed using MRM acquisition by monitoring the 293/275, 293/93 [retention time (RT) = 9.50, dwell time of 100 ms for each transition] for CnA, 295/81, 295/277 (RT = 10.08, dwell time of 100 ms) for CA, 187/141, 187/169 (RT = 6.51, dwell time of 161 ms) for 2-hydroxydecanoic acid. Acquisition of LC–MS data was performed using MassLynx v4.1 software (Waters).

Evaluation of *Arabidopsis* Plant Response to RKN Infection

To study the extent of nematode infection in WT, vector-only, and transgenic *Arabidopsis* lines, infected roots grown in monoxenic culture were collected at 28 dpi and analyzed following the procedure describe by Joshi et al. (2019, 2020) with minor modifications. Roots were gently harvested from the plates, agar was removed, and they were weighed. After cleaning, the roots were stained with acid fuchsin (Sigma-Aldrich) solution (17.5 mg acid fuchsin, 500 ml ethanol, 500 ml acetic acid) overnight. Stained roots were washed three times with distilled water, then mounted in water, and roots and galls were manually dissected under a stereomicroscope (Olympus SZX12, Tokyo, Japan). Different nematode development stages (J3/J4 and adult females) embedded in the roots and galls were manually dissected and counted for each root. Each treatment (Arabidopsis line) included 10 individual plates and the infection assays were repeated three times. Infection assay data were fitted with general linear mixed model in SPSS, by keeping samples as fixed factors and repeated assays as random factor. Further, Tukey *post-hoc* range test was applied to check significant differences ($p < 0.05$) among different samples.

Heterologous Expression of *LeDES* in Yeast

Full-length *LeDES* cDNA was cloned into the yeast expression vector pFL61 under the control of the constitutive yeast phosphoglycerate kinase (PGK) promoter (Minet et al., 1992). To generate yeast expression of the construct, *LeDES* cDNA was amplified from *pART27::LeDES* using *Not*I-containing primers (*DesNotF*: 5′-TTGCGGCCGCATGTCTTCTTATTCAGAG-3′ and *DesNotR*: 5′-AAGCGGCCGCCTATTTACTTGCTTTAGT-3′) and cloned into the pFL61 vector. *Saccharomyces cerevisiae* INVSc1 (MATa his3Δ1 leu2 trp1-289 ura3-52/MATα his3Δ1 leu2 trp1-289 ura3-52), procured from Invitrogen, was used as the host strain for yeast transformation. *S. cerevisiae* was transformed with the empty pFL61 vector (negative control) and with the *pFL61::LeDES* construct using the lithium acetate/polyethylene glycol transformation method (Sanadhya et al., 2015). Positive colonies were selected on synthetic dropout (SD) plates with synthetic defined medium lacking uracil (SD/-Ura; Clontech, Mountain View, CA, USA), and verified by PCR using gene-specific primers. Expression of *LeDES* in transgenic yeast clones was further confirmed by RT-PCR using cDNA.

Evaluating the Immotility Effect of Transgenic Yeast on J2s

The method used in this study to analyze the impact of the transgenic yeast harboring *LeDES* was adapted from Naor et al. (2018) with some minor modifications. *S. cerevisiae* cells transformed with *pFL61* and *pFL61::LeDES* were grown overnight at 28°C from individual colonies in 5 ml of SD/-Ura medium. The precultured yeast cells were pelleted by centrifugation and resuspended in 10 ml of induction medium: SD/-Ura with or without 9-HPODE or 13-HPODE to a final optical density at 600 nm of 2.0. After overnight incubation at 28°C with the respective oxylipin, 300 sterile J2s suspended in 0.01 M MES buffer were added to the cultures and incubated for additional 24 h at 25°C with shaking at 30 rpm. After 24 h incubation, the J2s in the suspensions were collected and subjected to 30-μm filtering (AD Sinun Technologies, Petach Tikvah, Israel) for 2 h (Sanadhya et al., 2018). J2s that actively passed through the filter were counted with nematode-counting slides (Chalex LLC, Portland, OR, USA) under the microscope (Wilovert Standard microscope, Helmut Hund GmbH, Wetzlar, Germany). To measure % motility, J2s counting in treatments included *pFL61* or *pFL61::LeDES* plasmids and the oxylipins 9-HPODE or 13-HPODE were divided by J2s counts following incubation with respective plasmids but without the respective oxylipins. Thus, the pure nematotoxic activity of *LeDES* could be assessed. Ten replicates were used for each treatment and experiments were performed three times independently. A general linear mixed model ANOVA test was applied to the data with similar results. Different letters above the columns indicate significant difference ($P \leq 0.05$) among the different treatments analyzed by Tukey *post-hoc* range test.

Sample Preparation From Transgenic Yeast for DVE Extraction and Analysis by LC–MS

colnelenic acid (CnA) and colneleic acid (CA) were produced from 9-HPODE by yeast lysate of transgenic and control yeast lines according to the method described by Kuroda with minor modifications (Kuroda et al., 2005). Yeast strains carrying empty vector and *LeDES* were precultured in SD/-Ura liquid medium at 28°C. After 16 h, the starter culture was added to a 250-ml flask containing 50 ml SD/-Ura liquid medium and incubated at 28°C for 24 h. The yeast cultures were centrifuged at 2,744 g

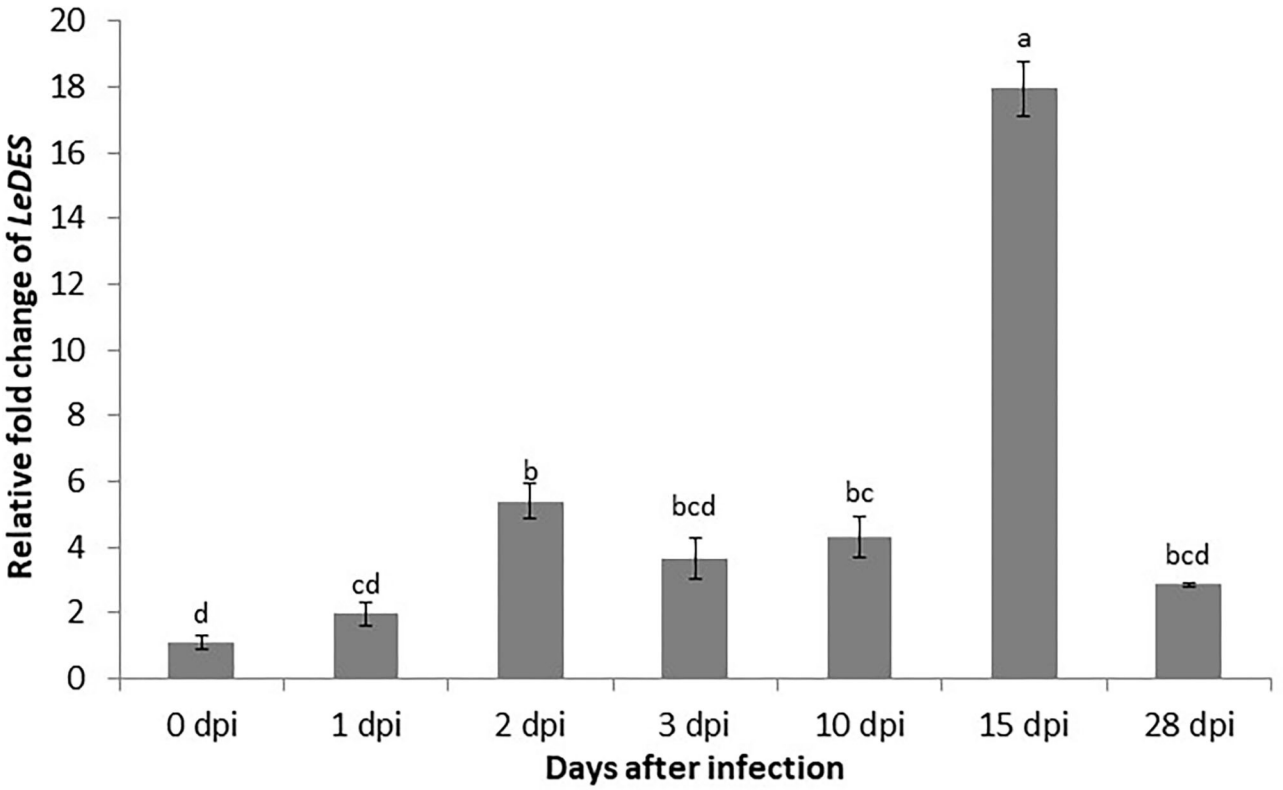

FIGURE 1 | Expression pattern of *LeDES* in tomato roots during the infection time course. To investigate the transcript levels of *LeDES* upon nematode infection, total RNA was isolated from each sample at 1, 2, 3, 10, 15, and 28 dpi or without infection; RNA was subjected to qRT-PCR and normalized to β-*tubulin* as the reference gene. Two biological replicates were taken and three independent qRT-PCRs were performed per sample, resulting in a total of six replicates for statistical analyses. The graph shows the mean and SD of the amount of *LeDES* transcript relative to non-inoculated samples. Error bars correspond to SD $n = 2$ while different letters above the bars denote a significant difference ($P \leq 0.05$, ANOVA) between different treatments as analyzed by Tukey–Kramer multiple comparison test.

for 10 min, and the pellet was weighed and then homogenized in 500 μl 50 mM phosphate buffer pH 7 by Bead Ruptor Elite (OMNI International, Kennesaw, GA, USA) and centrifuged. The lysate was collected and incubated with 5 μg/ml 9-HPODE at 30°C overnight. The reaction was terminated by adding an equal amount of 1 ppm 2-hydroxydecanoic acid in ethanol. LC–MS analyses of the lysates were conducted as described above.

RESULTS

Nematode-Induced *LeDES* Transcript Accumulation

To study the expression of *LeDES* in roots of tomato challenged with *M. javanica* J2s, qRT-PCR was performed with cDNA from root tissues collected 1, 2, 3, 10, 15, and 28 dpi. The nematodes induced activation of *LeDES,* as shown by a moderate course of increase in expression at all-time points upon inoculation (**Figure 1**). The relative fold changes in *LeDES* transcript in infected roots at 1, 2, 3, and 10 dpi were approximately 1.9, 5.3, 3.6, and 4.3, respectively, compared to non-inoculated roots. Transcript abundance of *LeDES* was dramatically induced at 15 dpi (17.9-fold), and was the highest for all-time points considered in this study (**Figure 1**). *LeDES* expression levels declined at 28 dpi, suggesting that *LeDES* has a role in the early defense mechanism induced by nematode penetration and migration, with expression peaking when the young developing galls form.

Spatiotemporal Expression and Distribution of *LeDES* Transcripts

In order to investigate the spatiotemporal activity of LeDES promoter, the 1,602-bp sequence upstream of the ATG start site of *LeDES* was fused to the GUS reporter gene, generating a *pLeDES::GUS* construct. The *pLeDES::GUS* reporter construct was then transformed into tomato via *R. rhizogenes*-mediated root transformation. Transgenic hairy roots that emerged from the cotyledons were confirmed to be carrying the *pLeDES::GUS* construct. *pLeDES*-driven GUS expression was monitored following wounding, exogenous application of defense-related signaling molecules, and in response to nematode infection conducted at specific time points after induction, in transgenic hairy roots by histochemical staining. In the absence of any stimulus, very intense GUS staining was typically observed in the root maturation zone (**Figures 2A,D**), whereas no GUS activity was found in the elongation zone (**Figures 2A,C**); notably, a very faint GUS signal could be observed in the root apex (**Figure 2B**). Strong GUS activity was also associated with the lateral root

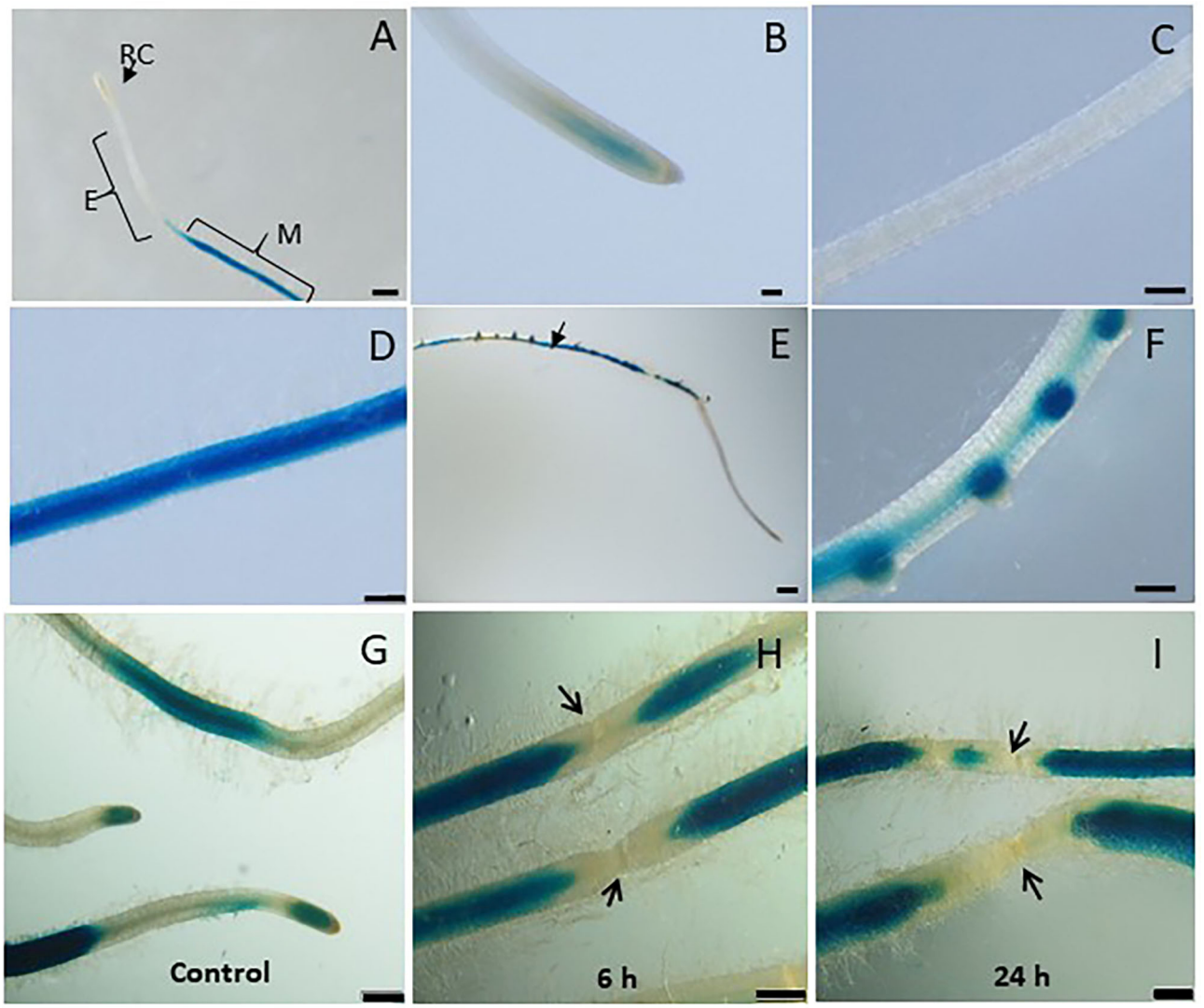

FIGURE 2 | Studying basal and wound induced *LeDES* GUS expression profile. Typical expression pattern of pLeDES::GUS in non-inoculated tomato root lines. **(A)** Basal GUS activity in roots. **(B–D)** Magnified image of root cap **(B)**, elongation zone **(C),** and maturation zone **(D)**. **(E,F)** Promoter–GUS activity observed in lateral root primordials in non-inoculated roots. RC, root cap; E, elongation zone; M, maturation zone. Bars: **(A,E)** 1 mm; **(B–D,F)** 250 μm. Expression analysis of pLeDES::GUS tomato root lines in response to wounding **(G–I).** Histochemical GUS staining of pLeDES::GUS in control roots **(G)** and in roots 6 h **(H)** and 24 h **(I)** after wounding. Bars: **(G–I)** 1 mm. Arrows indicate site of mechanical wounding.

primordium of the non-inoculated roots, suggesting a role for *LeDES* in genetic regulation of root growth and development (**Figures 2E,F**).

Tomato *LeDES* Expression Is Repressed Upon Wounding

Mechanical damage by wounding activates defense signaling pathways and alters hormonal levels in plants, which in turn protects the plant against injury and pathogen attack (Savatin et al., 2014). *LeDES* expression upon wounding was profiled by analyzing GUS expression in *pLeDES*::GUS roots of wounded and non-wounded roots 6 and 24 h after mechanical wounding. Whereas, a typical signal was observed along the root maturation zone (**Figure 2G**), no LeDES promoter activity was observed localized at the wound site at either 6 h (**Figure 2H**) or 24 h (**Figure 2I**) after wounding. It is clearly observed that a complete loss of GUS staining characterize the specific site of mechanical damage as observed (arrows in **Figures 2H,I**) 6 and 24 h after wounding, respectively. These results suggest wound-induced local suppression of *LeDES* at the site of the mechanical damage (**Figure 2**).

LeDES Mediates Me-SA and Auxin Phytohormone-Induced Response

To assess whether LeDES promoter is activated through phytohormone signaling, we used the phytohormone signaling

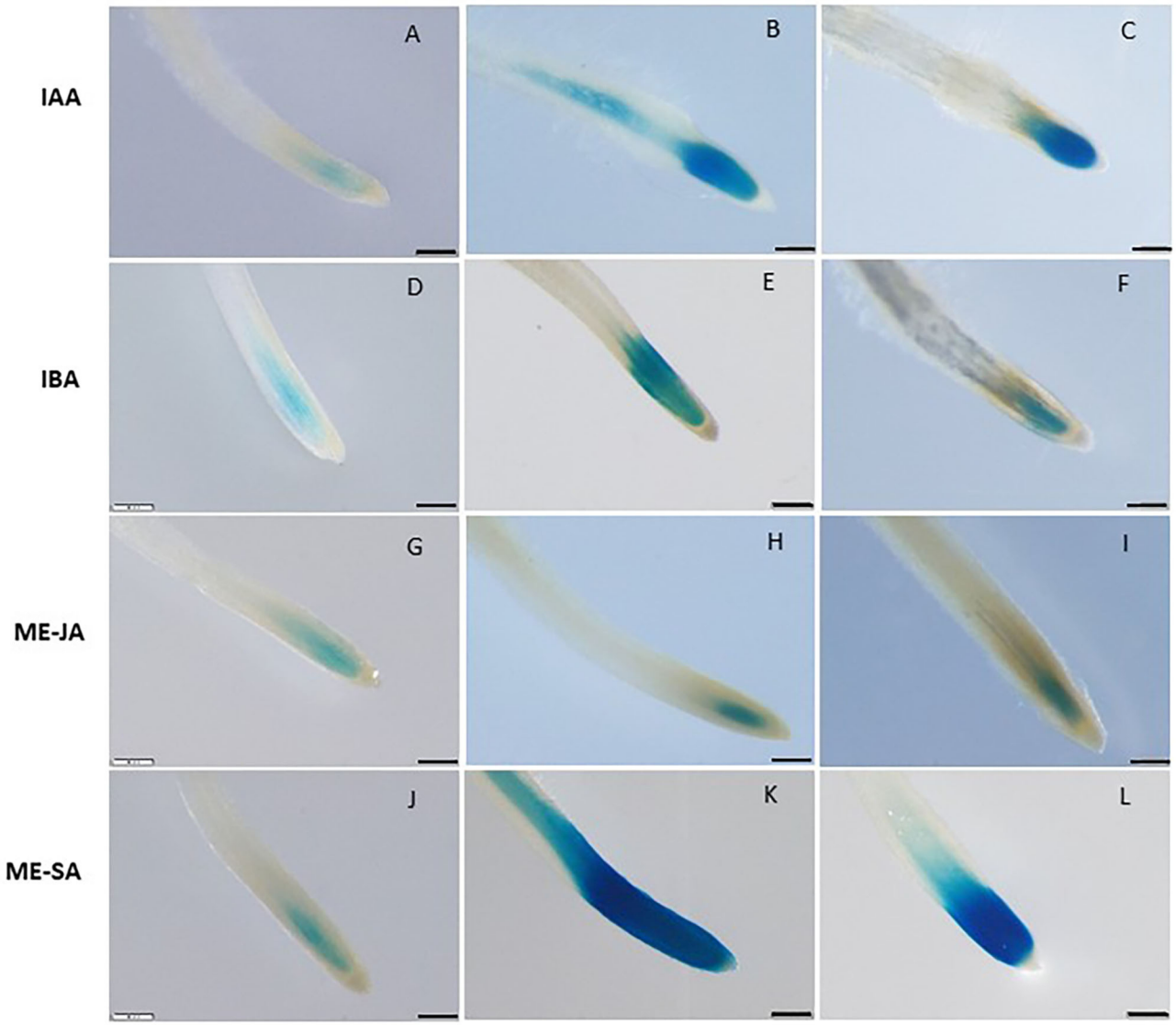

FIGURE 3 | GUS staining in transgenic tomato roots carrying pLeDES::GUS following exogenous phytohormone application. One-week-old roots were subjected to GB as a control **(A,D,G,J)** or to GB containing IAA [1 and 5 μM; **(B,C)**], IBA [1 and 10 μM; **(E,F)**], Me-JA [0.01 and 0.1 mM; **(H,I)**], or Me-SA [1 and 5 mM; **(K,L)**], for 16 h. GUS staining was monitored histochemically in root tips. Figures are representative of at least three independent experiments. Bars: 250 μm.

molecules IAA, IBA, Me-JA, and Me-SA in an LeDES::GUS promoter bioassay (**Figure 3**). GUS staining revealed high GUS expression in the root tips 16 h after treatment with the auxins (IAA and IBA) (**Figures 3B,C,E,F**) compared to the negative control (**Figures 3A,D**), and no activation of *LeDES* promoter by Me-JA (**Figures 3H,I**). Notably, strong induction of the GUS reporter gene was evident after Me-SA treatment, as observed in the root tip and elongation zone (**Figures 3K,L**). Our results suggest that various phytohormones coregulate *LeDES* expression, highlighting its possible role in mediating defense responses triggered by biotic stress.

Spatiotemporal Expression Pattern of *LeDES* Upon *M. javanica* Root Infection

Next, transcriptional activation of the GUS reporter gene driven by the LeDES promoter in the transgenic hairy roots of tomato was analyzed in a time-course analysis at 2, 3, 10, 15 and 28 dpi representing J2 (2 and 3 days), J3 and J4 (10 and 15 days) and female (28 days) stages of nematode development. Very strong staining was evident 2 and 3 dpi in the root elongation zone, the preferred site for nematode penetration, along with swelling and intensive root hair growth resulting from nematode penetration compared with non inoculated roots on the left panel (**Figures 4A–D**). An intense GUS signal was observed

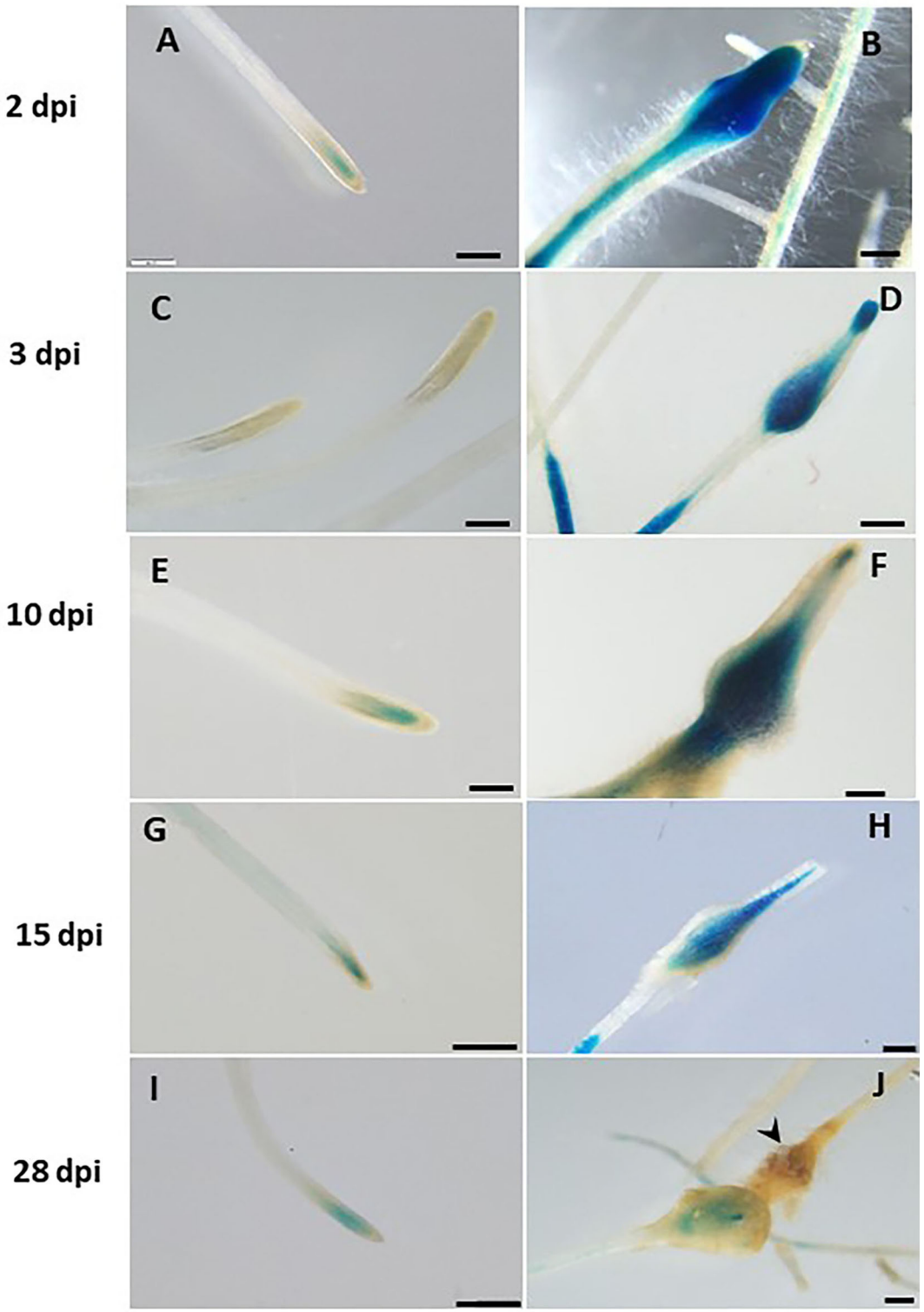

FIGURE 4 | Expression-pattern analysis of pLeDES::GUS root lines during nematode infection. Non-inoculated control root demonstrated consistent GUS staining in the apical meristem (cell-division zone) **(A,C,E,G,I)**. Increased GUS staining was detected in the infected swelling site located in the elongation zone on 2 dpi **(B)**, 3 dpi **(D),** and 10 dpi, premature developing gall **(F)**. Strong GUS staining was observed in the vasculature and vessels associated with the developed gall at 15 dpi **(H)**. At 28 dpi **(J)**, GUS staining intensity decreased and became localized specifically to the cells surrounding the developed nematode. Bars: **(A,C–E)** 250 μm; **(B,F)** 100 μm; **(G–J)** 500 μm.

in the bulging root tissue at the initial nematode penetration site, which is part of the developing gall (**Figure 4B**). High promoter activity continued to be observed in the maturing galls compared with their respective controls (**Figures 4E–H**) at 10 (**Figure 4F**) and 15 (**Figure 4H**) dpi, mainly confined to the deformed vascular bundles (**Figure 4H**). Notably, a significant reduction in promoter activity was evident at 28 dpi compared with the control roots (**Figures 4I,J**), whereas a very mild GUS signal associated with the vascular system connected to the developed female could be observed (**Figure 4J**).

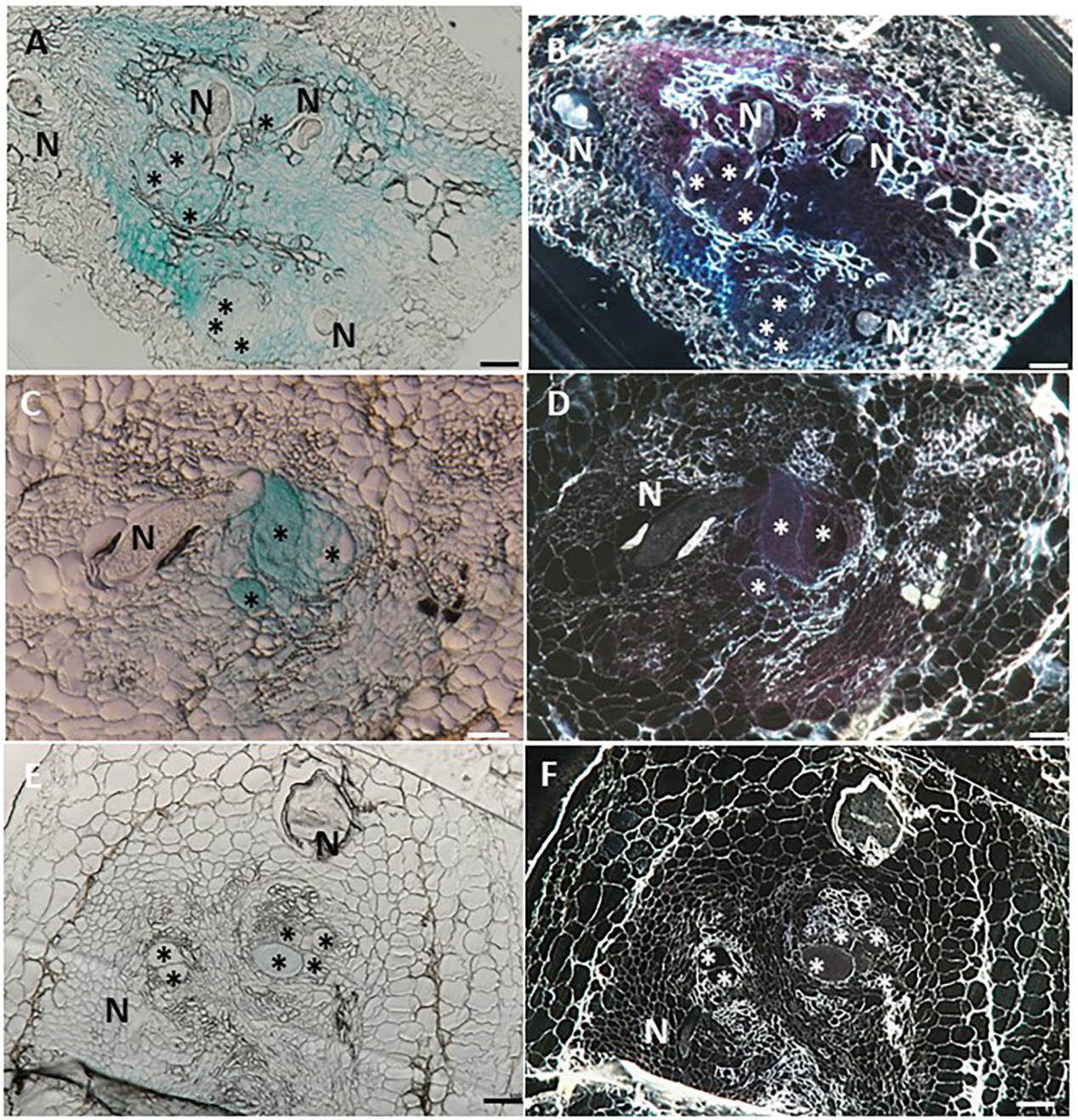

FIGURE 5 | Histological GUS localization within nematode feeding site. For histological GUS localization, galls were fixed and embedded in Technovit 7100 and 3-μm-thick cross sections were analyzed using a light microscope equipped with a Nikon digital camera. All giant cells were mature and nematodes developed to the J4 stage. Histological analysis of roots expressing pLeDES::GUS on 15 dpi clearly shows GUS expression restricted to the vascular systems bordering the feeding sites, the giant cells and cells surrounding the developing female body **(A,B)**. At 28 dpi, GUS signal is observed mostly in the mature feeding site **(C,D)** and **(E,F)**. GUS staining is observed as blue color in whole mounts, and as a red precipitate in the dark field micrographs of the sections. N, female nematode body; *giant cells. Bars: 100 μm.

Giant Cell-Specific Expression of *LeDES* Accompanying Premature Stages of *M. javanica* Infection

To investigate the spatial expression of *LeDES* at nematode feeding sites, thin sections of galls induced by *M. javanica*, 15 and 28 dpi, were prepared and analyzed. At 15 dpi, strong GUS staining showed a scattered signal distributed within the deformed stele harboring the feeding site and bounded by the endodermis cell layer, as observed under light and dark field, respectively (**Figures 5A,B**). At that time point, GUS signal was clearly visible in the giant cells, as well as in the surrounding xylem and phloem parenchyma cells. As infection progressed, GUS signal was significantly quenched, although it was predominantly retained within the developing giant cells (**Figures 5C,D**). However, as the female matured and the feeding site reached its maximum size, at 28 dpi, no GUS signal was observed in the adjacent parenchyma cells with only a very faint GUS signal in the feeding site (**Figures 5E,F**).

LeDES Heterologous Expression in *Arabidopsis* Attenuates Nematode Development

To further explore the role of *LeDES* in regulating plant responses to nematode infection, a plant binary vector containing a 1,437-bp *LeDES* ORF under the control of the CaMV 35S promoter was introduced into *A. thaliana* by floral-dip method for *Agrobacterium*-mediated transformation. From all of the independent kanamycin-resistant transgenic lines harboring the *35S:LeDES* construct, three homozygous lines (D1, D2, and D3) were validated by RT-PCR for *LeDES* heterologous expression, and used for nematode infection (**Figure 6A**). The transgenic plants did not show any phenotypic change in root or shoot growth compared to the WT Col-0 line (**Figure 6B**). To check for the presence of CnA and CA, indicative of active *DES* in the transgenic *Arabidopsis* plants, root lysates of transgenic and control plants were analyzed by LC–MS (**Figure 6C**). The root homogenates of transgenic and control plants were incubated with 9-HPODE and analyzed by LC–MS for the production

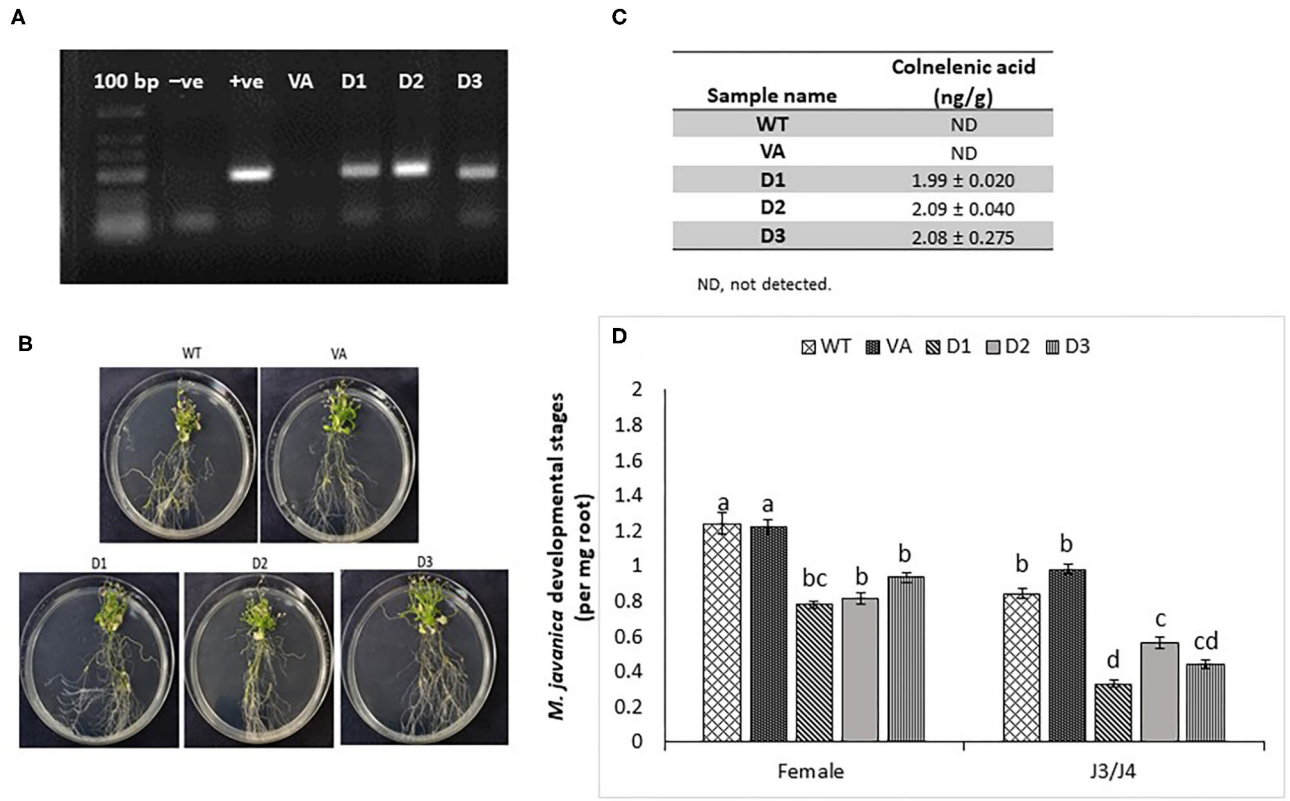

FIGURE 6 | Response of *Arabidopsis* plants overexpressing tomato *LeDES* to nematode infection. **(A)** RT-PCR confirmation of *LeDES* expression with DES-specific primers. Lane 1, negative control; lane 2, cloned *LeDES* template (positive control); Lane 3, independent transgenic line transformed with empty vector; lanes 4–6, independently generated transgenic lines for LeDES **(B)** *Arabidopsis* plants expressing *LeDES* 30 dpi; root systems of all plants show normal root with no phenotypic growth changes. **(C)** Quantification of colnelenic acid produced in transgenic *Arabidopsis* root homogenates as measured by LC-MS. **(D)** Disease development in *Meloidogyne*-infected roots of transgenic *Arabidopsis* plants expressing *LeDES* compared to control lines. All plants were inoculated with 300 sterile pre-parasitic J2s and the infected roots were assessed for J3/J4 and mature female development at 28 dpi through observation under the dissecting microscope following staining with acid fuchsin dye. General Linear Mixed Model test to infection assay data was applied. Different letters above the columns indicate significant difference ($P \leq 0.05$) among different *Arabidopsis* lines analyzed by Tukey *post-hoc* range test.

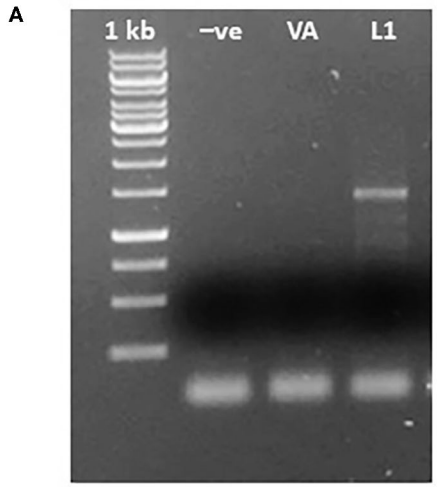

B

Sample name	Colnelenic acid (ng/g)
VA (pFL61)	ND
pFL61:DES	3.37 ± 0.060

ND, not detected.

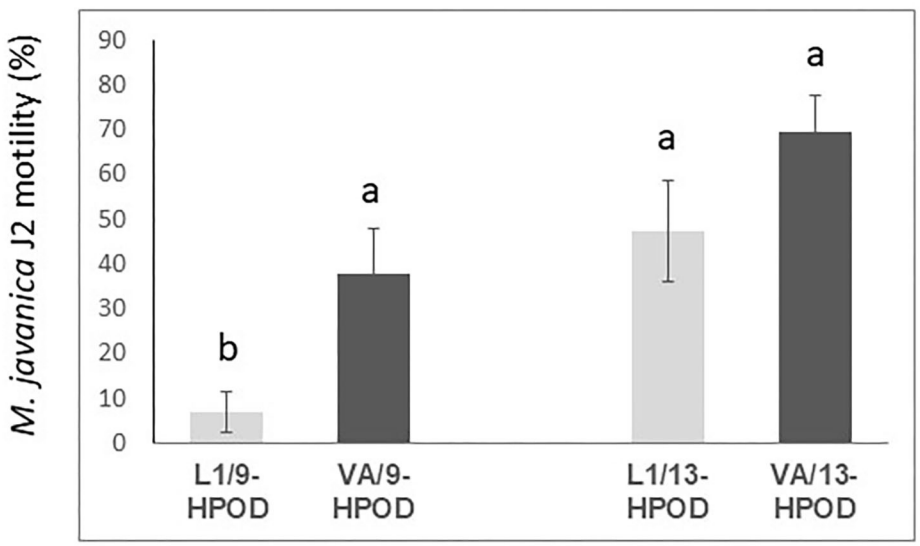

FIGURE 7 | Effect of recombinant yeast expressing *LeDES* on *M. javaniva* J2 viability. **(A)** RT-PCR confirmation of *LeDES* expression in yeast. Lane 1, negative control; lane 2, transgenic yeast cells with empty vector; lane 3, transgenic yeast containing *LeDES* (L1) **(B)** Quantification of colnelenic acid production in transgenic yeast by LC–MS. Values are means of duplicate measurements. **(C)** Yeast carrying *LeDES* display bionematostatic activity. J2s were incubated in SD medium containing yeast strain and 9-HPODE or 13-HPODE for 24 h, then 300 J2s were added to the reaction for 12 h then subjected for sieving followed by microscopic observation. Different letters above the columns indicate significant difference ($P \leq 0.05$) among the different treatments analyzed by Tukey *post-hoc* range test.

of CnA and CA. No CnA was observed in the control plants, but it was detected in the D1, D2, and D3 transgenic lines (**Figure 7C**). No accumulation of CA was identified through LC–MS in either the transgenic or control WT lines. To determine the effect of *LeDES* overexpression on disease development in *Arabidopsis* transgenic lines, 10 plants each from WT, vector-only, and three transgenic lines were inoculated with 300 J2s, and the nematode developmental stages (J3/J4 and females) were monitored at 28 dpi (**Figure 6D**). It is commonly observed that at 28 dai, analyzed infected roots, harbor mainly J3/J4, and mature female stages with or without egg masses. While, at this late time point after infection, J2s which were suppressed or arrested at the earlier time points, will be starved to death by then, and thus barely could be visible, at 28 dai. Disease development, as indicated by number of developmental stages (J3/J4 and females) on D1, D2, and D3 and control lines (WT and vector-only) indicated that *LeDES* overexpression restricts nematode infection, and results in significantly less nematodes molting into J3/J4 stages, as observed in *LeDES* transgenic lines compared to control lines at 28 dpi. Similarly, a decrease in the number of mature females was observed in transgenic lines overexpressing *LeDES* (**Figure 6D**). These results indicate that heterologous expression of *LeDES* in *Arabidopsis* plants results in attenuation of nematode disease development in the roots.

Infection assay data were fitted with general linear mixed model in SPSS, by keeping samples as fixed factors and repeated assays as random factor (**Supplementary Table 1**). Further, Tukey *post-hoc* range test was applied to check significant differences ($p < 0.05$) among different samples.

Functional Expression of *LeDES* in *Saccharomyces cerevisiae*, Product Analysis, and Nematotoxic Acitivity

To characterize the direct activity of DVEs against *M. javanica* J2s, *LeDES* cDNA was cloned into the yeast expression vector pFL61, under the control of the constitutive PGK promoter of *S. cerevisiae* to obtain the *pFL::LeDES* construct. Then, following yeast transformation, pFL::LeDES was expressed in *S. cerevisiae* strain INVSc1. To confirm the presence and expression of *LeDES*, transgenic yeast lines were analyzed by RT-PCR, revealing accumulation of *DES* transcripts exclusively in the positive transformed line L1 (**Figure 7A**). Then, CnA production by the recombinant yeast was determined by incubating transgenic yeast with 9-HPODE as a substrate. LC–MS was used to detect the presence of CnA. Accumulation of 3.37 ± 0.060 ng/g CnA was observed for the L1 recombinant yeast strain, whereas no accumulation was detected in the reaction containing extract from yeast cells with pFL61 vector (**Figure 7B**).

Hence, recombinant yeast clones transformed with the *pFL::LeDES* construct and a negative control, the void pFL61, were used to study the direct nematotoxicfunction of DVEs against *M. javanica* J2s. Following 24 h incubation of recombinant yeast strains expressing either pFL::LeDES or the empty vector pFL61 with 9-HPODE or 13-HPODE *M. javanica* J2s were added to the yeast reaction for an additional 12 h, then J2 viability/**motility** was evaluated through sieving followed by microscopy observation. There was a significant difference in percent **motility** of J2s following incubation with recombinant strain pFL::LeDES and 9-HPODE (7%), compared to that with the negative control yeast carrying the empty vector pFL61 and 9-HPODE (37%) (**Figure 7C**). These differences in J2 **motility** were not present when 13-HPODE was used as the substrate for either of the yeast strains.

DISCUSSION

Oxylipins are crucial compounds in plants, playing important roles in developmental processes and in plant defense mechanisms. The involvement of oxylipins such as jasmonic acid (JA) and its derivatives in defense responses against various fungal and bacterial pathogens has been widely recognized and well-studied (Deboever et al., 2020); however, reports demonstrating the role of oxylipin-mediated signaling involved in plant–parasitic nematode interactions are scarce (Gheysen and Mitchum, 2019). We previously showed that several oxylipins exhibit significant nematicidal activity against *M. javanica*, emphasizing their crucial role in the plant's defense response against nematode parasitism (Naor et al., 2018). In another more recent study, the involvement of 9-LOX and α-dioxygenase oxylipin pathways in tomato's defense against the biotrophic RKN *M. javanica* was observed, which was also evident with the accumulation of oxylipins at earlier stages of nematode parasitism (Fitoussi et al., 2021).

Oxylipin profiling of WT roots of tobacco plants exposed to *P. parasitica* var. *nicotianae* (*Ppn* race 0) also showed preferential upregulation of the 9-LOX pathway and accumulation of the two DVEs CA and CnA (Fammartino et al., 2007). Similarly, *NtLOX1*-antisense plants were more susceptible to *P. parasitica* var. *nicotianae* (Rancé et al., 1998) along with reduced accumulation of LOX downstream pathway products, especially CA and CnA, highlighting the potential role of these oxylipins in defense responses. Other studies, analyzing the oxylipin signature in potato leaves infected with late blight disease (Weber et al., 1999) or in elicited potato cell suspension cultures (Stumpe et al., 2001) revealed the dominant induction of the DES pathway downstream of the 9-lipoxygenation of polyenoic fatty acids.

Here, we chose to study *LeDES* on the basis of our previous report which demonstrated the nematicidal activity of the DVEs CA and CnA (Naor et al., 2018). In the current study, we showed that the DVE-biosynthesis pathway is activated at certain stages of *M. javanica* infection in tomato roots, as reflected by elevated *LeDES* expression. However, differences in temporal expression were detected, where the highest expression was observed at 15 dpi. Differences in transcript accumulation in response to RKN in the tomato host suggest differential control of RKN-induced DVE biosynthesis. Colneleic acid has been shown to attenuate 9-LOX (Corey et al., 1987; Itoh and Howe, 2001; Fammartino et al., 2007), thus it can be speculated that transcription of DVE fatty acids or other oxylipin (derived from 9-LOX) biosynthesis genes may be repressed by feedback from downstream metabolites. However, the synthesis of CA and CnA is highly specific and strongly induced in certain instances, such as infection (Itoh and Howe, 2001). We therefore isolated the promoter region (1,602 bp upstream from the start codon) to obtain insight into transcriptional reprogramming of *LeDES* expression in response to RKN parasitism.

The modulation of *LeDES* expression by nematode parasitism and signal molecules related to plant defense was monitored in transgenic tomato hairy-root lines expressing the GUS reporter gene driven by the *LeDES* promoter region. Notably, in non-inoculated control roots, GUS expression was not visible in the elongation zone, but was clearly detected in the apical meristem and maturation zone. Distinct GUS staining was also observed in lateral root primordia of developing roots, emphasizing the importance of *LeDES* in regulating root development. Lateral root emergence and meristem activation are crucial developmental mechanisms in roots which can modulate root architecture in response to stress, environmental, nutritional, and endogenous factors (Signora et al., 2001; de Smet et al., 2006). Vellosillo et al. (2007) also showed that external application of CA, can, or related oxylipins to *Arabidopsis* seedlings leads to loss of apical dominance and induces the development of lateral and adventitious roots. Thus, different oxylipins produced in response to pathogen infection are probably endogenous regulators of lateral root emergence and consequently, might be involved in reprogramming root system architecture upon pathogen infection.

Nematode penetration inflicts mechanical damage to the roots, which lead to the release of Damage-Associated Molecular Patterns (DAMPs) (Choi and Klessig, 2016; Holbein et al., 2016), which in turn initiate and perpetuate the innate immune responses mediated by JA, salicylic acid (SA), ethylene, auxin, and reactive oxygen species (ROS) (Holbein et al., 2019). Many reports have shown that the defense responses activated by pathogens closely mimic those to wounding (Savatin et al., 2014). Therefore, to assess the role of *LeDES* during the early infection stage, we analyzed the effect of wounding on transgenic roots after 6 and 24 h. Expression of the GUS gene was downregulated at the wounding site, indicating that this gene is not activated as part of the DAMP-triggered immunity through cell-wall damage and may be induced by other elicitors.

Phytohormones, namely SA, ethylene, JA, abscisic acid, auxin, brassinosteroid, gibberellic acid, and cytokinin, elicit defense responses by regulating the expression of defense-related genes (Santner et al., 2009; Jaillais and Chory, 2010; Pieterse et al., 2012). Among them, JA and SA are key components in mounting defense responses in plants in response to different biotic and abiotic stresses (Denancé et al., 2013). Treatment of transgenic roots with Me-JA showed no relevant effect on GUS signal. However, application of Me-SA very strongly induced the signal in the apical meristem and elongation zone. This result fits well with the notion that SA and JA act antagonistically on each other's pathways and biosynthesis upon sensing a pathogen (Lorenzo and Solano, 2005; Pieterse et al., 2012). Plants activate mainly the SA-signaling pathway to combat biotrophic pathogens, whereas JA is involved in defense against necrotrophs (Glazebrook, 2005). Similarly, *DES* transcript in garlic leaves was induced by SA but not Me-JA application (Stumpe et al., 2008), whereas *NtDES* was not induced by SA (Fammartino et al., 2007). Considering the biotrophic nature of RKNs, we can postulate a role for SA in modulating the expression of *LeDES*. This suggests that during the process of nematode infection, the *LeDES* branch of the 9-LOX pathway participates more in the systemic defense response than in the local one through production of CA and CnA. Whether, LeDES activation is indirectly mediated through potential Nematode Associated Molecular Pattern (NAMPs) molecules, which induce SA defense-signaling pathway, that is remained to be studied.

Furthermore, treatment with IBA and IAA also induced promoter activity in the root's apical meristem, thus indicating the potential role of auxins in manipulating *LeDES* expression under basal and stress conditions. Auxins are proposed to be involved in the formation of giant cells and galls, evidenced by its increased accumulation during the early stages of feeding-site development (Karczmarek et al., 2004; Cabrera et al., 2014; Kyndt et al., 2016).

The infection tests performed with the transgenic hairy roots further confirmed the specific role of *LeDES* during the progression of nematode infection. Interestingly, during early infection stages, high GUS activity was observed in developing galls. Strong promoter activity was also evident in the middle–late infection stage (15 dpi), which then decreased (28 dpi). Hence, the *pLeDES*::GUS activation pattern was consistent with our real-time PCR results, characterized by gradual increment and then a relative reduction in expression. In sections from the 15-day galls, LeDES promoter activity was diffuse, and found throughout the vascular bundle, extending from the pericycle to the pith and including the giant cells. GUS signal became constricted to the feeding sites as the nematodes molt into the female stage, and diminished when feeding system was completely mature. This specific induction of LeDES promoter in the galls and giant cells in response to RKN infection indicates a putative role in the defense response triggered by nematode attack. Alternatively, it may be that auxin or Me-SA, which were shown to activate *LeDES*, are responsible for the observed induction.

We further cloned and expressed *LeDES* in the model plant *A. thaliana* to investigate its role in regulating plant-parasitic nematode development. Heterologous expression of the gene in *A. thaliana* conferred increased resistance against the RKN, evidenced by the attenuation in J3/J4 and female stages measured in the infected roots. Similarly, Fammartino et al. (2007) demonstrated that *NtLOX1*-antisense plants, which are compromised in their resistance to Ppn race 0, display reduced accumulation of DVEs upon inoculation. However, studies showing contradictory results have also been published. Eschen-Lippold et al. (2007) showed that infection symptoms caused by *P. infestans* were unchanged in potato lines producing a reduced amount of CnA after RNAi inhibition of pathogen-inducible DES. Furthermore, Fauconnier et al. (2008) later also showed that changes in oxylipin synthesis upon *P. infestans* infection do not correlate with resistance in potato. These differences among the differential induction of DVEs in different pathosystems might be tissue-specific, in addition to its plant- or pathogen-specific features. Thus, the induced resistance observed in the *Arabidopsis*–nematode pathosystem might be the result of differential substrate availability for DES in transgenic *Arabidopsis* plants. Nevertheless, differences between Arabidopsis and tomato pathosystems might lead to misinterpretation regards LeDES function toward RKN in tomato host, thus in future, its function should be studied by further LeDES manipulation in tomato host.

In this study, recombinant expression of *LeDES* in *S. cerevisiae* resulted in the production of measurable amounts of CnA but not CA. Exposure of *M. javanica* J2s to yeast expressing *LeDES* when 9-HPODE is the substrate, resulted in reduced J2 motility. These results, along with previous ones showing that DVE is able to attenuate motility, therefore support our findings that these are good candidate defense compounds at early time points of the infection process, further emphasizing their potential as nematostatic compounds.

CONCLUDING REMARKS

The antimicrobial activity of different DVEs has been well-illustrated; however, there have been no reports of the involvement of DVEs in the defense response to biotic stress conditions, such as nematode infection. Our study reveals the functional role of *LeDES* by showing that this tomato gene can be overexpressed in economically important crops to improve resistance to RKNs. Furthermore, the potential of DVEs as nematostatic and signaling molecules was confirmed. However, their role in RKN resistance seems to be more complex, as they have been shown to have a nematostatic effect *in vitro*, but to play

several roles *in vivo*, including as a signaling molecule mediating the plant's defense response and in root development. Their importance in regulating root architecture along with a typical nematode-responsive pattern raises new questions regarding their function while the nematode is becoming established in the roots. Further analyses, particularly of pathways that are explicitly targeted by DVEs during infection, may provide a more in-depth understanding of their specific interactions with other components of the plant's defense arsenal. These pathways' regulation should be addressed to further discriminate the relative contribution of different classes of compounds to resistance *in planta*.

DATA AVAILABILITY STATEMENT

The raw data supporting the conclusions of this article will be made available by the authors, without undue reservation.

AUTHOR CONTRIBUTIONS

PS and SM conceived and designed the experiment. PS conducted all plants and yeasts transformation experiments, infection studies, gene expression studies, and wrote the manuscript. AK performed GUS staining experiments, galls thin sectioning, and microscopy work. NF constructed the LeDES promter:GUS plasmid. MC-W and PS performed the oxylipins analysis. PB performed the Nematicidal activity bioassay. MB is a key person in this manuscript as all the plants required for the experiments were as a result of his constant greenhouse care. All authors made substantial contributions to the final text and read and approved the final manuscript.

FUNDING

Funds received from the chief scientist, Ministry of Agriculture and Rural Development, were channeled toward understanding the function role of LeDES in regulating tomato response to RKN. Funds received from the Israeli Science Foundation were in part channeled toward studying the function role of LeDES in recombinant yeasts.

SUPPLEMENTARY MATERIAL

The Supplementary Material for this article can be found online at: https://www.frontiersin.org/articles/10.3389/fpls.2021.670772/full#supplementary-material

REFERENCES

Alkharouf, N. W., Klink, V. P., Chouikha, I. B., Beard, H. S., MacDonald, M. H., Meyer, S., et al. (2006). Timecourse microarray analyses reveal global changes in gene expression of susceptible *Glycine max* (soybean) roots during infection by *Heterodera glycines* (soybean cyst nematode). *Planta* 224, 838–852. doi: 10.1007/s00425-006-0270-8

Bar-Or, C., Kapulnik, Y., and Koltai, H. (2005). A broad characterization of the transcriptional profile of the compatible tomato response to the plant parasitic root knot nematode *Meloidogyne javanica*. *Eur. J. Plant Pathol.* 111, 181–192. doi: 10.1007/s10658-004-2134-z

Bird, D., Mc, K., Williamson, V. M., Abad, P., McCarter, J., Danchin, E. G. J., et al. (2009). The genomes of root-knot nematodes. *Annu. Rev. Phytopathol.* 47, 333–351. doi: 10.1146/annurev-phyto-080508-081839

Cabrera, J., Díaz-Manzano, F. E., Sanchez, M., Rosso, M. N., Melillo, T., Goh, T., et al. (2014). A role for LATERAL ORGAN BOUNDARIES-DOMAIN 16 during the interaction *Arabidopsis-Meloidogyne* spp. provides a molecular link between lateral root and root-knot nematode feeding site development. *New Phytol.* 203, 632–645. doi: 10.1111/nph.12826

Chinnapandi, B., Bucki, P., and Braun Miyara, S. (2017). SlWRKY45, nematode-responsive tomato WRKY gene, enhances susceptibility to the root knot nematode; *M. javanica* infection. *Plant Signal. Behav.* 12:e1356530. doi: 10.1080/15592324.2017.1356530

Chinnapandi, B., Bucki, P., Fitoussi, N., Kolomiets, M., Borrego, E., and Braun Miyara, S. (2019). Tomato SlWRKY3 acts as a positive regulator for resistance against the root-knot nematode *Meloidogyne javanica* by activating lipids and hormone-mediated defense-signaling pathways. *Plant Signal. Behav.* 14, 1–16. doi: 10.1080/15592324.2019.1601951

Choi, H. W., and Klessig, D. F. (2016). DAMPs, MAMPs, and NAMPs in plant innate immunity. *BMC Plant Biol.* 16:232. doi: 10.1186/s12870-016-0921-2

Clough, S. J., and Bent, A. F. (1998). Floral dip: a simplified method for *Agrobacterium*-mediated transformation of *Arabidopsis thaliana*. *Plant J.* 16, 735–743. doi: 10.1046/j.1365-313X.1998.00343.x

Corey, E. J., Nagata, R., and Wright, S. W. (1987). Biomimetic total synthesis of colneleic acid and its function as a lipoxygenase inhibitor. *Tetrahedron Lett.* 28, 4917–4920. doi: 10.1016/S0040-4039(00)96658-9

Croft, K. P. C., Jüttner, F., and Slusarenko, A. J. (1993). Volatile products of the lipoxygenase pathway evolved from *Phaseolus vulgaris* (L.) leaves inoculated with *Pseudomonas syringae* pv *phaseolicola*. *Plant Physiol.* 101, 13–24. doi: 10.1104/pp.101.1.13

Davis, E. L., Hussey, R. S., and Baum, T. J. (2004). Getting to the roots of parasitism by nematodes. *Trends Parasitol.* 20, 134–141. doi: 10.1016/j.pt.2004.01.005

de Smet, I., Zhang, H., Inzé, D., and Beeckman, T. (2006). A novel role for abscisic acid emerges from underground. *Trends Plant Sci.* 11, 434–439. doi: 10.1016/j.tplants.2006.07.003

Deboever, E., Deleu, M., Mongrand, S., Lins, L., and Fauconnier, M. L. (2020). Plant–pathogen interactions: underestimated roles of phyto-oxylipins. *Trends Plant Sci.* 25, 22–34. doi: 10.1016/j.tplants.2019.09.009

Denancé, N., Sánchez-Vallet, A., Goffner, D., and Molina, A. (2013). Disease resistance or growth: the role of plant hormones in balancing immune responses and fitness costs. *Front. Plant Sci.* 4:155. doi: 10.3389/fpls.2013.00155

Desaeger, J., Wram, C., and Zasada, I. (2020). New reduced-risk agricultural nematicides - rationale and review. *J. Nematol.* 52:e2020-91. doi: 10.21307/jofnem-2020-091

Eschen-Lippold, L., Rothe, G., Stumpe, M., Göbel, C., Feussner, I., and Rosahl, S. (2007). Reduction of divinyl ether-containing polyunsaturated fatty acids in transgenic potato plants. *Phytochemistry* 68, 797–801. doi: 10.1016/j.phytochem.2006.12.010

Estelle, D., Laurence, L., Marc, O., Caroline, D. C., Magali, D., and Marie-Laure, F. (2020). Linolenic fatty acid hydroperoxide acts as biocide on plant pathogenic bacteria: biophysical investigation of the mode of action. *Bioorg. Chem.* 100:103877. doi: 10.1016/j.bioorg.2020.103877

Fammartino, A., Cardinale, F., Göbel, C., Mène-Saffrané, L., Fournier, J., Feussner, I., et al. (2007). Characterization of a divinyl ether biosynthetic pathway specifically associated with pathogenesis in tobacco. *Plant Physiol.* 143, 378–388. doi: 10.1104/pp.106.087304

Fauconnier, M. L., Rojas-Beltran, J., Dupuis, B., Delaplace, P., Frettinger, P., Gosset, V., et al. (2008). Changes in oxylipin synthesis after *Phytophthora infestans* infection of potato leaves do not correlate with resistance. *Plant Physiol. Biochem.* 46, 823–831. doi: 10.1016/j.plaphy.2008.04.010

Feussner, I., and Wasternack, C. (2002). THE LIPOXYGENASE PATHWAY. *Annu. Rev. Plant Biol.* 53, 275–297. doi: 10.1146/annurev.arplant.53.100301.135248

Fitoussi, N., Borrego, E., Kolomiets, M. v., Qing, X., Bucki, P., et al. (2021). Oxylipins are implicated as communication signals in tomato–root-knot

nematode (*Meloidogyne javanica*) interaction. *Sci. Rep.* 11:326. doi: 10.1038/s41598-020-79432-6

Gheysen, G., and Mitchum, M. G. (2019). Phytoparasitic nematode control of plant hormone pathways. *Plant Physiol.* 179, 1212–1226. doi: 10.1104/pp.18.01067

Glazebrook, J. (2005). Contrasting mechanisms of defense against biotrophic and necrotrophic pathogens. *Annu. Rev. Phytopathol.* 43, 205–227. doi: 10.1146/annurev.phyto.43.040204.135923

Göbel, C., and Feussner, I. (2009). Methods for the analysis of oxylipins in plants. *Phytochemistry* 70, 1485–1503. doi: 10.1016/j.phytochem.2009.07.040

Göbel, C., Feussner, I., Schmidt, A., Scheel, D., Sanchez-Serrano, J., Hamberg, M., et al. (2001). Oxylipin profiling reveals the preferential stimulation of the 9-lipoxygenase pathway in elicitor-treated potato cells. *J. Biol. Chem.* 276, 6267–6273. doi: 10.1074/jbc.M008606200

Granér, G., Hamberg, M., and Meijer, J. (2003). Screening of oxylipins for control of oilseed rape (Brassica napus) fungal pathogens. *Phytochemistry* 63, 89–95. doi: 10.1016/S0031-9422(02)00724-0

Gullner, G., Künstler, A., Király, L., Pogány, M., and Tóbiás, I. (2010). Up-regulated expression of lipoxygenase and divinyl ether synthase genes in pepper leaves inoculated with *Tobamoviruses*. *Physiol. Mol. Plant Pathol.* 74, 387–393. doi: 10.1016/j.pmpp.2010.06.006

Hague, N. G. M., and Gowen, S. R. (1987). "Chemical control of nematodes," in *Principles and Practice of Nematode Control in Crops*, eds R. H. Brown and B. R. Kerry (Sydney, NSW: Academic Press), 131–178.

Holbein, J., Franke, R. B., Marhavý, P., Fujita, S., Górecka, M., Sobczak, M., et al. (2019). Root endodermal barrier system contributes to defence against plant-parasitic cyst and root-knot nematodes. *Plant J.* 100, 221–236. doi: 10.1111/tpj.14459

Holbein, J., Grundler, F. M. W., and Siddique, S. (2016). Plant basal resistance to nematodes: an update. *J. Exp. Bot.* 67, 2049–2061, doi: 10.1093/jxb/erw005

Hussey, R. S., and Baker, K. R. (1973). Comparison of methods of collecting inocula for *Meloidogyne* spp., including a new technique. *Plant Dis. Rep.* 57, 1025–1028.

Hwang, I. S., and Hwang, B. K. (2010). The pepper 9-lipoxygenase gene *CaLOX1* functions in defense and cell death responses to microbial pathogens. *Plant Physiol.* 152, 948–967. doi: 10.1104/pp.109.147827

Iberkleid, I., Sela, N., and Brown Miyara, S. (2015). *Meloidogyne javanica* fatty acid- and retinol-binding protein (Mj-FAR-1) regulates expression of lipid-, cell wall-, stress- and phenylpropanoid-related genes during nematode infection of tomato. *BMC Genomics* 16:272. doi: 10.1186/s12864-015-1426-3

Itoh, A., and Howe, G. A. (2001). Molecular cloning of a divinyl ether synthase. Identification as a CYP74 cytochrome P-450. *J. Biol. Chem.* 276, 3620–3627. doi: 10.1074/jbc.M008964200

Jaillais, Y., and Chory, J. (2010). Unraveling the paradoxes of plant hormone signaling integration. *Nat. Struct. Mol. Biol.* 17, 642–645. doi: 10.1038/nsmb0610-642

Jammes, F., Lecomte, P., de Almeida-Engler, J., Bitton, F., Martin-Magniette, M. L., Renou, J. P., et al. (2005). Genome-wide expression profiling of the host response to root-knot nematode infection in *Arabidopsis*. *Plant J.* 44, 447–458. doi: 10.1111/j.1365-313X.2005.02532.x

Jansen van Vuuren, R., and Woodward, B. (2001). The response of cassava cultivars to root-knot nematode infestation: an *in vitro* method. *Euphytica*. 120, 109–113. doi: 10.1023/A:1017524210671

Johnson, A. W., and Feldmesser, J. (1987). "Nematicides-a historical review," in Vistas on Nematology, eds J. A. Veech and D. W. Dickson (Hyattsville, MD: Society of Nematologists), 448–454.

Joshi, I., Kumar, A., Kohli, D., Singh, A. K., Sirohi, A., Subramaniam, K., et al. (2020). Conferring root-knot nematode resistance via host-delivered RNAi-mediated silencing of four Mi-msp genes in Arabidopsis. *Plant Sci.* 298:110592. doi: 10.1016/j.plantsci.2020.110592

Joshi, I., Kumar, A., Singh, A. K., Kohli, D., Raman, K. V., Sirohi, A., et al. (2019). Development of nematode resistance in Arabidopsis by HD-RNAi-mediated silencing of the effector gene Mi-msp2. *Sci. Rep.* 9:17404. doi: 10.1038/s41598-019-53485-8

Juhász, C., Tóbiás, I., Ádám, A. L., Kátay, G., and Gullner, G. (2015). Pepper 9- and 13-lipoxygenase genes are differentially activated by two *tobamoviruses* and by hormone treatments. *Physiol. Mol. Plant Pathol.* 92, 59–69. doi: 10.1016/j.pmpp.2015.08.004

Karczmarek, A., Overmars, H., Helder, J., and Goverse, A. (2004). Feeding cell development by cyst and root-knot nematodes involves a similar early, local and transient activation of a specific auxin-inducible promoter element. *Mol. Plant Pathol.* 5, 343–346. doi: 10.1111/j.1364-3703.2004.00230.x

Kuroda, H., Oshima, T., Kaneda, H., and Takashio, M. (2005). Identification and functional analyses of two cDNAs that encode fatty acid 9-/13-hydroperoxide lyase (CYP74C) in rice. *Biosci. Biotechnol. Biochem.* 69, 1545–1554. doi: 10.1271/bbb.69.1545

Kyndt, T., Goverse, A., Haegeman, A., Warmerdam, S., Wanjau, C., Jahani, M., et al. (2016). Redirection of auxin flow in *Arabidopsis thaliana* roots after infection by root-knot nematodes. *J. Exp. Bot.* 67, 4559–4570. doi: 10.1093/jxb/erw230

Livak, K. J., and Schmittgen, T. D. (2001). Analysis of relative gene expression data using real-time quantitative PCR and the 2-ΔΔCT method. *Methods* 25, 402–408. doi: 10.1006/meth.2001.1262

López-Ráez, J. A., Verhage, A., Fernández, I., García, J. M., Azcón-Aguilar, C., Flors, V., et al. (2010). Hormonal and transcriptional profiles highlight common and differential host responses to arbuscular mycorrhizal fungi and the regulation of the oxylipin pathway. *J. Exp. Bot.* 61, 2589–2601. doi: 10.1093/jxb/erq089

Lorenzo, O., and Solano, R. (2005). Molecular players regulating the jasmonate signalling network. *Curr. Opin. Plant Biol.* 8, 532–540. doi: 10.1016/j.pbi.2005.07.003

Mariutto, M., Fauconnier, M.-L., Ongena, M., Laloux, M., Wathelet, J.-P., Du Jardin, P., et al. (2014). Reprogramming of fatty acid and oxylipin synthesis in rhizobacteria-induced systemic resistance in tomato. *Plant Mol. Biol.* 84, 455–467. doi: 10.1007/s11103-013-0144-y

McCarter, J. P. (2009). Molecular *Approaches Toward Resistance* to *Plant Parasitic Nematodes. Cell Biology of Plant Nematode Parasitism.* Berlin: Springer-Verlag.

Mène-Saffrané, L., Esquerré-Tugayé, M. T., and Fournier, J. (2003). Constitutive expression of an inducible lipoxygenase in transgenic tobacco decreases susceptibility to *Phytophthora parasitica* var. *nicotianae*. *Mol. Breed.* 12, 271–282. doi: 10.1023/B:MOLB.0000006754.19398.d4

Minet, M., Dufour, M., and Lacroute, F. (1992). Complementation of *Saccharomyces cerevisiae* auxotrophic mutants by *Arabidopsis thaliana* cDNAs. *Plant J.* 2, 417–422. doi: 10.1046/j.1365-313X.1992.t01-38-00999.x

Murashige, T., and Skoog, F. (1962). A revised medium for rapid growth and bio assays with tobacco tissue cultures. *Physiol. Plant.* 15, 473–497. doi: 10.1111/j.1399-3054.1962.tb08052.x

Murray, M. G., and Thompson, W. F. (1980). Rapid isolation of high molecular weight plant DNA. *Nucleic Acids Res.* 8, 4321–4326. doi: 10.1093/nar/8.19.4321

Naor, N., Gurung, F. B., Ozalvo, R., Bucki, P., Sanadhya, P., and Miyara, S. B. (2018). Tight regulation of *allene oxide synthase (AOS)* and *allene oxide cyclase-3* (*AOC3*) promote *Arabidopsis* susceptibility to the root-knot nematode *Meloidogyne javanica*. *Eur. J. Plant Pathol.* 150, 149–165. doi: 10.1007/s10658-017-1261-2

Ozalvo, R., Cabrera, J., Escobar, C., Christensen, S. A., Borrego, E. J., Kolomiets, M., et al. (2014). Two closely related members of *Arabidopsis 13-lipoxygenases (13-LOXs), LOX3* and *LOX4*, reveal distinct functions in response to plant-parasitic nematode infection. *Mol. Plant Pathol.* 15, 319–332. doi: 10.1111/mpp.12094

Pieterse, C. M. J., van der Does, D., Zamioudis, C., Leon-Reyes, A., and van Wees, S. C. M. (2012). Hormonal modulation of plant immunity. *Annu. Rev. Cell Dev. Biol.* 28, 489–521. doi: 10.1146/annurev-cellbio-092910-154055

Prost, I., Dhondt, S., Rothe, G., Vicente, J., Rodriguez, M. J., Kift, N., et al. (2005). Evaluation of the antimicrobial activities of plant oxylipins supports their involvement in defense against pathogens. *Plant Physiol.* 139, 1902–1913. doi: 10.1104/pp.105.066274

Rancé, I., Fournier, J., and Esquerré-Tugayé, M. T. (1998). The incompatible interaction between *Phytophthora* parasitica var. nicotianae race 0 and tobacco is suppressed in transgenic plants expressing antisense lipoxygenase sequences. *Proc. Natl. Acad. Sci. U.S.A.* 95, 6554–6559. doi: 10.1073/pnas.95.11.6554

Sanadhya, P., Agarwal, P., Khedia, J., and Agarwal, P. K. (2015). A low-affinity K^+ transporter *AlHKT2;1* from recretohalophyte *Aeluropus lagopoides* confers salt tolerance in yeast. *Mol. Biotechnol.* 57, 489–498. doi: 10.1007/s12033-015-9842-9

Sanadhya, P., Bucki, P., Liarzi, O., Ezra, D., Gamliel, A., and Braun Miyara, S. (2018). Caenorhabditis elegans susceptibility to *Daldinia* cf. concentrica bioactive volatiles is coupled with expression activation of the stress-response transcription factor daf-16, a part of distinct nematicidal action. *PLoS ONE* 13:e0196870. doi: 10.1371/journal.pone.0196870

Santner, A., Calderon-Villalobos, L. I. A., and Estelle, M. (2009). Plant hormones are versatile chemical regulators of plant growth. *Nat. Chem. Biol.* 5, 301–307. doi: 10.1038/nchembio.165

Savatin, D. V., Gramegna, G., Modesti, V., and Cervone, F. (2014). Wounding in the plant tissue: the defense of a dangerous passage. *Front. Plant Sci.* 5:470. doi: 10.3389/fpls.2014.00470

Seo, H. S., Song, J. T., Cheong, J.-J., Lee, Y.-H., Lee, Y.-W., Hwang, I., et al. (2001). Jasmonic acid carboxyl methyltransferase: a key enzyme for jasmonate-regulated plant responses. *Proc. Natl. Acad. Sci. U. S. A.* 98, 4788–4793. doi: 10.1073/pnas.081557298

Signora, L., de Smet, I., Foyer, C. H., and Zhang, H. (2001). ABA plays a central role in mediating the regulatory effects of nitrate on root branching in *Arabidopsis*. *Plant J.* 28, 655–662. doi: 10.1046/j.1365-313x.2001.01185.x

Sijmons, P. C., Grundler, F. M. W., von Mende, N., Burrows, P. R., and Wyss, U. (1991). *Arabidopsis thaliana* as a new model host for plant-parasitic nematodes. *Plant J.* 1, 245–254. doi: 10.1111/j.1365-313X.1991.00245.x

Stumpe, M., Carsjens, J.-G., Göbel, C., and Feussner, I. (2008). Divinyl ether synthesis in garlic bulbs. *J. Exp. Bot.* 59, 907–915. doi: 10.1093/jxb/ern010

Stumpe, M., Kandzia, R., Göbel, C., Rosahl, S., and Feussner, I. (2001). A pathogen-inducible divinyl ether synthase (CYP74D) from elicitor-treated potato suspension cells. *FEBS Lett.* 507, 371–376. doi: 10.1016/S0014-5793(01)03019-8

Szakasits, D., Heinen, P., Wieczorek, K., Hofmann, J., Wagner, F., Kreil, D. P., et al. (2009). The transcriptome of syncytia induced by the cyst nematode *Heterodera schachtii* in *Arabidopsis* roots. *Plant J.* 57, 771–784. doi: 10.1111/j.1365-313X.2008.03727.x

Thomason, I. J. (1987). "Challenges facing nematology: environmental risks with nematicides and the need for new approaches," in *Vistas on Nematology*, eds J. A. Veech and D. W. Dickson (Hyattsville, MD: Society of Nematologists), 469–476.

Vellosillo, T., Martínez, M., López, M. A., Vicente, J., Cascón, T., Dolan, L., et al. (2007). Oxylipins produced by the 9-lipoxygenase pathway in *Arabidopsis* regulate lateral root development and defense responses through a specific signaling cascade. *Plant Cell* 19, 831–846. doi: 10.1105/tpc.106.046052

Weber, H., Chételat, A., Caldelari, D., and Farmer, E. E. (1999). Divinyl ether fatty acid synthesis in late blight-diseased potato leaves. *Plant Cell* 11, 485–493. doi: 10.1105/tpc.11.3.485

Wyss, U., Grundler, F. M. W., and Münch, A. (1992). The parasitic behaviour of second-stage juveniles of *Meloidogyne incognita* in roots of *Arabidopsis thaliana*. *Nematologica* 38, 98–111. doi: 10.1163/187529292X00081

Xu, R., and Li, Q. Q. (2008). Protocol: Streamline cloning of genes into binary vectors in *Agrobacterium* via the Gateway® TOPO vector system. *Plant Methods* 4, 1–7. doi: 10.1186/1746-4811-4-4

Conflict of Interest: The authors declare that the research was conducted in the absence of any commercial or financial relationships that could be construed as a potential conflict of interest.

Publisher's Note: All claims expressed in this article are solely those of the authors and do not necessarily represent those of their affiliated organizations, or those of the publisher, the editors and the reviewers. Any product that may be evaluated in this article, or claim that may be made by its manufacturer, is not guaranteed or endorsed by the publisher.

Copyright © 2021 Sanadhya, Kumar, Bucki, Fitoussi, Carmeli-Weissberg, Borenstein and Brown-Miyara. This is an open-access article distributed under the terms of the Creative Commons Attribution License (CC BY). The use, distribution or reproduction in other forums is permitted, provided the original author(s) and the copyright owner(s) are credited and that the original publication in this journal is cited, in accordance with accepted academic practice. No use, distribution or reproduction is permitted which does not comply with these terms.

frontiers in Plant Science

ORIGINAL RESEARCH
published: 26 August 2021
doi: 10.3389/fpls.2021.719587

The Synthesis of Pentyl Leaf Volatiles and Their Role in Resistance to Anthracnose Leaf Blight

*Zachary Gorman[1], Jordan P. Tolley[1,2], Hisashi Koiwa[2] and Michael V. Kolomiets[1]**

[1] Department of Plant Pathology and Microbiology, Texas A&M University, College Station, TX, United States, [2] Department of Horticultural Sciences, Texas A&M University, College Station, TX, United States

Volatiles are important airborne chemical messengers that facilitate plant adaptation to a variety of environmental challenges. Lipoxygenases (LOXs) produce a bouquet of non-volatile and volatile oxylipins, including C_6 green leaf volatiles (GLVs), which are involved in a litany of plant physiological processes. GLVs are emitted by a diverse array of plant species, and are the best-known group of LOX-derived volatiles. Five-carbon pentyl leaf volatiles (PLVs) represent another widely emitted group of LOX-derived volatiles that share structural similarity to GLVs, however, relatively little is known about their biosynthesis or biological activity. In this study, we utilized PLV-deficient mutants of maize and Arabidopsis and exogenous PLV applications to elucidate the biosynthetic order of individual PLVs. We further measured PLVs and GLVs after tissue disruption of leaves by two popular methods of volatile elicitation, wounding and freeze-thawing. Freeze-thawing distorted the volatile metabolism of both GLVs and PLVs relative to wounding, though this distortion differed between the two groups of volatiles. These results suggest that despite the structural similarity of these two volatile groups, they are differentially metabolized. Collectively, these results have allowed us to produce the most robust PLV pathway to date. To better elucidate the biological activity of PLVs, we show that PLVs induce maize resistance to the anthracnose pathogen, *Colletotrichum graminicola*, the effect opposite to that conferred by GLVs. Further analysis of PLV-treated and infected maize leaves revealed that PLV-mediated resistance is associated with early increases of oxylipin α- and γ-ketols, and later increases of oxylipin ketotrienes, hydroxytrienes, and trihydroxydienes. Ultimately, this study has produced the most up-to-date pathway for PLV synthesis, and reveals that PLVs can facilitate pathogen resistance through induction of select oxylipins.

Keywords: green leaf volatile (GLV), volatile organic compound (VOC), *Colletotrichum graminicola*, lipoxygenase (LOX), priming, oxylipin, ketol

OPEN ACCESS

Edited by:
Mario Serrano, National Autonomous University of Mexico, Mexico

Reviewed by:
Kenji Matsui, Yamaguchi University, Japan
Jian-Feng Li, Sun Yat-sen University, China

***Correspondence:**
Michael V. Kolomiets
kolomiets@tamu.edu

Specialty section:
This article was submitted to Plant Pathogen Interactions, a section of the journal Frontiers in Plant Science

Received: *02 June 2021*
Accepted: *26 July 2021*
Published: *26 August 2021*

Citation:
Gorman Z, Tolley JP, Koiwa H and Kolomiets MV (2021) The Synthesis of Pentyl Leaf Volatiles and Their Role in Resistance to Anthracnose Leaf Blight. Front. Plant Sci. 12:719587. doi: 10.3389/fpls.2021.719587

INTRODUCTION

Volatile-mediated signaling is an important aspect of plant life that allows plants to endure a plethora of environmental challenges. Plant volatile signaling facilitates inter- and intra-plant communication, as well as communication with insects and microbes (Allmann and Baldwin, 2010; Matsui et al., 2012). These communications allow plants to anticipate and pre-emptively prime defenses against a wide range of imminent stresses (Engelberth et al., 2004). There are several key groups of volatile organic compounds (VOC) that are integral to these processes, including green

leaf volatiles (GLV); a group of six-carbon, lipid-derived, volatile oxylipins that are synthesized in the hydroperoxide lyase (HPL) branch of the lipoxygenase (LOX) pathway (Matsui, 2006). These volatiles are widely emitted in response to a variety of different stresses and can induce widespread defense (Ameye et al., 2018). However, as our recent work showed, GLVs can also contribute to susceptibility of maize to the fungal agent of anthracnose disease, *Colletotrichum graminicola* (Gorman et al., 2020). While GLVs are a major component of VOC blends, they are not the only group of LOX-derived VOCs. Select jasmonates (Loughrin et al., 1995; Seo et al., 2001), and lesser-known five-carbon volatiles, henceforth referred to as pentyl leaf volatiles (PLVs), are also widely emitted LOX-derived volatile oxylipins.

Pentyl leaf volatiles are a group of volatiles that consist of five-carbon aldehydes, alcohols, ketones, and acetate conjugates produced in the LOX branch of the LOX pathway. Like GLVs, PLVs are emitted in response to a litany of abiotic and biotic stresses in numerous plant species (Fall et al., 2001; Heiden et al., 2003; Jardine et al., 2012; Mochizuki et al., 2016). Despite this, there has been little prior focus on the physiological functions of these volatiles or their synthesis. However, important roles of these volatiles in various plant species have been previously suggested, including priming of plant defenses against pathogens (Alméras et al., 2003; Song and Ryu, 2013; Choi et al., 2014; Song et al., 2015), aphid defense (Song and Ryu, 2013), and attraction of insects (van Tol et al., 2012; Song and Ryu, 2013; Roberts et al., 2019). Though PLVs include a diverse array of individual molecular species, little is known about the order of their synthesis.

Structurally, many PLV molecular species display distinct similarity to GLV molecular species (**Figure 1**), and are often co-emitted in response to stress (Fall et al., 2001; Heiden et al., 2003; Jardine et al., 2012; He et al., 2020). Both of these VOC groups depend on utilization of 13*S*-hydroperoxy octadecatrienoic acid (13*S*-HPOT) and 13*S*-hydroperoxy octadecadienoic acid (13*S*-HPOD), which are generated by LOX-mediated oxygenation of linolenic (C18:3) and linoleic acids (C18:2), respectively (Salch et al., 1995; Matsui, 2006). HPL acts on these hydroperoxides to produce the primary GLVs, (3*Z*)-hexenal and hexanal (Mukhtarova et al., 2018), as well as a non-volatile 12-carbon compound, (9*Z*)-traumatin (Hatanaka, 1993). (3*Z*)-Hexenal can be enzymatically or non-enzymatically isomerized to another aldehyde, (2*E*)-hexenal (Hatanaka, 1993; Kunishima et al., 2016; Spyropoulou et al., 2017), and both of these aldehydes can be enzymatically reduced to corresponding alcohols by NADH-dependent alcohol dehydrogenases (ADH) (Bate et al., 1998; Speirs et al., 1998) and NADPH-dependent cinnamaldehyde and hexenal reductase (CHR) (Tanaka et al., 2018). These alcohols can then be further converted to their respective acetate-conjugates by acetyl-CoA-dependent BAHD acetyl transferases (AT) (D'Auria et al., 2007).

Though LOXs oxygenate polyunsaturated fatty acids, they may also perform a secondary reaction on LOX-derived 13*S*-HPOT. This generates a radical that undergoes spontaneous β-scission to form a pentene allylic radical that rapidly forms the isomers, 1-penten-3-ol and (2*Z*)-pentenol. Pentanol may also be produced from 13*S*-HPOD substrate, although LOXs seem to have less affinity for this substrate (Salch et al., 1995). LOX-mediated cleavage of 13-hydroperoxides also generates a non-volatile 13-carbon compound, 13-oxo-9(*Z*)-11(*E*)-tridecadienoic acid (OTD) (Vliegenthart et al., 1975, 1977; Salch et al., 1995; Gao et al., 2008; He et al., 2020). (2*Z*)-Pentenol and 1-penten-3-ol can be metabolized into aldehydes or ketones, respectively, through the activity of ADHs (Gardner et al., 1996). Beyond this, little is known about derivatization of these volatiles, each of which may have their own distinct signaling activity. Since both GLVs and PLVs share common substrate, it is not surprising that the major PLV-producing LOX isoforms identified in maize, ZmLOX10 (He et al., 2020), Arabidopsis, AtLOX2 (Mochizuki et al., 2016), and tomato, TomLOXC (Shen et al., 2014) are also the sole GLV-producing LOX isoforms in these respective species (Christensen et al., 2013). Notably, ZmLOX6 of maize lacks the ability to generate fatty acid hydroperoxides, but can cleave them into PLVs and OTD (Gao et al., 2008). Soybean also appears to have two LOX isoforms that contribute to PLV synthesis (Kobayashi et al., 1995; Fisher et al., 2003).

Utilizing PLV-deficient mutants of maize and Arabidopsis alongside exogenous application of PLVs, we establish the biosynthetic order of PLVs in the LOX pathway and provide evidence that despite the similar structure of PLVs and GLVs, they are metabolized differently. We also provide evidence that freeze-thawing of plant tissues, a popular method of volatile analysis, distorts the volatile oxylipin profiles of plant tissues, and differentially effects metabolism of PLVs and GLVs. Lastly, we show that in maize, PLVs induce resistance to *Colletotrichum graminicola*, which stands in contrast to results of our recent study that revealed GLVs promote disease progression to this pathogen (Gorman et al., 2020). Furthermore, we show that PLV-mediated resistance correlates with the synthesis of oxylipin α- and γ-ketols, ketotrienes, hydroxytrienes, and trihydroxydienes.

MATERIALS AND METHODS

Plant and Fungal Materials and Growth Conditions

Mutant alleles of ZmLOX10 in maize were obtained by PCR screening of the *Mutator*-transposon insertional genetics resource at Corteva Agriscience, formerly DuPont-Pioneer[1], for insertions in these genes. The *lox10-3* mutant allele was confirmed as an exon-insertional knockout mutant (Christensen et al., 2013). Original *lox10-3* mutants were backcrossed into the B73 and W438 inbred line backgrounds and genetically advanced to the backcross 7 stage. Maize plants used in all experiments were grown to the V4 stage (plants having four fully expanded leaves) under growth lights (∼300 μmol m^{-2} s^{-1}) in a 14:10 h (light:dark) regime at 21–24°C. Maize plants were grown in TX-360 Metro Mix soil (Sun Gro Horticulture, Agawam, MA, United States).

Arabidopsis thaliana Col-0 and *Atlox2-1* mutants in the Col-0 background were grown for 4 weeks in LP5 potting medium (Sun Gro Horticulture, Bellevue, WA, United States) in a growth

[1]https://www.pioneer.com

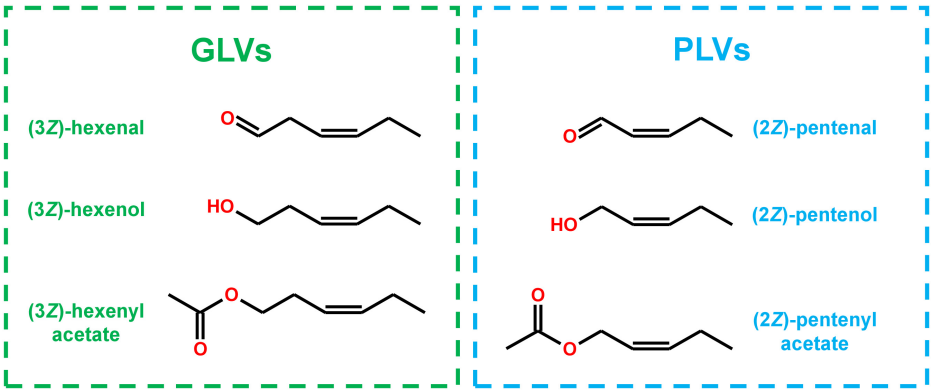

FIGURE 1 | Structural similarity of GLVs and PLVs.

chamber (~85 μmol m^{-2} s^{-1}) under a 12:12 h (light:dark) regime at 23°C (light): 21°C (dark), in 65% relative humidity. Screening of *Atlox2-1* mutant lines was performed as previously described by Glauser et al. (2009).

All *C. graminicola* plates used in infection assays were grown from culture stock (*C. graminicola* 1.001 strain) kept in a –80°C freezer. Cultures were grown on PDA plates for at least 2 weeks before conidia were collected for use in plant inoculations. Spore extractions were performed as previously described by Gao et al. (2007) and were used within 2 h of extraction.

PLV Metabolism Assays

For maize, fully expanded third leaves of wild type (WT) and *lox10-3* mutant in the B73 background were enclosed in 800 mL jars (one leaf per jar) alongside a cotton ball containing 2.5 μL of 100 mM of select PLVs dissolved in dichloromethane. For Arabidopsis, intact WT or *Atlox2-1* mutants were grown in small pots (~350 mL) (5 plants/pot), were enclosed in these jars with the respective treatments. Col-0 was exposed to 5 μL of treatments, *Atlox2-1* mutants were exposed to 2.5 μL. Four replicates for each plant/genotype/treatment were used. PLV treatments included purified chemical standards of (2*Z*)-pentenol, (2*E*)-pentenol, (2*E*)-pentenal, pentanol, pentanal, 1-penten-3-ol, 1-penten-3-one, 3-pentanol, and 3-pentanone (Sigma-Aldrich, St. Louis, MO, United States). Plants were incubated alongside the PLV treatments for 20 min, and then volatiles were collected onto HaySepQ filters containing 80–100 mesh (Supelco, Bellefonte, PA, United States) via dynamic airflow (1 L min^{-1}) for an additional 20 min. Volatiles were eluted off the HaySepQ filter traps with 250 μL of dichloromethane containing 100 μM of the internal standard, (4*Z*)-hexenol (Sigma-Aldrich, St. Louis, MO, United States). Volatiles were analyzed and quantified via gas chromatography mass spectrometry (GC-MS).

Volatile Analysis of Wounding and Freeze-Thawing

For volatile analysis of wounding responses, leaves of both maize and Arabidopsis were excised, quickly weighed out to 2 g, and cut into 1 cm pieces that were immediately placed into 800 mL jars (He et al., 2020). For maize, the 3rd and 4th leaves of B73, W438, and *lox10-3* mutants in these backgrounds were used (one plant/replicate, four replicates total). For Arabidopsis, all leaves of Col-0 were used (5–6 plants/rep, four reps total). Volatile analysis of freeze-thawing response was carried out similar to wounding, except instead of leaves being cut, they were briefly frozen in liquid N_2, and immediately placed into the jars for volatile collection. Volatiles were collected for 1 h as previously described.

Gas Chromatography-Mass Spectrometry

An Agilent 7890B gas chromatograph connected to an Agilent 5977B quadrupole mass spectrometer (Agilent, Santa Clara, CA, United States) was utilized to quantify volatiles. Two μL of liquid sample was injected splitless into a HP-5ms Ultra Inert column (Agilent, Santa Clara, CA, United States). The inlet temperature was set to 240°C for the duration of the run. The oven temperature was as follows: 40°C hold – 2 min, 3°C/min ramp to 160°C, 15°C/min ramp to 280°C, 280°C/min hold – 2 min. The solvent delay was 2.5 min. Analytes were fragmented by positive EI (230°C – source, 150°C – quadrupole, ionization energy – 70 eV, scan range – 25–500 amu). Most compounds were identified and quantified based off of retention times and spectra of pure external standards purchased from Sigma-Aldrich (St. Louis, MO, United States). The 4-oxo-(2*E*)-hexenal, (2*Z*)-pentenyl acetate, pentyl acetate, pentanoic acid, and 2-methyl-3-pentanone were identified based off matching of mass spectra and retention index (RI), calculated according to van Den Dool and Kratz (1963), in the NIST14 library. (2*Z*)-Pentenal and (2*Z*)-hexenal were identified by almost identical spectral matching to (2*E*)-pentenal and (2*E*)-hexenal, respectively, and retention times characteristic of other lipoxygenase-derived volatile (*E*/*Z*)-isomers. All volatiles were quantified based by utilizing internal and external standards.

Infection Assays

For disease assays, B73 and *lox10-3* mutant maize seedlings at the V4 developmental stage were exposed to PLVs for 2 h before being inoculated 1 h after volatile exposure ended. Six

plants of each genotype/treatment were placed into a 6 L glass container along with a cotton ball containing 100 μL of PLV or control treatment. PLV treatment consisted of a mixture containing 10 nmol of (2*Z*)-pentenol and 1-penten-3-ol dissolved in triacetin. Triacetin was used as control treatment. Chemical standards were purchased from Sigma-Aldrich (St. Louis, MO, United States). Plants were inoculated with *C. graminicola* by placing them in humidity chambers and applying 10 μL of spore suspension (10^6 spores mL^{-1}) at six different places on the third leaf of each plant. Plants were removed from humidity chambers 1 day after inoculation and placed back on growth shelves (Gao et al., 2007). For lesion area determination, plants were incubated in conditions as described above for 7 days following inoculation before the infected leaves were excised and scanned to produce digital images. Lesion area were determined from digital images using ImageJ software (Schneider et al., 2012).

For metabolite analysis of infected leaves, B73 plants were either exposed to PLV treatment or control treatment, and infected as described above. Infected leaf tissue was harvested 1 day post inoculation (dpi), 4 dpi, and 6 dpi and stored in −80°C until metabolites were extracted for analysis. Plants exposed to volatile treatments, but were not yet infected, were also collected (0 dpi).

Metabolite Extraction and Liquid Chromatography-Mass Spectrometry

A mortar and pestle were used to grind frozen plant material into a fine powder under liquid nitrogen. Hormones were extracted from tissue and quantified by liquid chromatography-mass spectrometry (LC-MS/MS) as previously described (Gorman et al., 2020). Five hundred μL of phytohormone extraction buffer (1-propanol/water/HCl [2:1:0.002 vol/vol/vol]) containing 500 nM of the internal standards d-JA (2,4,4-d_3; acetyl-2,2-d_2 JA (CDN Isotopes, Pointe-Claire, QC, Canada) and d_6-SA (Sigma-Aldrich, St. Louis, MO, United States). The samples were agitated in the dark for 30 min at 4°C. Five hundred μL dichloromethane was added to each sample and the samples were again agitated in the dark for 30 min at 4°C. The samples were then centrifuged at 17,000 × *g* for 5 min. The lower organic layer of each sample was transferred to a glass vial and evaporated by nitrogen gas. Samples were resuspended in 150 μL methanol, transferred to a separate tube, and centrifuged at 17,000 × *g* for 5 min to pellet any debris. Ninety μL of supernatant was transferred into autosampler vials for LC-MS/MS.

An Ascentis Express C-18 Column (3 cm × 2.1 mm, 2.7 μm) (Sigma-Aldrich, St. Louis, MO, United States) connected to an API 3200 LC-MS/MS (Sciex, Framingham, MA, United States) using electrospray ionization with multiple reaction mentoring was used. The injection volume was 10 μL and had a 450 μL min^{-1} mobile phase consisting of Solution A (0.2% acetic acid in water) and Solution B (0.2% acetic acid in acetonitrile) with a gradient consisting of (time – %B): 0.5–10%, 1.0–20%, 21.0–70%, 24.6–100%, 24.8–10%, 29 – stop. All oxylipins were quantified by comparison to deuterated internal standards.

RESULTS

Spontaneous Catabolism by PLVs

Previously, we analyzed volatiles emitted in B73 inbred WT maize in response to wounding and found a number of PLVs were emitted, although the biosynthetic order of their synthesis was not known (He et al., 2020). To resolve this gap in knowledge and generate a framework of PLV biosynthetic pathway, we incubated plant leaves with various individual PLVs and analyzing subsequent PLV emissions via gas chromatography-mass spectrometry. However, as PLVs are subject to atmospheric breakdown (Orlando et al., 2001), we first attempted to establish which PLVs can be non-enzymatically generated in the absence of plants. To accomplish this, we individually incubated various exogenous PLVs in empty jars, including (2*Z*)-pentenol, (2*E*)-pentenol, (2*E*)-pentenal, pentanol, pentanal, 1-penten-3-ol, 1-penten-3-one, 3-pentanol, or 3-pentanone, and found that several derivative PLVs were subsequently detected. Both (2*Z*)-pentenal and (2*E*)-pentenal were produced after (2*Z*)-pentenol treatment, as well as pentanol (**Table 1**). Furthermore, these were all produced in equal amounts. In response to (2*E*)-pentenol treatment, (2*E*)-pentenal and pentanol were both produced. Both (2*E*)-butenyl formate and (2*Z*)-butenyl formate were produced in response to (2*E*)-pentenal. Pentanal spontaneously converted to pentanol, as well as to pentanoic acid and to butyl formate. Oppositely, pentanal was produced after pentanol treatment. After 1-penten-3-ol treatment, 1-penten-3-one and 3-pentanol were detected. 3-Pentanone was detected after treatment with 1-penten-3-one, but not after 1-penten-3-ol treatment, despite that 1-penten-3-ol treatment produced 1-penten-3-one. Due to the trace quantities detected after 1-penten-3-one treatment, we concluded that non-enzymatic generation of 3-pentanone from 1-penten-3-one is not of significance. Contrastingly, relatively high amounts of 3-pentanone were detected after 3-pentanol treatment. 3-Pentanol also resulted in the generation of 2-methyl-3-pentanone. These results show that several PLVs can be non-enzymatically generated, although the degree that this process plays in generation of different PLV molecular species varies. Several non-enzymatic PLV derivatives detected in this analysis were not previously reported in either maize (He et al., 2020), Arabidopsis (Mochizuki et al., 2016), or tomato (Shen et al., 2014), including (2*E*)-butenyl formate, (2*Z*)-butenyl formate, butyl formate, pentanoic acid, and 2-methyl-3-pentanone. This suggests that these PLVs are an artifact of the high amounts of exogenous PLVs used in this experiment, and thus are excluded from further consideration in the following plant-based metabolism assays. Other PLVs detected in this experiment are able to be non-enzymatically synthesized. However, these other PLVs have been previously found to be emitted by plant tissues (Shen et al., 2014; Mochizuki et al., 2016; He et al., 2020). We next sought to evaluate how maize leaves metabolize exogenous PLVs.

Metabolism of PLVs by Maize

To elucidate maize metabolism of PLVs, we repeated the previous experiment, but we incubated PLVs in the presence of leaves of B73 WT. (2*Z*)-Pentenol was converted into the greatest number

TABLE 1 | Spontaneous catabolism of exogenous PLVs.

Analytes (nmol/h)	Treatment								
	(2*Z*)-pentenol	(2*E*)-pentenol	(2*E*)-pentenal	Pentanol	Pentanal	1-penten-3-ol	1-penten-3-one	3-pentanol	3-pentanone
(2*Z*)-pentenol									
(2*Z*)-pentenal	**1.1** ± 0.14								
(2*E*)-pentenol									
(2*E*)-pentenal	**1.1** ± 0.15	**1.9** ± 0.3							
(2*E*)-butenyl formate*			**0.5** ± 0.05						
(2*Z*)-butenyl formate*			**7.6** ± 0.79						
Pentanol	**1.1** ± 0.11	**7.1** ± 1.63			**0.6** ± 0.1				
Pentanal				**0.3** ± 0.03					
Pentanoic acid*					**49.2** ± 15.13				
Butyl formate*					**1.1** ± 0.21				
1-penten-3-ol									
1-penten-3-one						**0.6** ± 0.04			
3-pentanol						**0.1** ± 0.01			
3-pentenone							**0.1** ± 0.01	**19.1** ± 3.85	
2-methyl-3-pentanone*								**5.5** ± 0.85	

Various exogenous PLVs were incubated for 20 min in small glass jars before volatiles were collected and analyzed. Analytes detected (red cells) show mean ± SE (nmol per hour). Responses of the same analytes matching a respective volatile treatment were omitted (black cells). Empty cells indicate targets that were not detected. Asterisks after analyte names denote artificial PLVs.

of compounds (**Table 2** and **Figure 2**), likely due to its status as a primary PLV. (2*Z*)-Pentenol was most readily converted to (2*Z*)-pentenyl acetate, followed by (2*Z*)-pentenal, (2*E*)-pentenol, (2*E*)-pentenal, and pentanol, which were emitted in approximately equal amounts. (2*E*)-Pentenol exposure also resulted in the emission of (2*E*)-pentenal and pentanol, but produced higher amounts compared to (2*Z*)-pentenol (**Table 2**). The β-scission reaction proposed by Salch et al. (1995) suggests that pentanol is synthesized from 13*S*-HPOD, but these results show it can also be synthesized by the reduction of 13*S*-HPOT-derived 2-pentenol. Treatment with (2*Z*)-pentenol, (2*E*)-pentenol, and pentanol resulted in the emissions of (2*Z*)-pentenyl acetate, (2*E*)-pentenyl acetate, and pentyl acetate, respectively, suggesting these alcohols can all be acted upon by ATs. Interestingly, (2*Z*)-pentenyl acetate and pentyl acetate were more highly emitted after treatment with (2*Z*)-pentenol and pentanol, respectively, compared to (2*E*)-pentenyl acetate after (2*E*)-pentenol treatment. This suggests that PLV-metabolizing ATs prefer (2*Z*)-pentenol and pentanol as substrates. Importantly, PLV acetate conjugates were not detected after incubation of exogenous PLVs in empty jars, suggesting these PLVs are solely synthesized enzymatically. In addition to pentyl acetate, pentanol treatment also resulted in the emission of the aldehyde, pentanal. Conversely, exposure to pentanal resulted in the emission of pentanol and pentyl acetate. Similarly, (2*E*)-pentenal treatment resulted in the emission of (2*E*)-pentenol, (2*E*)-pentenyl acetate. These results suggest potential bi-directional interconversion of PLV aldehydes and alcohols, as well as the formation of PLV-derived esters. Treatment of B73 with the other primary PLV, 1-penten-3-ol, resulted in the emission of 1-penten-3-one, 3-pentanone, and to a much lesser extent, 3-pentanol. 1-Penten-3-one treatment also resulted in the emission of a small amount of 3-pentanol, and a large amount of 3-pentanone relative to treatment with 1-penten-3-ol. Exposure to 3-pentanol resulted in the emission of 3-pentanone. Oppositely, 3-pentanone resulted in minor emissions of 3-pentanol. No acetate or esterified derivatives of 1-penten-3-ol or any of its derivatives were detected, suggesting that the relevant AT(s) require a terminal hydroxyl group.

Since PLVs are released from leaves, we also treated PLV-deficient *lox10-3* mutants (He et al., 2020) with PLVs to rule out the emission of endogenous PLVs induced by exogenous PV treatments. Emission of select PLVs in response to treatment with specific PLVs was the same between WT B73 and *lox10-3* mutants (**Tables 2**, **3**), however, some PLVs were more lowly emitted in response to select PLV treatments. Most notably, acetate conjugates were emitted in lower amounts in *lox10-3* mutants relative to B73 WT. This suggests that ZmLOX10 positively regulates AT activity in maize. These results utilizing PLV-deficient *lox10-3* mutants confirm the previous B73 results, and show that ZmLOX10 positively regulates the AT(s) involved in the synthesis of various PLV acetates.

Metabolism of PLVs by Arabidopsis

Green leaf volatiles metabolism can greatly vary between different plant species (Matsui et al., 2000; Allmann and Baldwin, 2010; López-Gresa et al., 2018), therefore we also wanted to evaluate PLV metabolism in Arabidopsis. PLV metabolism was assessed in Arabidopsis Col-0 ecotype as described for maize. We found that overall, the same types of PLVs were emitted in response to select PLV treatments. There were, however, some notable differences regarding the relative amounts of emitted PLVs (**Figure 2**). After incubation with (2*Z*)-pentenol, equal amounts of (2*Z*)-pentenal and (2*Z*)-pentenyl acetate were recovered, followed by lower amounts of (2*E*)-pentenol and (2*E*)-pentenal (**Table 4**

TABLE 2 | Metabolism of exogenous PLVs by WT maize in the B73 background.

Analytes (nmol/h)	Treatment								
	(2Z)-pentenol	(2E)-pentenol	(2E)-pentenal	Pentanol	Pentanal	1-penten-3-ol	1-penten-3-one	3-pentanol	3-pentanone
(2Z)-pentenol			4.2 ± 0.5		2.4 ± 0.47				1.1 ± 0.29
(2Z)-pentenal	0.9 ± 0.12								
(2Z)-pentenyl acetate	7.6 ± 0.7								
(2E)-pentenol	0.7 ± 0.08								
(2E)-pentenal	0.8 ± 0.12	4.9 ± 0.37							
(2E)-pentenyl acetate		2.1 ± 0.32	0.6 ± 0.14						
Pentanol	0.8 ± 0.09	7.9 ± 1.43	1 ± 0.17						
Pentanal				0.4 ± 0.06					
Pentyl acetate				48.2 ± 6.37	8.7 ± 2.37				
1-penten-3-ol									
1-penten-3-one						1.1 ± 0.07			
3-pentanol						0.2 ± 0.02	0.1 ± 0.02		
3-pentenone						1.3 ± 0.14	11.5 ± 1.76	4.9 ± 0.32	

Leaves of B73 were incubated with various PLVs for 20 min before volatiles were collected and analyzed. Analytes detected (red cells) show mean ± SE (nmol per hour). Responses of the same analytes matching a respective volatile treatment were omitted (black cells). Empty cells indicate targets that were not detected.

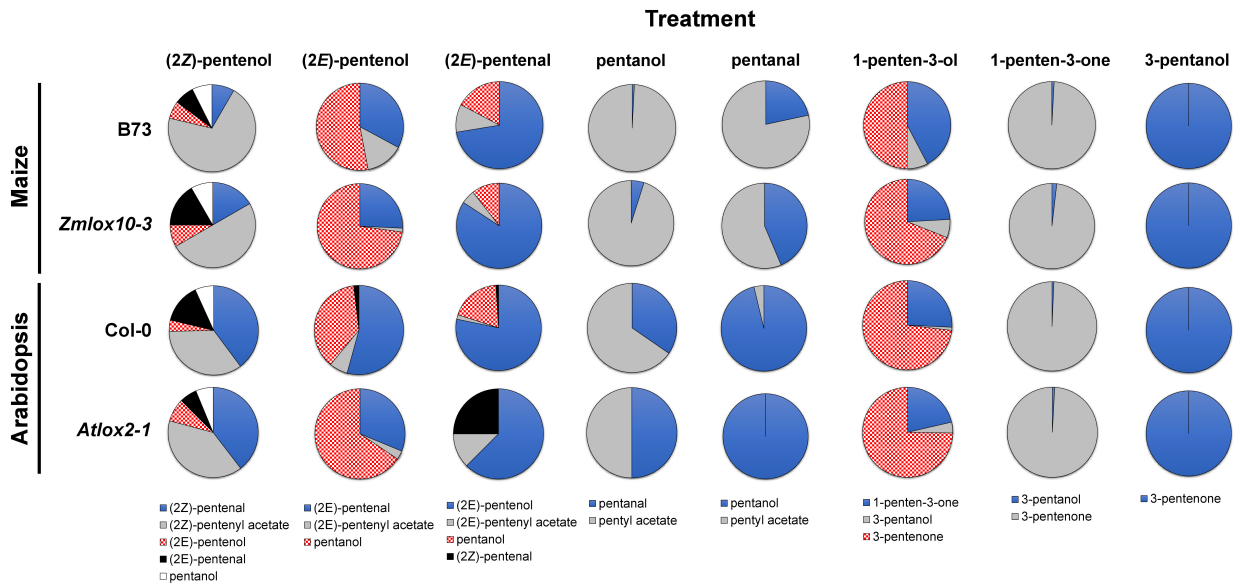

FIGURE 2 | Relative proportions of PLVs detected in maize (B73 and Zm*lox10-3* mutants) and Arabidopsis (Col-0 and *Atlox2-1* mutants) in response to treatment with different PLV molecular species. Colors and patterns representative of different PLVs are shown below individual treatments (top) and are consistent across all genotypes of a particular treatment.

and **Figure 2**). Notably, after (2*E*)-pentenal treatment, large amounts of (2*E*)-pentenol were retrieved. The ratio of pentyl acetate to pentanal produced after pentanol treatment was almost equal (**Table 4**), as opposed to the large difference observed in B73 maize (**Table 2**). 1-Penten-3-ol treatment resulted in 2–3 fold higher amounts of 3-pentanone relative to 1-penten-3-one (**Table 4**). This was substantially different than in maize, which emitted approximately amounts of these volatiles (**Tables 2**, **3**).

As for maize, we also utilized a PLV-deficient mutant of Arabidopsis, *Atlox2-1*, to rule out potential exogenous PLV-mediated induction of endogenous PLV synthesis (Mochizuki et al., 2016). As was the case between B73 WT and *lox10-3* mutant maize, we found few differences in the responses of Col-0 and *Atlox2-1* mutants (**Figure 2**). After treatment with (2*Z*)-pentenol, less (2*E*)-pentenal was recovered relative to the other metabolites detected than in Col-0 (**Tables 4**, **5** and **Figure 2**). After (2*E*)-pentenal treatment, there was less (2*E*)-pentanol and pentanol relative to (2*Z*)-pentenal, and (2*E*)-pentenyl acetate was not detected (**Table 5**). After pentanol treatment, there were approximately equal

TABLE 3 | Metabolism of exogenous PLVs by *lox10-3* mutants in the maize B73 background.

Analytes (nmol/h)	Treatment								
	(2*Z*)-pentenol	**(2*E*)-pentenol**	**(2*E*)-pentenal**	**Pentanol**	**Pentanal**	**1-penten-3-ol**	**1-penten-3-one**	**3-pentanol**	**3-pentanone**
(2*Z*)-pentenol									
(2*Z*)-pentenal	**0.8** ± 0.11								
(2*Z*)-pentenyl acetate	**2.4** ± 0.44								
(2*E*)-pentenol	**0.4** ± 0.12		**3.2** ± 0.97						
(2*E*)-pentenal	**0.8** ± 0.09	**3.5** ± 0.57							
(2*E*)-pentenyl acetate		**0.2** ± 0.1	**0.2** ± 0.08						
Pentanol	**0.4** ± 0.16	**9.9** ± 2.19	**0.4** ± 0.08		**2.4** ± 0.47				
Pentanal				**0.4** ± 0.03					
Pentyl acetate				**7.8** ± 1.46	**3.1** ± 0.65				
1-penten-3-ol									
1-penten-3-one						**0.7** ± 0.08			
3-pentanol						**0.2** ± 0.01	**0.2** ± 0.05		**1.5** ± 0.16
3-pentenone						**2** ± 0.09	**10.8** ± 3.71	**8.1** ± 1.61	

Leaves of lox10-3 mutants were incubated with various PLVs for 20 min before volatiles were collected and analyzed. Analytes detected (red cells) show mean ± SE (nmol per hour). Responses of the same analytes matching a respective volatile treatment were omitted (black cells). Empty cells indicate targets that were not detected.

TABLE 4 | Metabolism of exogenous PLVs by Arabidopsis.

Analytes (nmol/h)	Treatment								
	(2*Z*)-pentenol	**(2*E*)-pentenol**	**(2*E*)-pentenal**	**Pentanol**	**Pentanal**	**1-penten-3-ol**	**1-penten-3-one**	**3-pentanol**	**3-pentanone**
(2*Z*)-pentenol									
(2*Z*)-pentenal	**8.8** ± 2.11		**0.3** ± 0.06						
(2*Z*)-pentenyl acetate	**7.7** ± 1.19								
(2*E*)-pentenol	**0.9** ± 0.15		**23.4** ± 0.86						
(2*E*)-pentenal	**3.2** ± 0.69	**5.7** ± 0.88							
(2*E*)-pentenyl acetate		**0.7** ± 0.08	**0.5** ± 0.03						
Pentanol	**1.5** ± 0.19	**3.9** ± 0.57	**5.7** ± 0.24		**7.7** ± 1.78				
Pentanal				**0.9** ± 0.03					
Pentyl acetate		**0.2** ± 0.01		**1.7** ± 0.32	**0.3** ± 0.04				
1-penten-3-ol									
1-penten-3-one						**22.9** ± 3.1			
3-pentanol						**1** ± 0.2	**0.5** ± 0.05		**1.5** ± 0.25
3-pentenone						**65.1** ± 8.54	**72.8** ± 32.01	**140** ± 15.44	

Intact Arabidopsis, Col-0, were incubated with various PLVs for 20 min before volatiles were collected and analyzed. Analytes detected (red cells) show mean ± SE (nmol per hour). Responses of the same analytes matching a respective volatile treatment were omitted (black cells). Empty cells indicate targets that were not detected.

amounts of pentyl acetate and pentanal, which differed from the approximate 2:1 ratio of these volatiles found in Col-0. Collectively, these experiments show that PLV metabolism is largely similar in maize and Arabidopsis with regard to the types of individual molecular species that are synthesized in response to individual PLV treatments. However, these experiments also highlight particular PLVs are synthesized at different rates between species (**Figure 2**), indicating differential enzymatic activity across these two species. Collectively, these experiments establish the biosynthetic order of PLV synthesis within the LOX pathway and provide evidence of enzymatic and non-enzymatic synthesis of PLVs. Despite this, little is known about the enzymes behind PLV synthesis.

Volatile Analysis of Leaves Reveals Involvement of Different Enzymes in PLV and GLV Metabolism

One popular method of volatile elicitation, freeze-thawing, has been reported to irreversibly inactivate GLV-metabolizing ADH, and possibly AT enzymes, which generate GLV alcohol and acetate conjugates, respectively (Fall et al., 2001). However, wounding of plant leaves does not inhibit the function of these enzymes (He et al., 2020). Both GLVs (Bate et al., 1998; Speirs et al., 1998) and PLVs (Gardner et al., 1996) are reported to be acted upon ADHs. GLV aldehydes are also reported to be acted upon by a NADPH-dependent enzyme, CHR

TABLE 5 | Metabolism of exogenous PLVs by Arabidopsis.

Analytes (nmol/h)	Treatment								
	(2*Z*)-pentenol	(2*E*)-pentenol	(2*E*)-pentenal	Pentanol	Pentanal	1-penten-3-ol	1-penten-3-one	3-pentanol	3-pentanone
(2*Z*)-pentenol									
(2*Z*)-pentenal	**1.9** ± 0.26		**0.2** ± 0.02						
(2*Z*)-pentenyl acetate	**1.9** ± 0.23								
(2*E*)-pentenol	**0.4** ± 0.06		**0.5** ± 0.25						
(2*E*)-pentenal	**0.3** ± 0.03	**1** ± 0.16							
(2*E*)-pentenyl acetate		**0.1** ± 0.05							
Pentanol	**0.3** ± 0.02	**2.1** ± 0.46	**0.1** ± 0.05		**0.5** ± 0.25				
Pentanal				**0.6** ± 0.06					
Pentyl acetate				**0.6** ± 0.15					
1-penten-3-ol									
1-penten-3-one						**11.1** ± 1.55			
3-pentanol						**2** ± 0.41	**0.5** ± 0.05		**1.7** ± 0.27
3-pentenone						**38.8** ± 6.55	**58.5** ± 5.04	**77.9** ± 11.29	

Intact Arabidopsis, Atlox2-1 mutants in the Col-0 background, were incubated with various PLVs for 20 min before volatiles were collected and analyzed. Analytes detected (red cells) show mean ± SE (nmol per hour). Responses of the same analytes matching a respective volatile treatment were omitted (black cells). Empty cells indicate targets that were not detected.

(Tanaka et al., 2018). As such, we chose to employ both wounding and freeze-thawing with maize and Arabidopsis in order to determine if synthesis of PLV and GLV alcohols and acetates are similarly affected by freeze-thawing. We started by analyzing GLVs and PLVs from wounded and freeze-thawed leaves of WT and *lox10-3* mutants in the B73 and W438 maize inbred genetic backgrounds. Wounding resulted in the emission of diverse PLVs and GLVs in WTs of both backgrounds, with low amounts emitted by *lox10-3* mutants in both backgrounds (**Figure 3A**). Notably (2*E*)-pentenyl acetate and pentyl acetate were not emitted in these experiments, indicating that if they are emitted, it is only in trace quantities. Freeze-thawing of leaves resulted in dramatic increases of GLV aldehydes, including (3*Z*)-hexenal, hexanal, (2*E*)-hexenal, 4-hydroxy-(2*E*)-hexenal, 4-oxo-(2*E*)-hexenal (Matsui et al., 2012), and a newly identified GLV, (2*Z*)-hexenal (**Figure 3A**). Despite the significant increase of aldehyde substrate, freeze-thawing resulted in significantly lower amounts of GLV alcohols, including (3*Z*)-hexenol, (2*E*)-hexenol, and hexanol (**Figure 3A**). Emissions of the GLV acetates, (3*Z*)-hexenyl acetate and hexyl acetate, were similarly diminished after freeze-thawing.

Oppositely freeze-thawing of leaves resulted in much higher emissions of PLV alcohols, including (2*Z*)-pentenol, 1-penten-3-ol, and pentanol (**Figure 3B**). An exception to this trend was (2*E*)-pentenol, which was only slightly higher in *lox10-3* mutants in the B73 background, and WT in the W438 background. The PLV aldehydes, (2*Z*)-pentenal, (2*E*)-pentenal, pentanal, as well as the ketone, 1-penten-3-one, were all significantly higher after freeze-thawing in all genotypes. 3-Pentanone was elevated in response to freeze-thawing in WT and *lox10-3* mutants in the W438 background, but not the B73 background (**Figure 3B**). This represents an interesting difference in PLV synthesis between these different maize inbreds. It is possible that selective pressures have driven this difference, suggesting these volatiles are of consequence to maize fitness in response to different environmental challenges. Like GLV aldehydes, PLVs aldehydes were also more emitted by freeze-thawed leaves, but not to the degree of GLV aldehydes (**Figure 3**). The sole PLV that was decreased in response freeze-thawing was (2*Z*)-pentenyl acetate (**Figure 3B**). In fact, (2*Z*)-pentenyl acetate emissions in all genotypes were either completely, or almost completely, abolished by freeze-thawing, suggesting this treatment results in the inactivation of ATs.

To determine if the impact of freeze-thawing on PLV and GLV emissions is consistent throughout diverse plant species, we also analyzed GLVs and PLVs emitted by Arabidopsis Col-0 in response to wounding and freeze-thawing. As seen in maize, wounding elicited the emission of diverse GLVs and PLVs in Arabidopsis (**Figures 3C,D**). By comparing the relative proportions of maize and Arabidopsis volatiles emitted in response to wounding, it is clear that Arabidopsis favors formation of 1-penten-3-ol and its derivatives, whereas maize favors formation of (2*Z*)-pentenol and its derivatives (**Supplementary Figure 1**). This suggests that AtLOX2 and ZmLOX6 and/or ZmLOX10 may be able to preferentially direct synthesis of 1-penten-3-ol or (2*Z*)-pentenol from 13*S*-HPOT. GLV and PLV emissions after freeze-thawing, relative to wounding, were similar between maize and Arabidopsis. Aldehyde GLVs were increased, and GLV alcohols and acetates were diminished (**Figure 3C**). Correspondingly, (2*Z*)-pentenyl acetate was decreased, despite that most other PLVs displayed increased emissions after freeze-thawing (**Figure 3D**). Only pentanol, pentanal, (2*E*)-pentenol, and 1-penten-3-ol were not statistically increased by freeze-thawing, although the latter two displayed strong trends (**Figure 4B**). (2*Z*)-Pentenyl acetate was very lowly emitted by both maize and Arabidopsis after freeze-thawing, despite that its precursor, (2*Z*)-pentenol, was highly emitted. Similar responses of PLV and GLV acetates to freeze-thawing, coupled with the structural similarity of these VOCs, increases the likelihood that GLV-producing BAHD

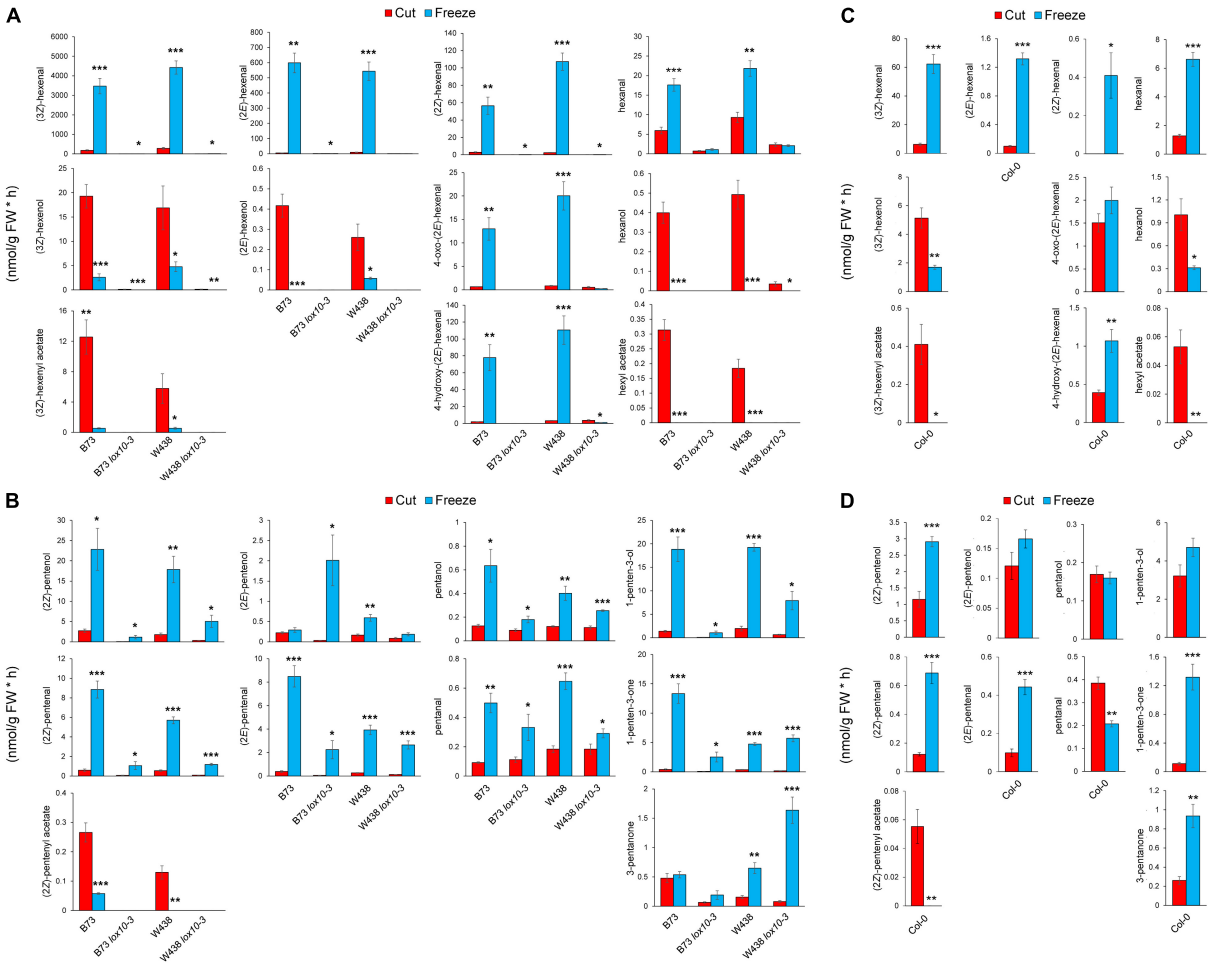

FIGURE 3 | Freezing differentially distorts GLV and PLV emissions of maize and Arabidopsis. Volatiles were collected for 1 h after leaves of two inbred lines of maize, B73 and W438, and *lox10-3* mutants in each respective background, and the Col-0 background of Arabidopsis, were either cut into 1 cm pieces (red) or briefly flash frozen in liquid nitrogen (blue). **(A,C)** Show GLV and **(B,D)** show PLV emissions in maize **(A,B)** and Arabidopsis **(C,D)** (mean ± SE, nmol per gram of fresh weight per hour). Student's *t*-test was performed to determine statistical difference between treatments for each individual genotype (*$p < 0.05$, **$p < 0.005$, ***$p < 0.0005$) ($n = 4$).

ATs also act on PLVs. Inactivation of GLV aldehyde-to-alcohol conversion, but not PLV alcohol-to-aldehyde conversion, suggest that the ADH(s), CHR, or other enzymes acting in these two pathways are different. Collectively, these results shed new light on PLV synthesis in both maize and Arabidopsis. We next focused on the impact of PLV-mediated signaling on maize defense.

PLVs Induce Maize Resistance to *C. graminicola*

Recently, we had shown that GLVs act as potent promoters of susceptibility to the causal agent of anthracnose disease in maize, *C. graminicola*, a fungal pathogen with a hemi-biotrophic life style (Gorman et al., 2020). Because PLVs are often co-emitted with GLVs (Fall et al., 2001; Heiden et al., 2003; Jardine et al., 2012; He et al., 2020), we examined the role of these volatiles in maize-*C. graminicola* interactions. To determine the impact of PLVs on *C. graminicola* infection, we pre-treated WT and PLV-deficient *lox10-3* mutants with a PLV mixture containing the primary PLVs, (2*Z*)-pentenol and 1-penten-3-ol, before inoculating their leaves. Plants were exposed to these volatiles for 2 h, and inoculated with spores of *C. graminicola* 1 h after volatile exposure ended. Surprisingly, we found that PLV treatment significantly increased resistance in WT B73 and W438 (**Figure 4**), the opposite effect observed after GLV treatment (Gorman et al., 2020). Surprisingly, *lox10-3* mutants in both backgrounds, which already display resistance to *C. graminicola* (Gorman et al., 2020; Wang et al., 2020a), had their resistance further enhanced by PLV exposure (**Figure 4**). Previously, we had shown that *lox10-3* mutant resistance is due to low levels of the biologically active jasmonate, jasmonic acid-isoleucine (JA-Ile), and elevated concentrations of salicylic acid (SA), the phytohormone known to govern resistance against (hemi)-biotrophic pathogens. Furthermore, we found that exogenous application of SA was unable to induce further resistance in these mutants (Gorman et al., 2020). This suggests

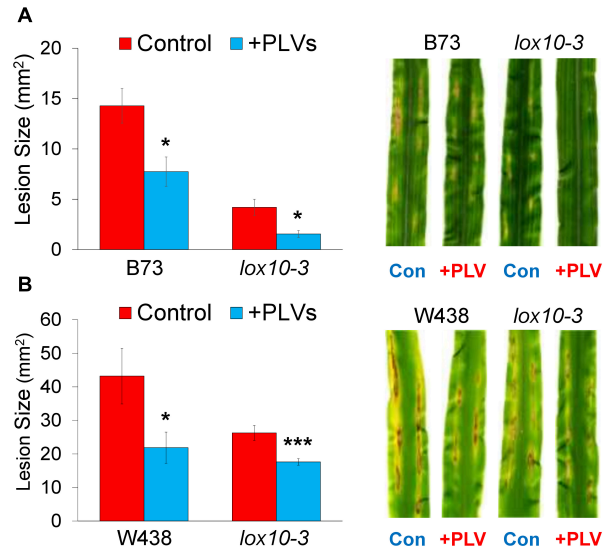

FIGURE 4 | Exogenous treatment with PLVs induces resistance of maize to *C. graminicola*. graph shows the mean area of lesions after inoculation of WT and *lox10-3* mutants in the B73 **(A)** and W438 **(B)** backgrounds after treatment with a PLV mixture containing (2*Z*)-pentenol and 1-penten-3-ol dissolved in triacetin, or control treatment (triacetin). Leaves were harvested after 7 dpi. Student's *t*-test was performed to determine statistical significance of lesion areas between control and PLV-treated plants within each genotype (*$p < 0.005$, ***$p < 0.0001$) ($n = 6$).

that SA-mediated resistance is already saturated in these mutants. Taking this into account, it is likely that PLV-mediated induction of resistance is not related to increases or decreases of SA or JA-Ile, respectively.

PLV-Mediated Resistance to *C. graminicola* Correlates With Increased Synthesis of Oxylipin Hydroxides and α- and γ-Ketols

In order to further investigate the potential biochemical mechanisms underlying PLV-mediated resistance to *C. graminicola* in maize, we used liquid chromatography mass spectrometry to measure a variety of different phytohormones and oxylipin metabolites in maize leaves infected with *C. graminicola* after treatment with PLVs. As hypothesized, the levels of JA-Ile and SA were not different between control and PLV-treated plants (**Supplementary Figure 2**). However, several 9- and 13-LOX-derived α- and γ-ketols, produced in the allene oxide synthase (AOS) branch of the LOX pathway, were higher in the infected plants exposed to PLVs (**Figure 5A**). Most ketols appeared to be elevated in the PLV-treated plants throughout the duration of infection, but many of these ketols, including 9-hydroxy-10-oxo-(12*Z*,15*Z*)-octadecadienoic acid (9,10-KODA), 9-hydroxy-12-oxo-(10*E*,15*Z*)-octadecadienoic acid (9,12-KODA), 13-hydroxy-12-oxo-(9*Z*,15*Z*)-octadecadienoic acid (13,12-KODA), and 13-hydroxy-12-oxo-(9*Z*)-octadecadienoic acid (13,12-KOMA), were most significantly increased at 1 day post inoculation (dpi). 9-hydroxy-12-oxo-(10*E*)-octadecenoic acid (9,12-KOMA) appeared to be higher at most timepoints in infected PLV-treated plants, but was not statistically higher, though it was close at 1 dpi ($p = 0.0697$) and 6 dpi ($p = 0.0805$). Only 13-hydroxy-10-oxo-(11*E*,15*Z*)-octadecadienoic acid (13,10-KODA) did not come close to statistical difference at this timepoint, but was significantly higher in PLV-treated plants at 4 dpi. Importantly, we have previously shown that exogenous treatments with several of these ketols, including the α-ketol 9,10-KODA (Wang et al., 2020a), and the γ-ketols, 9,12-KOMA and 9,12-KODA (Wang et al., 2020b), strongly increase maize resistance to *C. graminicola*.

In addition to LOX-derived oxylipin ketols, several 13*S*-HPOT-derived oxylipin hydroxytrienes and ketotrienes were increased in PLV-treated plants throughout the course of infection (**Figure 5B**). Other oxylipins were also increased over the course of infection in plants exposed to PLVs. This includes 9-hydroxy-(10*E*,12*Z*,15*Z*)-octadecatrienoic acid (9-HOT) and 13-hydroxy-(9*Z*,11*E*,15*Z*)-octadecatrienoic acid (13-HOT), produced in the reductase (RED) and peroxygenase (POX) branches of the LOX pathway (Blée, 2002), and 9-oxo-(10*E*,12*Z*,15*Z*)-octadecatrienoic acid (9-KOT) and 13-oxo-(9*Z*,11*E*,15*Z*)-octadecatrienoic acid (13-KOT), which are produced in the LOX (Vollenweider et al., 2000), RED, and POX (Chechetkin et al., 2004) branches of the LOX pathway. Collectively, the greatest differences in these oxylipins between control and PLV-treated plants were observed at the two latest timepoints, 4 and 6 dpi, though there were some exceptions. 9-HOT was already induced by PLV treatment prior to infection, 0 dpi, but was not statistically higher at later timepoints, though it was close at 4 dpi ($p = 0.0636$) and 6 dpi ($p = 0.0680$). Additionally, while 13-KOT was statistically higher in PLV-treated plants at 6 dpi, it was not at 4 dpi. Lastly, 9,10,13-trihydroxy-(11*E*,15*Z*)-octadecadienoic acid (9,10,13-THOD) and 9,12,13-trihydroxy-(10*E*,15*Z*)-octadecadienoic acid (9,12,13-THOD), two trihydroxydienes produced in the epoxy alcohol synthase (EAS) branch of the LOX pathway (Blée, 2002), were also higher at 4 and 6 dpi in PLV-treated plants (**Figure 5C**). Collectively, these results suggest that several oxylipins, including α- and γ-ketols, ketotrienes, hydroxytrienes, and trihydroxydienes, are involved in PLV-mediated defense against *C. graminicola* in maize.

DISCUSSION

Pentyl leaf volatiles represent a widely emitted group of plant volatiles, though little is known regarding their synthesis or biological roles. Aspects of PLV metabolism had been previously hypothesized (Gardner et al., 1996), but lacked a full experimental examination of the pathway. In order to determine the biosynthetic order of individual PLVs, we exposed both maize and Arabidopsis to exogenous PLVs and analyzed subsequent PLV emissions. Deuterated exogenous PLV standard are not available, therefore, in order to demostrate that PLVs detected in these experiments were from exogenous PLV standards and not endogenous PLVs, we applied high concentrations of exogenous PLVs and employed the use of

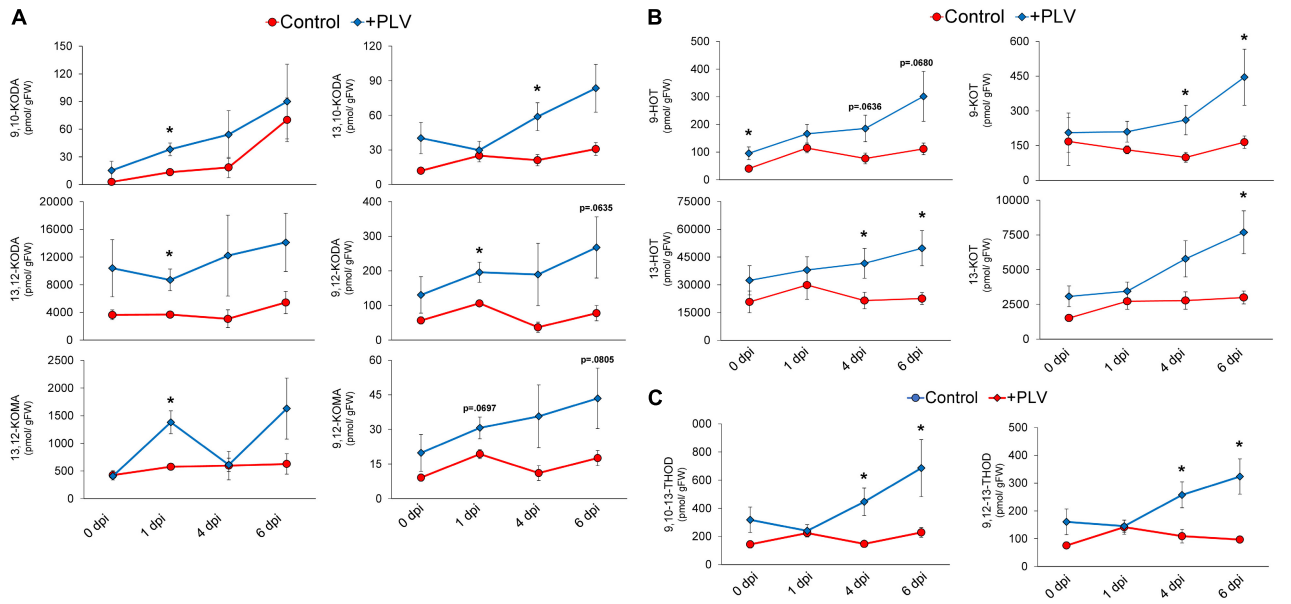

FIGURE 5 | Pentyl leaf volatiles induce synthesis of oxylipin ketols, hydroxytrienes, ketotrienes, and trihydroxydienes in response to *C. graminicola* infection. The graph shows the mean amount of various oxylipin ketols **(A)** and hydroxytrienes and ketotrienes **(B)** and trihydroxydienes **(C)** throughout *C. graminicola* infection of B73 leaves after treatment with a PLV mixture [(2*Z*)-pentenol and 1-penten-3-ol] dissolved in triacetin, or control treatment (triacetin). Plants were exposed to treatments for 2 h prior to inoculation and inoculated with *C. graminicola* spores 1 h after volatile exposure was halted. Oxylipins were analyzed after 1, 4, and 6 days post inoculation (dpi), as well as before infection, 0 dpi. Student's *t*-test was performed to determine statistical significance between control and PLV-treated plants at each timepoint ($p < 0.05$) ($n = 6$).

PLV-deficient mutants in both maize, *lox10-3* (He et al., 2020) and Arabidopsis, *Atlox2-1* (Mochizuki et al., 2016). Treatment with (2*Z*)-pentenol and 1-penten-3-ol produced most other PLVs (**Tables 2–5**), validating their predicted status as primary PLVs (Salch et al., 1995). Importantly, no exogenous PLV treatments resulted in the production of either of these volatiles, suggesting that PLV-mediated signaling does not induce PLV biosynthesis. This observation, in addition to the utilization of PLV-deficient mutants, confirmed that PLVs detected after treatment are derived from exogenous PLVs. The artificially high amount of PLVs used in these experiments also made it necessary to determine which PLVs detected in these experiments were a result of plant absorption, metabolism, and re-emission, and which were produced by non-enzymatic degradation unrelated to plant tissues. By incubating PLVs in the absence of plants, we identified several artificial PLVs (**Table 1**), including pentanoic acid, but(en)yl formates, 3-methyl-2-pentanone, and excluded them from further analyses. We also identified several PLVs that were non-enzymatically synthesized, but have been previously reported to be emitted by plant tissues (Shen et al., 2014; Mochizuki et al., 2016; He et al., 2020). Though these PLVs are able to be non-enzymatically generated, the impact of enzymatic vs. non-enzymatic synthesis of these PLVs *in planta* is difficult to discern, as PLVs are known to be sequestered in plant tissues by binding to non-volatile metabolites (Sugimoto et al., 2015).

Treatment with all PLV alcohols, including (2*Z*)-pentenol, (2*E*)-pentenol, 1-penten-3-ol, and pentanol, resulted in their oxidation to their respective aldehyde and ketone derivatives (**Tables 2–5**). Previously, generation of (2*Z*)-pentenal and (2*E*)-pentenal from (2*Z*)-pentenol was reported to be catalyzed by an ADH(s) (Gardner et al., 1996), however, we also found that non-enzymatic generation plays a part in their generation (**Table 1**). This was also true of pentanal and 3-pentanone generated from pentanol and 3-pentanol, respectively. Prior analysis of atmospheric decomposition by PLV alcohols supports these findings (Orlando et al., 2001). Interestingly, while conversion of (2*E*)-pentenol to (2*E*)-pentenal occurred, the opposite reaction also occurred, suggesting that stoichiometry dictates the observed reaction (**Tables 2–5**). This was also true of pentanol and pentanal. Interestingly, various alkene PLVs were reduced to alkanes. This was unexpected, as reduction of carbon-carbon double bonds in GLVs, which are better characterized and similarly structured (**Figure 1**), has not been reported. These reactions seemed to be largely driven by spontaneous, non-enzymatic decomposition of PLVs (**Table 1**), though this does not rule out the possible existence of a PLV-specific reductase. Similar to GLVs, PLV alcohols are able to be metabolized into more chemically stable acetate conjugates (**Tables 2–5**), likely through the activity of the same AT(s). Notably, the relevant ATs are more active on PLV alkenes than alkanes, and requires PLV substrate to possess a terminal hydroxyl group. In response to 1-penten-3-ol and 3-pentanol, 1-penten-3-one and 3-pentanone appeared more readily synthesized by Arabidopsis (**Tables 2–5** and **Figure 2**). Conversely, maize seemed to produce more PLV acetate conjugates in response to volatile treatments. These observations were supported by observations of volatile emissions between the two species (**Figure 3**). These observations suggest selective pressure on PLV synthesis in plants for, as

of yet, unknown purposes. When comparing the overall effect of ZmLOX10 and AtLOX2 on PLV metabolism in maize and Arabidopsis, respectively, the only notable difference was the relative quantity of PLV acetates, with both mutants possessing lesser proportions of these volatiles in response to treatment with various PLV alcohols (**Figure 2**). Both of these LOX isoforms are the major 13-oxylipin producers in their respective species, and one or many of these oxylipins could directly or indirectly affect expression or function of AT(s) relevant to GLV and PLV synthesis. Based on these collective results, we have summarized the biosynthetic pathway of PLVs in **Figure 6**.

GLV and PLV analysis of wounded and freeze-thawed leaves of maize and Arabidopsis helped establish the biosynthetic order of PLVs, as well as identify PLVs that are most likely relevant to biological processes. We found that wounding of both species resulted in emission of several GLVs and PLVs (**Figure 3**). We were surprised to find GLV emissions in Arabidopsis Col-0, which was reported to possess a natural mutation in its AtHPL1 gene that renders it non-functional (Duan et al., 2005), though the quantities were very low. This analysis also confirmed that ZmLOX10 is critical for GLV and PLV synthesis in both the W438 and B73 backgrounds (Christensen et al., 2013; He et al., 2020). We also identified a GLV, (2*Z*)-hexenal, and a PLV, (2*Z*)-pentenyl acetate, that have not been previously reported to be emitted by plants. Furthermore, these volatiles were emitted by both Arabidopsis and maize. Emissions of (2*Z*)-pentenol and (2*E*)-pentenal in both species strongly correlated, but not with (2*E*)-pentenol. This indicates that (2*E*)-pentenol is likely derived from (2*E*)-pentenal, which is in turn derived from (2*Z*)-pentenol, rather than from (2*Z*)-pentenol directly. Several PLVs identified in the PLV metabolism assays were not found in volatile analysis of plant tissues, including (2*E*)-pentenyl acetate, pentyl acetate, and 3-pentanol (**Figure 3**). This suggests that they are likely only synthesized and emitted in trace quantities.

Another important finding from this study is that the widely used method of volatile analyses by freeze-thawing tissues may lead to consequential distortions of volatile profiles. These two methods differ in the number of cells they disrupt, with freeze-thawing disturbing all cells in the leaf tissue and wounding disturbing a fewer number of cells. Volatile elicitation by complete tissue disruption, including freeze-thawing, is often used for analysis of volatiles, despite that it has been previously reported to eliminate emissions of GLV alcohols, likely through inactivation of enzymes involved in volatile metabolism, such as ADH (Fall et al., 2001; Matsui et al., 2012) and CHR (Tanaka et al., 2018). ADHs (Bate et al., 1998; Speirs et al., 1998) and CHR (Tanaka et al., 2018), which utilize the cofactors NADH and NADPH, respectively, are known to facilitate conversion of GLV aldehydes to alcohols. Importantly, CHR was found to be more important for metabolism of aldehydes in intact tissues (Tanaka et al., 2018). ADHs are also reported to convert PLV alcohols to aldehydes (Gardner et al., 1996), though very little is known about these enzymes. Thus, we expected emission of PLV aldehydes and GLV alcohols and acetate conjugates to be low in response to freeze-thawing. This hypothesis was only partially supported, with freeze-thawing resulting in significantly diminished levels of GLV alcohols and acetates (**Figure 3**). Conversely, both GLV and PLV aldehydes, as well as PLV alcohols, were increased in response to freeze-thawing (**Figure 3**). This suggests that despite ADHs having reported activity in both GLV and PLV metabolism, and the structural similarity of these two groups, these reactions are potentially catalyzed by different enzymes. GLV and PLV alcohols did not share similar responses to freeze-thawing, but emissions of acetate conjugates of both groups were significantly reduced (**Figure 3**). This suggests that the AT(s) that acts on GLVs may also metabolize PLVs. Additionally, since (2*Z*)-pentenyl acetate is derived from (2*Z*)-pentenol, which was more highly emitted after freeze-thawing, these results suggest that function of both ADHs and ATs are negatively impacted by freezing. The exact identity of the enzymes involved in PLV metabolism remains unknown and should be further investigated. ADHs and BAHD ATs constitute large families of enzymes, making it likely that a wide range of volatiles are impacted by freeze-thawing. Taking this into account, utilization of freeze-thawing to elicit volatile emissions should be used with caution in the future.

Though GLVs and PLVs are often co-emitted, they also share clear antagonism. This is evidenced by increases in PLV emission in *hpl* mutants (Vancanneyt et al., 2001; Salas et al., 2006; Shen et al., 2014). Since GLV and PLV synthesis requires substrate from the same LOXs, this is not surprising. Previously, both GLVs and PLVs have been implicated in susceptibility (Scala et al., 2013) and resistance (Song et al., 2015) of Arabidopsis to infection by *P. syringae*, respectively. In this study, we found that PLVs induced greater resistance to *C. graminicola* in two inbred backgrounds of maize (**Figure 4**). Furthermore, PLVs were able to further enhance resistance in already-resistant *lox10-3* mutants in both inbred backgrounds. Previously, we revealed that GLVs strongly promoted anthracnose disease progression caused by this same pathogen through induction of JA-Ile and suppression of SA (Gorman et al., 2020). Upon investigation of the biochemical mechanisms underlying PLV-mediated resistance, we did not find that JA-Ile or SA levels were significantly altered in PLV-treated plants at any point throughout infection (**Supplementary Figure 2**). Despite this, it is still possible these phytohormones are involved in PLV-mediated responses to other stresses. However, we did find that a variety of LOX-derived oxylipins, including α- and γ-ketols, ketotrienes, hydroxytrienes, and trihydroxydienes, were increased in PLV-treated plants throughout the time course of infection (**Figure 5**). Though there were slight differences, most ketols were significantly increased at the earliest timepoint after inoculation, 1 dpi (**Figure 5A**). Contrarily, ketotrienes, hydroxytrienes, and trihydroxydienes were, overall, significantly elevated in PLV-treated plants at later timepoints in the infection process, 4 and 6 dpi (**Figures 5B,C**). We previously showed that the α-ketol 9,10-KODA (Wang et al., 2020a), and the γ-ketols, 9,12-KOMA and 9,12-KODA (Wang et al., 2020b), act as potent priming agents that induce resistance to *C. graminicola*. The ketotriene, 9-KOT, has been shown to provide resistance to pathogens (Vicente et al., 2012) as well as inhibit their *in vitro* vegetative growth (Prost et al., 2005). The hydroxytriene, 9-HOT, is involved in the regulation of defense gene expression (Vellosillo et al., 2007). Importantly, *C. graminicola* switches from a phase of biotrophic growth to necrotrophic growth approximately

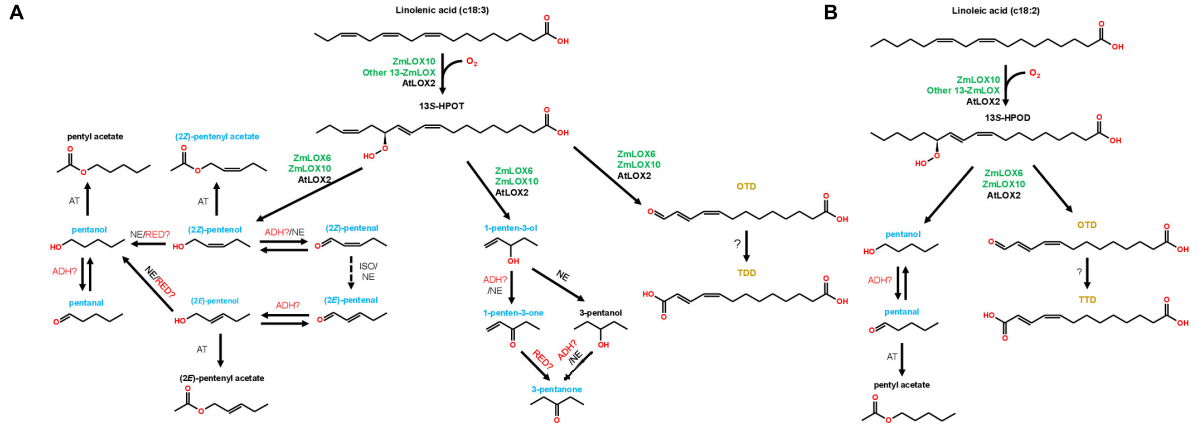

FIGURE 6 | Working model of the PLV pathway in maize (green gene names) and Arabidopsis (black gene names). The graph shows both C18:3-derived **(A)** and C18:2-derived **(B)** PLV synthesis. Dashed arrows indicate hypothetical reactions. Alcohol dehydrogenase (ADH), acetyl transferase (AT), reductase (RED), non-enzymatic (NE), isomerase (ISO). The names of biologically relevant PLVs are blue, the names of trace PLVs are black, and the names of 13-carbon compounds (Gao et al., 2008) are orange. Adapted from Gardner et al. (1996).

48–72 h after inoculation, where it begins to form visible lesions (Bergstrom and Nicholson, 1999; Mims and Vaillancourt, 2002; Vargas et al., 2012). Collectively, these results indicate that ketols may be effective at mediating resistance to this pathogen during the biotrophic phase of infection by *C. graminicola*, and ketotrienes, hydroxytrienes, and trihydroxydienes may be involved in defense during its necrotrophic phase of growth. Determining the specific roles of these oxylipins in maize-*C. graminicola* interactions should be the subject of future studies. These results support previous findings that PLVs induce resistance to biotrophic and hemi-biotrophic pathogens (Song and Ryu, 2013; Choi et al., 2014; Song et al., 2015), and provide another example of their antagonism to GLVs.

Green leaf volatiles emissions are known to significantly vary in composition and abundance across the plant kingdom (Engelberth and Engelberth, 2020), and this is likely also the case for PLV emissions because of their biosynthetic antagonism with GLVs (Vancanneyt et al., 2001; Salas et al., 2006; Shen et al., 2014). These differences in volatile emissions are likely a result of selective pressures that each plant species has faced throughout their respective evolutionary histories. For example, GLVs mediate maize susceptibility to *C. graminicola* and other hemi-biotrophic pathogens (Gorman et al., 2020; Wang et al., 2020a), but GLVs are critical for defense against insect herbivory (Rojas et al., 2018). Maize is one of the highest GLV-producing monocots (Engelberth and Engelberth, 2020) and has historically experienced significant insect herbivory, suggesting that GLV-mediated susceptibility to *C. graminicola* could be an unintended consequence of evolutionary response to insect pressure or breeding efforts. Oppositely, there are some plants that emit little-to-no GLVs (Engelberth and Engelberth, 2020), and are therefore likely to have increased PLV emissions, which could be a consequence of greater biotrophic or hemi-biotrophic pathogen pressures. As of now, these hypotheses remain untested, and should be the focus of future studies.

This work provides a solid framework of the PLV metabolic pathway in plants that future studies can build upon to elucidate the enzymes involved in PLV synthesis, and establish additional biological effects of these volatiles. Importantly, this work suggests that structure of the PLV pathway is conserved across diverse plant species, but that the enzymes involved in PLV metabolism can vary, even across different genetic backgrounds of the same species. This suggests selective pressure on PLV synthesis, which is supported by their ability to induce resistance to pathogens and insects, including the economically costly maize pathogen, *C. graminicola*. Ultimately, this work will facilitate future studies into this widely emitted, yet enigmatic group of oxylipin volatiles.

DATA AVAILABILITY STATEMENT

The original contributions presented in the study are included in the article/**Supplementary Material**, further inquiries can be directed to the corresponding author.

AUTHOR CONTRIBUTIONS

ZG and MK designed the all experiments. ZG executed the all experiments, performed the all analyses, and wrote the manuscript. JT grew and screened Arabidopsis for the experiments. All the authors reviewed the manuscript.

FUNDING

This study was supported by USDA-NIFA (2017-67013-26524) grant awarded to MK.

SUPPLEMENTARY MATERIAL

The Supplementary Material for this article can be found online at: https://www.frontiersin.org/articles/10.3389/fpls.2021.719587/full#supplementary-material

REFERENCES

Allmann, S., and Baldwin, I. T. (2010). Insects betray themselves in nature to predators by rapid isomerization of green leaf volatiles. *Science* 329, 1075–1078. doi: 10.1126/science.1191634

Alméras, E., Stolz, S., Vollenweider, S., Reymond, P., Mène-Saffrané, L., and Farmer, E. E. (2003). Reactive electrophile species activate defense gene expression in *Arabidopsis*. *Plant J.* 34, 205–216.

Ameye, M., Allmann, S., Verwaeren, J., Smagghe, G., Haesaert, G., Schuurink, R. C., et al. (2018). Green leaf volatile production by plants: a meta-analysis. *New Phytol.* 220, 666–683. doi: 10.1111/nph.14671

Bate, N. J., Riley, J. C., Thompson, J. E., and Rothstein, S. J. (1998). Quantitative and qualitative differences in C6-volatile production from the lipoxygenase pathway in an alcohol dehydrogenase mutant of *Arabidopsis thaliana*. *Physiol. Plant.* 104, 97–104. doi: 10.1034/j.1399-3054.1998.1040113.x

Bergstrom, G. C., and Nicholson, R. L. (1999). The biology of corn anthracnose: knowledge to exploit for improved management. *Plant Dis.* 83, 596–608. doi: 10.1094/pdis.1999.83.7.596

Blée, E. (2002). Impact of phyto-oxylipins in plant defense. *Trends Plant Sci.* 7, 315–322. doi: 10.1016/s1360-1385(02)02290-2

Chechetkin, I. R., Medvedeva, N. V., and Grechkin, A. N. (2004). The novel pathway for ketodiene oxylipin biosynthesis in Jerusalem artichoke (*Helianthus tuberosus*) tubers. *Biochim. Biophys. Acta BBA Mol. Cell Biol. Lipids* 1686, 7–14. doi: 10.1016/j.bbalip.2004.07.001

Choi, H. K., Song, G. C., Yi, H. S., and Ryu, C. M. (2014). Field evaluation of the bacterial volatile derivative 3-pentanol in priming for induced resistance in pepper. *J. Chem. Ecol.* 40, 882–892. doi: 10.1007/s10886-014-0488-z

Christensen, S. A., Nemchenko, A., Borrego, E., Murray, I., Sobhy, I. S., Bosak, L., et al. (2013). The maize lipoxygenase, ZmLOX10, mediates green leaf volatile, jasmonate and herbivore-induced plant volatile production for defense against insect attack. *Plant J.* 74, 59–73. doi: 10.1111/tpj.12101

D'Auria, J. C., Pichersky, E., Schaub, A., Hansel, A., and Gershenzon, J. (2007). Characterization of a BAHD acyltransferase responsible for producing the green leaf volatile (Z)-3-hexen-1-yl acetate in *Arabidopsis thaliana*. *Plant J.* 49, 194–207. doi: 10.1111/j.1365-313x.2006.02946.x

Duan, H., Huang, M. Y., Palacio, K., and Schuler, M. A. (2005). Variations in CYP74B2 (hydroperoxide lyase) gene expression differentially affect hexenal signaling in the Columbia and Landsberg erecta ecotypes of *Arabidopsis*. *Plant Physiol.* 139, 1529–1544. doi: 10.1104/pp.105.067249

Engelberth, J., Alborn, H. T., Schmelz, E. A., and Tumlinson, J. H. (2004). Airborne signals prime plants against insect herbivore attack. *Proc. Natl. Acad. Sci. U.S.A.* 101, 1781–1785. doi: 10.1073/pnas.0308037100

Engelberth, J., and Engelberth, M. (2020). Variability in the capacity to produce damage-induced aldehyde green leaf volatiles among different plant species provides novel insights into biosynthetic diversity. *Plants* 9:213. doi: 10.3390/plants9020213

Fall, R., Karl, T., Jordan, A., and Lindinger, W. (2001). Biogenic C5 VOCs: release from leaves after freeze–thaw wounding and occurrence in air at a high mountain observatory. *Atmos. Environ.* 35, 3905–3916. doi: 10.1016/s1352-2310(01)00141-8

Fisher, A. J., Grimes, H. D., and Fall, R. (2003). The biochemical origin of pentenol emissions from wounded leaves. *Phytochemistry* 62, 159–163. doi: 10.1016/s0031-9422(02)00521-6

Gao, X., Shim, W. B., Göbel, C., Kunze, S., Feussner, I., Meeley, R., et al. (2007). Disruption of a maize 9-lipoxygenase results in increased resistance to fungal pathogens and reduced levels of contamination with mycotoxin fumonisin. *Mol. Plant Microbe Interact.* 20, 922–933. doi: 10.1094/mpmi-20-8-0922

Gao, X., Stumpe, M., Feussner, I., and Kolomiets, M. (2008). A novel plastidial lipoxygenase of maize (Zea mays) ZmLOX6 encodes for a fatty acid hydroperoxide lyase and is uniquely regulated by phytohormones and pathogen infection. *Planta* 227, 491–503. doi: 10.1007/s00425-007-0634-8

Gardner, H. W., Grove, M. J., and Salch, Y. P. (1996). Enzymic pathway to ethyl vinyl ketone and 2-pentenal in soybean preparations. *J. Agric. Food Chem.* 44, 882–886. doi: 10.1021/jf950509r

Glauser, G., Dubugnon, L., Mousavi, S. A., Rudaz, S., Wolfender, J. L., and Farmer, E. E. (2009). Velocity estimates for signal propagation leading to systemic jasmonic acid accumulation in wounded *Arabidopsis*. *J. Biol. Chem.* 284, 34506–34513. doi: 10.1074/jbc.m109.061432

Gorman, Z., Christensen, S. A., Yan, Y., He, Y., Borrego, E., and Kolomiets, M. V. (2020). Green leaf volatiles and jasmonic acid enhance susceptibility to anthracnose diseases caused by *Colletotrichum graminicola* in maize. *Mol. Plant Pathol.* 21, 702–715. doi: 10.1111/mpp.12924

Hatanaka, A. (1993). The biogeneration of green odour by green leaves. *Phytochemistry* 34, 1201–1218. doi: 10.1016/0031-9422(91)80003-j

He, Y., Borrego, E. J., Gorman, Z., Huang, P. C., and Kolomiets, M. V. (2020). Relative contribution of LOX10, green leaf volatiles and JA to wound-induced local and systemic oxylipin and hormone signature in Zea mays (maize). *Phytochemistry* 174:112334. doi: 10.1016/j.phytochem.2020.112334

Heiden, A. C., Kobel, K., Langebartels, C., Schuh-Thomas, G., and Wildt, J. (2003). Emissions of oxygenated volatile organic compounds from plants Part I: emissions from lipoxygenase activity. *J. Atmos. Chem.* 45, 143–172.

Jardine, K., Barron-Gafford, G. A., Norman, J. P., Abrell, L., Monson, R. K., Meyers, K. T., et al. (2012). Green leaf volatiles and oxygenated metabolite emission bursts from mesquite branches following light–dark transitions. *Photosynth. Res.* 113, 321–333. doi: 10.1007/s11120-012-9746-5

Kobayashi, A., Tsuda, Y., Hirata, N., Kubota, K., and Kitamura, K. (1995). Aroma constituents of soybean [*Glycine max* (L.) Merril] milk lacking lipoxygenase isoenzymes. *J. Agric. Food Chem.* 43, 2449–2452. doi: 10.1021/jf00057a025

Kunishima, M., Yamauchi, Y., Mizutani, M., Kuse, M., Takikawa, H., and Sugimoto, Y. (2016). Identification of (Z)-3:(E)-2-hexenal isomerases essential to the production of the leaf aldehyde in plants. *J. Biol. Chem.* 291, 14023–14033. doi: 10.1074/jbc.m116.726687

López-Gresa, M. P., Payá, C., Ozáez, M., Rodrigo, I., Conejero, V., Klee, H., et al. (2018). A new role for green leaf volatile esters in tomato stomatal defense against *Pseudomonas syringe* pv. tomato. *Front. Plant Sci.* 9:1855. doi: 10.3389/fpls.2018.01855

Loughrin, J. H., Manukian, A., Heath, R. R., and Tumlinson, J. H. (1995). Volatiles emitted by different cotton varieties damaged by feeding beet armyworm larvae. *J. Chem. Ecol.* 21, 1217–1227. doi: 10.1007/bf02228321

Matsui, K. (2006). Green leaf volatiles: hydroperoxide lyase pathway of oxylipin metabolism. *Curr. Opin. Plant Biol.* 9, 274–280. doi: 10.1016/j.pbi.2006.03.002

Matsui, K., Sugimoto, K., Mano, J. I., Ozawa, R., and Takabayashi, J. (2012). Differential metabolisms of green leaf volatiles in injured and intact parts of a wounded leaf meet distinct ecophysiological requirements. *PLoS One* 7:e36433. doi: 10.1371/journal.pone.0036433

Matsui, K., Ujita, C., Fujimoto, S. H., Wilkinson, J., Hiatt, B., Knauf, V., et al. (2000). Fatty acid 9-and 13-hydroperoxide lyases from cucumber. *FEBS lett.* 481, 183–188. doi: 10.1016/s0014-5793(00)01997-9

Mims, C. W., and Vaillancourt, L. J. (2002). Ultrastructural characterization of infection and colonization of maize leaves by *Colletotrichum graminicola*, and by a *C. graminicola* pathogenicity mutant. *Phytopathology* 92, 803–812. doi: 10.1094/phyto.2002.92.7.803

Mochizuki, S., Sugimoto, K., Koeduka, T., and Matsui, K. (2016). *Arabidopsis* lipoxygenase 2 is essential for formation of green leaf volatiles and five-carbon volatiles. *FEBS Lett.* 590, 1017–1027. doi: 10.1002/1873-3468.12133

Mukhtarova, L. S., Brühlmann, F., Hamberg, M., Khairutdinov, B. I., and Grechkin, A. N. (2018). Plant hydroperoxide-cleaving enzymes (CYP74 family) function as hemiacetal synthases: structural proof of hemiacetals by NMR spectroscopy.

Biochim. Biophys. Acta BBA Mol. Cell Biol. Lipids 1863, 1316–1322. doi: 10.1016/j.bbalip.2018.08.011

Orlando, J. J., Tyndall, G. S., and Ceazan, N. (2001). Rate coefficients and product yields from reaction of OH with 1-penten-3-ol, (Z)-2-penten-1-ol, and allyl alcohol (2-propen-1-ol). *J. Phys. Chem. A* 105, 3564–3569. doi: 10.1021/jp0041712

Prost, I., Dhondt, S., Rothe, G., Vicente, J., Rodriguez, M. J., Kift, N., et al. (2005). Evaluation of the antimicrobial activities of plant oxylipins supports their involvement in defense against pathogens. *Plant Physiol.* 139, 1902–1913. doi: 10.1104/pp.105.066274

Roberts, J. M., Kundun, J., Rowley, C., Hall, D. R., Douglas, P., and Pope, T. W. (2019). Electrophysiological and behavioral responses of adult vine weevil, *Otiorhynchus sulcatus* (Coleoptera: Curculionidae), to host plant odors. *J. Chem. Ecol.* 45, 858–868. doi: 10.1007/s10886-019-01108-x

Rojas, J. C., Kolomiets, M. V., and Bernal, J. S. (2018). Nonsensical choices? Fall armyworm moths choose seemingly best or worst hosts for their larvae, but neonate larvae make their own choices. *PloS One* 13:e0197628. doi: 10.1371/journal.pone.0197628

Salas, J. J., García-González, D. L., and Aparicio, R. (2006). Volatile compound biosynthesis by green leaves from an *Arabidopsis thaliana* hydroperoxide lyase knockout mutant. *J. Agric. Food Chem.* 54, 8199–8205. doi: 10.1021/jf061493f

Salch, Y. P., Grove, M. J., Takamura, H., and Gardner, H. W. (1995). Characterization of a C-5, 13-cleaving enzyme of 13 (S)-hydroperoxide of linolenic acid by soybean seed. *Plant Physiol.* 108, 1211–1218. doi: 10.1104/pp.108.3.1211

Scala, A., Mirabella, R., Mugo, C., Matsui, K., Haring, M. A. and Schuurink, R. C. (2013). E-2-hexenal promotes susceptibility to Pseudomonas syringae by activating jasmonic acid pathways in *Arabidopsis*. *Front. Plant Sci.* 4:74. doi: 10.3389/fpls.2013.00074

Schneider, C. A., Rasband, W. S., and Eliceiri, K. W. (2012). NIH image to imageJ: 25 years of image analysis. *Nat. Methods* 9:671. doi: 10.1038/nmeth.2089

Seo, H. S., Song, J. T., Cheong, J. J., Lee, Y. H., Lee, Y. W., Hwang, I., et al. (2001). Jasmonic acid carboxyl methyltransferase: a key enzyme for jasmonate-regulated plant responses. *Proc. Natl. Acad. Sci. U.S.A.* 98, 4788–4793. doi: 10.1073/pnas.081557298

Shen, J., Tieman, D., Jones, J. B., Taylor, M. G., Schmelz, E., Huffaker, A., et al. (2014). A 13-lipoxygenase, TomloxC, is essential for synthesis of C5 flavour volatiles in tomato. *J. Exp. Bot.* 65, 419–428. doi: 10.1093/jxb/ert382

Song, G. C., Choi, H. K., and Ryu, C. M. (2015). Gaseous 3-pentanol primes plant immunity against a bacterial speck pathogen, *Pseudomonas syringae* pv. tomato via salicylic acid and jasmonic acid-dependent signaling pathways in *Arabidopsis*. *Front. Plant Sci.* 6:821. doi: 10.3389/fpls.2015.00821

Song, G. C., and Ryu, C. M. (2013). Two volatile organic compounds trigger plant self-defense against a bacterial pathogen and a sucking insect in cucumber under open field conditions. *Int. J. Mol. Sci.* 14, 9803–9819. doi: 10.3390/ijms14059803

Speirs, J., Lee, E., Holt, K., Yong-Duk, K., Scott, N. S., Loveys, B., et al. (1998). Genetic manipulation of alcohol dehydrogenase levels in ripening tomato fruit affects the balance of some flavor aldehydes and alcohols. *Plant Physiol.* 117, 1047–1058. doi: 10.1104/pp.117.3.1047

Spyropoulou, E. A., Dekker, H. L., Steemers, L., van Maarseveen, J. H., de Koster, C. G., Haring, M. A., et al. (2017). Identification and characterization of (3Z):(2E)-hexenal isomerases from cucumber. *Front. Plant Sci.* 8:1342. doi: 10.3389/fpls.2017.01342

Sugimoto, K., Matsui, K., and Takabayashi, J. (2015). Conversion of volatile alcohols into their glucosides in *Arabidopsis*. *Commun. Integr. Biol.* 8:e992731. doi: 10.4161/19420889.2014.992731

Tanaka, T., Ikeda, A., Shiojiri, K., Ozawa, R., Shiki, K., Nagai-Kunihiro, N., et al. (2018). Identification of a hexenal reductase that modulates the composition of green leaf volatiles. *Plant Physiol.* 178, 552–564. doi: 10.1104/pp.18.00632

van Den Dool, H., and Kratz, P. D. (1963). A generalization of the retention index system including linear temperature programmed gas-liquid partition chromatography. *J. Chromatogr.* 11, 463–471. doi: 10.1016/s0021-9673(01)80947-x

van Tol, R. W., Bruck, D. J., Griepink, F. C., and De Kogel, W. J. (2012). Field attraction of the vine weevil *Otiorhynchus sulcatus* to kairomones. *J. Econ. Entomol.* 105, 169–175. doi: 10.1603/ec11248

Vancanneyt, G., Sanz, C., Farmaki, T., Paneque, M., Ortego, F., Castañera, P., et al. (2001). Hydroperoxide lyase depletion in transgenic potato plants leads to an increase in aphid performance. *Proc. Natl. Acad. Sci. U.S.A.* 98, 8139–8144. doi: 10.1073/pnas.141079498

Vargas, W. A., Martín, J. M. S., Rech, G. E., Rivera, L. P., Benito, E. P., Díaz-Mínguez, J. M., et al. (2012). Plant defense mechanisms are activated during biotrophic and necrotrophic development of *Colletotricum graminicola* in maize. *Plant Physiol.* 158, 1342–1358. doi: 10.1104/pp.111.190397

Vellosillo, T., Martínez, M., López, M. A., Vicente, J., Cascón, T., Dolan, L., et al. (2007). Oxylipins produced by the 9-lipoxygenase pathway in *Arabidopsis* regulate lateral root development and defense responses through a specific signaling cascade. *Plant Cell* 19, 831–846. doi: 10.1105/tpc.106.046052

Vicente, J., Cascón, T., Vicedo, B., García-Agustín, P., Hamberg, M., and Castresana, C. (2012). Role of 9-lipoxygenase and α-dioxygenase oxylipin pathways as modulators of local and systemic defense. *Mol. Plant* 5, 914–928. doi: 10.1093/mp/ssr105

Vliegenthart, J. F. G., de Groot, J. J. M. C., Veldink, G. A., Boldingh, J., Wever, R., and Van Gelder, B. F. (1975). Demonstration by EPR spectroscopy of the functional role of iron in soybean lipoxygenase-1. *Biochim. Biophys. Acta* 377, 71–79. doi: 10.1016/0005-2744(75)90287-9

Vliegenthart, J. F. G., Verhagen, J., Bouman, A. A., and Boldingh, J. (1977). Conversion of 9-D-and 13-L-hydroperoxylinoleic acids by soybean lipoxygenase-1 under anaerobic conditions. *Biochim. Biophys. Acta* 486, 114–120. doi: 10.1016/0005-2760(77)90075-3

Vollenweider, S., Weber, H., Stolz, S., Chételat, A., and Farmer, E. E. (2000). Fatty acid ketodienes and fatty acid ketotrienes: Michael addition acceptors that accumulate in wounded and diseased *Arabidopsis* leaves. *Plant J.* 24, 467–476. doi: 10.1111/j.1365-313x.2000.00897.x

Wang, K. D., Borrego, E. J., Kenerley, C. M., and Kolomiets, M. V. (2020a). Oxylipins other than jasmonic acid are xylem-resident signals regulating systemic resistance induced by *Trichoderma virens* in maize. *Plant Cell* 32, 166–185. doi: 10.1105/tpc.19.00487

Wang, K. D., Gorman, Z., Huang, P. C., Kenerley, C. M., and Kolomiets, M. V. (2020b). *Trichoderma virens* colonization of maize roots triggers rapid accumulation of 12-oxophytodienoate and two ?-ketols in leaves as priming agents of induced systemic resistance. *Plant Signal. Behav.* 15:1792187. doi: 10.1080/15592324.2020.1792187

Conflict of Interest: The authors declare that the research was conducted in the absence of any commercial or financial relationships that could be construed as a potential conflict of interest.

Publisher's Note: All claims expressed in this article are solely those of the authors and do not necessarily represent those of their affiliated organizations, or those of the publisher, the editors and the reviewers. Any product that may be evaluated in this article, or claim that may be made by its manufacturer, is not guaranteed or endorsed by the publisher.

Copyright © 2021 Gorman, Tolley, Koiwa and Kolomiets. This is an open-access article distributed under the terms of the Creative Commons Attribution License (CC BY). The use, distribution or reproduction in other forums is permitted, provided the original author(s) and the copyright owner(s) are credited and that the original publication in this journal is cited, in accordance with accepted academic practice. No use, distribution or reproduction is permitted which does not comply with these terms.

frontiers in Plant Science

ORIGINAL RESEARCH
published: 07 September 2021
doi: 10.3389/fpls.2021.699146

Transcriptome and Oxylipin Profiling Joint Analysis Reveals Opposite Roles of 9-Oxylipins and Jasmonic Acid in Maize Resistance to Gibberella Stalk Rot

Qing Wang[1,2,3†], *Yali Sun*[1,2,3†], *Fang Wang*[1,2,3], *Pei-Cheng Huang*[4], *Yinying Wang*[1,2,3], *Xinsen Ruan*[1,2,3], *Liang Ma*[1,2,3], *Xin Li*[1,2,3], *Michael V. Kolomiets*[4] *and Xiquan Gao*[1,2,3*]

[1] State Key Laboratory for Crop Genetics and Germplasm Enhancement, Nanjing Agricultural University, Nanjing, China, [2] Jiangsu Collaborative Innovation Center for Modern Crop Production, Nanjing Agricultural University, Nanjing, China, [3] College of Agriculture, Nanjing Agricultural University, Nanjing, China, [4] Department of Plant Pathology and Microbiology, Texas A&M University, College Station, TX, United States

OPEN ACCESS

Edited by:
Dilantha Fernando,
University of Manitoba, Canada

Reviewed by:
Autar Krishen Mattoo,
Agricultural Research Service (USDA), United States
Ana Badea,
Agriculture and Agri-Food Canada, Canada

***Correspondence:**
Xiquan Gao
xgao@njau.edu.cn

[†] These authors have contributed equally to this work

Specialty section:
This article was submitted to Plant Pathogen Interactions, a section of the journal Frontiers in Plant Science

Received: 22 April 2021
Accepted: 11 August 2021
Published: 07 September 2021

Citation:
Wang Q, Sun Y, Wang F, Huang P-C, Wang Y, Ruan X, Ma L, Li X, Kolomiets MV and Gao X (2021) Transcriptome and Oxylipin Profiling Joint Analysis Reveals Opposite Roles of 9-Oxylipins and Jasmonic Acid in Maize Resistance to Gibberella Stalk Rot. Front. Plant Sci. 12:699146. doi: 10.3389/fpls.2021.699146

Gibberella stalk rot caused by *Fusarium graminearum* is one of the devastating diseases of maize that causes significant yield losses worldwide. The molecular mechanisms regulating defense against this pathogen remain poorly understood. According to recent studies, a major oxylipin hormone produced by 13-lipoxygenases (LOX) namely jasmonic acid (JA) has been associated with maize susceptibility to GSR. However, the specific roles of numerous 9-LOX-derived oxylipins in defense against Gibberella stalk rot (GSR) remain unexplained. In this study, we have shown that disruption of a 9-LOX gene, *ZmLOX5*, resulted in increased susceptibility to GSR, indicating its role in defense. To understand how *ZmLOX5* regulates GSR resistance, we conducted transcriptome and oxylipin profiling using a *zmlox5-3* mutant and near-isogenic wild type B73, upon infection with *F. graminearum*. The results showed that JA biosynthetic pathway genes were highly up-regulated, whereas multiple 9-LOX pathway genes were down-regulated in the infected *zmlox5-3* mutant. Furthermore, oxylipin profiling of the mutant revealed significantly higher contents of several jasmonates but relatively lower levels of 9-oxylipins in *zmlox5-3* upon infection. In contrast, B73 and W438, a more resistant inbred line, displayed relatively lower levels of JAs, but a considerable increase of 9-oxylipins. These results suggest antagonistic interaction between 9-oxylipins and JAs, wherein 9-oxylipins contribute to resistance while JAs facilitate susceptibility to *F. graminearum*.

Keywords: 9-oxylipins, lipoxygenase, ketols, transcriptome, *Fusarium graminearum*

INTRODUCTION

Gibberella stalk rot caused by *Fusarium graminearum* (*teleomorph Gibberella zeae*) severely impacts maize (*Zea mays*) production worldwide, leading to dramatic yield losses (Mueller and Wise, 2015). Major efforts are devoted to breeding Gibberella stalk rot (GSR)-resistant varieties because the application of certain agronomic practices and fungicides in GSR control are either less effective or harmful to the environment.

A few reports are dealing with GSR resistance mechanisms. For instance, disruption of *ZmCCT*, a candidate gene for *qRfg1*, reduced *Fusarium* spp. resistance (Wang et al., 2017), while *ZmAuxRp1*, a candidate gene for *qRfg2*, exerts its function *via* balancing the growth and defense by regulating DIMBOA content upon *F. graminearum* infection (Ye et al., 2019). Despite these findings, the complex mechanisms underlying maize resistance to GSR remain largely unexplored.

Increasing reports have suggested that plant oxylipins play crucial roles in defense response to pathogens, serving as signaling molecules or having direct toxicity for microbes (Howe and Schilmiller, 2002; Famer et al., 2003; Deboever et al., 2020). Oxylipins represent a large family of oxidized fatty acids, mainly generated from linoleic acid (C18:2) or α-linolenic acid (C18:3), the catalysis of which is initiated by lipoxygenases (LOXs) and α-dioxygenases (DOX) (Blee, 2002; Feussner and Wasternack, 2002; Andreou et al., 2009). According to the oxidized position of carbon (C), LOXs are divided into 9- and 13-LOXs (Feussner and Wasternack, 2002; Schneider et al., 2007). Jasmonic acid (JA) biosynthesis is initiated by oxidation of α-linolenic acid by 13-LOXs followed by the action of allene oxide synthase (AOS) and allene oxide cyclase (AOC) resulting in the production of a JA precursor, 12-oxo-phytodienoic acid (12-OPDA). Afterward, 12-OPDA is reduced by 12-OPDA reductase (OPR) followed by three rounds of beta-oxidation to produce (+)-7-iso-JA (Wasternack, 2007; Borrego and Kolomiets, 2016). Then, (+)-7-iso-JA is conjugated to isoleucine by the JAR1 enzyme resulting in the synthesis of the biologically active JA-Ile. On the other hand, 9-LOXs catalyze the formation of a series of 9-oxylipins, such as (9*S*, 10*E*, 12*Z*)-9-hydroperoxy-10, 12-octadecadienoic acid (9*S*-HPODE) and others (Feussner and Wasternack, 2002; Howe and Schilmiller, 2002).

It has been well-documented that 13-oxylipins, including JAs and their derivatives, play diverse roles in plant-pathogen interactions (Bate and Rothstein, 1998; Birkett et al., 2000; Turner et al., 2002; Wasternack and Feussner, 2018; Deboever et al., 2020). For instance, two maize 13-LOXs, e.g., ZmLOX10 and ZmLOX11, were shown to be highly induced by pathogen infection (Nemchenko et al., 2006). Disruption of *ZmOPR7* and *ZmOPR8*, two key genes responsible for JA biosynthesis in maize, resulted in complete loss of immunity against soil-borne necrotrophic pathogens, e.g., *Pythium* spp. (Yan et al., 2012), and *Fusarium verticillioides* (Christensen et al., 2014), but increased resistance to the hemibiotrophic *Colletotrichum graminicola* (Gorman et al., 2020). Furthermore, jasmonic acid-isoleucine (JA-Ile) was induced in response to various biotic stresses (Howe et al., 2018). Interestingly, accumulating evidence suggested that the JA precursor, 12-OPDA, could function as a signaling molecule independent of JA-Ile. Most recently, 12-OPDA and α-ketol of octadecadienoic acid (KODA) were identified as critical xylem-mobile signaling molecules to activate induced systemic resistance (ISR) triggered by maize root colonization of the beneficial fungus, *Trichoderma virens* (Wang et al., 2020).

The functions of the majority of 9-oxylipins in plant biotic stress responses are largely unexplored compared with JAs (Deboever et al., 2020). Nevertheless, increasing evidence showed that 9-oxylipins also play a role in plant-pathogen interactions. For example, disruption of a tobacco 9-LOX gene led to the loss of hypersensitive reaction (HR)-mediated resistance to *Phytophthora parasitica* (Rance et al., 1998). This result is likely due to the reduced levels of 9-LOX derived colnelenic and colnelenic acids (Fammartino et al., 2007). Furthermore, 9-KOT was strongly induced upon infection by *Pseudomonas syringae* pv. tomato (*Pst*) in Arabidopsis (Vicente et al., 2012). In maize, ZmLOX1, 2, 3, 4, 5, and 12 comprise the 9-LOX category (Christensen et al., 2014; Borrego and Kolomiets, 2016). Functional analysis of *zmlox3-4* mutant showed that the oxylipins produced by this specific 9-LOX are required for fungal pathogenesis by *F. verticillioides* and other pathogens of leaf, stem, and root (Gao et al., 2007; Isakeit et al., 2007; Pathi et al., 2020), Increased resistance of *zmlox3-4* mutant to *F. verticillioides* was explained by the over-expression of other 9-LOXs, *ZmLOX4*, *ZmLOX5*, and *ZmLOX12*, as *zmlox4*, *zmlox5*, and *zmlox12* mutants were more susceptible to *F. verticillioides*, due to decreased JA levels in response to infection (Christensen et al., 2014; Battilani et al., 2018). However, the roles of 9-oxylipins in maize resistance to GSR remain unexplored.

In this study, we tested *zmlox5-3* mutant and its corresponding wild type (WT) maize line B73, for resistance to GSR. Disruption of *ZmLOX5* resulted in increased GSR disease severity. RNA-seq transcriptome analyses revealed that the mutant responded to *F. graminearum* infection by increased transcript accumulation of the genes related to JA synthesis and signal transduction pathways yet decreased expression of the 9-LOX pathway genes in *zmlox5* mutant compared with WT. In agreement with this, *zmlox5-3* accumulated significantly higher levels of JA-Ile and other JAs, but lower levels of several 9-oxylipins upon infection. Thus, it is concluded that ZmLOX5-produced 9-oxylipins contribute to GSR resistance, whereas JAs appear to facilitate *F. graminearum* virulence.

MATERIALS AND METHODS

Plant Material and Fungal Strain

The seeds of maize lines W438, B73, and the transposon element-insertional mutant zmlox5-3 of B73, provided by Prof. Kolomiets laboratory, were sown in the soil in PVC cylinders (5 cm in diameter and 20 cm in depth) and grown under the condition of day/night of 14/10 h photoperiod at 26 ± 2°C and 75% humidity on a growth shelf. Two-week-old seedlings were transferred to a culture room for phenotypic assay.

Fusarium graminearum strain 0609, provided by Prof. Mingliang Xu, China Agricultural University, was initially cultured on potato dextrose agar (PDA) media for 7 days and then maintained at 4°C until use. There were 10 pieces of 0.5 cm^3 PDA plug freshly excised from the agar plate, then cultured in 40 ml fresh mung bean broth on a rotary shaker at 25°C and 200 rpm for 3–4 days. The concentration of spore suspension was adjusted to 1×10^6 macroconidia per ml supplemented with Tween-20 to a final concentration at 0.001%.

Inoculation Assay, Sampling, and Disease Phenotyping

The fungal inoculum and artificial inoculation of seedlings were conducted according to our previous study (Sun et al., 2018). Prior to inoculation, maize seedlings were lawn down in a plastic

square tray (100 × 80 × 10 cm) and a hole was punched by a 1 ml sterile syringe needle on the middle of the stem of the seedling. Afterward, 20-μl spore suspension was carefully dropped onto the wounded site and the square tray was sealed by saran wrap to keep the humidity. The culture condition was maintained at 24 ± 2°C, with 14 h light/10 h dark period and 200 lux light intensity.

For RNA-seq and qRT-PCR analysis, 12 uninfected or infected stems from each line were collected at 0, 12, 24, and 48 h after infection (hai) respectively, then stored in −80°C for further study. For fungal biomass quantification, 10 infected maize stems from each line were collected at 72 hai. Gibberella stalk rot disease symptoms were scored using 20 seedlings per genotype at 3 days post-inoculation (dpi) according to a five-level seedling GSR scale, ranging from 1 (most resistant) to 5 (most susceptible) (Sun et al., 2018). The statistical analysis was performed by using SPSS (14.0) (IBM, Stanford, USA) for ANOVA and Student's *t*-test, with the significance level of $p \leq 0.05$.

Isolation of Genomic DNA and Quantification of Fungal Biomass

The isolation of genomic DNA (gDNA) was carried out using maize stems by a CTAB (cetyl trimethylammonium bromide)-based method described by the study of Brandfass and Karlovsky (2008). The gDNA of the inoculated seedling stem was diluted to a 50 ng/μl working solution for the quantification of stem and fungal biomass. The gDNA of the non-inoculated stem was used as an external DNA standard in the reference gene-based qRT-PCR analysis, by diluting to a series of concentrations, i.e., 100, 50, 25, 6.25, 1.5625, and 0.39 ng of DNA per microliter.

For fungal biomass quantification, Potato dextrose broth was inoculated with 5 ml of 1×10^6 macroconidia suspension of *F. graminearum* 0609 and incubated on a rotary shaker at 25°C for 3–5 days. The mycelium was harvested and freeze-dried, and gDNA was isolated as described by the study of Brandfass and Karlovsky (2008), as *Fusarium* standard in the reference gene-based qRT-PCR. The genomic DNA was diluted to a series of concentrations at 50, 10, 5, 1, 0.5, and 0.1 ng of *F. graminearum* DNA per μl and kept at −20°C until use.

The qRT-PCR was performed on a CFX96 real-time PCR system (Bio-rad, Hercules, CA, USA). Primers of *F. graminearum* Tubulin and maize *β-Tubulin 4* gene (Zm00001d013612) used to quantify *F. graminearum* and maize biomass, respectively (listed in **Supplementary Table 1**). The amplification mix consisted of 1 μl of template DNA, 5 μl of universal SYBR green master (Monad, Suzhou, China), 2 μl of double-distilled water, and 1 μl each of forward and reverse primer (10 pmol/μl). The qRT-PCR was performed according to the description of the study by Wang et al. (2015), with a cycle at initial denaturation step at 94°C for 1.5 min, followed by 35 cycles of 94°C for 30 s, 60°C for 45 s, and 72°C for 45 s, and elongation at 72°C for 5 min. The average amount of *F. graminearum* in maize stem and the infection percentage of stem samples (relative fungal biomass) were calculated based on the description in the study conducted by Brunner et al. (2009). The infection index was calculated as the average of three biological replicates.

RNA-Seq and qRT-PCR Analysis

Total RNA was extracted from *F. graminearum*-inoculated and uninoculated B73 and *zmlox5-3* seedling stems at different time points using Trizol reagent (Invitrogen, CA, USA), then purified with the RNeasy Mini Kit (Qiagen, Hilden, Germany). Following the quality control of RNA samples using Illumina TruSeq RNA library prep kit v2, RNA sequencing was performed with Illumina HiSeq 2000 (Illumina Inc., Berry, Beijing).

Paired-end RNA sequence reads of 150 bases were generated, and all clean reads were mapped to the reference genome of maize inbred B73 (RefGen_V4) and the reference genome dataset of *F. graminearum* (FGS 5b) using HISAT2 (version 2.2.1.0) (https://daehwankimlab.github.io/hisat2/). The gene expression values were normalized as gene counts. To identify differentially expressed genes (DEGs), DESeq2 (version 1.32.0) (https://bioconductor.org/packages/release/bioc/html/DESeq2.html) was used with the threshold of a false-discovery rate (FDR) <0.05. DEGs were annotated according to maize genome from NCBI and were subjected to Gene Ontology (GO) enrichment (www.geneontology.org) (Ashburner et al., 2000) and KEGG pathway analyses (www.genome.jp/kegg) (Kanehisa et al., 2016). Three independent biological replicates were conducted with each sample containing at least six seedlings.

To verify the dynamic change of key genes in the 9- and 13-LOX pathway of three genotypes, 20 genes were selected to conduct quantitative RT–PCR analysis using the CFX96 real-time PCR system (Bio-rad, Hercules, CA, U.S.A.) (**Supplementary Table 1**). Complementary DNA (cDNA) synthesis was carried out using 1 μg of total RNA. The PCR reaction mix consisted of 1 μl of template cDNA, 5 μl of universal SYBR green master, 2 μl of double-distilled water, and 1 μl each of forward and reverse primer (10 pmol/μl). PCR was performed according to the following protocol: initial denaturation for 10 min at 94°C, followed by 44 cycles with 45 s at 94°C, 45 s at 60°C, and 45 s at 72°C, and the final elongation at 72°C for 5 min. Fluorescence was determined during the annealing step of each cycle. Following amplification, the melting curves were acquired by heating the samples to 95°C for 15 s, cooling to 60°C for 1 min, and then slowly increasing the temperature from 60 to 95°C at a rate of 0.5°C per second, with continuous measurement of the fluorescence, cooling to 60°C for 15 s. The relative expression levels of target genes were normalized by the maize *β-Tubulin 4* gene (Zm00001d013612) and relative to the sample at 0 hai by using the $2^{-\Delta\Delta Ct}$ method. All qRT–PCR reactions were performed with three biological replicates for each sample.

Oxylipin Profiling

Oxylipin profiling was conducted according to the description in previous studies (Wang et al., 2020; Ma et al., 2021), with some modifications. In brief, non-inoculated (control) and inoculated maize stem tissues were collected at 24 and 48 hai from the three genotypes, then immediately frozen with liquid nitrogen and stored in −80°C. Afterward, 100 mg of stem tissue was finely ground using liquid nitrogen and mixed with 500 μl extraction buffer (1-propanol/water/HCl [2:1:0.002 vol/vol/vol]) containing 10 μl of 5 μM isotopically-labeled internal standards.

The samples were processed and injected into an API 3200 (Sciex, Framingham, MA, USA) LC-MS/MS using electrospray ionization in negative mode with multiple reactions mentoring (MRM). The chromatography was performed with an Ascentis Express C-18 Column (3 cm × 2.1 mm, 2.7 μm) (Sigma-Aldrich, St. Louis, MO, USA). The mobile phase was set at 400 ml per minute consisting of Solution A (0.02% acetic acid in water) and Solution B (0.02% acetic acid in acetonitrile) with a gradient consisting of (time in min—%B):0.5–10%, 1–20%, 21–70%, 24.6–100%, 24.8–10%, 29–stop. The peaks and retention times of oxylipins were then determined by comparing levels of endogenous metabolites to isotopically labeled standards from Sigma-Aldrich (St. Louis, MO, USA), Cayman Chemical (Ann Arbor, MI, USA), and Larodan AB (Solna, Sweden), with appropriate response factors (Muller and Munne-Bosch, 2011; Christensen et al., 2014). Using unsupervised principal component analysis (PCA), significantly regulated metabolites in each genotype and between three genotypes during the infection period were determined by one-way and two-way ANOVA analysis and were analyzed using MetaboAnalyst (version 5.0) (https://www.metaboanalyst.ca/) (Chong et al., 2019).

RESULTS

zmlox5-3 Mutant Is Shown to Be Susceptible to Gibberella Stalk Rot

To elucidate the function of 9-oxylipins in GSR resistance of maize, we deployed *zmlox5-3*, a *Mutator*-insertional mutant of *ZmLOX5*, one of the 9-LOX gene (Park et al., 2010), and its near-isogenic WT, to the inbred line B73. Mutant *zmlox5-3* was previously reported to display increased susceptibility to *F. verticillioides* (Battilani et al., 2018). **Figures 1A,B** show that *zmlox5-3* was significantly more susceptible to *F. graminearum* exhibiting a disease index of 4.6, compared with 3.9 for B73. Moreover, qRT-PCR-based quantification of the fungal biomass indicated that *zmlox5-3* contained 34.7% more fungal RNA compared with B73 (**Figure 1C**). The increased disease severity in *zmlox5-3* suggests that *ZmLOX5* is essential for maize resistance to GSR.

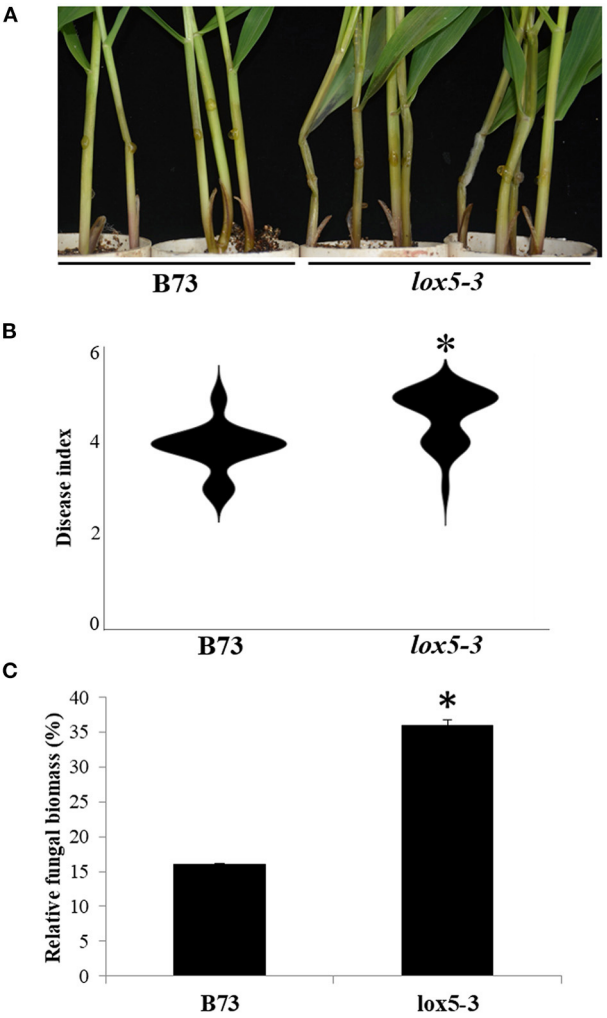

FIGURE 1 | Phenotyping of *zmlox5-3* and B73 stems at 3 days post-infection with *F. graminearum*. **(A)** Representative images of B73 (left) and *lox5-3* (right) at 72 h after infection (hai) with *F. graminearum*. **(B)** Gibberella stalk rot (GSR) disease index of B73 and *zmlox5-3* at 72 hai. The disease was quantified using 20 seedlings per genotype. **(C)** Fungal biomass quantification of *F. graminearum* by qRT-PCR at 72 hai for B73 and *zmlox5-3*. The data were shown as the average of 10 plants per genotype. The experiments were replicated three times, with similar results obtained. Stars above the bars indicate the statistical significance at $p < 0.05$.

Transcriptomic Analysis of Maize in Response to *F. graminearum* Infection

To identify the key genes potentially regulated by the *ZmLOX5*-derived oxylipins and their involvement in maize–*F. graminearum* interaction, Illumina-based RNA-seq was conducted using stems collected from B73 and *zmlox5-3* seedlings at 12 and 24 h post-infection with *F. graminearum*. In total, the transcriptome sequencing of 12 libraries produced clean reads ranging from 33,576,369 to 19,936,838 (average 26,454,227) with a length of 150 bp among the samples after filtering out low-quality reads, adaptor reads, and high unknown base (N) reads. Using HISAT to map the reads against the B73 genome as a reference, more than 85 and 88% alignment rates were obtained in B73 and *zmlox5-3*, respectively (**Supplementary Table 2**). Pearson's correlation between biological replicates for each time point was higher than 77 and 85% in B73 and *zmlox5-3*, respectively, indicating good repeatability of the sequencing data (**Supplementary Figure 1**).

Differentially expressed genes were then identified with a threshold of $p < 0.05$ and log2 Fold Change (FC) > 1. Compared with the controls, 474 and 2,028 up-regulated DEGs and 444 and 1,407 down-regulated DEGs were identified in B73. On the other hand, only 217 and 1,299 up-regulated DEGs and 161 and 476 down-regulated DEGs were recorded in *zmlox5-3* at 12 and 24 hai, respectively (**Figure 2A**). In total, 506 up-regulated and 321 down-regulated DEGs were uniquely expressed in *zmlox5-3*, whereas 1,335 up-regulated and 1,389 down-regulated DEGs

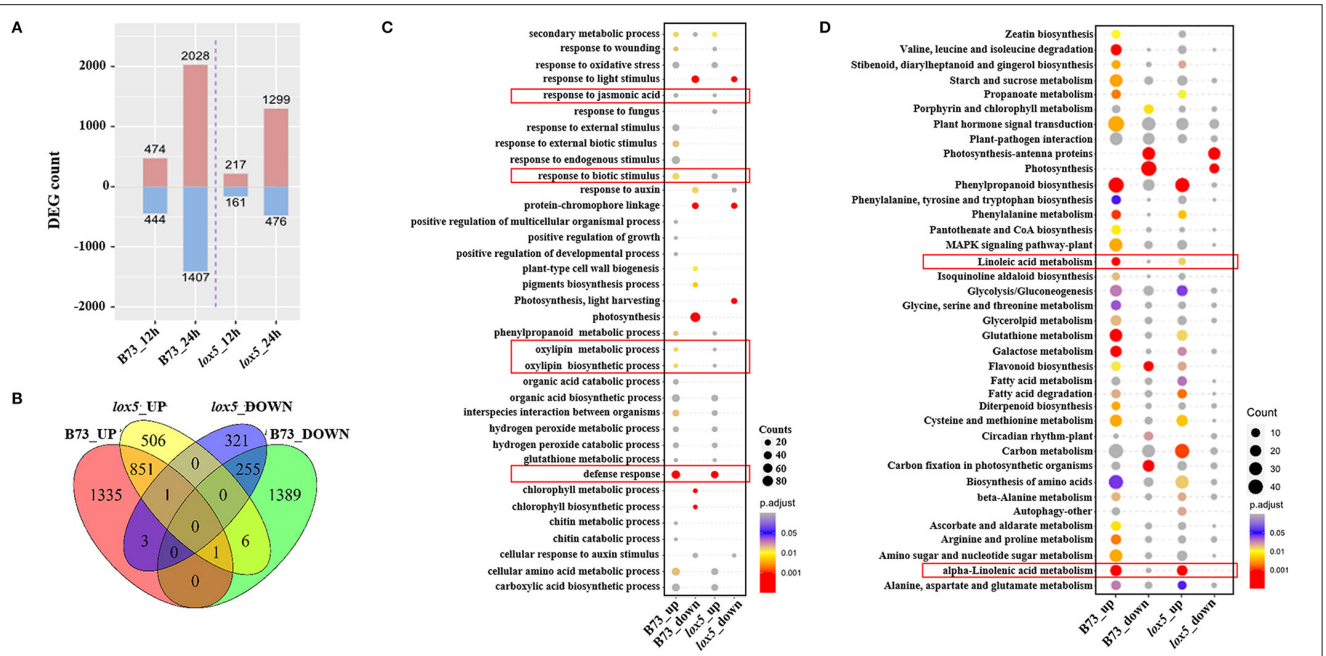

FIGURE 2 | RNA-seq analysis of B73 and *zmlox5-3* upon *F. graminearum* infection. **(A)** Differentially expressed genes (DEGs) at 12 and 24 hai in B73 and *zmlox5-3*, respectively. DEGs were determined by comparing the expression of candidate genes in samples infected at 12 and 24 hai and that of mock samples, respectively. **(B)** The Venn diagram represented the specific and common DEGs between B73 and *zmlox5-3*. **(C)** GO term enrichment of up- and down-regulated DEGs significantly enriched in biological process (BP) in B73 and *zmlox5-3*. The terms associated with disease resistance are highlighted in the red rectangle. **(D)** Significantly enriched KEGG pathways of up- and down-regulated DEGs in B73 and *zmlox5-3*. The linoleic and alpha-linolenic acid metabolism were highlighted in the red rectangle. The size of the dot indicates the number of gene counts. The DEGs were selected with the criteria at adjusted *p* (*p*.adj) < 0.05 shown in the colored sidebar.

were specifically identified in B73. There were 851 common up-regulated DEGs and 255 common down-regulated DEGs in B73 and *zmlox5-3* (**Figure 2B**).

To further determine the DEGs potentially relevant for GSR resistance or susceptibility, we conducted GO analysis for the up- and down-regulated genes in B73 and *zmlox5-3* (**Figure 2C**). It showed that GO terms of biological processes (BP) "chlorophyll metabolic process" and "chlorophyll biosynthetic process," as well as "response to external biotic stimulus," were only up-regulated in B73. Whereas, "photosynthesis" was the most down-regulated in B73 but not in *zmlox5-3*. On the contrary, "photosynthesis, light-harvesting" was only down-regulated in *zmlox5-3* but not in B73. Furthermore, multiple defense response-related processes, including "defense response," "response to biotic stress," "cellular amino acid metabolic process," "phenylpropanoid metabolic process," "response to jasmonic acid," "oxylipin metabolic process," and "oxylipin biosynthetic process" were all up-regulated in both genotypes.

To better understand the relative biological functions of DEGs in the two lines upon infection with *F. graminearum*, KEGG pathway analysis was conducted and enrichment of the pathways that were up-regulated or down-regulated was analyzed. As shown in **Figure 2D**, up-regulated DEGs were highly enriched in pathways such as "phenylpropanoid biosynthesis," "phenylalanine metabolism," "glutathione metabolism," and "galactose metabolism" in both lines, whereas down-regulated DEGs were mainly enriched in the photosynthesis-related pathways, including "photosynthesis-antenna protein," "photosynthesis," and "carbon fixation pathways" (**Figure 2D**). Notably, "linoleic acid metabolism" and "α-linolenic acid metabolism" pathways were also found to be highly enriched for up-regulated DEGs in both lines (**Figure 2D**).

Oxylipin Profiling of the Seedling Response to Infection With *F. graminearum*

To identify oxylipins that may explain decreased resistance of *zmlox5-3* mutant, we performed oxylipin quantification in the mutant and B73 at different time points upon infection with *F. graminearum*. To hone-in a subset of oxylipins associated with GSR resistance, we included the GSR resistant inbred line W438 (Sun et al., 2021) in the panel subjected to oxylipin profiling. The principal component analysis showed a clear trend of separation between control and infected samples for all three lines. Interestingly, infected *zmlox5-3* at 48 hai was clearly separated from the uninfected control, compared with B73 and W438, suggesting that multiple oxylipins might be associated with GSR resistance or susceptibility (**Figure 3A**).

In total, we have measured 51 compounds. Two-way ANOVA analysis identified 42 metabolites that were significantly different at $p \leq 0.05$ (**Supplementary Table 3**). The majority of these compounds showed distinct patterns in the three genotypes during the infection period (**Figure 3B**). Several 9-oxylipins were

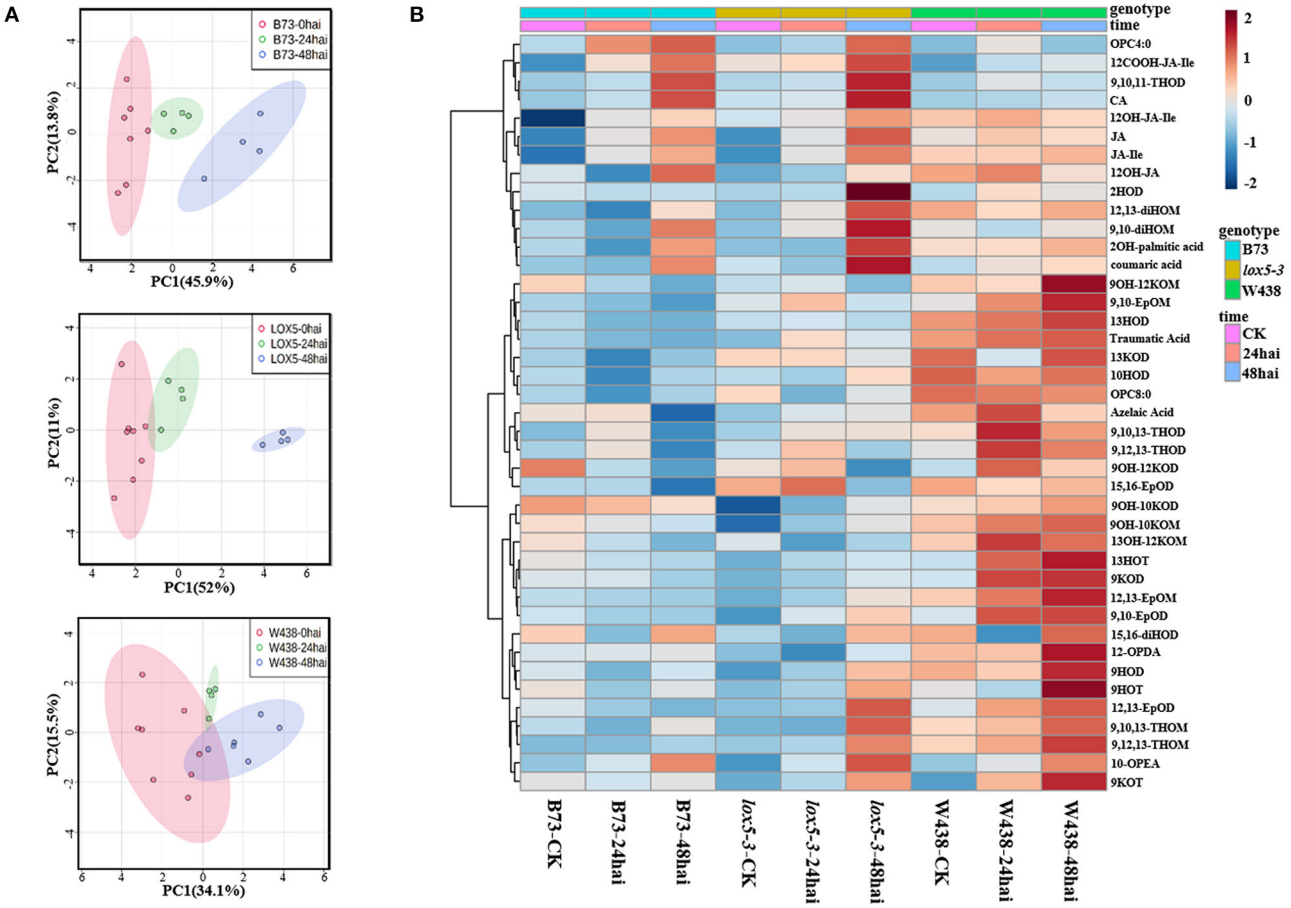

FIGURE 3 | Oxylipins profiling in stem tissue of W438, B73, and *zmlox5-3* at 24 and 48 h and corresponding controls at 0 h post-infection with *F. graminearum*. **(A)** PCA score plot based on the metabolite profiling of W438, B73, and *lox5-3*. **(B)** Heatmap of significantly altered oxylipins between W438, B73, and *zmlox5-3* upon infection with *F. graminearum*. The sidebars on the left of the heatmap represent genotypes and time points, respectively. Statistical analysis was conducted by Two-way ANOVA (interaction $p \leq 0.01$).

strongly induced in W438 at both 24 and 48 hai. For instance, the contents of 9OH-10KOM, 9,10-EpOM (9(*R*), 10(*S*)-Epoxy-12(*Z*)-octadecenoic acid), 9-HOT, and 9-HOD at 48 hai were 6.9, 3.8, 3.5, and 2.2 times higher in W438 than that in *lox5-3,* underlining the potential relevance of 9-oxylipins for defense against *F. graminearum*.

Higher Jasmonates Levels Correlate With Increased Susceptibility to GSR

In contrast to 9-oxylipins, most JA derivatives, including OPC4:0 [3-oxo-2-(2-pentenyl) cyclopentane-1-butanoic acid], JA, JA-Ile, 12OH-JA, 12COOH-JA-Ile, and 12OH-JA-Ile, were significantly induced in *lox5-3* at 48 hai and to a lesser extent in B73. Remarkably, the levels of jasmonates remained unchanged in the resistant inbred W438. To better understand the potential interaction between JA and other oxylipins, we examined metabolites that were related to JA. All jasmonates showed a positive correlation as expected. On the contrary, 15,16-EpOD, 9OH-12KOM, 9OH-12KOD, 9OH-Tan, and 13OH-12KOD negatively correlated with JA (**Figure 4A**), suggesting that these oxylipins may be antagonistic to JAs.

To understand how JAs and other 13-oxylipins are impacted by *ZmLOX5* mutation at the transcriptional and metabolic levels, we conducted the joint analysis of metabolites and gene expression levels of 13-oxylipin pathways in WT and *zmlox5-3* mutant. While the majority of the compounds in the JA biosynthetic pathways, including OPC4:0, JA, and JA derivatives, especially JA-Ile, were produced at a relatively lower level in the infected W438, these metabolites were significantly induced in *lox5-3* (**Figure 4B**). Surprisingly, the concentration of the compounds upstream of OPC:0, such as 12-OPDA and OPC8:0, were maintained at higher levels in W438 but not in *zmlox5-3*. Among those compounds, JA-Ile levels increased ∼14.8-fold and 43.5-fold in *zmlox5-3* at 24 and 48 hai, and 22.7-fold to 43.2-fold in B73, respectively, whereas only 0.9-fold to 2.7-fold

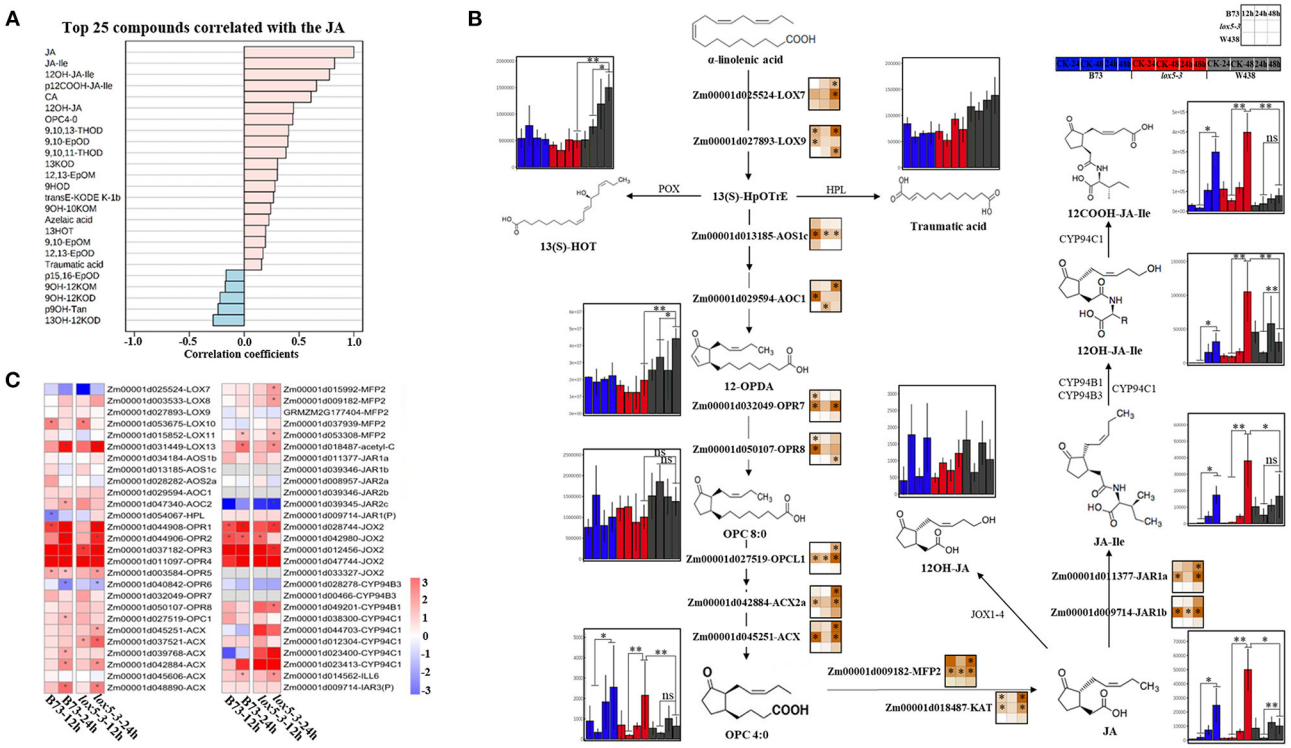

FIGURE 4 | Integrated analysis of transcriptome and 13-oxylipins profiling of stem tissues of W438, B73, and *lox5-3* at 24 and 48 h post-infection with *F. graminearum*. The corresponding control was the samples collected at 0 hai. **(A)** Correlation coefficient analysis of oxylipins associated with JA between W438, B73, and *zmlox5-3* upon *F. graminearum* infection. **(B)** Diagram of main oxylipins and expression of related genes involved in JA biosynthesis pathway. The change of oxylipin contents was indicated as a box plot at the side of the compound name, and the heat map at the side of the gene name represented the expression levels of selected genes. The stars indicate statistical significance at $p < 0.05$. **(C)** Expression pattern of genes involved in the 13-LOX pathway in B73 and *zmlox5-3* at 12 and 24 hai. The different colors represent the log2 fold-change of each gene at different time points, and stars indicate the statistical significance at $p < 0.05$.

increases were observed in W438 at 24 and 48 hai, respectively (**Supplementary Table 4**).

In line with the results of oxylipin profiling, the key genes encoding proteins converting JA to JA-Ile are *Jasmonate resistant 1* (*JAR1a*, Zm00001d011377) and *JAR1b* (Zm00001d009714) and the two putative JA-Ile conjugating enzymes in maize (Borrego and Kolomiets, 2016), which were highly expressed at most time points in *zmlox5-3* but induced only at 48 hai in B73. Moreover, two genes encoding proteins metabolizing OPC4:0 to JA, which are *glyoxysomal fatty acid beta-oxidation multifunctional protein MFP-a* (*MFP2*, Zm00001d009182) and *acetyl-CoA acyltransferase* (*KAT*, Zm00001d018487), were both up-regulated in B73 and *lox5-3*. However, all these genes were not induced throughout all time points in W438 (**Figure 4B**), supporting the notion that increased JA is associated with increased susceptibility to GSR.

Surprisingly, the precursor compounds of the JA biosynthetic pathway, such as 12-OPDA and OPC8:0, accumulated to higher levels in W438, compared with the susceptible genotypes (**Figure 4B**), which may be due to reduced conversion of these precursors to JA in W438. Interestingly, several key genes encoding enzymes catalyzing the formation of JA precursors, including *LOX9* (Zm00001d027893), *AOC1* (Zm00001d029594), and *OPR8* (Zm00001d050107), were up-regulated earlier at 12 hai in *zmlox5-3*, but at later time points at 24 and 48 hai in B73 and W438, respectively. Moreover, most of the genes engaged in three-step β-oxidation, including *OPC-8:0 CoA ligase 1* (*OPCL1*, Zm00001d027519), *Acyl-coenzyme A oxidase* (*ACX*, Zm00001d045251), *MFP2*, and *KAT*, were highly expressed in *zmlox5-3* and to a lesser extent in B73, but not in W438 (**Figure 4B**). Taken together, these results suggest that JA biosynthesis pathway genes downstream of 12-OPDA were induced in *zmlox5-3* and B73 but not in resistant W438. This again points to JA-Ile as a potential susceptibility factor promoting virulence of this pathogen, a scenario similar to a recent study showing that JAs contribute to susceptibility toward another hemibiotrophic maize pathogen, *Colletotrichum graminicola* (Gorman et al., 2020).

Accumulation of 9-Oxylipins Is Associated With Reduced Susceptibility

Given that ZmLOX5 is a 9-LOX, we investigated whether 9-oxylipins could be associated with GSR resistance. Quantification of 9-oxylipins showed that an α-ketol, 10-oxo-9-hydroxy-12(*Z*) and 15(*Z*)-octadecadienoic acid (9OH-10KOD), which is recently identified as a mobile ISR signal (Wang et al.,

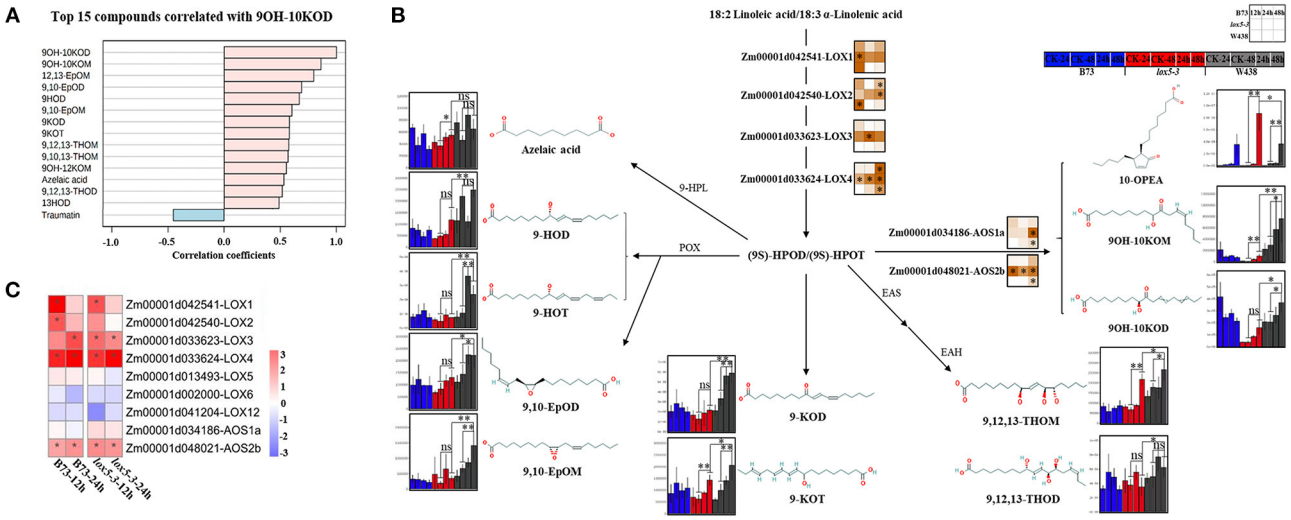

FIGURE 5 | Integrated analysis of transcriptome and 9-oxylipins profiling of stem tissues of W438, B73, and *lox5-3* at 24 and 48 h post-infection with *F. graminearum*. The corresponding control was the samples collected at 0 hai. **(A)** Correlation coefficient analysis of oxylipins associated with 9OH-10KOD between W438, B73, and *lox5-3* upon *F. graminearum* infection. **(B)** Diagram of main oxylipins and expression of related genes involved in the 9-LOX pathway. The change of oxylipin contents is indicated as a box plot at the side of the compound name, and the heat map at the side of the gene name represented the expression levels of selected genes. The stars indicate the statistical significance at $p < 0.05$. **(C)** Expression pattern of genes involved in the 9-LOX pathway in B73 and *lox5-3* at 12 and 24 hai. Different colors represent log2 fold-change of each gene at different time points, and stars indicate the statistical significance at $p < 0.05$.

2020), was the most significantly induced compound in W438 (**Supplementary Table 3**). Therefore, we further examined which other oxylipins correlated with 9OH-10KOD (**Figure 5A**). It was clearly shown that 11 out of 14 oxylipins identified in this study produced through the 9-LOX pathway highly correlated with 9OH-10KOD, whereas traumatin was the only compound negatively correlated with 9OH-10KOD (**Figure 5A**). These 9-oxylipins, which are mainly produced by 9-POX, 9-AOS, EAS, EAH, 9-HPL, and 9-LOX branch pathways, were significantly induced in W438 but displayed moderate or no change in B73, and much lower basal levels in the *lox5-3* mutant (**Figure 5B**). Moreover, the contents of the two ketols, 9OH-10KOM and 9OH-10KOD, were 6.87- and 2.45-fold higher in W438 than in *zmlox5-3* at 48 hai (**Figure 5B**). Similarly, 9,10-EpoM and 9-HOT levels were 3.75- and 3.45-fold higher in W438 than in *zmlox5-3* at 48 hai (**Supplementary Table 4**).

Intriguingly, the so-called "death acid" 10-oxo-11-phytodienoic acid (10-OPEA) accumulated to higher levels in *zmlox5-3* than in B73 or W438 at 48 hai. The analysis of qRT-PCR showed that the expression levels of the 9-LOXs and putative death acid producers, which are *ZmLOX1* (Zm00001d042541), *ZmLOX2* (Zm00001d042540), *ZmLOX3* (Zm00001d033623), and *ZmLOX4* (Zm00001d033624), were higher in *zmlox5-3*. Whereas, in W438, *ZmLOX1* and *ZmLOX2* were strongly induced only at the earlier time point at 12 hai and *ZmLOX4* was highly expressed at 48 hai (**Figure 5B**). Similar to 9-LOXs, putative ketol- and death acid-producing *AOS2b* (Zm00001d048021) also displayed higher expression levels in the *zmlox5-3* mutant (**Figure 5B**). Together, these results suggest that the cell death process mediated by "death acids" could be associated with the increased susceptibility of *zmlox5-3* observed.

DISCUSSION

Compared with JAs, the role of a large number of 9-oxylipins generated *via* the 9-LOX pathways in plant resistance to pathogens remains less explored. Among the well-studied maize 9-LOXs, *zmlox3* mutant displayed enhanced resistance to multiple pathogens, including *Cochliobolus heterostrophus*, *F. verticillioides*, *C. graminicola*, and *Ustilago maydis*. This reveals that this specific gene is a susceptibility factor in response to these pathogens (Gao et al., 2007; Battilani et al., 2018; Pathi et al., 2020). On the contrary, the other 9-LOX genes, *ZmLOX4*, *ZmLOX5*, and *ZmLOX12* were reported to be required for defense against *F. verticillioides* in maize, as *lox4* and *lox5* mutants were susceptible to *F. verticillioides*, accompanied by decreased levels of JAs (Park, 2012; Christensen et al., 2014; Battilani et al., 2018, Lanubile et al., 2021). The present study showed that ZmLOX5 is involved in defense against GSR and revealed an opposite role of 9-oxylipins and JAs in response to *F. graminearum*. Similar to these findings, Wang et al. (2020) have also demonstrated contrasting roles of 9-LOX-derived ketols and JA in maize resistance to anthracnose leaf blight pathogen, *C. graminicola*. In that study, while the treatment of maize with an α-ketol, 9,10-KODA resulted in increased resistance to *C. graminicola*, JA facilitated virulence of this pathogen. The negative role of JA in defense against *C. graminicola* was explained by its antagonistic interaction with SA as a JA-deficient mutant of maize was more resistant to this pathogen and accumulated increased levels of SA (Gorman et al., 2020). It is important to note, that both *F. graminearum* and *C. graminicola* are well-established hemibiotrophic pathogens, the defense against which primarily relies on SA signaling. Thus,

it appears that individual molecular species of oxylipins exert their function in disease resistance or susceptibility in a pathogen species-dependent manner.

Increased JA Correlates With Increased Susceptibility to *F. graminearum*

Oxylipin profiling performed in this study showed that the majority of jasmonates were highly induced in *zmlox5-3* compared with WT in response to *F. graminearum* infection, far exceeding the levels found in the resistant line W438 (**Figure 4B**). This suggests a positive correlation of JAs with enhanced GSR susceptibility in *zmlox5* mutant. Increased JA synthesis in the mutant was further supported by increased expression of both JA biosynthesis genes and the genes regulated by JA in the *zmlox5-3* mutant. These results also revealed that the 9-oxylipins produced by ZmLOX5 have a profound suppressive effect on the biosynthesis of JAs in response to *F. graminearum*. A strong antagonism between JA, 13-oxylipins, and 9-oxylipins has been recently demonstrated for wound responses of maize JA-deficient *opr7opr8* double mutant and a mutant in the major 13-LOX gene, *ZmLOX10* (He et al., 2020). That study showed that deletion of 13-oxylipins resulted in overproduction of a number of wound-induced 9-oxylipins.

Jasmonic acids and their derivatives have been repeatedly mentioned for their roles in defense against necrotrophic pathogens in various plant species (Howe, 2001; Stintzi et al., 2001; Wasternack and Hause, 2013; Borrego and Kolomiets, 2016; Wasternack and Feussner, 2018; Deboever et al., 2020). However, multiple lines of evidence in multiple plant species suggest that JA promotes disease progression by biotrophic and hemibiotrophic pathogens due to the well-characterized antagonism between JA and SA signaling (Glazebrook, 2005). One of the strongest illustrations of JA signaling serving to promote pathogen virulence is the discovery that some pathovars of *Pseudomonas suringae* take advantage of JA-SA antagonism by producing coronatine, a structural and functional mimic of JA-Ile, to induce host JA signaling, which in turn results in the down-regulation of SA-mediated defenses (Robert-Seilaniantz et al., 2011; Pieterse et al., 2012). In the case of this study, due to the hemibiotrophic lifestyle of *F. graminearum*, overproduction of JAs is beneficial for *F. graminearum* to promote disease progression at the necrotrophic phase, e.g., after 48 h post-infection. We hypothesize that JA promotes disease progression at the necrotrophic phase of infection by its well-known capacity to induce cell death processes in diverse plant species including maize (Mur et al., 2006; Yan et al., 2012). The finding that JA promotes susceptibility to GSR is supported by the recent study showing the increased resistance against *F. graminearum* in the *COI1* and JA-deficient mutants of maize (Ma et al., 2021), and by the previous study in Arabidopsis that *coi1* mutant is more resistant to wilt disease caused by *F. oxysporum* (Thatcher et al., 2009). The results in the present study, together with previous findings, support a strong negative relationship between JA pathways and resistance to diseases caused by *Fusarium* spp.

In this study, the levels of bioactive JA-Ile in the susceptible lines, *zmlox5-3* and B73, were excessively high in comparison to the resistant line W438 (**Figure 4B**). This might be due to the limitation of over-synthesis of JA-Ile in resistant line (Staswick and Tiryaki, 2004; Stitz et al., 2011; Caarls et al., 2017; Smirnova et al., 2017). Another reason for increased JAs in *zmlox5-3* might be the constant catalysis via β-oxidation, the process that appears to be exerted at a much lower level in W438, as evident from both transcript levels of β-oxidation genes and actual JA precursors' contents.

A recent study showed that upon activation of induced systemic resistance (ISR) by *Trichoderma virens* in B73, 12-OPDA levels increased, while JA biosynthetic genes downstream of 12-OPDA, such as *ACX*, *MFP* and *KAT*, and JA responsive genes were down-regulated. In here, as well as in the application of exogenous JA and JA-Ile, it resulted in increased susceptibility to *C. graminicola* (Wang et al., 2020). These results, together with the present data of this study, suggest that individual steps in JA biosynthetic pathways seem to be tightly controlled in a pathogen-dependent manner to produce diverse intermediate products, whose functions might be distinct from those of the final functional jasmonates JA-Ile. Additionally, pathogens might also produce JA, JA-Ile, and JA-Ile analogs to facilitate their pathogenicity (Gao and Kolomiets, 2009; Brodhun et al., 2013; Cole et al., 2014; Geng et al., 2014; Patkar et al., 2015; Gimenez-Ibanez et al., 2016; Deboever et al., 2020). Thus, it is reasonable to propose that the bioactive hormone JA-Ile is likely regulated by ZmLOX5 in a resistant line to avoid its overproduction. Although the exact mechanisms behind *ZmLOX5*-mediated suppression of jasmonates synthesis are not fully understood, our results provided genetic evidence that this gene and its products play a vital role in defense against GSR via negative regulation of JA and JA-Ile biosynthesis.

ZmLOX5-Derived 9-Oxylipins Contribute to Resistance to GSR

It has been shown that 9-oxylipins possessed strong activity in defense against various pathogens in several plant species (Christensen et al., 2015; Deboever et al., 2020). For instance, 9-hydroxy-10*E*,12*Z*-octadecadienoic acid (9-HOD) was found to be 20-fold higher in WT than in the susceptible mutant of *Nicotiana attenuata* upon bacterial infection (Schuck et al., 2014). Moreover, a greater 9-KOT level was shown to correlate with increased resistance (Vicente et al., 2012), while (9*S*, 10*E*, 12*Z*, 15*Z*)-9-hydroxy-10,12,15-octadecatrienoic acid (9-HOT) was suggested to participate in defensive responses and cell wall modification during the reaction to hemibiotrophic bacteria in Arabidopsis (Vellosillo et al., 2013). Similarly, in the present study, the contents of multiple 9-oxylipins, including 9OH-10KOM, 9OH-10KOD, 9-HOT, 9-HOD, 9-KOD, and 9-KOT, were much higher in the resistant line W438 than in susceptible *zmlox5-3*, emphasizing the important role of 9-oxylipins in resistance to GSR.

Another 9-oxylipin, 10-OPEA, has been reported to act as a phytoalexin and an inducer of plant programmed cell death (PCD) to suppress some fungal pathogens (Christensen et al., 2015; He et al., 2019). However, our results did not support such a role for this molecule in maize interaction

with *F. graminearum*. We showed that this oxylipin and the putative biosynthetic gene encoding a 9-AOS, *AOS2b*, were more strongly induced in *zmlox5-3* compared with B73 and W438 (**Figure 5B**). One possible reason behind such opposite roles of 10-OPEA is that high 10-OPEA content was related with PCD caused by infection of necrotrophic pathogen *Cochliobolus heterostrophus* in the previous study, despite the minor effect of 10-OPEA on fungal growth *in vitro* (Christensen et al., 2015), whereas *F. graminearum* possess hemibiotrophic lifestyle. This is reminiscent of the widely published contrasting roles of JA-Ile in resistance to necrotrophs, but in susceptibility to hemibiotrophs. However, further experiments will be needed to show whether higher levels of 10-OPEA are indeed associated with enhanced susceptibility of *zmlox5-3* mutants.

In summary, this study has shown that *zmlox5-3* mutant accumulates higher amounts of diverse jasmonates together with greater expression levels of JAs, but lower levels of 9-oxylipins and reduced gene expression of *9-LOXs*. On the contrary, lower amounts of JAs but higher levels of multiple 9-oxylipins were found in the resistant line. These findings indicate that 9-oxylipins and JAs pathways might antagonize each other and that *ZmLOX5*-regulated 9-oxylipins contribute to resistance, whereas JAs seem to play a negative role in maize defense against GSR.

DATA AVAILABILITY STATEMENT

The data presented in the study are deposited in the NCBI GEO database, accession number GSE174508.

AUTHOR CONTRIBUTIONS

XG and MK: conceptualization and resources. QW, P-CH, and YW: data curation. QW, YS, FW, and P-CH: formal analysis. XG: funding acquisition, project administration, and supervision. QW, YS, FW, P-CH, XR, LM, and XL: investigation. QW, YS, P-CH, and XR: methodology. QW and YS: validation. QW and XG: writing-original draft preparation. QW, XG, and MK: writing-review and editing. All authors read and approved the final manuscript.

FUNDING

This work was supported financially by the grants from The National Key Research and Development Program of China (No. 2016YFD0101002), National Natural Science Foundation of China (Nos. 31671702 and 31471508), and Jiangsu Collaborative Innovation Center for Modern Crop Production (JCIC-MCP).

ACKNOWLEDGMENTS

The bioinformatics analysis of this work was supported in part by the high-performance computing platform of Bioinformatics Center, Nanjing Agricultural University. The authors are grateful to Prof. Wolfgang Friedt, Institute of Plant Breeding, Justus Liebig University of Giessen, Germany, for his great help with language editing.

SUPPLEMENTARY MATERIAL

The Supplementary Material for this article can be found online at: https://www.frontiersin.org/articles/10.3389/fpls.2021.699146/full#supplementary-material

Supplementary Figure 1 | RNA-seq data correlation of different replicates from B73 and *zmlox5-3* at 0, 12 and 24 h post-*F. graminearum* inoculation.

Supplementary Figure 2 | Gene Ontology (GO) term enrichment of up- and down-regulated differentially expressed genes (DEGs) significantly enriched in **(A)** Cellular component (CC) and **(B)** Molecular function (MF) in B73 and *zmlox5-3*.

Supplementary Table 1 | List of primers for qRT-PCR used in this study.

Supplementary Table 2 | Statistics of all samples mapped to the B73 reference genome.

Supplementary Table 3 | Two-way ANOVA (genotype × time) statistical analysis of oxylipins identified in this study.

Supplementary Table 4 | Content fold change of oxylipins identified in B73, *lox5-3*, and W438 at 24 and 48 hai. The fold changes of oxylipins were calculated based on the contents in infected samples over that in control samples at 24 and 48 hai, respectively.

REFERENCES

Andreou, A., Brodhun, F., and Feussner, I. (2009). Biosynthesis of oxylipins in non-mammals. *Prog. Lipid Res.* 48, 148–170. doi: 10.1016/j.plipres.2009.02.002

Ashburner, M., Ball, C. A., Blake, J. A., Botstein, D., Butler, H., Cherry, J. M., et al. (2000). Gene ontology: tool for the unification of biology. The gene ontology consortium. *Nat. Genet.* 25, 25–29. doi: 10.1038/75556

Bate, N. J., and Rothstein, S. J. (1998). C6-volatiles derived from the lipoxygenase pathway induce a subset of defense-related genes. *Plant J.* 16, 561–569. doi: 10.1046/j.1365-313x.1998.00324.x

Battilani, P., Lanubile, A., Scala, V., Reverberi, M., Gregori, R., Falavigna, C., et al. (2018). Oxylipins from both pathogen and host antagonize jasmonic acid-mediated defence via the 9-lipoxygenase pathway in *Fusarium verticillioides* infection of maize. *Mol. Plant Pathol.* 19, 2162–2176. doi: 10.1111/mpp.12690

Birkett, M. A., Campbell, C. A. M., Chamberlain, K., Guerrieri, E., Hick, A. J., Martin, J. L., et al. (2000). New roles for cis-jasmoneas an insect semiochemical and in plant defense. *Proc. Natl. Acad. Sci. U.S.A.* 97, 9329–9334. doi: 10.1073/pnas.160241697

Blee, E. (2002). Impact of phyto-oxylipins in plant defense. *Trends Plant Sci.* 7, 315–322. doi: 10.1016/s1360-1385(02)02290-2

Borrego, E. J., and Kolomiets, M. V. (2016). Synthesis and functions of jasmonates in maize. *Plants* 5:41. doi: 10.3390/plants5040041

Brandfass, C., and Karlovsky, P. (2008). Upscaled CTAB-based DNA extraction and real-time PCR assays for *Fusarium culmorum* and *F. graminearum* DNA in plant material with reduced sampling error. *Int. J. Mol. Sci.* 9, 2306–2321. doi: 10.3390/ijms9112306

Brodhun, F., Cristobal-Sarramian, A., Zabel, S., Newie, J., Hamberg, M., and Feussner, I. (2013). An iron 13S-lipoxygenase with an alpha-linolenic acid specific hydroperoxidase activity from *Fusarium oxysporum*. *PLoS ONE* 8:e64919. doi: 10.1371/journal.pone.0064919

Brunner, K., Kovalsky Paris, M. P., Paolino, G., Burstmayr, H., Lemmens, M., Berthiller, F., et al. (2009). A reference-gene-based quantitative PCR method as a tool to determine Fusarium resistance in wheat. *Anal. Bioanal. Chem.* 395, 1385–1394. doi: 10.1007/s00216-009-3083-3

Caarls, L., Elberse, J., Awwanah, M., Ludwig, N. R., de Vries, M., Zeilmaker, T., et al. (2017). Arabidopsis JASMONATE-INDUCED OXYGENASES

down-regulate plant immunity by hydroxylation and inactivation of the hormone jasmonic acid. *Proc. Natl. Acad. Sci. U.S.A.* 114, 6388–6393. doi: 10.1073/pnas.1701101114

Chong, J., Wishart, D. S., and Xia, J. (2019). Using MetaboAnalyst 4.0 for comprehensive and integrative metabolomics data analysis. *Curr. Protoc. Bioinformatics*. 68:e86. doi: 10.1002/cpbi.86

Christensen, S. A., Huffaker, A., Kaplan, F., Sims, J., Ziemann, S., Doehlemann, G., et al. (2015). Maize death acids, 9-lipoxygenase-derived cyclopente(a)nones, display activity as cytotoxic phytoalexins and transcriptional mediators. *Proc. Natl. Acad. Sci. U.S.A.* 112, 11407–11412. doi: 10.1073/pnas.1511131112

Christensen, S. A., Nemchenko, A., Park, Y. S., Borrego, E., Huang, P. C., Schmelz, E. A., et al. (2014). The novel monocot-specific 9-lipoxygenase *ZmLOX12* is required to mount an effective jasmonate-mediated defense against *Fusarium verticillioides* in maize. *Mol. Plant Microbe Interact.* 27, 1263–1276. doi: 10.1094/MPMI-06-13-0184-R

Cole, S. J., Yoon, A. J., Faull, K. F., and Diener, A. C. (2014). Host perception of jasmonates promotes infection by *Fusarium oxysporum* formae speciales that produce isoleucine- and leucine-conjugated jasmonates. *Mol. Plant Pathol.* 15, 589–600. doi: 10.1111/mpp.12117

Deboever, E., Deleu, M., Mongrand, S., Lins, L., and Fauconnier, M. L. (2020). Plant-pathogen interactions: underestimated roles of phyto-oxylipins. *Trends Plant Sci.* 25, 22–34. doi: 10.1016/j.tplants.2019.09.009

Famer, E. E., Almeras, E., and Krishnamurthy, V. (2003). Jasmonates and related oxylipins in plant responses to pathogenesis and herbivory. *Curr. Opin. Plant Biol.* 6, 372–378. doi: 10.1016/s1369-5266(03)00045-1

Fammartino, A., Cardinale, F., Gobel, C., Mene-Saffrane, L., Fournier, J., Feussner, I., et al. (2007). Characterization of a divinyl ether biosynthetic pathway specifically associated with pathogenesis in tobacco. *Plant Physiol.* 143, 378–388. doi: 10.1104/pp.106.087304

Feussner, I., and Wasternack, C. (2002). The lipoxygenase pathway. *Annu. Rev. Plant Biol.* 53, 275–297. doi: 10.1146/annurev.arplant.53.100301.135248

Gao, X., and Kolomiets, M. V. (2009). Host-derived lipids and oxylipins are crucial signals in modulating mycotoxin production by fungi. *Toxin Rev.* 28, 79–88. doi: 10.1080/15569540802420584

Gao, X., Shim, W. B., Gobel, C., Kunze, S., Feussner, I., Meeley, R., et al. (2007). Disruption of a maize 9-lipoxygenase results in increased resistance to fungal pathogens and reduced levels of contamination with mycotoxin fumonisin. *Mol. Plant Microbe Interact.* 20, 922–933. doi: 10.1094/MPMI-20-8-0922

Geng, X., Jin, L., Shimada, M., Kim, M. G., and Mackey, D. (2014). The phytotoxin coronatine is a multifunctional component of the virulence armament of *Pseudomonas syringae*. *Planta* 240, 1149–1165. doi: 10.1007/s00425-014-2151-x

Gimenez-Ibanez, S., Chini, A., and Solano, R. (2016). How microbes twist jasmonate signaling around their little fingers. *Plants* 5:10009. doi: 10.3390/plants5010009

Glazebrook, J. (2005). Contrasting mechanisms of defense against biotrophic and necrotrophic pathogens. *Annu. Rev. Phytopath.* 43, 205–227. doi: 10.1146/annurev.phyto.43.040204.135923

Gorman, Z., Christensen, S. A., Yan, Y., He, Y., Borrego, E., and Kolomiets, M. V. (2020). Green leaf volatiles and jasmonic acid enhance susceptibility to anthracnose diseases caused by *Colletotrichum graminicola* in maize. *Mol. Plant Pathol.* 21, 702–715. doi: 10.1111/mpp.12924

He, Y., Borrego, E. J., Gorman, Z., Huang, P. C., and Kolomiets, M. V. (2020). Relative contribution of LOX10, green leaf volatiles and JA to wound-induced local and systemic oxylipin and hormone signature in *Zea mays* (maize). *Phytochem* 74:112334. doi: 10.1016/j.phytochem.2020.112334

He, Y., Karre, S., Johal, G. S., Christensen, S. A., and Balint-Kurti, P. (2019). A maize polygalacturonase functions as a suppressor of programmed cell death in plants. *BMC Plant Biol.* 19:310. doi: 10.1186/s12870-019-1897-5

Howe, G. A. (2001). Cyclopentenone signals for plant defense: remodeling the jasmonic acid response. *Proc. Natl. Acad. Sci. U.S.A.* 98, 12317–12319. doi: 10.1073/pnas.231480898

Howe, G. A., Major, I. T., and Koo, A. J. (2018). Modularity in jasmonate signaling for multistress resilience. *Annu. Rev. Plant Biol.* 69, 387–415. doi: 10.1146/annurev-arplant-042817-040047

Howe, G. A., and Schilmiller, A. L., (2002). Oxylipin metabolism in responseto stress. *Curr. Opin. Plant Biol.* 5, 230–236. doi: 10.1016/s1369-5266(02)00250-9

Isakeit, T., Gao, X., and Kolomiets, M. (2007). Increased resistance of a maize mutant lacking the 9-lipoxygenase gene, *ZmLOX3*, to root rot caused by exserohilum pedicellatum. *J. Phytopathol.* 155, 758–760. doi: 10.1111/j.1439-0434.2007.01301.x

Kanehisa, M., Sato, Y., Kawashima, M., Furumichi, M., and Tanabe, M. (2016). KEGG as a reference resource for gene and protein annotation. *Nucleic Acids Res.* 44, D457–D462. doi: 10.1093/nar/gkv1070

Lanubile, A., Borrelli, V. M. G., Soccio, M., Giorni, P., Stagnati, L., Busconi, M., et al. (2021). Loss of ZmLIPOXYGENASE4 decreases *Fusarium verticillioides* resistance in maize seedlings. *Genes* 12:335. doi: 10.3390/genes 12030335

Ma, L., Sun, Y., Ruan, X., Huang, P. C., Wang, S., Li, S., et al. (2021). Genome-wide characterization of jasmonates signaling components reveals the essential role of *ZmCOI1a-ZmJAZ15* action module in regulating maize immunity to gibberella stalk rot. *Int. J. Mol. Sci.* 22:20870. doi: 10.3390/ijms22020870

Mueller, D. S., and Wise, K. A. (2015). *Corn disease loss estimates from the United States and Ontario, Canada-2014. Diseases of Corn. BP-96-14-W*. West Lafayette, IN: Purdue University.

Muller, M., Munne-Bosch, S. (2011). Rapid and sensitive hormonal profiling of complex plant samples by liquid chromatography coupled to electrospray ionization tandem mass spectrometry. *Plant Methods.* 7:37. doi: 10.1186/1746-4811-7-37

Mur, L. A., Kenton, P., Atzorn, R., Miersch, O., and Wasternack, C. (2006). The outcomes of concentration-specific interactions between salicylate and jasmonate signaling include synergy, antagonism, and oxidative stress leading to cell death. *Plant Physiol.* 140, 249–262. doi: 10.1104/pp.105.072348

Nemchenko, A., Kunze, S., Feussner, I., and Kolomiets, M. (2006). Duplicate maize 13-lipoxygenase genes are differentially regulated by circadian rhythm, cold stress, wounding, pathogen infection, and hormonal treatments. *J. Exp. Bot.* 57, 3767–3779. doi: 10.1093/jxb/erl137

Park, Y. S. (2012). *Diverse Functions of the Two Segmentally Duplicated 9-Lipoxygenase Zmlox4 and Zmlox5 of Maize*. [Doctoral dissertation]. College Station, TX: Texas A & M University.

Park, Y. S., Kunze, S., Ni, X., Feussner, I., and Kolomiets., M. V. (2010). Comparative molecular and biochemical characterization of segmentally duplicated 9-lipoxygenase genes ZmLOX4 and ZmLOX5 of maize. *Planta* 231, 1425–1437. doi: 10.1007/s00425-010-1143-8

Pathi, K. M., Rink, P., Budhagatapalli,. N., Betz, R., Saado, I., Hiekel, S., et al. (2020). Engineering Smut Resistance in Maize by Site-Directed Mutagenesis of LIPOXYGENASE 3. *Front. Plant Sci.* 11:543895. doi: 10.3389/fpls.2020.543895

Patkar, R. N., Benke, P. I., Qu, Z., Chen, Y. Y., Yang, F., Swarup, S., et al. (2015). A fungal monooxygenase-derived jasmonate attenuates host innate immunity. *Nat. Chem. Biol.* 11, 733–740. doi: 10.1038/nchembio.1885

Pieterse, C. M. J., van der Does, A., Zamioudis, C., Leon Reyes, H. A., and van Wees, S. C. M. (2012). Hormonal modulation of plant immunity. *Annu. Rev. Cell Dev. Biol.* 28, 489–521. doi: 10.1146/annurev-cellbio-092910-154055

Rance, I., Fournier, J., and Esquerre-Tugaye, M. T. (1998). The incompatible interaction between *Phytophthora parasitica var. nicotianae race 0* and tobacco is suppressed in transgenic plants expressing antisense lipoxygenase sequences. *Proc. Natl. Acad. Sci. U.S.A.* 95, 6554–6559. doi: 10.1073/pnas.95.11.6554

Robert-Seilaniantz, A., Grant, M., and Jones, J. D. (2011). Hormone crosstalk in plant disease and defense: more than just jasmonate-salicylate antagonism. *Annu. Rev. Phytopath.* 49, 317–343. doi: 10.1146/annurev-phyto-073009-114447

Schneider, C., Pratt, D. A., Porter, N. A., and Brash, A. R. (2007). Control of oxygenation in lipoxygenase and cyclooxygenase catalysis. *Chem. Biol.* 14, 473–488. doi: 10.1016/j.chembiol.2007.04.007

Schuck, S., Kallenbach, M., Baldwin, I. T., and Bonaventure, G. (2014). The Nicotiana attenuata GLA1 lipase controls the accumulation of *Phytophthora parasitica*-induced oxylipins and defensive secondary metabolites. *Plant Cell Environ.* 37, 1703–1715. doi: 10.1111/pce.12281

Smirnova, E., Marquis, V., Poirier, L., Aubert, Y., Zumsteg, J., Menard, R., et al. (2017). Jasmonic acid oxidase 2 hydroxylates jasmonic acid and represses basal defense and resistance responses against *Botrytis cinerea* infection. *Mol. Plant.* 10, 1159–1173. doi: 10.1016/j.molp.2017.07.010

Staswick, P. E., and Tiryaki, I. (2004). The oxylipin signal jasmonic acid is activated by an enzyme that conjugates it to isoleucine in Arabidopsis. *Plant Cell.* 16, 2117–2127. doi: 10.1105/tpc.104.023549

Stintzi, A., Weber, H., Raymond, P., Browse, J., and Farmer, E. E. (2001). Plant defense in the absence of jasmonic acid: the role of cyclopentenones. *Proc. Natl. Acad. Sci. U.S.A.* 98, 12837–12842. doi: 10.1073/pnas.211311098

Stitz, M., Baldwin, I. T., and Gaquerel, E. (2011). Diverting the flux of the JA pathway in *Nicotiana attenuata* compromises the plant's defense metabolism and fitness in nature and glasshouse. *PLoS ONE*. 6:e25925. doi: 10.1371/journal.pone.0025925

Sun, Y., Ruan, X., Ma, L., Wang, F., and Gao, X. (2018). Rapid screening and evaluation of maize seedling resistance to stalk rot caused by *Fusarium* spp. *Bio-protocol* 8:e2859. doi: 10.21769/BioProtoc.2859

Sun, Y., Ruan, X., Wang, Q., Zhou, Y., Ma, L., Wang, F., et al. (2021). Integrated gene co-expression analysis and metabolites profiling highlight the important role of ZmHIR3 in maize resistance to Gibberella stalk rot. *Front. Plant Sci.* 12:664733. doi: 10.3389/fpls.2021.664733

Thatcher, L. F., Manners, J. M., and Kazan, K. (2009). *Fusarium oxysporum* hijacks COI1-mediated jasmonate signaling to promote disease development in Arabidopsis. *Plant J.* 58, 927–939. doi: 10.1111/j.1365-313x.2009.03831.x

Turner, J. G., Ellis, C., and Devoto, A. (2002). The jasmonate signal pathway. *Plant Cell* 14, S153–S164. doi: 10.1105/tpc.000679

Vellosillo, T., Aguilera, V., Marcos, R., Bartsch, M., Vicente, J., Cascon, T., et al. (2013). Defense activated by 9-lipoxygenase-derived oxylipins requires specific mitochondrial proteins. *Plant Physiol.* 161, 617–627. doi: 10.1104/pp.112.207514

Vicente, J., Cascon, T., Vicedo, B., Garcia-Agustin, P., Hamberg, M., and Castresana, C. (2012). Role of 9-lipoxygenase and alpha-dioxygenase oxylipin pathways as modulators of local and systemic defense. *Mol. Plant.* 5, 914–928. doi: 10.1093/mp/ssr105

Wang, C., Yang, Q., Wang, W., Li, Y., Guo, Y., Zhang, D., et al. (2017). A transposon-directed epigenetic change in *ZmCCT* underlies quantitative resistance to Gibberella stalk rot in maize. *New Phytol.* 215, 1503–1515. doi: 10.1111/nph.14688

Wang, K. D., Borrego, E. J., Kenerley, C. M., and Kolomiets, M. V. (2020). Oxylipins other than jasmonic acid are xylem-resident signals regulating systemic resistance induced by *Trichoderma virens* in Maize. *Plant Cell.* 32, 166–185. doi: 10.1105/tpc.19.00487

Wang, Q., Vera Buxa, S., Furch, A., Friedt, W., and Gottwald, S. (2015). Insights into *Triticum aestivum* seedling root rot caused by *Fusarium graminearum*. *Mol. Plant Microbe Interact.* 28, 1288–1303. doi: 10.1094/MPMI-07-15-0144-R

Wasternack, C. (2007). Jasmonates: an update on biosynthesis, signal transduction and action in plant stress response, growth and development. *Ann. Bot.* 100, 681–697. doi: 10.1093/aob/mcm079

Wasternack, C., and Feussner, I. (2018). The oxylipin pathways: biochemistry and function. *Annu. Rev. Plant Biol.* 69, 363–386. doi: 10.1146/annurev-arplant-042817-040440

Wasternack, C., and Hause, B. (2013). Jasmonates: biosynthesis, perception, signal transduction and action in plant stress response, growth and development. An update to the 2007 review in Annals of Botany. *Ann Bot.* 111, 1021–1058. doi: 10.1093/aob/mct067

Yan, Y., Christensen, S., Isakeit, T., Engelberth, J., Meeley, R., Hayward, A., et al. (2012). Disruption of OPR7 and OPR8 reveals the versatile functions of jasmonic acid in maize development and defense. *Plant Cell.* 24, 1420–1436. doi: 10.1105/tpc.111.094151

Ye, J., Zhong, T., Zhang, D., Ma, C., Wang, L., Yao, L., et al. (2019). The auxin-regulated protein *ZmAuxRP1* coordinates the balance between root growth and stalk rot disease resistance in maize. *Mol. Plant.* 12, 360–373. doi: 10.1016/j.molp.2018.10.005

Conflict of Interest: The authors declare that the research was conducted in the absence of any commercial or financial relationships that could be construed as a potential conflict of interest.

Publisher's Note: All claims expressed in this article are solely those of the authors and do not necessarily represent those of their affiliated organizations, or those of the publisher, the editors and the reviewers. Any product that may be evaluated in this article, or claim that may be made by its manufacturer, is not guaranteed or endorsed by the publisher.

Copyright © 2021 Wang, Sun, Wang, Huang, Wang, Ruan, Ma, Li, Kolomiets and Gao. This is an open-access article distributed under the terms of the Creative Commons Attribution License (CC BY). The use, distribution or reproduction in other forums is permitted, provided the original author(s) and the copyright owner(s) are credited and that the original publication in this journal is cited, in accordance with accepted academic practice. No use, distribution or reproduction is permitted which does not comply with these terms.

frontiers in Plant Science

ORIGINAL RESEARCH
published: 27 October 2021
doi: 10.3389/fpls.2021.731694

Green Leaf Volatile-Burst in *Selaginella moellendorffii*

*Moena Tanaka, Takao Koeduka and Kenji Matsui**

Graduate School of Sciences and Technology for Innovation, Yamaguchi University, Yamaguchi, Japan

Green leaf volatiles (GLVs) consist of six-carbon volatile aldehydes, alcohols, and their esters. They are formed from polyunsaturated fatty acids and are involved in the defense of plants against herbivores and pathogens. GLVs generally have low concentrations in intact healthy plant tissues, but the biosynthetic pathway to form GLVs is quickly activated by mechanical damage to tissues, an event called the GLV-burst. Most seed plants have the ability to implement GLV-burst; however, this potential in non-seed plants has not been extensively researched. In this study, we examined the GLV-burst capacity of monilophytes, lycophytes, and bryophytes, and confirmed that monilophytes and lycophytes showed substantial GLV-burst ability, while bryophytes did not, with a few exceptions. When the genome sequence of a model lycophyte, *Selaginella moellendorffii* was reviewed, 10 genes were found that showed high similarity with the non-canonical cytochrome P450 enzymes, CYP74s, specialized in oxylipin formation. Recombinant proteins expressed with *Escherichia coli* showed that one of them had the ability to encode allene oxide synthase, and another encoded hydroperoxide lyase (HPL), preferring linolenic acid 13-hydroperoxide, and it was inferred that this gene was responsible for GLV-burst in *S. moellendorffii*. Based on the phylogenetic tree constructed with CYP74s of non-seed and seed plants, we hypothesized that HPL was acquired independently in the lycophyte and seed plants through diversification of CYP74 genes.

Keywords: green leaf volatiles (GLV), hydroperoxide lyase, CYP74 enzymes, non-seed plants, *Selaginella moellendorffii* (Spikemoss)

OPEN ACCESS

Edited by:
Michael V. Kolomiets,
Texas A&M University, United States

Reviewed by:
Masaharu Mizutani,
Kobe University, Japan
Lei Wang,
Kunming Institute of Botany, Chinese Academy of Sciences (CAS), China

***Correspondence:**
Kenji Matsui
matsui@yamaguchi-u.ac.jp

Specialty section:
This article was submitted to Plant Metabolism and Chemodiversity, a section of the journal Frontiers in Plant Science

Received: *28 June 2021*
Accepted: *06 October 2021*
Published: *27 October 2021*

Citation:
Tanaka M, Koeduka T and Matsui K (2021) Green Leaf Volatile-Burst in Selaginella moellendorffii. Front. Plant Sci. 12:731694. doi: 10.3389/fpls.2021.731694

INTRODUCTION

Oxylipins are biological compounds formed from fatty acids and their esters through at least one step of dioxygenation reaction. They are synthesized *de novo* when cells are activated by mechanical trauma or by specific stresses but are generally not stored in healthy cells. Most oxylipins are signaling molecules that act as autocrine, paracrine, or even endocrine, and in certain cases of volatile oxylipins found in fungi and plants, they can mediate communication between organisms. The fatty acid substrate mainly used for oxylipin formation depends on the kingdom to which the organism belongs. Animals prefer arachidonic acid for the biosynthesis of prostaglandins and leukotrienes (Funk, 2001), whereas fungi normally use linoleic acid to form precocious sexual inducers and volatile eight-carbon alcohols (Brodhun and Feussner, 2011). The biosynthesis of jasmonates and green leaf volatiles (GLVs) in vascular plants is generally performed with the use of α-linolenic acid (Wasternack and Feussner, 2018), although arachidonic acid is more often used for oxylipin formation in bryophytes (Croisier et al., 2010).

Green leaf volatiles consist of six-carbon aldehydes, alcohols, and their esters (Matsui, 2006; Ameye et al., 2018). In intact and healthy, unstressed plant tissues, the GLV levels are generally low, but they are quickly formed when plant tissues are mechanically damaged (D'Auria et al., 2007; Mochizuki and Matsui, 2018). The free form of α-linolenic acid or the form esterified with glycerolipids is oxygenated by lipoxygenase to yield 13-hydroperoxides, which are further metabolized by the cytochrome P450 enzyme (CYP74B) fatty acid hydroperoxide lyase (HPL) (**Figure 1**). HPL forms (*Z*)-3-hexenal and 12-oxo-(*Z*)-9-dodecenoic acid from the 13-hydroperoxide of α-linolenic acid. The enzymatic conversion of α-linolenic acid (and its esters) quickly progresses when the cells are damaged by mechanical wounding from herbivores or pathogens. A portion of the (*Z*)-3-hexenal formed in the injured tissues diffuses out to the neighboring intact tissues, where it is efficiently reduced by cinnamaldehyde and hexenal reductase (CHR) to yield (*Z*)-3-hexen-1-ol (Tanaka et al., 2018), which is further converted into (*Z*)-3-hexen-1-yl acetate by acetyl CoA:(*Z*)-3-hexen-1-ol acetyltransferase (CHAT) (D'Auria et al., 2007).

This quick formation of GLVs, termed the GLV-burst in this study, is detectable within seconds after mechanical wounding of Arabidopsis leaves (D'Auria et al., 2007). GLVs are directly and indirectly involved in plant defense against herbivores and pathogens (Matsui, 2006; Ameye et al., 2018). Depletion of HPL in potato plants increases aphid performance (Vancanneyt et al., 2001). Overexpression of the HPL gene in *Arabidopsis* plants enhances defense against the necrotrophic fungal pathogen *Botrytis cinerea* (direct defense) and promotes attraction of parasitic wasps to herbivores feeding on the transgenic *Arabidopsis* leaves (indirect defense) (Shiojiri et al., 2006). To efficiently exert these defensive effects, rapid formation of GLVs is desirable.

The aim of this study was to determine when plants acquired GLV-burst ability. A comprehensive survey of 37 plant species, including bryophytes, monilophytes, and spermatophytes, showed that almost all vascular plants formed GLVs after disruption of the green tissues; however, one bryophyte, *Pogonatum inflexum*, revealed little GLV formation after damage (Hatanaka et al., 1978). The survey was furthered by examining 23 species of mosses collected in Switzerland and Germany (Croisier et al., 2010), most of which showed vigorous activity to form 1-octen-3-ol, but presented negligible GLV formation after freeze-thaw treatment, except for two species (*Neckera complanate* and *Dicranum scoparium*). HPL genes have been identified and studied in various seed plants (Matsui, 2006; Ameye et al., 2018), whereas there is only one report on the HPL gene in a non-seed plant, and that was from the moss *Physcomitrella patens* (Stumpe et al., 2006). This HPL (PpHPL) is largely involved in the formation of nine-carbon volatiles from linoleic acid 9-hydroperoxide and arachidonic acid 12-hydroperoxide (Stumpe et al., 2006); thus, its involvement in GLV-burst is implausible. Previously, we analyzed the genome sequences of *Marchantia polymorpha* and *Klebsormidium nitens* (formerly *K. flaccidum*), and revealed two and one CYP74 genes, respectively, all of which encoding allene oxide synthases (AOSs) but not HPL (Koeduka et al., 2015).

AOS is an enzyme that shares the substrate with HPL and converts linolenic acid 13-hydroperoxide into an unstable allene oxide (**Figure 1**), which when acted on by allene oxide cyclase is converted into 12-oxo-phytodienoic acid, which is further metabolized to yield jasmonic acid (Wasternack and Feussner, 2018). AOSs also belong to the CYP74 family and have high sequence similarity with HPLs. CYP74s are non-canonical cytochrome P450 enzymes that use hydroperoxides as opposed to molecular oxygen, which is characteristically used by canonical cytochrome P450 enzymes. CYP74s are almost exclusively found in plants (Brash, 2009). In addition to HPL and AOS, divinyl ether synthase (DES) and epoxyalcohol synthase (EAS) (**Figure 1**) belong to the CYP74 family with high sequence similarity. The enzymes grouped in the CYP74 family are quite similar to each other, and small amino acid exchange between them is often enough to interconvert their enzyme function (Lee et al., 2008; Toporkova et al., 2008, 2019; Scholz et al., 2012).

The ability of GLV-burst had likely been acquired between bryophytes and monilophytes, namely lycophytes, through innovation of the HPL that forms (*Z*)-3-hexenal as one of the products, by modifying the CYP74 genes available at that time. We collected several species of lycophytes, monilophytes, and bryophytes, and examined their GLV-burst ability. We also used the genome sequence of *Selaginella moellendorffii*, a lycophyte that has revealed a strong GLV-burst capacity. *S. moellendorffii* has 10 CYP74-like genes, six of which have been characterized as AOS, DES, or EAS (Gorina et al., 2016; Pratiwi et al., 2017; Toporkova et al., 2018). After examining the remaining four genes, we found that at least one of them encoded HPL and could be responsible for the GLV-burst. Based on the results shown in this study, the manner in which the plant lineage evolved the GLV-burst ability is discussed.

MATERIALS AND METHODS

Plant Materials

Selaginella moellendorffii (provided by Dr. Xiaonan Xie, Utsunomiya University, Japan) was cultivated in a growth chamber at 22°C under 14 h of light/day (fluorescent lights at 62.5 μmol m^{-2} s^{-1}) in normal potting soil mixed with Akadama and Hyuga soils (TACHIKAWA HEIWA NOUEN, Tochigi, Japan) in the ratio of 1:1:1. *Physcomitrella patens* (Gransden2004, provided by Prof. Mitsuyasu Hasebe, National Institute for Basic Biology, Japan) were grown in Jiffy pots (SAKATA SEED, Kanagawa, Japan) in a plant box (As One, Osaka, Japan). *Marchantia polymorpha* males (Takaragaike-1) were grown on half-strength Gamborg B5 medium (pH 5.5) with 1.0% agar at 22°C under continuous white light (fluorescent lights at 35 μmol m^{-2} s^{-1}). *Sphagnum palustre* (purchased from a local market) was grown on peat moss (SAKATA SEED, Kanagawa, Japan) in the same growth chamber as *S. moellendorffii*. The list of plants used in this study is shown in **Supplementary Table 1**, and their phylogenetic relationship is illustrated in **Supplementary Figure 1**.

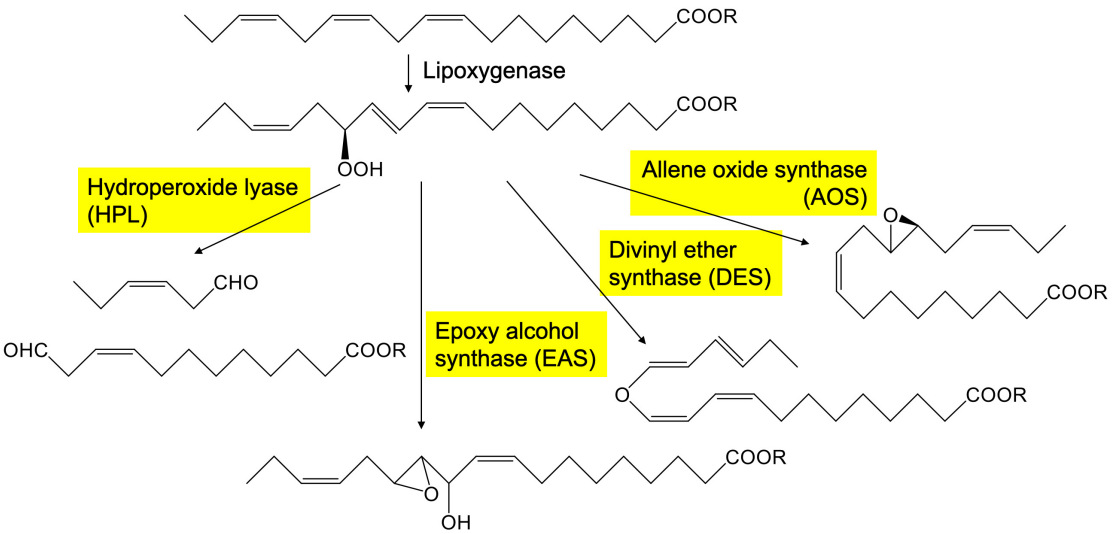

FIGURE 1 | Representative pathway to form oxylipins from 13-hydroperoxide of linolenate catalyzed by CYP74s in plants. The enzymes with yellow background belong to CYP74 family.

Volatile Analysis

Plant leaves or thalli (100 mg fresh weight) were ground with 2 mL of 50 mM MES-KOH (pH 6.3) for 1 or 5 min with a mortar and pestle. The enzyme reactions were terminated by the addition of 2 mL of methyl *tert*-butyl ether containing 0.001% butylated hydroxytoluene and 5 nmol mL^{-1} tetralin (internal standard). After centrifugation, the resultant green supernatant was directly subjected to GC-MS analysis. To determine the amounts in intact tissues, the tissues were frozen in liquid nitrogen immediately after harvest and powdered with a Micro Smash MS-100R cell disruptor (TOMY, Tokyo, Japan) with stainless steel beads (1 mm). The volatiles in the frozen powder were immediately extracted with the solvent containing the internal standard. The volatiles were analyzed using GC-MS (QP-2010, Shimadzu, Kyoto, Japan) with a DB-WAX column (30 m length × 0.25 mm diameter × 0.25 μm film thickness, Agilent Technologies, Santa Clara, CA, United States). Injection was performed using a splitless mode with a sampling time of 1 min at 240°C. A column temperature of 40°C was held for 5 min and increased by 5.0°C min^{-1} to 200°C. The carrier gas (He) was delivered at 44.8 cm s^{-1}. The MS was operated in electron ionization mode with an ionization energy of 70 eV, and the temperatures of the ion source and interface were 200 and 240°C, respectively, with a continuous scan from *m/z* 40–350. For quantification, calibration curves were constructed with (*Z*)-3-hexenal (provided by Zeon Co., Tokyo, Japan), (*E*)-2-hexenal, and *n*-hexanal (both from FUJIFILM Wako Pure Chemical Co., Tokyo, Japan).

In order to compare volatiles in intact and partially wounded tissues, an SPME (solid phase micro extraction) fiber (50/30-μm DVB/Carboxen/PDMS; Supelco, MilliporeSigma, Burlington, MA, United States) was used essentially as described previously (Matsui et al., 2012; Tanaka et al., 2018). In brief, 150–200 mg fresh weight of shoots and roots of *S. moellendorffii* were left intact or cut into pieces (1–2 mm wide) with scissors and immediately placed in a glass vial (22 mL, Perkin Elmer, Waltham, MA, United States). The vial was sealed tightly with a butyl stopper and a crimp-top seal. The SPME fiber was exposed to the headspace of the vial for 30 min at 25°C. Thereafter, the fiber was inserted into the insertion port of the GC-MS system shown above but with the SPME Sleeve (Supelco) for the glass insert. The sampling time was 1 min with the splitless injection mode. The fiber was held in the injection port for 10 min to fully remove compounds from the matrix. Chromatography was carried out as shown above.

Expression of Recombinant Enzymes in *Escherichia coli*

Total genomic DNA was extracted from the aboveground parts of *S. moellendorffii* and used as the template for PCR with primers designed based on the genome sequence in Phytozome[1]. Primers used in this study are listed in **Supplementary Table 2**. The resultant product was cloned into the expression vector pET100/D-TOPO (Invitrogen, Waltham, MA, United States) using the TOPO cloning strategy. *Escherichia coli* BL21 Star (DE3) was used as the host for the expression of recombinant proteins. An overnight culture (500 μL) of the cells was added to 300 mL of fresh LB with ampicillin (100 μg mL^{-1}) and incubated at 37°C to an OD600 of 0.6. Isopropyl β-D-1-thiogalactopyranoside and 5-aminolevulinic acid (Cosmo Bio, Tokyo, Japan) were added to the cultures at 1 and 20 mM, respectively. After additional culture for 24 h at 16°C, the cells were harvested by centrifugation and disrupted with a sonicator (ULTRASONIC DISRUPTOR, TOMY, Tokyo, Japan) in 50 mM Tris–Cl (pH 8.0) buffer containing 1 mM EDTA, 100 mM NaCl, 0.4 mM phenylmethylsulfonyl fluoride, and 0.27 mg mL^{-1} lysozyme (FUJIFILM Wako Pure Chemical Co.). The lysate was

[1]https://phytozome.jgi.doe.gov/

centrifuged at 5,000 rpm for 5 min, and the resultant supernatant was re-centrifuged at 50,000 rpm (CS100FX, Eppendorf Himac, Ibaraki, Japan) for 60 min to obtain the membrane fraction, which was then resuspended in 50 mM Tris-Cl (pH 8.0) buffer containing 1 mM EDTA and 100 mM NaCl. BL21 Star (DE3) harboring pET15b (Takara Bio, Shiga, Japan) was used as the empty vector control.

Enzyme Assay and Product Analysis

Hydroperoxide lyase activity was measured by following the decrease in absorption at 234 nm. The *E. coli* membrane fraction was mixed separately with 30 μM each of (9*Z*,11*E*,15*Z*)-13-hydroperoxyoctadeca-9,11,15-trienoic acid (13HPOT), (10*E*,12*Z*,15*Z*)-9-hydroperoxyoctadeca-10,12,15-trienoic acid (9HPOT), (9*Z*,11*E*)-13-hydroperoxyoctadeca-9,11-dienoic acid (13HPOD), and (10*E*,12*Z*)-9-hydroperoxyoctadeca-10,12-dienoic acid (9HPOD) in 50 mM MES-KOH (pH 6.0) at 25°C. The HPO substrates were prepared from α-linolenic acid and linoleic acid (MilliporeSigma) with soybean lipoxygenase-1 partially purified from soybean seeds and *Magnaporthe salvinii* lipoxygenase provided by Novozyme Japan (Chiba, Japan) as described previously (Koeduka et al., 2015; Sugio et al., 2018). The compositions of HPOs were analyzed using the straight-phase HPLC system after reducing the hydroperoxide group to hydroxide with triphenylphosphine (Sugio et al., 2018). The contamination of the positional and geometrical isomers in each HPO preparation was mostly negligible except for 9HPOT, which contained 26.2% of 13HPOT (**Supplementary Figure 2**).

To determine HPL activity, the initial velocity of decrease in absorption at 234 nm was followed for 10 s using an absorption coefficient of 25 mM^{-1} cm^{-1}. The volatile products were analyzed by GC-MS as described above after extraction with methyl *tert*-butyl ether. For analyses of non-volatile products with LC-MS/MS, the reaction was terminated by the addition of 1 mL of methanol. The mixture was centrifuged at 2,000 rpm for 10 min. The resultant supernatant was directly used for LC-MS/MS (3200 Q-TRAP LC-MS/MS System, AB Sciex, Framingham, MA, United States, equipped with a Prominence UFLC, Shimadzu, Kyoto, Japan). The products were separated on a Mightysil RP18 column (150 mm × 2 mm inner diameter) with a binary gradient consisting of water/formic acid (100:0.1, v/v, solvent A) and acetonitrile/formic acid (100:0.1, v/v, solvent B). The run consisted of a linear increase from 20% B to 95% B over 30 min at a flow rate of 0.2 mL min^{-1}. Compounds were detected with a photodiode array detector (SPD-M20A, Shimadzu) and by MS/MS using the negative ion mode with ion spray voltage −4,500 V, nitrogen as both the curtain gas (set to 40 arbitrary units) and collision gas (set to "high"), collision energy −10 V, scan range *m/z* 100–500, scan speed 4,000 Da s^{-1}, and declustering potential −30 V. Recombinant CaHPL was expressed with *E. coli* and purified as described previously (Matsui et al., 1996). The 12-Oxo-(*Z*)-9-dodecenoic acid and 12-oxo-phytodienoic acid were purchased from Larodan AB (Solna, Sweden).

Quantitative Real-Time RT-PCR Analysis

For mechanical wounding the shoots and roots were cut into pieces (1–2 mm long) with scissors, and placed on a sheet of wet paper towel at 25°C. Total RNA was isolated using the Qiagen RNeasy Plant Mini Kit according to the manufacturer's instructions. Total RNA (0.25 μg) was then reverse transcribed with 2.5 μM aliquots of oligo$(dT)_{15}$ primer (Invitrogen) and ReverTra Ace (derived from Moloney murine leukemia virus reverse transcriptase; Toyobo, Osaka, Japan) according to the manufacturer's instructions. Real-time quantitative PCR was performed with the StepOne System (Thermo Fisher Scientific, Waltham, MA, United States). Ct values for the genes of interest were normalized to means of the reference gene for the ubiquitin gene (*XP_002966475*). Expression levels were calculated as relative amounts by using relative standard curves. The lowest value in each experiment was set at 1. Primers for RT-PCR are shown in **Supplementary Table 2**. Under the current RT-PCR condition SmHPL1a and SmHPL1b were indistinguishable.

Phylogenetic Tree

Phylogenetic analyses were carried out using the Maximum Likelihood method based on the LG model + G + I in MEGAX (Kumar et al., 2018). Amino acid sequences were aligned using MAFFT v7.475 and Gblocks Server v0.91b. Genbank accession numbers of each CYP74 protein used for phylogenetic analysis are listed in **Supplementary Table 3**.

Statistics

All values are presented as the mean ± SEM in triplicate at minimum. Statistical analyses were performed using Excel Toukei in Microsoft Excel (Social Survey Research Information Co., Tokyo, Japan). The statistical methods used are described in the figure captions.

RESULTS

Distribution of Green Leaf Volatile-Burst Ability Among Monilophytes, Lycophytes, and Bryophytes

As one of the representative plant species in the missing link between bryophytes and monilophytes, we focused on a lycophyte, *S. moellendorffii*, because of the availability of genome resources of this species (Banks et al., 2011; Ferrari et al., 2020). The leaves were completely ground in a mortar, and the volatile compounds formed in the homogenate were analyzed by GC-MS after 1 and 5 min of grinding (**Figure 2**). Small amounts of *n*-hexanal, (*Z*)-3-hexenal, (*E*)-2-hexenal, and 1-octen-3-ol were detected in the intact leaves as found with intact Arabidopsis leaves and *Nicotiana attenuata* leaves (Scala et al., 2013; Mochizuki et al., 2016; Joo et al., 2018), and, apart from 1-octen-3-ol, their levels increased substantially after 1 min of milling, which is a typical feature of the GLV-burst (D'Auria et al., 2007; Mochizuki and Matsui, 2018). Terpene compounds detected in stressed *S. moellendorffii* plants (Li et al., 2012) were not detected here. (*Z*)-3-Hexen-1-yl acetate, which is generally

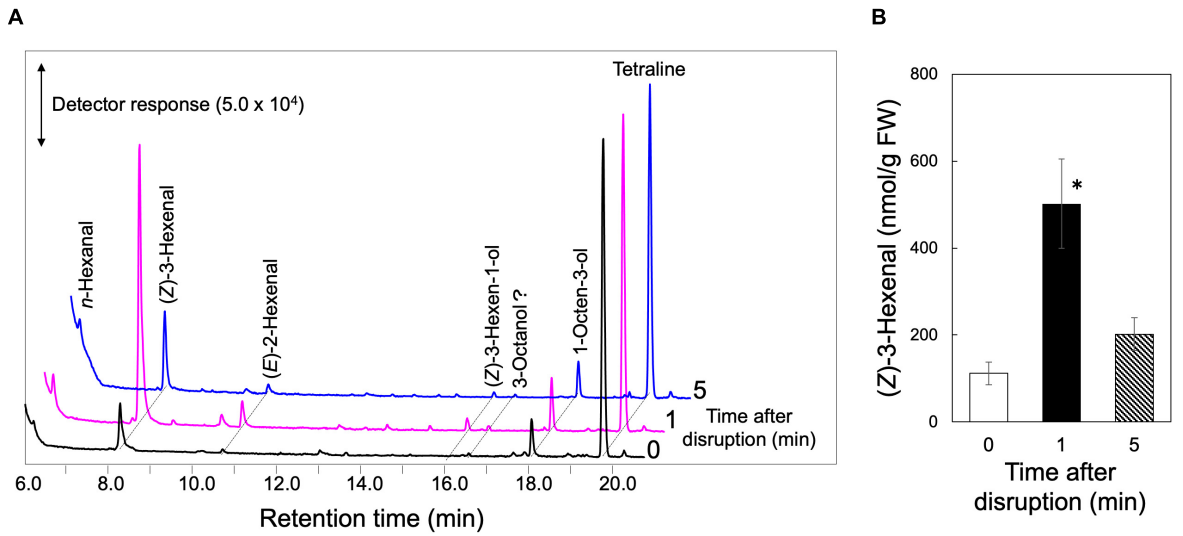

FIGURE 2 | GLV-burst with *S. moellendorffii*. The upper ground parts of *S. moellendorffii* were ground in a mortar and pestle. After 1 and 5 min, the volatiles were extracted for GC-MS analyses. Intact leaves were also analyzed and shown at 0 min after disruption. **(A)** Representative chromatograms of volatiles found in the extracts. **(B)** The amounts of (*Z*)-3-hexenal found in the extracts. Mean values ± SE are shown ($n = 3$, biological replicates). Asterisk shows significant differences (one-way ANOVA, Tukey, $P < 0.05$).

identified in partially wounded angiosperm leaves (Matsui et al., 2012) was not found in the completely disrupted *S. moellendorffii* leaves in our study. (Z)-3-Hexenyl acetate was not detected even with the partially damaged leaves (**Supplementary Figure 3**).

The GLV-burst abilities were evaluated with the leaf or thalli of three species of monilophytes, seven species of lycophytes, and six species of bryophytes with GC-MS analyses after disruption of the organs, and the results are shown as a heat map (**Figure 3**, each result is summarized in **Supplementary Dataset 1**). As reported previously (Hatanaka et al., 1978), all plant species belonging to monilophytes showed substantial GLV-burst abilities, and lycophytes also showed capacity. In contrast, GLVs were not detected in four species of bryophytes, whereas *Dicranum scoparium* revealed a high propensity to form (*Z*)-3-hexenal, (*E*)-2-hexenal, (*Z*)-3-hexen-1-ol, and 4-oxo-(*E*)-2-hexenal. Similar observations have been reported for *D. scoparium* samples from Europe (Croisier et al., 2010). The intact thalli of *Sphagnum palustre* contained substantial amounts of *n*-hexanal and (*Z*)-3-hexenal, but their amounts scarcely increased after disruption of the thalli. The bryophytes, except for *Marchantia polymorpha*, formed a substantial amount of 1-octen-3-ol after grinding of their thalli, as reported (Croisier et al., 2010).

Gene Mining

The results shown above suggest that GLV-burst ability was acquired when lycophytes diverged from the first vascular plants. The acquisition or development of gene(s) encoding HPL could account for the procurement of the ability to conduct the GLV-burst. We have previously determined that all the CYP74 genes found in the *M. polymorpha* and *Klebsormidium nitens* genomes encoded AOSs (Koeduka et al., 2015), and that no gene-encoding HPL has been identified in the liverwort and chalophyte to date. PpHPL found in *Physcomitrella patens* is specialized for the formation of nine-carbon volatiles such as (*E*)-2-nonenal; therefore, its involvement in the GLV-burst is excluded. As *S. moellendorffii* has been established as a model lycophyte (Weng and Noel, 2013) that has shown a substantial GLV-burst ability (**Figure 2**), we examined the genome sequence (Banks et al., 2011) and the expression atlas of *S. moellendorffii* (Ferrari et al., 2020) to mine CYP74 genes that could encode HPL.

Using BLASTP search on the *S. moellendorffii* v1.0 proteome database in Phytozome[2] with AtHPL (At4g15440) as a query, we found more than 10 CYP74-like genes with E-values less than 2.4×10^{-87} (**Supplementary Table 4**) as reported previously (Koeduka et al., 2015). Among these, four genes have been confirmed as SmAOS2, SmDES1, SmDES2, and SmEAS1 through analysis of the catalytic activities of the corresponding recombinant proteins expressed in *E. coli* (Gorina et al., 2016; Pratiwi et al., 2017; Toporkova et al., 2018). The other two genes highly homologous to SmAOS2 were tentatively assigned as SmAOS1 and SmAOS3 (Pratiwi et al., 2017). The expression profile search in the CoNekT database[3] constructed by a comprehensive gene expression analysis with *S. moellendorffii* (Ferrari et al., 2020) showed that, among the remaining four genes, Smo133317 (SmCYP74J1) and Smo92382 (SmCYP74L1) showed substantial expression in the aerial parts of *S. moellendorffii*, while the other two genes, Smo98717 (CYP74L2) and Smo413157 (CYP74L3), were expressed specifically in the roots (**Supplementary Figure 4**). The volatile analyses with intact and partially wounded roots and shoots indicated that the GLV-burst was predominantly detected

[2]phytozome.jgi.doe.gov/pz/portal.html

[3]https://conekt.sbs.ntu.edu.sg/

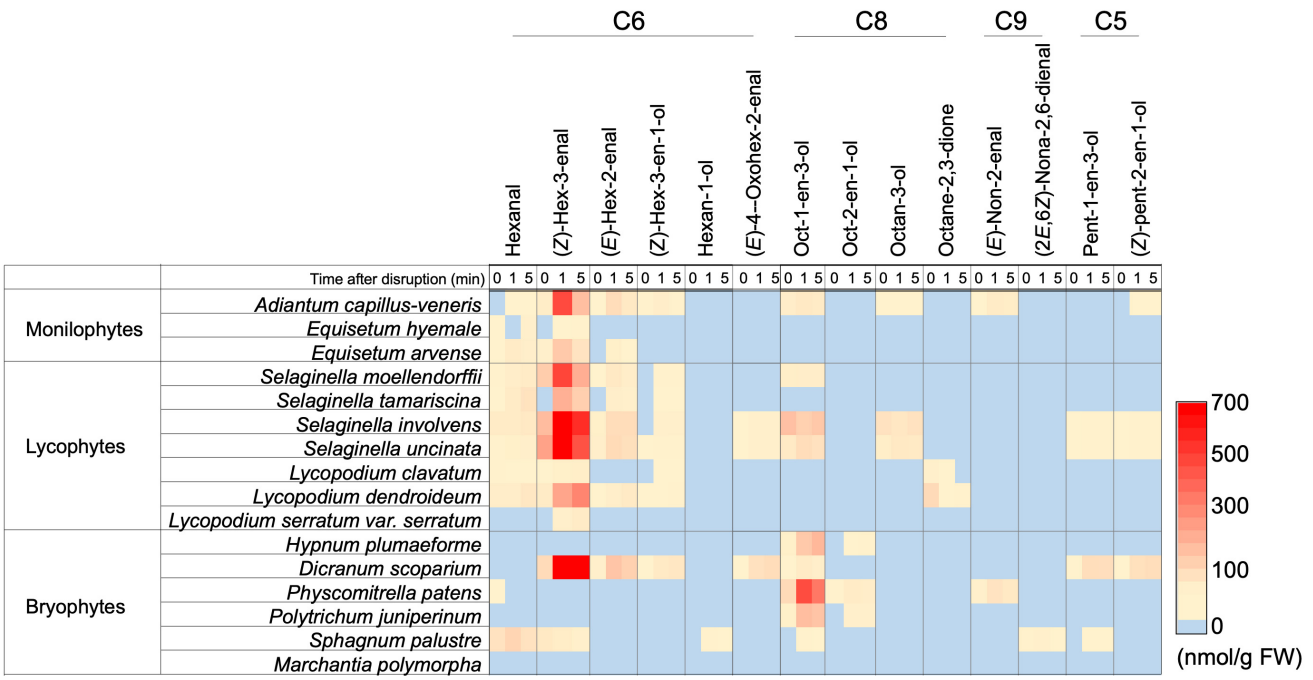

FIGURE 3 | Distribution of the ability to form oxylipin volatiles among a subset of monilophyte, lycophyte, and bryophyte plant species. The amount of each compound is shown with color. The detailed values are shown in **Supplementary Dataset 1**.

in the green aerial parts (**Supplementary Figure 3**); therefore, we assumed that the genes expressed in the green part of the plant were involved in the GLV-burst. Accordingly, we focused on Smo133317 (SmCYP74J1) and Smo92382 (SmCYP74L1).

Smo133317 (SmCYP74J1) Encodes 13AOS

When Smo133317 (SmCYP74J1) was expressed in *E. coli* cells, the activity to degrade 13HPOT was detected in the membrane fraction prepared from the *E. coli* lysate through monitoring by following the decrease in absorption at 234 nm. GC-MS analysis of the products showed the formation of a trace amount of (*Z*)-3-hexenal that was equivalent to that of the reaction mixture with the heat-denatured membrane fraction. LC-MS/MS analysis indicated the formation of 12-oxo-phytodienoic acid (OPDA), 13-hydroxy-12-oxo-(9*Z*,15*Z*)-octadecadienoic acid (α-ketol), and 9-hydroxy-12-oxo-(10*E*,15*Z*)-octadecadienoic acid (γ-ketol) in the reaction of 13HPOT with the membrane fraction (Yanagi et al., 2011; **Figure 4**). No other peak corresponding to divinyl ether (*m/z* of 291.2) or epoxy alcohol (*m/z* of 309.2) that would be formed *via* DES or EAS activity on 13HPOT was detected. Accordingly, we named Smo133317 (SmCYP74J1) as SmAOS4. Recombinant SmAOS4 showed the highest activity at pH 5.5. Under representative reaction conditions with 40 μM of the substrate, the recombinant SmAOS4 showed the highest activity with 13HPOD, followed by 13HPOT (**Table 1**), whereas 9HPOD showed only 14% activity with 13HPOD.

Smo92382 (SmCYP74L1) and Its Variant Encode 13HPL

The open reading frame of SmCYP74L1 was obtained by PCR cloning of genomic DNA and sequenced. Two clones were retained, one had 100% similarity to the sequence reported in the genome database, while the other showed nine nucleotide substitutions resulting in the substitution of six amino acids (**Supplementary Figure 5**). We tentatively named the identical gene to that in the database as *SmCYP74L1a* and its allelic gene *SmCYP74L1b*. The membrane fraction prepared from *E. coli* lysate expressing recombinant proteins derived from the open reading frame of these two genes degraded 13HPOT *in vitro*. GC-MS analyses of the products obtained from the reaction of the membrane fraction harboring recombinant SmCYP74L1a or SmCYP74L1b protein with 13HPOT showed the formation of (*Z*)-3-hexenal as the main product (**Figure 5**). LC-MS/MS analyses of the non-volatile products indicated the formation of 12-oxo-(*Z*)-9-dodecenoic acid with both recombinant enzymes (**Figure 4**). No peaks corresponding to the products of AOS, DES, or EAS activities were detected. Accordingly, we retained the name SmHPL1a for SmCYP74L1a and SmHPL1b for SmCYP74L1b.

Escherichia coli membrane expressing recombinant SmHPL1b showed higher HPL activity (**Figure 5**); therefore, we further analyzed its properties. The highest activity was observed at pH 5.5, and under standard conditions with 40 μM of the four HPOs, recombinant SmHPL1b showed the greatest activity with 13HPOT (**Table 1**). In contrast, 13HPOD had only 6% activity with 13HPOT, whereas 9HPOT and 9HPOD

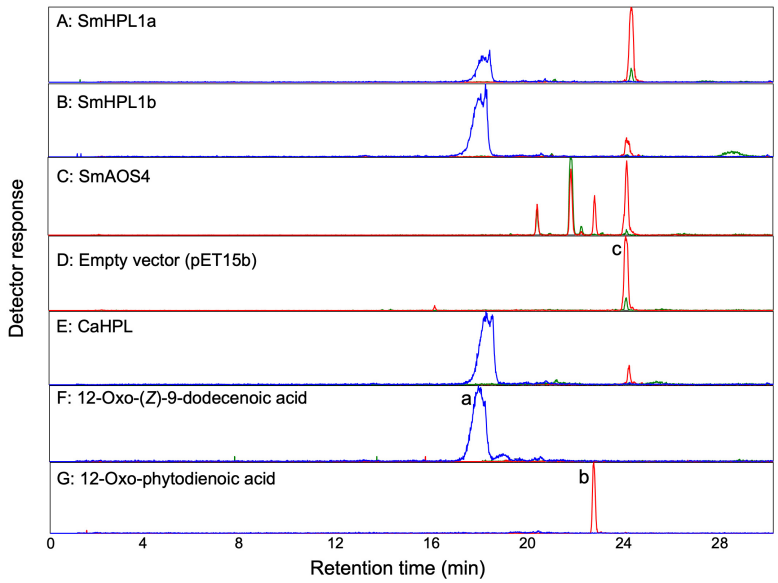

FIGURE 4 | LC-MS/MS analyses of products formed by **(A)** recombinant SmHPL1a, **(B)** recombinant SmHPL1b, **(C)** recombinant SmAOS4, **(E)** recombinant bell pepper HPL (CaHPL) from 13HPOT. As the empty vector control, the membrane fraction of the *E. coli* cells harboring pET15b was reacted with 13HPOT **(D)**. Authentic standards of 12-oxo-(*Z*)-9-dodecenoic acid (peak a) **(F)** and 12-oxo-phytodienoic acid (OPDA) (peak b) **(G)** were also analyzed. The substrate, 13HPOT, is shown with peak c. The red trace shows extracted ion chromatograms with *m/z* of 291.2 ± 0.5 for hydroperoxides of linolenic acid $[M\text{-}H_3O^+]^-$, 12-oxo-phytodienoic acid $[M\text{-}H^+]$, or colnelenic acid $[M\text{-}H^+]^-$. The blue trace is with *m/z* of 211.1 ± 0.5 for 12-oxo-(*Z*)-9-dodecenoic acid $[M\text{-}H^+]^-$. The green trace is with *m/z* of 309.2 ± 0.5 for hydroperoxides of linolenic acid $[M\text{-}H^+]^-$, α- and γ-ketols $[M\text{-}H^+]^-$, or epoxy alcohol $[M\text{-}H^+]^-$.

TABLE 1 | Substrate specificities of recombinant SmHPL1b and SmAOS4.

	SmHPL1b	SmAOS4
Substrate	**Relative activity (%)**	**Relative activity (%)**
13HPOT	100	52.6 ± 2.63
13HPOD	6.10 ± 1.22	100
9HPOT	2.18 ± 0.98	14.9 ± 0.88
9HPOT	2.32 ± 0.85	14.0 ± 0.98

were only slightly catalyzed by recombinant SmHPL1b. The recombinant enzyme followed Michaelis-Menten kinetics, and the *Km* value with 13HPOT was estimated to be 31.4 μM (**Supplementary Figure 6**).

Gene Expression

RT-qPCR analyses showed that the transcription levels of *SmAOS2* and *SmAOS4* in the shoots were higher than those in the roots, while that of *SmAOS3* in the roots was higher than that in the shoots (**Figure 6**). The level of *SmAOS3* in the shoots slightly increased after mechanical wounding. The expression level of *SmAOS4* immediately dropped after mechanical wounding and slowly returned to the original level after 60 min of wounding. Expression of *SmHPL1a/b* was rather specific to the shoots and the expression in the roots was not detected. The expression level varied slightly after mechanical wounding on the shoots, but no obvious induction or suppression after wounding was observed.

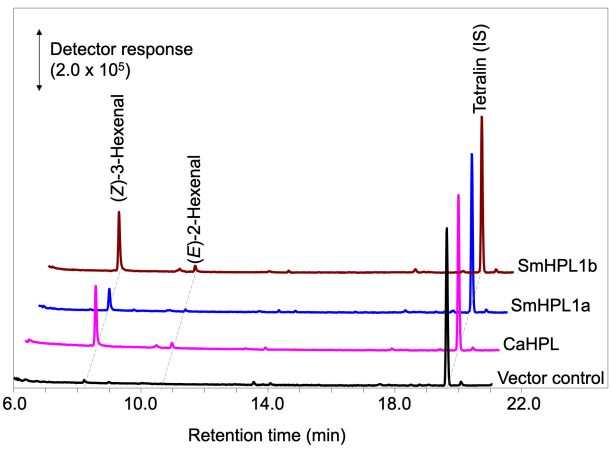

FIGURE 5 | GC-MS analyses of the volatile products formed by recombinant SmHPL1a (blue) and SmHPL1b (brown) from 13HPOT. As the positive control, volatile products formed by bell pepper HPL (CaHPL) from 13HPOT are also shown (magenta). The vector control was run with the membrane fraction of *E. coli* cells harboring pET15b (black).

The transcription level of *SmOPR5* increased after mechanical wounding as reported previously (Pratiwi et al., 2017).

Phylogenetic Tree

The phylogenetic tree with SmHPL1a, SmHPL1b, and SmAOS4, together with representatives of functionally characterized plant

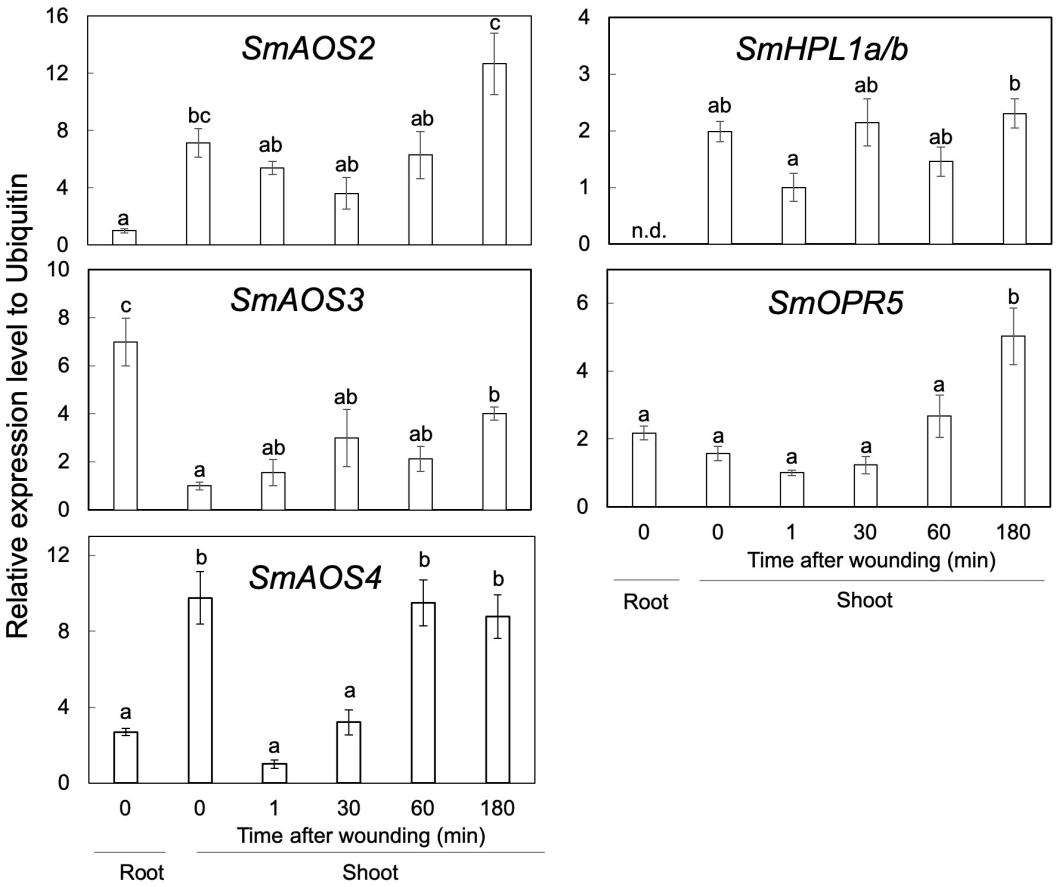

FIGURE 6 | Gene-expression profiles of *SmAOS2*, *SmAOS3*, *SmAOS4*, *SmHPL1a/b*, and *SmOPR5* in the roots and the shoots. Those in the shoots after mechanical wounding are also shown. The expression data represent the mean ± standard error of four biological replicates. Different letters indicate significant difference ($P < 0.05$, one-way ANOVA, Tukey-Kramer). n.d., not detected.

CYP74s and CYP74-like genes found with the transcriptome data of *Adiantum capillus-veneris* (Ni et al., 2020) showed that SmHPL1a and b were grouped with DES and EAS from *S. moellendorffii*, which consisted of a clade distinctive to the clade with seed plant HPLs. SmAOS4 is located in another clade closely related to the one consisting of angiosperm AOSs and 9/13HPLs (**Figure 7**). The six CYP74-like proteins found with the transcriptome data of *A. capillus-veneris* were divided into two groups, one in the angiosperm HPL clade and the other in the bryophyte AOS clade.

DISCUSSION

Based on the results presented in this study and those in previous reports (Hatanaka et al., 1978; Croisier et al., 2010), the ability of GLV-burst appears to have been acquired when the lycophyte species diverged from the plant lineage. GLVs are involved in the defense against pathogens and herbivores in angiosperms (Matsui, 2006; Ameye et al., 2018). The quick formation of GLVs at the damaged sites accounts for the efficient defensive effects through methods such as deterring actively feeding herbivores or attracting carnivores that prey on these herbivores. Cues strategically emitted from the appropriate place and time should provide reliable information for guiding carnivores to their prey. The fossil records indicate that lycophytes from the Permian to Triassic periods were attacked by various kinds of herbivores (Labandeira et al., 2016); thus, the plants at those geological ages would have employed several defensive strategies, including GLV-burst.

Interestingly, most bryophytes showed the ability to quickly form 1-octen-3-ol as opposed to GLVs after mechanical wounding of their thalli. This compound is a common volatile among fungi, and its involvement in the defense against fungivores, including arthropods and nematodes, is assumed (Inamdar et al., 2020). It is likely that this rapid formation of 1-octen-3-ol after mechanical wounding could also be part of the defense against bryophyte feeders, although direct evidence of this is lacking. Among vascular plants, the distribution of 1-octen-3-ol is limited, and it is found only in some angiosperms of the orders Fabales and Lamiales (Matsui et al., 2018; Lawson et al., 2021). Some lycophytes formed 1-octen-3-ol, but this ability appeared indistinct in vascular plants. In summary, the ability to form 1-octen-3-ol appeared to be replaced by GLV-burst when the lycophytes emerged from the plant lineage. Labeling experiments supported that C20 fatty acids, such as arachidonic

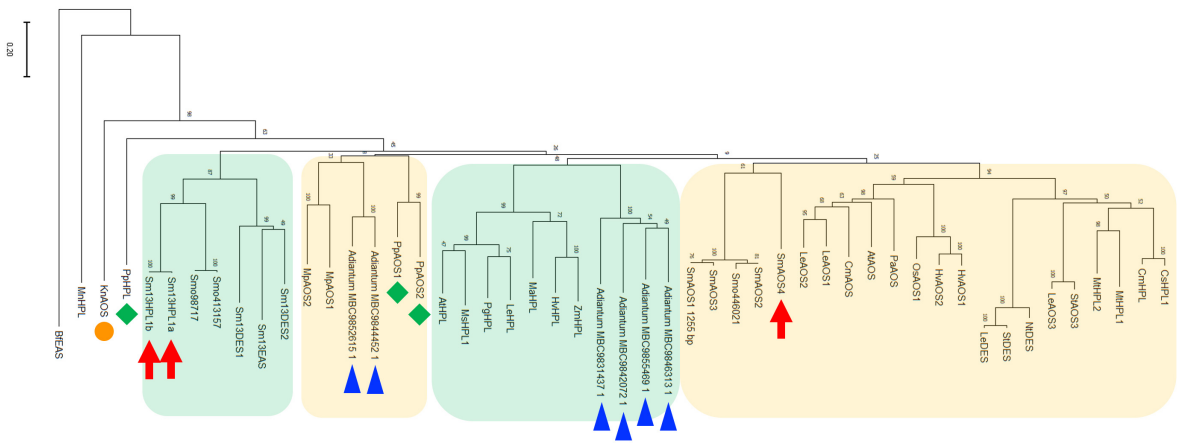

FIGURE 7 | Phylogenetic analysis of SmHPL1a and b and SmAOS4 with the CYP74 enzymes from different species. Phylogenetic analysis was performed in MEGAX using the maximum likelihood method. The details of the sequences used here are shown in **Supplementary Table 3**. SmHPL1a/b and SmAOS4 are highlighted with red arrows. HPL and AOSs from *P. patens* are highlighted with green diamonds, and *K. nitens* AOS is with an orange circle. The genes found with transcriptome analyses on *A. capillus-veneris* are highlighted with blue triangles. The clade consisting of HPL, DES, and EAS from *S. moellendorffii*, and the one of seed plant HPLs are shown with green background, respectively. The clade mainly consisting of bryophyte AOSs, and the one of land plant AOSs, DESs, and 9/13HPLs are shown with orange background, respectively.

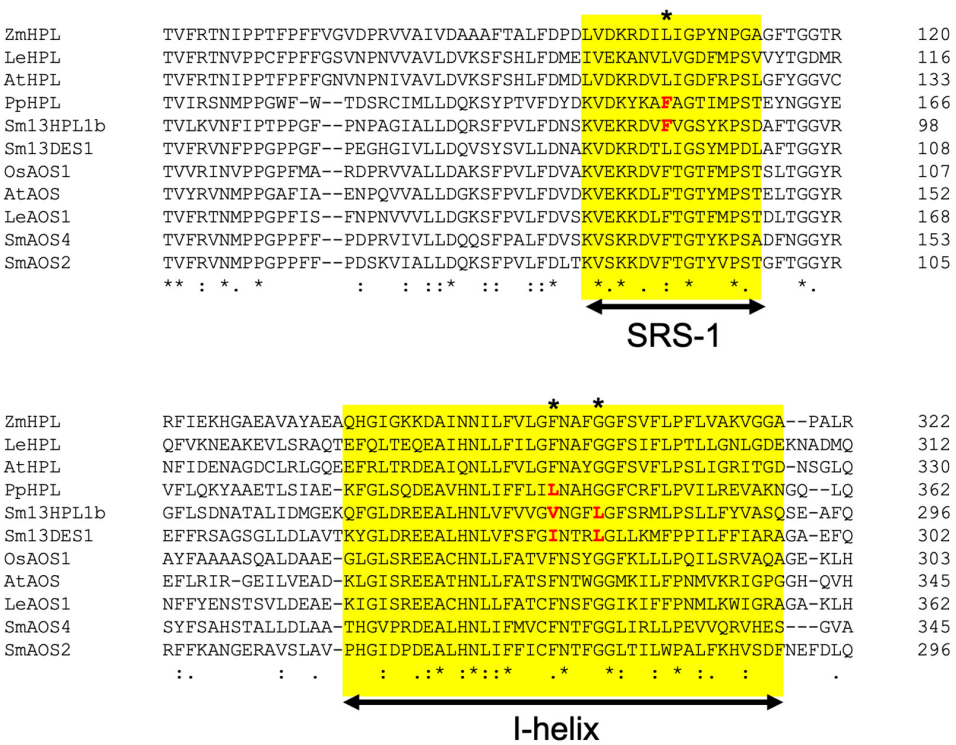

FIGURE 8 | Multialignment of representative seed plant HPLs and AOSs with SmHPL1b, SmDES1, SmAOS4, and SmAOS2. The substrate recognition site (SRS)-1 and I-helix are highlighted with yellow background. The amino acids specific to non-seed CYP74s are shown in red. The position of F/L toggle is shown with asterisk.

acid and icosapentaenoic acid, were the predominant precursors for 1-octen-3-ol formation in bryophytes (Croisier et al., 2010). With a moss *Physcomitrella patens,* disruption of the *PpHPL* that was essential to formation of (*E*)-2-nonenal showed no effect on the ability to form 1-octen-3-ol (Stumpe et al., 2006). Therefore, PpHPL is not involved in 1-octen-3-ol formation, but the a multifunctional lipoxygenase catalyzes the oxygenation of arachidonic acid to 12-hydroperoxide as well as the subsequent cleavage reaction to form 1-octen-3-ol (Senger et al., 2005). Arachidonic acid and icosapentaenoic acid are common in

bryophytes but are rare in vascular plants (Lu et al., 2019). Accordingly, the timing of the change from 1-octen-3-ol to GLVs coincides to a degree with the loss of C20 fatty acids, as well as with the period when the distribution of arachidonic acid began showing an inverse correlation with jasmonic acid (Gachet et al., 2017). The composition of oxylipins is modified in response to changes in the fatty acid composition during plant evolution. Accordingly, the enzyme systems that form oxylipin volatiles should be replaced from those related to 1-octen-3-ol to those involved in GLV-burst, justifying the acquisition of SmHPL1a and SmHPL1b as part of this process. The notable exception found with *Dicranum scoparium* that showed the substantial ability of GLV-burst should not be ignored. Another example of the exception was reported with *Neckera complanata* (Croisier et al., 2010). These are two species found among 29 species of bryophytes examined so far. *N. complanata* belongs to Hypnales and *D. scoparium* belongs to Dicranales, and they are distant from each other in the evolutionary tree. In the genome of the model bryophytes *M. polymorpha* and *P. pantens*, no gene encoding 13HPL has been found (Scholz et al., 2012; Koeduka et al., 2015). Taking together, it is likely that *D. scoparium* and *N. complanata* acquired GLV-burst capabilities due to convergent evolution. An example of the acquisition of metabolic capacity through convergent evolution was recently reported in a moss *Calohypnum plumiforme* (formerly *Hypnum plumaeforme*) (Hypnales) (Mao et al., 2020). This hypothesis should be examined as one of our next challenges.

Klebsormidium nitens has only one CYP74 gene in its genome and it encodes 13AOS (Koeduka et al., 2015). BLASTP analysis with genome sequences of the nine species belonging to Chlorophytes available in Phytozome 13 yielded no genes that were significantly similar to either *K. nitens* AOS or SmHPL1a/b. It has been reported that *Spirogloea muscicola* gen. nov., belonging to subaerial Zygnematophyceae, diversified after Klebsormidium, has one gene related to AOS in its genome (Cheng et al., 2019); therefore, it is suggested that *K. nitens* AOS is likely the closest to the common ancestor of the CYP74 genes that are widely found in extant terrestrial plants (**Figure 7**). In the moss *P. patens*, PpHPL that has the HPL activity moderately specific to linoleic acid 9-hydroperoxide (Stumpe et al., 2006) was first acquired from the ancestral CYP74 gene. *S. moellendorffii* likely adopted the CYP74 gene related to PpHPL that was further diversified into 13HPL, DES, and EAS. Another diversification of PpHPL-related ancestral gene resulted in three clades consisting of bryophyte AOS, angiosperm 13HPL, and vascular plant AOS/DES/HPL (**Figure 7**). Unexpectedly, genes found with a monilophyte *Adiantum capillus-veneris* locate in the clade of bryophyte AOS and that of vascular plant AOS/DES/HPL. Based on these results, it is suggested that 13HPL might have been acquired independently in *S. moellendorffii* and angiosperms. In fact, SmHPL1a/b does not follow the "F/L toggle rule" exclusively conserved among angiosperm HPL and AOS (Lee et al., 2008; Scholz et al., 2012; Toporkova et al., 2019; **Figure 8**). The structural analysis unambiguously indicated that the Phe residue located in the active site of AtAOS stabilized an intermediary-formed carbon-centered radical that led to allene oxide, and Leu at the same position led to hemiacetal that finally caused the formation of HPL products (Lee et al., 2008). SmHPL1a/b are the exception among HPLs that have Phe at the toggle in the substrate recognition site (SRS)-1 domain (**Figure 8**), and other than SmHPL1a/b, only PpHPL contains Phe at the toggle. Amino acid replacements unique to PpHPL, SmHPL1a/b, or SmDES1 are also found in the I-helix, which is referred to as the oxygen-binding domain (**Figure 8**). Accordingly, it is assumed that the structural determinants strictly followed by HPL and AOS in angiosperms are not applicable to those of bryophytes and lycophytes, which supports the hypothesis that HPL genes were independently acquired in *S. moellendorffii* and angiosperms.

Overall, all CYP74s in the plant lineage could be derived from a common ancestral gene close to *K. nitens* AOS. CYP74 is characterized as the P450 that lacks monooxygenase activity, and instead has the ability to rearrange fatty acid hydroperoxides through the homolytic scission of the hydroperoxyl group (Brash, 2009). All enzymes belonging to CYP74s share the first part of the reaction, that is, the homolytic scission of the hydroperoxyl group to form epoxyallylic radicals. The fate of the reactive carbon-centered radical intermediate is the determinant of the products, which confirms whether the enzyme of each CYP74 is denoted as HPL or AOS. The fate is likely determined by a few amino acid residues located at the active site (Lee et al., 2008; Scholz et al., 2012; Toporkova et al., 2019). Therefore, site-directed mutagenesis of a few amino acid residues at the active site allowed the interconversion of HPL to AOS and HPL/EAS to AOS (Lee et al., 2008; Scholz et al., 2012; Toporkova et al., 2019). This characteristic feature of CYP74s shows that HPL could have developed independently in *S. moellendorffii* and angiosperms, allowing for the diversification of CYP74 enzymes, with the interconversion of their catalytic activities. It is also possible that 13HPL was acquired independently in *N. complanata* and *D. scoparium*. Further collection of 13HPL genes in non-seed plants should be conducted to elucidate the structural basis of how the development of 13HPL in lycophytes and monilophytes proceeded.

This hypothesis, in turn, indicates that the GLV-burst plays a significant role in improving plant fitness during evolution after the loss of the ability to form 1-octen-3-ol. The advantageous effects of the GLV-burst have been well documented in angiosperms to date (Matsui, 2006; Ameye et al., 2018). In lycophytes, this ability is expected to increase their fitness, but further studies are needed to determine the benefits to this group. The ability of the GLV-burst in a few bryophytes found in this study is substantial, and it is expected that these bryophyte species employed convergent evolution to convert CYP74s encoding 9HPL or AOS into 13HPL to benefit from the GLV-burst. This is the hypothesis that requires further study.

DATA AVAILABILITY STATEMENT

The datasets presented in this study can be found in online repositories. The names of the repository/repositories and accession number(s) can be found in the article/**Supplementary Material**.

AUTHOR CONTRIBUTIONS

KM and MT participated in the design of the experiment. MT performed the majority of the experiments. KM, MT, and TK wrote the manuscript. All authors contributed to the article and approved the submitted version.

FUNDING

This work was partly supported by JSPS KAKENHI Grant Numbers 19H02887 and 16H03283 (to KM).

ACKNOWLEDGMENTS

We would like to thank Mitsuharu Hasebe, National Institute of Basic Biology, Japan, for providing *Physcomitrella patens*, and Xionan Xie, Utsunomiya University, Japan, for providing *Selaginella moellendorffii*.

SUPPLEMENTARY MATERIAL

The Supplementary Material for this article can be found online at: https://www.frontiersin.org/articles/10.3389/fpls.2021.731694/full#supplementary-material

REFERENCES

Ameye, M., Allmann, S., Verwaeren, J., Smagghe, G., Haesaert, G., Schuurink, R. C., et al. (2018). Green leaf volatile production by plants: a meta-analysis. *N. Phytol.* 220, 666–683. doi: 10.1111/nph.14671

Banks, J. A., Nishiyama, T., Hasebe, M., Bowman, J. L., Gribskov, M., dePamphillis, C., et al. (2011). The compact Selaginella genome identifies changes in gene content associated with the evolution of vascular plants. *Science* 332, 960–963.

Brash, A. R. (2009). Mechanistic aspects of CYP74 allene oxide synthases and related cyrochrome P450 enzymes. *Phytochemistry* 70, 1522–1531. doi: 10.1016/j.phytochem.2009.08.005

Brodhun, F., and Feussner, I. (2011). Oxylipins in fungi. *FEBS J.* 278, 1047–1063. doi: 10.1111/j.1742-4658.2011.08027.x

Cheng, S., Xian, W., Fu, Y., Marin, B., Keller, J., Wu, T., et al. (2019). Genomes of subaerial Zygnematophyceae provide insights into land plant evolution. *Cell* 179, 1057–1067. doi: 10.1016/j.cell.2019.10.019

Croisier, E., Rempt, M., and Pohnert, G. (2010). Survey of volatile oxylipins and their biosynthetic precursors in bryophytes. *Phytochemistry* 71, 574–580. doi: 10.1016/j.phytochem.2009.12.004

D'Auria, J. C., Pichersky, E., Schaub, A., Hansel, A., and Gershenzon, J. (2007). Characterization of a BAHD acyltransferase responsible for producing the green leaf volatile (*Z*)-3-heen-1-yl acetate in *Arabidopsis thaliana*. *Plant J.* 49, 194–207. doi: 10.1111/j.1365-313x.2006.02946.x

Ferrari, C., Shivhare, D., Hanse, B. O., Pasha, A., Esteban, E., Provart, N. J., et al. (2020). Expression atlas of *Selaginella moellendorffii* provides insights into the evolution of vasculature, secondary metabolism, and roots. *Plant Cell* 32, 853–870. doi: 10.1105/tpc.19.00780

Funk, C. D. (2001). Prostaglandins and leukotrienes: advances in eicosanoid biology. *Science* 294, 1871–1875. doi: 10.1126/science.294.5548.1871

Gachet, M. S., Schubert, A., Calarco, S., Boccard, J., and Gertsch, J. (2017). Targeted metabolomics shows plasticity in the evolution of signaling lipids and uncovers old and new endocannabinoids in the plant kingdom. *Sci. Rep.* 7:41177. doi: 10.1038/srep41177

Gorina, S. S., Toporkova, Y. Y., Mukhatarova, L. S., Smirnova, E. O., Chechetkin, I. R., Khairutdinov, B. I., et al. (2016). Oxylipin biosynthesis in spikemoss *Selaginella moellendorffii*: molecular cloning and identification of divinyl ether synthases CYP74M1 and CYP74M3. *Biochim. Biophys. Acta* 1861, 301–309. doi: 10.1016/j.bbalip.2016.01.001

Hatanaka, A., Sekiya, J., and Kajiwara, T. (1978). Distribution of an enzyme system producing *cis*-3-hexenal and *n*-hexanal from linolenic and linoleic acids in some plants. *Phytochemistry* 17, 869–872.

Inamdar, A. A., Morath, S., and Bennett, J. W. (2020). Fungal volatile organic compounds: more than just a funky smell? *Ann. Rev. Microbiol.* 74, 101–116. doi: 10.1146/annurev-micro-012420-080428

Joo, Y., Schuman, M. C., Goldberg, J. K., Wissgott, A., Kim, S. G., and Baldwin, I. T. (2018). Herbivory elicits changes in green leaf volatile production via jasmonate signaling and the circadian clock. *Plant Cell Environ.* 42, 972–982.

Koeduka, T., Ishizaki, K., Mwenda, C. M., Hori, K., Sasaki-Sekimoto, Y., Ohta, H., et al. (2015). Biochemical characterization of allene oxide synthases from the liverwort *Marchantia polymorpha* and green microalgae *Klebsormidium flaccidum* provides insight into the evolutionary divergence of the plant CYP74 family. *Planta* 242, 1175–1186. doi: 10.1007/s00425-015-2355-8

Kumar, S., Stecher, G., Li, M., Knyaz, C., and Tamura, K. (2018). MEGA X: molecular evolutionary genetics analysis across computing platforms. *Mol. Biol. Evol.* 35, 1547–1549. doi: 10.1093/molbev/msy096

Labandeira, C. C., Kustatscher, E., and Wappler, T. (2016). Floral assemblages and patterns of insect herbivory during the Permian to Triassic of northeastern Italy. *PLoS One* 11:40165205. doi: 10.1371/journal.pone.0165205

Lawson, S. K., Satyal, P., and Setzer, W. N. (2021). The volatile phytochemistry of seven native American aromatic medicinal plants. *Plants* 10:1061. doi: 10.3390/plants10061061

Lee, D. S., Nioche, P., Hamberg, M., and Raman, C. S. (2008). Structural insights into the evolutionary paths of oxylipin biosynthetic enzymes. *Nature* 455, 363–368. doi: 10.1038/nature07307

Li, G., Köllner, T. G., Yin, Y., Jiang, Y., Chen, H., Xu, Y., et al. (2012). Nonseed plant *Selaginella moellendorffii* has both seed plant and microbial types of terpene synthases. *Proc. Natl. Acad. Sci. U. S. A.* 109, 14711–14715. doi: 10.1073/pnas.1204300109

Lu, Y., Eiriksson, F. F., Thorsteinsóttir, M., and Simonsen, H. T. (2019). Valuable fatty acids in bryophytes – production, biosynthesis, analysis and applications. *Plants* 8:524. doi: 10.3390/plants8110524

Mao, L., Kawaide, H., Higuchi, T., Chen, M., Miyamoto, K., Hirata, Y., et al. (2020) Genomic evidence for convergent evolution of gene clusters for momilactone biosynthesis in land plants. *Proc. Natl. Acad. Sci. U. S. A.* 117, 12472–12480. doi: 10.1073/pnas.1914373117

Matsui, K. (2006). Green leaf volatiles: hydroperoxide lyase pathway of oxylipin metabolism. *Curr. Opin. Plant Biol.* 9, 274–280. doi: 10.1016/j.pbi.2006.03.002

Matsui, K., Shibutani, M., Hase, T., and Kajiwara, T. (1996). Bell pepper fruit fatty acid hydroperoxde lyase is a cytochrome P450 (CYP74B). *FEBS Lett.* 394, 21–24. doi: 10.1016/0014-5793(96)00924-6

Matsui, K., Sugimoto, K., Mano, J., Ozawa, R., and Takabayashi, J. (2012). Differential metabolisms of green leaf volatiles in injured and intact parts of a wounded leaf meet distinct ecophysiological requirements. *PLoS One* 7:e36433. doi: 10.1371/jurnal.pone.0036433

Matsui, K., Takemoto, H., Koeduka, T., and Ohnishi, T. (2018). 1-Octen-3-ol is formed from its glycoside during processing of soybean [*Glycine max* (L.) Merr.] seeds. *J. Agric. Food Chem.* 66, 7409–7416. doi: 10.1021/acs.jafc.8b01950

Mochizuki, S., and Matsui, K. (2018). Green leaf volatile-burst in Arabidopsis is governed by galactolipid oxygenation by a lipoxygenase that is under control of calcium ion. *Biochem. Biophys. Res. Comm.* 505, 939–944. doi: 10.1016/j.bbrc.2018.10.042

Mochizuki, S., Sugimoto, S., Koeduka, T., and Matsui, K. (2016). Arabidopsis lipoxygenase 2 is essential for formation of green leaf volatiles and five-carbon volatiles. *FEBS Lett.* 590, 1017–1027. doi: 10.1002/1873-3468.12133

Ni, R., Zhu, T. T., Zhang, X. S., Wang, P. Y., Sun, C. J., Qia, Y. N., et al. (2020). Identification and evolutionary analysis of chalcone isomerase-fold proteins in ferns. *J. Exp. Bot.* 71, 290–304. doi: 10.1093/jxb/erz425

Pratiwi, P., Tanaka, G., Takahashi, T., Xie, X., Yoneyama, K., Matsuura, H., et al. (2017). Identification of jasmonic acid and jasmonoyl-isoleucine, and

characterization of AOS, AOC, OPR and JAR1 in the model lycophyte *Selaginella moellendorffii*. *Plant Cell Physiol.* 58, 789–801. doi: 10.1093/pcp/pcx031

Scala, A., Allmann, S., Mirabella, R., Haring, M. A., and Schuurink, R. (2013). Green leaf volatiles: a plnat's multifunctional weapon against herbivores and pathogen. *Int. J. Mol. Sci.* 14, 17781–17811. doi: 10.3390/ijms140917781

Scholz, J., Brodhu, F., Hornung, E., Herrfurth, C., Stumpe, M., Beike, A. K., et al. (2012). Biosynthesis of allene oxide in *Physcomitrella patens*. *BMC Plant Biol.* 12:228. doi: 10.1186/1471-2229-12-228

Senger, T., Wichard, T., Kunze, S., Göbel, C., Lerchl, J., Pohnert, G., et al. (2005). A multifunctional lipoxygenase with fatty acid hydroperoxide cleaving activity from the moss *Physcomitrella patens*. *J. Biol. Chem.* 280, 7588–7596. doi: 10.1074/jbc.m411738200

Shiojiri, K., Kishimoto, K., Ozawa, R., Kugimiya, S., Urashimo, S., Arimura, G., et al. (2006). Changing green leaf volatile biosynthesis in plants: an approach for improving plant resistance against both herbivores and pathogens. *Proc. Natl. Sci. Acad. U. S. A.* 103, 16672–16676.

Stumpe, M., Bode, J., Göbel, C., Wichard, T., Schaaf, A., Frank, W., et al. (2006). Biosynthesis of C9-aldehydes in the moss *Physcomitrella patens*. *Biochim. Biophys. Acta* 1761, 301–312. doi: 10.1016/j.bbalip.2006.03.008

Sugio, A., Østergaard, L. H., Matsui, K., and Takagi, S. (2018). Characterization of two fungal lipoxygenases expressed in *Aspergillus oryzae*. *J. Biosci. Bioeng.* 126, 436–444.

Tanaka, T., Ikeda, A., Shiojiri, K., Ozawa, R., Shiki, K., Nagai-Kunihiro, N., et al. (2018). Identification of a hexenal reductase that modulates the composition of green leaf volatiles. *Plant Physiol.* 178, 552–564. doi: 10.1104/pp.18.00632

Toporkova, Y. Y., Gogolev, Y. V., Mukhtarova, L. S., and Grechkin, A. N. (2008). Determinants governing the CYP74 catalysis: conversion of allene oxide synthase into hydroperoxide lyase by site-directed mutagenesis. *FEBS Lett.* 582, 3423–3428. doi: 10.1016/j.febslet.2008.09.005

Toporkova, Y. Y., Smirnova, E. O., Gorina, S. S., Mukhtarova, L. S., and Grechkin, A. N. (2018). Detection of the first higher plant exoxyalcohol synthase: molecular cloning and characterization of the CYP74M2 enzyme of spikemoss *Selaginella moellendorffii*. *Phytochemistry* 156, 73–82. doi: 10.1016/j.phytochem.2018.08.010

Toporkova, Y. Y., Smirnova, E. O., Mukhtarova, L. S., Gorina, S. S., and Grechkin, A. N. (2019). Catalysis by allene oxide synthase (CYP74A and CYP74C): alterations by the Phe/Leu mutation at the SRS-1 region. *Phytochemistry* 169:112152. doi: 10.1016/j.phytochem.2019.112152

Vancanneyt, G., Sanz, C., Farmaki, T., Paneque, M., Ortego, F., Castanera, P., et al. (2001). Hydroperoxide lyase depletion in transgenic potato plants leads to an increase in aphid performance. *Proc. Natl. Acad. Sci. U. S. A.* 98, 8139–8144. doi: 10.1073/pnas.141079498

Wasternack, C., and Feussner, I. (2018). The oxylipin pathways: biochemistry and function. *Ann. Rev. Plant Biol.* 69, 363–386. doi: 10.1146/annurev-arplant-042817-040440

Weng, J.-K., and Noel, J. P. (2013). Chemodiversity in *Selaginella*: a reference system for parallele and convergent metabolic evolution in terrestrial plants. *Front. Plant Sci.* 4:119. doi: 10.3389/fpls.2013.00119

Yanagi, K., Sugimoto, K., and Matsui, K. (2011). Oxylipin-specific cytochrome P450s (CYP74s) in *Lotus japonicus*: their implications in response to mechanical wounding and nodule formation. *J. Plant Interact.* 6, 255–264. doi: 10.1080/17429145.2011.562985

Conflict of Interest: The authors declare that the research was conducted in the absence of any commercial or financial relationships that could be construed as a potential conflict of interest.

Publisher's Note: All claims expressed in this article are solely those of the authors and do not necessarily represent those of their affiliated organizations, or those of the publisher, the editors and the reviewers. Any product that may be evaluated in this article, or claim that may be made by its manufacturer, is not guaranteed or endorsed by the publisher.

Copyright © 2021 Tanaka, Koeduka and Matsui. This is an open-access article distributed under the terms of the Creative Commons Attribution License (CC BY). The use, distribution or reproduction in other forums is permitted, provided the original author(s) and the copyright owner(s) are credited and that the original publication in this journal is cited, in accordance with accepted academic practice. No use, distribution or reproduction is permitted which does not comply with these terms.

frontiers in Plant Science

MINI REVIEW
published: 28 October 2021
doi: 10.3389/fpls.2021.720867

Lipid Peroxide-Derived Reactive Carbonyl Species as Mediators of Oxidative Stress and Signaling

*Md. Sanaullah Biswas[1] and Jun'ichi Mano[2]**

[1] Department of Horticulture, Bangabandhu Sheikh Mujibur Rahman Agricultural University, Gazipur, Bangladesh, [2] Science Research Center, Yamaguchi University, Yamaguchi, Japan

Oxidation of membrane lipids by reactive oxygen species (ROS) or O_2/lipoxygenase leads to the formation of various bioactive compounds collectively called oxylipins. Reactive carbonyl species (RCS) are a group of oxylipins that have the α,β-unsaturated carbonyl structure, including acrolein and 4-hydroxy-(*E*)-2-nonenal. RCS provides a missing link between ROS stimuli and cellular responses in plants via their electrophilic modification of proteins. The physiological significance of RCS in plants has been established based on the observations that the RCS-scavenging enzymes that are overexpressed in plants or the RCS-scavenging chemicals added to plants suppress the plants' responses to ROS, i.e., photoinhibition, aluminum-induced root damage, programmed cell death (PCD), senescence, abscisic acid-induced stomata closure, and auxin-induced lateral root formation. The functions of RCS are thus a key to ROS- and redox-signaling in plants. The chemical species involved in distinct RCS signaling/damaging phenomena were recently revealed, based on comprehensive carbonyl determinations. This review presents an overview of the current status of research regarding RCS signaling functions in plants and discusses present challenges for gaining a more complete understanding of the signaling mechanisms.

Keywords: environmental stress responses, plant hormone signaling, reactive electrophile species, reactive oxygen species, redox signaling

OPEN ACCESS

Edited by:
Silke Allmann,
University of Amsterdam, Netherlands

Reviewed by:
Thomas Roach,
University of Innsbruck, Austria
Yanjie Xie,
Nanjing Agricultural University, China

****Correspondence:***
Jun'ichi Mano
mano@yamaguchi-u.ac.jp

Specialty section:
This article was submitted to Plant Physiology, a section of the journal Frontiers in Plant Science

Received: *05 June 2021*
Accepted: *01 October 2021*
Published: *28 October 2021*

Citation:
Biswas MS and Mano J (2021) Lipid Peroxide-Derived Reactive Carbonyl Species as Mediators of Oxidative Stress and Signaling. Front. Plant Sci. 12:720867. doi: 10.3389/fpls.2021.720867

INTRODUCTION

The production of reactive oxygen species (ROS) such as superoxide radical ($O_2^{\bullet-}$), hydrogen peroxide (H_2O_2), and singlet oxygen ($^1O_2$) is intrinsically associated with redox reactions in aerobic cells (Halliwell and Gutteridge, 2015). In plants, intracellular ROS levels are changed by environmental stress, biotic stress, phytohormones, and developmental signals, and increases in ROS cause reprogramming of cells to enable them to survive in new conditions (oxidative signaling) or cell death (oxidative stress). Specifically, ROS are critical agents in determining cell fates in various physiological situations (Mittler, 2017; Mhamdi and Van Breusegem, 2018; Waszczak et al., 2018). Because ROS production sites are often associated with membranes (Asada, 2006), fatty acids [especially polyunsaturated fatty acids (PUFAs)] are oxidized by ROS to lipid peroxides (LOOHs). LOOHs are also produced via the lipoxygenase (LOX)-catalyzed oxygenation of PUFAs. Subsequently, LOOHs are metabolized or non-enzymatically decompose to a variety of aldehydes and ketones (collectively designated as "oxylipin carbonyls") (Blée, 1998). A carbonyl group can form a Schiff's base with an amino group and hence are potential protein modifiers (**Figure 1**).

Among the oxylipin carbonyls, those that have the α,β-unsaturated bond are grouped as reactive carbonyl species (RCS) (Mano, 2012; Mano et al., 2019a) or oxylipin reactive electrophile species (RES) (Farmer and Mueller, 2013) because they can form a Michael adduct with a nucleophilic group on proteins (Cys, His, or Lys residue) or nucleic acids (guanine base) due to the high electrophilicity of their β-carbon (Esterbauer et al., 1991). This chemical property gives RCS a potential ability to mediate ROS-initiated signals/damage to proteins, implying that RCS can cause both "eustress" and "distress" to organisms depending on their intracellular levels, as can ROS (Kranner et al., 2010). For animals, the physiological importance of RCS in oxidative stress was established in the 1990s (Esterbauer et al., 1991). The role of RCS was initially regarded as cell-damaging agents, and more recently their functions as cellular signals to regulate gene expression have been recognized (Schopfer et al., 2011; Bachi et al., 2013; Parvez et al., 2018).

For plants, the occurrence of a wide variety of carbonyls including RCS (Schauenstein et al., 1977) and the toxicity of carbonyl compounds are known (Reynolds, 1977), but their physiological functions have been investigated only sparsely until the 1990s (Gardner et al., 1990). The possibility that oxylipin carbonyls evoke physiological responses in plants was tested with experiments in which certain carbonyls were poured or fumigated on plants. Bate and Rothstein (1998) showed the (*E*)-2-hexenal, a C6 RCS, induced defense gene in *Arabidopsis thaliana.* Edward E. Farmar's group demonstrated that acrolein and methylvinyl ketone (MVK), which are also types of RCS, induced distinct groups of genes (Alméras et al., 2003; Weber et al., 2004). The endogenous formation of RCS such as 4-hydroxy-(*E*)-2-nonenal (HNE) was detected in *Daucus carota* cultured cells and the bell pepper fruit (Deighton et al., 1997, 1999).

In those studies, oxylipin carbonyls were investigated as end products of the LOX-dependent formation of LOOHs in the context of plant responses to biotic stressors (e.g., infection and wounding) that activate LOXs. In contrast, in abiotic (environmental) stress studies, thiobarbituric acid-reactive substances (TBARS), which mainly detect the RCS malondialdehyde (MDA), were frequently employed as a marker of lipid oxidation due to ROS. The physiological effects of MDA and a variety of other RCS — including the more toxic acrolein and HNE — have not received broad attention until recently.

There has been substantial progress in our understanding of the functions of RCS in the plant stress responses during the past decade (Farmer and Mueller, 2013; Mano et al., 2019a). This progress is due to advances in the comprehensive analysis of carbonyls in plant tissues and the use of RCS-scavenging enzymes in transgenic plants (described below). The roles of RCS, ranging from signaling agents to cell-damaging toxins in a continuum of effects, have been discovered in a variety of physiological responses of plants (**Table 1**).

In this review, we present an overview of current research on RCS metabolism in plants (formation and scavenging) (section "Occurrence and Metabolism of Reactive Carbonyl Species in Plants"), the potential effects of RCS on plants (section "Response of Plants to Exogenously Added Reactive Carbonyl Species") and plant functions (section "Physiological Roles of Endogenously Generated Reactive Carbonyl Species That Are Verified by the Measurement of Reactive Carbonyl Species Contents"), and the target proteins of RCS (section "Target Proteins of Reactive Carbonyl Species"). We then discuss present challenges in the elucidation of the RCS signaling mechanisms (and therewith the ROS- and redox signaling mechanisms) in plants.[1]

OCCURRENCE AND METABOLISM OF REACTIVE CARBONYL SPECIES IN PLANTS

Determination of Carbonyls in Plants

More than a dozen oxylipin carbonyls are present in plants (Schauenstein et al., 1977). Typical oxylpin carbonyls and RCS are shown in **Figure 1**. Although they are common as carbonyls, the chemical reactivities of distinct species are very different (LoPachin and Ganvin, 2014), as are their biological effects (Reynolds, 1977; Alméras et al., 2003; Weber et al., 2004; Mano et al., 2009; Yamauchi et al., 2015). For investigations of the roles of RCS, it is necessary to know their levels in tissues and their changes in response to various physiological stimuli. The measurement of TBARS (Steward and Bewley, 1980; Hodges et al., 1999) is generally thought to represent the MDA level, but this method is not specific to MDA, and it cannot detect many RCS that are more highly reactive, and thus biologically more active, than MDA (Esterbauer et al., 1991).

For a comprehensive carbonyl determination, a separation of the hydrazone derivatives of carbonyls by high-performance liquid chromatography (HPLC) is suitable (Esterbauer et al., 1989). Because carbonyls are unstable (they are prone to reduction by reductants contained in plant extract, oxidation by ROS and O_2, and adduct formation with nucleophilic molecules), the extracted carbonyls should be stabilized by derivatization with 2,4-dinitrophenylhydrazine (DNPH). The resulting hydrazone derivatives of carbonyls can be sensitively determined spectrophotometrically (with an absorbance peak ranging from 300 to 380 nm) after separation on a reverse-phase HPLC column (Esterbauer et al., 1989). With a protocol optimized for the extraction of hydrophilic RCS from plant tissues, it is possible to determine the content of 19 types of carbonyls including the most toxic RCS acrolein and HNE (Mano and Biswas, 2018). More than a dozen types of oxylipin carbonyls were identified in leaves and roots, and their significant increases in response to stress treatments were observed (Mano et al., 2010; Yin et al., 2010). DNPH-derivatized carbonyls are also determined efficiently by liquid chromatography-mass spectrometry (LC-MS). The mass spectrometer is operated in

[1]The term "RCS" sometimes includes, in addition to the LOOH-derived α,β-unsaturated carbonyls, the sugar-derived dicarbonyls methylglyoxal and glyoxal (a broad definition of RCS). In this review article, however, we adopt a narrow definition of RCS; we exclude these dicarbonyls because we believe that they should be distinguished from oxylipin-derived carbonyls in terms of both physiology and chemistry. A review article is available on these sugar-derivided dicarbonyls in plants (Hoque et al., 2016).

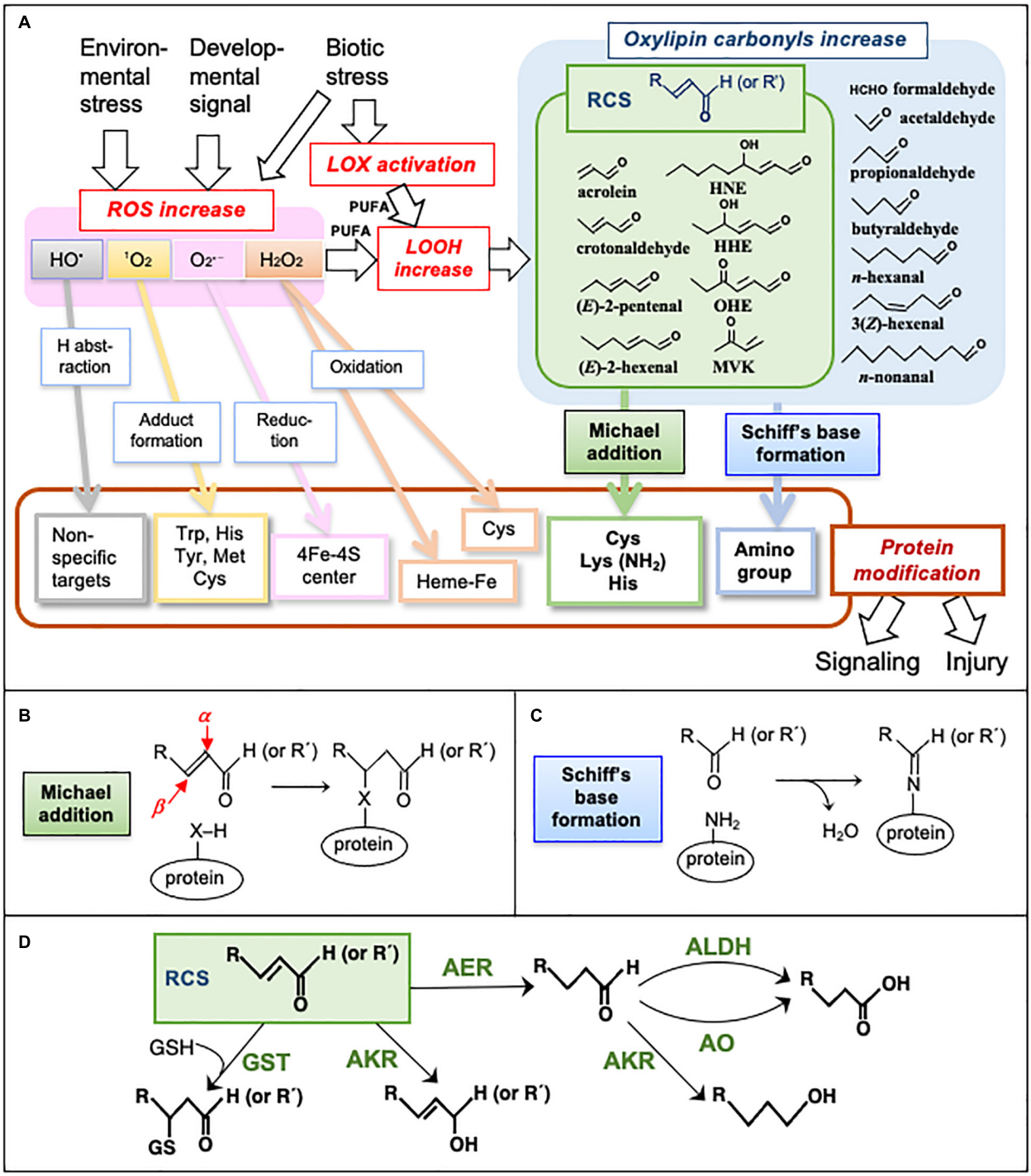

FIGURE 1 | Metabolism and reactions of oxylipin carbonyls. **(A)** Formation of ROS and oxylipin carbonyls and their actions causing signaling and injury via protein modification. $HO^{\bullet}$ is highly reactive and non-specifically oxidizes almost all biomolecules. $^1O_2$ is also highly reactive, and it prefers adduct formation on a double bond and a sulfur atom. $O_2^{\bullet-}$, a relatively less reactive ROS, can reductively destroy the 4Fe-4S center in some enzymes such as aconitase (Halliwell and Gutteridge, 2015). H_2O_2 is also less reactive and may oxidize the Fe atom in the heme proteins such as ascorbate peroxidase or guaiacol peroxidase to inactivate them (Miyake and Asada, 1996). Oxylipin carbonyls and RCS, produced via the oxidation of PUFA by ROS, react with proteins in different manners from ROS. **(B)** Formation of the Michael adduct on a protein. The α- and β-carbons in an RCS molecule are indicated by red arrows. X, a nucleophilic atom. **(C)** Schiff's base formation on a protein. **(D)** Enzymes to scavenge carbonyls and RCS in plants. AER, 2-alkenal reductase; AKR, aldo-keto reductase; ALDH, aldehyde dehydrogenase; AO, aldehyde oxidase; GST, glutathione transferase.

TABLE 1 | Plant responses to oxidative stimuli that are relevant to RCS.

Stimulus/response[a]	Plant species	Modulation of RCS			References
		Method[b]	RCS level changes[c]	Physiological outcome	
Drought stress/leaf damage	*Nicotiana tabacum*	OE of AKR	Suppression of increase in MDA (as TBARS)	Suppression of damage	Oberschall et al., 2000
Cd stress, chilling stress/leaf damage	*N. tabacum*	OE of AKR	Suppression of increase in MDA (as TBARS)	Suppression of damage	Hegedüs et al., 2004
Heat stress, MV/leaf damage	*N. tabacum*	OE of AKR	Suppression of increase in MDA (as TBARS)	Suppression of damage	Turóczy et al., 2011
Heavy metal stress (Cu, Cd), H_2O_2 stress/damage	*Arabidopsis thaliana*	OE of ALDH	Suppression of increase in MDA (as TBARS)	Suppression of damage	Sunkar et al., 2003
NaCl stress/damage	*A. thaliana*	KO of *ALDH3*	Enhanced increase in MDA (as TBARS)	Enhancement of damage	Kotchoni et al., 2006
Strong light/leaf damage	*N. tabacum*	OE of AER	Suppression of increase in acrolein and (*E*)-2-hexenal	Suppression of photoinhibition	Mano et al., 2010
$AlCl_3$ stress/root damage	*N. tabacum*	OE of AER	Suppression of increase in acrolein, (*E*)-2-hexenal, HNE and HHE	Suppression of damage	Yin et al., 2010
MV/leaf damage	*A. thaliana*	KO of *AOR*	Enhanced increase in acrolein	Enhancement of damage	Yamauchi et al., 2012
Heat stress/leaf damage	*Cyclamen persicum*	KD of *CpFAD7*	Suppression of increases in acrolein, (*E*)-2-hexenal and MVK	Suppression of leaf injury	Kai et al., 2012
H_2O_2/PCD of cultured cells	*N. tabacum*	carnosine added	Suppression of increases in acrolein and HNE	Suppression of PCD initiation	Biswas and Mano, 2015
Darkness/senescence of siliques	*A. thaliana*	KO of *AAO4*	Increases in acrolein and MDA	Senescence facilitated	Srivastava et al., 2017
ABA/stomata closure	*N. tabacum*	OE of AER	Suppression of increases in acrolein, (*E*)-2-hexenal, HNE and HHE	Inhibition of stomata closure	Islam et al., 2016
MeJA/stomata closure	*N. tabacum*	OE of AER	Suppression of increases in acrolein, HNE, HHE and (*E*)-2-heptenal	Inhibition of stomata closure	Islam et al., 2020
Auxin/LR formation	*A. thaliana*	carnosine added	Suppression of increases in acrolein, crotonaldehyde and HNE	Inhibition of LR formation	Biswas et al., 2019

[a] *ABA, abscisic acid; LR, lateral root; MeJA, methyl jasmonate; MV, methylviologen; PCD, programmed cell death.*
[b] *AAO4, Arabidopsis aldehyde oxidase 4; AER, 2-alkenal reductase; AKR, aldo-keto reductase; ALDH, aldehyde dehydrogenase; AOR, alkenal/one oxidoreductase; CpFAD, chloroplastic fatty acid desaturate; KD, knock-down; KO, knock-out; OE, overexpression.*
[c] *HHE, 4-hydroxy-(E)-2-hexenal; HNE, 4-hydroxy-(E)-2-hexenal; MDA, malondialdehyde; MVK, methylvinyl ketone, TBARS, thiobarbituric acid-reactive substances.*

negative ion mode with multiple reactions monitoring (MRM) (Roach et al., 2017). Significant increases in the levels of RCS such as acrolein, MDA, (*E*)-2-hexenal, and (*E*)-2-pentenal were detected in photoautotrophic *Chlamydomonas reinhardtii* LHCSR3-deficient strain *npq4* under high light conditions (500 μmol photons m^{-2} s^{-1}) (Roach et al., 2017), on $^1O_2$ exposure (Roach et al., 2018), and under a high-O_2 atmosphere (Roach, 2020).

Gas chromatography-mass spectrometry (GC-MS) is also used for determining RCS and oxylipin carbonyls (Michalski et al., 2008). The exposure of *A. thaliana* plants to high light (1,500 μmol photons m^{-2} s^{-1}) at low temperature (7°C) for 24 h increased the levels of 4-hydroxy-2-hexenal (HHE), HNE, and hexenal (Rac et al., 2021). The C3–C17 volatile compounds emitted during wounding were determined quantitatively in the leaves of five tropical crops (Portillo-Estrada et al., 2021). The medicinal plant *Rhodiola semenowii* when exposed to chilling stress, benzeneacetaldehyde and ketones such as 4-cyclopentene-1,3-dione and 1,2-cyclopentanedione were increased in the shoots; whereas plants under water-deficit stress showed decreased accumulations of ketones such as 2-propanone and 1-(acetyloxy)-2-propanone in the root (Terletskaya et al., 2021). Solid-phase micro-extraction fiber-trapped volatiles were measured by GC-time of flight (TOF)-MS and highly sensitive GC-quadrupole (Q)TOF-MS (Spyropoulou et al., 2017). GC-MS is also applicable for analyses of non-volatile oxylipin carbonyls after their derivatization (Kawai et al., 2007).

Reactive Carbonyl Species Generation Mechanism

The endogenous level of an RCS is determined by the balance between its generation rate and the scavenging rate. We will explain the mechanism of RCS generation in plant cells and then describe the scavenging mechanisms for RCS.

RCS are formed through the oxidative degradation of LOOH. LOOH are generated by two distinct mechanisms: the enzymatic oxygenation of lipids, and the non-enzymatic oxidation of PUFAs by ROS. In an enzymatic process, lipoxygenase (LOX), a key enzyme of the oxidation of PUFAs such as α-linolenic acid, converts them to either 9- or 13-hydroperoxy-octadecatrienoic acids, or a mixture of both. Corresponding 9- and 13-hydroperoxide lyases act on 9- and 13-hydroperoxides, respectively, to form C6-C9 aldehydes and 9- and 13-oxoacid, including jasmonic acid and 12-oxo-phytodienoic acid (OPDA) (Matsui, 2006; Mosblech et al., 2009; Vincenti et al., 2019). OPDA has an α,β-unsaturated carbonyl structure and is therefore also

an RCS. (*Z*)-3-Hexenal, the primary C6 product of the hydroperoxide lyase-catalyzed degradation of 13-hydroperoxide, is converted to (*E*)-2-hexenal, an RCS, by an isomerase (Kunishima et al., 2016; Spyropoulou et al., 2017). The enzymatic lipid oxidation and oxylipin metabolism in plants have been extensively studied as cellular responses relevant to infection and wounding.

The non-enzymatic lipid peroxidation process is explained in *in vitro* studies of oil deterioration under heat (Vliegenthart, 1979; Grosch, 1987). The highly oxidizing ROS, such as hydroxyl radical ($HO^{\bullet}$), starts the oxidation of a lipid molecule by abstracting a hydrogen atom from the pentadiene structure in a PUFA moiety, such as linoleic acid (18:2) and linolenic acid (18:3).

ROS are constitutively generated via the reduction of molecular oxygen (O_2) in almost all of the subcellular compartments, among which chloroplasts and peroxisomes generate large fluxes of ROS formation in photosynthetic tissues under light, whereas the mitochondria contribute mainly to the flux in non-photosynthetic tissues (Foyer and Noctor, 2003; Mittler et al., 2004). In the chloroplast, the energy transfer from the triplet state of the primary electron donor ($^3P680^*$) in photosystem II (PSII) to ground state O_2 generates $^1O_2$, and the electron transfer from photosystem I (PSI)-ferredoxin to O_2 produces $O_2^{\bullet-}$ (Asada, 2006). Under high light conditions, $^1O_2$ occupies a major portion of the ROS generated in leaves (Triantaphylidès et al., 2008; Waszczak et al., 2018). $O_2^{\bullet-}$ is also produced in the mitochondrial electron transport chain when electrons from complexes I and II are overloaded (Huang et al., 2016). In the presence of superoxide dismutase (SOD), $O_2^{\bullet-}$ is disproportionated to form H_2O_2 and O_2. In the peroxisome, H_2O_2 generated by the glycolate oxidase activity during photorespiration is also a major source of ROS in C3 plants (Foyer and Noctor, 2003). $HO^{\bullet}$ is formed via the Fenton reaction in any part of the cell when H_2O_2 is reduced by metal catalysts such as Fe^{2+} ion (Mittler, 2017).

The NADPH oxidase complex (also known as the respiratory burst oxidase homolog; RBOH) on the plasma membrane is another important source of ROS. The *A. thaliana* genome contains 10 genes for the RBOH isoforms, which are expressed in a tissue-specific manner (Chapman et al., 2019). RBOHs are latent under normal conditions and activated when the cell receives stimuli, e.g., a pathogen attack or developmental signal (Mittler et al., 2011; Waszczak et al., 2018). The RBOH complex then reduces O_2 to $O_2^{\bullet-}$ in the apoplast by consuming NADPH in the cytosol. The $O_2^{\bullet-}$ is then converted to H_2O_2 and O_2 by the SOD in the apoplast.

The ROS thus generated in the close vicinity of membranes will oxidize the PUFA part of lipids in the membranes. Radicals, i.e., $HO^{\bullet}$ and $O_2H^{\bullet}$ (the protonated form of superoxide radical) are neutral species and are capable of hydrogen abstraction from lipid molecules. The generated lipid radical reacts with O_2 and forms a lipid peroxyl radical, which then oxidizes neighboring lipid molecules to cause radical chain oxidation to lipid peroxidation (Grosch, 1987). In addition to the radical chain reaction, the addition of $^1O_2$ to a PUFA also generates a LOOH (Triantaphylidès et al., 2008). The subsequent fragmentation of LOOHs by the enzymatic and non-enzymatic processes forms dozens of oxylipin carbonyls, including RCS of various carbon-chain lengths and different extents of oxygenation (Farmer and Mueller, 2013; Yalcinkaya et al., 2019a).

Reactive Carbonyl Species Scavenging Compounds and Enzymes

Plant cells are enriched with non-enzymatic and enzymatic scavenging systems to control the endogenous levels of RCS. As low-molecular-weight scavengers, the thiol-compounds cysteine and the reduced form of glutathione (GSH) can efficiently trap RCS by forming an RCS-conjugate (Esterbauer et al., 1975). With aluminum (Al) stress treatment, transgenic *A. thaliana* plants with higher levels of GSH exhibited less increases in RCS and other oxylipin carbonyls in roots and showed higher tolerance to Al toxicity compared to the wildtype plants (Yin et al., 2017). GSH may be critical for the scavenging of certain types of RCS because plants have glutathione transferase (GST) isozymes that show narrow specificities to selected types of RCS (Mano et al., 2019b, described below). Polyphenols (which are rich in plants) are also candidate RCS scavengers. Certain types of polyphenols such as phloretin in tea leaf and apple fruit (Zhu et al., 2009), pelargonidin in brown rice (Colzani et al., 2018), and catechins in tea leaf (Sugimoto et al., 2021) can trap acrolein and HNE *in vitro*, but their *in planta* function to scavenge RCS has not been verified.

Enzymatic reactions to scavenge RCS and non-RCS carbonyls in plants are classified into five types (**Figure 1D**) as follows: (*i*) 2-Alkenal reductase (AER) (Mano et al., 2002, 2005), and alkenal/one oxidoreductase (AOR) (Yamauchi et al., 2011) specifically reduce the α,β-unsaturated bond of an RCS molecule to form the corresponding saturated species. This type of enzyme does not react with the carbonyl group. AER from *A. thaliana* shows a higher affinity to longer-chain RCS than smaller RCS such as acrolein. (*ii*) Aldo-keto reductases (AKR) catalyze the reduction of a carbonyl to alcohol (Oberschall et al., 2000). AKR isozymes have a relatively broad substrate specificity for various carbonyls (Yamauchi et al., 2011). (*iii*) Aldehyde dehydrogenase (ALDH) catalyzes the oxidation of a carbonyl to a carboxylic acid (Kotchoni et al., 2006). (*iv*) GST catalyzes the formation of the covalent bond between an electrophilic compound (such as an RCS) and GSH to detoxify the former (Gronwald and Plaisance, 1998). The specificity to the electrophile substrate differs by isozymes. In the *A. thaliana* genome, there are about 50 isogenes of GST. Ten of the 28 total Tau-class GST isozymes can recognize acrolein or HNE or both as the substrate (Mano et al., 2017, 2019b), suggesting that GST is also an important enzyme for RCS detoxification. (*v*) Aldehyde oxidase (AO) catalyzes the oxidation of a carbonyl to carboxylate using O_2 as the electron acceptor (Srivastava et al., 2017). *A. thaliana* has four AO isozymes. An extensive comparison of the substrate specificity of these RCS-scavenging enzymes is available in a recent article (Mano et al., 2019b).

RESPONSE OF PLANTS TO EXOGENOUSLY ADDED REACTIVE CARBONYL SPECIES

Reactive Carbonyl Species Can Modify Proteins

As shown in **Figure 1**, RCS can form Michael adducts or Schiff's base with proteins, resulting in the modification of the Cys, Lys, His, and amino groups. Saturated carbonyls are capable of Schiff's base formation but do not form Michael adducts. In contrast, methylglyoxal, and glyoxal, which are dialdehydes generated mainly through sugar metabolism, appear to modify Arg residues preferentially on the target proteins (Armed et al., 2005; Gao and Wang, 2006). The protein modification by RCS is thus distinct from that by saturated carbonyls and dialdehydes. On the other hand, ROS can react with amino acid residues which are not targeted by carbonyls, e.g., Trp, Tyr, and Met. $HO^{\bullet}$ can oxidize any type of organic compounds indiscriminately (Møller et al., 2007; Parvez et al., 2018). In addition, metal centers such as 4Fe-4S center and heme iron in proteins are sensitive to $O_2^{\bullet -}$ and H_2O_2, respectively (Halliwell and Gutteridge, 2015).

Regarding the known H_2O_2 sensor proteins such as OxyR in bacteria and Yap1 in yeast, a specific Cys residue(s) is oxidized by H_2O_2 to the sulfenic acid (Cys-SOH), causing protein structural changes that result in the alteration of their physiological functions (Reczek and Chandel, 2015). Redox-reversible Cys residues on a protein can thus be affected by both ROS and RCS, but the chemical structures of the reaction products are different (**Figure 1A**). The modification of Cys residues in a protein may result in either its inactivation or activation, depending on the protein and the modifying compound (Wible and Sutter, 2017).

Toxicity of Reactive Carbonyl Species

Because of their reactivity, carbonyl compounds are generally toxic to living cells. Reynolds (1977) compared the toxicity of various carbonyl compounds to lettuce seeds and showed that RCS are more toxic than saturated carbonyls. For example, the IC50 concentration to inhibit seed germination was 0.043 mM for acrolein and 13.7 mM for propionaldehyde. The exposure of *A. thaliana* plants to volatile RCS such as acrolein, methylvinyl ketone (MVK), and (*E,Z*)-2,6-nonadienal (Alméras et al., 2003) or (*E*)-2-hexenal (Matsui et al., 2012) caused a decrease in PSII activity. Acrolein caused the inactivation of PSII under light in the cyanobacterium *Synechocystis* sp. (Shimakawa et al., 2013). The infiltration of HNE into tobacco leaves caused necrosis (Mano et al., 2005).

The toxicity of RCS can be attributed to the inactivation of certain target enzymes. Pea mitochondria, alternative oxidase (Winger et al., 2005), and lipoate enzymes such as the H-subunit of glycine decarboxylase complex (Taylor et al., 2002) are highly sensitive to exogenously added HNE. In spinach chloroplasts, the addition of RCS resulted in the inactivation of photosynthesis. A comparison of various RCS and oxylipin carbonyls of C3–C9 revealed that an RCS is more toxic than the corresponding saturated carbonyl (as shown for seed germination). The most toxic RCS was acrolein, followed by HNE (Mano et al., 2009).

Alteration of Gene Expression by Exogenous Reactive Carbonyl Species

At lower doses, exogenously added RCS can alter plant gene expression. *A. thaliana* plants upon exposure to (*E*)-2-hexenal, activated a wide range of genes to protect against pathogen attack (Bate and Rothstein, 1998; Kishimoto et al., 2005). An exogenous application of low levels of MDA (4 μmol L^{-1} air volume) to *A. thaliana* strongly upregulated many defense genes against abiotic/environmental stress (e.g., *ROF1*, *XERO2*, and *DREB2A*) (Weber et al., 2004). Acrolein and MVK upregulated the pathogenesis-related gene *HEL* (*PR4*) in *A. thaliana* plants (Alméras et al., 2003). The addition of OPDA, a C12 RCS, to *A. thaliana* liquid culture induced a set of defense genes that are distinct from those activated by jasmonate and MeJA, which are non-RCS downstream products of OPDA (Taki et al., 2005). The fumigation of *A. thaliana* plants with an RCS of carbon-chain length 4–8 expressed heat stress-related genes (*HSFA2*, *MBF1c*) and drought stress-related genes (*DREB2A*, *ZAT*s) and thus enhanced abiotic stress tolerance (Yamauchi et al., 2015). Salt-sensitive glycophyte *A. thaliana* and its close relative *Eutrema parvulum,* a salt-tolerant halophyte, responded differently after exposure to various concentrations of RCS. Applications of acrolein, HHE, and HNE increased the activity of various ROS scavenging enzymes such as catalase and ascorbate peroxidase in *A. thaliana* but not in *E. parvulum*. The gene expressions of the membrane-bound *SOS1* and tonoplast-localized *NHX1* and *NHX5* were upregulated by RCS, depending on the RCS type and concentrations (Yalcinkaya et al., 2019b).

In mammals, transcription factor Nrf2 is a master regulator of cellular responses against environmental stressors, which induces the expression of detoxification genes. Under normal conditions, the Nrf2 level in the cell is kept low by the action of Keap1 (Kelch-like ECH-associated protein 1), an adaptor subunit of Cullin 3-based E3 ubiquitin ligase. Keap1 catalyzes the ubiquitination of Nrf2 and facilitates its degradation. Under oxidative stress, HNE modifies Keap1 on its Cys residues 151, 273, and 288 and inhibits its ubiquitin ligase activity. HNE thus raises the Nrf2 level and thereby activates the target genes (Suzuki and Yamamoto, 2017). A similar RCS-mediated gene regulation mechanism may well be present in plants. The exposure of *C. reinhardtii* cells to a low concentration of acrolein (600 ppm) increased the glutathione content and the expression of the GST isogene *GSTS1*. These responses protected the algal cells from $^1O_2$ generated under high light (Roach et al., 2017). The $^1O_2$-tolerance was induced by acrolein at as low as 125 ppm, while acrolein at higher than 900 ppm caused damage to cells, representing a typical continuum of the effect of RCS from eustress to distress (Roach et al., 2018). The 8 base-pair palindromic sequence CAACGTTG (electrophile-responsive element; ERE) in the promoter region is required for the (*E*)-2-hexenal-responsive expression of *GSTS1* (Fischer et al., 2012) and other defense genes including *IFR1* (Venkanna et al., 2017) in *C. reinhardtii*. SINGLET OXYGEN RESISTANT 1 (SOR1),

a bZIP-type putative transcription factor, is a candidate to be bound to ERE as a repressor because the *SOR1*-deficient mutant *sor1* shows overexpression of the electrophile-responsive genes (Fischer et al., 2012). It has yet to be clarified whether the SOR1 protein is the (*E*)-2-hexenal sensor or additional factors mediate the RCS signal to SOR1.

PHYSIOLOGICAL ROLES OF ENDOGENOUSLY GENERATED REACTIVE CARBONYL SPECIES THAT ARE VERIFIED BY THE MEASUREMENT OF REACTIVE CARBONYL SPECIES CONTENTS

Reactive Carbonyl Species Are Causative Agents of Oxidative Injury in Plants

In the early 2000s, pioneering work was published regarding the damage-causing effect of endogenously produced carbonyls, in which the overexpression of carbonyl-scavenging enzymes such as ALDH and AKR conferred tolerance against environmental stressors in transgenic plants (Oberschall et al., 2000; Sunkar et al., 2003; Hegedüs et al., 2004; see **Table 1**). The toxicity of the endogenous carbonyls was further supported by the observations of the transgenic plants with suppressed ALDH levels. When the expressions of *ALDH7* and *ALDH3* genes were suppressed in *A. thaliana,* the plants showed greater sensitivity to NaCl (Kotchoni et al., 2006). Similarly, the suppression of *ALDH7* expression in rice made the plants hypersensitive to NaCl and chilling (Shin et al., 2009). The silencing of *NbALDH2C4* in *Nicotiana benthamiana* enhanced the sensitivity of the plants to low temperature with higher accumulations of ROS and MDA, and in potatoes, the overexpression of *ALDH2B7a* lowered the level of aldehydes and enhanced the cold stress tolerance (Guo et al., 2020). In these studies, the TBARS level and the extent of tissue injury were shown to be correlated in both wildtype and transgenic lines. This evidence strongly supported the participation of the endogenous oxylipin carbonyls in the injury, but it was unclear which carbonyl species were increased and damaged the cells.

HPLC-based comprehensive analyses of carbonyls identified the carbonyl species involved in tissue injury, as follows (Mano et al., 2010; Yin et al., 2010; Kai et al., 2012; Yamauchi et al., 2012; see **Table 1**). The application of photoinhibitory intensity light to wildtype tobacco leaves caused significant accumulations of RCS such as acrolein, (*E*)-2-pentenal, and (*E*)-2-hexenal prior to the appearance of photoinhibition symptoms; whereas transgenic tobacco plants that overproduced AER accumulated lower levels of these RCS, and eventually their leaves suffered less damage (Mano et al., 2005, 2010). Conversely, the knock-out of chloroplastic AOR in *A. thaliana* resulted in hypersensitivity to methylviologen, in association with a higher accumulation of acrolein (Yamauchi et al., 2012).

The treatment of tobacco roots with aluminum chloride ($AlCl_3$) increased the ROS level in the elongation zone and eventually caused cell death (Yamamoto et al., 2002). The $AlCl_3$ treatment also increased the RCS acrolein, HNE, and HHE by 1.2 nmol (g tissue)$^{-1}$ and also less-reactive non-RCS carbonyls; for example, formaldehyde was increased by 40 nmol (g tissue)$^{-1}$. In contrast, in AER-overexpression (OE) plants, the $AlCl_3$-induced increases of RCS and non-RCS carbonyls were significantly suppressed and the transgenic plants suffered less injury by the Al ion (Yin et al., 2010). Importantly, the absorption of Al ion and the enhancement of the ROS level at the target site (the elongation zone) in the $AlCl_3$-treated roots were not affected by the overexpression of AER. These results support the possibility that the protection of cells in AER-OE plants is attributable solely to RCS scavenging. In other words, the RCS produced downstream of ROS caused tissue injury.

Heat-stress treatment of wildtype cyclamen plants (*Cyclamen persicum* Mill.) resulted in accumulations of (*E*)-2-hexenal, acrolein, and MVK, and the leaves were consequently damaged. An RNAi-suppression of *CpFAD7* (chloroplastic fatty acid desaturase 7) in cyclamen plants resulted in lower trienoic fatty acids contents and thus less accumulation of these three RCS. These RNAi lines did not show any visible damage symptoms under heat stress (Kai et al., 2012). The formation of these RCS was therefore related to the heat-induced damage in the leaves.

Signaling Functions of the Endogenously Generated Reactive Carbonyl Species

The signaling functions of endogenously generated RCS have also been verified by the measurement of RCS contents and by the modulation of RCS levels with a scavenging enzyme or a chemical scavenger, as follows (Biswas and Mano, 2015; Islam et al., 2016, 2020; Srivastava et al., 2017; Biswas et al., 2019; see **Table 1**). Programmed cell death (PCD) is a genetically regulated process that directs a cell to eliminate itself in an organized way, as a strategy used by plants to survive stressful conditions. The cells damaged by biotic or abiotic stressors accumulate ROS, which accelerates the PCD process (Petrov et al., 2015). For our studies of ROS signaling mechanisms, we used H_2O_2-induced PCD in tobacco BY-2 cells, an experimental model system, and we tested the hypothesis that RCS are involved in the ROS signaling for initiating PCD (Biswas and Mano, 2015). The addition of H_2O_2 to BY-2 cells caused increases in RCS such as acrolein, HNE, and HHE and non-RCS carbonyls such as acetaldehyde, propionaldehyde, and *n*-hexanal within 2 h, while typical PCD symptoms (TUNEL-positive nuclei, DNA laddering, and cytoplasm shrinkage) appeared 5 h after H_2O_2 treatment. The addition of the chemical carbonyl scavengers carnosine and hydralazine suppressed increases in both RCS and PCD symptoms in H_2O_2-treated cells, without affecting the levels of ROS and LOOH in the cells. Therefore, these chemicals suppressed the H_2O_2-induced PCD by scavenging RCS. Our investigation also demonstrated that the overexpression of AER in tobacco prevented root epidermis PCD under salt stress (Biswas and Mano, 2015). Specifically, the RCS generated in the

ROS-stimulated cells acted as the signal to turn on the death program of plant cells.

Senescence is the aging process of various parts of the plant body, and internal and external stimuli initiate the cell death program characterized by the expression of senescence-related genes. RCS were also shown to be involved in the senescence of Arabidopsis siliques, as follows. The Arabidopsis aldehyde oxidase 4 (AAO4) can detoxify RCS and non-RCS carbonyls. The siliques of knockout mutant *aao4* accumulated higher levels of acrolein and MDA in darkness and a higher level of MDA after UV-C exposure compared to the wildtype and showed accelerated senescence (Srivastava et al., 2017). The involvement of RCS in the senescence was further supported by the observation that exogenously added acrolein and HNE enhanced silique senescence in *aao4*, but not in the wildtype.

Functions of RCS in hormone signaling are also being revealed. ROS is involved in auxin-triggered lateral root (LR) formation (Orman-Ligeza et al., 2016), but the ROS signaling mechanism had been poorly understood. We observed that the addition of auxin to *A. thaliana* roots caused increases in the levels of various oxylipin carbonyls (such as HNE, crotonaldehyde, formaldehyde, and butyraldehyde) prior to the apparent LR emergence. Importantly, the simultaneous addition of the carbonyl scavenger carnosine and auxin to roots suppressed both the increase in the carbonyl levels and LR formation. When an RCS such as acrolein or crotonaldehyde was added to roots, the degradation of the auxin signaling repressor Aux/IAA protein was facilitated, and the auxin-responsive genes for LR formation were activated at the LR-forming sites (Biswas et al., 2019). These results demonstrate that RCS reinforce the auxin signaling for LR formation, by facilitating the degradation of Aux/IAA.

In the stomata closure induced by abscisic acid (ABA) and methyl jasmonate (MeJA), the production of ROS in guard cells is involved as a signal (Pei et al., 2000; Suhita et al., 2004). The addition of H_2O_2 and ABA (Islam et al., 2016, 2019) and MeJA (Islam et al., 2020) to leaf epidermis increased the levels of acrolein, HNE, and HHE; the addition of HNE to leaf epidermis caused stomata closure (Islam et al., 2016) preceded by the typical $[Ca^{2+}]$ elevation in the guard cells (Islam et al., 2019). The AER-OE tobacco leaves accumulated fewer RCS in response to MeJA, ABA, and H_2O_2 and exhibited smaller stomatal closure responses. These findings indicate that RCS generated in the guard cells, downstream of H_2O_2, acted as a signal for stomatal closure in the ABA and MeJA signals.

The above-described results suggest that RCS are critical signaling molecules involved in plant growth and development and cell death. However, to elucidate the functional mechanisms of RCS, it is necessary to determine which carbonyl is the most important player for each RCS-induced response. Considering the evidence obtained thus far, we can see that different physiological responses have different requirements for carbonyls. For example, the heat-shock response genes were induced by fumigation with RCS of C4–C8 chain length but the C3 RCS acrolein did not exert this effect (Yamauchi et al., 2015). For the promotion of LR formation, strong effects were observed for the RCS acrolein, HNE, and crotonaldehyde, in that order. Interestingly, butyraldehyde and propionaldehyde, which are non-RCS carbonyls, also induced LR formation at higher doses than RCS. In contrast, *n*-hexanal, another non-RCS carbonyl, inhibited LR formation (Biswas et al., 2019).

Not only the strength but also the intracellular level of a carbonyl will determine its contribution to plant responses. In Al-stressed roots, many types of RCS and non-RCS carbonyls were increased. The formaldehyde content in the stressed cells was 100-fold higher than the acrolein content (Yin et al., 2010). Considering that formaldehyde is 400-fold less toxic than acrolein (Reynolds, 1977), we can estimate the former's contribution is 1/4 of the latter. Similarly, in H_2O_2-stimulated BY-2 cells, multiple types of RCS and non-RCS carbonyls were increased. In the stressed cells, acrolein was increased to 2.5 nmol/g cells, whereas n-hexanal was increased to 18 nmol/g cells. Because the PCD-inducing strength of acrolein is 15-fold higher than that of n-hexanal (Biswas and Mano, 2015), the contribution of n-hexanal is estimated as roughly half of that of acrolein. The significance of non-RCS carbonyls is therefore not negligible, at least in these responses.

TARGET PROTEINS OF REACTIVE CARBONYL SPECIES

Once the involvement of RCS in a physiological phenomenon (e.g., metabolic pathways such as respiration, or signaling pathways such as ABA-induced stomata closure) is identified, the next step for the elucidation of the mechanism is to determine the target protein that is primarily modified by the RCS. There are two approaches for the identification of target proteins: the functional approach and the comprehensive approach.

Functional Approach

In the functional approach, the number of candidate RCS target proteins in the RCS-sensitive biochemical pathway of interest is narrowed down by examining the RCS effect on partial reactions of distinct enzymes. Millar and Leaver (2000) observed that the addition of HNE to potato mitochondria inactivated respiration, and they identified the most sensitive target as glycine decarboxylase complex. Taylor et al. (2002) revealed that HNE was covalently bound to the lipoic acid in the active site of the H protein of the complex and blocked the catalytic activity. In the mitochondrial inner membrane, uncoupling protein 1 was observed to be sensitive to HNE (Winger et al., 2005). Regarding photosynthesis, the addition of acrolein to spinach chloroplasts inactivated the CO_2-fixation activity, whereas the thylakoid electron transport chain was not affected (Mano et al., 2009). Specifically, the primary target site was in the Calvin cycle, and it was finally revealed that the thiol-regulated enzymes phosphoribulokinase, fructose-bisphoshatase, and glyceraldehyde-3-phosphate dehydrogenase were the sensitive targets. On the other hand, acrolein added to Synechococcus

cells under light caused the inactivation of the PSII reaction. A proposed mechanism is that the photoproduced $HO^{\bullet}$ reacted with acrolein and was bound to the PSII complex (Shimakawa et al., 2013).

Wounding treatment in jasmonate biosynthesis-deficient *A. thaliana* mutants showed that OPDA, a precursor RCS to jasmonate, functions as a signaling molecule for diverse physiological processes in plants (Taki et al., 2005). OPDA also repressed cell-cycle regulation and cell growth in Arabidopsis cell cultures (Eckardt, 2008) and suppressed the root growth induced by TGA transcription factors (Stotz et al., 2013). It has been suggested that cellular GSH and redox potentials play a potential role in OPDA signaling, and cyclophilin 20-3 was shown to bind OPDA to maintain the cellular redox homeostasis in stress responses via the formation of cysteine synthase complex (Park et al., 2013).

RCS are involved in the ABA- and MeJA-dependent signaling for stomata closure (Islam et al., 2016, 2020). The action site of RCS in the ABA signaling pathway should reside upstream of the activation of the putative Ca^{2+} channel because exogenous addition of acrolein stimulated the Ca^{2+} influx into the guard cell (Islam et al., 2019). Interestingly, the Arabidopsis mutant *tgg1tgg2*, deficit of two myrosinases TGG1 and TGG2, was insensitive to acrolein with regard to the stimulation of Ca^{2+} influx, indicating that these myrosinases are required for the acrolein signaling (Rahman et al., 2020). It has yet to be clarified whether the myrosinases are the RCS targets.

In tobacco BY-2 cells, the addition of the PCD-initiating level of H_2O_2 stimulated the activities of caspase-1-like protease (C1LP) and caspase-3-like protease (C3LP), which are cysteine proteases that are known to trigger PCD in plants (Ye et al., 2013; Hatsugai et al., 2015). A lethal dose of acrolein increased the activity of C3LP (Biswas and Mano, 2016). Acrolein and HNE added to cell-free extracts stimulated the C3LP and C1LP activities, but H_2O_2 could not (Biswas and Mano, 2016). These proteases are thus direct targets of RCS. C3LP activity is displayed by two different proteins: the β1 subunit of 20S proteasome (Hatsugai et al., 2015) and cathepsin B (Ge et al., 2016). The RCS-responsive C3LP activity has been attributed to the former protein on the basis of an inhibitor study (Biswas et al., 2020).

In the auxin signaling for LR formation, RCS promote the degradation of the Aux/IAA repressor protein, which is a key step in auxin signaling (Biswas et al., 2019). In the *slr1* mutant of *A. thaliana* (which does not form LRs because an amino acid change in IAA14 protein prevents its degradation by the proteasome; Fukaki et al., 2002), RCS was ineffective to promote LR formation. These results indicate that the primary RCS action site resides in-between the auxin recognition by the receptor TIR1 and the degradation of Aux/IAA (Biswas et al., 2019). One possible target is TIR1. Cys140 in the TIR protein can be modified by nitric oxide (NO), and this modification increases the affinity of the TIR1-Aux/IAA complex to auxin. This explains NO's ability to promote LR formation (Terrile et al., 2012). Because both NO and RCS are electrophiles, RCS may be bound to the same Cys residue and facilitate the auxin signaling by the same mechanism. Alternatively, IAA14 protein may be the RCS sensor.

Comprehensive Approach

In the comprehensive approach, RCS-modified proteins are identified by proteomic analysis. The plants or cells of interest are treated with oxidative agents, and the RCS-modified proteins in cell extracts are marked or collected by an anti-RCS antibody for the subsequent proteomic analysis. Winger et al. (2007) detected HNE-modified proteins in *A. thaliana* mitochondria by western blotting with an anti-HNE antibody after two-dimensional electrophoresis. The immunoreactive proteins increased by the treatment of cells with H_2O_2, antimycin A, and menadione were extracted from the gels and sequenced. The list of the HNE-modified proteins in oxidative stressed cells largely overlapped with the proteins in the cells treated directly with HNE, indicating that RCS preferentially modifies certain proteins.

Mano et al. (2014) collected HNE-modified proteins by antibody affinity trapping from the leaves of *A. thaliana* and compared the amount of each of the proteins between the NaCl-stressed samples and the control samples by a differential quantitative proteomics technique. Seventeen proteins were observed to be more frequently (more than twofold) modified with the endogenously produced HNE under salt stress. Based on the identities of these target proteins, it was observed that under NaCl stress, HNE affected proteins in the cytosol, peroxisome, chloroplast, mitochondrion, and (interestingly) apoplast. This intracellular distribution of the HNE target proteins suggests that under stress conditions, membranes of various organelles and the plasma membrane are oxidized and produce RCS.

An advanced comprehensive analysis has been applied to investigate the various types of oxidative modifications of proteins in legume nodules (Matamoros et al., 2018). In this method, a carbonyl moiety on a protein, which is formed due to oxidation or RCS addition (Møller et al., 2007), is labeled with a biotin probe. The labeled protein fragments are collected by avidin affinity chromatography and then analyzed with LC-ESI-Orbitrap-MS, which allows identification of the modified peptide, the modified amino acid residue, and the type of carbonylation. In the root nodules, 12 types of carbonylations affecting six amino acid residues were identified in 238 proteins. Interestingly, Lys was the most commonly carbonylated amino acid and accounted for 58% of all modifications, followed by His, Cys, Arg, Thr, and Pro (Matamoros et al., 2018). It is also possible to investigate the difference of the extent of modification extent on the same target protein in samples treated differently. This method has a great potential to investigate the RCS target proteins that are involved in plant responses to oxidative stimuli.

The comprehensive approach is useful for creating a list of potential targets of RCS, but the significance of the RCS modification or each target protein should be investigated in separate experiments. An examination of the effects of RCS on the biochemical activity of the purified target protein should be conducted, and in clarifying the physiological significance of the RCS modification of a target protein, a genetic analysis using a mutant is preferable.

DISCUSSION

As described thus far, the significance of RCS as signal mediators downstream of ROS is evident. There is an open question about the ROS signaling mechanism: how can ROS, the only four species, transmit signals to specific targets in different physiological situations? (Møller and Sweetlove, 2010). The variety of RCS species, which is greater than that of ROS, may provide a clue to this specificity problem if the relationships between the ROS types and the downstream RCS types are revealed. Because RCS have comparatively longer lifetimes than ROS (Parvez et al., 2018), they are suitable for conveying signals within a cell and between cells. Considering the critical significance of ROS in a wide range of physiological phenomena in plants from cell division to pollination, seed germination to fruit ripening (Mittler, 2017; Mhamdi and Van Breusegem, 2018; Waszczak et al., 2018), and stress responses (Gill and Tuteja, 2010; Schippers et al., 2016), further explorations of the physiology of RCS will surely uncover many interesting facts.

For investigations of the involvement of RCS in a physiological phenomenon, a recommended starter experiment is to examine the effect of carbonyl scavengers on the phenomenon, as was done for PCD in BY-2 cells (Biswas and Mano, 2015). If RCS are involved, the increase in the endogenous RCS levels should be associated with the examined phenomenon, and the addition of carbonyl scavengers should suppress the RCS levels and the response of the cell. Because carnosine reaction has the bias for distinct RCS, it is necessary to clarify which carbonyl species are decreased. One important precaution is that most of the compounds known as carbonyl scavengers, e.g., the dipeptide carnosine, may have antioxidant effects (Aldini et al., 2007; Zhu et al., 2011). Thus, if the scavenger suppresses the tested phenomenon, it is necessary to confirm that the ROS levels are not affected. The LOOH level test with the fluorescent dye Spy-LHP (Khorobrykh et al., 2011) will provide another negative control for determining whether or not a carbonyl scavenger affects the formation of LOOHs.

For further examinations of the RCS function in the above-verified phenomenon, analyses of the carbonyls and the identification of the target proteins is necessary. The HPLC (or LC-MS) analysis of carbonyls allows the simultaneous determination of multiple types of carbonyls in one sample, but it requires the extraction of carbonyls from samples of at least tens of mg fresh weight of plant tissue. This requirement practically limits the carbonyl analysis in a specialized type of cells such as guard cells or the LR primodia cells. The visualization and detection of carbonyls in the tissues and distinct cells by chemical probe-based observations or a mass spectrometry imaging system would be a critical technique in the understanding of RCS physiology in plants. The identification of target proteins also requires certain amounts of samples. The most advanced single-cell proteomics (Kelly, 2020) in combination with proper methods for the in situ labeling of the modified proteins as described above (Matamoros et al., 2018) may provide a breakthrough.

Last but not least, there is an almost untouched but very critical issue regarding RCS: the relationship of RCS signaling with other reactive species, i.e., ROS, reactive nitrogen species (RNS), and reactive sulfur species (RSS). Nitric oxide has an electrophilic nature and can form a covalent bond with the thiol group. Specifically, RCS and NO may compete for Cys on the target proteins. RNS can react with lipids to form nitro-fatty acids (Sánchez-Calvo et al., 2013), but their metabolism and physiological significance in plants have scarcely been investigated. RSS include hydrogen sulfide and persulfides (R-SSH), which are endogenously produced and act as signaling molecules (Aroca et al., 2018). Regarding the chemical properties of RSS, they are nucleophiles as potent as thiol compounds (Benchoam et al., 2020), and accordingly, they may modulate RCS signals. Conversely, RCS may modulate RSS signaling. These reactive species, i.e., ROS, RNS, RCS, and RSS (RONCSS; De Tullio and Asard, 2012) are critical factors for determining cell fates, because not only are they bioactive agents but also do they react with antioxidants to alter the redox status of the cell in a rapid and microlocal manner, which may eventually affect the global redox responses of cells in the tissue. It will be a challenging task to delineate the cellular logic of reactive molecules, in which all RONCSS in the same samples are comprehensively analyzed.

AUTHOR CONTRIBUTIONS

JM conceived and supervised the review topics. MB wrote the first draft. Both authors contributed to the article and approved the submitted version.

FUNDING

This work was supported by a grant from the Japan Society for the Promotion of Science (JSPS) KAKENHI (No. 20H03278).

ACKNOWLEDGMENTS

We thank Koichi Sugimoto for critical reading of the manuscript.

REFERENCES

Aldini, G., Delle-Done, I., Facino, R. M., Mizani, A., and Carini, M. (2007). Intervention strategies to inhibit protein carbonylation by lipoxydation-derived reactive carbonyls. *Med. Res. Rev.* 27, 817–868. doi: 10.1002/med.20073

Alméras, E., Stolz, S., Vollenweider, S., Reymond, P., Mène-Saffrané, L., and Farmer, E. E. (2003). Reactive electrophile species activate defense gene expression in *Arabidopsis*. *Plant J.* 34, 205–216. doi: 10.1046/j.1365-313x.2003.01718.x

Armed, N., Dobler, D., Dean, M., and Thronalley, P. J. (2005). Peptide mapping identifies hotspot site of modification in human serum albumin by methylglyoxal involved in ligand binding and esterase activity. *J. Biol. Chem.* 280, 5724–5732. doi: 10.1074/jbc.M410973200

Aroca, A., Gotor, C., and Romero, L. C. (2018). Hydrogen sulfide signaling in plants: emerging roles of protein persulfidation. *Front. Plant Sci.* 9:1369. doi: 10.3389/fpls.2018.01369

Asada, K. (2006). Production and scavenging of reactive oxygen species in chloroplasts and their functions. *Plant Physiol.* 141, 391–396. doi: 10.1104/pp.106.082040

Bachi, A., Dalle-Donne, I., and Scaloni, A. (2013). Redox proteomics: chemical principles, methodological approaches and biological/biomedical promises. *Chem. Rev.* 113, 596–698. doi: 10.1021/cr300073p

Bate, N. J., and Rothstein, S. J. (1998). C6-volatiles derived from the lipoxygenase pathway induce a subset of defense-related genes. *Plant J.* 16, 561–569. doi: 10.1046/j.1365-313x.1998.00324.x

Benchoam, D., Semelak, J. A., Cuevasanta, E., Mastrogiovanni, M., Grassano, J. S., Ferrer-Sueta, G., et al. (2020). Acidity and nucleophilic reactivity of glutathione persulfide. *J. Biol. Chem.* 295, 15466–15481. doi: 10.1074/jbc.RA120.014728

Biswas, M., Terada, R., and Mano, J. (2020). Inactivation of carbonyl-detoxifying enzymes by H2O2 is a trigger to increase carbonyl load for initiating programmed cell death in plants. *Antioxidants* 9:141. doi: 10.3390/antiox9020141

Biswas, M. S., Fukaki, H., Mori, I. C., Nakahara, K., and Mano, J. (2019). Reactive oxygen species and reactive carbonyl species constitute a feed-forward loop in auxin signaling for lateral root formation. *Plant J.* 100, 536–548. doi: 10.1111/tpj.14456

Biswas, M. S., and Mano, J. (2015). Lipid peroxide-derived short-chain carbonyls mediate hydrogen peroxide-induced and salt-induced programmed cell death in plants. *Plant Physiol.* 168, 885–898. doi: 10.1104/pp.115.256834

Biswas, M. S., and Mano, J. (2016). Reactive carbonyl species activate caspase-3-like protease to initiate programmed cell death in plants. *Plant Cell Physiol.* 57, 1432–1442. doi: 10.1093/pcp/pcw053

Blée, E. (1998). Phytooxylipins and plant defense reactions. *Prog. Lipid Res.* 37, 33–72. doi: 10.1016/s0163-7827(98)00004-6

Chapman, J. M., Muhlemann, J. K., Gayomba, S. R., and Muday, G. K. (2019). RBOH-dependent ROS synthesis and ROS scavenging by plant specialized metabolites to modulate plant development and stress responses. *Chem. Res. Toxicol.* 32, 370–396. doi: 10.1021/acs.chemrestox.9b00028

Colzani, M., Regazzoni, L., Criscuolo, A., Baron, G., Carini, M., Vistoli, G., et al. (2018). Isotopic labelling for the characterization of HNE-sequestering agents in plant-based extracts and its application for the identification of anthocyanidins in black rice with giant embryo. *Free Rad. Res.* 52, 896–906. doi: 10.1080/10715762.2018.1490735

De Tullio, M., and Asard, H. (2012). Molecules tell stories: reactive oxygen, nitrogen, carbonyl and sulfur species take center stage. *Plant Physiol. Biochem.* 59, 1–2. doi: 10.1016/j.plaphy.2012.07.025

Deighton, N., Magill, W. J., Brenner, D. H., and Benson, E. E. (1997). Malondialdehyde and 4-Hydroxy-2-nonenal in plant tissue cultures: LC-MS determination of 2, 4-dinitrophenylhydrazone derivatives. *Free Rad. Res.* 27, 255–265. doi: 10.3109/10715769709065764

Deighton, N., Muckenschnabel, I., Goodman, B. A., and Williamson, B. (1999). Lipid peroxidation and the oxidative burst associated with infection of *Capsicum annuum* by *Botrytis cinerea*. *Plant J.* 20, 485–492. doi: 10.1046/j.1365-313x.1999.00622.x

Eckardt, N. A. (2008). Oxylipin signaling in plant stress responses. *Plant Cell* 20, 495–497. doi: 10.1105/tpc.108.059485

Esterbauer, H., Schaur, R., and Zollner, J. H. (1991). Chemistry and biochemistry of 4-hydroxynonenal, malonaldehyde and related aldehydes. *Free Radic. Biol. Med.* 11, 81–128. doi: 10.1016/0891-5849(91)90192-6

Esterbauer, H., Zollner, H., and Schaur, R. J. (1989). "Aldehydes formed by lipid peroxidation: mechanisms of formation, occurrence, and determination," in *Membrane Lipid Oxidation*, ed. C. Vigo-Pelfrey (Boca Raton, FL: CRC Press), 239–268.

Esterbauer, H., Zollner, J., and Scholz, N. (1975). Reaction of glutathione with conjugated carbonyls. *Z. Naturforsch.* 3s0, 466–473.

Farmer, E. E., and Mueller, M. J. (2013). ROS-mediated lipid peroxidation and RES-activated signaling. *Annu. Rev. Plant Biol.* 64, 429–450. doi: 10.1146/annurev-arplant-050312-120132

Fischer, B., Ledford, H., Wakao, S., Huang, S. G., Casero, D., Pellegrini, M., et al. (2012). SINGLET OXYGEN RESISTANT 1 links reactive electrophile signaling to singlet oxygen acclimation in *Chlamydomonas reinhardtii*. *Proc. Natl. Acad. Sci. U.S.A* 109, E1302–E1311. doi: 10.1073/pnas.1116843109

Foyer, C. H., and Noctor, G. (2003). Redox sensing and signalling associated with reactive oxygen in chloroplasts, peroxisomes and mitochondria. *Physiol. Plant.* 119, 355–364. doi: 10.1034/j.1399-3054.2003.00223.x

Fukaki, J., Tameda, S., Masuda, H., and Tasaka, M. (2002). Lateral root formation is blocked by a gain-of-function mutation in the SOLITARY-ROOT/IAA14 gene of *Arabidopsis*. *Plant J.* 29, 153–168. doi: 10.1046/j.0960-7412.2001.01201.x

Gao, U., and Wang, Y. (2006). Site-selective modifications of arginine residues in human hemoglobin induced by methylglyoxal. *Biochemistry* 45, 15654–15660. doi: 10.1021/bi061410o

Gardner, H. W., Dombois, D. L. Jr., and Desjardins, A. E. (1990). Hexanal, trans-2-hexenal, and trans-2-nonenal inhibit soybean, *Glycine max*, seed germination. *J. Agr. Food Chem.* 38, 1316–1320. doi: 10.1021/jf00096a005

Ge, Y., Cai, Y., Bonneau, L., Rotari, V., Danon, A., McKenzie, E. A., et al. (2016). Inhibition of cathepsin B by caspase-3 inhibitors blocks programmed cell death in *Arabidopsis*. *Cell Death Differen.* 25, 1532. doi: 10.1038/s41418-018-0136-1

Gill, S. S., and Tuteja, N. (2010). Reactive oxygen species and antioxidant machinery in abiotic stress tolerance in crop plants. *Plant Physiol. Biochem.* 48, 909–930. doi: 10.1016/j.plaphy.2010.08.016

Gronwald, J. W., and Plaisance, K. L. (1998). Isolation and characterization of glutathione S-transferase isozymes from sorghum. *Plant Physiol.* 117, 877–892. doi: 10.1104/pp.117.3.877

Grosch, W. (1987). "Reactions of hydroperoxides—Products of low molecular weight," in *Autoxidation of Unsaturated Lipids*, ed. H. W.-S. Chan (London: Academic Press), 95–139.

Guo, J., Sun, W., Liu, H., Chi, J., Odiba, A. S., and Li, G. (2020). Aldehyde dehydrogenase plays crucial roles in response to lower temperature stress in *Solanum tuberosum* and *Nicotiana benthamiana*. *Plant Sci.* 297, 110525. doi: 10.1016/j.plantsci.2020.110525

Halliwell, B., and Gutteridge, J. M. C. (2015). *Free Radicals in Biology and Medicine*, 5th Edn. London: Oxford Univ. Press, 257–265. doi: 10.1093/acprof:oso/9780198717478.001.0001

Hatsugai, N., Yamada, K., Goto-Yamada, S., and Hara-Nishimura, I. (2015). Vacuolar processing enzyme in plant programmed cell death. *Front. Plant Sci.* 6:234. doi: 10.3389/fpls.2015.00234

Hegedüs, A., Erdei, S., Janda, T., Tóth, E., Horváth, G., and Dudits, D. (2004). Transgenic tobacco plants overproducing alfalfa aldose/aldehyde reductase show higher tolerance to low temperature and cadmuim stress. *Plant Sci.* 166, 1329–1333.

Hodges, D. M., DeLong, J. M., Forney, C. F., and Prange, R. K. (1999). Improving the thiobarbituric acid-reactive-substances assay for estimating lipid peroxidation in plant tissues containing anthocyanin and other interfering compounds. *Planta* 207, 604–611. doi: 10.1007/s004250050524

Hoque, T. S., Hossain, M. A., Mostofa, M. G., Burritt, D. H., Fujita, M., and Tran, L.-S. P. (2016). Methylglyoxal: an emerging signaling molecule in plant abiotic stress responses and tolerance. *Front. Plant Sci.* 13:1341. doi: 10.3389/fpls.2016.01341

Huang, S., Van Aken, O., Schwarzländer, M., Belt, K., and Millar, A. H. (2016). The roles of mitochondrial reactive oxygen species in cellular signaling and stress response in plants. *Plant Physiol.* 171, 1551–1559. doi: 10.1104/pp.16.00166

Islam, M. M., Ye, W., Akter, F., Rhaman, M. S., Matsushima, D., Munemasa, S., et al. (2020). Reactive carbonyl species mediate methyl jasmonate-induced stomatal closure. *Plant Cell Physiol.* 61, 1788–1797. doi: 10.1093/pcp/pcaa107

Islam, M. M., Ye, W., Matsushima, D., Munemasa, S., Okuma, E., Nakamura, Y., et al. (2016). Reactive carbonyl species mediate abscisic acid signaling in guard cells. *Plant Cell Physiol.* 57, 2552–2563. doi: 10.1093/pcp/pcw166

Islam, M. M., Ye, W., Matsushima, D., Rhaman, M. S., Munemasa, S., Okuma, E., et al. (2019). Reactive carbonyl species function as signal mediators downstream of H_2O_2 production and regulate $[Ca^{2+}]$cyt elevation in ABA signal pathway in *Arabidopsis* guard cells. *Plant Cell Physiol.* 60, 1146–1159. doi: 10.1093/pcp/pcz031

Kai, H., Hirashima, K., Matsuda, O., Ikegami, H., Winkelmann, T., Nakahara, T., et al. (2012). Thermotolerant cyclamen with reduced acrolein and methyl vinyl ketone. *J. Exp. Bot.* 63, 4143–4150. doi: 10.1093/jxb/ers110

Kawai, Y., Takeda, S., and Terao, J. (2007). Lipidomic analysis for lipid peroxidation-derived aldehydes using gas chromatography-mass spectrometry. *Chem. Res. Toxicol.* 20, 99–107. doi: 10.1021/tx060199e

Kelly, R. T. (2020). Single-cell proteomics; progress and prospects. *Mol. Cell. Proteom.* 19, 1739–1748. doi: 10.1074/mcp.R120.002234

Khorobrykh, S. A., Khorobrykh, A. A., Yanykin, D. V., Ivanov, B. N., Klimov, V. V., and Mano, J. (2011). Photoproduction of catalase-insensitive peroxides on the donor side of manganese-depleted photosystem II: evidence with a specific fluorescent probe. *Biochemistry* 50, 10658–10665. doi: 10.1021/bi200945v

Kishimoto, K., Matsui, K., Ozawa, R., and Takabayashi, J. (2005). Volatile C6-aldehydes and allo-ocimene activate defense genes and induce resistance against *Botrytis cinerea* in *Arabidopsis thaliana*. *Plant Cell Physiol.* 46, 1093–1102. doi: 10.1093/pcp/pci122

Kotchoni, S. O., Kuhns, C., Ditzer, A., Kirch, H.-H., and Bartels, D. (2006). Overexpression of different aldehyde dehydrogenase genes in *Arabidopsis thaliana* confers tolerance to abiotic stress and protects plants against lipid peroxidation and oxidative stress. *Plant Cell Environ.* 29, 1033–1048. doi: 10.1111/j.1365-3040.2005.01458.x

Kranner, I., Minibayeva, F. V., Bekett, R. P., and Seal, C. E. (2010). What is stress? Concepts, definitions and applications in seed science. *New Phytol.* 188, 655–673. doi: 10.1111/j.1469-8137.2010.03461.x

Kunishima, M., Yamauchi, Y., Mizutani, M., Kuse, M., Takikawa, H., and Sugimoto, Y. (2016). Identification of (Z)-3:(E)-2-hexenal isomerases essential to the production of the leaf aldehyde in plants. *J. Biol. Chem.* 291, 14023–14033. doi: 10.1074/jbc.M116.726687

LoPachin, R. M., and Ganvin, T. (2014). Molecular mechanisms of aldehyde toxicity: a chemical perspective. *Chem. Res. Toxicol.* 27, 1081–1091.

Mano, J. (2012). Reactive carbonyl species: their production from lipid peroxides, action in environmental stress, and the detoxification mechanism. *Plant Physiol. Biochem.* 59, 90–97. doi: 10.1016/j.plaphy.2012.03.010

Mano, J., Belles-Boix, E., Babiychuk, E., Inzé, D., Hiraoka, E., Takimoto, K., et al. (2005). Protection against photooxidative injury of tobacco leaves by 2-alkenal reductase. detoxication of lipid peroxide-derived reactive carbonyls. *Plant Physiol.* 139, 1773–1783. doi: 10.1104/pp.105.070391

Mano, J., and Biswas, M. S. (2018). "Analysis of reactive carbonyl species generated under oxidative stress," in *Plant Programmed Cell Death: Methods and Protocols*, eds L. De Gara and V. Locato (New York, NY: Springer), 117–124. doi: 10.1007/978-1-4939-7668-3_11

Mano, J., Biswas, M. S., and Sugimoto, K. (2019a). Reactive carbonyl species: a missing link in ROS signaling. *Plants* 8:391. doi: 10.3390/plants8100391

Mano, J., Ishibashi, A., Muneuchi, H., Morita, C., Sakai, H., Biswas, S., et al. (2017). Acrolein-detoxifying isozymes of glutathione transferase in plants. *Planta* 245, 255–264. doi: 10.1007/s00425-016-2604-5

Mano, J., Kanameda, S., Kuramitsu, R., Matsuura, N., and Yamauchi, Y. (2019b). Detoxification of reactive carbonyl species by glutathione transferase *Tau isozymes*. *Front. Plant Sci.* 10:487. doi: 10.3389/fpls.2019.00487

Mano, J., Miyatake, F., Hiraoka, E., and Tamoi, M. (2009). Evaluation of the toxicity of stress-related aldehydes to photosynthesis in chloroplasts. *Planta* 230, 639–648. doi: 10.1007/s00425-009-0964-9

Mano, J., Nagata, M., Okamura, S., Shiraya, T., and Mitsui, T. (2014). Identification of oxidative-modified proteins in salt-stressed *Arabidopsis*: a carbonyl-targeted proteomics approach. *Plant Cell Physiol.* 55, 1233–1244. doi: 10.1093/pcp/pcu072

Mano, J., Tokushige, K., Mizoguchi, H., and Khorobrykh, S. A. (2010). Accumulation of lipid peroxide-derived, toxic α,β-unsaturated aldehydes (E)-2-pentenal, acrolein and (E)-2-hexenal in leaves under photoinhibitory illumination. *Plant Biotechnol.* 27, 193–197.

Mano, J., Torii, Y., Hayashi, S., Takimoto, K., Matsui, K., Nakamura, K., et al. (2002). The NADPH:quinone oxidoreductase P1-ζ-crystallin in *Arabidopsis catalyzes* the α,β-hydrogenation of 2-alkenals: detoxication of the lipid peroxide-derived reactive aldehydes. *Plant Cell Physiol.* 43, 1445–1455. doi: 10.1093/pcp/pcf187

Matamoros, M. A., Kim, A., Peñuelas, M., Ihling, C., Greisser, E., Hoffmann, R., et al. (2018). Protein carbonylation and glycation in legume nodules. *Plant Physiol.* 177, 1510–1528. doi: 10.1104/pp.18/00533

Matsui, K. (2006). Green leaf volatiles: hydroperoxide lyase pathway of oxylipin metabolism. *Curr. Opin. Plant Biol.* 9, 274–280. doi: 10.1016/j.pbi.2006.03.002

Matsui, K., Sugimoto, K., Mano, J. I., Ozawa, R., and Takabayashi, J. (2012). Differential metabolisms of green leaf volatiles in injured and intact parts of a wounded leaf meet distinct ecophysiological requirements. *PLoS One* 7:e36433. doi: 10.1371/journal.pone.0036433

Mhamdi, A., and Van Breusegem, F. (2018). Reactive oxygen species in plant development. *Development* 145:dev164376. doi: 10.1242/dev.164376

Michalski, M.-C., Calzada, C., Makino, A., Michaud, S., and Guichardant, M. (2008). Oxidation products of polyunsaturated fatty acids in infant formulas compared to human milk – A preliminary study. *Mol. Nutr. Food Res.* 52, 1478–1485. doi: 10.1002/mnfr.200700451

Millar, A. H., and Leaver, C. J. (2000). The cytotoxic lipid peroxidation product, 4-hydroxy-2-nonenal, specifically inhibits decarboxylating dehydrogenases in the matrix of plant mitochondria. *FEBS Lett.* 481, 117–121.

Mittler, R. (2017). ROS are good. *Trends Plant Sci.* 22, 11–19. doi: 10.1016/j.tplants.2016.08.002

Mittler, R., Vanderauwera, S., Gollery, M., and Van Breusegem, F. (2004). Reactive oxygen gene network of plants. *Trends Plant Sci.* 9, 490–498. doi: 10.1016/j.tplants.2004.08.009

Mittler, R., Vanderauwera, S., Suzuki, N., Miller, G., Tognetti, V. B., Vandepoele, K., et al. (2011). ROS signaling: the new wave? *Trends Plant Sci.* 16, 300–309. doi: 10.1016/j.tplants.2011.03.007

Miyake, C., and Asada, K. (1996). Inactivation mechanism of ascorbate peroxidase at low concentrations of ascorbate; Hydrogen peroxide decomposes compound I of ascorbate peroxidase. *Plant Cell Phyisol.* 37, 423–430. doi: 10.1093/oxfordjournals.pcp.a028963

Møller, I. A., Jensen, P. E., and Hansson, A. (2007). Oxidative modifications to cellular components in plants. *Annu. Rev. Plant Biol.* 58, 459–481. doi: 10.1146/annurev.arplant.58.032806.103946

Møller, I. M., and Sweetlove, L. J. (2010). ROS signalling: specificity is required. *Trends Plant Sci.* 15, 370–374. doi: 10.1016/j.tplants.2010.04.008

Mosblech, A., Feussner, I., and Heilmann, I. (2009). Oxylipins: structurally diverse metablotites from fatty acid oxidation. *Plant Physiol. Biochem.* 47, 511–517. doi: 10.1016/j.plaphy.2008.12.011

Oberschall, A., Deák, M., Török, K., Sass, L., Vass, I., Kovács, I., et al. (2000). A novel aldose/aldehyde reductase protects transgenic plants against lipid peroxidation under chemical and drought stresses. *Plant J.* 24, 437–446. doi: 10.1111/j.1365-313x.2000.00885.x

Orman-Ligeza, B., Parizot, B., De Rycke, R., Fernandez, A., Himschoot, E., Van Breusegem, F., et al. (2016). RBOH-mediated ROS production facilitates lateral root emergence in *Arabidopsis*. *Development* 143, 3328–3339. doi: 10.1242/dev.136465

Park, S.-W., Li, W., Viehhauser, A., He, B., Kim, S., Nilsson, A. K., et al. (2013). Cyclophilin 20-3 relays a 12-oxo-phytodienoic acid signal during stress responsive regulation of cellular redox homeostasis. *Proc. Natl. Acad. Sci. USA* 110, 9559–9564. doi: 10.1073/pnas.1218872110

Parvez, S., Long, M. J. C., Poganik, J. R., and Aye, Y. (2018). Redox signaling by reactive electrophiles and oxidants. *Chem. Rev.* 118, 8798–8888. doi: 10.1021/acs.chemrev.7b00698

Pei, Z. M., Murata, Y., Benning, G., Thomine, S., Klüster, B., Allen, G. J., et al. (2000). Calcium channels activated by hydrogen peroxide mediate abscisic acid sinaliing in guard cells. *Nature* 406, 731–734. doi: 10.1038/35021067

Petrov, V., Hille, J., Mueller-Roeber, B., and Gechev, T. S. (2015). ROS-mediated abiotic stress-induced programmed cell death in plants. *Front. Plant Sci.* 6:69. doi: 10.3389/fpls.2015.00069

Portillo-Estrada, M., Okereke, C. N., Jiang, Y., Talts, E., Kaurilind, E., and Niinemets, Ü (2021). Wounding-induced VOC emissions in five tropical agricultural species. *Molecules* 26:2602. doi: 10.3390/molecules26092602

Rac, M., Shumbe, L., Oger, C., Guy, A., Vigor, C., Ksas, B., et al. (2021). Luminescence imaging of leaf damage induced by lipid peroxidation products and its modulation by β-cyclocitral. *Physiol. Plant.* 171, 246–259. doi: 10.1111/ppl.13279

Rahman, M. S., Nakamura, T., Nakamura, Y., Munemasa, S., and Murata, Y. (2020). The myrosinases TGG1 and TGG2 function redundantly in reactive carbonyl species signaling in *Arabidopsis* guard cells. *Plant Cell Physiol.* 61, 967–977. doi: 10.1093/pcp/pcaa024

Reczek, C. R., and Chandel, N. S. (2015). ROS-dependent signal transduction. *Curr. Opin Cell Biol.* 33, 8–13. doi: 10.1016/j.ceb.2014.09.010

Reynolds, T. (1977). Comparative effects of aliphatic compounds on inhibition of lettuce fruit germination. *Ann. Bot.* 41, 637–648. doi: 10.1093/oxfordjournals.aob.a085333

Roach, T. (2020). LHCSR3-Type NPQ Prevents photoinhibition and slowed growth under fluctuating light in *Chlamydomonas reinhardtii*. *Plants* 9:1604. doi: 10.3390/plants9111604

Roach, T., Baur, T., Stöggl, W., and Krieger-Litszkay, A. (2017). Chlamydomonas reinhardtii responding to high light: a role for 2-propenal (acrolein). *Physiol. Plant.* 161, 75–87. doi: 10.1111/ppl.12567

Roach, T., Stöggl, W., Baur, T., and Kranner, I. (2018). Distress and eustress of reactive electrophiles and relevance to light stress acclimation via stimulation of thiol/disulphide-based redox defences. *Free Radic. Biol. Med.* 122, 65–73. doi: 10.1016/j.freeradbiomed.2018.03.030

Sánchez-Calvo, B., Barroso, J. B., and Cropas, F. J. (2013). Hypothesis: nitro-fatty acids play a role in plant metabolism. *Plant Sci.* 199-200, 1–6. doi: 10.1016/j.plantsci.2012.10.006

Schauenstein, E., Esterbauer, H., and Zollner, H. (1977). *Aldehyde in Biological Systems: Their Natural Occurrence and Biological Activities*. London: Pion, 589–590.

Schippers, J. H., Foyer, C. H., and van Dongen, J. T. (2016). Redox regulation in shoot growth, SAM maintenance and flowering. *Curr. Opin. Plant Biol.* 29, 121–128. doi: 10.1016/j.pbi.2015.11.009

Schopfer, F. J., Cipollina, C., and Freeman, B. A. (2011). Formation and signaling actions of electrophilic lipids. *Chem. Rev.* 111, 5997–6021. doi: 10.1021/cr200131e

Shimakawa, G., Iwamoto, T., Mabuchi, T., Saito, R., Yamamoto, H., Amako, K., et al. (2013). Acrolein, an α,β-unsaturated carbonyl, inhibits both growth and PSII activity in the cyanobacterium *Synechocystis* sp. PCC 6803. *Biosci. Biotechnol. Biochem.* 77, 1655–1660.

Shin, J.-H., Kim, S.-R., and An, G. (2009). Rice aldehyde dehydrogenase7 is needed for seed maturation and viability. *Plant Physiol.* 149, 905–915.

Spyropoulou, E. A., Dekker, H. L., Steemers, L., van Maarseveen, J. H., de Koster, C. G., and Haring, M. A. (2017). Identification and characterization of (3Z):(2E)-hexenal isomerases from cucumber. *Front. Plant Sci.* 8:1342. doi: 10.3389/fpls.2017.01342

Srivastava, S., Brychkova, C., Yarmolinsky, D., Soltabayeva, A., Samani, T., and Sagi, M. (2017). Aldehyde oxidase 4 plays a critical role in delaying silique senescence by catalyzing aldehyde detoxification. *Plant Physiol.* 173, 1977–1997. doi: 10.1104/pp.16.01939

Steward, R. C., and Bewley, J. D. (1980). Lipid peroxidation associated with accelerated aging of soybean axes. *Plant Physiol.* 65, 245–248. doi: 10.1104/pp.65.2.245

Stotz, H. U., Mueller, S., Zoeller, M., Mueller, M. J., and Berger, S. (2013). TGA transcription factors and jasmonate-independent COI1 signalling regulate specific plant responses to reactive oxylipins. *J. Exp. Bot.* 64, 963–975. doi: 10.1093/jxb/ers389

Sugimoto, K., Matsuoka, Y., Sakai, K., Fujiya, N., Fujii, H., and Mano, J. (2021). Catechins in green tea powder (matcha) are heat-stable scavengers of acrolein, a lipid peroxide-derived reactive carbonyl species. *Food Chem.* 355, 129403. doi: 10.1016/j.foodchem.2021.129403

Suhita, D., Ragavendra, A. S., Kwak, J. M., and Vavasseur, A. (2004). Cytoplasmic alkalization precedes reactive oxygen species production during methyl jasmonate- and abscisic acid-induced stomatal closure. *Plant Physiol.* 134, 1536–1545. doi: 10.1104/pp.103.032250

Sunkar, R., Bartels, D., and Kirch, H.-H. (2003). Overexpression of a stress-inducible aldehyde dehydrogenase gene from *Arabidopsis thaliana* in transgenic plants improves stress tolerance. *Plant J.* 35, 452–464. doi: 10.1046/j.1365-313x.2003.01819.x

Suzuki, T., and Yamamoto, M. (2017). Stress-sensing mechanisms and the physiological roles of the Keap1–Nrf2 system during cellular stress. *J. Biol. Chem.* 292, 16817–16824. doi: 10.1074/jbc.R117.800169

Taki, N., Sasaki-Sekimoto, Y., Obayashi, T., Kikuta, A., Kobayashi, K., Ainai, T., et al. (2005). 12-Oxo-phytodienoic acid triggers expression of a distinct set of genes and plays a role in wound-induced gene expression in *Arabidopsis*. *Plant Physiol.* 139, 1268–1283. doi: 10.1104/pp.105.067058

Taylor, N. L., Day, D. A., and Millar, A. H. (2002). Environmental stress causes oxidative damage to plant mitochondria leading to inhibition of glycine decarboxylase. *J. Biol. Chem.* 277, 42662–42668. doi: 10.1074/jbc.M204761200

Terletskaya, N. V., Korbozova, N. K., Kudrina, N. O., Kobylina, T. N., Kurmanbayeva, M. S., Meduntseva, N. D., et al. (2021). The influence of abiotic stress factors on the morphophysiological and phytochemical aspects of the acclimation of the plant Rhodiola semenowii Boriss. *Plants* 10, 1196. doi: 10.3390/plants10061196

Terrile, M. C., París, R., Calderón-Villalobos, L. I., Iglesias, M. J., Lamattina, L., Estelle, M., et al. (2012). Nitric oxide influences auxin signaling through S-nitrosylation of the *Arabidopsis* TRANSPORT INHIBITOR RESPONSE 1 auxin receptor. *Plant J.* 70, 492–500. doi: 10.1111/j.1365-313X.2011.04885.x

Triantaphylidès, C., Krischke, M., Hoeberichts, F. A., Ksas, B., Gresser, G., Havaux, M., et al. (2008). Singlet oxygen is the major reactive oxygen species involved in photooxidative damage to plants. *Plant Physiol.* 148, 960–968. doi: 10.1104/pp.108.125690

Turóczy, Z., Kis, P., Török, K., Cserháti, M., Lendvai, A., Dudits, D., et al. (2011). Overproduction of a rice aldo-keto reductase increases oxidative and heat stress tolerance by malondialdehyde and methylglyoxal detoxification. *Plant Mol. Biol.* 75, 399–412. doi: 10.1007/s11103-011-9735-7

Venkanna, D., Südfeld, C., Baier, T., Homburg, S. V., Patel, A. V., Wobbe, L., et al. (2017). Knock-down of the IFR1 protein perturbs the homeostasis of reactive electrophile species and boosts photosynthetic hydrogen production in *Chlamydomonas reinhardtii*. *Front. Plant Sci.* 8:1347. doi: 10.3389/fpls.2017.01347

Vincenti, S., Mariani, M., Alberti, J.-C., Jacopini, S., Brunini-Bronzini de Caraffa, V., Berti, L., et al. (2019). Biocatalytic synthesis of natural green leaf volatiles using the lipoxygenase metabolic pathway. *Catalysts* 9:873. doi: 10.3390/catal9100873

Vliegenthart, J. F. G. (1979). Enzymic and non enzymic oxidation of polyunsaturated fatty acids. *Chem. Ind.* 7, 241–251.

Waszczak, C., Carmody, M., and Kangasjärvi, J. (2018). Reactive oxygen species in plant signaling. *Annu. Rev. Plant Biol.* 69, 209–236.

Weber, H., Chételat, A., Reymond, P., and Farmer, E. E. (2004). Selective and powerful stress gene expression in *Arabidopsis* in response to malondialdehyde. *Plant J.* 37, 877–888. doi: 10.1111/j.1365-313x.2003.02013.x

Wible, R. S., and Sutter, T. R. (2017). Soft cysteine signaling network: the functional significance of cysteine in protein function and the soft acids/bases thiol chemistry that facilitates cysteine modification. *Chem. Res. Toxicol.* 30, 729–762. doi: 10.1021/acs.chemrestox.6b00428

Winger, A. M., Millar, A. H., and Day, D. A. (2005). Sensitivity of plant mitochondrial terminal oxidases to the lipid peroxidation product 4-hydroxy-2-nonenal (HNE). *Biochem. J.* 387, 865–870. doi: 10.1042/BJ20042044

Winger, A. M., Taylor, N. L., Heazlewood, J. L., Day, D. A., and Millar, A. H. (2007). The cytotoxic lipid peroxidation product 4-hydroxy-2-nonenal covalently modifies a selective range of proteins linked to respiratory function in plant mitochondria. *J. Biol. Chem.* 282, 37436–37447. doi: 10.1074/jbc.M702385200

Yalcinkaya, T., Uzilday, B., Ozgur, R., and Turkan, I. (2019b). The roles of reactive carbonyl species in induction of antioxidant defence and ROS signalling in extreme halophytic model Eutrema parvulum and glycophytic model *Arabidopsis thaliana*. *Exp. Environ. Bot.* 160, 81–91. doi: 10.1016/j.envexpbot.2019.01.009

Yalcinkaya, T., Uzilday, B., Ozgur, R., Turkan, I., and Mano, J. (2019a). Lipid peroxidation-derived reactive carbonyl species (RCS): their interaction with ROS and cellular redox during environmental stresses. *Environ. Exp. Bot.* 165, 139–149. doi: 10.1016/j.envexpbot.2019.06.004

Yamamoto, Y., Kobayashi, Y., Devi, S. R., Rikiishi, S., and Matsumoto, H. (2002). Aluminum toxicity is associated with mitochondrial dysfunction and the production of reactive oxygen species in plant cells. *Plant Physiol.* 128, 63–72.

Yamauchi, Y., Hasegawa, A., Mizutani, M., and Sugimoto, Y. (2012). Chloroplastic NADPH dependent alkenal/one oxidoreductase contributes to the detoxification of reactive carbonyls produced under oxidative stress. *FEBS Lett.* 586, 1208–1213. doi: 10.1016/j.febslet.2012.03.013

Yamauchi, Y., Hasegawa, A., Taninaka, A., Mizutani, M., and Sugimoto, Y. (2011). NADPH-dependent reductases involved in the detoxification of reactive carbonyls in plants. *J. Biol. Chem.* 286, 6999–7009. doi: 10.1074/jbc.M110.202226

Yamauchi, Y., Kunishima, M., Mizutani, M., and Sugimoto, Y. (2015). Reactive short-chain leaf volatiles act as powerful inducers of abiotic stress-related gene expression. *Sci. Rep.* 5:8030. doi: 10.1038/srep08030

Ye, Y., Li, Z., and Xing, D. (2013). Nitric oxide promotes MPK6-mediated caspase-3-like activation in cadmium-induced *Arabidopsis thaliana* programmed cell death. *Plant Cell Environ.* 36, 1–15. doi: 10.1111/j.1365-3040.2012.02543.x

Yin, L., Mano, J., Wang, S., Tsuji, W., and Tanaka, K. (2010). The involvement of lipid peroxide-derived aldehydes in aluminum toxicity of tobacco roots. *Plant Physiol.* 152, 1406–1417. doi: 10.1104/pp.109.151449

Yin, Y., Mano, J., Tanaka, K., Wang, S., Zhanga, M., Denga, X., et al. (2017). High level of reduced glutathione contributes to detoxification of lipid peroxide-derived reactive carbonyl species in transgenic *Arabidopsis* overexpressing glutathione reductase under aluminum stress. *Physiol. Plant.* 161, 211–223. doi: 10.1111/ppl.12583

Zhu, Q., Sun, Z., Jian, Y., Chen, F., and Wang, M. (2011). Acrolein scavengers: reactivity, mechanism and impact on health. *Mol. Nutr. Food Res.* 55, 1375–1390. doi: 10.1002/mnfr.201100149

Zhu, Q., Zheng, Z.-P., Cheng, K.-W., Wu, J.-J., Zhang, S., Tang, Y. S., et al. (2009). Natural polyphenols as direct trapping agents of lipid peroxidation-derived acrolein and 4-hydroxy-trans-2-nonenal. *Chem. Res. Toxicol.* 22, 1721–1727. doi: 10.1021/tx900221s

Conflict of Interest: The authors declare that the research was conducted in the absence of any commercial or financial relationships that could be construed as a potential conflict of interest.

Publisher's Note: All claims expressed in this article are solely those of the authors and do not necessarily represent those of their affiliated organizations, or those of the publisher, the editors and the reviewers. Any product that may be evaluated in this article, or claim that may be made by its manufacturer, is not guaranteed or endorsed by the publisher.

Copyright © 2021 Biswas and Mano. This is an open-access article distributed under the terms of the Creative Commons Attribution License (CC BY). The use, distribution or reproduction in other forums is permitted, provided the original author(s) and the copyright owner(s) are credited and that the original publication in this journal is cited, in accordance with accepted academic practice. No use, distribution or reproduction is permitted which does not comply with these terms.

frontiers in Plant Science

ORIGINAL RESEARCH
published: 16 November 2021
doi: 10.3389/fpls.2021.721572

Processing of Airborne Green Leaf Volatiles for Their Glycosylation in the Exposed Plants

Koichi Sugimoto[1], Yoko Iijima[2], Junji Takabayashi[3] and Kenji Matsui[4]*

[1] Tsukuba-Plant Innovation Research Center, University of Tsukuba, Tsukuba, Japan, [2] Department of Applied Chemistry, Kogakuin University, Tokyo, Japan, [3] Center for Ecological Research, Kyoto University, Kyoto, Japan, [4] Graduate School of Sciences and Technology for Innovation, Yamaguchi University, Yamaguchi, Japan

Green leaf volatiles (GLVs), the common constituents of herbivore-infested plant volatiles (HIPVs), play an important role in plant defense and function as chemical cues to communicate with other individuals in nature. Reportedly, in addition to endogenous GLVs, the absorbance of airborne GLVs emitted by infested neighboring plants also play a major role in plant defense. For example, the exclusive accumulation of (*Z*)-3-hexenyl vicianoside in the HIPV-exposed tomato plants occurs by the glycosylation of airborne (*Z*)-3-hexenol (Z3HOL); however, it is unclear how plants process the other absorbed GLVs. This study demonstrates that tomato plants dominantly accumulated GLV–glycosides after exposure to green leaf alcohols [Z3HOL, (*E*)-2-hexenol, and *n*-hexanol] using non-targeted LC–MS analysis. Three types of green leaf alcohols were independently glycosylated without isomerization or saturation/desaturation. Airborne green leaf aldehydes and esters were also glycosylated, probably through converting aldehydes and esters into alcohols. Further, we validated these findings in Arabidopsis mutants- (*Z*)-3-hexenal (Z3HAL) reductase (*chr*) mutant that inhibits the conversion of Z3HAL to Z3HOL and the acetyl-CoA:(*Z*)-3-hexen-1-ol acetyltransferase (*chat*) mutant that impairs the conversion of Z3HOL to (*Z*)-3-hexenyl acetate. Exposure of the *chr* and *chat* mutants to Z3HAL accumulated lower and higher amounts of glycosides than their corresponding wild types (Col-0 and L*er*), respectively. These findings suggest that plants process the exogenous GLVs by the reductase(s) and the esterase(s), and a part of the processed GLVs contribute to glycoside accumulation. Overall, the study provides insights into the understanding of the communication of the plants within their ecosystem, which could help develop strategies to protect the crops and maintain a balanced ecosystem.

Keywords: green leaf volatiles (GLVs), glycosylation, bioconversion, specialized metabolism, aldehyde reductase, esterase

OPEN ACCESS

Edited by:
Wanchai De-Eknamkul, Chulalongkorn University, Thailand

Reviewed by:
Thomas J. Bach, Université de Strasbourg, France
Jurgen Engelberth, University of Texas at San Antonio, United States

****Correspondence:***
Koichi Sugimoto
sugimoto.koichi.gu@u.tsukuba.ac.jp

Specialty section:
This article was submitted to Plant Metabolism and Chemodiversity, a section of the journal Frontiers in Plant Science

Received: *07 June 2021*
Accepted: *14 October 2021*
Published: *16 November 2021*

Citation:
Sugimoto K, Iijima Y, Takabayashi J and Matsui K (2021) Processing of Airborne Green Leaf Volatiles for Their Glycosylation in the Exposed Plants. Front. Plant Sci. 12:721572. doi: 10.3389/fpls.2021.721572

INTRODUCTION

Plant-derived volatile organic compounds play an important role in the interactions between volatile-emitting plants and herbivores, microorganisms, neighboring plants, and different parts of the damaged plants (Arimura et al., 2009). For example, fruit and flower volatiles attract seed dispersers and pollinators, respectively, whereas the vegetative volatiles of herbivore-infested plants

not only attract carnivorous natural enemies of herbivores but also prime the defense response in the neighboring receiver plants (Arimura et al., 2009). Green leaf volatiles (GLVs) are the major constituents of herbivore-infested plant volatiles (HIPVs). Through intensive studies in recent decades, the involvement of GLVs in plant–plant interactions has been widely explored. Some GLVs, such as (*E*)-2-hexenal (E2HAL), (*Z*)-3-hexenal (Z3HAL), and (*Z*)-3-hexenol (Z3HOL) are known to induce the accumulation of jasmonic acid (Engelberth et al., 2004; Hu et al., 2019), the expression of defense genes (Farag et al., 2005; Kishimoto et al., 2005), the biosynthesis of defensive compounds (Kishimoto et al., 2006; Kikuta et al., 2011), the emission of *de novo* synthesized volatiles (Farag and Paré, 2002), and the reemissions of absorbed volatiles (Matsui et al., 2012). In certain cases, GLVs emitted by neighboring herbivore-infested plants can serve as aerial messengers to attract natural enemies of the herbivores. For example, in our previous study, we have shown that airborne Z3HOL (emitted by neighboring infested plants) is absorbed and subsequently converted into (*Z*)-3-hexenyl vicianoside (Z3HexVic), a defensive glycoside against common cutworm larvae (Sugimoto et al., 2014).

Green leaf volatiles have a six-carbon backbone derived from unsaturated fatty acids (**Figure 1**), and they are categorized into three forms: monounsaturated (*Z*)- and (*E*)-, and saturated *n*-forms (shown as green, blue, and orange background, respectively, in **Figure 1**). They have three functional groups, aldehyde, alcohol, and esters. It has been shown that the six-carbon Z3HAL, one of the most abundant GLVs from the damaged leaves, and its oxoacid derivative are formed by the cleavage of 13-hydroperoxide (HPOT) by 13-hydroperoxide lyase (HPL, Matsui et al., 1996). HPOT is produced through the oxidization of linolenic acid (LNA) by 13-lipoxygenases (LOX, Halitschke and Baldwin, 2003; Chen et al., 2004). A variety of GLVs are produced by the reduction of aldehyde moiety to form alcohol moiety and subsequent acetylation of alcohol moiety to form esters using the cinnamaldehyde and hexenal reductase (CHR, Tanaka et al., 2018) and acetyl-CoA:(*Z*)-3-hexen-1-ol acetyltransferase (CHAT, D'Auria et al., 2007), respectively. The (*E*)-form of GLVs is formed from its (*Z*)-form by Z3:E2-hexenal isomerase (HI, Kunishima et al., 2016; Spyropoulou et al., 2017). Additionally, when linoleic acid (LA) is processed through this pathway instead of LNA, the saturated *n*-form of GLVs are produced. Some of the GLVs endogenously produced in the leaf tissues accumulate as glycosides, for example, (*Z*)-3-hexenyl primeveroside (Z3HexPri) in the tea leaves (Ohgami et al., 2015; Jing et al., 2019). As evident from these studies, the biosynthetic pathways of endogenous GLVs have been extensively explored; however, little is known about how exogenous airborne GLVs are processed in plants.

In this study, we performed exposure experiments using various GLV species in tomato plants to analyze the metabolic changes in the exposed plants. The expected processing pathways of exogenous GLVs were tested using Arabidopsis mutant plants. The findings of this study could be helpful in the understanding of the communication of the plants within their ecosystem and, therefore, could assist in developing strategies to protect the crops and the natural flora, and maintain a balanced ecosystem.

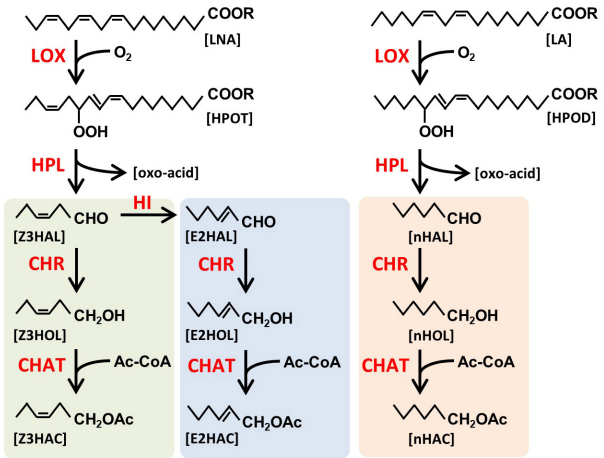

FIGURE 1 | Biosynthetic pathway of green leaf volatiles (GLVs). GLVs are fatty acid-derived volatiles. Linolenic acid (LNA) and linoleic acid (LA) are oxidized by lipoxygenases (LOX) to form 13-hydroperoxy octadecatrienoic acid (HPOT) and 13-hydroperoxy octadecadienoic acid (HPOD), respectively, and subsequently cleaved by hydroperoxide lyase (HPL) to form green leaf aldehydes, (*Z*)-3-hexenal (Z3HAL), and *n*-hexanal (nHAL), respectively. Z3HAL could be converted into (*E*)-2-hexenal (E2HAL) by Z3:E2-hexenal isomerase (HI). Three forms of green leaf aldehydes [Z3HAL (green), E2HAL (blue), and nHAL (orange)] are reduced by cinnamaldehyde and hexenal reductase (CHR) to form green leaf alcohols [(*Z*)-3-hexenol (Z3HOL), (*E*)-2-hexenol (E2HOL), and *n*-hexanol (nHOL), respectively]. The green leaf alcohols are subsequently acylated by acetyl CoA:(*Z*)-3-hexen-1-ol acetyltransferase (CHAT) to form (*Z*)-3-hexenyl acetate (Z3HAC), (*E*)-2-hexenyl acetate (E2HAC), and *n*-hexyl acetate (nHAC) with acetyl CoA as an acyl donor.

MATERIALS AND METHODS

Plants and Growth Conditions

Tomato plants (*Solanum lycopersicum*) cv. Micro-Tom were grown on potting soil in a growth room at 25°C with 14 h of fluorescent light (100 μE m^{-2} s^{-1}) and for 10 h in the dark. *Arabidopsis thaliana* wild-type Columbia (Col-0), Nossen (No-0), and Landsberg *erecta* (L*er*) were grown on half-strength MS plates in a growth chamber at 22°C with 16 h of fluorescent light (80 μE m^{-2} s^{-1}) and 8 h in the dark. Arabidopsis T-DNA insertion mutants of hexenal reductase (*chr*, Tanaka et al., 2018) and acetyl CoA:(*Z*)-3-hexen-1-ol acetyltransferase (*chat*, D'Auria et al., 2007) were developed by the previous work and kindly provided by Prof. J. D'Auria at Texas Tech University, respectively. A pair of the mutant and the corresponding wild-type was grown on a same plate to minimize the environmental effects on their growth and metabolisms.

Chemicals and Chemical Treatments

Volatile compounds were purchased from Wako Chemicals (Osaka, Japan), except for Z3HAL, which was kindly provided by Zeon Corporation (Tokyo, Japan). Formononetin, an internal standard for liquid chromatography-mass spectrometry (LC–MS) analysis, was purchased from Sigma-Aldrich (St. Louis, MO, United States). For volatile exposure, plants were enclosed

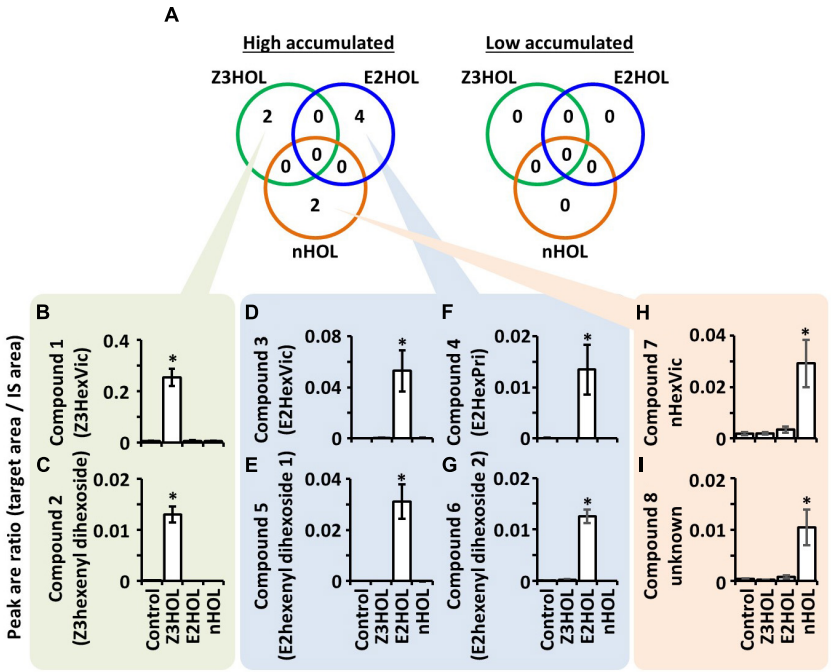

FIGURE 2 | Differentially accumulated compounds in tomato leaves exposed to the green leaf alcohols. **(A)** Numbers in the green, blue, and orange circles represent the differentially accumulated compounds in Z3HOL-, E2HOL-, and nHOL-exposed tomato leaves, respectively. The number of high-accumulated compounds in Z3HOL-, E2HOL-, and nHOL-exposed samples (2, 4, and 2, respectively). No overlapping compounds were found among exposed volatile species. **(B–I)** The relative quantity of each compound is shown in bar graphs (*$p < 0.05$; Dunnett test). The raw data is available in the **Supplementary Data**.

in a 2-L glass jar or a 10-L plexiglass box with the volatile-permeated cotton swab at 1 μM (22.4 ppmV) final concentration and exposed for 6 h. Sample leaves were excised from the exposed plants, flash-frozen in liquid nitrogen, and stored at −80°C until use.

Metabolite Extraction and Liquid Chromatography-Mass Spectrometry Analyses

Metabolite analyses were performed as described by Sugimoto et al. (2014). Briefly, leaf metabolites were extracted by adding 3 × volume of MeOH containing 1 μg mL^{-1} formononetin to ca. 100 mg of ground frozen leaf powder. The extract was injected into the LC-MS (3200 QTRAP, SCIEX, Framingham, MA, United States) or LC-high resolution-mass spectrometry (LC-HRMS; Finnigan LTQ-FT, Thermo Fisher Scientific, Waltham, MA, United States). Chromatographic separation was performed using 0.1% formic acid in water (solvent A) and 0.1% formic acid in acetonitrile (solvent B). The gradient program was started with 20% B for the initial 10 min, 20 to 50% for the next 10 min, followed by an increase from 50 to 95% in 20 min, and a constant 95% B for the final 5 min, with a constant flow rate of 0.2 mL min^{-1} and with an ODS column (Mightysil RP-18, 5 μm, 2 mm × 150 mm, Kanto Chemical, Tokyo, Japan) for LC-MS analysis. The gradient program for LC-HRMS analysis was started with 10% B, followed by an increase to 50% in 50 min, then 90% in 10 min followed by a constant 90% B for the final 5 min with a constant flow rate at 0.5 mL min^{-1}, and the separation was achieved with an ODS column (TSK-gel ODS-100V, 5 μm, 4.6 mm × 250 mm, TOSOH, Japan).

Data Analysis

Pairwise data between mutant and wild-types were compared by *t*-test. Multiple comparisons of the control and volatile treatments were analyzed by Dunnett's test, wherein, those of the genotype and wounding treatments were analyzed using Tukey's test. All the statistical analyses were performed using R software (R 4.0.3, R Core Team, 2021) with a threshold of $P < 0.05$. Metabolomic profiles were analyzed using a permutation test with MultiQuant software (SCIEX) with a threshold adjusted at $P < 0.05$.

RESULTS

Specific Changes of Tomato Leaf Metabolites by Exposure to Structurally Different Green Leaf Alcohols

Metabolite profiles of tomato leaf extracts were compared with LC-MS when the plants were exposed to the structurally different green leaf alcohols, Z3HOL, (*E*)-2-hexenol (E2HOL), and *n*-hexanol (nHOL). Data processing is summarized in **Supplementary Figure 1**. Single quadrupole LC-MS analysis detected 2,491 ions in the extracts (**Supplementary Data 1**).

Among 2,491 ions, 19, 15, and 20 ions were high in Z3HOL-, E2HOL-, and nHOL-exposed samples, respectively, compared with the control-exposed samples (**Supplementary Data 2**). Zero, one, and eight ions were lower in Z3HOL-, E2HOL-, and nHOL-exposed samples, respectively (**Supplementary Data 3**). The differentially accumulated ions had no overlap among the exposed volatile species. To obtain the rigid dataset, reproducible analysis was performed by LC-HRMS with independent extracts. In Z3HOL-exposed samples, nine ions of the nineteen candidates were reproducibly detected by LC-HRMS (**Supplementary Data 4**, green colors) and four ions of nine reproduced ones were statistically different from the control-exposed samples (**Supplementary Data 4**, dark green color). Similarly, nine of the 15 ions were reproducibly detected (**Supplementary Data 4**, blue colors), and six of the nine reproduced ions were statistically validated (**Supplementary Data 4**, dark blue color) in high accumulated ions in E2HOL-exposed plants. Seven of 20 in high accumulated ions in nHOL-exposed plants were reproducibly detected (**Supplementary Data 4**, orange colors) and three of the seven reproduced ions were statistically validated (**Supplementary Data 4**, dark orange color). On the other hand, no peaks were statistically validated in low accumulated ions even though two ions were reproducibly detected by LC-HRMS (**Supplementary Data 5**). Finally, four, six, and three reproducible ions were integrated into two, four, and two compounds in Z3HOL-, E2HOL-, and nHOL-exposed samples, respectively (**Figure 2**, **Supplementary Data 6**, and **Supplementary Figure 1**), by considering the retention times (RTs) with chromatographic patterns, isotopic ions, and different adducts as described below.

It is already known that the Z3HOL-exposed tomato plants accumulate both Z3HexVic (**Figure 3A**, peak a) and Z3HexPri (**Figure 3A**, peak b) (Sugimoto et al., 2014). In this analysis, E2HOL-exposed tomato showed a similar chromatographic pattern to Z3HOL-exposed plants with a 1-min delay at *m/z* = 417 (**Figure 3A**, peaks c and d). Considering the biosynthesis of Z3HexVic and Z3HexPri in Z3HOL-exposed plants, e.g., absorbing and converting the airborne Z3HOL into its glycoside, the peak c and d of **Figure 3A** in E2HOL-exposed plants putatively derived from the conversion of airborne E2HOL, and were (*E*)-2-hexenyl vicianoside (E2HexVic) and (*E*)-2-hexenyl primeveroside (E2HexPri), respectively (**Supplementary Data 6**). The similarity of MS and MS/MS spectra of Z3HexVic and E2HexVic gave the additional support to this conclusion. The MS spectrum of Z3HexVic (**Figure 3A**, peak a) indicated its molecular ion $[(M + H)^+ = 395.19]$, adduct ions with ammonium $[(M + NH_4)^+ = 412.22]$, sodium $[(M + Na)^+ = 417.17]$ and potassium $[(M + K)^+ = 433.15]$, and its isotopic ions $\{[M(^{13}C) + Na]^+ = 418.18, [M(^{13}C \times 2) + Na]^+ = 419.18\}$ (**Supplementary Figure 2A**, MS spectra). The MS spectrum of E2HexVic (**Figure 3A**, peak c) consisted of the same patterns as Z3HexVic (**Supplementary Figure 2B**, MS spectra) since the aglycon of two compounds were isomers. The MS/MS fragments of Z3HexVic consisted of a dehydrated ($-H_2O$) ion (*m/z* = 377.10), a single sugar-deleted ion (*m/z* = 198.28, **Supplementary Figure 2A**, MS/MS spectra)

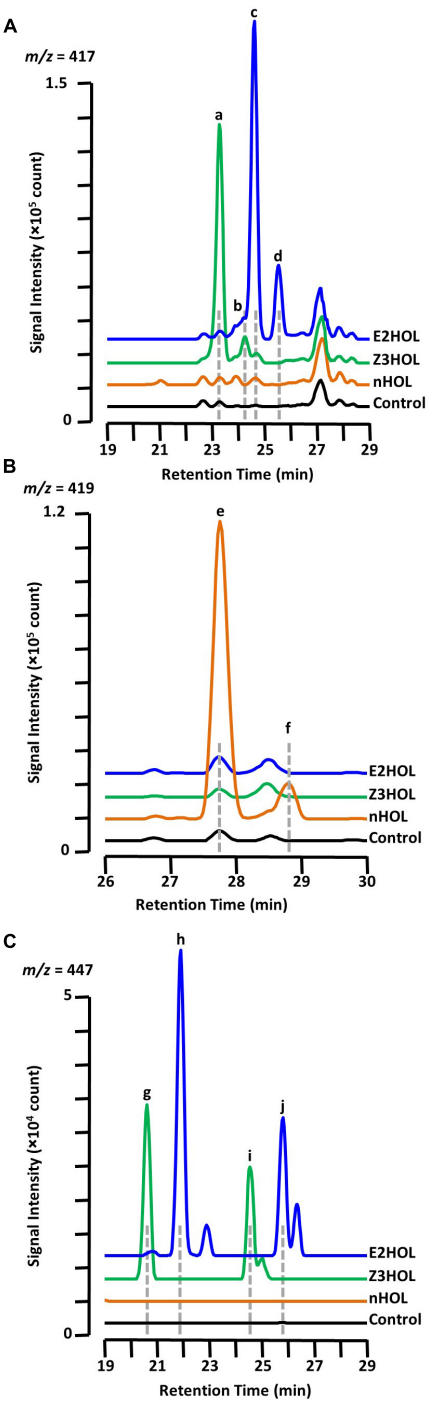

FIGURE 3 | Chromatographic analysis of glycoside accumulation in the green leaf alcohol-exposed tomato. Chromatograms from Z3HOL-, E2HOL-, and nHOL-exposed leaf extracts (green, blue, and orange lines, respectively) were compared at the *m/z* = 417 **(A)**, 419 **(B)**, and 447 **(C)**, corresponding to the green leaf alcohol-diglycoside conjugates. The chromatogram of the control leaf extract is shown by the black line. Peaks a and b are (*Z*)-3-hexenyl vicianoside and (*Z*)-3-hexenyl primeveroside, respectively. Peaks c through f are (*E*)-2-hexenyl vicianoside, (*E*)-2-hexenyl primeveroside, *n*-hexyl vicianoside, and *n*-hexyl primeveroside, respectively. Peaks g and i were (*Z*)-3-hexenyl dihexosides, and peaks h and j are (*E*)-2-hexenyl dihexosides.

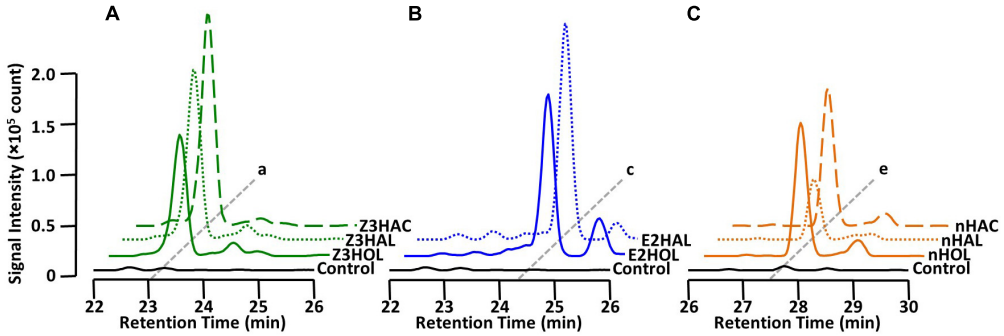

FIGURE 4 | Diglycoside accumulation in GLV-exposed tomato. Comparison of the chromatograms from **(A)** Z3HAL-, Z3HOL-, and Z3HAC-exposed leaf extracts at *m/z* = 417. (*Z*)-3-Hexenyl vicianoside (a) accumulated in the (*Z*)-form GLVs exposed plants. **(B)** E2HAL- and E2HOL-exposed leaf extracts at *m/z* = 417. (*E*)-2-Hexenyl vicianoside (c) was accumulated in both (*E*)-forms of GLV- exposed plants. **(C)** nHAL-, nHOL-, and nHAC-exposed leaf extracts at *m/z* = 419. *n*-Hexyl vicianoside (e) was accumulated in the *n*-form GLVs exposed plants. The chromatogram of the control leaf extract is shown by the black line.

with two unassigned ions (*m/z* = 219.08 and 233.09). The MS/MS fragments of E2HexVic consisted of the same assigned ions (**Supplementary Figure 2B**, MS/MS spectra) with two unassigned ions (*m/z* = 233.17 and 295.01). Under the same concept, nHOL exposure caused similar peak patterns at *m/z* = 419 with a 4.5-min delay from Z3HexVic and Z3HexPri (**Figure 3B**, peaks e and f). This also suggests that airborne nHOL was likely to be converted into *n*-hexyl vicianoside (nHexVic) and *n*-hexyl primeveroside (nHexPri), reflecting two more hydrogens in nHOL (monoisotopic mass = 102.104) compared with Z3HOL and E2HOL (100.089) (**Supplementary Figure 2**, structure). The MS spectrum of nHexVic (**Figure 3B**, peak e) consisted of its molecular ion $[(M + H)^+ = 397.21]$, adduct ions with ammonium $[(M + NH_4)^+ = 414.23]$, sodium $[(M + Na)^+ = 419.19]$ and potassium $[(M + K)^+ = 435.16]$, and its isotopic ions $\{[M(^{13}C) + Na]^+ = 420.19, [M(^{13}C \times 2) + Na]^+ = 421.19\}$ (**Supplementary Figure 2C**, MS spectra). Another ion was detected with high accumulation in nHOL-exposed tomato, which was unassigned by HRMS; therefore the compound remained as an "unknown" compound even with its coelution with nHexVic (**Supplementary Data 6**).

Under the same context, Z3HOL-exposed plants showed other marginally and significantly accumulated ions with *m/z* = 447 at RT = 20.86 and 24.81 min, respectively (**Figure 3C**, peaks g and i), which were predicted as hexenyl dihexosides by HRMS. The ions with the same *m/z* were also detected in E2HOL-exposed plants with a 1-min delay in their RTs (**Figure 3C**, peaks h and j), which was also predicted as hexenyl dihexosides by HRMS. The similar chromatographic patterns between Z3HOL- and E2HOL-exposure implied that these ions were formed by the conversion of airborne volatiles and predicted as (*Z*)-3- or (*E*)-2-hexenyl dihexosides.

Glycoside Accumulation by Exposure to Different Green Leaf Volatiles

It has been shown that in addition to green leaf alcohols, other groups of GLVs, such as aldehydes and esters, also make the exposed plants defensive (Kishimoto et al., 2005; Frost et al., 2008; Hu et al., 2019; Su et al., 2020). In this study, we tested whether airborne green leaf aldehydes and esters were converted into their corresponding defensive glycosides. The findings demonstrated that exposure of the tomato plants to Z3HAL and (*Z*)-3-hexenyl acetate (Z3HAC) accumulated Z3HexVic similar to Z3HOL exposure (**Figure 4A**). Similarly, exposure to E2HAL accumulated the same compound found in E2HOL exposed plants, and the exposure of nHAL and *n*-hexyl acetate (nHAC) led to the accumulation of the same compound found in nHOL-exposed plants (**Figures 4B,C**).

Estimation of the Z3HexVic Biosynthetic Route From Non-alcohol Green Leaf Volatiles

Like the endogenous Z3HOL biosynthesis process in plants, the aldehyde moiety of the exogenous Z3HAL is reduced to alcohols. Here, to understand the effect of the mutation on glycoside accumulation, we used a Z3HAL reductase mutant of *Arabidopsis thaliana* (Tanaka et al., 2018). It has been shown that the Col-0 ecotype with a natural mutation in *HPL* gene that cannot produce GLVs (Duan et al., 2005) accumulates (*Z*)-3-hexenyl glucoside (Z3HexGlc) rather than Z3HexVic by Z3HOL exposure (Sugimoto et al., 2015). In addition, we also show that exposure of the Col-0 plants to Z3HAL, Z3HOL, and Z3HAC, accumulated Z3HexGlc (**Figure 5A**). On the contrary, exposure of the Z3HAL reductase mutant plants (*chr*) to Z3HAL accumulated a lower amount of Z3HexGlc than the Z3HAL-exposed Col-0 plants. However, the *chr* and Col-0 plants accumulated similar levels of Z3HexGlc after Z3HOL and Z3HAC exposure (**Figure 5A**). It is also known that Z3HOL is esterified by acetyl-CoA:(*Z*)-3-hexen-1-ol acetyltransferase (CHAT) for Z3HAC production. The CHAT mutant (*chat*) and its parental ecotype (L*er*) showed similar levels of Z3HexGlc accumulation following Z3HOL and Z3HAC exposure; however, the *chat* mutant accumulated higher amounts of Z3HexGlc compared with L*er* after Z3HAL exposure (**Figure 5B**). Additionally, the amount of Z3HexGlc was measured in another *chr* mutant in the No-0 ecotype, which

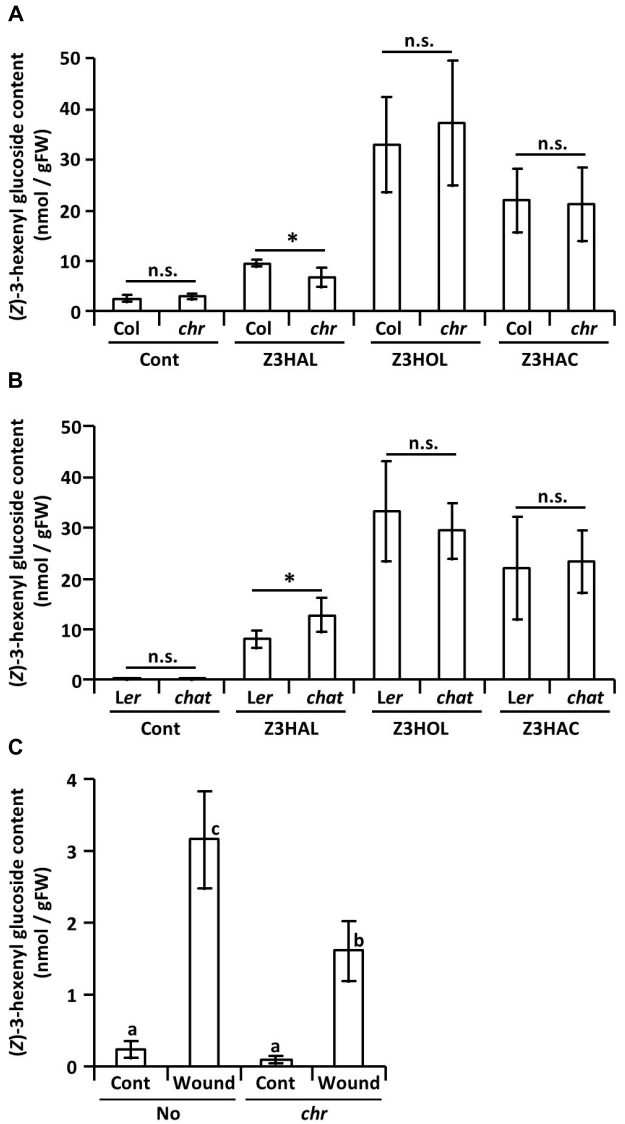

FIGURE 5 | Accumulation of (*Z*)-3-hexenyl glucoside in GLV-exposed and wounded Arabidopsis plants. Comparison of the amount of (*Z*)-3-hexenyl glucoside between **(A)** the *chr* mutant and its corresponding wild type (Col) plants and **(B)** the *chat* mutant and its corresponding wild type (L*er*) plants after (*Z*)-3-GLVs exposure. Wild types and mutants are exposed together in the same plexiglass box as described in Materials and Methods. Data are shown as mean ± SE (N = 5–7). The difference between the wild types and mutants was analyzed by t-test (*$p < 0.05$). **(C)** The amount of (*Z*)-3-hexenyl glucoside in the *chr* mutant and its corresponding wild type (No) plants with or without wounding (Wound/Cont) was compared, data are shown as mean ± SE (N = 6–20). Different letters indicate the significant difference ($p < 0.05$; Tukey's multiple comparisons).

enables the production of endogenous GLVs to test whether the endogenously produced Z3HAL was converted into Z3HexGlc through the Z3HOL biosynthetic pathway. The No-0 plants accumulated Z3HexGlc by wounding treatment; in contrast, the *chr* mutant plants accumulated significantly lower amounts of Z3HexGlc under the wounded conditions (**Figure 5C**).

DISCUSSION

Potential Involvement of the Processing of Volatiles in Defense Induction

Metabolomic analysis of the GLV-exposed tomato leaves indicated that only a limited number of changes occurred, predominantly the glycosylation of exogenous volatiles (**Figure 3** and **Supplementary Data**). Nevertheless, GLV-exposure induces diverse defensive responses against pathogens and herbivores. For example, Arabidopsis plants exposed to Z3HAL and E2HAL elicit a defense against the necrotrophic fungus, *Botrytis cinerea*, with the upregulation of various defense genes (Kishimoto et al., 2005, 2006; Yamauchi et al., 2015). GLV-exposed maize plants show enhanced defensive traits against insect herbivory, *S. littoralis* (Hu et al., 2019) by jasmonate accumulation (Engelberth et al., 2004, 2007; Hu et al., 2019; Gorman et al., 2020), volatile emissions (Farag et al., 2005; Ruther and Kleier, 2005; Yan and Wang, 2006; Hu et al., 2019), and gene expression (Farag et al., 2005; Engelberth et al., 2013; Hu et al., 2019). Z3HAC also elicits an enhanced defense against herbivory in exposed maize plants with primed JA accumulation and gene expression of benzoxazinoid biosynthesis, a specialized defense chemical in maize (Engelberth et al., 2007; Hu et al., 2019). Additionally, Z3HOL exposure in tea plants creates prime conditions for defense gene expression and plant defense against subsequent infestation by the tea geometrid, *Ectropis obliqua* (Xin et al., 2019). Z3HOL exposure also provides tomato plants with increased defense against *Tomato yellow leaf curl virus* transmission by the whitefly, *Bemisia tabaci*, with primed defense gene expression and metabolite accumulation (Su et al., 2020). The large gap between the limited metabolic changes and the diverse defense responses suggest that the processing of GLVs might be involved in defense induction in plants. On the contrary, the substantial accumulation of Z3HexVic begins to be detected ca. 0.5–1 h in the Z3HOL-exposed tomato plants (Sugimoto et al., 2014). This period is much longer than the known "early responses," such as the change in membrane potential occurring within seconds in the Z3HAL-, E2HAL-, and Z3HAC-exposed tomato plants (Zebelo et al., 2012). Reportedly, MAPK activation was observed around 3 min after the exposure of GLVs in *Lolium* plants (Dombrowski and Martin, 2018), and cytosolic calcium influx was detected at 10 min after E2HAL- and Z3HAC-exposure (Zebelo et al., 2012). Therefore, further studies are required to test whether GLV-glycosylation/-processing is involved in defense induction.

Processing Pathway of Exogenous Green Leaf Volatiles

Glycosylation of exogenous Z3HOL is known in various plant species including tomato, Arabidopsis, and tea plants (Sugimoto et al., 2014, 2015; Jing et al., 2019); however, the information on how plants process exogenous green leaf aldehydes and esters is limited. The emission of Z3HOL and Z3HAC by Z3HAL-exposed Arabidopsis plants suggested that the conversion of exogenous aldehyde occurs *via* a pathway similar to that of GLV biosynthesis (Matsui et al., 2012).

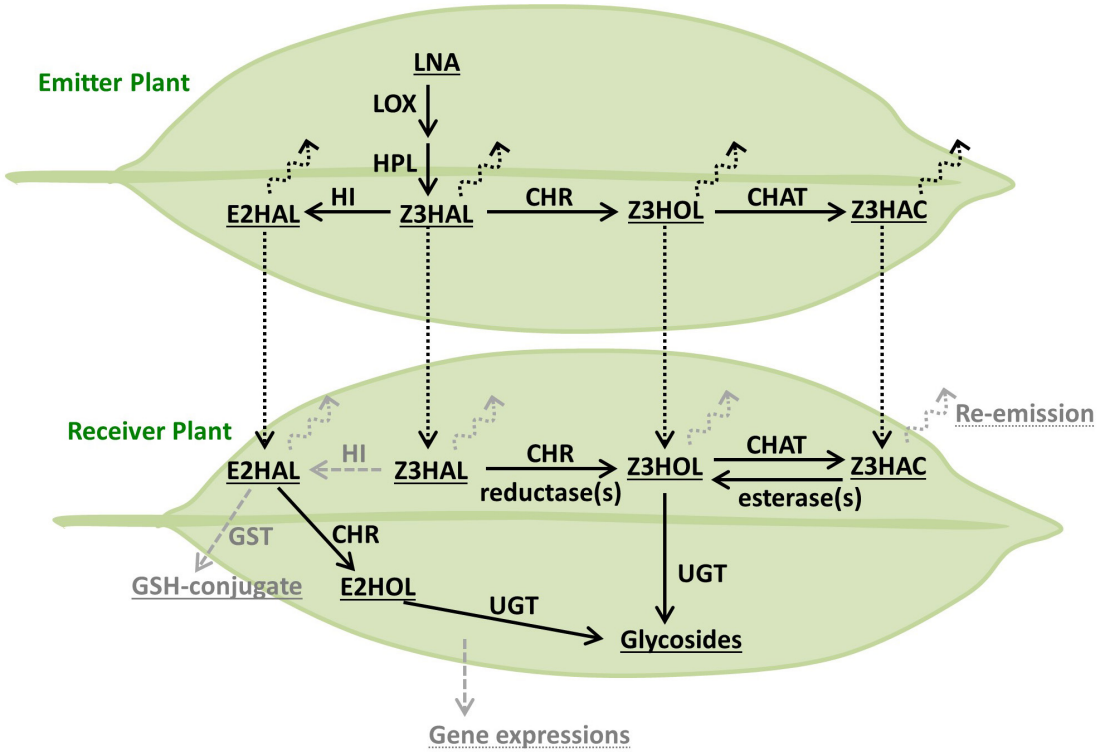

FIGURE 6 | Model of the processing route of green leaf volatiles. The biosynthetic pathway of GLVs originated from LNA is depicted in the emitter plant (top leaf). Processing of exogenous GLVs is depicted in the receiver plant (bottom leaf). The compounds, enzymes, and other processes are described as underlined, plain, and dotted-underlined text, respectively. The enzymatic conversion and airborne transfer are indicated as solid and dotted arrows, respectively. The potential components, which were not found or tested in this study, are shown in gray.

Here, we showed that the exogenous green leaf aldehydes were converted into their glycosides (**Figure 4**), and the conversion pathway was partly controlled by the CHR enzyme (**Figures 5A**, **6**), as evident from the mutant analysis. Notably, the findings demonstrated that the *chr* mutant accumulated some Z3HexGlc after exposure to high amounts of Z3HAL or wounding in the Z3HAL producing ecotype. Therefore, it is expected that (an)other enzyme(s) might be involved in the conversion of exogenous Z3HAL into Z3HOL, such as alcohol dehydrogenase (Bate et al., 1998; Speirs et al., 1998).

Interestingly, Z3HAC-exposure accumulated Z3HexGlc in Arabidopsis plants (**Figures 4**, **5**), suggesting the presence of an opposite reaction of GLV biosynthesis mediated by an unidentified enzyme. Z3HAC hydrolysis has also been suggested by Z3HexVic accumulation in Z3HAC-exposed wheat plants (Ameye et al., 2020). The *chat* mutant accumulated significantly higher amounts of Z3HexGlc upon Z3HAL-exposure (**Figure 5B**), probably because the *chat* mutant impaired the conversion of Z3HOL into Z3HAC, which might cause overaccumulation of Z3HOL, allowing the excess amount of Z3HOL to be used for Z3HexGlc production. This indicates that exogenous Z3HAL is serially converted into Z3HOL and Z3HAC by CHR and CHAT enzymes, respectively. This result supports the previous prediction regarding the re-emission of Z3HOL and Z3HAC from the Z3HAL-exposed plants (Matsui et al., 2012).

Future Prospects of Green Leaf Volatile-Glycosylation in Plant Defense

Glycosylation of GLVs is a widely deployed defense mechanism in plants (Sugimoto et al., 2014; Jing et al., 2019; Ameye et al., 2020), and the purified Z3HexVic functions as a defensive chemical against herbivory (Sugimoto et al., 2014). Although other defensive glycosides such as hydroxygeranyllinalool diterpene glycosides (HGL-DTGs) accumulated in wild tobacco, *Nicotiana attenuata* (Heiling et al., 2010), have toxic effects (Poreddy et al., 2015), the mode of action of Z3HexVic and other GLV-glycosides remains unknown. Additionally, simultaneous quantitative analysis of the glycosides, the volatiles, and other GLV-derived compounds clarified the complete fate of the exogenous/endogenous GLVs (**Figure 6**). For example, the absorbed exogenous GLVs are partly reemitted as volatiles and converted to other GLVs (Matsui et al., 2012) and stored as non-volatile compounds such as glycosides (**Figures 3**, **4**; Sugimoto et al., 2014) and glutathione-conjugates (Davoine et al., 2006). To obtain an adequate substrate for glycosylation, absorbed GLVs should be processed through the biosynthetic pathway (Z3HAL to Z3HOL) and its' reverse pathway (Z3HAC to Z3HOL), depending on the type of airborne GLVs. In this analysis,

Z3HAL-exposed tomato plants accumulated an undetectable amount of E2HexVic, even though the functional Z3:E2-hexenal isomerase was present in the tomato genome (Kunishima et al., 2016; Spyropoulou et al., 2017). A potential explanation is that tomato plants might have a low HI activity and therefore emit a reduced amount of (*E*)-2-form GLVs compared with (*Z*)-3-form GLV emission (Degenhardt et al., 2010; Sugimoto et al., 2014). Another possibility is the difference in volatile processing against endogenous GLV production occurring within minutes (D'Auria et al., 2007), and exogenous GLV glycosylation is detectable within hours (Sugimoto et al., 2014). It will also be a future challenge to investigate and understand how exogenous volatiles induce defense responses. Furthermore, the exact mechanism of the absorption/penetration of the airborne GLVs should be explored to clarify the complete mechanism of the defensive roles of GLVs.

DATA AVAILABILITY STATEMENT

The datasets presented in this study can be found in online repositories. The names of the repository/repositories and accession number(s) can be found in the article/ **Supplementary Material**.

AUTHOR CONTRIBUTIONS

KS designed the research and analyzed the data. KS and YI performed the experiments. KS, JT, and KM wrote the manuscript. All authors contributed to the article and approved the submitted version.

FUNDING

The authors are also grateful for the grant support for priority area (S) from the Ministry of Education, Culture, Sports, Science, and Technology of Japan; Research Fellowships for Young Scientists (24·841) from the Japan Society for the Promotion of Science; and Cooperative Research Grant #13-Jikkenn-2 and #2109 of the Plant Transgenic Design Initiative (PTraD) by Tsukuba-Plant Innovation Research Center, University of Tsukuba.

ACKNOWLEDGMENTS

The authors would like to thank Saunia Withers at the Duke University for her native English language corrections. The authors would also like to thank Editage (www.editage.com) for English language editing.

SUPPLEMENTARY MATERIAL

The Supplementary Material for this article can be found online at: https://www.frontiersin.org/articles/10.3389/fpls.2021.721572/full#supplementary-material

REFERENCES

Ameye, M., van Meulebroek, L., Meuninck, B., Vanhaecke, L., Smagghe, G., Haesaert, G., et al. (2020). Metabolomics reveal induction of ROS production and glycosylation events in wheat upon exposure to the green leaf colatile Z-3-hexenyl acetate. *Front. Plant Sci.* 11:596271. doi: 10.3389/fpls.2020.596271

Arimura, G.-I., Matsui, K., and Takabayashi, J. (2009). Chemical and molecular ecology of herbivore-induced plant volatiles: proximate factors and their ultimate functions. *Plant Cell Physiol.* 50, 911–923. doi: 10.1093/pcp/pcp030

Bate, N. J., Riley, J. C. M., Thompson, J. E., and Rothstein, S. J. (1998). Quantitative and qualitative differences in C_6-volatile production from the lipoxygenase pathway in an alcohol dehydrogenase mutant of *Arabidopsis thaliana*. *Physiol. Plant.* 104, 97–104. doi: 10.1034/j.1399-3054.1998.1040113.x

Chen, G., Hackett, R., Walker, D., Taylor, A., Lin, Z., and Grierson, D. (2004). Identification of a specific isoform of tomato lipoxygenase (TomloxC) incolved in the generation of fatty acif-derived flavor compounds. *Plant Physiol.* 136, 2641–2651. doi: 10.1104/pp.104.041608

D'Auria, J. C., Pichersky, E., Schaub, A., Hansel, A., and Gershenzon, J. (2007). Characterization of a BAHD acyltransferase responsible for producing the green leaf volatile (Z)-3-hexen-1-yl acetate in *Arabidopsis thaliana*. *Plant J.* 49, 194–207. doi: 10.1111/j.1365-313X.2006.02946.x

Davoine, C., Falletti, O., Douki, T., Iacazio, G., Ennar, N., Montillet, J.-L., et al. (2006). Adducts of oxylipin electrophiles to glutathione reflect a 13 specificity of the downstream lipoxygenase pathway in the tobacco hypersensitive response. *Plant Physiol.* 140, 1484–1493. doi: 10.1104/pp.105.074690

Degenhardt, D. C., Refi-Hind, S., Stratmann, J. W., and Lincoln, D. E. (2010). Systemin and jasmonic acid regulate constitutive and herbivore-induced systemic volatile emissions in tomato, *Solanum lycopersicum*. *Phytochemistry* 71, 2024–2037. doi: 10.1016/j.phytochem.2010.09.010

Dombrowski, J. E., and Martin, R. C. (2018) Activation of MAP kinases by green leaf volatiles in grasses. *BMC Res. Notes* 11:79. doi: 10.1186/s13104-017-3076-9

Duan, H., Huang, M. Y., Palacio, K., and Schuler, M. A. (2005). Variations in CYP74B2 (hydroperoxide lyase) gene expression differentially affect hexenal signaling in the Columbia and *Landsberg erecta* ecotypes of *Arabidopsis*. *Plant Physiol.* 139, 1529–1544. doi: 10.1104/pp.105.067249

Engelberth, J., Alborn, H. T., Schmelz, E. A., and Tumlinson, J. H. (2004). Airborne signals prime plants against insect herbivore attack. *Proc. Natl. Acad. Sci. U.S.A.* 101, 1781–1785. doi: 10.1073/pnas.0308037100

Engelberth, J., Contreras, C. F., Calvi, C., Li, T., and Engelberth, M. (2013). Early transcriptome analyses of Z-3-hexenol-treated *Zea mays* revealed distinct transcriptional networks and anti-herbivore defense potential of green leaf volatiles. *PLoS One* 8:e77465. doi: 10.1371/journal.pone.0077465

Engelberth, J., Seidl-Adams, I., Schultz, J. C., and Tumlinson, J. H. (2007).) Insect elicitors and exposure to green leafy volatiles differentially upregulate major octadecanoids and transcripts of 12-oxo phytodienoic acid reductases in *Zea mays*. *Mol. Plant Microbe Interact.* 20, 707–716. doi: 10.1094/MPMI -20-6-0707

Farag, M. A., Fokar, M., Abd, H., Zhang, H., Allen, R. D., and Paré, P. W. (2005). (Z)-3-Hexenol induces defense genes and downstream metabolites in maize. *Planta* 220, 900–909. doi: 10.1007/s00425-004-1404-5

Farag, M. A., and Paré, P. W. (2002). C_6-Green leaf volatiles trigger local and systemic VOC emissions in tomato. *Phytochemistry* 61, 545–554. doi: 10.1016/S0031-9422(02)00240-6

Frost, C. J., Mescher, M. C., Dervinis, C., Davis, J. M., Carlson, J. E., and De Moraes, C. M. (2008). Priming defense genes and metabolites in hybrid poplar by the green leaf volatile cis-3-hexenyl acetate. *New Phytol.* 180, 722–734. doi: 10.1111/j.1469-8137.2008.02599.x

Gorman, Z., Christensen, S. A., Yan, Y., He, Y., Borrego, E., and Kolomiets, M. V. (2020). Green leaf volatiles and jasmonic acid enhance susceptibility to

anthracnose diseases caused by *Colletotrichum graminicola* in maize. *Mol. Plant Pathol.* 21, 702–715. doi: 10.1111/mpp.12924

Halitschke, R., and Baldwin, I. T. (2003). Antisense LOX expression increases herbivore performance by decreasing defense responses and inhibiting growth-related transcriptional reorganization in *Nicotiana attenuate*. *Plant J.* 36, 794–807. doi: 10.1046/j.1365-313x.2003.01921.x

Heiling, S., Schuman, M. C., Schoettner, M., Mukerjee, P., Berger, B., Schneider, B., et al. (2010). Jasmonate and ppHsystemin regulate key malonylation steps in the biosynthesis of 17-hydroxygeranyllinalool diterpene glycosides, an abundant and effective direct defense against herbivores in *Nicotiana attenuate*. *Plant Cell* 22, 273–292. doi: 10.1105/tpc.109.071449

Hu, L., Ye, M., and Erb, M. (2019). Integration of two herbivore-induced plant volatiles results in synergistic effects on plant defence and resistance. *Plant Cell Environ.* 42, 959–971. doi: 10.1111/pce.13443

Jing, T., Zhang, N., Gao, T., Zhao, M., Jin, J., Chen, Y., et al. (2019). Glucosylation of (Z)-3-hexenol informs intraspecies interactions in plants: a case study in *Camellia sinensis*. *Plant Cell Environ.* 42, 1352–1367. doi: 10.1111/pce.13479

Kikuta, Y., Ueda, H., Nakayama, K., Katsuda, Y., Ozawa, R., Takabayashi, J., et al. (2011). Specific regulation of pyrethrin biosynthesis in *Chrysanthemum cinerariaefolium* by a blend of volatiles emitted from artificially damaged conspecific plants. *Plant Cell Physiol.* 52, 588–596. doi: 10.1093/pcp/pcr017

Kishimoto, K., Matsui, K., Ozawa, R., and Takabayashi, J. (2005). Volatile C6-aldehydes and allo-ocimene activate defense genes and induce resistance against *Botrytis cinereal* in *Arabidopsis thaliana*. *Plant Cell Physiol.* 46, 1093–1102. doi: 10.1093/pcp/pci122

Kishimoto, K., Matsui, K., Ozawa, R., and Takabayashi, J. (2006). ETR-, JAR1- and PAD2-dependent signaling pathway are involved in C6-aldehyde-induced defense responses of Arabidopsis. *Plant Sci.* 171, 415–423. doi: 10.1016/j.plantsci.2006.05.004

Kunishima, M., Yamauchi, Y., Mizutani, M., Kuse, M., Takikawa, H., and Sugimoto, Y. (2016). Identification of (Z)-3:(E)-2-hexenal isomerases essential to the production of the leaf aldehyde in plants. *J. Biol. Chem.* 291, 14023–14033. doi: 10.1074/jbc.M116.726687

Matsui, K., Shibutani, M., Hase, T., and Kajiwara, T. (1996). Bell pepper fruit fatty acid hydroperoxide lyase is a cytochrome P450 (CYP74B). *FEBS Lett.* 394, 21–24. doi: 10.1016/0014-5793(96)00924-6

Matsui, K., Sugimoto, K., Mano, J., Ozawa, R., and Takabayashi, J. (2012). Differential metabolisms of green leaf volatiles in injured and intact parts of a wounded leaf meed distinct ecophysiological requirements. *PLoS One* 7:e36433. doi: 10.1371/journal.pone.0036433

Ohgami, S., Ono, E., Hirokawa, M., Murata, J., Totsuka, K., Toyonaga, H., et al. (2015). Volatile glycosylation in tea plants: sequential glycosylations for the biosynthesis of aroma β-primeverosides are catalyzed by two *Camellia sinensis* glycosyltransferases. *Plant Physiol.* 168, 464–477. doi: 10.1104/pp.15.00403

Poreddy, S., Mitra, S., Schöttner, M., Chandran, J., Schneider, B., Baldwin, I. T., et al. (2015). Detoxification of hostplant's chemical defence rather than its anti-predator co-option drives b-glucosidase-mediated lepidopteran counteradaptation. *Nat. Commun.* 6:8525. doi: 10.1038/ncomms9525

R Core Team (2021). *R: A Language and Environment for Statistical Computing*. Vienna: R Foundation for Statistical Computing. Available online at: https://www.R-project.org/

Ruther, J., and Kleier, S. (2005). Plant-plant signaling: ethylene synergizes volatile emission in *Zea mays* induced by exposure to (Z)-3-hexen-1-ol. *J. Chem. Ecol.* 31, 2217–2222. doi: 10.1007/s10886-005-6413-8

Speirs, J., Lee, E., Holt, K., Yong-Duk, K., Scott, N. S., Loveys, B., et al. (1998). Genetic manipulation of alcohol dehydrogenase levels in ripening tomato fruit affects the balance of some flavor aldehydes and alcohols. *Plant Physiol.* 117, 1047–1058. doi: 10.1104/pp.117.3.1047

Spyropoulou, E. A., Dekker, H. L., Steemers, L., van Maarseveen, J. H., de Koster, C. G., Haring, M. A., et al. (2017). Identification and characterization of (3Z):(2E)-hexenal isomerases from cucumber. *Front. Plant Sci.* 8:1342. doi: 10.3389/fpls.2017.01342

Su, Q., Yang, F., Zhang, Q., Tong, H., Hu, Y., Xhang, X., et al. (2020). Defence priming in tomato by the green leaf volatile (Z)-3-hexenol reduces whitefly transmission of a plant virus. *Plant Cell Environ.* 43, 2797–2811. doi: 10.1111/pce.13885

Sugimoto, K., Matsui, K., Iijima, Y., Akakabe, Y., Muramoto, S., Ozawa, R., et al. (2014). Intake and transformation to a glycoside of (Z)-3-hexenol from infested neighbors reveals a mode of plant odor reception and defense. *Proc. Natl. Acad. Sci. U.S.A.* 111, 7144–7149. doi: 10.1073/pnas.1320660111

Sugimoto, K., Matsui, K., and Takabayashi, J. (2015). Conversion of volatile alcohols into their glucosides in *Arabidopsis*. *Comm. Integr. Biol.* 8:e992731. doi: 10.4161/19420889.2014.992731

Tanaka, T., Ikeda, A., Shiojiri, K., Ozawa, R., Shiki, K., Nagai-Kunihiro, N., et al. (2018). Identification of a hexenal reductase that modulates the composition of green leaf volatiles. *Plant Physiol.* 178, 552–564. doi: 10.1104/pp.18.00632

Xin, Z., Ge, L., Chen, S., and Sun, X. (2019). Enhanced transcriptome responses in herbivore-infested tea plants by the green leaf volatile (Z)-3-hexenol. *J. Plant Res.* 132, 285–293. doi: 10.1007/s10265-019-01094-x

Yamauchi, Y., Kunishima, M., Mizutani, M., and Sugimoto, Y. (2015). Reactive short-chain leaf volatiles act as powerful inducers of abiotic stress-related gene expression. *Sci. Rep.* 5:8030. doi: 10.1038/srep08030

Yan, Z.-G., and Wang, C.-Z. (2006). Wound-induced green leaf volatiles cause the release of acetylated derivatives and a terpenoid in maize. *Phytochemistry* 67, 34–42. doi: 10.1016/j.phytochem.2005.10.005

Zebelo, S. A., Matsui, K., Ozawa, R., and Maffei, M. E. (2012). Plasma membrane potential depolarization and cytosolic calcium flux are early events involved in tomato (*Solanum lycopersicon*) plant-to-plant communication. *Plant Sci.* 196, 93–100. doi: 10.1016/j.plantsci.2012.08.006

Conflict of Interest: The authors declare that the research was conducted in the absence of any commercial or financial relationships that could be construed as a potential conflict of interest.

Publisher's Note: All claims expressed in this article are solely those of the authors and do not necessarily represent those of their affiliated organizations, or those of the publisher, the editors and the reviewers. Any product that may be evaluated in this article, or claim that may be made by its manufacturer, is not guaranteed or endorsed by the publisher.

Copyright © 2021 Sugimoto, Iijima, Takabayashi and Matsui. This is an open-access article distributed under the terms of the Creative Commons Attribution License (CC BY). The use, distribution or reproduction in other forums is permitted, provided the original author(s) and the copyright owner(s) are credited and that the original publication in this journal is cited, in accordance with accepted academic practice. No use, distribution or reproduction is permitted which does not comply with these terms.

Advantages of publishing in Frontiers

OPEN ACCESS
Articles are free to read for greatest visibility and readership

FAST PUBLICATION
Around 90 days from submission to decision

HIGH QUALITY PEER-REVIEW
Rigorous, collaborative, and constructive peer-review

TRANSPARENT PEER-REVIEW
Editors and reviewers acknowledged by name on published articles

Frontiers
Avenue du Tribunal-Fédéral 34
1005 Lausanne | Switzerland

Visit us: www.frontiersin.org
Contact us: frontiersin.org/about/contact

REPRODUCIBILITY OF RESEARCH
Support open data and methods to enhance research reproducibility

DIGITAL PUBLISHING
Articles designed for optimal readership across devices

FOLLOW US
@frontiersin

IMPACT METRICS
Advanced article metrics track visibility across digital media

EXTENSIVE PROMOTION
Marketing and promotion of impactful research

LOOP RESEARCH NETWORK
Our network increases your article's readership